



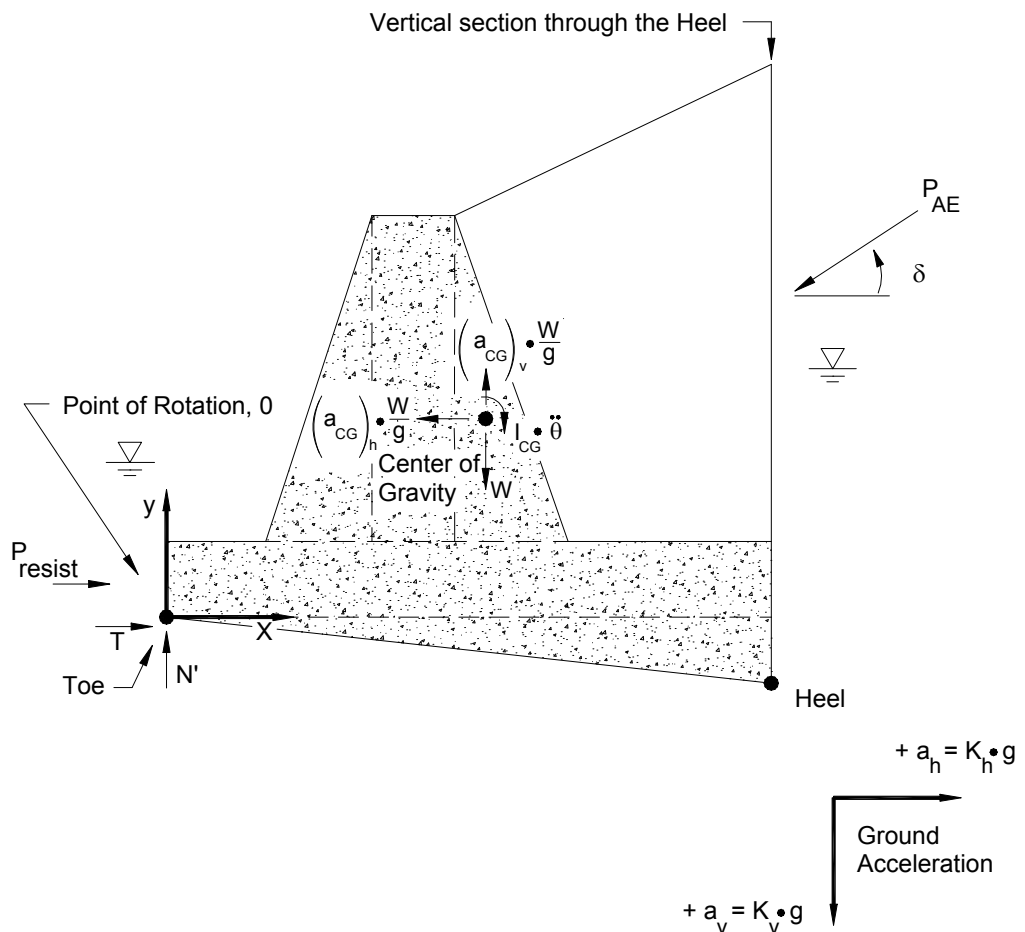
**US Army Corps  
of Engineers®**  
Engineer Research and  
Development Center

*Infrastructure Technology Research Program  
Navigation Systems Research Program*

# Rotational Response of Toe-Restrained Retaining Walls to Earthquake Ground Motions

Robert M. Ebeling and Barry C. White

December 2006



# **Rotational Response of Toe-Restrained Retaining Walls to Earthquake Ground Motions**

Robert M. Ebeling and Barry C. White

*Information Technology Laboratory  
U.S. Army Engineer Research and Development Center  
3909 Halls Ferry Road  
Vicksburg, MS 39180-6199*

Final report

Approved for public release; distribution is unlimited.

Prepared for U.S. Army Corps of Engineers  
Washington, DC 20314-1000

Under Work Unit 4402JC

**Abstract:** This research report describes the engineering formulation and corresponding software developed for the rotational response of rock-founded, toe-restrained Corps retaining walls to earthquake ground motions. The PC software  $C_{\text{corps}}W_{\text{all}}\text{Rotate}$  (sometimes referred to as  $CWR_{\text{rotate}}$ ) was developed to perform an analysis of permanent wall rotation for each proposed retaining wall section to a user-specified earthquake acceleration time-history. A particular formulation of the permanent sliding (i.e., translational) displacement response of retaining walls is also described. The resulting engineering methodology and corresponding software are applicable to a variety of retaining walls that are buttressed at their toes by a structural feature (e.g., navigation walls retaining earth, spillway chute walls, spillway discharge channel walls, approach channel walls to outlet works structures, highway and railway relocation retaining walls, and floodwall channels).  $C_{\text{corps}}W_{\text{all}}\text{Rotate}$  is particularly applicable to L-walls and T-walls (cantilever retaining walls) and may also be used to predict permanent, seismically induced displacements on retaining walls with or without a toe restraint.

Formal consideration of the permanent seismic wall displacement in the seismic design process for Corps-type retaining structures is given in Ebeling and Morrison (1992). The key aspect of the engineering approach presented in this 1992 document is that simplified procedures for computing the seismically induced earth loads on Corps retaining structures are also dependent upon the amount of permanent wall displacement expected to occur for each specified design earthquake. The Ebeling and Morrison simplified engineering procedures for Corps retaining structures, including waterfront retaining structures, are geared towards hand calculations. The engineering formulation and corresponding PC software  $C_{\text{corps}}W_{\text{all}}\text{Rotate}$  discussed in this report extend simplified procedures to walls that rotate or slide during earthquake shaking and make possible the use of acceleration time-histories in the Corps' design/analysis process when time-histories are made available on Corps projects. The engineering methods contained in this report and implemented within  $C_{\text{corps}}W_{\text{all}}\text{Rotate}$  allow the engineer to rapidly determine if a given retaining wall system has a tendency to rotate or to slide for a specified seismic event.

**DISCLAIMER:** The contents of this report are not to be used for advertising, publication, or promotional purposes. Citation of trade names does not constitute an official endorsement or approval of the use of such commercial products. All product names and trademarks cited are the property of their respective owners. The findings of this report are not to be construed as an official Department of the Army position unless so designated by other authorized documents.

**DESTROY THIS REPORT WHEN NO LONGER NEEDED. DO NOT RETURN IT TO THE ORIGINATOR.**

# Contents

<b>Figures and Tables</b> .....	<b>viii</b>
<b>Preface</b> .....	<b>xii</b>
<b>1 Introduction to Rotational or Sliding Response of Toe-Restrained Retaining Walls to Earthquake Ground Motions</b> .....	<b>1</b>
1.1 Introduction .....	1
1.1.1 Pseudo-static methods with a preselected seismic coefficient.....	4
1.1.2 Stress-deformation methods.....	7
1.1.3 Sliding block methods.....	11
1.2 Rotational analysis of a retaining structure modeled as a rigid block—existing methodologies.....	20
1.3 New rotational analysis model based on a rigid block problem formulation.....	26
1.4 Seismic design criteria for Corps retaining structures.....	28
1.5 Axial load capacity of spillway invert slabs .....	29
1.6 Background and research objective .....	31
1.7 Organization of report.....	32
<b>2 Existing Rotational Analysis Models of a Retaining Wall Rotating About a Point Along its Base</b> .....	<b>35</b>
2.1 Introduction.....	35
2.2 Nadim and Whitman rigid block model of a gravity wall with earthquake-induced, permanent rotation about a center of rocking located along the base of the wall .....	36
<i>Limiting acceleration of a wall – sliding</i> .....	41
<i>Limiting acceleration of a wall—lift-off of its base in rotation</i> .....	43
<i>Nadim and Whitman (1984) observations</i> .....	45
<i>Summary observations regarding the Nadim and Whitman formulation by other researchers</i> .....	45
2.3 Siddharthan, Ara, Anderson, Gowda, and Norris rigid block model of a gravity wall with earthquake-induced, coupled permanent rotation and sliding about a center of rotation located along the base of the wall .....	46
<i>Uncoupled equation for rotation</i> .....	51
<i>Foundation response</i> .....	53
<i>Summary observations regarding the Siddharthan et al. formulation by other researchers</i> .....	53
2.4 Fishman and Richards rigid block model of a bridge abutment with earthquake-induced, coupled permanent rotation and translation for free and fixed connections to bridge decks .....	54
2.5 Steedman and Zeng rigid block model of a gravity wall with earthquake-induced rotation about its toe .....	57
<i>Limiting acceleration of a wall – lift-off of its base in rotation</i> .....	60
<i>Angular acceleration and rotation of a wall</i> .....	61
<i>Limiting acceleration of a wall sliding</i> .....	62

	<i>Zeng and Steedman (1996 and 2000) observations</i> .....	64
<b>3</b>	<b>New Rotational Analysis Model of a Retaining Wall Rotating About Its Toe and Buttressed by a Reinforced Concrete Slab</b> .....	<b>65</b>
3.1	Introduction .....	65
3.2	Acceleration of rigid mass center (CG) .....	67
3.3	Threshold value of acceleration corresponding to incipient lift-off of the base of the wall in rotation .....	72
3.4	Angular acceleration of the retaining wall structural wedge – general formulation .....	75
3.5	Dynamic active earth pressure force $P_{AE}$ .....	79
3.6	Moments due to external forces acting about the toe of the structural wedge .....	83
3.7	Angular acceleration of the retaining wall structural wedge – formulation implemented in $C_{orps}W_{all}Rotate$ .....	84
3.8	Numerical method for computing the rotational time-history of a rigid block retaining structure rotating about its toe .....	85
3.8.1	<i>Introduction to a step-by-step solution scheme</i> .....	85
3.8.2	<i>Positive angular accelerations <math>\alpha_0</math> and <math>\alpha_1</math> at times <math>t_i</math> and <math>t_{i+1}</math></i> .....	87
3.8.3	<i>Positive angular acceleration <math>\alpha_0</math> at time <math>t_i</math> and negative angular acceleration <math>\alpha_1</math> at <math>t_{i+1}</math></i> .....	89
3.8.4	<i>Negative angular accelerations <math>\alpha_0</math> and <math>\alpha_1</math> at times <math>t_i</math> and <math>t_{i+1}</math></i> .....	95
3.8.5	<i>Positive angular acceleration <math>\alpha_0</math> at time <math>t_i</math> and negative angular acceleration <math>\alpha_1</math> at <math>t_{i+1}</math></i> .....	99
3.8.6	<i>Starting the <math>C_{orps}W_{all}Rotate</math> analysis and the initiation of wall rotation during a <math>DT</math> time-step</i> .....	104
3.8.7	<i>Cessation of wall rotation</i> .....	105
3.9	New rotational analysis model of a wall retaining a partially submerged backfill and rotating about its toe and buttressed by a reinforced concrete slab .....	106
3.9.1	<i>Threshold value of acceleration corresponding to incipient lift-off of the base of the wall in rotation—partially submerged backfill</i> .....	108
3.9.2	<i>Moments due to external forces acting about the toe of the structural wedge—partially submerged backfill</i> .....	110
3.9.3	<i>Angular acceleration of the structural wedge wall retaining a partially submerged backfill—formulation implemented in <math>C_{orps}W_{all}Rotate</math></i> .....	111
3.9.4	<i>Numerical method for computing the rotational time-history of a rigid block retaining structure rotating about its toe</i> .....	112
3.10	Effective vertical acceleration constant value for the incipient lift-off in rotation evaluation process .....	112
<b>4</b>	<b>New Translational Block Analysis Model of a Retaining Structure Buttressed by a Reinforced Concrete Slab</b> .....	<b>116</b>
4.1	Introduction .....	116
4.2	Contrasting a translational with the rotational analysis of a rigid block .....	117
4.3	Maximum transmissible acceleration .....	118
4.4	Time-history of permanent wall displacement.....	123
4.4.1	<i>Introduction to a step-by-step solution scheme</i> .....	124
4.4.2	<i>Positive relative accelerations <math>relAO</math> and <math>relA1</math> at times <math>t_i</math> and <math>t_{i+1}</math></i> .....	126

4.4.3 Positive relative acceleration $relA0$ at time $t_i$ and negative relative acceleration $relA1$ at $t_{i+1}$ .....	129
4.4.4 Negative relative accelerations $relA0$ and $relA1$ at times $t_i$ and $t_{i+1}$ .....	135
4.4.5 Positive relative acceleration $relA0$ at time $t_i$ and negative relative acceleration $relA1$ at $t_{i+1}$ .....	139
4.4.6 Starting the $C_{orpsWallRotate}$ analysis and the initiation of wall translation during a $DT$ time-step .....	144
4.4.7 Cessation of wall translation .....	145
4.5 New translational analysis model of a wall retaining a partially submerged backfill and buttressed by a reinforced concrete slab .....	145
4.5.1 Introduction .....	145
4.5.2 Threshold value of acceleration corresponding to incipient lift-off of the base of the wall in rotation—partially submerged backfill.....	148
4.5.3 Numerical method for computing the translational time-history of a rigid block retaining structure.....	153
4.6 Vertical acceleration in the new translational analysis model of a wall retaining a partially submerged backfill and buttressed by a reinforced concrete slab.....	153
<b>5 The Visual Modeler and Visual Post-Processor — <math>C_{orpsWallRotate}</math>.....</b>	<b>157</b>
5.1 Introduction .....	157
5.2 Visual modeler and visual post-processor .....	157
5.2.1 Introduction to the visual modeling environment.....	157
5.2.2 Earthquake time-history input .....	158
5.2.3 Structural geometry input.....	161
5.2.4 Structural wedge data.....	172
5.2.5 Driving wedge data .....	177
5.2.6 Analysis results and visual post-processor.....	181
5.2.7 Example 1 — Earth retaining wall at a dry soil site — No reinforced concrete slab buttress at the wall's toe .....	185
5.2.8 Example 2 — Earth retaining wall at a dry soil site — 1-foot thick reinforced concrete slab buttress at the wall's toe.....	193
<b>6 Summary, Conclusions, and Recommendations.....</b>	<b>205</b>
6.1 Summary and conclusions.....	205
6.2 Recommendations for future research .....	207
<b>References.....</b>	<b>210</b>
<b>Appendix A: Computation of the Dynamic Active Earth Pressure Forces for a Partially Submerged Retained Soil Using the Sweep-Search Wedge Method.....</b>	<b>215</b>
A.1 Introduction .....	215
A.2 Dynamic Active Earth Pressure Force, $P_{AE}$ — Effective Stress Analysis.....	217
A.2.1 Calculation of Water Pressure Forces for a Hydrostatic Water Table .....	219
A.2.2 Static Water Pressure Forces Acting on the Wedge.....	219
A.2.3 Equilibrium of Vertical Forces.....	220
A.2.4 Equilibrium of Forces in the Horizontal Direction.....	220
A.3 Static Active Earth Pressure Force, $P_A$ — Effective Stress Analysis .....	222

A.4 Dynamic Active Earth Pressure Force, $P_{AE}$ — Total Stress Analysis .....	225
A.5 Static Active Earth Pressure Force, $P_A$ — Total Stress Analysis .....	226
A.6 Weight Computation of a Soil Wedge with a Bilinear Ground Surface .....	228
A.6.1 $\alpha$ greater than $\alpha_{corner}$ .....	228
A.6.2 $\alpha_{corner}$ greater than $\alpha$ .....	233
<b>Appendix B: An Abbreviated Review of Dynamics of a Rigid Body .....</b>	<b>240</b>
B.1 Dynamic Equilibrium of a Particle under Planar Motion .....	240
B.2 Dynamic Equilibrium of a Rigid Mass under Planar Motion.....	243
B.3 Mass of a Rigid Body.....	246
B.4 Equation of Rotational Motion of a Rigid Mass .....	248
B.5 Equations of Motion: Rotation about a Fixed Axis .....	252
B.6 Planar Kinematics of a Rigid Body: Noncentroidal Rotation about a Fixed Axis.....	256
B.7 Planar Kinetics of a Rigid Body.....	257
<b>Appendix C: An Approach for Computing the Dynamic Active Earth Pressure Distribution for a Partially Submerged Retained Soil .....</b>	<b>259</b>
C.1 Earth Pressure Distribution for the Dynamic Active Earth Pressure Force, $P_{AE}$ , of a Partially Submerged, Cohesionless, Level Backfill — Effective Stress Analysis with $c'$ Equal to Zero .....	259
Step 1: Convert the static active earth pressure force, $P_A$ , into an equivalent active earth pressure diagram .....	260
Step 2: Create an incremental dynamic force component pressure diagram .....	263
Step 3: Create the dynamic active earth pressure diagram.....	264
Step 4: Complete the pressure diagram by adding in the pore water pressure distribution.....	264
C.2 Earth Pressure Distribution for the Static Active Earth Pressure Force, $P_A$ , component of $P_{AE}$ of a Cohesionless, Backfill with a Sloping or a Bilinear Ground Surface — Effective Stress Analysis with $c'$ Equal to Zero .....	266
C.2.1 The Basic Procedure to Compute the Active Effective Stress Distribution Corresponding to $P_A$ for a Moist Retained Soil with a Sloping Ground Surface .....	267
C.2.2 The Basic Procedure to Compute the Active Effective Stress Distribution Corresponding to $P_A$ for a Partially Submerged Retained Soil with a Sloping Ground Surface .....	268
C.2.3 The Basic Procedure to Compute the Active Effective Stress Distribution Corresponding to $P_A$ for a Partially Submerged Retained Soil with a Bilinear Ground Surface .....	271
C.3 Earth Pressure Distribution for the Dynamic Active Earth Pressure Force, $P_{AE}$ , for a Backfill with Mohr-Coulomb Shear Strength Parameters $c'$ and $\phi'$ — Effective Stress Analysis .....	273
C.3.1 The Basic Procedure to Compute the Active Effective Stress Distribution Corresponding to $P_A$ for a Partially Submerged Retained Soil with a Sloping Ground Surface .....	280
C.3.2 The Basic Procedure to Compute the Active Effective Stress Distribution Corresponding to $P_A$ for a Partially Submerged Retained Soil with a Bilinear Ground Surface .....	282
C.4 Earth Pressure Distribution for the Dynamic Active Earth Pressure Force, $P_{AE}$ , for a Backfill with Mohr-Coulomb Shear Strength Parameters, $S_u$ — Total Stress Analysis.....	284

C.4.1 The Basic Procedure to Compute the Active Total Stress Distribution Corresponding to $P_A$ for a Partially Submerged Retained Soil with a Sloping Ground Surface .....	289
C.4.2 The Basic Procedure to Compute the Active Total Stress Distribution Corresponding to $P_A$ for a Partially Submerged Retained Soil with a Bilinear Ground Surface .....	291
<b>Appendix D: Water Pressures Acting on a Partially Submerged Structural Wedge .....</b>	<b>294</b>
D.1 Steady-State Water Pressures Acting on the Structural Wedge.....	294
D.2 The Westergaard Procedure for Computing Hydrodynamic Water Pressures.....	298
<b>Appendix E: Mass Moment of Inertia Computation .....</b>	<b>302</b>
E.1 Mass Moment of Inertia of a Rectangle .....	302
E.2 Mass Moment of Inertia of a Triangle.....	306
E.3 Mass Moment of Inertia of the Structural Wedge .....	307
<b>Appendix F: Listing and Description of <math>C_{\text{orps}}W_{\text{all}}\text{Rotate}</math> ASCII Input Data File (file name: CWROTATE.IN) .....</b>	<b>308</b>
First line/First column – Designate this data input is for a $C_{\text{orps}}W_{\text{all}}\text{Rotate}$ analysis.....	308
Group 1 – Global Geometry of the Structural Wedge that Contains the Retaining Wall .....	308
Group 2 – Base of Structural Wedge.....	309
Group 3 – Resisting Force Normal to a Vertical Plane Extending up Through the Toe of the Structural Wedge.....	309
Group 4 – Driving Wedge in the Retained Soil.....	310
Group 5 – Water Table Height in the Retained Soil and Pool Height, with Input in Four Parts.....	311
Group 6 – Acceleration Time-Histories with Input in Two Parts .....	313
Group 7 – Analysis Controls .....	314
Group 8 – Units for Output of Acceleration, Velocity, and Displacement Time-Histories .....	315
<b>Appendix G: Listing of <math>C_{\text{orps}}W_{\text{all}}\text{Rotate}</math> ASCII Output Files.....</b>	<b>317</b>
<b>Appendix H: Earth Pressure Distribution and Depth of Cracking in a Cohesive Retained Soil – Static Active Earth Pressures .....</b>	<b>320</b>
H.1 Example No. 1: Effective Stress Analysis of a Cohesive Soil.....	321
H.2 Example No. 2: Total Stress Analysis of a Cohesive Soil.....	323



# Figures and Tables

## Figures

Figure 1.1. Rotational response of a cantilever retaining wall with a permanent earthquake-induced rotation, $\theta_r$ .....	2
Figure 1.2. Translational response of a cantilever retaining wall with a permanent earthquake-induced sliding displacement, $\Delta_s$ .....	3
Figure 1.3. Rock-founded cantilever retaining wall bordering a spillway channel. ....	4
Figure 1.4. Gravity retaining wall and driving soil wedge treated as a rigid body.....	5
Figure 1.5. Simplified “driving” wedge method of analysis and the Mononobe-Okabe active earth pressure force relationship. ....	7
Figure 1.6. Elements of the Newmark (rigid) sliding block method of analysis (from Hynes-Griffin and Franklin (1984)). ....	13
Figure 1.7. Gravity retaining wall and failure wedge treated as a sliding block (after Whitman (1990)).....	17
Figure 1.8. Incremental failure by base sliding (adapted from Richards and Elms (1979)).....	18
Figure 1.9. Permanent, seismically induced displacement of a rock-founded cantilever wall retaining moist backfill and with toe restraint, computed using CorpsWallRotate. ....	20
Figure 1.10. Forces and accelerations of a rigid block model of a gravity retaining wall with rotation during horizontal shaking of the rigid base (after Zeng and Steedman (2000)).....	22
Figure 1.11. The acceleration of point c relative to point o expressed in terms of normal and tangential components. ....	24
Figure 1.12. Permanent, seismically induced displacement due to the rotation about the toe of a rock-founded cantilever retaining wall and with toe restraint, computed using CorpsWallRotate. ....	27
Figure 2.1. Rotating gravity retaining wall (after Nadim and Whitman (1984)).....	37
Figure 2.2. Dynamic forces acting on the retaining wall per the Nadim formulation .....	42
Figure 2.3. The Siddharthan, Ara, Anderson, Gowda, and Norris simplified rigid block model for seismically induced wall displacement (after Siddharthan, Ara, and Anderson (1990)). ....	46
Figure 2.4. Forces and moments acting on a rigid block model of a gravity wall (after Siddharthan, Ara, and Anderson (1990)). ....	48
Figure 2.5. Free-body diagram of bridge abutment with free connection to bridge deck (after Fishman and Richards (1998)). ....	55
Figure 2.6. Free-body diagram of bridge abutment with fixed connection to bridge deck (after Fishman and Richards (1997)).....	57
Figure 2.7. Forces and accelerations of a rigid block model of a gravity retaining wall with rotation during horizontal shaking of the rigid base (after Zeng and Steedman (2000)).....	58
Figure 2.8. Forces and acceleration of a rigid block model of a gravity retaining wall with sliding (i.e., translation) during horizontal shaking of the rigid base (after Zeng and Steedman (2000)). ....	63

Figure 3.1. Idealized permanent, seismically-induced displacement due to the rotation about the toe of a rock-founded wall retaining moist backfill, with toe restraint, computed using $C_{\text{ CorpsWallRotate}}$ .....	66
Figure 3.2. Free-body and kinetic diagrams of a rigid block model of a cantilever wall retaining moist backfill with rotation about the toe of the wall during horizontal and vertical shaking of the rigid level base. ....	69
Figure 3.3. Tangential, normal, and angular accelerations of the center of mass (of a rigid block model of a cantilever wall retaining moist backfill) relative to the point of rotation during horizontal and vertical shaking of the rigid level base.....	71
Figure 3.4. Horizontal and vertical components of the tangential and normal acceleration of the center of mass (of a rigid block model of a cantilever wall retaining moist backfill) relative to the point of rotation during horizontal and vertical shaking of the rigid level base. ....	72
Figure 3.5. Inertia forces and resultant force vectors acting on a rigid block model of a cantilever wall retaining moist backfill with rotation about the toe of the wall during horizontal and vertical shaking of the rigid level base. ....	74
Figure 3.6. Equivalent kinetic diagrams for the rigid block model of a cantilever wall retaining moist backfill with rotation about the toe of the wall during horizontal and vertical shaking of the rigid level base. ....	77
Figure 3.7. Structural wedge with toe resistance retaining a driving soil wedge with a moist slope (i.e., no water table) analyzed by effective stress analysis with full mobilization of $(c', \phi')$ shear resistance within the backfill.....	80
Figure 3.8. Resultant location of $P_{\text{AE}}$ based on the positions and magnitudes of the static active earth pressure force, $P_{\text{A}}$ , and incremental dynamic active earth pressure force, $\Delta P_{\text{AE}}$ , of a moist, level, backfill (after Ebeling and Morrison (1992)).....	82
Figure 3.9. The computation of equivalent earth pressures acting on a rigid block model of a cantilever wall retaining moist, level, granular (with $c'=0$ ) backfill (after Ebeling and Morrison (1992)).....	83
Figure 3.10. Complete equations for rotational motions over time increment $DT$ based on linearly varying angular acceleration.....	87
Figure 3.11. Rotational velocity and rotations at the end of time increment $DT$ based on linearly varying angular acceleration.....	89
Figure 3.12. Two possible outcomes for the case of a negative angular acceleration at time $t_i$ and a positive angular acceleration at time $t_{i+1}$ . ....	91
Figure 3.13. Two possible outcomes for the case of negative angular accelerations at times $t_i$ and $t_{i+1}$ .....	96
Figure 3.14. Two possible outcomes for the case of a positive angular acceleration at time $t_i$ and a negative angular acceleration at time $t_{i+1}$ . ....	101
Figure 3.15. Control points, water pressures, and corresponding resultant forces acting normal to faces of the three regions of a structural wedge rotating about its toe—effective stress analysis. ....	107
Figure 3.16. Inertia forces and resultant force vectors acting on a rigid block model of a (inclined base) cantilever wall retaining a partially submerged backfill with rotation about the toe of the wall during horizontal and vertical shaking of the inclined rigid base—effective stress analysis.....	108
Figure 4.1. Permanent, seismically induced displacement of a rock-founded cantilever wall retaining moist backfill and with toe restraint, computed using $C_{\text{ CorpsWallRotate}}$ . ....	117

Figure 4.2. Inertia forces and resultant force vectors acting on a rigid block model of a cantilever wall retaining moist backfill with sliding along its base during horizontal and vertical shaking of the inclined rigid base. ....	119
Figure 4.3. Complete equations for relative motions over time increment $DT$ based on linearly varying acceleration.....	127
Figure 4.4. Relative velocity and displacements at the end of time increment $DT$ based on linearly varying relative acceleration. ....	128
Figure 4.5. Two possible outcomes for the case of a negative relative acceleration at time $t_i$ and a positive relative acceleration at time $t_{i+1}$ . ....	130
Figure 4.6. Two possible outcomes for the case of negative relative accelerations at times $t_i$ and $t_{i+1}$ . ....	136
Figure 4.7. Two possible outcomes for the case of a positive relative acceleration at time $t_i$ and a negative relative acceleration at time $t_{i+1}$ . ....	140
Figure 4.8. Control points, water pressures, and corresponding resultant forces acting normal to faces of the three regions of a structural wedge sliding along its base—effective stress analysis. ....	147
Figure 4.9. Inertia forces and resultant force vectors acting on a rigid block model of a (inclined base) cantilever wall retaining a partially submerged backfill with sliding along the base of the wall during earthquake shaking of the inclined rigid base—effective stress analysis.....	148
Figure 5.1. The <b>Introduction</b> tab features and idealized structural wedge diagram. ....	159
Figure 5.2. A strong earthquake time-history ground motion shown in the <b>Earthquake</b> tab.....	162
Figure 5.3. Dynamic forces acting on the free-body section of the structural wedge and its material regions.....	163
Figure 5.4. Examples of width and height definition for each of the ten structural wedge material regions.....	164
Figure 5.5. Examples of structural wedge material regions.....	165
Figure 5.6. The input <b>Geometry</b> tab in action. ....	171
Figure 5.7. Boundary water pressure diagram — full contact along the base of the retaining wall with its foundation in a sliding block analysis.....	172
Figure 5.8. Boundary water pressure diagram — loss of contact (i.e., development of a gap) along the base of the retaining wall with its foundation in a rotational analysis.....	173
Figure 5.9. Summary of the user-defined geometry and computed weight, mass and moments of inertia for the structural wedge as defined in the <b>Geometry</b> tab. ....	174
Figure 5.10. Defining the material properties using the <b>Structural Wedge</b> tab for an effective stress analysis.....	175
Figure 5.11. Defining the material properties using the <b>Structural Wedge</b> tab for a total stress analysis. ....	176
Figure 5.12. Defining the material parameter for the <b>Driving Wedge</b> tab — effective stress method of analysis.....	179
Figure 5.13. Defining the material properties for the <b>Driving Wedge</b> tab — total stress method of analysis.....	180
Figure 5.14. The <b>Analysis</b> tab. ....	182
Figure 5.15. Rock-founded earth retaining wall for Example 1. ....	186
Figure 5.16. Data contained within the input <b>Geometry</b> tab for Example 1. ....	187
Figure 5.17. The final <b>Analysis</b> tab for Example 1.....	190

Figure 5.18. Time-history of the evaluation of the effective vertical acceleration. ....	191
Figure 5.19. Newmark sliding block time-history results for Example 1.....	192
Figure 5.20. Rock-founded earth retaining wall buttressed at the toe of the wall by a 1-ft-thick reinforced concrete slab for Example 2. ....	194
Figure 5.21. The input <b>Geometry</b> tab for Example 2. ....	195
Figure 5.22. The third iteration <b>Analysis</b> tab settings for Example 2 – Sliding Evaluation. ....	198
Figure 5.23. The second iteration <b>Analysis</b> tab settings for Example 2 – Rotational Evaluation. ....	199
Figure 5.24. The rotational <b>Analysis</b> tab settings for final Example 2 – Computation. ....	201
Figure 5.25. Rotational block time-history results for Example 2. ....	202
Figure 5.26. Permanent rotation of the rigid block after earthquake shaking ends for Example 2. ....	203

## Tables

Table 1.1. Approximate magnitudes of movements required to reach minimum active earth pressure conditions (after Clough and Duncan (1991)) .....	6
Table 5.1. Assessment of constant Y acceleration, the effective vertical acceleration for Example 1. ....	189
Table 5.2. Assessment of constant Y acceleration, the effective vertical acceleration for Example 2 – Sliding Evaluation. ....	196
Table 5.3. Assessment of constant Y acceleration, the effective vertical acceleration for Example 2 – Rotational Evaluation. ....	197

## Preface

Funding to initiate this research was provided by the U.S. Army Engineer District (USAED), Los Angeles. Robert Conley, Chief, Cost and Structural Engineering Section, USAED, Los Angeles, was the project monitor. Additional funding for continued product development and broadened scope of research was provided by Headquarters, U.S. Army Corps of Engineers (HQUSACE), as part of the Infrastructure Technology Research Program. Funding to conclude this research task, including software development, was provided by the Navigation Systems Research Program. The research was performed under Work Unit 4402JC, entitled “Soil-Structure Interaction for Seismic Evaluation of Earth-Retaining Lock and Cantilever Walls.” The HQUSACE Technical Monitor was Anjana Chudgar.

James E. Clausner, Coastal and Hydraulics Laboratory (CHL), U.S. Army Engineer Research and Development Center (ERDC), was the Navigation Systems Research Program Manager. Dr. Michael K. Sharp, Geotechnical and Structures Laboratory, ERDC, was the Acting Technical Director for Navigation. Angela Premo, USAED, South Atlantic, was the Navigation Business Line Leader for HQUSACE. Dr. Robert M. Ebeling, Engineering Informatics Systems Division (EISD), Information Technology Laboratory (ITL), ERDC, Vicksburg, MS, was the Principal Investigator.

This report was prepared by Dr. Ebeling and Barry C. White, Computational Science and Engineering Branch, EISD. Dr. Ebeling was author of the scope of work for this research. The report was prepared under the supervision of Dr. Cary D. Butler, Chief, EISD, and Dr. Jeffery P. Holland, Director, ITL. During publication of this report Mr. John E. West was Acting Assistant Director of ITL, and Dr. Deborah F. Dent was Acting Director.

COL Richard B. Jenkins was Commander and Executive Director of ERDC. Dr. James R. Houston was Director.

### Considerations for Assigning Shear Strength Parameters

A key item in the permanent deformation and permanent rotation analysis of a Corps earth retaining structure using the PC-based software, CorpsWallRotate, described in this report, is the selection of suitable shear strength parameters. In an effective stress analysis, the issue of the suitable friction angle is particularly troublesome when the peak friction angle is significantly greater than the residual friction angle. In the displacement controlled approach examples given in Section 6.2 of Ebeling and Morrison (1992), effective stress based shear strength parameters (i.e., effective cohesion  $c'$  and effective angle of internal friction  $\phi'$ ) were used to define the shear strength of the dilative granular backfills, *with  $c'$  set equal to zero in all cases due to the level of deformations anticipated in a sliding block analysis during seismic shaking*. In 1992 Ebeling and Morrison concluded that it is conservative to use the residual friction angle in a sliding block analysis, and this should be the usual practice for displacement based analysis of granular retained soils. The primary author of this report would broaden the concept to the assignment of effective (i.e.,  $c'$  and  $\phi'$ ) or total (i.e., undrained  $S_u$ ) shear strength parameters for the retained soil to be consistent with the level of shearing-induced deformations encountered for each design earthquake in a rotational analysis and note that active earth pressures are used to define the loading imposed on the structural wedge by the driving soil wedge. (Refer to Table 1.1 in this report for guidance regarding wall movements required to fully mobilize the shear resistance within the retained soil during earthquake shaking.) In an effective stress analysis, engineers are cautioned to carefully consider the reasonableness of including a nonzero value for effective cohesion  $c'$  in their permanent deformation and permanent rotation analyses.

### Assumption Made for the Soil Driving Wedge in a Cohesive Soil

$C_{\text{orps}}W_{\text{allRotate}}$  performs a permanent displacement analysis of a retaining wall due to earthquake shaking. Reversal in the direction of the horizontal component of the time-history of earthquake ground shaking occurs many times during the typical tens of seconds of ground motion. Consequently, a reversal in direction of the inertial force imparted to the structural wedge and to the soil driving wedge occurs many times during the course of the analysis using  $C_{\text{orps}}W_{\text{allRotate}}$ . In a traditional soil wedge formulation for static loading, a crack is typically considered to exist within the upper portion of the soil driving wedge for a cohesive soil (with shear strength,  $S_u$ , specified in a total stress analysis or  $c'$  specified in an effective stress analysis) and the planer wedge slip surface is terminated when it intersects the zone of cracking at a depth,  $d_{\text{crack}}$ , below the ground surface (e.g., see Appendix H in EM 1110-2-2502). This assumption is not made in the  $C_{\text{orps}}W_{\text{allRotate}}$  formulation for *dynamic loading*. Instead, it is assumed that in the dynamic wedge formulation, the crack within the zone of cracking at the top of the retained cohesive soil of the driving wedge will not remain open during earthquake shaking *due to the inertial load direction reversals* during this time-history based  $C_{\text{orps}}W_{\text{allRotate}}$  analysis. So, even for cohesive soils the planar slip surface, obtained from the sweep-search method of analysis of the driving wedge used by  $C_{\text{orps}}W_{\text{allRotate}}$  to obtain a value for the earthquake induced resultant driving force  $P_{\text{AE}}$  (acting on the structural wedge), extends uninterrupted within the driving soil wedge (in the retained soil) to the ground surface and is not terminated by a vertical crack face to the ground surface when it enters the zone of cracking.

In order to assign a location to  $P_{\text{AE}}$ , the static value for active earth pressure force,  $P_A$ , is needed (refer to Equation 3.24 for the level ground, moist backfill case and to Appendix C for all other cases).  $C_{\text{orps}}W_{\text{allRotate}}$  proceeds with the computation of  $h_{\text{PAE}}$ , the location of the resultant force  $P_{\text{AE}}$ , using the value for  $P_A$  computed by procedure discussed in Appendix A. The computation of  $h_{\text{PAE}}$  by  $C_{\text{orps}}W_{\text{allRotate}}$  is described in Appendix C.

In a traditional soil wedge formulation for static loading, a crack is typically considered to exist within the upper portion of the soil driving wedge for a cohesive soil and the planer wedge slip surface is terminated when it intersects the zone of cracking at a depth,  $d_{\text{crack}}$ , below the ground surface (e.g., see Appendix H in EM 1110-2-2502). This assumption is made in the  $C_{\text{orps}}W_{\text{allRotate}}$  formulation for static loading force  $P_A$  (but not when computing  $P_{\text{AE}}$  for dynamic loading). A sweep-search wedge method of analysis as discussed in Appendix A is used by the  $C_{\text{orps}}W_{\text{allRotate}}$  to determine the value of the active earth pressure force,  $P_A$ .

Earth pressure distributions and depth of cracking: The earth pressure distribution applied to the structural wedge by the driving soil wedge in a  $C_{orps}W_{all}Rotate$  analysis is made up of two components, the earth pressure distribution due to the static active earth pressures and a trapezoidal earth pressure distribution due to the incremental dynamic force component,  $\Delta P_{AE}$  (with  $\Delta P_{AE} = P_{AE} - P_A$ ). The methodologies discussed in Appendix A are used by  $C_{orps}W_{all}Rotate$  to first determine the resultant earth pressure forces  $P_A$  and  $P_{AE}$  and then the methodologies discussed in Appendix C are used to compute the resulting earth pressure distributions for  $P_A$  and  $\Delta P_{AE}$ , respectively. In order to compute values of  $P_{AE}$  and  $P_A$  by the dynamic and static sweep-search solutions of trial soil wedges, a depth of cracking needs to be specified in each sweep-search analysis made by  $C_{orps}W_{all}Rotate$  of a cohesive soil. Initial sweep-search soil wedge solutions are always made assuming a zero depth of crack. This is deemed sufficient for all  $P_{AE}$  computations, as discussed previously. However, an iterative procedure is used to determine the value for the depth of cracking in the analysis of  $P_A$  in cohesive soils and the corresponding earth pressure distribution (which includes both compression as well as tensile stresses). After the resulting static earth pressure force,  $P_A$ , computation is completed, a resulting earth pressure distribution is constructed and new depth of cracking for static loading is determined.  $C_{orps}W_{all}Rotate$  then proceeds with second sweep-search trial wedge analysis of the retained soil for a new value for  $P_A$  corresponding to this new, nonzero crack depth value. A new static earth pressure distribution and a third value for crack depth is then determined. The process is repeated until the depth of cracking used in the sweep-search trial wedge analysis and the depth of cracking determined from the static active earth pressure distribution are nearly the same value.

In the special case of cohesive soils, the  $C_{orps}W_{all}Rotate$  analysis disregards the tensile stresses when defining the static active earth pressures and the corresponding resulting static active earth pressure force to be applied to the structural wedge, as well as when computing the resulting force location  $h_{PA}$  of this modified stress distribution. A trapezoidal earth pressure distribution is used to define  $\Delta P_{AE}$  for cohesive as well as cohesionless soils.



# 1 Introduction to Rotational or Sliding Response of Toe-Restrained Retaining Walls to Earthquake Ground Motions

## 1.1 Introduction

Engineering formulations and software provisions based on sound seismic engineering principles are needed for a wide variety of the Corps retaining walls that (1) rotate or (2) slide (i.e., translate) during earthquake shaking and (3) for massive concrete retaining walls constrained to rocking. The engineering formulation discussed in this report was developed to address the first two of these three modes of retaining wall responses to earthquake shaking.

This research report describes the engineering formulation developed for the permanent rotational response of rock-founded, toe-restrained retaining walls to earthquake ground motions as idealized in Figure 1.1. The corresponding PC software,  $C_{\text{Corps}}W_{\text{all}}\text{Rotate}$ , developed to perform a rotating or sliding analysis of each user-specified retaining wall section is also discussed. Baseline-corrected, horizontal and vertical acceleration time-histories are used to represent the earthquake ground motions in this formulation. They are user input to  $C_{\text{Corps}}W_{\text{all}}\text{Rotate}$ . A particular formulation of the permanent sliding displacement response of retaining walls (Figure 1.2) for a user-specified earthquake acceleration time-history is also described. (Note that a more versatile, simplified sliding block formulation that eliminates the need for an acceleration time-history,  $C_{\text{Corps}}W_{\text{all}}\text{SLIP}$ , has also been developed and is discussed in Ebeling et al. (2007).) The engineering methodology and software are particularly applicable to rock-founded L-walls and T-walls (usually referred to as cantilever retaining walls) and semi-gravity walls. Figure 1.3 shows an example of retaining walls that border a spillway channel in which the base slab will act as a strut during a seismic event.  $C_{\text{Corps}}W_{\text{all}}\text{Rotate}$  is applicable to a variety of retaining walls buttressed at their toe by a structural feature such as a reinforced concrete slab. The presence of the structural feature at the toe of the retaining wall may result in a tendency for the earth retaining structure to rotate rather than slide during earthquake shaking. Other examples of Corps earth retaining structures having this structural feature include navigation walls, spillway chute

walls, spillway discharge channel walls, approach channel walls to outlet works structures, highway and railway relocation retaining walls, and floodwall channels.  $C_{orps}W_{all}Rotate$  may also be used to predict permanent seismically induced (rotational or translational) displacements of retaining walls with or without toe restraint.

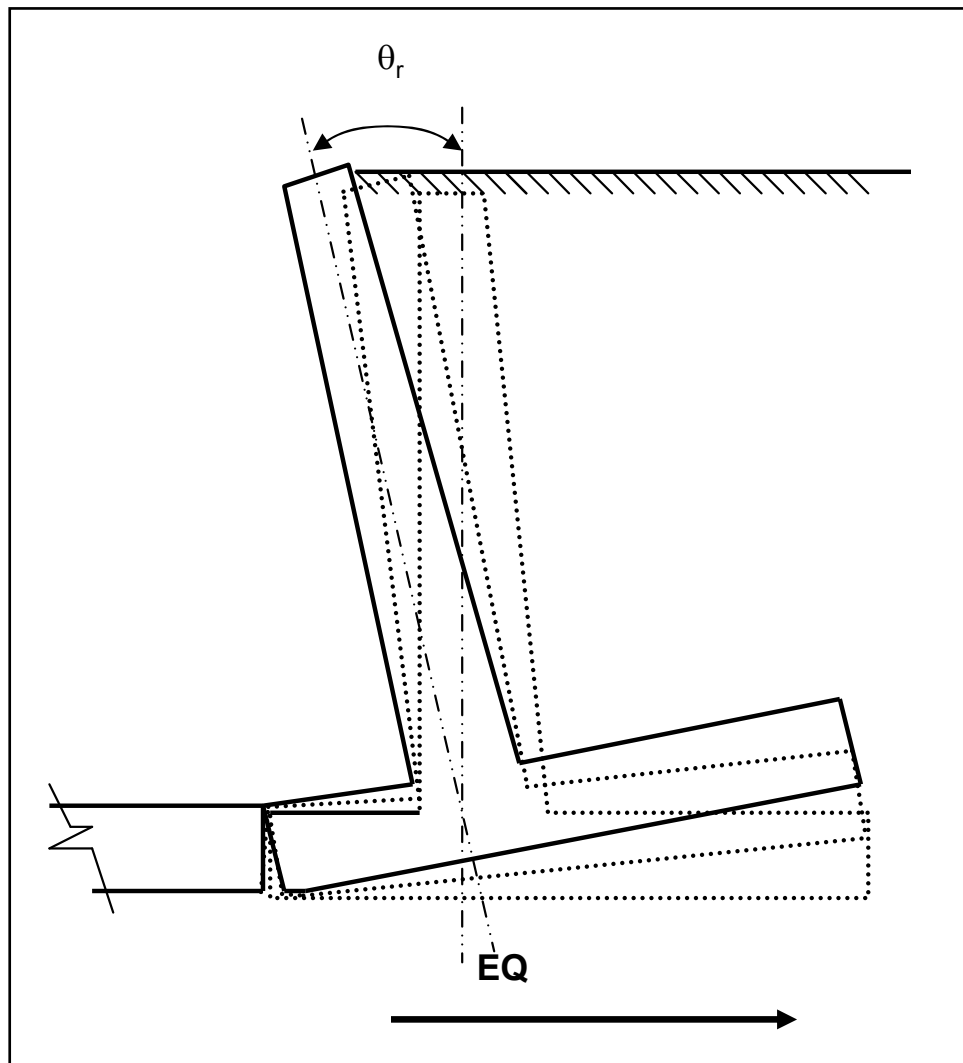


Figure 1.1. Rotational response of a cantilever retaining wall with a permanent earthquake-induced rotation,  $\theta_r$ .

There are three categories of analytical approaches used to perform a seismic stability analysis. They are listed in order of sophistication and complexity:

- Pseudo-static methods with a preselected seismic coefficient
- Sliding block methods
- Stress-deformation methods

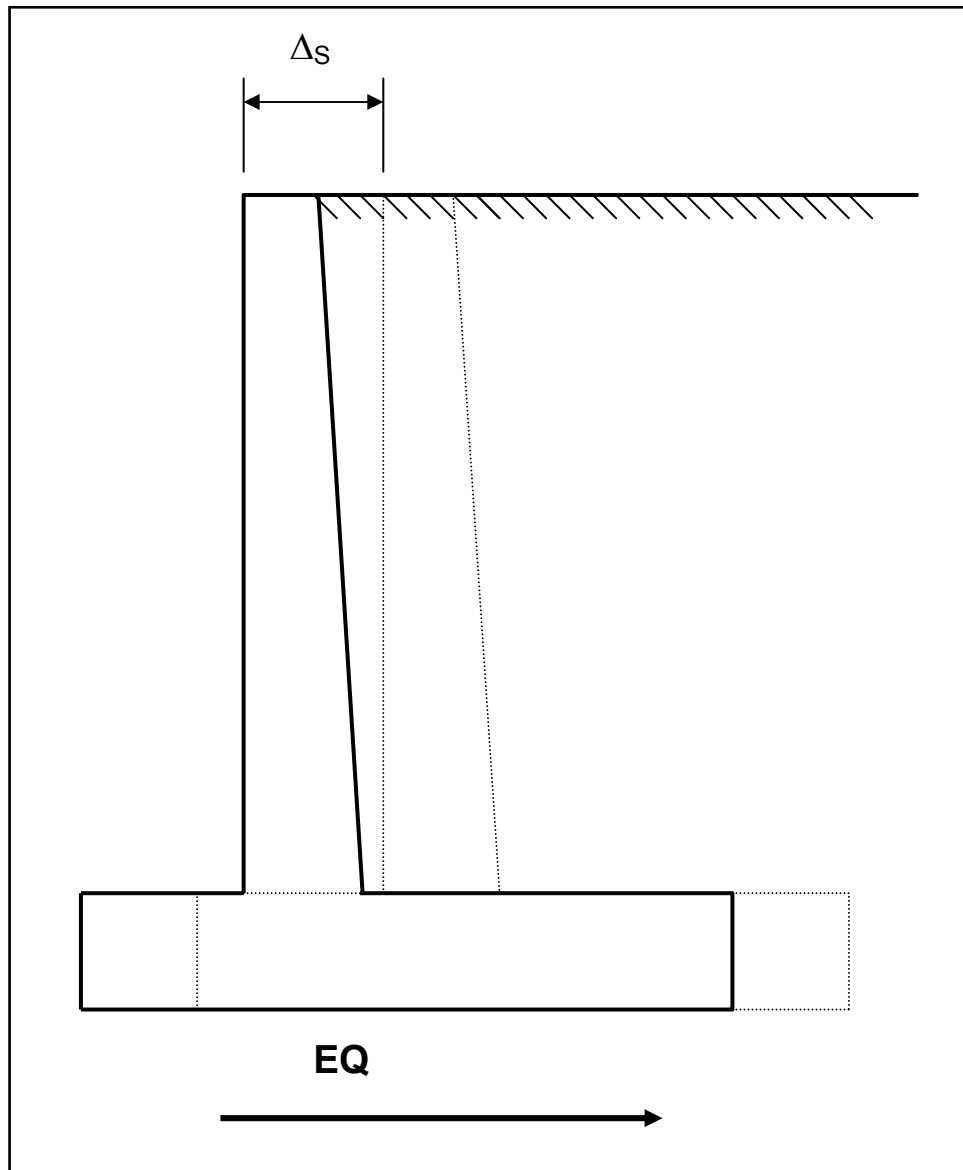


Figure 1.2. Translational response of a cantilever retaining wall with a permanent earthquake-induced sliding displacement,  $\Delta_s$ .

Each category will be subsequently discussed. Because sliding block methods are the focus of this report, this category will be discussed last. The sliding block method of analysis serves as a basis for introducing the analysis of permanent wall rotation due to seismic loading.

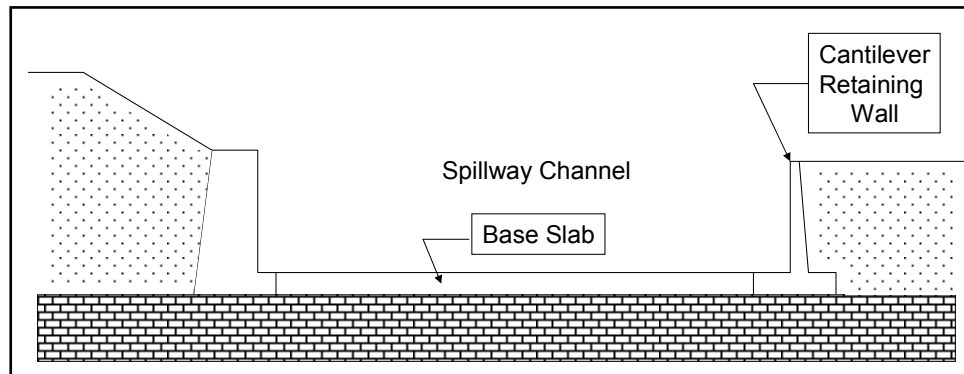


Figure 1.3. Rock-founded cantilever retaining wall bordering a spillway channel.

### 1.1.1 Pseudo-static methods with a preselected seismic coefficient

Pseudo-static methods with a preselected seismic coefficient in the horizontal and in the vertical direction often require bold assumptions about the manner in which the earthquake shaking is represented and the simplifications made for their use in stability computations. Essentially, pseudo-static methods are force-equilibrium methods of analysis expressing the safety and stability of an earth retaining structure to dynamic earth forces in terms of (1) the factor of safety against sliding along the base of the wall, (2) the ability of the wall to resist the earth forces acting to overturn the wall, and (3) the factor of safety against a bearing capacity failure or crushing of the concrete or rock at the toe in the case of a rock foundation. An example using 1992 Corps criteria (now outdated) is discussed in Section 6.2 of Chapter 6 in Ebeling and Morrison (1992). Pseudo-static methods with horizontal and vertical preselected seismic coefficients represent earthquake loading as static forces. In these types of computations, the earthquake “demand” is represented by (1) a horizontal seismic coefficient and (2) a vertical seismic coefficient (sometimes specified as zero) acting at mass centers. Values for these coefficients (typical symbols are  $k_h$  and  $k_v$ ) are dimensionless numbers that, when multiplied times the weight of some body, give a pseudo-static inertia force for use in analysis or design. The horizontal and vertical inertia forces are applied to the mass center of the body as shown in Figure 1.4. The coefficients  $k_h$  and  $k_v$  are, in effect, decimal fractions of the acceleration of gravity ( $g$ ). For some analyses, it is appropriate to use acceleration values of  $k_h g$  and  $k_v g$  smaller than the horizontal and vertical peak accelerations, respectively, anticipated during the design earthquake event. It is important to recognize that this category of method of analysis does not provide quantitative information regarding seismically-induced displacements.

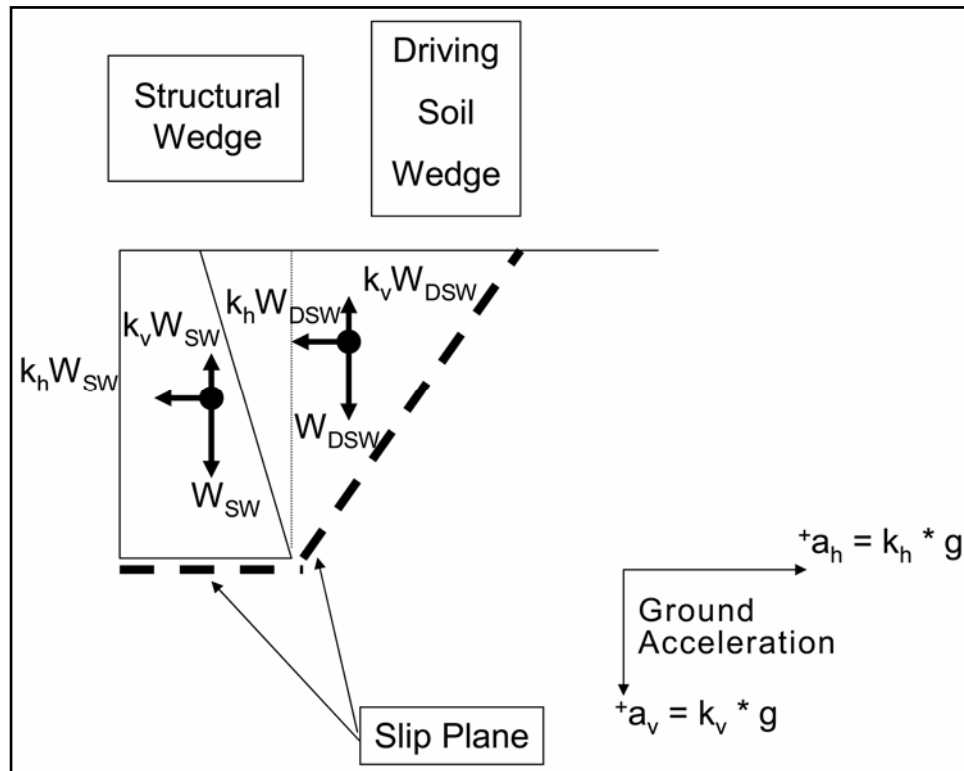


Figure 1.4. Gravity retaining wall and driving soil wedge treated as a rigid body.

For retaining walls in which the permanent relative motion of the retaining structure and retained soil (i.e., the backfill) are sufficient to fully mobilize the shear strength in the soil, soil wedge solutions in which a wedge of soil bounded by the structural wedge and by an assumed failure plane within the retained soil are considered to move as a rigid body and with the same horizontal acceleration (Figure 1.4). Table 1.1 lists the approximate magnitudes of movements required to reach minimum active earth pressure conditions. Although this Clough and Duncan guidance is for static loading, after careful evaluation Ebeling and Morrison (1992, in Section 2.2.2) concluded that the Table 1.1 values may also be used as rough guidance for minimum retained soil seismic displacement to fully mobilize a soil's shear resistance, resulting in dynamic active earth pressures.

**Table 1.1. Approximate magnitudes of movements required to reach minimum active earth pressure conditions (after Clough and Duncan (1991))**

Type of Retained Soil	Values of Y/H <sup>a</sup>
	Active
Dense Sand	0.001
Medium-Loose Sand	0.002
Loose Sand	0.004
<sup>a</sup> Y = movement of top of wall required to reach minimum active pressure, by tilting or lateral translation. H = height of wall.	

A commonly cited expression for the forces the driving soil wedge exerts on the structural wedge was first proposed by Okabe (1924, 1926) and Mononobe and Matsuo (1929). A form of their expression for  $P_{AE}$  in use today (see Chapter 4 in Ebeling and Morrison (1992)) is given in Figure 1.5. Their formulation is referred to as Mononobe-Okabe with  $P_{AE}$  expressed in terms of an active earth pressure coefficient,  $K_{AE}$ , with the subscript A designating active and the subscript E designating earthquake. The Mononobe-Okabe formulation is an extension of Coulomb's theory of static active earth pressures with a horizontal seismic coefficient and a vertical seismic coefficient acting at the center of a Coulomb's "driving" soil wedge mass of a moist retained soil (i.e., with no water table), as shown in this figure. Equation 36 in Chapter 4 of Ebeling and Morrison (1992) gives the Mononobe-Okabe relationship for  $K_{AE}$ . The general wedge solution resulting in this same value for  $P_{AE}$  as can be calculated by the Mononobe-Okabe relationship is given in Appendix A of Ebeling and Morrison (1992). For retaining wall problems analyzed using the simplified wedge method, EM 1110-2-2100 in Section 5-5, part (3)b provides guidance on assumptions regarding the magnitude of the seismic coefficient  $k_h$  that may be used as a fraction of peak ground acceleration. Guidance is also given regarding the magnitude of the seismic coefficient,  $k_v$ , expressed as a fraction of the value for  $k_h$ . *Minimum*  $k_h$  values are cited in Table G-1, Section G-4 of Appendix G, part (a) in EM 1110-2-2100, according to the seismic zone in which the project resides.

Because seismically induced deformations are not an explicit part of this computational process and given that pseudo-static methods represent earthquake loads by static forces, the results are difficult to interpret. This is because displacement is more closely related to assessment of the *seismic performance* for a retaining structure than are factors of safety.

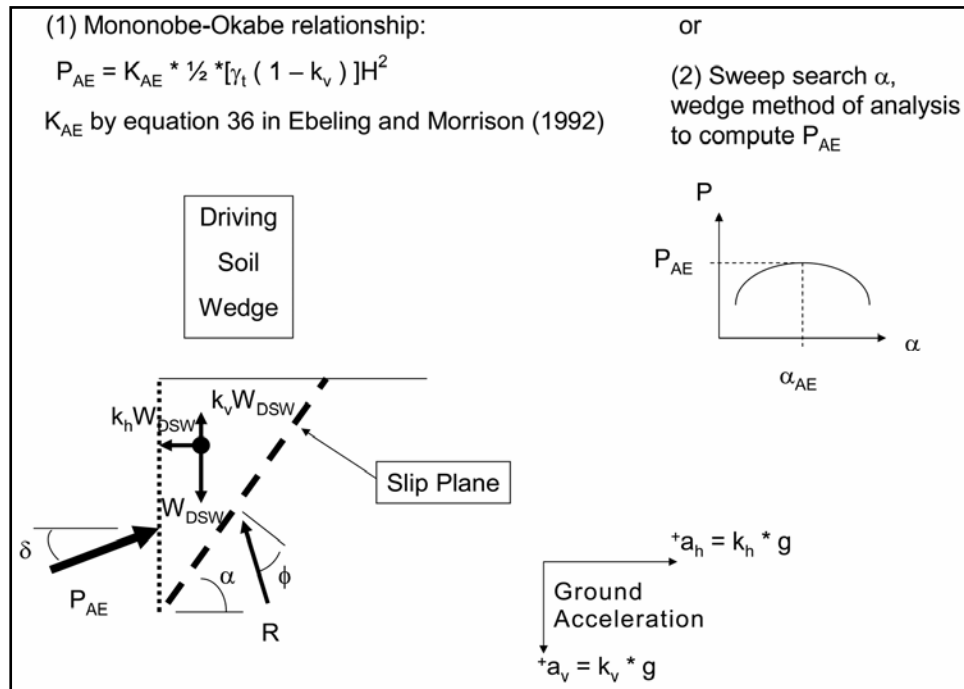


Figure 1.5. Simplified “driving” wedge method of analysis and the Mononobe-Okabe active earth pressure force relationship.

### 1.1.2 Stress-deformation methods

Stress-deformation methods are specialized applications of finite element or finite difference programs for the dynamic analysis of earth retaining structures to seismic loading using numerical techniques to account for the nonlinear engineering properties of soils. The problem being analyzed is often referred to as a soil-structure interaction (SSI) problem.

Acceleration time-histories are typically used to represent the earthquake ground motions in this type of formulation. The general procedure of stress-deformation dynamic analysis is straightforward and follows the usual engineering approach: (1) define the problem, (2) idealize the physical system, (3) set up the equations of motion for the dynamic problem, (4) characterize the dynamic engineering properties of the (structure, soil, and/or rock) materials as per the constitutive material model(s) being used, (5) solve the equations of motion, and (6) evaluate the results. Steps (1), (2), (4), and (6) are handled by the engineer while steps (3) and (5) are dealt with by the engineering software. A partial listing of computer-based codes for dynamic analysis of soil systems is given in Appendix D of Ebeling and Morrison (1992). Use of this type of advanced engineering software requires specialized knowledge in the fields of geotechnical and structural engineering dynamics as well as in

numerical methods. Two computer programs, FLUSH and FLAC, will briefly be discussed to give the reader a sense of what is involved with the application of computationally complex numerical codes in a complete soil-structure interaction dynamic analysis and the numerous input and modeling considerations required.

#### *1.1.2.1 FLUSH*

The ASCE Standard 4-86 (1986) states that SSI denotes the phenomenon of coupling between a structure and its supporting soil or rock medium during earthquake shaking. The resulting dynamic soil pressures are a result of the degree of interactions that occur between the structure and the soil. This response is dependent on (1) the characteristics of the ground motion, (2) the retained and foundation soils (or rock), and (3) the structure itself. One method of analysis for SSI is referred to as the direct method and treats the structure and the surrounding retained soil and foundation medium in a single analysis step. FLUSH is a classic example of this category of software which uses the finite element method in this dynamic analysis (Lysmer, Udaka, Tsai, and Seed 1975).

Two-dimensional (2-D) cross sections of the retaining structure and portions of the retained soil and foundation are typically modeled in the FLUSH analysis. Nonlinear soil behavior is treated through equivalent linearization of the shear stiffness of each soil element with the effective shear strains that develop during earthquake shaking for the user-specified earthquake acceleration time-history. Material damping is assigned to each soil (and/or rock) element and to each structural element comprising the mesh. Material damping is strain-compatible for each soil, rock, and structural material type. FLUSH solves the equation of motion in the frequency domain. The acceleration time-history is introduced through the base nodes of the mesh; fictitious (artificial) boundary conditions allow for the introduction of vertically propagating shear waves resulting in horizontal motion of the nodes of the mesh during earthquake shaking and for vertically propagating compression waves that allow for the vertical motion of the nodes. Lateral boundaries, referred to as transmitting boundaries, are imposed on the 2-D mesh to allow for energy absorbing boundary conditions to be specified. Because it is essentially a wave propagation problem being solved, great care is exercised by the seismic engineer to size the mesh so that moderate to high wave frequencies are not artificially excluded in the dynamic numerical analysis. Sizing of the 2-D mesh as it pertains to the height of the elements and with regard to



the maximum shear wave frequency vertically transmitted by the elements first involves the analysis of representative 1-D soil columns.

To assess the maximum frequency that may be transmitted by a user-proposed 2-D finite element mesh in a FLUSH analysis, representative imaginary sections within the 2-D model problem are first analyzed by the vertical shear wave propagation program SHAKE (Schnabel, Lysmer, and Seed 1972) and by a 1-D finite element column using FLUSH. Strain-compatible shear stiffness results from the SHAKE analyses are used to determine the maximum height of the soil elements for the maximum frequency of the vertically propagating shear wave needed to be transmitted in the FLUSH (2-D) analysis. A 1-D soil column is then constructed using finite elements and analyzed using FLUSH to verify that the required vertically propagating shear wave frequencies are being transmitted by the FLUSH mesh. The wavelength associated with the highest frequency transmitted by the mesh is related to the heights of the elements and to the strain-compatible shear wave velocities via the strain-compatible shear stiffness of each of the elements. Recall that FLUSH accounts for nonlinear response of soils during earthquake shaking through adjustments of the soil shear stiffness and material damping parameters as a function of shear strain that develop in each element of the finite element mesh. Note that the results of this assessment are dependent on the characteristics of the acceleration time-history used in the analysis.

FLUSH output obtained via the extraction mode includes time-histories of the dynamic stresses within each element and dynamic displacements at each node in the finite element model. Time-histories of nodal point forces may also be obtained using specialized software. The computed dynamic stresses are then superimposed on the static stresses so as to attain the total stresses. Static stresses are typically obtained from a SOILSTRUCT finite element analysis (Ebeling, Peters, and Clough 1992).

In a static analysis using SOILSTRUCT, the nonlinear stress-strain behavior of soils is accounted for in an incremental, equivalent linear method of analysis in which the sequential excavation (if any), followed by sequential construction of the structure and incremental placement of retained soil, is made. Examples of this application to Corps structures for static loading(s) are given in Clough and Duncan (1969), Ebeling et al. (1993), Ebeling and Mosher (1996), Ebeling, Peters, and Mosher (1997),

Ebeling and Wahl (1997), and Ebeling, Pace, and Morrison (1997). The mesh used in the FLUSH dynamic analysis will be the basis for the mesh used in the SOILSTRUCT static analysis, for the convenience of combining results.

#### *1.1.2.2 FLAC*

The Corps recently completed its first research application of FLAC to the seismic analysis of a cantilever retaining wall (Green and Ebeling 2002). FLAC is a commercially available, 2-D, explicit finite difference program written primarily for geotechnical applications. The basic formulation of FLAC is plane-strain. Dynamic analyses can be performed with FLAC using the optional dynamic calculation module, wherein user-specified acceleration, velocity, or stress time-histories can be input as an exterior boundary condition or as an interior excitation. FLAC allows for energy absorbing boundary conditions to be specified, which limits the numerical reflection of seismic waves at the model perimeter. The nonlinear constitutive models (10 are built-in), in conjunction with the explicit solution scheme, in FLAC give stable solutions to unstable physical processes, such as sliding or overturning of a retaining wall. FLAC solves the full dynamic equations of motion, even for essentially static systems, which enables accurate modeling of unstable processes, e.g., retaining wall failures.

FLAC, like FLUSH, has restrictions associated with the wavelength associated with the highest frequency transmitted within the grid. A procedure similar to that used to design the FLUSH mesh and involving 1-D soil column analyses, via SHAKE, is used to lay out the FLAC grid for the dynamic retaining wall problem analyzed and for the specified acceleration time-history. Section 3.3.4 of Green and Ebeling (2002) discusses the dimensions of the finite difference grid and the maximum frequency that can pass through without numerical distortion.

A disadvantage of FLAC is the long computational times, particularly when modeling stiff materials, which have large physical wave speeds. The size of the time-step depends on the dimension of the elements, the wave speed of the material, and the type of damping specified (i.e., mass proportional or stiffness proportional), where stiffness proportional to include Rayleigh damping, requires a much smaller time-step. The critical time-step for numerical stability and accuracy considerations is automatically computed by FLAC, based on these factors listed. For those

readers unfamiliar with the concept of critical time-step for numerical stability and accuracy considerations in a seismic time-history engineering analysis procedure, please refer to Ebeling (1992, Part V), or to Ebeling, Green, and French (1997). The Lagrangian formulation in FLAC updates the grid coordinates each time-step, thus allowing large cumulative deformations to be modeled. This is in contrast to Eulerian formulation in which the material moves and deforms relative to a fixed grid, and is therefore limited to small deformation analyses.

#### 1.1.2.3 FLUSH versus FLAC

The advantages of FLUSH are that it has considerably faster run times than FLAC and has been applied to a number of dynamic SSI problems. FLUSH is now freely downloadable from the Internet. The major disadvantage of FLUSH is that it does not allow for *permanent* displacement of the wall (although strain softening associated with earthquake-induced soil or rock deformations is accounted for in the analysis). A disadvantage of FLAC is that the earthquake engineering community and the Corps are just now developing modeling procedures for the application of FLAC to dynamic SSI problems, learning how to perform the analyses and interpret the computed results.

#### 1.1.3 Sliding block methods

Sliding block methods of analysis of earth retaining structures can be viewed as a compromise between the simplistic pseudo-static methods with a preselected seismic coefficient and the computationally complex stress-deformation methods of analysis (e.g., via FLUSH, FLAC, etc.). Sliding block methods of analysis calculate a permanent deformation of a retaining structural system due to a user-specified design earthquake event.

The numerous variations of rigid sliding block methods of seismic analysis as applied to slopes, earthen dams, retaining wall systems, and foundations have their roots in the methodology outlined in Newmark (1965) and what has come to be known as the Newmark sliding block

model.<sup>1</sup> This problem was first studied in detail by Newmark (1965) using the sliding block on a sloping plane analogy. Procedural refinements were contributed by Franklin and Chang (1977), Wong (1982), Whitman and Liao (1985), Ambraseys and Menu (1988), and others. Makdisi and Seed (1978) and Idriss (1985, Figure 47), proposed relationships based on a modification to the Newmark permanent displacement procedure to allow for the dynamic response of embankments.

#### *1.1.3.1 Concepts of Newmark's sliding (rigid) block method of analysis*

Franklin and Chang (1977) and Hynes-Griffin and Franklin (1984) illustrate key concepts of a Newmark sliding block analysis using a potential sliding mass within an embankment under earthquake loading. The problem engineering idealization is shown in Figure 1.6. The Figure 1.6.a potential sliding mass is in a condition of incipient sliding with full mobilization of the shear resistance for the soil along the slip plane shown in this figure. The corresponding sliding factor of safety is equal to unity. This condition results from the acceleration of the earthen mass into the embankment (i.e., to the left) and away from the cut.  $W$  is the weight of the sliding mass. The force  $N$  times  $W$  in this figure is the inertia force required to reduce the sliding factor of safety to unity. By D'Alembert's principle, the inertia force,  $N$  times  $W$ , is applied pseudostatically to the soil mass in a direction opposite to acceleration of the mass,  $N$  times  $g$ , with  $N$  being a decimal fraction of the acceleration of gravity,  $g$  (the universal gravitational constant). The acceleration of the soil mass contained within the slip plane shown in Figure 1.6.a is limited to an acceleration value of  $N$  times  $g$  because the shear stress required for equilibrium along the slip plane can never be less than the shear strength of the soil. To state this in another way, the sliding factor of safety can never be less than 1.0. So if the earthquake-induced ground acceleration should increase to a value greater than the value  $N$  times  $g$ , the Figure 1.6.a mass above this slip plane would move downhill relative to the embankment. During this permanent slope displacement, the "sliding"

---

<sup>1</sup> An interesting footnote in seismic engineering history is given in Whitman (2000): Dr. Robert Whitman, Professor Emeritus of MIT, in 1953 performed a calculation of the permanent displacement of a slope as a result of earthquake-induced ground motions using a sliding block concept for a consulting job that Professor Donald Taylor (of MIT) had with the U.S. Army Corps of Engineers. Professor Newmark was part of the same consulting panel and sent word back to Dr. Whitman that he found this approach to be interesting, and that if he (Whitman) did not pursue it, he (Newmark) would. Dr. Whitman did not, and Professor Newmark did. Professor Newmark's research culminated in his now classic 1965 *Geotechnique* paper on this topic, the fifth Rankine lecture.

mass would only feel the acceleration value  $N$  times  $g$  and not the ground acceleration values.

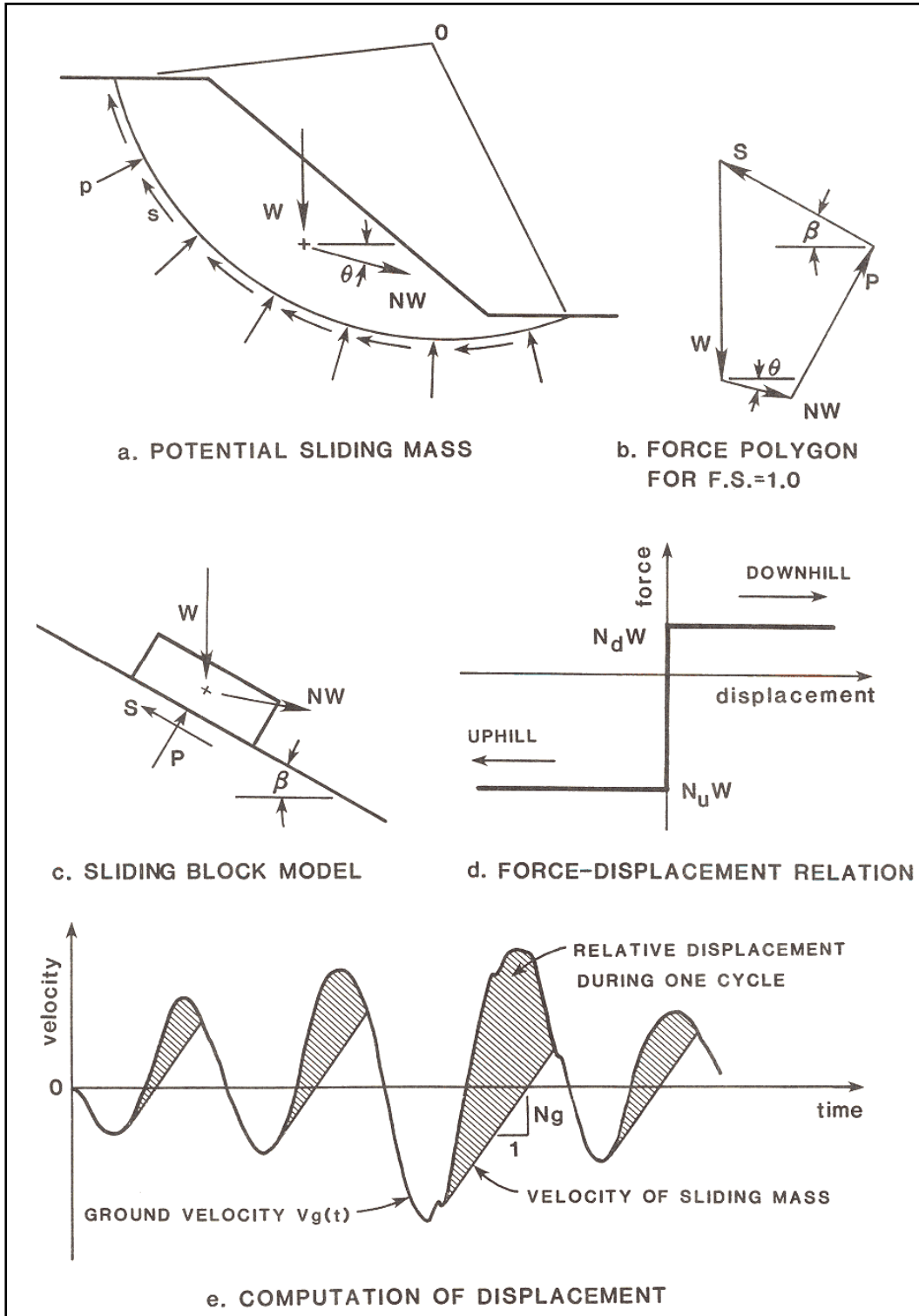


Figure 1.6. Elements of the Newmark (rigid) sliding block method of analysis (from Hynes-Griffin and Franklin 1984).

Figure 1.6.b shows the force polygon for the “sliding” soil mass. The inclination angle  $\theta$  of the inertia force may be found as the angle that is most critical, that is, the angle that minimizes  $N$ . Franklin and Chang (1977) and Hynes-Griffin and Franklin (1984) state that the angle  $\theta$  is typically set equal to zero in seismic slope stability analyses. The angle  $\beta$  is the direction of the resultant force,  $S$ , of the distributed shear stresses along the interface and is determined during the course of the slope stability analyses to determine the value of  $N$  that results in a sliding factor of safety of 1.0 for the slope’s sliding mass. The force  $P$  is the resultant of the normal forces. The Figure 1.6.b force polygon for the slope mass is applied to an “idealized” sliding rigid block model on a plane inclined at an angle  $\beta$  to horizontal in Figure 1.6.c. This idealization is the basis for the designation as the Newmark’s sliding (rigid) block method of analysis, representing the sliding mass of the embankment.

Figure 1.6.d is an idealization of the limiting force versus displacement relationships applied to this problem. The resistance to sliding is assumed to be rigid-plastic, as shown in this figure. This resistance to sliding is unsymmetrical because the block can slide downhill more easily than uphill. It is the usual practice to assume that uphill sliding never occurs, i.e., a worst-case assumption, and results in the greatest permanent displacement (downhill).

Figure 1.6.e shows a time-history plot of the velocity of the embankment during earthquake shaking. Not shown is the corresponding (ground/embankment) acceleration time-history for this particular earthquake event. (Earthquake shaking is usually represented by an acceleration time-history. Since the ground acceleration varies with time, let ground acceleration be represented by variable fraction  $A$  times the constant acceleration of gravity,  $g$ . Recall that the integral of the acceleration time-history is equal to the Figure 1.6.e velocity time-history.) For an embankment that suffers a slope failure from seismic ground motions, the total permanent displacement of a sliding mass relative to the base is the sum of the increments of displacement occurring during a number of individual pulses of ground motion. These incremental relative displacements are determined as follows. For each time the acceleration of the embankment, equal to  $A$  times  $g$ , is greater than the constant  $N$  times  $g$ , relative displacements (between the slope mass and the embankment) will *initiate*. There are four of these incremental, permanent displacement pulses occurring in Figure 1.6.e. During slope displacements, the sliding

mass will move at a slower velocity than will the embankment (designated the ground velocity in this figure). The integral of the difference in velocities between the sliding mass and the embankment velocity is equal to the incremental, relative displacement of the sliding mass. The total permanent downhill displacement is the sum of the four incremental displacement cycles depicted in this figure. Note that incremental sliding of the slope terminates when the velocities of the embankment and of the sliding mass converge to the same value.

**Summary:** The idealized engineering problem depicted in Figure 1.6 describes the essential features of the Newmark sliding (rigid) block method of analysis as first applied to slopes: (1) There is a level of earthquake shaking as characterized in terms of a value of acceleration designated  $N$  times  $g$ , which fully mobilizes the shear resistance along a sliding plane of a potential sliding mass, corresponding to a factor of safety against sliding of 1.0 for that mass. (2) For a given embankment (or equivalently, ground) acceleration time-history in which accelerations exceed the value of  $N$  times  $g$ , incremental permanent displacements will occur. (3) The magnitude of the incremental displacements may be numerically quantified using the procedure outlined in Figure 1.6.e. (4) Total permanent displacement is equal to the sum of the incremental displacement pulses. Although this procedure has been applied to other types of structures, the essential features of the Newmark (rigid) sliding block method of analysis remain the same.

#### 1.1.3.2 Sliding block method of analysis applied to retaining structures

A variation proposed on the Newmark sliding block method of analysis for earth retaining structures is the displacement controlled approach (Section 6.3 in Ebeling and Morrison (1992)). It incorporates retaining wall movements explicitly in the stability analysis of earth retaining structures. This methodology is applied as either (1) the displacement controlled *design* of a new retaining wall or as (2) an *analysis* of earthquake-induced displacements of an existing retaining wall.

**The displacement controlled *design* of retaining wall:** In this approach the retaining wall geometry is the primary variable. It is, in effect, a procedure for choosing a seismic coefficient based upon explicit choice of an allowable permanent displacement. Once the seismic coefficient is selected, the usual stability analysis against sliding is performed, including the use of the Mononobe-Okabe equations (or,

alternatively, a sweep-search, soil wedge solution). The wall is proportioned to resist the applied earth and inertial force loadings. No safety factor is required to be applied to the required weight of wall evaluated by this approach; the appropriate level of safety is incorporated into the step used to calculate the horizontal seismic coefficient. This procedure of analysis represents an improved alternative to the conventional equilibrium method of analysis that expresses the stability of a rigid wall (of prescribed geometry and material properties) in terms of a pseudo-static method with a preselected seismic coefficient and preselected factor of safety against sliding along its base, discussed in Section 1.1.1. Section 6.3.1 in Ebeling and Morrison (1992) outlines the computational steps in the (seismic) displacement controlled design of a retaining wall.

**The analysis of earthquake-induced displacements of a retaining wall:** The retaining wall geometry and material properties are typically first established for the usual, unusual, and extreme load cases with nonseismic loadings. In the subsequent seismic analysis of the retaining wall using the earthquake-induced displacement approach, the primary variable is the permanent displacement. The seismic inertia coefficient  $N^*$  that reduces the sliding factor of safety for the driving soil wedge and the structural wedge to unity is first determined. (Ebeling and Morrison (1992) designated the value for a retaining wall's maximum transmissible acceleration as  $N^*g$ .) Figure 1.7 shows the driving soil wedge and structural wedge treated as a single rigid block in this approach. The resulting permanent seismic displacement of the retaining wall is subsequently determined for the earthquake specified by the design engineer. Section 6.3.2 in Ebeling and Morrison (1992) outlines the computational steps in the analysis of earthquake-induced displacements of a retaining wall (with specified geometry and material properties).

The analytical procedure that was developed by Richards and Elms (1979) recognizes that for some limiting value of horizontal acceleration, identified as  $N^*g$  in Figure 1.7, the horizontal inertia force acting on a retaining wall with no toe fill will nominally exceed the shear resistance provided by the foundation along the interface between the base of the wall and the foundation. This implies that although the soil base (i.e., the foundation to the wall) may be accelerating horizontally at values greater than  $N^*g$ , the wall will be sliding along the base under the action of the horizontal inertial force that corresponds to the horizontal acceleration,



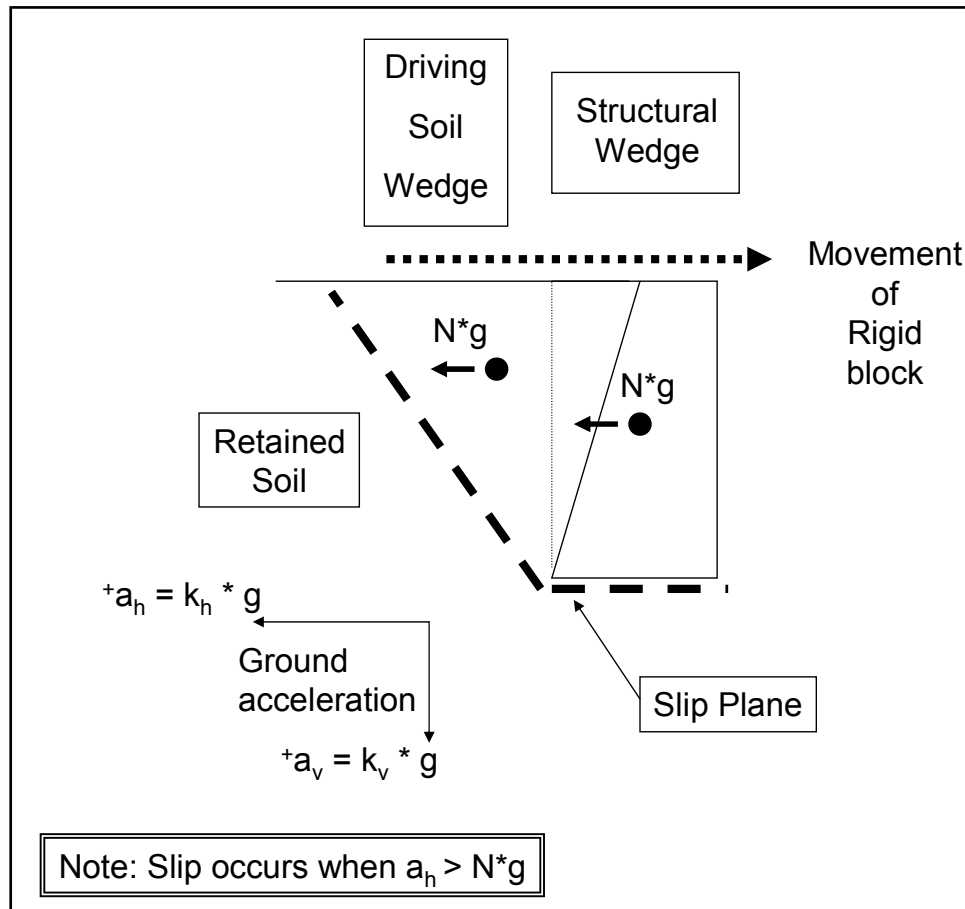


Figure 1.7. Gravity retaining wall and failure wedge treated as a sliding block (after Whitman 1990).

$N * g$ . This results in movement of the soil base relative to the movement of the wall and vice versa. The relative movement *commences* at the point in time designated as point a in the first time-history shown in Figure 1.8 and continues until the (absolute) velocity of the base is equal to the (absolute) velocity of the wall, designated as time point b in the second time-history of this same figure. The (absolute) velocity of the soil base is equal to the integral over time of the soil acceleration, and the (absolute) velocity of the wall between time points a and b is equal to the integral of the wall acceleration, which is a constant  $N * g$ . The *relative* velocity of the wall,  $v_r$ , shown in the third time-history is equal to the integral of the difference between the base acceleration and the constant wall acceleration,  $N * g$ , between time points a and b, as shown in Figure 1.8. The relative displacement of the wall is the fourth time-history and equal to the integral of the relative velocity of the wall, which occurs between the two points in time labeled a and b in Figure 1.8. Note that at time point b when the wall is stopping its first increment of relative movement, the

acceleration is less than  $N^*g$  as shown in the first time-history. This observation demonstrates that the relative velocity of the wall (shown in the third time-history) controls the *cessation* of the seismically induced incremental wall movement. Additional incremental relative displacements occur for the wall between the two later points in time labeled c and d in Figure 1.8 with the residual relative wall displacements,  $d_r$ , equal to the cumulative relative displacements computed during the entire time of earthquake shaking (labeled as point d in the fourth time-history). Lastly,  $N^*g$  is referred to as either the maximum transmissible acceleration or the yield acceleration.

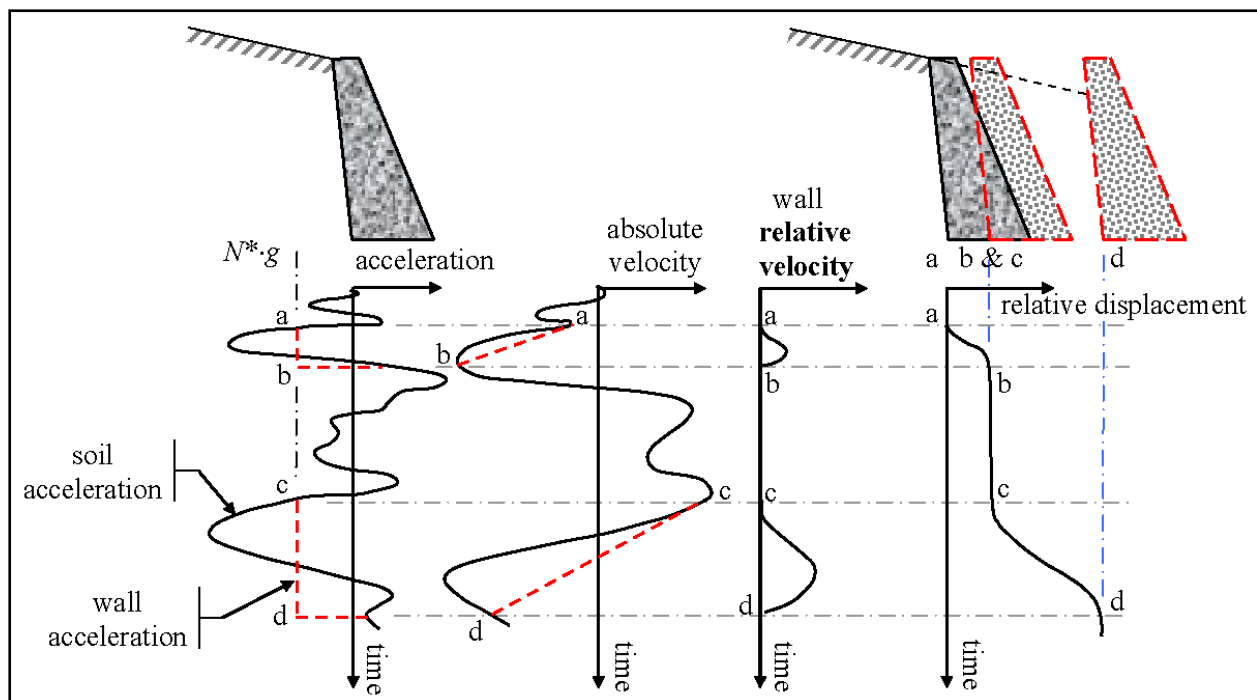


Figure 1.8. Incremental failure by base sliding (adapted from Richards and Elms 1979).

Ebeling and Morrison (1992) observe that the approach has been reasonably well validated for the case of walls retaining granular, moist backfills (i.e., no water table). A key item is the selection of suitable shear strength parameters. In an effective stress analysis, the issue of the suitable friction angle is particularly troublesome when the peak friction angle is significantly greater than the residual friction angle. In the displacement controlled approach examples given in Section 6.2 of Ebeling and Morrison (1992), effective stress based shear strength parameters (i.e., effective cohesion  $c'$  and effective angle of internal friction  $\phi'$ ) were used to define the shear strength of the dilative granular backfills, with  $c'$  set equal to zero in all cases because of the level of

deformations anticipated in a sliding block analysis during seismic shaking. In 1992 Ebeling and Morrison concluded that it is conservative to use the residual friction angle in a sliding block analysis, and this should be the usual practice for displacement-based analysis of granular retained soils. For this report the primary author would broaden the concept to the assignment of effective (or total) shear strength parameters for the retained soil to be consistent with the level of shearing-induced deformations encountered for each design earthquake in a rotational analysis and note that active earth pressures are used to define the loading imposed on the structural wedge by the driving soil wedge. (Refer to Table 1.1 for guidance regarding wall movements required to fully mobilize the shear resistance within the retained soil during earthquake shaking.)

$C_{\text{orpsWallRotate}}$  has the ability to perform a sliding analysis of a user-specified retaining wall section such as the rock-founded retaining wall shown in Figure 1.9. This retaining wall is an idealization of the Figure 1.3 cantilever retaining wall problem. Besides the overall wall and retained soil geometry and material properties, the engineer provides as input baseline-corrected, horizontal and vertical acceleration time-histories that are used to represent the earthquake ground motions.  $C_{\text{orpsWallRotate}}$  represents the effect of the invert spillway slab on the toe of the cantilever wall through a user-specified, limiting resisting force,  $P_{\text{resist}}$ . The magnitude of the  $P_{\text{resist}}$  may be estimated using the simplified procedure developed by Strom and Ebeling (2004). Details regarding the sliding block method of analysis formulated in  $C_{\text{orpsWallRotate}}$  are given in Chapter 4 of this report.

In most sliding block formulations, including that used in  $C_{\text{orpsWallRotate}}$ , an active earth pressure force is applied to the structural wedge in the permanent displacement analysis. Table 1.1 lists the approximate magnitudes of movements required to reach minimum active earth pressure conditions. Although this Clough and Duncan guidance is for static loading, after careful evaluation Ebeling and Morrison (1992, in Section 2.2.2) concluded that the Table 1.1 values may also be used as rough guidance for minimum retained soil seismic displacement to fully mobilize a soil's shear resistance, resulting in dynamic active earth pressures. That is, the permanent displacements computed using  $C_{\text{orpsWallRotate}}$  must equal or exceed the Table 1.1 values (given as displacement-normalized wall heights in this table). If not, then the dynamic earth pressures are underestimated in the analysis.

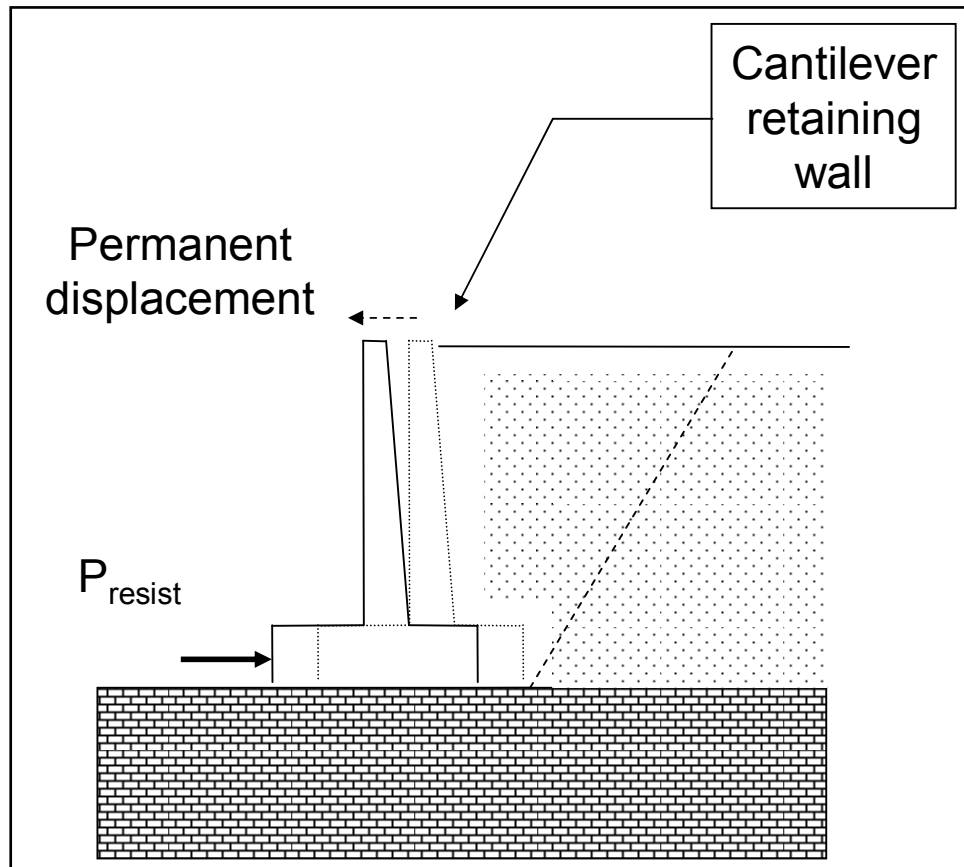


Figure 1.9. Permanent, seismically induced displacement of a rock-founded cantilever wall retaining moist backfill and with toe restraint, computed using CorpsWallRotate.

## 1.2 Rotational analysis of a retaining structure modeled as a rigid block—existing methodologies

The permanent displacement of retaining structures is not restricted to walls that slide along their base as a result of inertial forces imparted during earthquake shaking. For some retaining wall system configurations and material properties, permanent displacements may instead result from the rotation of a retaining wall about a point along its wall-to-foundation interface. The limited research in this topic has focused on methodologies that calculate the permanent displacement caused by seismically induced rotation of a retaining wall modeled as a rigid block. Published analytical methods include those of Nadim and Whitman (1984), Siddharthan et al. (1992), Richards et al. (1996), Steedman and Zeng (1996), and Zeng and Steedman (2000). Figure 1.10 shows the Steedman and Zeng (1996) or, equivalently, the Zeng and Steedman (2000), rotating block methodology for computing permanent rotation and thus displacements of a gravity retaining wall using a horizontal

acceleration time-history to represent earthquake shaking. Key formulation features include a gravity retaining wall modeled as a rigid block; the gravity wall rotating about its toe and on a rigid foundation; a gravity wall retaining moist backfill; and sufficient wall movements away from the retained soil such that the shear strength of the soil is fully mobilized, resulting in the active earth pressure force,  $P_{AE}$ . All these formulations use the Mononobe-Okabe relationship to compute the value of  $P_{AE}$ , which is expressed in terms of an active earth pressure coefficient,  $K_{AE}$ . Vertical ground accelerations are ignored, for simplicity in their formulation. Note that with the point of rotation assigned to the toe of the gravity wall, the resultant foundation-to-wall reaction forces,  $F_s$  and  $N$ , act through this point as well.

A rotation  $\theta$  about the toe of the Figure 1.10 wall is developed once a wall-specific threshold acceleration is exceeded during earthquake shaking represented by a ground acceleration,  $a_{ground}$ .<sup>1</sup> During rotation, the angular acceleration of the mass center (labeled point  $c$ ) of rigid body is  $\alpha$ . (Recall that mass is equal to the weight  $W$  divided by the acceleration of gravity  $g$ .) The  $x$ - and  $y$ -axis accelerations of (rigid) mass center point  $c$  during rotation are labeled  $(a_c)_x$  and  $(a_c)_y$  in this figure. This results in the accumulation of permanent wall rotation with time during further (horizontal) acceleration of the rigid base. When ground acceleration drops below the threshold acceleration for rotation for the wall, restoring forces and moments will act to slow the speed of angular rotation down, thus reducing the rate of increase of the tilt angle about the toe. Wall rotation ceases when the angular rotational velocity (of the mass center about point  $o$ ) returns to zero. Additional increments of wall rotation  $\Delta\theta$  occur each time a (horizontal) ground acceleration pulse exceeds the threshold acceleration for rotation for the wall in the same manner that permanent sliding displacements accumulate for a Newmark rigid sliding block model.

---

<sup>1</sup> The reader is cautioned that the notation given in this section is the same as that used by Steedman and Zang (1996) and is not universally consistent with the notation adopted by the authors of this report for the new formulation that is discussed in Chapter 3 and implemented in  $C_{orpsWallRotate}$ .

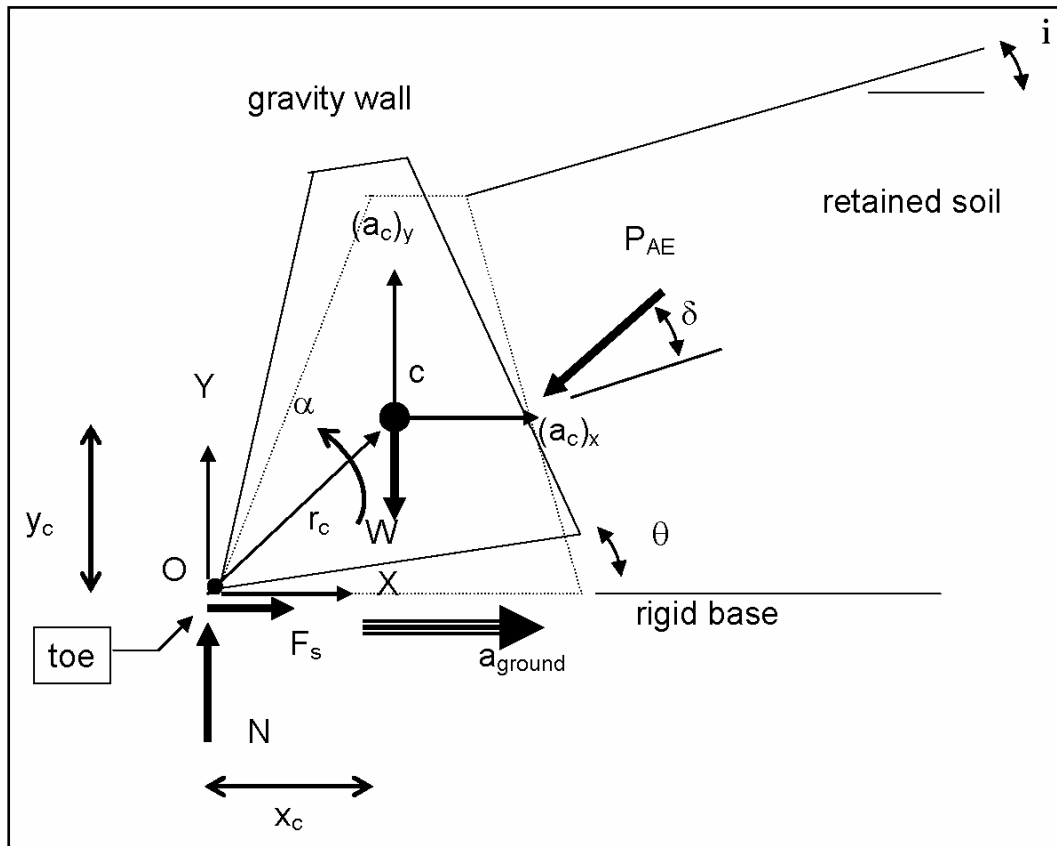


Figure 1.10. Forces and accelerations of a rigid block model of a gravity retaining wall with rotation during horizontal shaking of the rigid base (after Zeng and Steedman 2000).

An important difference between the Newmark sliding block method of analysis for earth retaining structures (i.e., the displacement controlled approach that is discussed in Section 1.1.3) and the rotational analysis of a retaining structure modeled as a rigid block is the acceleration imparted to the rigid block. When a rigid block undergoes permanent *sliding* displacement during earthquake shaking, the largest magnitude horizontal acceleration felt by the rigid block (and the retaining structure contained within the rigid block) is  $N^*g$ , which is less than the peak value for ground acceleration. The maximum transmissible acceleration,  $N^*g$ , is sometimes referred to as the yield acceleration; it is not the user-defined, horizontal ground (or, equivalently, the rigid base) acceleration. For a rigid block that undergoes *rotation* during earthquake shaking, the accelerations felt by this rigid block during shaking are those of the ground acceleration time-history. This is because continuous contact between the rigid block undergoing rotation and the ground is maintained at the point of rotation, i.e., point o, during the entire earthquake shaking process.

Relative-motion analysis of the rigid body model of the Figure 1.10 retaining wall is used to establish the acceleration of (rigid) mass center point  $c$  by establishing the relationship between the acceleration of point  $c$  and the acceleration of point  $o$  (the point of rotation at toe of the wall). In the Zeng and Steedman (2000) Figure 1.10 retaining wall problem, the (translational) acceleration of point  $o$  at the toe of the retaining wall is set equal to the horizontal acceleration vector of the ground,  $a_{\text{ground}}$ , and is a known, user-specified quantity. (Note that its value is established by the user-defined acceleration time-history and changes in magnitude and possibly direction at each increment in time during earthquake shaking.) At each instant in time, the acceleration of the center of mass at point  $c$ ,  $a_c$ , in Figure 1.10 is expressed in terms of the (translational) acceleration of point  $o$ ,  $a_o$ , plus the acceleration of point  $c$  *relative to* point  $o$ ,  $a_{c/o}$ ,

$$a_c = a_o + a_{c/o} \quad 1.1$$

Note that accelerations  $a_c$  and  $a_o$  are absolute accelerations of the two respective points on the rigid body. If the vectors  $a_c$  and  $a_o$  are equal in magnitude and direction, the rigid body undergoes pure translation. In all other cases, rotation of the rigid body will occur. The acceleration of point  $c$  relative to point  $o$ , designated  $a_{c/o}$ , may be expressed in terms of normal and tangential components, respectively, of the acceleration of point  $c$  *relative to* point  $o$ ,

$$a_{c/o} = (a_{c/o})_{\text{tangent}} + (a_{c/o})_{\text{normal}} \quad 1.2$$

Thus, the accelerations felt at the Figure 1.10 mass center  $c$  are the sum of three components:

$$a_c = a_{\text{ground}} + (a_{c/o})_{\text{tangent}} + (a_{c/o})_{\text{normal}} \quad 1.3$$

Figure 1.11 shows these relative acceleration vectors acting at point  $c$ . As the mass center rotates about the toe of the wall,  $(a_{c/o})_{\text{tangent}}$  is the acceleration vector of the rigid mass tangent to the path of rotation of the center of the rigid mass rotating about this point  $o$ ,

$$(a_{c/o})_{\text{tangent}} = \alpha \times r_c \quad 1.4$$

in which

- $\alpha$  = the angular acceleration of the center of rigid mass, point c, about the point of rotation, point o
- $r_c$  = the vector from the point of rotation, point o, to the center of rigid mass, point c

Note that the direction of vector  $(a_{c/o})_{\text{tangent}}$  is consistent with the direction of vector  $\alpha$ .

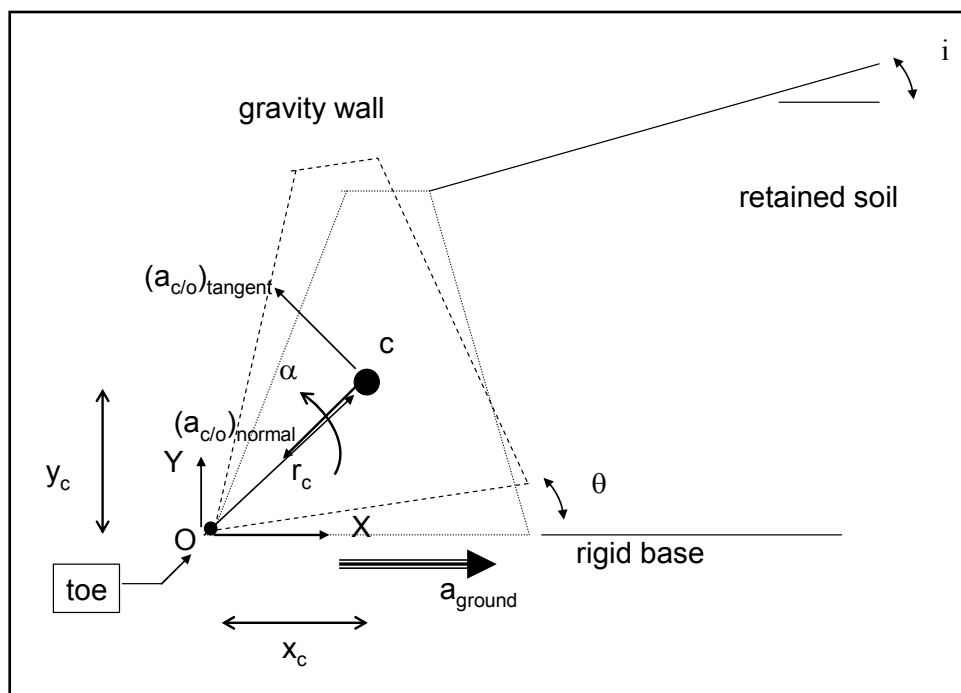


Figure 1.11. The acceleration of point c relative to point o expressed in terms of normal and tangential components.

Additionally, as the mass center rotates about the toe of the wall, the normal acceleration is defined as

$$(a_{c/o})_{\text{normal}} = \omega \times (\omega \times r_c) \quad 1.5$$

in which  $\omega$  the angular velocity of (rigid) mass center point c about its point of rotation, point o. The vector  $a_{\text{normal}}$  is the time rate of change of the change in velocity's direction at point c as it rotates about point o. The direction of  $(a_{c/o})_{\text{normal}}$  is always towards point o, the center of the circular path of rotation as shown in Figure 1.11.



Introducing Equations 1.4 and 1.5, Equation 1.3 becomes

$$a_c = a_{\text{ground}} + \alpha \times r_c - \omega^2 r_c \quad 1.6$$

From Figures 1.10 and 1.11, the horizontal and vertical acceleration components of the center of the rigid mass, point c, are

$$(a_c)_x = a_{\text{ground}} - \alpha \bullet y_c - \omega^2 \bullet x_c \quad 1.7$$

and

$$(a_c)_y = \alpha \bullet x_c - \omega^2 \bullet y_c \quad 1.8$$

Thus for a rigid block that undergoes *rotation* during earthquake shaking, the horizontal acceleration of (rigid) mass center point c is a function not only of the horizontal ground acceleration but it is also a function of the angular acceleration and the angular velocity during rotation of point c about point o. This differs from the situation of a rigid block that undergoes permanent *sliding* displacement during earthquake shaking; the largest magnitude horizontal acceleration felt by this rigid block is  $N \cdot g$ . Recall that  $N \cdot g$ , the maximum transmissible acceleration, is sometimes referred to as the yield acceleration; it is not the user-defined, horizontal ground (or, equivalently, rigid base) acceleration. Unlike the sliding (rigid) block model, which effectively isolates the sliding block from the shaking base below, the rotating rigid block model continues to transmit horizontal acceleration through the “pin,” located at the toe of the wall, into the wall.

For the Steedman and Zeng (1996) (rigid) gravity wall formulation, vertical ground accelerations are ignored. However, for a rigid block that undergoes *rotation* during earthquake shaking, vertical acceleration of (rigid) mass center point c will occur, but is not a function of the horizontal ground acceleration: The vertical acceleration of point c is solely a function of the angular acceleration and the angular velocity during rotation. The Steedman and Zeng rotational model for the prediction of permanent displacement has been validated by comparison with experimental data of a large gravity wall constrained to rock and subjected to a series of damaging earthquakes in centrifuge testing, as described in Steedman and Zeng (1996).

### 1.3 New rotational analysis model based on a rigid block problem formulation

An engineering formulation developed for the rotational response of rock-founded, toe-restrained retaining walls to earthquake ground motions is given in this report. Rock-founded, cantilever walls retaining moist backfills of the type shown in Figure 1.3 that are buttressed at their toe by an invert spillway slab exemplify this category of retaining structure. (Recall that this new engineering procedure and corresponding software are not limited to cantilever walls.) The analysis of the earthquake-induced permanent rotation of the rock-founded retaining wall is idealized in Figure 1.12. The buttressing effect of e.g. an invert spillway slab is represented by the user-specified force  $P_{\text{resist}}$  acting on a vertical section extending upwards from the toe of the wall; Strom and Ebeling (2004) present a simplified engineering procedure to estimate the magnitude of  $P_{\text{resist}}$ . As in Zeng and Steedman (2000), rotation of a rigid block model of the structural retaining wall system is assumed in this new formulation to occur about the toe of the structure (i.e., the rigid block is “pinned” to the rigid, rock foundation base at its toe). However, this new procedure differs from the Steedman and Zeng formulation by (1) formal consideration of a toe-restraint in the analysis (due to the presence of a reinforced concrete slab against the toe of the wall); (2) the ability of the user to assign a vertical acceleration time-history in addition to a horizontal acceleration time-history; (3) consideration of a pool of water in front of the wall, a submerged foundation and a partially submerged retained soil; and (4) the implementation of this formulation within corresponding PC software  $C_{\text{orps}}W_{\text{all}}\text{Rotate}$  using a graphical user interface (GUI) for input of geometry, input of material properties, input/verification of earthquake time-history files, and visualization of results. In addition, (5) a sweep-search wedge formulation within the retained soil is used to determine the value of  $P_{\text{AE}}$  rather than relying on the Mononobe-Okabe relationship (cited in the Steedman and Zeng (1996) formulation). Recall that the Mononobe-Okabe relationship is valid for a retained soil with a constant surface slope and whose strength is characterized by the Mohr-Coulomb shear strength parameter  $\phi$  (e.g., refer to Equations 33 through 35 in Ebeling and Morrison (1992)). The advantage of the sweep-search method as formulated in this report is that it allows for (a) the analysis of bilinear ground surfaces for the retained soil and/or (b) the analysis of cohesive ( $S_u$ ) soils. Details regarding the rotating block method of analysis formulated in  $C_{\text{orps}}W_{\text{all}}\text{Rotate}$  are given in Chapter 3 of this report.

$C_{\text{CorpsWallRotate}}$  applies an active earth pressure force to the structural wedge in the permanent rotation analysis, as is done in most sliding block formulations for retaining walls. Table 1.1 lists the approximate magnitudes of movements required to reach minimum active earth pressure conditions. Although this Clough and Duncan guidance is for static loading, after careful evaluation Ebeling and Morrison (1992, in Section 2.2.2) concluded that the Table 1.1 values may also be used as rough guidance for minimum retained soil seismic displacement to fully mobilize a soils shear resistance, resulting in dynamic active earth pressures. That is, the permanent displacements resulting from rotations computed using  $C_{\text{CorpsWallRotate}}$  must equal or exceed the Table 1.1 values (given as displacement-normalized wall heights in this table). If not, then the dynamic earth pressures are underestimated in the analysis.

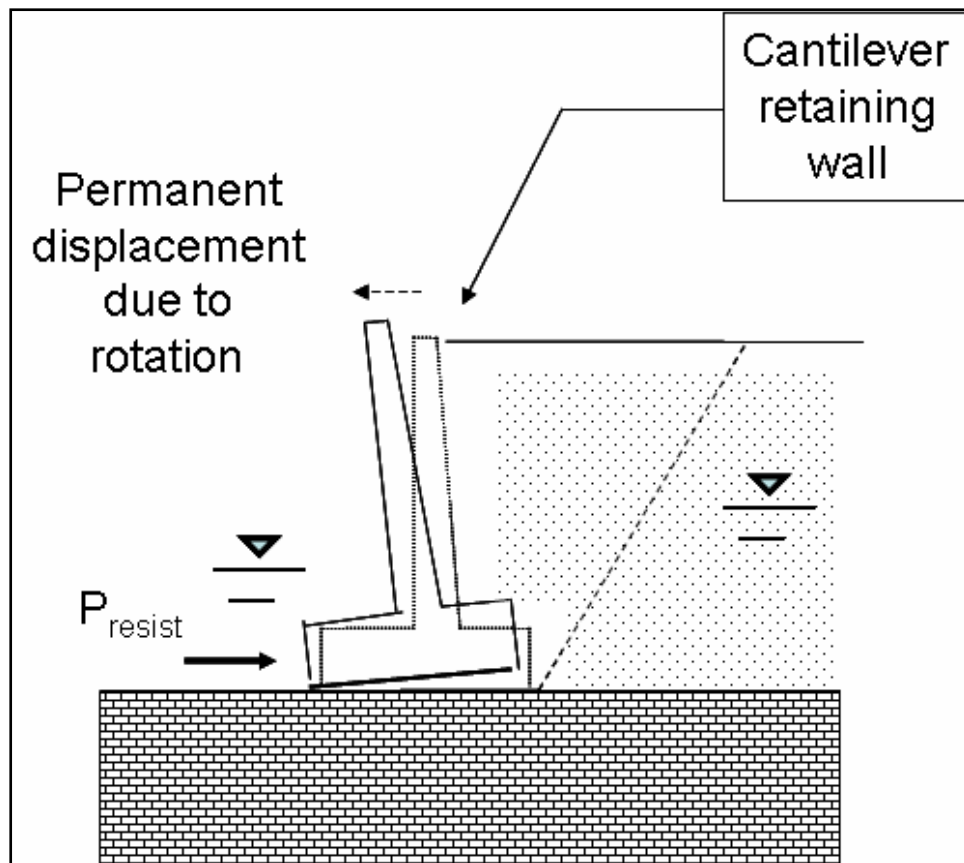


Figure 1.12. Permanent, seismically induced displacement due to the rotation about the toe of a rock-founded cantilever retaining wall and with toe restraint, computed using  $C_{\text{CorpsWallRotate}}$ .

## 1.4 Seismic design criteria for Corps retaining structures

Current Corps engineering methodology is to evaluate retaining walls for usual, unusual, and extreme loadings. Consideration of earthquake loadings is part of the design process for Corps earth retaining structures. Engineering Regulation (ER) 1110-2-1806 provides requirements governing the seismic design and evaluation of structures located at Corps projects. The engineering procedures outlined in this Corps document are applicable to the analysis of existing, or the design of new earth retaining structures. The Corps regulation for earthquake loadings, ER 1110-2-1806, specifies two *project specific* earthquakes, the Operational Basis Earthquake (OBE) and the Maximum Design Earthquake (MDE).

The OBE is an earthquake that can reasonably be expected to occur within the service life of the project, that is, with a 50-percent probability of exceedance during the service life. (This corresponds to a return period of 144 years for a project with a service life of 100 years.) The associated performance requirement is that the project functions with little or no damage, and without interruption of function. The purpose of the OBE is to protect against economic losses from damage or loss of service, and therefore alternative choices of return period for the OBE may be based on economic considerations. The OBE is determined by a Probabilistic Seismic Hazard Analysis (PSHA). The OBE is classified as an unusual event. Retaining walls are expected to remain serviceable and operable immediately following an OBE event, or immediately following any earthquake that can reasonably be expected to occur within the service life of the project.

The MDE is the maximum level of ground motion for which a structure is designed or evaluated. The associated performance requirement is that the project performs without catastrophic failure, such as an uncontrolled release of a reservoir, although severe damage or economic loss may be tolerated. For *critical features*, the MDE is the same as the Maximum Credible Earthquake (MCE). [Section 5(a) and Table B-1 in ER 1110-2-1806 outlines the assessment of the hazard potential classification of Civil Works projects and is related to the consequences of project failure. *Critical features* are the engineering structures, natural site conditions, or operating equipment and utilities at high hazard projects whose failure during earthquake could result, in loss of life.] For all other features, the MDE shall be selected as a lesser earthquake than the MCE which provides economical designs meeting appropriate safety standards. The MDE is the

maximum level of ground motion for which a structure is designed or evaluated. Although not formally stated in the ER, recent (limited) application to select, normal Corps (non-critical) structures is to assume the MDE is an earthquake that has a 10 percent chance of being exceeded in a 100-year period (or a 950-year return period). The MDE for non-critical structures is established for each project on an individual basis, often in consultation with CE-CW (Headquarters). The MDE for normal structures is determined by PSHA. For critical structures the MDE is the MCE, which is determined by a deterministic seismic hazard assessment (DSHA). The MCE is defined as the greatest earthquake that can reasonably be expected to be generated on a specific source, on the basis of seismological and geological evidence. Significant damage resulting from an MDE event can be considered as acceptable provided the damaged structure can be repaired and put back in service without risk to life.

Factors of safety and safety requirements for retaining walls subject to seismic loading conditions are provided in EM 1110-2-2100. This supersedes the stability guidance for retaining walls contained in EM 1110-2-2502 (but *not* the engineering procedures, which are based on the simplified pseudo-static procedure of analysis).

Factors of safety for sliding and flotation, and the safety provisions related to resultant location and allowable bearing capacity contained in EM 1110-2-2100 are dependent on:

- Load condition category (usual, unusual, or extreme),
- Site information knowledge (well-defined, ordinary, or limited), and
- Structure importance (normal, or critical).

EM 1110-2-2100 associates each of the three load condition categories to a range in annual probability (or, equivalently, a range in return period). Additional “structure specific” information related to load condition categories and probabilities are contained in Appendix B of EM 1110-2-2100.

## **1.5 Axial load capacity of spillway invert slabs**

Reinforced concrete slabs provide an important contribution to the overall seismic stability of retaining walls. Figure 1.3 shows for example, an invert spillway buttressing a cantilever retaining wall that borders a spillway channel. Key to the seismic performance of this spillway retaining wall is

the stabilizing force that the channel invert slab exerts at the toe of this wall. The magnitude of this stabilizing force will depend on the limit state axial load capacity of this invert slab.

Invert slabs can be founded on earth or rock. Types of construction used by the Corps include an “independent block plan” and a “continuous reinforcing plan.” Invert slabs when loaded axially can exhibit either short column, or long column behavior with the later referring to slabs whose axial capacity is reduced by second-order deformations (i.e.,  $P \bullet \Delta$  effects).

Slab capacity in terms of axial load versus moment interaction is determined based on ultimate strength design principles, which can be applied to both unreinforced (plain concrete) and reinforced concrete invert slab sections. Influences from the subgrade reaction, slab dead load, and axial load eccentricity when considered in a second-order analysis suggest the axial load capacity can be based on a short column design with second-order displacements due to  $P \bullet \Delta$  effects having little if any effect on column axial load capacity, according to Strom and Ebeling (2004).

The axial load resistance  $P_{\text{resist}}$  provided by the Figure 1.3 invert slab is illustrated in Figure 1.12. Limited investigations, by Strom and Ebeling (2004), based on the Corps minimum thickness for invert slabs constructed on rock and earth, and for both continuous reinforcing plans and independent block plans, indicate the limit state axial load capacity, or ultimate axial load resistance of the slab ( $P_{\text{resist}}$ ) may be on the order of:

- 120 kips per foot width of slab for a 1.0-foot-thick invert slab on rock.
- 240 kips per foot width of slab for a 2.0-foot-thick invert slab on soil.

The above values are valid for both anchored and unanchored invert slabs, and for the minimum contraction joint spacings typically found on Corps projects. However, a site-specific evaluation of the limiting axial resisting force due to the buttressing effect of the any type of slab on the toe of a retaining wall is required. Refer to Strom and Ebeling (2004) for a simplified engineering methodology for the assessment of  $P_{\text{resist}}$  for all types of slabs buttressing all types of retaining structures, including the Figure 1.3 invert spillway slab.

## 1.6 Background and research objective

Engineer Manual 1110-2-2502 Retaining and Flood Walls gives engineering procedures that are currently being used by District Engineers in their *initial* assessment of seismic wall performance of existing earth retaining structures and the (preliminary) sizing of new retaining structures. The engineering procedures given in EM 1110-2-2502 for retaining walls make extensive use of the simplified pseudo-static procedure of analysis of earth retaining structures and expresses wall performance criteria in terms of computed factors of safety against sliding and bearing failure, and base area in compression. The simplified pseudo-static procedure of analysis makes it difficult to interpret the actual wall performance for Corps projects subjected to “strong” design ground motions because of simplifications made in the procedure of analysis. In a pseudo-static analysis an oversimplification occurs when the engineer is forced to render the complex, horizontal and vertical earthquake acceleration time-history events to constant values of accelerations and assume a constant direction for each. These constant values are denoted as the pseudo-static acceleration coefficients in the horizontal and vertical directions (refer to Section 1.1.1 of this report). The engineer is also required to assume a constant direction for each of these components. An acceleration time-history, in actuality, varies both in magnitude and in direction with time.

The simplified pseudo-static procedure does not allow for interpretation of *actual* wall performance by District Engineers. Intense shaking imparted by the OBE and MCE design events makes the interpretation of the simplified procedure of analysis even more difficult. The more important questions for the wall are whether the wall slides into the spillway basin, or rotates into the spillway basin, or even tips over onto its side during the earthquake event. The simplified pseudo-static procedure of analysis is not capable of answering these questions. The answers depend on the magnitude of the pseudo-static coefficient used in the calculations compared to the magnitude of the peak values for the acceleration pulses as well as the number and duration of these strong shaking acceleration pulses in the design earthquake event time-history. When considering both horizontal and vertical accelerations, the resulting wall response is further complicated by the time-history of phasing between the pulses of horizontal and vertical accelerations. Only the permanent wall sliding displacement/wall rotation method of time-history analysis can answer

these questions. Again, wall displacements will influence the seismic earth pressure forces imparted on the wall by the retained soil.

Formal consideration of the permanent seismic wall displacement in the seismic design process for Corps-type retaining structures is given in Ebeling and Morrison (1992). The key aspect of the engineering approach presented in this Corps document is that simplified procedures for computing the seismically induced earth loads on retaining structures are also dependent upon the amount of permanent wall displacement that is expected to occur for each specified design earthquake. The Ebeling and Morrison simplified engineering procedures for Corps retaining structures are geared towards hand calculations. The engineering formulation and corresponding PC software  $C_{\text{Corps}}W_{\text{all}}\text{Rotate}$  discussed in this report extend these simplified procedures to walls that rotate during earthquake shaking and make possible the use of acceleration time-histories in the Corps design/analysis process when time-histories are made available on Corps projects.  $C_{\text{Corps}}W_{\text{all}}\text{Rotate}$  may be used to predict permanent seismically induced rotational or translational displacements of walls retaining backfill, with or without a toe restraint. It is particularly applicable to rock-founded L-walls and T-walls (i.e., cantilever retaining walls) which border spillway channels (Figure 1.3).

The engineering methods contained in this report and implemented within  $C_{\text{Corps}}W_{\text{all}}\text{Rotate}$  allow the engineer to determine if a given retaining wall has a tendency to rotate or to slide for a specified seismic event. This is a new capability for the seismic design/evaluation process for Corps retaining structures.

## 1.7 Organization of report

Chapter 2 discusses four existing rotational analysis models of a retaining wall rotating about a point along its base. All of these engineering formulations involved retaining walls *without toe restraint*.

Chapter 3 describes the new engineering formulation for the seismic analysis of the permanent rotation of a retaining structure modeled as a rigid block *with toe restraint*. The numerical method used to compute the rotation time-history of the rigid block model about its toe is presented.

Chapter 4 describes a new translational block analysis model of a retaining structure buttressed by a reinforced concrete slab. It is a special variation



of the engineering formulation for the seismic analysis of the permanent displacement of a retaining structure modeled as a rigid sliding block but with a toe restraint. The numerical method used to compute the sliding displacement time-history of the rigid block model is presented.

Chapter 5 describes key aspects of the visual modeler and visual post-processor  $C_{\text{orps}}W_{\text{all}}\text{Rotate}$ . Specifically, a description of the GUI for input of geometry, input of material properties, input/verification of earthquake time-history files, and for visualization of results is presented to make the user familiar with its operation.

Chapter 6 presents a summary, conclusions, and recommendations for additional research.

Appendix A presents a derivation of the dynamic active earth pressure force using the sweep-search wedge method which is implemented in  $C_{\text{orps}}W_{\text{all}}\text{Rotate}$  to calculate  $P_{\text{AE}}$ .

Appendix B provides an abbreviated review of dynamics of a rigid body.

Appendix C describes an approach used for computing the dynamic active earth pressure distribution for a partially submerged, retained soil.

Appendix D describes the procedures used to compute the water pressures acting on the structural wedge, including the computation of hydrodynamic water pressures due to earthquake shaking of a pool (when present) in front of the retaining wall. With most Corps hydraulic structures that act as earth retaining structures possessing a vertical face in contact with the pool (when present), hydrodynamic water pressures are approximated in the  $C_{\text{orps}}W_{\text{all}}\text{Rotate}$  using the Westergaard (1931) procedure.

Appendix E outlines the mass moment of inertia computation made by  $C_{\text{orps}}W_{\text{all}}\text{Rotate}$  for the structural wedge.

Appendix F lists and describes the contents of the ASCII input data file to the FORTRAN engineering computer program portion of  $C_{\text{orps}}W_{\text{all}}\text{Rotate}$ . This data file, always designated as CWROTATE.IN, is created by the GUI, the visual modeler portion of  $C_{\text{orps}}W_{\text{all}}\text{Rotate}$ .

Appendix G lists the CorpsWallRotate ASCII output files.

Appendix H discusses two example computations of static, active earth pressure distributions and depth of cracking in cohesive soils.

## 2 Existing Rotational Analysis Models of a Retaining Wall Rotating About a Point Along its Base

### 2.1 Introduction

The permanent displacement of retaining structures is not restricted to walls that slide along their base as a result of inertial forces imparted during earthquake shaking. For some retaining wall system configurations and material properties, permanent displacements may instead result from the rotation of a retaining wall about a point along its wall-to-foundation interface. The limited research on this general topic has focused on engineering methodologies that calculate the permanent displacement due to seismically induced rotation of a retaining wall modeled as a rigid block. Published analytical methods include those of Nadim and Whitman (1984), Siddharthan et al. (1992), Fishman and Richards (1997, 1998), Steedman and Zeng (1996), and Zeng and Steedman (2000). All four studies involve engineering formulations for retaining walls *without toe restraint*. This chapter reviews key aspects of these existing, simplified formulations used to analyze seismically-induced permanent displacement due to rotation of a rigid block retaining wall about a point along its base.<sup>1</sup>

**The reader is cautioned that the notation given in each of the sections is the same as that used by the developers of each of the formulations being discussed (as used in their cited papers) and is not universally consistent with the notation adopted by the authors of this report for the new formulation that is discussed in Chapter 3 and implemented in CorpsWallRotate.**

During ground shaking, inertial forces are induced on the retaining wall system. Acceleration time-histories are used to represent ground shaking in these simplified models of retaining wall systems. The time-varying inertial forces lead to elastic deformations which can ultimately result in permanent rotation of the wall or sliding of the wall. In the case of permanent rotation of a rigid block model of the retaining wall system,

---

<sup>1</sup> Appendix B provides an abbreviated review of dynamics of a rigid body.

(1) inertial forces vary in magnitude and direction with time, and (2) their magnitudes are proportional to the value of acceleration at any given instant in time but act in the direction opposite to acceleration. Additionally, a rotational acceleration about a point of rotation develops once the threshold acceleration for lift-off of the base of the wall in rotation is exceeded, which leads to permanent rotation of the wall relative to the top-of-foundation. When the ground acceleration drops below this threshold acceleration value, restoring forces and moments will act to slow the speed of rotation, reducing the rate of increase of the angle of wall rotation. An increment of permanent wall rotation occurs during this interval in time. Additional permanent rotation will be induced during further cycles of ground acceleration if the threshold acceleration for lift-off of the base of the wall in rotation is again exceeded. The angle of permanent wall rotation accumulates with each of these excursion cycles in a manner similar to the accumulation of permanent sliding displacement in Newmark's sliding block method, briefly discussed in Chapter 1 and discussed in detail in Chapter 4. The primary author of this report observes that for a retaining wall system of specified geometry and material properties (i.e., unit weights and shear strength parameters, etc.) the threshold values of acceleration corresponding to incipient lift-off of the base of the wall in rotation (about a specified point of rotation) and for incipient sliding of the wall are not the same.

## **2.2 Nadim and Whitman rigid block model of a gravity wall with earthquake-induced, permanent rotation about a center of rocking located along the base of the wall**

One of the earliest formulations of a rigid block that rotates during earthquake shaking about a point along its base was developed by Nadim and Whitman (1984). Figure 2.1 depicts the idealized problem of a retaining wall that develops incremental, permanent rotations about a user-specified point of rotation during earthquake shaking. Nadim and Whitman termed this point as the "center of rocking," and it is designated point O in this figure. Note that in this simplified formulation, there is no incremental rotation into the backfill; all incremental, permanent rotations that develop are directed away from the backfill. Acceleration time-histories are used to characterize earthquake shaking of the ground in this formulation.

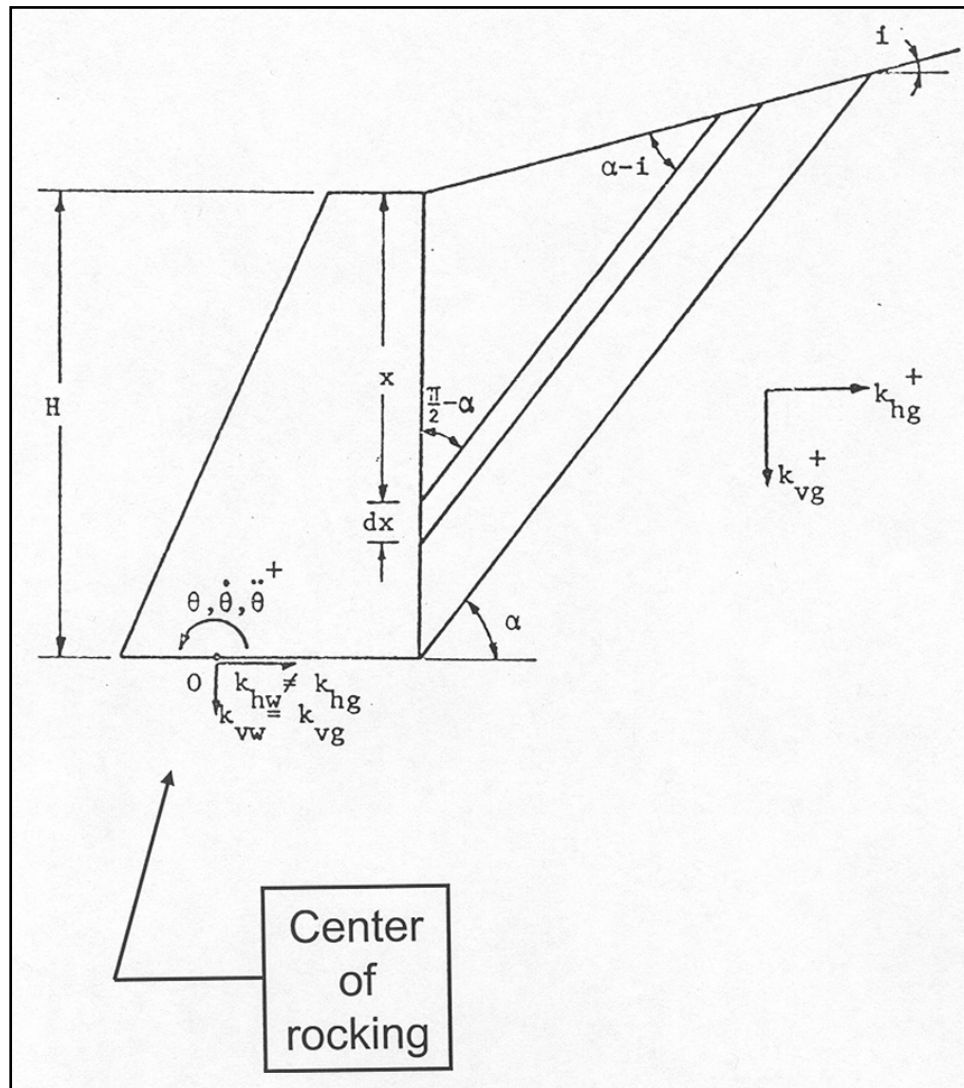


Figure 2.1. Rotating gravity retaining wall (after Nadim and Whitman (1984)).

The sign convention adopted by Nadim and Whitman (1984) for user-specified horizontal  $k_{hg}g$  and vertical  $k_{vg}g$  ground acceleration time-histories are shown in the right-hand side of Figure 2.1. Positive horizontal ground acceleration is directed towards the retained soil and positive vertical acceleration is directed towards the foundation.<sup>1</sup> Recall that  $g$  is the universal gravitational constant, while  $k_{hg}$  and  $k_{vg}$  are the respective *time-histories* of the horizontal and vertical ground accelerations, expressed in decimal fraction. Notation with regards to the parameter “ $k$ ” is as follows; the first subscript “ $h$ ” or “ $v$ ” means “horizontal” or “vertical,”

<sup>1</sup> The primary author of this report is of the opinion that this sign convention used is for the convenience of calculating the thrust force  $P_{AE}$  provided by the driving soil wedge and not based on considerations associated with the structural wedge.

and the second subscript “g” or “w” means “ground” or “wall.” The earthquake shaking is represented by user-specified ground acceleration time-histories in this formulation. The components of wall acceleration are  $k_{hw}$  and  $k_{vw}$  at the center of rocking. In this figure the notation of  $k_{hw}$  not equal to  $k_{hg}$  is meant to highlight the fact that the horizontal acceleration of the wall is not equal to the horizontal acceleration of the ground. It is assumed that there are no rotational movements of the ground so  $\ddot{\theta}$  in this figure is the absolute rotational acceleration as well as the rotational relative acceleration of the wall.

Incremental, permanent wall rotations can occur during “strong” earthquake acceleration “pulses” (i.e., sequences in the acceleration time-history that contain high amplitude acceleration wave forms and usually of short duration) in which horizontal ground acceleration thrusts are directed towards the retained soil (i.e., acting in the Figure 2.1 positive  $k_{hg}$  direction). The resulting incremental, permanent wall movements will be directed away from the retained soil. When these incremental wall movements occur, they are assumed to be of sufficient magnitude to fully mobilize the shear resistance in the retained soil. Active earth pressures are assumed to act on the retained side of the wall during these incremental wall rotations. In order to satisfy continuity, Nadim and Whitman (1984) assumed the backfill soil is allowed to move in planes parallel to the plane of failure as shown in this figure. There are an infinite number of failure planes, all of which are parallel. The total active thrust acting on the back of the retaining wall is equal to the sum of the wall-to-retained soil interface incremental forces of each of the Figure 2.1 soil slices within the retained soil. The angle that the rupture plane makes with horizontal  $\alpha$  is established in this formulation using the Zarrabi (1979) relationship for  $\alpha$ , which is based on the single, rigid-plastic active wedge used in the Mononobe-Okabe formulation with a potential failure plane that goes through the heel of the wall. In order to find the inclination  $\alpha$  of the failure planes, Nadim and Whitman assume that the (resultant) active thrust from all of the Figure 2.1 soil slices is equivalent to the value of  $P_{AE}$  computed using the Mononobe-Okabe formulation. Nadim (1980) observes that this assumption is equivalent to using the Mononobe-Okabe equation with an average  $k_{hb}$  and  $k_{vb}$  for the entire rigid-plastic soil mass.

For a specified value of  $\alpha$  the resultant active force  $P_{AE}$  and its line of action  $L$  (above the heel of the wall) are given by Nadim and Whitman (1984) as:

$$P_{AE} = \frac{1}{2} \cdot \gamma \cdot H^2 \cdot c \cdot \left[ b - \frac{a \cdot \ddot{\theta}}{3} \right] \quad 2.1$$

$$L = \frac{H}{3} \cdot \left[ \frac{b - a \cdot \ddot{\theta} / 2}{b - a \cdot \ddot{\theta} / 3} \right] \quad 2.2$$

where

$$a = \frac{H \cdot \cos(\phi)}{g \cdot \cos(\alpha)} \quad 2.3$$

$$b = \sin(\alpha - \phi) \cdot [1 - k_{vg} - k_{hg} \cdot \tan(\alpha)] + k_{hw} \cdot \frac{\cos(\phi)}{\cos(\alpha)} \quad 2.4$$

$$c = \frac{\cos(i) \cdot \cos(\alpha)}{\sin(\alpha - i) \cdot \cos(\alpha - \phi_w - \phi)} \quad 2.5$$

- H = height of wall
- g = constant of gravitational acceleration
- i = backfill slope
- $\alpha$  = inclination of failure planes in retained soil
- $\phi$  = friction angle of retained soil
- $\phi_w$  = friction angle of wall-backfill interface
- $\gamma$  = unit weight of backfill
- $\ddot{\theta}$  = rotational acceleration of the wall

When there is no rotational acceleration, the value of  $P_{AE}$  would become identical to  $P_{AE}$  computed using the Mononobe-Okabe equation (refer to Figure 1.5), provided that the correct inclination of rupture plane  $\alpha$  within the retained soil is used in Equations 2.1 through 2.4. Rotational acceleration causes an additional term in the equation for  $P_{AE}$ . This term depends on the assumption made regarding continuity; in order for  $P_{AE}$  to remain positive,  $b$  must be greater than  $\frac{a \cdot \ddot{\theta}}{3}$  at each time-step in the time-history response analysis.

Equation 2.2 for the line of action  $L$  suggests that when  $\ddot{\theta}$  is positive (i.e., the wall is rotating away from the retained soil),  $P_{AE}$  lies below the lower

third point. Nadim (1980) notes that this conclusion is contrary to all previous results obtained by different investigators (also see Section 4.2.2 in Ebeling and Morrison (1992)). Physically, as the wall tilts, each slice of soil in the backfill experiences a different acceleration. The soil close to the bottom of the wall is slipping least relative to the ground, hence its acceleration is largest. The topmost soil is lagging furthest behind the ground and has the lowest acceleration. Thus, the bottom soils contribute more to the lateral pressures and cause the resultant force below the lower third point. Conversely, as soon as the wall decelerates (i.e., when  $\ddot{\theta}$  is negative), the situation is reversed. Now the resultant force,  $P_{AE}$ , lies well above the third point. So the *point of application of the resultant force*  $P_{AE}$  changes, but the results of calculations made by Nadim (1980) indicate that on average, it falls slightly above the lower third point.

In the Nadim and Whitman (1984) formulation, the center of rocking is restricted to a point along the base of the wall. Note that they did not restrict this fixed point of rotation, i.e., the center of rocking in their vocabulary, to the toe of the wall in their formulation. However, this center of rocking, about which permanent rotation will occur during earthquake shaking, was fixed at a user-specified location along the base of the wall for the duration of each time-history analysis. In subsequent analyses, the user could then repeat the time-history analysis of permanent wall rotation for the same acceleration time-history but specifying another location of the center of rocking along the base of the wall. The center of rocking location that results in the largest permanent wall rotation is considered the solution for the problem by Nadim and Whitman. It is envisioned by the primary author of this report that a center of rocking location other than at the toe of the wall implies a flexible and somewhat compliant foundation. A soil foundation would satisfy this characterization. Nadim and Whitman refer to a soil foundation (versus a rock foundation) in their formulation discussions.

Figure 2.2.a shows the dynamic forces acting on the Nadim and Whitman retaining wall. The wall has a weight per unit length of  $W_w$  and a mass moment of inertia per unit length  $I_{CG}$  about the wall's center of gravity, CG. The friction angle at the base of the wall is  $\phi_b$  and the wall-to-retained soil interface friction angle is  $\phi_w$ . The vertical acceleration of the rigid wall at the point of rocking (point O),  $k_{vw}g$ , is the same as the vertical acceleration of the ground,  $k_{vg}g$ . By definition, only sliding may take place at point O; the horizontal acceleration of point O,  $k_{hw}g$ , would be different during



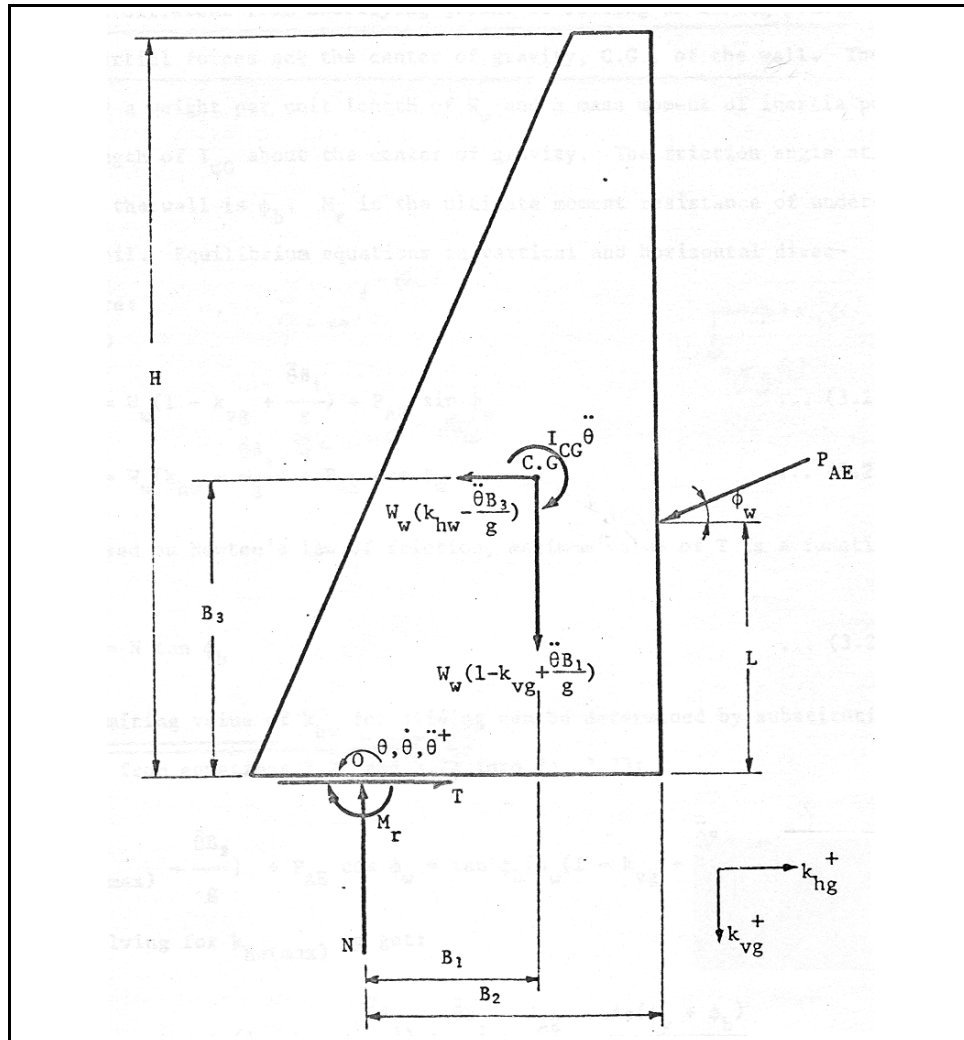
sliding from the horizontal acceleration of the ground,  $k_{hg}$ . The inertial forces act at the center of gravity of the wall.  $N$  and  $T$  are the foundation's normal and shear reaction forces, respectively.  $M_r$  is the ultimate moment resistance of underlying "soil" foundation. The principal author of this report observes that the foundation reaction moment,  $M_r$ , in conjunction with the normal force,  $N$ , implies an eccentricity of the location of the foundation's resultant reaction force  $N$  with respect to the user-defined center of rocking, as shown in Figure 2.2.b.

For "large"  $k_{hg}$  horizontal ground acceleration thrusts towards the retained soil (acting in the Figures 2.1 and 2.2.a positive  $k_{hg}$  direction), incremental wall rotations initiate when a limiting wall acceleration value for the wall is exceeded. (Recall that the inertial force acts opposite to the direction of acceleration, away from the retained soil for positive horizontal acceleration thrusts. Inertia forces have been applied according to D'Alembert's principle which permits the problem to be treated as a static problem.) Thus, large horizontal acceleration thrusts in the direction of the retained soil will attempt to destabilize the wall, possibly resulting in incremental wall rotations in the positive  $\theta$  direction shown in this figure (i.e., rotation outward) and corresponding incremental, permanent wall movements directed away from the retained soil. For a given retaining wall system configuration and material properties, there is a unique value of limiting acceleration for sliding and a unique value of limiting acceleration for lift-off of a wall in rotation about a point along its base. For any given retaining wall system, the values of these two limiting accelerations are typically not the same.

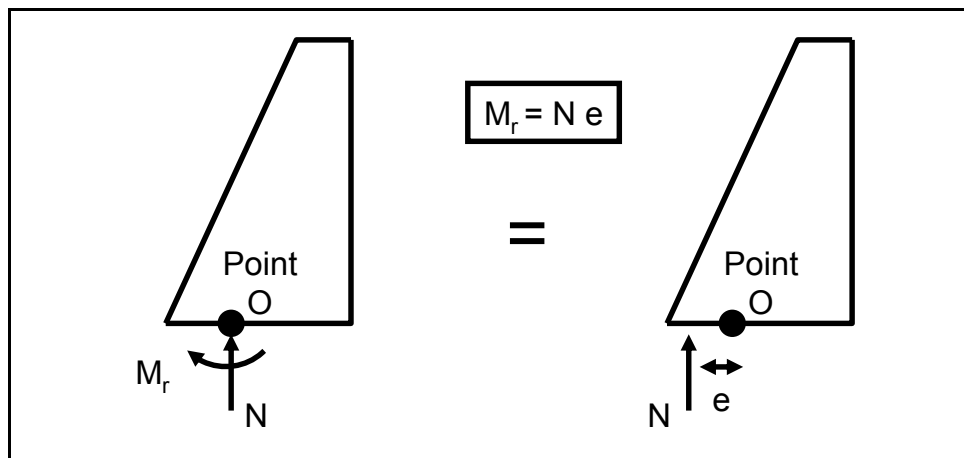
### Limiting acceleration of a wall – sliding

When ground acceleration thrusts exceed a limiting value of sliding acceleration the wall will begin to slide. The limiting acceleration of the wall can be determined from the equilibrium equations of the wall. The equation of horizontal equilibrium for the Figure 2.2.a wall is

$$T = W_w \left( k_{hw} - \frac{\ddot{\theta} B_3}{g} \right) + P_{AE} \bullet \cos(\phi_w) \quad 2.6$$



a. Dynamic forces acting on the retaining wall (after Nadim 1980).



b. Foundation reaction resultant force N eccentric to the point of rotation by a distance e.

Figure 2.2. Dynamic forces acting on the retaining wall per the Nadim formulation

and the equation of vertical equilibrium is

$$N = W_w \left( 1 - k_{vg} + \frac{\ddot{\theta} B_1}{g} \right) + P_{AE} \bullet \sin(\phi_w) \quad 2.7$$

Coulomb's law of friction relates the maximum value of T to N by

$$T_{\max} = N \bullet \tan(\phi_b) \quad 2.8$$

By setting

$$k_{hw} = (k_{hw})_{\text{slide}} \quad 2.9$$

the limiting horizontal acceleration value of  $(k_{hw})_{\text{slide}}$  for *(incipient) sliding* is determined by introducing Equations 2.6 and 2.7 into Equation 2.8, and solving for  $(k_{hw})_{\text{slide}}$ ,

$$(k_{hw})_{\text{slide}} = \tan(\phi_b) \bullet \left( 1 - k_{vg} + \frac{\ddot{\theta} B_1}{g} \right) + \frac{\ddot{\theta} B_3}{g} - \frac{P_{AE}}{W_w} \bullet \frac{\cos(\phi_w + \phi_b)}{\cos(\phi_b)} \quad 2.10$$

Permanent, incremental wall translations initiate when horizontal ground acceleration,  $k_{hg}g$ , thrusts towards the retained soil exceed the limiting horizontal wall acceleration value,  $(k_{hw})_{\text{slide}}$ .

### Limiting acceleration of a wall—lift-off of its base in rotation

When ground acceleration thrusts exceed a limiting value of acceleration, the wall will begin to lift off of its foundation, rotating about the center of rocking (i.e., point O) at the base of the wall. The limiting acceleration of the wall can be determined from equilibrium equations of the wall. The moment equilibrium equation about point O is

$$\begin{aligned} I_{CG} \ddot{\theta} + W_w \left( 1 - k_{vg} + \frac{\ddot{\theta} B_1}{g} \right) B_1 - W_w \left( k_{hw} - \frac{\ddot{\theta} B_3}{g} \right) B_3 \\ - P_{AE} \bullet \cos(\phi_w) \bullet L + P_{AE} \bullet \sin(\phi_w) \bullet B_2 + M_r = 0 \end{aligned} \quad 2.11$$

Solving for  $\ddot{\theta}$ ,

$$\ddot{\theta} = \frac{P_{AE} \cdot (L \cdot \cos(\phi_w) - B_2 \cdot \sin(\phi_w)) + W_w \cdot [k_{hw} \cdot B_3 - (1 - k_{vg}) \cdot B_1] - M_r}{I_{rot}} \quad 2.12$$

with

$$I_{rot} = I_{CG} + \frac{W_w}{g} \cdot (B_1^2 + B_3^2) \quad 2.13$$

$I_{rot}$  is the mass moment of inertia about point O. If the applied moment from  $P_{AE}$  and wall inertia is less than  $M_r$ , no permanent rotation takes place and  $\ddot{\theta}$  is zero.

By setting

$$k_{hw} = (k_{hw})_{tilt} \quad 2.14$$

the limiting horizontal acceleration value of  $(k_{hw})_{tilt}$  for (incipient) lift-off of a wall in rotation about point O is determined by introducing Equation 2.14 into Equation 2.12 and setting the numerator equal to zero. (Recall wall rotations occur when a nonzero  $\ddot{\theta}$  value is achieved.) Thus, a wall's value of *limiting yield acceleration* is

$$(k_{hw})_{tilt} = \frac{M_r + P_{AE} \cdot (B_2 \cdot \sin(\phi_w) - L \cdot \cos(\phi_w)) + W_w \cdot (1 - k_{vg}) \cdot B_1}{W_w \cdot B_3} \quad 2.15$$

Since a key item of interest is the horizontal limiting acceleration, Nadim and Whitman set  $k_{vg}$  equal to 0 in Equation 2.15, resulting in

$$(k_{hw})_{tilt} = \frac{M_r + P_{AE} \cdot (B_2 \cdot \sin(\phi_w) - L \cdot \cos(\phi_w)) + W_w \cdot B_1}{W_w \cdot B_3} \quad 2.16$$

Rotational acceleration of the wall is zero for values of horizontal ground acceleration less than or equal to  $(k_{hw})_{tilt}g$ . At a time-step  $t_i$  into the ground acceleration time-history, when the horizontal ground acceleration value  $k_{hgg}$  is equal to or greater than  $(k_{hw})_{tilt}g$ , incremental rotation commences (i.e., the wall's rotational acceleration  $\ddot{\theta}$  is nonzero). The time-history of rotational velocity  $\dot{\theta}$  is obtained by numerical integration of the wall's  $\ddot{\theta}$

time-history. Incremental, permanent wall rotations stop when the value of  $\dot{\theta}$  returns to zero. No wall rotations into the retained soil are allowed in the Nadim and Whitman (1984) formulation. The time-history of incremental, permanent wall rotation  $\theta$  (about point O) is obtained by numerical integration of the  $\dot{\theta}$  time-history. After (1) this first pulse of wall rotations conclude and (2) should the horizontal ground acceleration value,  $k_{hg}g$ , be equal to or greater than  $(k_{hw})_{tilt}g$  at a later time,  $t_j$ , then a second pulse of incremental, permanent wall rotations would commence. Several incremental pulses of permanent wall rotation occur during the course of a typical earthquake time-history analysis. The total permanent wall rotation at the end of earthquake shaking is equal to the sum of the incremental wall rotation pulses.

#### **Nadim and Whitman (1984) observations**

(1) Studies performed by Nadim (1980) show that when sliding starts before tilting [i.e.,  $(k_{hw})_{slide} < (k_{hw})_{tilt}$ ] *only sliding movements* take place, but when tilting starts before sliding, usually the wall movement is coupled tilting and sliding, with *tilting movements dominating* the displacement pattern. (2) The location of the critical center of rocking (i.e., point O) depends on the variation of the ultimate moment capacity of the *foundation soil*,  $M_r$ , and the moment of inertia of the wall with distance at the base of the wall.

#### **Summary observations regarding the Nadim and Whitman formulation by other researchers**

Along with others, Fishman and Richards (1997) observe that Nadim and Whitman (1984) employed coupled equations of motion to study the problem of seismically induced tilting of gravity retaining walls. Based on the work of Nadim and Whitman (1984), Siddharthan et al. (1990, 1991, and 1992) developed a method to predict the seismic performance of retaining walls considering both rotation and translation deformation modes. Their coupled equations of motion were, in turn, updated and extended by Fishman and Richards (1997) for the analysis of bridge abutments with a pin connection at the intersection of the top of wall and the bridge deck. Key aspects of these two studies are summarized in the subsequent subsections.

### 2.3 Siddharthan, Ara, Anderson, Gowda, and Norris rigid block model of a gravity wall with earthquake-induced, coupled permanent rotation and sliding about a center of rotation located along the base of the wall

Nadim and Whitman (1984) employed coupled equations of motion to study the problem of seismically induced tilting of gravity retaining walls. Based on the work of Nadim and Whitman (1984), Siddharthan et al. (1990, 1991, and 1992) developed a method to predict the seismic performance of retaining walls considering both rotation and translation deformation modes as shown in Figure 2.3.

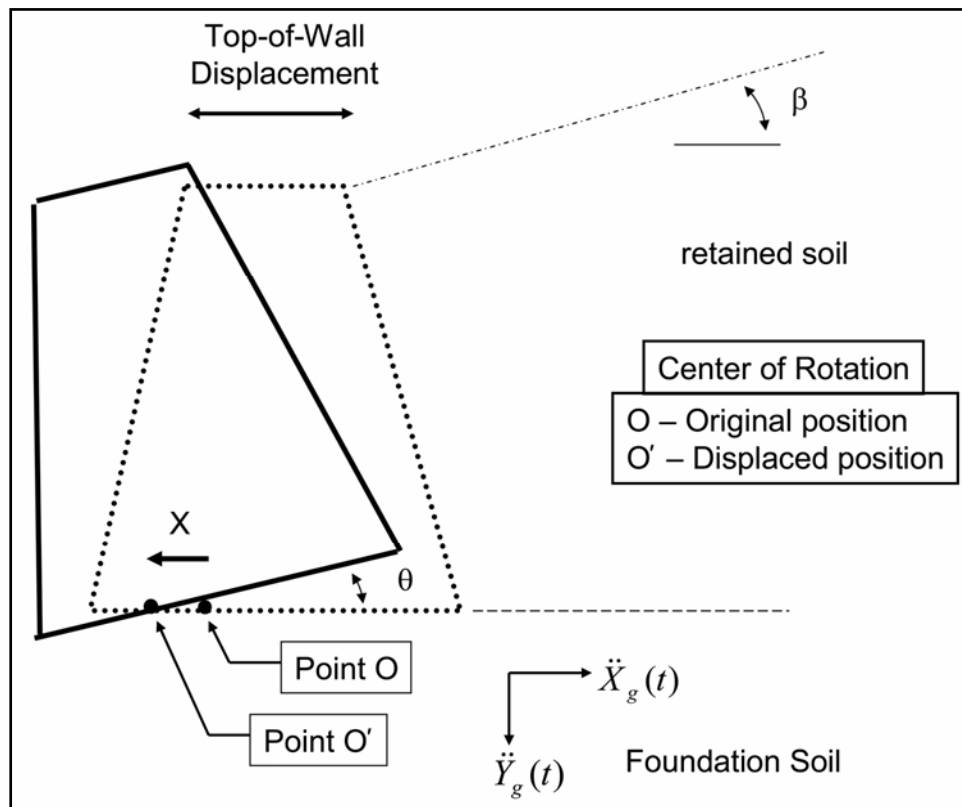


Figure 2.3. The Siddharthan, Ara, Anderson, Gowda, and Norris simplified rigid block model for seismically induced wall displacement (after Siddharthan, Ara, and Anderson (1990)).

In the Siddharthan et al. (1990, 1991, and 1992) type of analysis, the permanent wall *translation and rotation* about a point along the base, referred to as the center of rotation, are designated as the primary unknowns. The center of rotation is selected prior to starting the dynamic analysis and sliding and rotation of the wall about this point are computed. From these results, the top-of-wall permanent displacement is evaluated as a function of time. In subsequent time-history analyses in

which the location of the center of rotation along the wall's base is changed to another position (which is fixed for the duration of each time-history analysis), a number of top-of-wall permanent displacement values at the end of shaking are computed and tabulated. The maximum of these computed top-of-wall permanent displacement values is considered to be the design wall displacement. (This approach of altering the center of rotation so as to find the maximum permanent displacement is consistent with that used by Nadim and Whitman (1984).)

Figure 2.4 shows a rigid retaining wall of height  $H$  subjected to base excitation, represented by horizontal and vertical ground accelerations,  $\ddot{x}_g(t)$  and  $\ddot{y}_g(t)$ , respectively. Note the sign convention for horizontal and vertical ground accelerations in this formulation is the same as assumed by Nadim and Whitman (1984); positive horizontal ground acceleration is directed towards the retained soil and positive vertical acceleration is directed towards the foundation. Inertia forces have been (again) applied according to D'Alembert's principle which permits the problem to be treated as a static problem. The response of the wall is given in terms of wall translation  $x$  (relative to the input excitation), and rotation  $\theta$  about the center of rotation point  $O$ , which is located along the base of the wall.  $CG$  is the center of gravity of the wall;  $R$  is the distance from rotation point  $O$  to  $CG$ ;  $I_{CG}$  is the mass moment of inertia of the wall about the  $CG$ ;  $\delta$  is the wall-to-retained soil friction angle;  $\alpha$  is the angle the back of the wall makes with respect to vertical;  $W$  is the weight of the wall; and  $P_{AE}$  is the total dynamic active thrust on the wall. In their formulation the Mononobe-Okabe relationship is used to compute the value of  $P_{AE}$ . The point of application of the *total* active force  $P_{AE}$  is assigned to a height  $mH$  above the heel of the wall, with  $m$  being a value less than one. Its point of application is based on the Seed-Whitman guidelines as described in Section 4.2.2 in Ebeling and Morrison (1992), but with the incremental dynamic force,  $\Delta P_{AE}$ , assigned to  $0.52H$  above the base rather than  $0.6H$  as per Seed and Whitman (1970). (Recall that in the Seed-Whitman formulation the total force  $P_{AE}$  is the sum of the static force component,  $P_A$ , plus an incremental dynamic component,  $\Delta P_{AE}$ .  $P_{AE}$  is computed using the Mononobe-Okabe relationship and  $P_A$  is computed using the Coulomb active earth pressure force relationship; with  $\Delta P_{AE} = P_{AE} - P_A$ . Please refer to Figure 4.10 in Chapter 4 of Ebeling and Morrison (1992).) The base reaction is given in terms of the vertical and horizontal forces  $P_v$  and  $P_h$  and a moment of resistance,  $M_O$ .

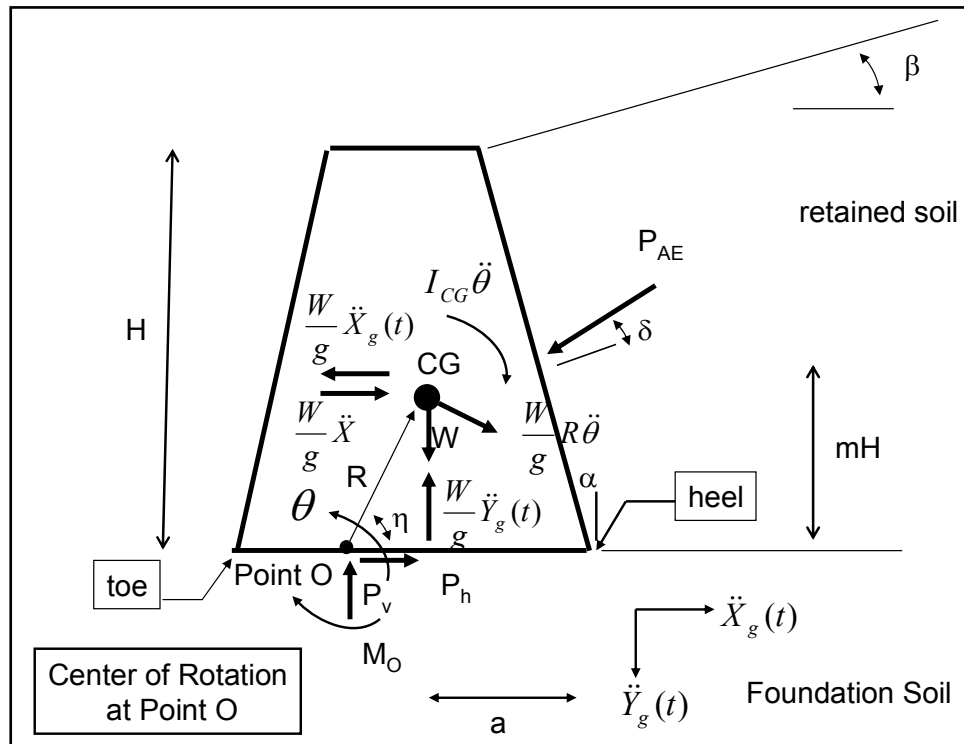


Figure 2.4. Forces and moments acting on a rigid block model of a gravity wall (after Siddharthan, Ara, and Anderson (1990)).

The equation of horizontal equilibrium for the Figure 2.4 wall is

$$\sum F_x = \frac{W}{g} \ddot{X} + P_h - \frac{W}{g} \ddot{X}_g(t) - P_{AE} \cdot \cos(\delta + \alpha) + \frac{W}{g} \cdot R \cdot \ddot{\theta} \cdot \sin(\eta) \quad 2.17$$

and the equation of vertical equilibrium is

$$\sum F_y = W - P_v - \frac{W}{g} \ddot{Y}_g(t) + P_{AE} \cdot \sin(\delta + \alpha) + \frac{W}{g} \cdot R \cdot \ddot{\theta} \cdot \cos(\eta) \quad 2.18$$

Coulomb's law of friction relates the maximum value of  $P_h$  to  $P_v$  by

$$(P_h)_{\max} = P_v \cdot \tan(\phi_b) \quad 2.19$$

Solving Equations 2.17 and 2.18 for  $P_h$  and  $P_v$ , respectively, results in

$$P_h = \frac{W}{g} \ddot{X}_g(t) - \frac{W}{g} \ddot{X} + P_{AE} \cdot \cos(\delta + \alpha) - \frac{W}{g} \cdot R \cdot \ddot{\theta} \cdot \sin(\eta) \quad 2.20$$



$$P_v = W - \frac{W}{g} \ddot{Y}_g(t) + P_{AE} \bullet \sin(\delta + \alpha) + \frac{W}{g} \bullet R \bullet \ddot{\theta} \bullet \cos(\eta) \quad 2.21$$

Combining Equations 2.20 and 2.21 into Equation 2.19 results in

$$\begin{aligned} & \frac{W}{g} \ddot{X}_g(t) - \frac{W}{g} \ddot{X} + P_{AE} \bullet \cos(\delta + \alpha) - \frac{W}{g} \bullet R \bullet \ddot{\theta} \bullet \sin(\eta) = \\ & \left[ W - \frac{W}{g} \ddot{Y}_g(t) + P_{AE} \bullet \sin(\delta + \alpha) + \frac{W}{g} \bullet R \bullet \ddot{\theta} \bullet \cos(\eta) \right] \bullet \tan(\phi_b) \end{aligned} \quad 2.22$$

Rearranging, Equation 2.22 becomes

$$\begin{aligned} & \frac{W}{g} \ddot{X}_g(t) - \frac{W}{g} \ddot{X} + P_{AE} \bullet \cos(\delta + \alpha) \\ & - \left[ W - \frac{W}{g} \ddot{Y}_g(t) + P_{AE} \bullet \sin(\delta + \alpha) \right] \bullet \tan(\phi_b) = \\ & \frac{W}{g} \bullet R \bullet \ddot{\theta} \bullet \sin(\eta) + \frac{W}{g} \bullet R \bullet \ddot{\theta} \bullet \cos(\eta) \bullet \tan(\phi_b) \end{aligned} \quad 2.23$$

Introducing the trigonometric identity

$$\tan(\phi_b) = \frac{\sin(\phi_b)}{\cos(\phi_b)} \quad 2.24$$

to the second term of the right-hand side of Equation 2.23 and rearranging terms results in

$$\frac{W}{g} \bullet R \bullet \ddot{\theta} \bullet \left\{ \sin(\eta) \bullet \left[ \frac{\cos(\phi_b)}{\cos(\phi_b)} \right] + \cos(\eta) \bullet \left[ \frac{\sin(\phi_b)}{\cos(\phi_b)} \right] \right\} \quad 2.25$$

Introducing the trigonometric identity

$$\sin(\eta) \bullet \cos(\phi_b) + \cos(\eta) \bullet \sin(\phi_b) = \sin(\eta + \phi_b) \quad 2.26$$

Equation 2.25 becomes

$$\frac{W}{g} \bullet R \bullet \ddot{\theta} \bullet \frac{\sin(\eta + \phi_b)}{\cos(\phi_b)} \quad 2.27$$

Replacing the right-hand side of Equation 2.23 with Equation 2.27 and rearranging terms results in

$$\begin{aligned} & \frac{W}{g} \ddot{X}_g(t) + P_{AE} \bullet \cos(\delta + \alpha) \\ & - \left[ W - \frac{W}{g} \ddot{Y}_g(t) + P_{AE} \bullet \sin(\delta + \alpha) \right] \bullet \tan(\phi_b) = \quad 2.28 \\ & \frac{W}{g} \ddot{X} + \frac{W}{g} \bullet R \bullet \ddot{\theta} \bullet \frac{\sin(\eta + \phi_b)}{\cos(\phi_b)} \end{aligned}$$

Siddharthan, Ara, and Norris (1990) observe that this equation (2.28), which gives the equation of motion in the horizontal direction, can be uncoupled by omitting the last term,

$$\frac{W}{g} \bullet R \bullet \ddot{\theta} \bullet \frac{\sin(\eta + \phi_b)}{\cos(\phi_b)} \quad 2.27 \text{ bis}$$

(i.e., the rotation term), from the right hand side of this equation. Note that the resulting uncoupled equation is the same equation as used by Richards and Elm (1979) and given in Chapter 4 of this report.

The equation of moment equilibrium for the Figure 2.4 wall is

$$\sum M_o = I_o \bullet \ddot{\theta} = \left( I_{CG} + \frac{W}{g} \bullet R^2 \right) \bullet \ddot{\theta} \quad 2.29$$

which becomes

$$\begin{aligned} & \frac{W}{g} \ddot{X} \bullet R \bullet \sin(\eta) + \left( I_{CG} + \frac{W}{g} \bullet R^2 \right) \ddot{\theta} = \frac{W}{g} \ddot{X}_g(t) \bullet R \bullet \sin(\eta) \\ & - \frac{W}{g} [g - \ddot{Y}_g(t)] \bullet R \bullet \cos(\eta) + P_{AE} \bullet (mH) \bullet \cos(\delta + \alpha) \quad 2.30 \\ & - P_{AE} \bullet \sin(\delta + \alpha) \bullet [R \bullet \cos(\eta) + a - mH \bullet \tan(\alpha)] - M_o \end{aligned}$$

in which  $a$  is the horizontal distance between the CG and the heel of the wall,  $\eta$  is the angle that the line joining points O and CG makes with the horizontal.  $\phi_b$  is the friction angle at the interface between the wall base

and foundation soil,  $M_{y0}$  is the yield moment of resistance, and  $mH$  is the location of the line of action of the backfill thrust from the base.

Equations 2.28 and 2.30 are *coupled equations* for  $d^2x/dt^2$  and  $d^2\theta/dt^2$ . A step-by-step solution scheme is followed in order to obtain the wall translation,  $x$ , and rotation,  $\theta$ , in the time domain. This step-by-step solution scheme is outlined in Siddharthan, Ara, and Anderson (1990).

Siddharthan, Ara, and Norris (1992) note that it is customary in dynamic analyses to describe the response of a system in terms of generalized coordinates which may be displacements, rotations, or a combination of both. The generalized coordinates should be independent of each other, and one should be able to represent the response at any other point in terms of the generalized coordinates. For the retaining wall problem, it is necessary to specify a point about which the wall translation and rotation (generalized coordinates) need to be computed. This point is referred to as the center of rotation. Nadim and Whitman (1984) selected this point to be located at the base of the wall. In a linear problem, the displacement response at any point will not depend on the selection of the center of rotation. On the other hand, the retaining wall response is statically indeterminate and nonlinear.

Siddharthan, Ara, and Norris (1992) observe that the resistance against rotation offered by the foundation soil and moment of inertia about the point of rotation depends on the selection of the center of rotation. Therefore, the center of rotation will affect the computed wall displacement. In the procedure adopted here, the center of rotation is selected before starting the dynamic analysis and the sliding and rotation of the wall about this point are computed. From these results, the top-of-wall displacement is evaluated as a function of time. By varying the location of the center of rotation along the base of the wall and repeating the time-history analyses for the same ground motion, a number of top-of-wall displacement values at the end of the excitation are noted. The maximum of these top-of-wall displacement values is considered to be the design displacement.

#### **Uncoupled equation for rotation**

Siddharthan, Ara, and Norris (1992) note that Equation 2.30 (in this report), which gives the rotational equation of motion, can be uncoupled by omitting the first term

$$\frac{W}{g} \ddot{X} \bullet R \bullet \sin(\eta) \quad 2.31$$

(i.e., the sliding term) from the left-hand side of the equation, resulting in the uncoupled equation for rotation about the center of rotation, point O,

$$\begin{aligned} \left( I_{CG} + \frac{W}{g} \bullet R^2 \right) \ddot{\theta} &= \frac{W}{g} \ddot{X}_g(t) \bullet R \bullet \sin(\eta) \\ -\frac{W}{g} [g - \ddot{Y}_g(t)] \bullet R \bullet \cos(\eta) &+ P_{AE} \bullet (mH) \bullet \cos(\delta + \alpha) \\ -P_{AE} \bullet \sin(\delta + \alpha) \bullet [R \bullet \cos(\eta) &+ a - mH \bullet \tan(\alpha)] - M_o \end{aligned} \quad 2.32$$

The complete derivation of Siddharthan et al. (1990, 1991, and 1992) equations of motion is also given in Appendix A of Fishman and Richards (1997).

To compare the Nadim and Whitman Equation 2.11 (this report) formulation for the Figure 2.2.a retaining structure to the Siddharthan et al. uncoupled Equation 2.32 for the Figure 2.4 retaining structure, some geometrical conversions are required:  $\alpha$  is set equal to zero degree for the Figure 2.4 retaining wall in order to obtain a vertical wall-to-retained soil interface and the radius R and angle  $\eta$  in Figure 2.4 are converted into the Figure 2.2.a geometry designations by

$$R^2 = B_1^2 + B_3^2 \quad 2.33$$

$$R \bullet \cos(\eta) = B_1 \quad 2.34$$

$$\sin(\delta + \alpha) \bullet [R \bullet \cos(\eta) + a - mH \bullet \tan(\alpha)] = \sin(\delta) \bullet B_2 \quad 2.35$$

$$R \bullet \sin(\eta) = B_3 \quad 2.36$$

and

$$mH \bullet \cos(\delta + \alpha) = L \bullet \cos(\delta) \quad 2.37$$

when  $\alpha$  is equal to zero. Introducing these geometry designations into the uncoupled Equation 2.32 and recognizing the differences in notation used for several of the variables, it is concluded that the resulting relationship is

the same as Nadim and Whitman's Equation 2.11. Thus, the *uncoupled* Siddharthan et al. formulation for rotation is the same as the Nadim and Whitman formulation.

### **Foundation response**

One of the input parameters is  $M_{y0}$  which is assessed by Siddharthan et al. (1990, 1991, 1992) by assuming the foundation soil is represented by Winkler springs, and these springs are not bonded to the foundation. The resisting moment is determined by modeling the base as a strip footing resting on Winkler springs. Equations are given in Siddharthan, Ara, and Norris (1992) and Siddharthan, Gowda, and Norris (1991). Both full contact and partial contact (lift-off) were considered.  $P_v$  and  $P_h$  are the foundation's normal and shear reaction forces, respectively. The principal author of this report observes that the foundation reaction moment,  $M_{y0}$ , in conjunction with the normal force,  $P_v$ , implies an eccentricity of the location of the foundation's resultant reaction force,  $P_v$ , with respect to the user-defined center of rocking.

Fishman and Richards (1997) question the use of the Winkler spring model once the soil reaches its ultimate bearing pressure. Fishman and Richards (1997) present an alternative formulation for assessing the force and moment provided by the soil foundation to the wall; key aspects of their formulation are discussed in the subsequent subsection.

### **Summary observations regarding the Siddharthan et al. formulation by other researchers**

Fishman and Richards (1997) observe that the advantage to the Siddharthan, Gowda, and Norris (1991) equations of motion is that they involve much less computational work than those originally proposed by Nadim and Whitman (1984) where they (i.e., Nadim and Whitman) assume that the locations and magnitudes of the wall forces (i.e.,  $P_{AE}$ ) vary as a function of sliding and rotating wall acceleration. Recall that the only unknown variables in Equations 2.28 and 2.32 are  $\dot{X}(t)$  and  $\ddot{\theta}(t)$ .

## **2.4 Fishman and Richards rigid block model of a bridge abutment with earthquake-induced, coupled permanent rotation and translation for free and fixed connections to bridge decks**

Siddharthan et al. (1990, 1991, and 1992) and Whitman (1992) proposed the use of coupled equations of motion to predict seismic-induced permanent deformation of retaining walls. These equations can be used to describe mixed modes of deformation including sliding and/or tilting. Equations of motion are cast in terms of relative acceleration between the retaining wall and foundation soil. Relative displacement and rotations are computed by double integration of the equations of motion with respect to time, similar to Newmark (1965) and Richards and Elms (1979). Specifically, Fishman and Richards (1997, 1998) modified these Siddharthan et al. coupled equations of motion (discussed in the previous subsection) and included the following modifications; (1) calculation of seismic bearing capacity (and, specifically, the possibility of seismic loss of bearing capacity); (2) estimation of the moment resistance of the foundation soil; and (3) extension of the equations to consider bridge abutments that may be forced to rotate about a point of fixity at the top of the abutment at the connection to the bridge deck. The Fishman and Richards (1997, 1998) free-body diagram of bridge abutment with a free connection to bridge deck is shown in Figure 2.5. Note the sign convention for horizontal and vertical ground accelerations in this formulation is the same as assumed by Nadim and Whitman (1984) and Siddharthan et al. (1990, 1991, and 1992); positive horizontal ground acceleration is directed towards the retained soil and positive vertical acceleration is directed towards the foundation.

The inertial forces are applied according to D'Alembert's principle. Fishman and Richards (1998) note that much like the Richards and Elms (1979) approach to translating walls, Newton's fundamental laws of motion are applied to arrive at the coupled equations of motion proposed by Siddharthan et al. (1990, 1991, and 1992) and described in the previous section. The Siddharthan et al. coupled equations of motion for the Figure 2.5 notation are

$$\begin{aligned} & \frac{W}{g} \ddot{X}_g(t) + P_{AE} \bullet \cos(\delta) \\ & - \left[ W - \frac{W}{g} \ddot{Y}_g(t) + P_{AE} \bullet \sin(\delta) + F_{DV} \right] \bullet \tan(\phi_b) \qquad \qquad \qquad 2.38 \\ & = \frac{W}{g} \ddot{X} + \frac{W}{g} \bullet R \bullet \ddot{\theta} \bullet \frac{\sin(\eta + \phi_b)}{\cos(\phi_b)} \end{aligned}$$

$$\begin{aligned} & \frac{W}{g} \ddot{X} \bullet R \bullet \sin(\eta) + \left( I_{CG} + \frac{W}{g} \bullet R^2 \right) \ddot{\theta} = \frac{W}{g} \ddot{X}_g(t) \bullet R \bullet \sin(\eta) \\ & - \frac{W}{g} [g - \ddot{Y}_g(t)] \bullet R \bullet \cos(\eta) + P_{AE} \bullet (mH) \bullet \cos(\delta) \qquad \qquad \qquad 2.39 \\ & - P_{AE} \bullet \sin(\delta) \bullet [R \bullet \cos(\eta) + a] - F_{DV} \bullet [a + R \bullet \cos(\eta)] - M_o \end{aligned}$$

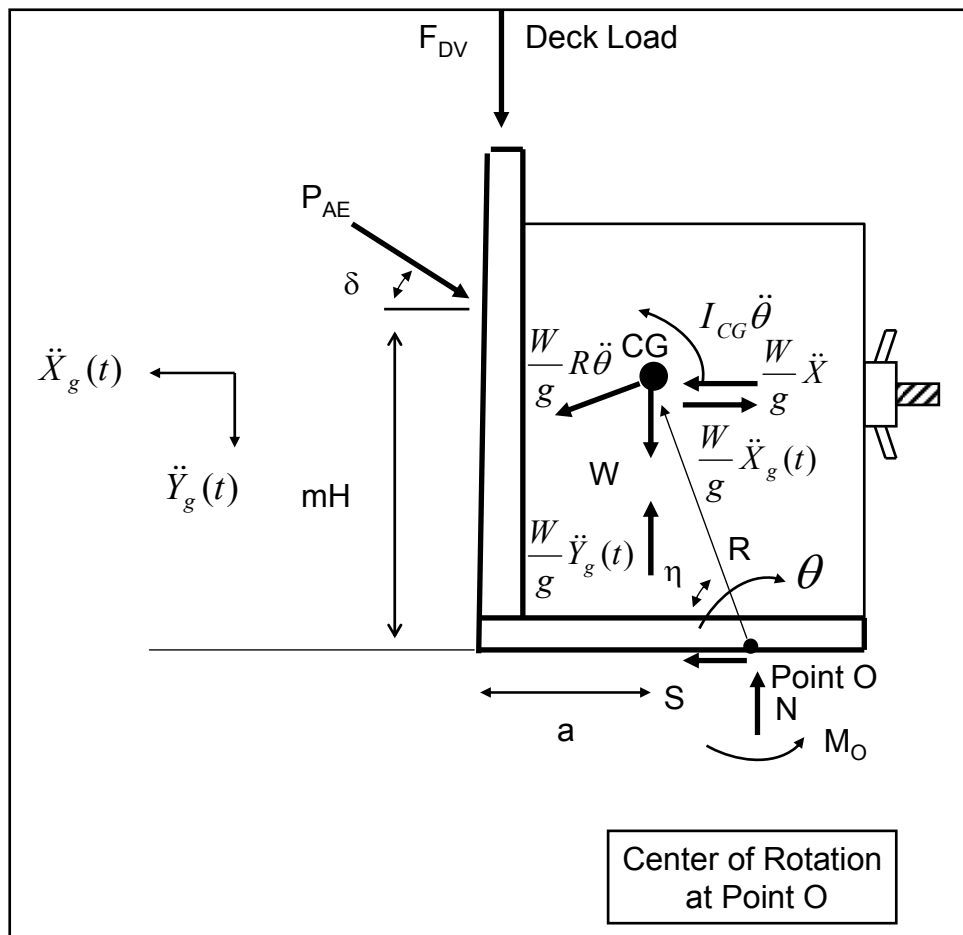


Figure 2.5. Free-body diagram of bridge abutment with free connection to bridge deck (after Fishman and Richards (1998)).

Note that by taking  $\alpha$  equal to zero degrees and adding in the vertical deck load  $F_{DV}$ , the Siddharthan et al. equations (Equations 2.28 and 2.30) match Equations 2.38 and 2.39, respectively.  $P_{AE}$  is the total dynamic active thrust on the wall. In their formulation the Mononobe-Okabe relationship is used to compute the value of  $P_{AE}$ . Vertical acceleration can be included quite easily by using  $k_h/(1-k_v)$  instead of  $k_h$  when computing  $P_{AE}$  and  $W$  becomes  $(1-k_v)W$  in the equilibrium equations (e.g., see Appendix A or Equation 33 and Figure 4.1a in Chapter 4 of Ebeling and Morrison (1992)). The point of application of the *total* active force  $P_{AE}$  is assigned to a height  $mH$  above the heel of the wall, with  $m$  being a value less than one. Fishman and Richards (1997) assume that  $P_{AE}$  acts at the wall mid-height, consistent with a Richards and Elms (1979) suggestion. An additional detail in their computations is that until the base moves creating an active situation, it acts as a “rigid” wall retaining “non-yielding” backfill (in Ebeling and Morrison (1992) terminology). Citing results from Wood (1975) analyses, Fishman and Richards (1997) assume the seismic lateral pressure increment is parabolic with a thrust force  $P_{RE}$  roughly twice the Mononobe-Okabe value and with the wall/retained soil interface friction angle,  $\delta$ , is close to zero for this special case.

Siddharthan et al. equations of motion apply to a retaining wall, but not to a *pin-connected* bridge abutment of the type shown in Figure 2.6. This figure shows the free-body diagram of the bridge abutment problem solved by Fishman and Richards.

Derivation of the equation of motion for an abutment pinned at the top is presented in Appendix B of Fishman and Richards (1997). Summing moments about the pin results in

$$\begin{aligned} \sum M_{pin} = & I_{CG} \cdot \ddot{\theta} + \frac{W}{g} \cdot R^2 \cdot \ddot{\theta} - \frac{W}{g} \ddot{X}_g(t) \cdot R \cdot \sin(\eta) \\ & + W \cdot R \cdot \cos(\eta) - P_{AE} \cdot h \cdot \cos(\delta) - N \cdot b + S \cdot H \end{aligned} \quad 2.40$$

where  $N$  is the vertical soil resistance and  $S$  is the horizontal soil resistance.

Rearranging the equation of motion results in,



$$\left( I_{CG} + \frac{W}{g} \cdot R^2 \right) \ddot{\theta} = \frac{W}{g} \ddot{X}_g(t) \cdot R \cdot \sin(\eta) \quad 2.41$$

$$-W \cdot R \cdot \cos(\eta) + P_{AE} \cdot h \cdot \cos(\delta) + N \cdot b - S \cdot H$$

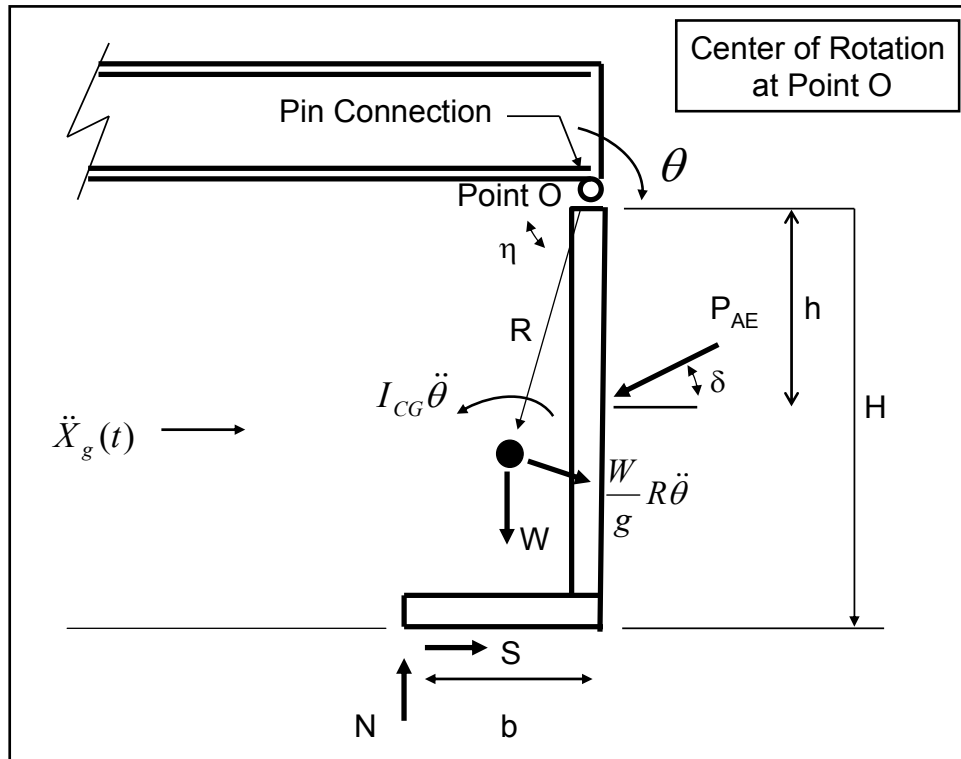


Figure 2.6. Free-body diagram of bridge abutment with fixed connection to bridge deck (after Fishman and Richards (1997)).

Numerical methods, as described in Fishman and Richards (1997), are used to solve for the acceleration components  $\ddot{X}(t)$  and  $\ddot{\theta}(t)$ . Specifically, a step-by-step solution scheme is followed in order to obtain the wall translation,  $x$ , and rotation,  $\theta$ , in the time domain. A key aspect of their formulation is formal consideration of seismic bearing capacity of the foundation soil.

## 2.5 Steedman and Zeng rigid block model of a gravity wall with earthquake-induced rotation about its toe

Figure 2.7 shows the Steedman and Zeng (1996) or, equivalently, the Zeng and Steedman (2000) rotating block methodology for computing permanent rotation and thus displacements of a gravity retaining wall using a horizontal acceleration time-history to represent earthquake shaking. Key formulation features include; a gravity retaining wall

modeled as a rigid block; the gravity wall rotates about its toe and on a *rigid foundation*; a gravity wall retaining moist backfill; and sufficient wall movements away from the retained soil occur such that the shear strength of the soil is fully mobilized, resulting in the active earth pressure force  $P_{AE}$ . Only a horizontal ground acceleration time-history is used to represent earthquake shaking, i.e., vertical ground accelerations are ignored for simplicity in their formulation. Note that with the point of rotation assigned to the toe of the gravity wall, the resultant foundation-to-base of wall reaction forces  $F_s$  and  $N$  act through this point as well.

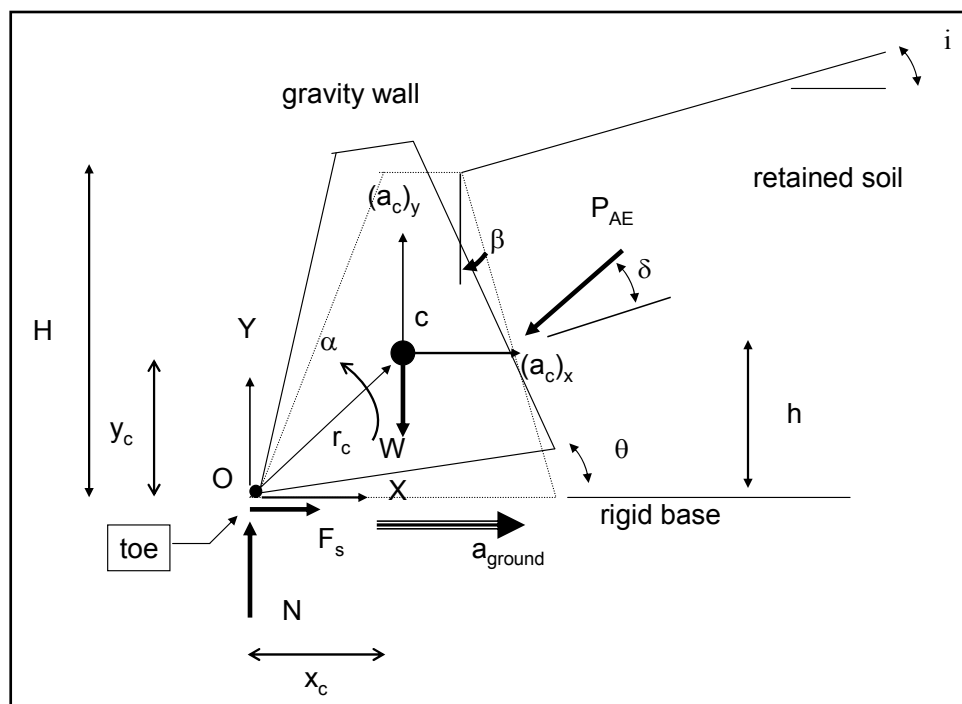


Figure 2.7. Forces and accelerations of a rigid block model of a gravity retaining wall with rotation during horizontal shaking of the rigid base (after Zeng and Steedman (2000)).

A rotation  $\theta$  about the toe of the Figure 2.7 wall develops once a wall-specific threshold acceleration is exceeded during earthquake shaking that is represented by a horizontal ground acceleration  $a_{\text{ground}}$ , as depicted in this figure. During rotation, the angular acceleration of the mass center (labeled point  $c$ ) of rigid body is  $\alpha$ . (Recall that mass is equal to the weight,  $W$ , divided by the acceleration of gravity,  $g$ .) The  $x$ - and  $y$ -axis accelerations of (rigid) mass center point  $c$  during rotation are labeled  $(a_c)_x$  and  $(a_c)_y$  in this figure. This results in the accumulation of permanent wall rotation with time during further (horizontal) acceleration of the rigid base. When ground acceleration drops below the threshold acceleration for rotation for the wall, restoring forces and moments will act to slow the

speed of angular rotation, thus reducing the rate of increase of the tilt angle about the toe. Wall rotation ceases when the angular rotational velocity (of the mass center about point O) returns to zero. Additional increments of wall rotation  $\Delta\theta$  occur each time a (horizontal) ground acceleration pulse exceeds the threshold acceleration for rotation for the wall in the same manner that permanent sliding displacements accumulate for a Newmark rigid sliding block model.

The equation for the acceleration of the Figure 2.7 (rigid) mass center point c was shown in Section 1.2 to be

$$a_c = a_{\text{ground}} + \alpha \times r_c - \omega^2 r_c \quad 1.6 \text{ bis}$$

with the horizontal and vertical acceleration components of  $a_c$  are

$$(a_c)_x = a_{\text{ground}} - \alpha \bullet y_c - \omega^2 \bullet x_c \quad 1.7 \text{ bis}$$

and

$$(a_c)_y = \alpha \bullet x_c - \omega^2 \bullet y_c \quad 1.8 \text{ bis}$$

These three equations demonstrate that for a rigid block that undergoes *rotation* during earthquake shaking, the horizontal acceleration of (rigid) mass center point c is a function not only of the horizontal ground acceleration but it is also a function of the angular acceleration  $\alpha$  and the angular velocity  $\omega$  during rotation of point c about point O. Recall that this differs from the situation of a rigid block that undergoes permanent *sliding* displacement during earthquake shaking; the largest magnitude horizontal acceleration felt by this rigid block is the maximum transmissible acceleration,  $N^*g$ , as discussed in previous chapters.  $N^*g$  is sometimes referred to as the yield acceleration. Note that  $N^*g$  is not the user-defined, horizontal ground (or, equivalently, rigid base) acceleration. Unlike the sliding (rigid) block model, which effectively isolates the sliding block from the shaking base below, the rotating rigid block model *continues* to transmit horizontal acceleration through the “pin,” located at the toe of the wall, into the wall.

In the Steedman and Zeng (1996) (rigid) gravity wall formulation, vertical ground acceleration is ignored. However, Equation 1.8 demonstrates for a

rigid block that undergoes *rotation* during earthquake shaking, vertical acceleration of (rigid) mass center point *c* will occur, but is not a function of the horizontal ground acceleration: The vertical acceleration of point *c* is solely a function of the angular acceleration and the angular velocity during rotation. The Steedman and Zeng rocking model for the prediction of permanent displacement has been validated by comparison with experimental data of a large gravity wall constrained to rock and subjected to a series of damaging earthquakes in centrifuge testing, as described in Steedman and Zeng (1996).

### Limiting acceleration of a wall – lift-off of its base in rotation

When ground acceleration thrusts exceed a limiting value of acceleration, the wall will begin to lift off of its rigid foundation, rotating about the center of rocking (i.e., point *O*) at the toe of the wall. The inertial forces are applied according to D'Alembert's principle and earth pressure force invoked by the (assumed pseudo-static) acceleration field. The limiting acceleration of the wall can be determined from equilibrium equations of the wall. For the Figure 2.7 gravity retaining wall subject to pure rotation, the onset of lift-off from its foundation in rotation, the rotating moment

$$M_{rotation} = k_{tr} \bullet W \bullet y_c + P_{AE} \bullet \cos(\delta + \beta) \bullet h \quad 2.42$$

exactly equals the restoring moment

$$M_{restoring} = W \bullet x_c + P_{AE} \bullet \sin(\delta + \beta) \bullet (B - h \bullet \tan \beta) \quad 2.43$$

where *W* is the weight of the wall,  $k_{tr}$  is the threshold acceleration coefficient in lift-off of the wall from its base (with a corresponding acceleration  $a_{tr} = k_{tr}$  times *g*),  $P_{AE}$  is the Mononobe-Okabe active earth pressure force,  $\delta$  is the wall-to-retained soil friction angle;  $\beta$  is the angle the back of the wall makes with respect to vertical, *h* the location of the line of action of the backfill thrust from the base, and *B* is the width of the wall at its base. Equating Equations 2.42 and 2.43 results in the relationship for the threshold acceleration coefficient in lift-off of the wall from its base

$$k_{tr} = \frac{\left[ \begin{array}{c} W \bullet x_c + P_{AE} \bullet \sin(\delta + \beta) \bullet \\ (B - h \bullet \tan \beta) - P_{AE} \bullet \cos(\delta + \beta) \bullet h \end{array} \right]}{\left[ W \bullet y_c \right]} \quad 2.44$$

### Angular acceleration and rotation of a wall

The equation for moment equilibrium about the center of rotation (assigned to toe) of the Figure 2.7 wall is

$$\sum M_o = -y_c \cdot \left(\frac{W}{g}\right) \cdot (a_c)_x + x_c \cdot \left(\frac{W}{g}\right) \cdot (a_c)_y + I_c \cdot \alpha \quad 2.45$$

in which  $I_c$  is the mass moment of inertia of the wall about its centroid (point c). Summing moments of the forces about the toe of the wall, the left-hand side of Equation 2.45 becomes

$$\begin{aligned} \sum M_o = & P_{AE} \cdot \cos(\delta + \beta) \cdot h - W \cdot x_c \\ & - P_{AE} \cdot \sin(\delta + \beta) \cdot [B - h \cdot \tan \beta] \end{aligned} \quad 2.46$$

Introducing Equation 2.46 into Equation 2.45, substituting Equations 1.7 and 1.8, and solving for the rotational acceleration  $\alpha$ , results in

$$\alpha = \frac{\left\{ P_{AE} \cdot \cos(\delta + \beta) \cdot h + \left(\frac{W}{g}\right) \cdot a_g \cdot y_c - W \right\} \cdot x_c - P_{AE} \cdot \sin(\delta + \beta) \cdot [B - h \cdot \tan \beta]}{\left\{ I_c + \left(\frac{W}{g}\right) \cdot r^2 \right\}} \quad 2.47$$

To calculate  $\alpha$ , dynamic earth pressure  $P_{AE}$  is calculated by using the horizontal ground acceleration  $a_g$  ( $=k_h g$ ) rather than the limiting value of acceleration  $a_{tr}$  when the wall will begin to lift off of its rigid foundation ( $=k_{tr} g$ ). Note that at each time-step  $i$  during wall rotation, the value for  $P_{AE}$  changes and is computed using the value for  $k_h$  ( $=a_g/g$ ) consistent with that time-step.

Zeng and Steedman (2000) observe that in the rotating block method, this threshold acceleration for rotating,  $a_{tr}$ , does *not* represent the *true* acceleration of any particular points in the retaining wall system. In fact, the acceleration of points within the retaining wall system will vary throughout the rigid body. With regard to the calculation of the value for  $P_{AE}$ , Zeng and Steedman assume the acceleration is uniform in the backfill and it is the same as the ground acceleration.

The velocity of rotation or angular velocity, is determined by integration of the acceleration of rotation

$$\omega = \int_0^t \alpha \, dt \text{ when } \omega \text{ is greater than zero} \quad 2.48$$

or

$$\omega = 0 \text{ when Equation 2.48 gives } \omega \text{ less than zero} \quad 2.49$$

The angle of permanent (incremental) rotation is the integration of the angular velocity of rotation over the period of time being considered,

$$\theta = \int_0^t \omega \, dt \quad 2.50$$

Note that the cycle of permanent wall rotation through an angle  $\theta$  ceases when the angular velocity  $\omega$  is zero. The increment in permanent wall rotation ceases until the threshold acceleration for rotation  $a_{tr}$  is exceeded again. In practical application of the Steedman and Zang procedure to earthquake ground motions, numerical methods would be applied to perform these integrations. The final tilting angle is the accumulation of incremental tilting angles during the entire earthquake.

### Limiting acceleration of a wall sliding

Zeng and Steedman (2000) also considered the possibility of a gravity retaining wall sliding along the rigid base during earthquake shaking. When ground acceleration thrusts exceed a limiting value of sliding acceleration the wall will begin to slide. The limiting acceleration of the wall can be determined from the equilibrium equations of the wall. Following established methods (discussed in previous chapters), sliding of the wall will occur when the mobilized frictional force at the base reaches a maximum and the earth pressure evoked by the assumed pseudo-static acceleration value of limiting sliding acceleration. For the Figure 2.8 wall at the instant when sliding starts, equilibrium of forces in the horizontal direction results in

$$[k_{ts} \bullet W + P_{AE} \bullet \cos(\delta + \beta)] = [W + P_{AE} \bullet \sin(\delta + \beta)] \bullet \tan \delta_b \quad 2.51$$

where  $\delta_b$  is the wall-to-base friction angle. The threshold sliding acceleration coefficient,  $k_{ts}$ , is

$$k_{ts} = \{ [W + P_{AE} \cdot \sin(\delta + \beta)] \cdot \tan \delta_b - P_{AE} \cdot \cos(\delta + \beta) \} / W \quad 2.52$$

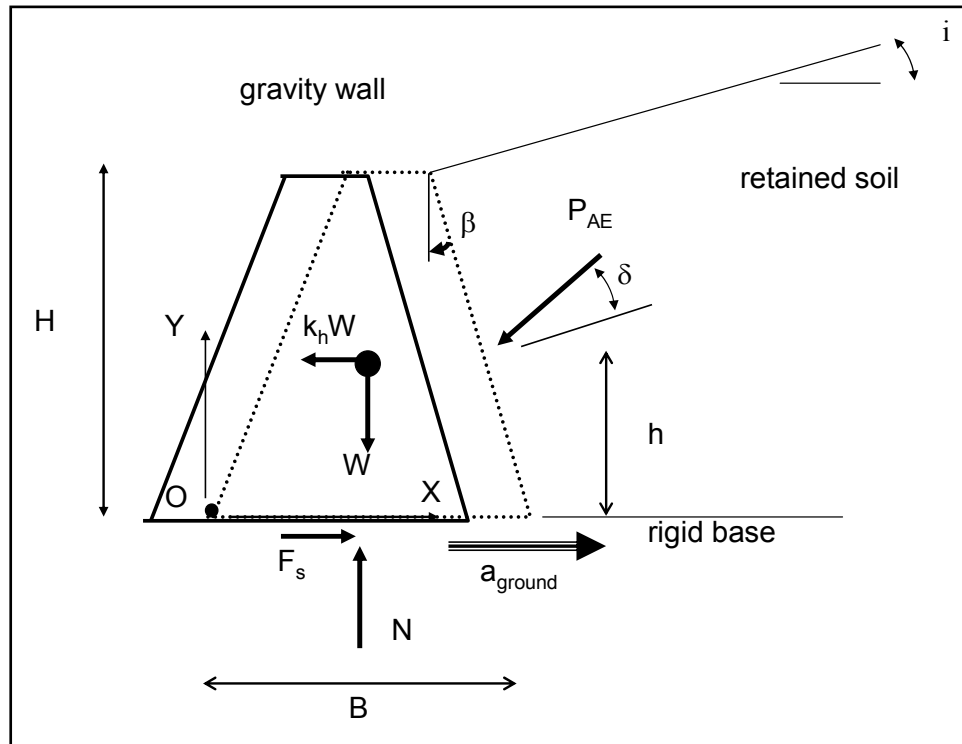


Figure 2.8. Forces and acceleration of a rigid block model of a gravity retaining wall with sliding (i.e., translation) during horizontal shaking of the rigid base (after Zeng and Steedman (2000)).

An increment of sliding of the rigid block model of the gravity wall will initiate when the (horizontal) ground acceleration,  $a_g$ , is equal to the threshold sliding acceleration,  $a_{ts}$  ( $= k_{ts}$  times  $g$ ). Sliding will terminate when the velocity of the wall is equal to the velocity of the ground, as depicted in Figure 1.8. The increment in permanent wall translation ceases until the threshold acceleration for sliding,  $a_{ts}$ , is exceeded again. In practical application of the Steedman and Zang procedure to earthquake ground motions, numerical methods would be applied to perform these integrations. The final translation is the accumulation of incremental sliding displacements during the entire earthquake.

**Zeng and Steedman (1996 and 2000) observations**

When the maximum ground acceleration is larger than the threshold accelerations for both sliding and rotation, lateral displacement and tilting may occur simultaneously. The sliding movement and tilting will interfere with each other and will affect both the threshold acceleration and the overall displacements. (1) Zeng and Steedman concluded that for a wall in which sliding is initiated first, the tilting of the wall is not possible. (2) Additionally, they concluded that if rotation starts first, the rotational motion will increase the threshold acceleration for sliding and, hence, reduce the total sliding displacement. An iterative, numerical procedure is briefly summarized in Zeng and Steedman (2000) for performing coupled rotation and displacement computations. (3) Steedman and Zeng (1996) observe that although the angle of friction on the base of the wall is clearly not significant in rocking, even a small tensile capacity on this surface will have an important effect on the onset of outward movement, raising the threshold for first yield. No tensile capacity was assumed in their models.



### **3 New Rotational Analysis Model of a Retaining Wall Rotating about its Toe and Buttressed by a Reinforced Concrete Slab**

#### **3.1 Introduction**

This chapter describes a new engineering formulation developed for computing the rotational response to earthquake ground motions of *toe-restrained*, rock-founded retaining walls. The resulting engineering formulation is implemented within corresponding PC software `CorpsWallRotate` using a graphical user interface (GUI) for input of geometry, input of material properties, input/verification of earthquake time-history files, and visualization of results. (Key aspects of the visual modeler and visual post-processor `CorpsWallRotate` are described in Chapter 5.)

The permanent displacement of retaining structures is not restricted to walls that slide along their base as a result of inertial forces imparted during earthquake shaking. For some retaining wall system configurations and material properties, permanent displacements may instead result from the rotation of a retaining wall about a point along its wall-to-foundation interface. Chapter 2 reviewed key aspects of four existing, simplified engineering formulations used to analyze seismically induced permanent displacement due to rotation of a rigid block retaining wall about a point along its base. These four formulations involve retaining walls *without toe restraint*.

The idealized permanent displacement due to rigid body noncentroidal rotation of a retaining wall about its toe during earthquake shaking and with toe restraint is shown in Figure 3.1.<sup>1</sup> The buttressing effect of a reinforced concrete slab is represented in this simplified dynamic model by the user-specified force  $P_{\text{resist}}$  acting on a vertical section extending upwards from the toe of the wall as per Strom and Ebeling (2004).

---

<sup>1</sup> The planar kinematics of rigid body noncentroidal rotation about a fixed axis is described in Section B.6 of Appendix B.

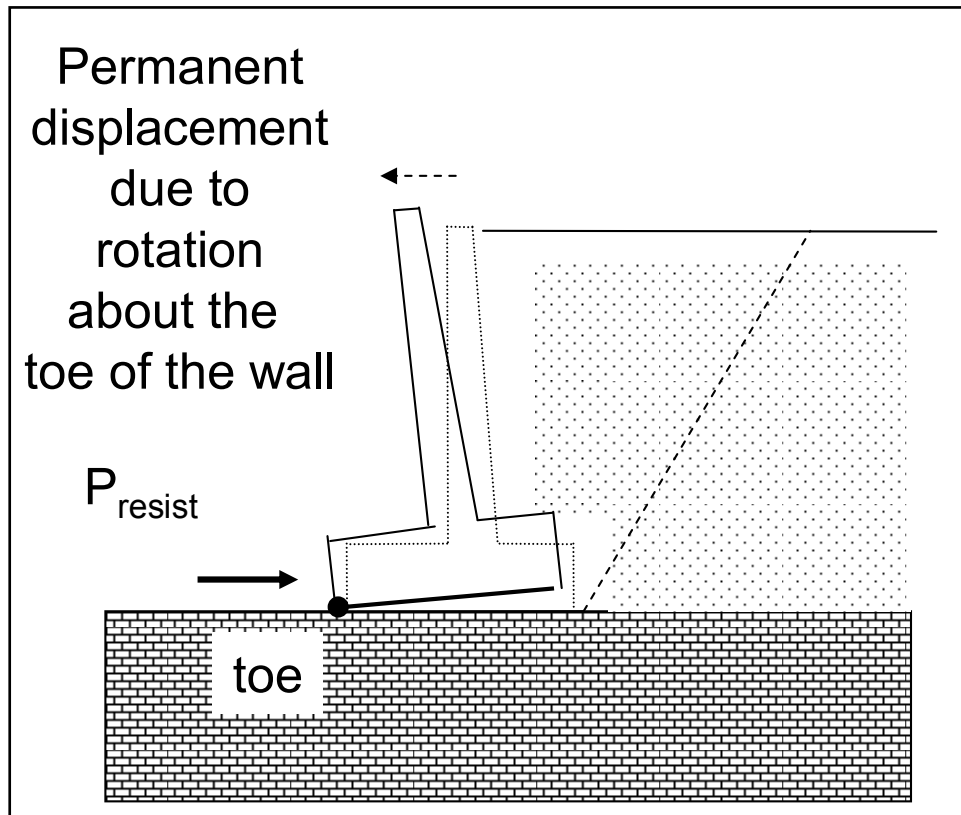


Figure 3.1. Idealized permanent, seismically induced displacement due to the rotation about the toe of a rock-founded wall retaining moist backfill, with toe restraint, computed using CorpsWallRotate.

The Figure 1.3 cantilever retaining wall that is buttressed by an invert spillway slab (which is a reinforced concrete slab) exemplifies this category of retaining structure system for Corps retaining walls. The primary author of this report is of the opinion that the assignment of the point of rotation to the toe of the wall becomes a reasonable simplifying assumption because of the constraint provided by the Figure 1.3 invert spillway slab to lateral translations, combined with the effects of the stiff, competent rock foundation.<sup>1</sup> A key result of a CorpsWallRotate analysis idealized in Figure 3.1 is the permanent, earthquake-induced displacement of a retaining wall due to rotation about the toe of the wall.

As in the Zeng and Steedman (2000) formulation discussed in Section 2.5, rotation of a rigid block model of the structural retaining wall system in this new formulation is assumed to occur about the toe of the wall (i.e., the

<sup>1</sup> A competent, rigid base is assumed in this initial formulation for CorpsWallRotate. Future improvements to CorpsWallRotate will include automated procedures to evaluate the bearing capacity for the rock foundation material.

rigid block is “pinned” to the rigid base at its toe). This new procedure differs from the Steedman and Zeng formulation by (1) formal consideration of a toe restraint in the analysis (caused by the presence of a reinforced concrete slab against the toe of the wall); (2) the ability of the user to assign a vertical acceleration time-history in addition to a horizontal acceleration time-history; (3) consideration of a pool of water in front of the wall, a submerged foundation and a partially submerged retained soil; and (4) the implementation of this formulation within corresponding PC software `CorpsWallRotate` using a GUI for input of geometry, input of material properties, input/verification of earthquake time-history files, and visualization of results. In addition, a sweep-search wedge formulation within the retained soil is used to determine the value of  $P_{AE}$  rather than relying on the Mononobe-Okabe relationship (cited in the Steedman and Zeng (1996) formulation). Recall that the Mononobe-Okabe relationship is valid for a retained soil with a constant surface slope and whose strength is characterized by the Mohr-Coulomb shear strength parameter  $\phi$  (e.g., refer to Equations 33 through 35 in Ebeling and Morrison (1992)). The advantage of the sweep-search method as formulated in this report is that it allows for (a) the analysis of bilinear ground surfaces and/or (b) the analysis of “cohesive” ( $S_u$ ) soils.<sup>1</sup>

The derivation for a rock-founded wall retaining moist backfill is presented first. This is followed by the formulation for a rock-founded wall retaining a partially submerged backfill and for the case of a pool in front of the retaining wall.

### 3.2 Acceleration of rigid mass center (CG)

An important difference between the Newmark (1965) sliding block method of analysis for earth retaining structures (i.e., the displacement controlled approach that is discussed in Section 1.1.3) and the rotational analysis of a retaining structure modeled as a rigid block is the acceleration imparted to the rigid block. When a rigid block undergoes permanent *sliding* displacement during earthquake shaking, the largest magnitude horizontal acceleration felt by the rigid block (and the retaining structure contained within the rigid block) is  $N^*g$ , which is less than the

---

<sup>1</sup> In the formulation described in this report, a cohesive soil refers to a total stress analysis in which the shear strength of the soil is characterized in terms of its undrained shear strength,  $S_u$ . Note that minimum wall movements needed to fully mobilize the shear resistance of the soil, on the order of those listed in Table 1.1, will impact the characterization of the retained soil shear strength parameters used in the permanent displacement analysis.

peak value for ground acceleration. The maximum transmissible acceleration  $N \cdot g$  is sometimes referred to as the yield acceleration; it is not the user-defined, horizontal ground (or, equivalently, the rigid base) acceleration. For a rigid block that undergoes *rotation* during earthquake shaking, the accelerations felt by this rigid block during shaking are those of the ground acceleration time-history plus the contribution of angular acceleration and angular velocity during rotation of the rigid body about its point of rotation. This is because continuous contact between the rigid block undergoing rotation and the ground is maintained at the point of rotation, i.e., point  $o$ , during the entire earthquake shaking process. Thus, large horizontal acceleration thrusts in the direction of the retained soil will attempt to destabilize the wall, possibly resulting in incremental wall rotations in the positive  $\theta$  direction shown in Figure 3.2 (i.e., rotation outward) and corresponding incremental, permanent wall movements directed away from the retained soil.

Relative-motion analysis of the rigid body model of the Figure 3.2 wall retaining moist backfill is used to establish the acceleration of (rigid) mass center point  $CG^1$  by establishing the relationship between the acceleration of point  $CG$  and the acceleration of point  $o$ . In the  $C_{\text{orps}}W_{\text{all}}\text{Rotate}$  formulation, the acceleration of point  $o$  at the toe of the retaining wall is set equal to acceleration of the ground,  $a_{\text{ground}}$ , and is a known, user-specified quantity. The horizontal and vertical components of the ground acceleration,  $a_{\text{ground}}$ , are designated as  $a_h$  and  $a_v$  in this figure, with subscript “h” or “v” meaning “horizontal” or “vertical.”<sup>2</sup>

The sign convention adopted for ground acceleration,  $a_{\text{ground}}$ , by Nadim and Whitman (1984), Siddharthan et al. (1990, 1991, and 1992), and Fishman and Richards (1997, 1998) for user-specified horizontal  $a_h = k_h g$  and vertical  $a_v = k_v g$  ground acceleration time-histories was adopted for this formulation and shown in Figure 3.2 as the rigid base accelerations. Positive horizontal ground acceleration is directed towards the retained soil and positive vertical acceleration is directed downward into the rigid

---

<sup>1</sup> Computation of the center of mass as well as mass of the structural wedge by  $C_{\text{orps}}W_{\text{all}}\text{Rotate}$  is outlined in Section B.3.

<sup>2</sup> Note that values of  $a_h$  and  $a_v$  are established by a pair of user-defined horizontal and vertical acceleration time-histories in  $C_{\text{orps}}W_{\text{all}}\text{Rotate}$ , each of which changes in magnitude and possibly direction at each increment in time during earthquake shaking.

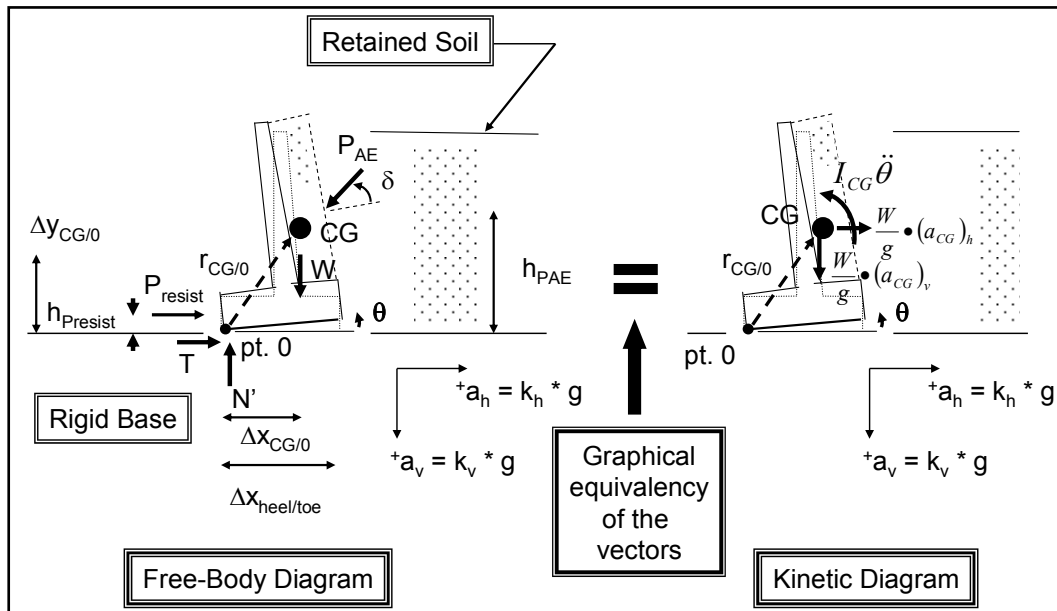


Figure 3.2. Free-body and kinetic diagrams of a rigid block model of a cantilever wall retaining moist backfill with rotation about the toe of the wall during horizontal and vertical shaking of the rigid level base.

base foundation.<sup>1</sup> Recall that  $g$  is the universal gravitational constant while  $k_h$  and  $k_v$  are the respective *time-histories* of the horizontal and vertical ground accelerations, expressed in decimal fraction. The acceleration of the center of gravity of the retaining wall structural system is designated by the subscript “CG.” Incremental, permanent wall rotations can occur during “strong” earthquake acceleration “pulses” (i.e., sequences in the acceleration time-history that contain high-amplitude acceleration wave forms and usually of short duration) in which horizontal ground acceleration thrusts are directed towards the retained soil (i.e., acting in the Figure 3.2 positive  $a_h$  direction) and/or vertical ground acceleration thrusts are directed towards the rigid base (i.e., acting in the Figure 3.2 positive  $a_v$  direction). The resulting incremental, permanent wall movements will be directed away from the retained soil. When these incremental wall movements occur, they are assumed to be of sufficient magnitude to fully mobilize the shear resistance in the retained soil. Active earth pressures are assumed to act on the retained side of the wall during these incremental wall rotations.

<sup>1</sup> The sign convention used in CorpsWallRotate is for the convenience of calculating the thrust force  $P_{AE}$  provided by the driving soil wedge and not based on considerations associated with the structural wedge shown in Figure 3.2. Appendix A describes the  $P_{AE}$  computation.

Referring to Figure 3.2, the rigid mass center is designated point CG and the center of rotation is point o. The acceleration response of mass center point CG,  $a_{CG}$ , will differ from the acceleration of point o, equal to the ground acceleration,  $a_{ground}$ , according to the relationship

$$a_{CG} = a_{ground} + a_{CG/o} \quad 3.1$$

where  $a_{CG/o}$  is the acceleration of the center of mass relative to toe of the wall (i.e., point o). Note that accelerations  $a_{CG}$  and  $a_o$  are absolute accelerations of the two respective points on the rigid body. If the vectors  $a_{CG}$  and  $a_o$  are equal in magnitude and direction, the rigid body undergoes pure translation. In all other cases, rotation of the rigid body will occur. The acceleration of point CG relative to point o, designated  $a_{CG/o}$ , may be expressed in terms of normal and tangential components, respectively, of the acceleration of point CG *relative to* point o,

$$a_{CG/o} = (a_{CG/o})_{\text{tangent}} + (a_{CG/o})_{\text{normal}} \quad 3.2$$

Note that the direction of vector  $(a_{CG/o})_{\text{tangent}}$  is consistent with the Figure 3.3 angular acceleration vector  $\alpha$  while the vector  $(a_{CG/o})_{\text{normal}}$  is always directed from CG towards the point of rotation, point o, regardless of the direction of  $\omega$ .<sup>1,2,3</sup> The accelerations felt at the Figure 3.3 mass center CG are the sum of three components:

$$a_{CG} = a_{ground} + (a_{CG/o})_{\text{tangent}} + (a_{CG/o})_{\text{normal}} \quad 3.3$$

Introducing the cross product definitions of the tangential and normal acceleration vectors,  $(a_{CG/o})_{\text{tangent}}$  and  $(a_{CG/o})_{\text{normal}}$ , (i.e., Equations 3.4 and 3.5 or, equivalently, Equation B.23) and referring to their Figure 3.4 horizontal and vertical vector direction components, Equation 3.3 becomes

<sup>1</sup> See Section B.5 in Appendix B.

<sup>2</sup> Recall that the angular velocity,  $\omega$ , is  $d\theta/dt = \dot{\theta}$  and the angular acceleration,  $\alpha$ , is  $d\omega/dt = d^2\theta/dt^2 = \ddot{\theta}$ .

<sup>3</sup> Consistency in the direction of the vectors  $(a_{CG/o})_{\text{tangent}}$  and  $\alpha$  is provided by evoking the right-hand rule in the derivation of

$$(a_{CG/o})_{\text{tangent}} = \alpha \times r_{CG/o} \quad 3.4$$

and that the direction of vector  $(a_{CG/o})_{\text{normal}}$  is in the same direction as vector  $-r_{CG/o}$

$$(a_{CG/o})_{\text{normal}} = \omega \times (\omega \times r_{CG/o}) = -(\omega)^2 r_{CG/o} \quad 3.5$$

as discussed in Hibbler (2001) on pages 294-295.

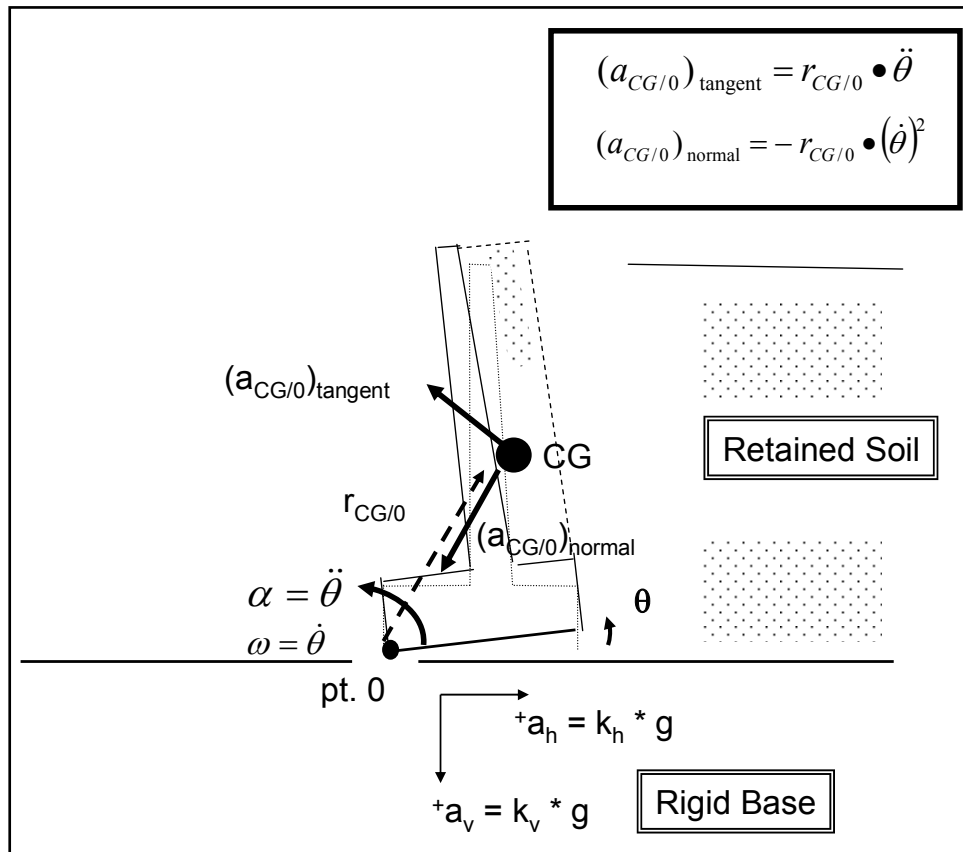


Figure 3.3. Tangential, normal, and angular accelerations of the center of mass (of a rigid block model of a cantilever wall retaining moist backfill) relative to the point of rotation during horizontal and vertical shaking of the rigid level base.

$$(a_{CG})_h = a_h - \alpha \cdot \Delta y_{CG/0} - \omega^2 \cdot \Delta x_{CG/0} \tag{3.6}$$

and

$$(a_{CG})_v = a_v - \alpha \cdot \Delta x_{CG/0} + \omega^2 \cdot \Delta y_{CG/0} \tag{3.7}$$

Equation 3.6 demonstrates that the horizontal acceleration of point CG is solely a function of (a) the horizontal ground acceleration, (b) the angular acceleration, and (c) the angular velocity during rotation. Note that the horizontal acceleration of (rigid) mass center point CG is not a function of the vertical ground acceleration. Equation 3.7 demonstrates that the vertical acceleration of point CG is solely a function of (a) the vertical ground acceleration, (b) the angular acceleration, and (c) the angular velocity during rotation. Note that the vertical acceleration of (rigid) mass center point CG is not a function of the horizontal ground acceleration.

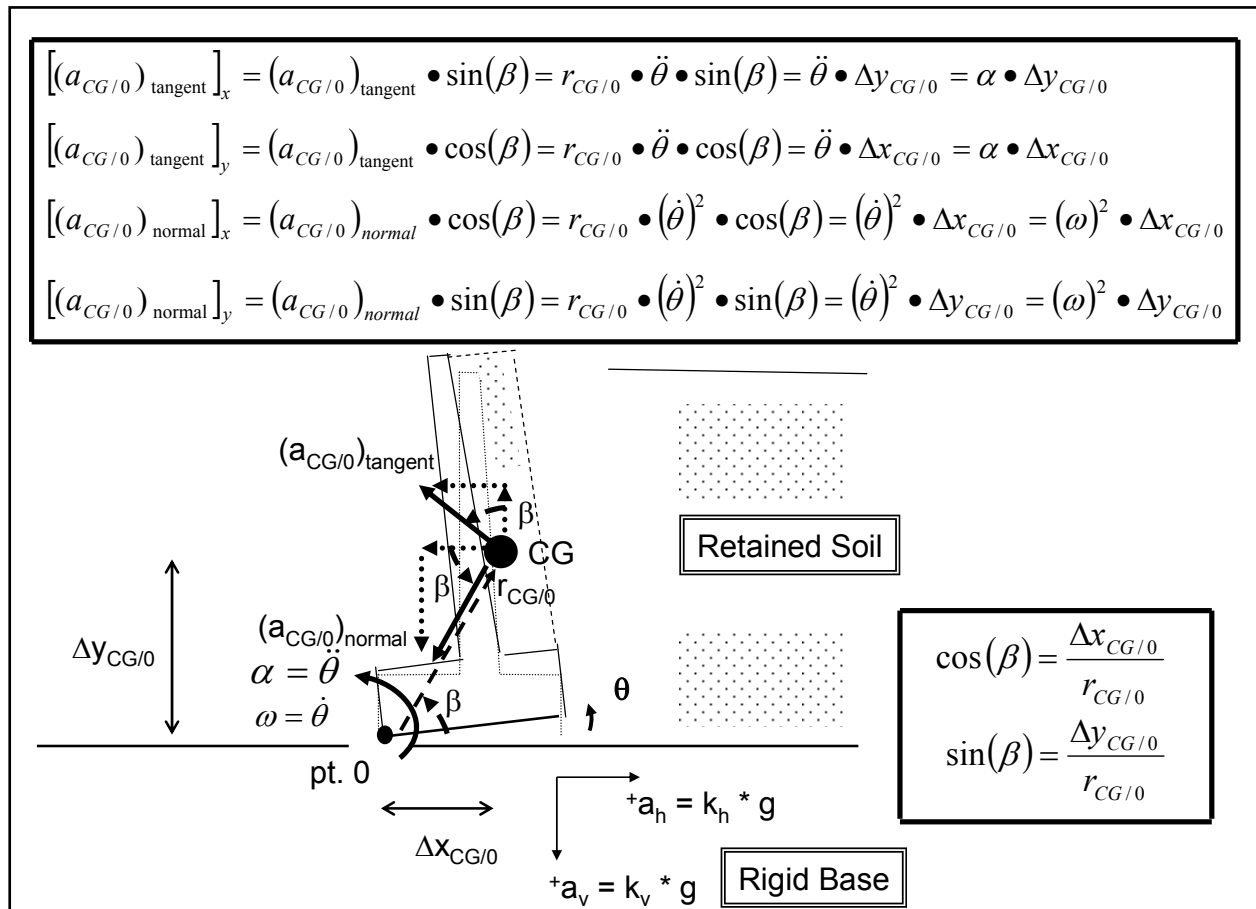


Figure 3.4. Horizontal and vertical components of the tangential and normal acceleration of the center of mass (of a rigid block model of a cantilever wall retaining moist backfill) relative to the point of rotation during horizontal and vertical shaking of the rigid level base.

### 3.3 Threshold value of acceleration corresponding to incipient lift-off of the base of the wall in rotation

During ground shaking, inertial forces are induced on the retaining wall system. Acceleration time-histories are used to represent ground shaking in the simplified CorpsWallRotate model of a retaining wall system. The time-varying inertial forces lead to elastic deformations, which can ultimately result in permanent rotation of the wall or sliding of the wall. In the case of permanent rotation of a rigid block model of the retaining wall system, (1) inertial forces vary in magnitude and direction with time and (2) their magnitudes are proportional to the value of acceleration at any given instant in time but acting in the direction opposite to acceleration. Additionally, a rotational acceleration about a point of rotation develops once the threshold acceleration for lift-off of the base of the wall in rotation is exceeded, which leads to permanent rotation of the wall relative to the top-of-foundation. When the ground acceleration drops below this



threshold acceleration value, restoring forces and moments will act to slow the speed of rotation, reducing the rate of increase of the angle of wall rotation. An increment of permanent wall rotation occurs during this interval in time. Additional permanent rotation will be induced during further cycles of ground acceleration if the threshold acceleration for lift-off of the base of the wall in rotation is again exceeded. The angle of permanent wall rotation accumulates with each of these excursion cycles in a manner similar to the accumulation of permanent sliding displacement in Newmark's sliding block method, briefly discussed in Chapter 1 and discussed in detail in a subsequent chapter. The primary author of this report observes that for a retaining wall system of specified geometry and material properties (i.e., unit weights and shear strength parameters, etc.) the threshold values of acceleration corresponding to incipient lift-off of the base of the wall in rotation (rotating about the toe of the wall in a  $C_{orps}W_{all}Rotate$  analysis) and for incipient sliding of the wall are not the same.

So the first step in determining if the retaining wall will rotate prior to sliding during earthquake shaking, or vice versa, is to compute: (1) the value of acceleration that is needed for lift-off of the wall from its base in rotation about the toe of the wall (discussed in this chapter); and (2) the limiting acceleration required to reduce the factor of safety against sliding to a limiting value of 1.0 (commonly referred to as the maximum transmissible acceleration,  $N \cdot g$ , sometimes referred to as the yield acceleration and discussed in Chapter 4). The second step is to compare these limiting acceleration values. For the simplified decoupled analyses outlined in this report, the mode of deformation is dictated by the smaller of the two acceleration values.

The free-body and kinetic diagrams of Figure 3.2 are combined in Figure 3.5 into a single figure showing the dynamic forces acting on a rigid block model of the structural wedge with rotation about the toe of the wall during horizontal and vertical shaking of the rigid base.<sup>1</sup> This cantilever wall retaining moist backfill is subjected to the five external forces of the weight of the structural wedge,  $W$ , the dynamic active earth pressure force,  $P_{AE}$ , the resisting force,  $P_{resist}$ , provided by the reinforced concrete slab at the toe of the wall, and the horizontal and vertical components of the rigid

---

<sup>1</sup> The inertial forces are applied according to D'Alembert's principle. The advantage of the inertia-force method based on D'Alembert's principle is that it converts a dynamics problem into an equivalent problem in equilibrium.

base-to-wall reaction forces  $T$  and  $N'$ , respectively, acting through the toe of the wall.

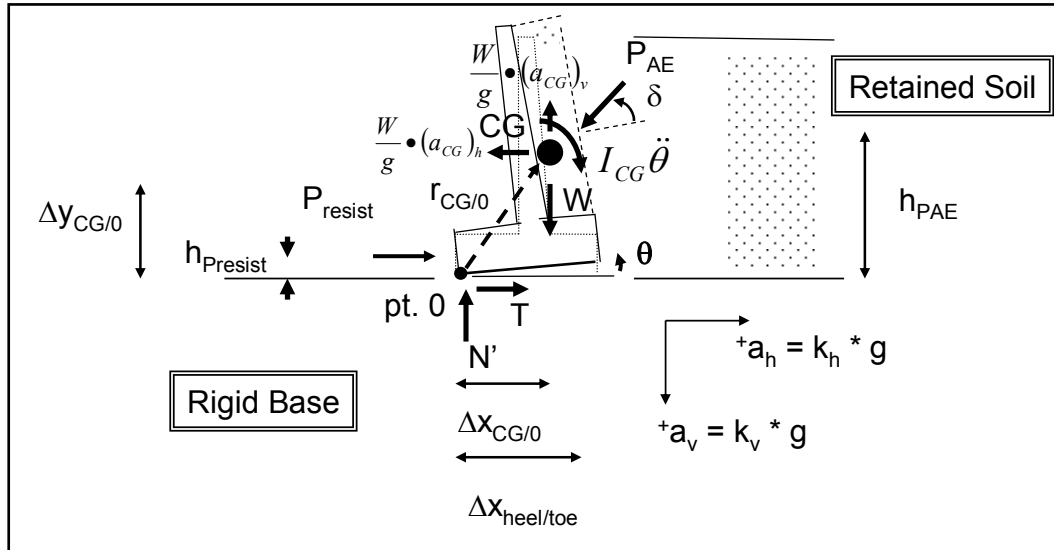


Figure 3.5. Inertia forces and resultant force vectors acting on a rigid block model of a cantilever wall retaining moist backfill with rotation about the toe of the wall during horizontal and vertical shaking of the rigid level base.

At the onset of lift-off of the base of the Figure 3.5 retaining wall (with level base) subject to pure rotation about its toe, the rotating (i.e., overturning) moment equals the stabilizing (i.e., restoring) moment. The summation of moments about point o of the Figure 3.5 forces acting on the rigid body results in

$$\begin{aligned} \frac{W}{g} \cdot (a_{CG})_h \cdot \Delta y_{CG/0} + \frac{W}{g} \cdot (a_{CG})_v \cdot \Delta x_{CG/0} + P_{AE} \cdot \cos(\delta) \cdot h_{PAE} = \\ P_{resist} \cdot h_{Presist} + W \cdot \Delta x_{CG/0} + P_{AE} \cdot \sin(\delta) \cdot \Delta x_{heel/toe} \end{aligned} \quad 3.8$$

Note that  $\ddot{\theta}$  is a very small number at the *onset* of lift-off and is set equal to zero as its limiting value when deriving this relationship. The component of the threshold acceleration occurring at lift-off of the base is designated as

$$(a_{CG})_{threshold-rotation-h} = (k_{CG})_{threshold-rotation-h} \cdot g \quad 3.9$$

where  $(k_{CG})_{threshold-rotation-h}$  is a value of horizontal ground acceleration, expressed in decimal fraction. Note that the horizontal acceleration value  $[(k_{CG})_{threshold-rotation-h} \text{ times } g]$  is not a user-specified constant. Since the

horizontal limiting acceleration is of interest, one option is to set the vertical component of acceleration occurring at lift-off in rotation equal to zero, as done by Nadim and Whitman (1984).<sup>1</sup> By making this assumption and introducing Equation 3.9, Equation 3.8 becomes

$$(k_{CG})_{\text{threshold-rotation-h}} = \frac{P_{\text{resist}} \cdot h_{\text{presist}} + W \cdot \Delta x_{CG/0} + P_{AE} \cdot \sin(\delta) \cdot \Delta x_{\text{heel/toe}} - P_{AE} \cdot \cos(\delta) \cdot h_{PAE}}{W \cdot \Delta y_{CG/0}} \quad 3.10$$

Because of the inclusion of acceleration in  $P_{AE}$  formulation (refer to Appendix A),  $C_{\text{orps}}W_{\text{all}}\text{Rotate}$  solves Equation 3.10 using a trial-and-error numerical approach. Observe that this relationship agrees with the Nadim and Whitman equation (Equation 2.16) and the Steedman and Zang equation (Equation 2.44) when  $P_{\text{resist}}$  is set equal to zero.

### 3.4 Angular acceleration of the retaining wall structural wedge – general formulation

If the maximum ground acceleration exceeds a threshold value of acceleration corresponding to incipient lift-off of the base of the wall in rotation,  $(a_{CG})_{\text{threshold-rotation-h}}$ , then permanent rotation of the wall will occur. For the retaining wall shown in Figure 3.2, the equation of motion when rotation has initiated is

$$\sum M_o = I_{CG} \cdot \alpha - \frac{W}{g} \cdot (a_{CG})_h \cdot \Delta y_{CG/0} - \frac{W}{g} \cdot (a_{CG})_v \cdot \Delta x_{CG/0} \quad 3.11$$

in which  $\sum M_o$  is the summation of moments about point o of external forces (including the weight of the structural wedge,  $W$ ) acting on the rigid body (counterclockwise positive); and  $I_{CG}$  is the mass moment of inertia about the center of gravity point, CG (refer to Equations B.15 or B.16).<sup>2</sup> Recall inertia forces have been applied according to D'Alembert's principle which permits the problem to be treated as a static problem. Introducing Equations 3.6 and 3.7, results in

<sup>1</sup> Another option, implemented in  $C_{\text{orps}}W_{\text{all}}\text{Rotate}$ , is to assign a constant value to the vertical acceleration component. A procedure for determining the value for this constant is discussed in Sections 3.9 and 3.10.

<sup>2</sup> Computation of the mass moment of inertia in  $C_{\text{orps}}W_{\text{all}}\text{Rotate}$  is described in Appendix E.

$$\begin{aligned} \Sigma M_o = I_{CG} \cdot \alpha - \frac{W}{g} \cdot [a_h - \alpha \cdot \Delta y_{CG/0} - \omega^2 \cdot \Delta x_{CG/0}] \cdot \Delta y_{CG/0} \\ - \frac{W}{g} \cdot [a_v - \alpha \cdot \Delta x_{CG/0} + \omega^2 \cdot \Delta y_{CG/0}] \cdot \Delta x_{CG/0} \end{aligned} \quad 3.12$$

Collecting terms, Equation 3.12 becomes

$$\begin{aligned} \Sigma M_o = \alpha \cdot \left\{ I_{CG} + \frac{W}{g} \cdot [(\Delta y_{CG/0})^2 + (\Delta x_{CG/0})^2] \right\} \\ + \frac{W}{g} \cdot \omega^2 \cdot [\Delta x_{CG/0} \cdot \Delta y_{CG/0} - \Delta y_{CG/0} \cdot \Delta x_{CG/0}] \\ - \frac{W}{g} \cdot [a_h \cdot \Delta y_{CG/0} + a_v \cdot \Delta x_{CG/0}] \end{aligned} \quad 3.13$$

which reduces to

$$\begin{aligned} \Sigma M_o = \alpha \cdot \left\{ I_{CG} + \frac{W}{g} \cdot [(\Delta y_{CG/0})^2 + (\Delta x_{CG/0})^2] \right\} \\ - \frac{W}{g} \cdot [a_h \cdot \Delta y_{CG/0} + a_v \cdot \Delta x_{CG/0}] \end{aligned} \quad 3.14$$

By referring to Figure 3.6, introducing

$$(r_{CG/0})^2 = (\Delta y_{CG/0})^2 + (\Delta x_{CG/0})^2 \quad 3.15$$

and recognizing that the mass moment of inertia about the point o (the of rotation) is

$$I_o = I_{CG} + \frac{W}{g} \cdot (r_{CG/0})^2 \quad 3.16$$

Equation 3.14 becomes

$$\Sigma M_o = \alpha \cdot I_o - \frac{W}{g} \cdot [a_h \cdot \Delta y_{CG/0} + a_v \cdot \Delta x_{CG/0}] \quad 3.17$$

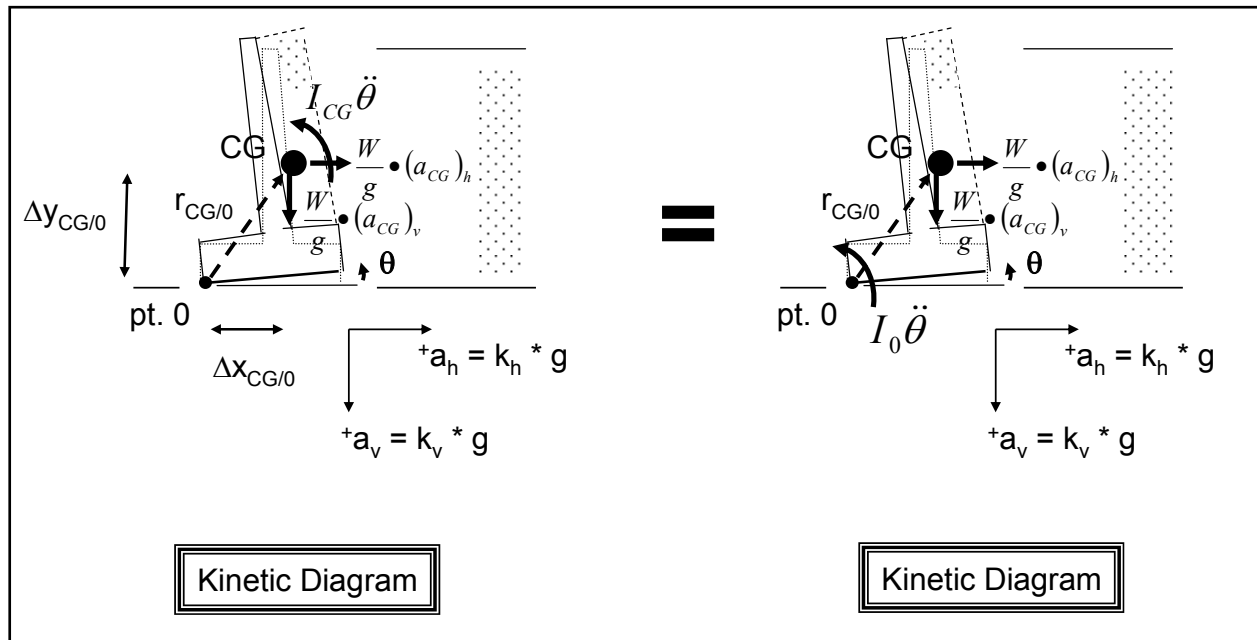


Figure 3.6. Equivalent kinetic diagrams for the rigid block model of a cantilever wall retaining moist backfill with rotation about the toe of the wall during horizontal and vertical shaking of the rigid level base.

Solving for the retaining wall’s angular acceleration, Equation 3.17 becomes

$$\alpha = \frac{\sum M_0 + \frac{W}{g} \cdot [a_h \cdot \Delta y_{CG/0} + a_v \cdot \Delta x_{CG/0}]}{I_0} \tag{3.18}$$

or, equivalently,  $\alpha$  is given by

$$\alpha = \frac{\sum M_0 + \frac{W}{g} \cdot [(k_h \cdot g) \cdot \Delta y_{CG/0} + (k_v \cdot g) \cdot \Delta x_{CG/0}]}{I_0} \tag{3.19}$$

Thus, Equation 3.18 or, equivalently, Equation 3.19 provides for the calculation of the angular acceleration of the wall at every increment in time during earthquake shaking once the threshold value of acceleration corresponding to incipient lift-off of the base of the wall in rotation is exceeded and the wall is rotating. When the ground acceleration drops below  $(a_{CG})_{\text{threshold-rotation-h}}$ , restoring forces and moments will act to slow the speed of the angular rotation, thus reducing the rate of increase of the permanent angle of rotation. Wall rotation ceases when the angular

rotational velocity of the center of gravity returns to zero. Additional increments of wall rotation occur each time a ground acceleration pulse exceeds  $(a_{CG})_{\text{threshold-rotation-h}}$  in the same manner that permanent sliding displacements accumulate in a rigid block analysis.

The velocity of rotation (i.e., angular velocity) is computed by integration of the angular acceleration during each segment of wall rotation (that initiates when the threshold acceleration is exceeded)

$$\omega = \int_0^t \alpha dt \quad \text{when } \omega > 0 \quad 3.20$$

or

$$\omega = 0 \quad \text{when Equation 3.17 gives } \omega \text{ less than } 0 \quad 3.21$$

Note that  $C_{\text{orps}}W_{\text{allRotate}}$  assumes that the wall cannot rotate back into the retained soil, which is expressed by Equation 3.20. The permanent rotation of the wall is the integration of the angular velocity of rotation

$$\theta = \int_0^t \omega dt \quad 3.22$$

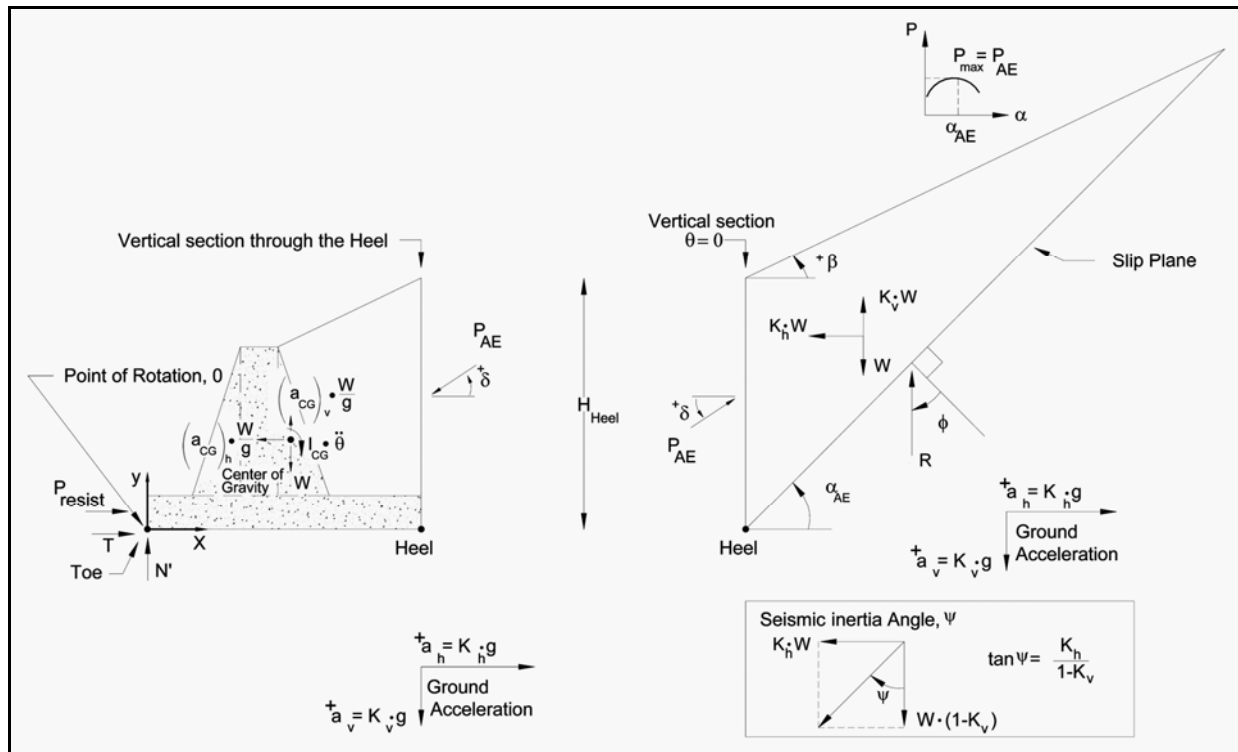
This series of computations using Equations 3.18 through 3.22 are repeated for each sequence of wall rotations that occurs for the duration of earthquake shaking. The experience of the primary author of this report is that when the acceleration time-histories used as input to  $C_{\text{orps}}W_{\text{allRotate}}$  are based on previously recorded earthquake events (a typical scenario), the permanent rotation occurs during several, separate pulses occurring throughout the duration of shaking.

Unlike the sliding (rigid) block model (discussed in Chapter 4), which effectively isolates the sliding block from the shaking base below, the rotating rigid block model continues to transmit horizontal acceleration through the “pin,” located at the toe of the wall, into the wall. The center of gravity wall accelerations during rotation are computed at each time increment during wall rotation using the value for angular velocity,  $\omega$ , and angular acceleration,  $\alpha$ , at that same instant in time using Equations 3.6 and 3.7.

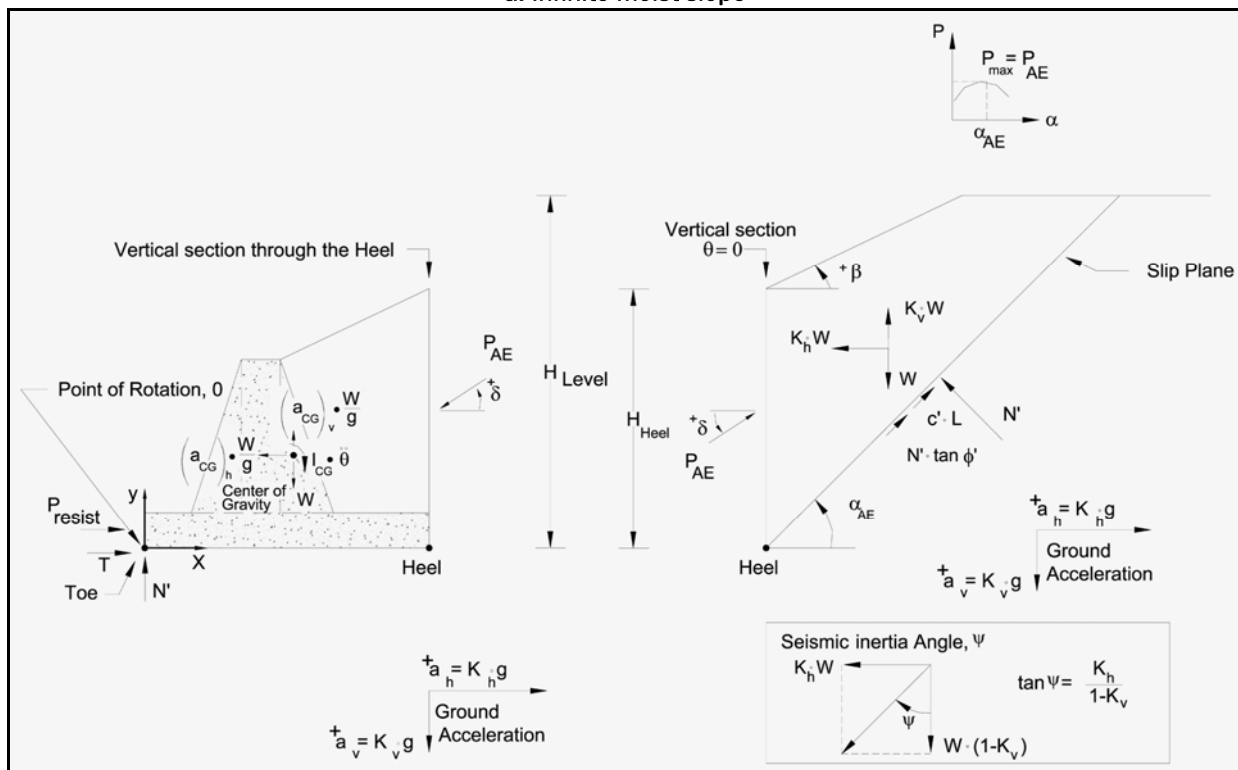
### 3.5 Dynamic active earth pressure force $P_{AE}$

Figure 3.5 shows an idealized structural wedge containing a cantilever retaining wall retaining moist backfill with externally applied forces acting on it during the seismically-induced rotation  $\theta$  of the wall about its toe, point o. One of the forces identified in this figure is the dynamic active resultant earth pressure force exerted by the driving soil wedge on the structural wedge,  $P_{AE}$ . Rather than relying on the Mononobe-Okabe relationship, a sweep-search wedge formulation within the retained soil is used to determine the value of  $P_{AE}$ . Recall that the Mononobe-Okabe relationship is valid for a retained soil with a constant surface slope (including the case of a level backfill) and whose strength is characterized by the Mohr-Coulomb shear strength parameter  $\phi$  (e.g., refer to Equations 33 through 35 in Ebeling and Morrison (1992)). The computed value for  $P_{AE}$  via the Figure 3.7.a sweep-search method in a cohesionless backfill will agree with the value computed using the Mononobe-Okabe relationship. The advantage of the sweep-search method as formulated in this report and implemented in  $C_{orps}W_{all}Rotate$  is that it allows for (1) the analysis of the more practical case of the bilinear ground surface depicted in Figure 3.7.b and/or (2) the analysis of “cohesive” ( $S_u$ ) soils. Sufficient wall movement during earthquake shaking to fully mobilize the shear resistance within the retained soil as per Table 1.1 criteria is assumed in this formulation. The sweep-search formulation implemented within  $C_{orps}W_{all}Rotate$  is given in Appendix A for effective shear strength ( $c'$ ,  $\phi'$ ) and for undrained ( $S_u$ ) shear strength soil parameters.

The effect of an earthquake on the driving soil wedge is incorporated through the use of the user-specified horizontal and vertical components of the ground acceleration time-histories,  $a_h (= k_h g)$  and  $a_v (= k_v g)$ , respectively. Recall that  $g$  is the universal gravitational constant, while  $k_h$  and  $k_v$  are the respective *time-histories* of the horizontal and vertical ground accelerations, expressed in decimal fraction. No potential site amplification effects are considered in this simplified formulation so the ground acceleration time-histories are assumed to act within the driving soil wedge as well. So, at each instant in time during earthquake shaking, the horizontal and vertical inertia forces ( $k_h$  times soil wedge weight,  $W$ , and  $k_v$  times soil wedge weight,  $W$ , respectively) acts at the center of mass of the soil wedge and in the direction opposite to that in which their respective component ground acceleration acts (refer to the right-hand side of Figures 3.7.a and b).



a. Infinite moist slope



b. Bilinear moist slope

Figure 3.7. Structural wedge with toe resistance retaining a driving soil wedge with a moist slope (i.e., no water table) analyzed by effective stress analysis with full mobilization of  $(c', \phi')$  shear resistance within the backfill.



The Mononobe-Okabe analysis procedure does not provide a means for calculating the point of action of the resulting force  $P_{AE}$ , nor does the sweep-search soil wedge method of analysis. Limited tests results involving dry sands (as discussed on page 63 in Ebeling and Morrison, 1992) indicate that the vertical position of  $P_{AE}$  ranges from 0.4 to 0.55 times the height of the wall (above the heel).  $P_{AE}$  acts at a higher position along the back of the wall than the static active earth pressure force due to the concentration of soil mass comprising the sliding wedge above the mid-wall height (Figure 3.8). With the static force component of  $P_{AE}$  acting below mid-wall height and the inertia force component of  $P_{AE}$  acting above mid-wall height, the vertical position of the resultant force  $P_{AE}$  will depend upon the magnitude of the accelerations applied to the mass comprising the soil wedge. Following the approach taken by Seed and Whitman (1970),  $P_{AE}$  is defined as the sum of the initial static active earth pressure force,  $P_A$ , and the dynamic active earth pressure force increment,  $\Delta P_{AE}$ ,

$$P_{AE} = P_A + \Delta P_{AE} \quad 3.23$$

as depicted in Figure 3.8. The sweep-search method is also used in `CorpsWallRotate` to compute the resultant static active earth pressure force  $P_A$ . After reviewing the various results, Seed and Whitman (1970) suggested applying the dynamic force component  $\Delta P_{AE}$  at 0.6 times  $H$ . Based on this recommendation, computation of the location of the resultant force  $P_{AE}$  along the imaginary vertical section extending upwards from the heel of the wall is made using

$$h_{PAE} = \frac{P_A \cdot \left(\frac{H}{3}\right) + \Delta P_{AE} \cdot (0.6 \cdot H)}{P_{AE}} \quad 3.24$$

with  $P_A$  acting at  $H/3$  for moist, *level*, granular (with  $c'=0$ ) backfill.<sup>1</sup> Note that the magnitude of  $P_{AE}$  and thus, the magnitude of  $h_{PAE}$  is a function of the seismic coefficient used in the driving wedge seismic analysis. The solution process implemented in `CorpsWallRotate` is to first compute  $P_{AE}$  and  $P_A$ , solve for  $\Delta P_{AE}$  using Equation 3.23, then solve for  $h_{PAE}$  using Equation 3.24.

---

<sup>1</sup> Appendix C outlines procedures for determining the point of application of  $P_A$  for other backfill cases. Appendix H discusses two example computations of static, active earth pressure distributions and depth of cracking in cohesive soils.

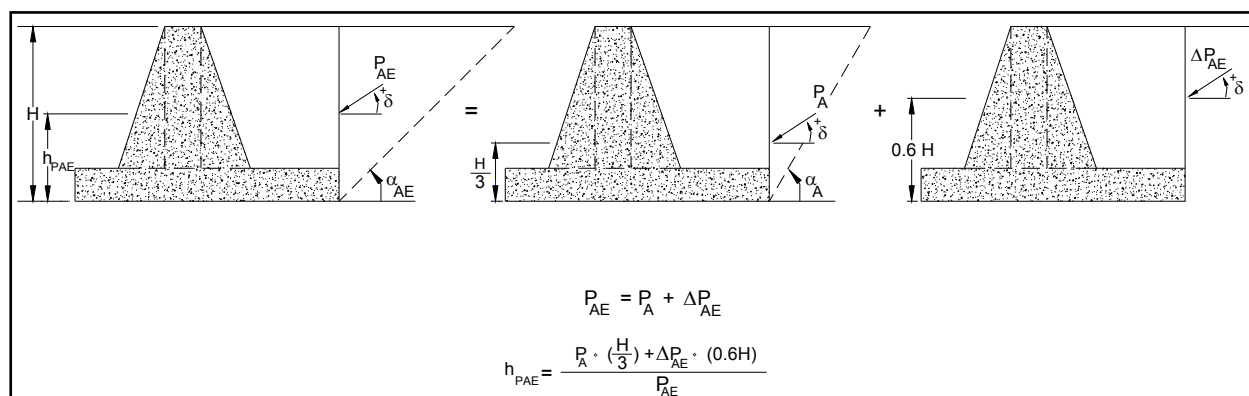


Figure 3.8. Resultant location of  $P_{AE}$  based on the positions and magnitudes of the static active earth pressure force,  $P_A$ , and incremental dynamic active earth pressure force,  $\Delta P_{AE}$ , of a moist, level, backfill (after Ebeling and Morrison (1992)).

Once the magnitude and location of  $P_{AE}$  that act on the back of the rigid block model of the structural wedge are determined, an approach such as the procedure described in Ebeling and Morrison (1992) and shown in Figure 3.9 may be used to convert this force into equivalent pressure diagram. Key to this Ebeling and Morrison approach is the use of *pressure distributions* for each of the static  $P_A$  and for  $\Delta P_{AE}$  force components that are consistent not only in their magnitudes but also consistent with their Figure 3.8  $P_A$  and  $\Delta P_{AE}$  force positions. The resulting total pressure distribution acting on the structural wedge is the sum of the triangular distribution of static active earth pressures that are consistent with  $P_A$  for the moist granular backfill shown in the figure plus the trapezoidal stress distribution consistent with  $\Delta P_{AE}$  acting at 0.6 times  $H$ .<sup>1</sup>

A key item is the selection of suitable shear strength parameters. In an effective stress analysis, the issue of the suitable friction angle is particularly troublesome when the peak friction angle is significantly greater than the residual friction angle. In the displacement-controlled approach examples given in Section 6.2 of Ebeling and Morrison (1992), effective stress-based shear strength parameters (i.e., effective cohesion  $c'$  and effective angle of internal friction  $\phi'$ ) were used to define the shear strength of the dilative granular backfills, with  $c'$  set equal to zero in all

<sup>1</sup> In the case of a water table and an effective stress analysis in which the effective shear strength parameters  $c'$  and  $\phi'$  are assigned to the (granular) retained soil, this approach is altered by changing the distribution of equivalent static earth pressures representing  $P_A$  to account for pore water pressures in the backfill in the usual manner for geotechnical engineering. This is demonstrated in Figure 7.10 in Ebeling and Morrison (1992) and discussed in Appendix C of this report. In the case of a total stress analysis, boundary water pressures (due to the presence of a water table in the retained soil) are not applied along the imaginary interface between the driving (soil) wedge and the structural wedge.

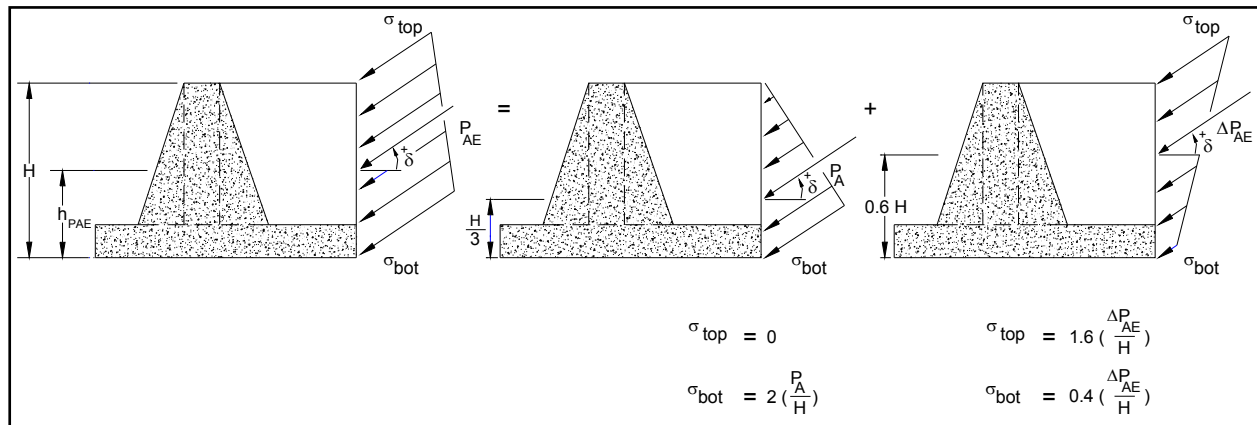


Figure 3.9. The computation of equivalent earth pressures acting on a rigid block model of a cantilever wall retaining moist, level, granular (with  $c'=0$ ) backfill (after Ebeling and Morrison 1992).

cases due to the level of deformations anticipated in a sliding block analysis during seismic shaking. In 1992, Ebeling and Morrison concluded that it is conservative to use the residual friction angle in a sliding block analysis, and this should be the usual practice for displacement based analysis of granular retained soils. The primary author of this report would broaden the concept to the assignment of effective (or total) shear strength parameters for the retained soil to be consistent with the level of shearing-induced deformations encountered for each design earthquake in a rotational analysis and note that active earth pressures are used to define the loading provided to the structural wedge by the driving soil wedge. (Refer to Table 1.1 for guidance regarding wall movements required to fully mobilize the shear resistance within the retained soil during earthquake shaking.)

### 3.6 Moments due to external forces acting about the toe of the structural wedge

The Figure 3.5 cantilever wall, with level base, retaining moist backfill is subjected to the five external forces of the weight of the structural wedge,  $W$ , the dynamic active earth pressure force,  $P_{AE}$ , the resisting force,  $P_{\text{resist}}$ , provided by the reinforced concrete slab at the toe of the wall, and the horizontal and vertical components of the rigid base-to-wall reaction forces  $T$  and  $N'$ , respectively, acting through the toe of the wall. The moment due to these external forces about the point  $o$  at toe of the wall (counterclockwise positive, as previously stated) is

$$\begin{aligned} \sum M_o = & -W \bullet \Delta x_{CG/o} - P_{resist} \bullet h_{Presist} - P_{AE} \\ & \bullet \sin(\delta) \bullet \Delta x_{heel/toe} + P_{AE} \bullet \cos(\delta) \bullet h_{PAE} \end{aligned} \quad 3.25$$

Since the foundation reaction shear force T and normal force N' act through point o during rotation, they do not contribute to the moment. At each instant in time during earthquake shaking, the horizontal and vertical accelerations vary in direction. Thus, the magnitudes of  $P_{AE}$  and  $h_{PAE}$  vary as well.

### 3.7 Angular acceleration of the retaining wall structural wedge – formulation implemented in **C<sub>orps</sub>W<sub>all</sub>Rotate**

The relationship defining the angular acceleration of the retaining wall structural wedge that is implemented in **C<sub>orps</sub>W<sub>all</sub>Rotate** is derived by introducing Equation 3.25 into Equation 3.19. When rotation has initiated, the angular acceleration of the structural wedge (with level base) is

$$\alpha = \frac{\left\{ \begin{array}{l} -W \bullet \Delta x_{CG/o} - P_{resist} \bullet h_{Presist} - P_{AE} \bullet \sin(\delta) \\ \bullet \Delta x_{heel/toe} + P_{AE} \bullet \cos(\delta) \bullet h_{PAE} \\ + \frac{W}{g} \bullet [(k_h \bullet g) \bullet \Delta y_{CG/o} + (k_v \bullet g) \bullet \Delta x_{CG/o}] \end{array} \right\}}{I_o} \quad 3.26$$

with the mass moment of inertia about the point o (the of rotation) given by

$$I_o = I_{CG} + \frac{W}{g} \bullet (r_{CG/o})^2 \quad \text{bis 3.16}$$

Recall  $\alpha$  (or, equivalently,  $\ddot{\theta}$ ) is the angular acceleration of the structural wedge of (total) mass M (=W/g) about point of rotation, point o. The resulting engineering formulation is implemented in the corresponding PC software **C<sub>orps</sub>W<sub>all</sub>Rotate** and will perform a rotating analysis of each user-specified retaining wall section.

Equation 3.26 agrees with the uncoupled Nadim and Whitman (1984) equation (Equation 2.12), with the Siddharthan et al. equation (Equation 2.32), when  $P_{resist}$  is set equal to zero and with the Steedman

and Zeng equation (Equation 2.47) when the vertical ground acceleration is set equal to zero.<sup>1</sup>

### 3.8 Numerical method for computing the rotational time-history of a rigid block retaining structure rotating about its toe

#### 3.8.1 Introduction to a step-by-step solution scheme

Earthquake acceleration time-histories are used to represent the earthquake demand in this formulation, as is the case for all rotating wall formulations discussed in Chapter 2. Again, baseline-corrected, horizontal and vertical acceleration time-histories are to be used to represent the earthquake ground motions in  $C_{\text{orps}}W_{\text{allRotate}}$ .<sup>2</sup> It is the experience of the primary author of this report that the duration of ground acceleration time-histories used on Corps projects is on the order of tens of seconds, and up to about one minute of earthquake shaking. The number of time increments (i.e., discrete acceleration point values) contained in the acceleration time-history corresponds to the number of solutions made in the rotational wall analysis by  $C_{\text{orps}}W_{\text{allRotate}}$ . The number of time increments is defined by the duration of earthquake shaking and the time increment  $DT$  used in digitization of the acceleration time-history.

<sup>1</sup> Note: In order to compare Equation 3.26 with (1) Nadim and Whitman (Equation 2.12), recognize that the equivalent geometry designations are

$$\Delta x_{CG/O} = B_1 \quad 3.27$$

$$\Delta y_{CG/O} = B_3 \quad 3.28$$

$$h_{PAE} = L \quad 3.29$$

and

$$\Delta x_{heel/toe} = B_2 \quad 3.30$$

for a point of rotation specified about the toe, point O, to match the  $C_{\text{orps}}W_{\text{allRotate}}$  formulation. In order to compare Equation 3.26 with (2) Siddharthan et al. (Equation 2.32) for a point of rotation specified about the toe, the equivalent geometry designations are

$$\Delta x_{CG/O} = R \cdot \cos(\eta) \quad 3.31$$

$$\Delta y_{CG/O} = R \cdot \sin(\eta) \quad 3.32$$

$$h_{PAE} = mH \quad 3.33$$

$$h_{PAE} \cdot \cos(\delta) = mH \cdot \cos(\delta + \alpha) \quad 3.34$$

$$\Delta x_{heel/toe} \cdot \sin(\delta) = \sin(\delta + \alpha) \cdot [R \cdot \cos(\eta) + a - mH \cdot \tan(\alpha)] \quad 3.35$$

but with  $\alpha$  equal to zero to match the  $C_{\text{orps}}W_{\text{allRotate}}$  structural wedge geometry. In order to compare Equation 3.26 with (3) Steedman and Zeng (Equation 2.47), the equivalent geometry designations are

$$\Delta x_{CG/O} = X_c \quad 3.36$$

$$\Delta y_{CG/O} = Y_c \quad 3.37$$

$$\Delta x_{heel/toe} \cdot \sin(\delta) = \sin(\delta + \beta) \cdot [B - h \cdot \tan(\beta)] \quad 3.38$$

but with  $\beta$  equal to zero to match the  $C_{\text{orps}}W_{\text{allRotate}}$  structural wedge geometry.

<sup>2</sup> Note that  $C_{\text{orps}}W_{\text{allRotate}}$  requires the time-step  $DT$  for the horizontal and vertical acceleration time-histories used in the same analysis be the same value.

There is no standard time increment  $DT$  for the digitization and subsequent processing of acceleration time-histories for Corps projects. However, Ebeling, Green, and French (1997) observe that a  $DT$  equal to 0.02, 0.01, or 0.005 second is the most common. For example, an earthquake acceleration time-history with 40 seconds of shaking and a time-step of 0.02 second will contain 2,000 discretized acceleration points. If the acceleration time-history was processed with a  $DT$  equal to 0.01 or 0.005 second, then the discretized acceleration time-histories would contain 4,000, and 8,000 acceleration points, respectively.

A step-by-step solution scheme is followed in order to obtain the wall's rotational velocity,  $\omega$ , and rotation,  $\theta$ , in the time domain by  $C_{\text{CorpsWallRotate}}$ . An overview of the characteristics of this numerical formulation is depicted in Figure 3.10. A key feature of the numerical formulation used is the assumption of a *linear* variation in angular acceleration  $\alpha$  over time-step  $DT$ , from time  $t_i$  to time  $t_{i+1}$ . Values of  $\alpha$  are computed using Equation 3.26 at each time-step. This idealized figure assumes that the wall is undergoing positive angular acceleration, positive rotational (i.e., angular) velocity, and positive (permanent) rotation at time  $t_i$ , which continues through time  $t_{i+1}$ . (Other cases will be considered later.) It also assumes that the angular acceleration increases in magnitude over this time-step,  $DT$ , as depicted in this figure. Recall the velocity of rotation (i.e., angular velocity) is computed by integrating the angular acceleration during each segment of wall rotation (refer to Equation 3.20). So for a linear variation in angular acceleration over time-step  $DT$ , the rotational velocity,  $\omega$ , is a quadratic relationship. Similarly, with the permanent rotation of the wall being the integration of the angular velocity of rotation (refer to Equation 3.21), the rotation of the wall about its toe is a cubic relationship. The value for angular acceleration, rotational velocity  $\omega$  and (permanent wall) rotation  $\theta$  at any point in time  $\Delta t$  after  $t_i$  and before time  $t_{i+1}$  are given by the linear, quadratic, and cubic relationships contained on the right-hand side of these three figures (with  $\Delta t$  less than or equal to  $DT$ ).

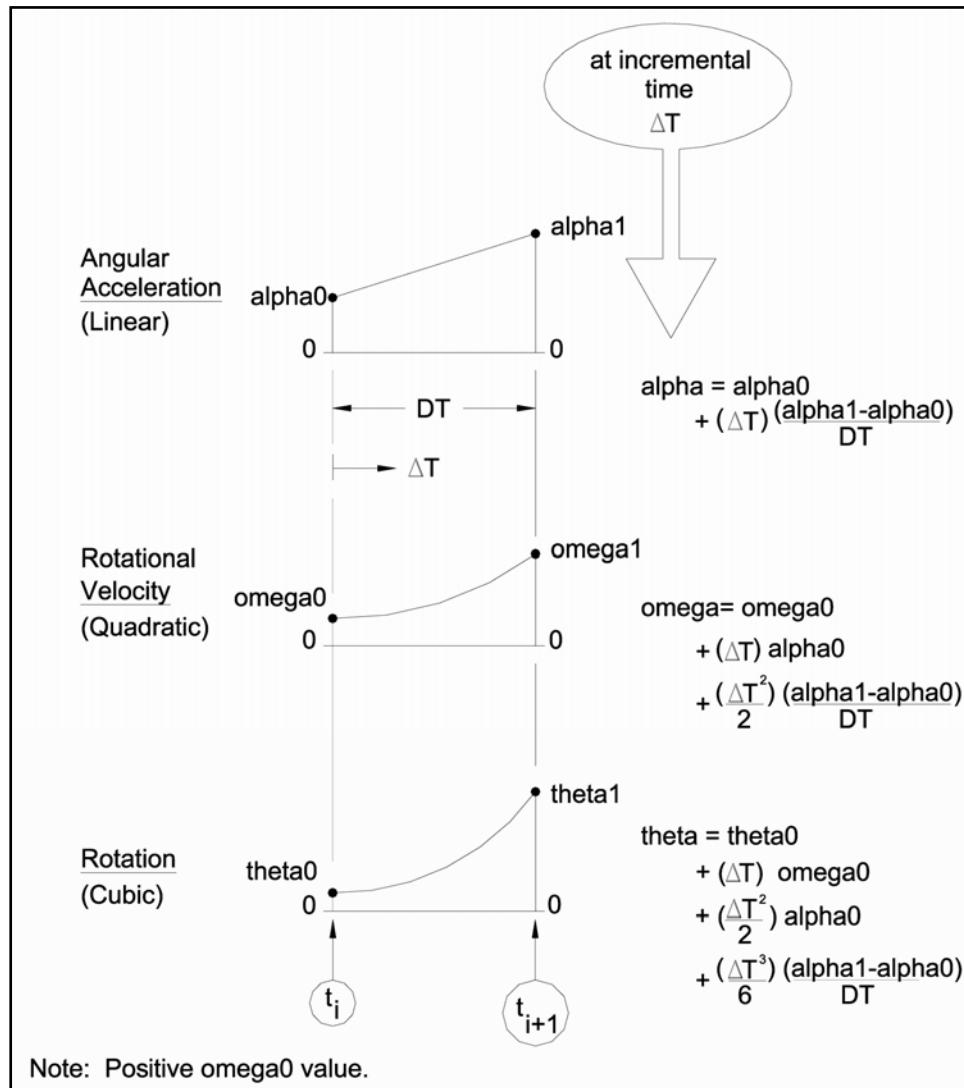


Figure 3.10. Complete equations for rotational motions over time increment  $\Delta T$  based on linearly varying angular acceleration.

### 3.8.2 Positive angular accelerations $\alpha_0$ and $\alpha_1$ at times $t_i$ and $t_{i+1}$

Expanding on the details of the computations for the numerical formulation depicted in Figure 3.10, the computation of the angular acceleration,  $\alpha$ , rotational velocity,  $\omega$ , and rotation,  $\theta$ , at time  $t_{i+1}$  are made as follows: Values for  $\alpha$ ,  $\omega$ ,  $\theta$ , at time  $t_i$  are known from the previous computation step in the step-by-step solution scheme.<sup>1</sup> The value for  $\alpha$  at time  $t_{i+1}$  (designated  $\alpha_1$  in the figure) is computed using Equation 3.26. Referring to Figure 3.11, the rotational velocity  $\omega$  at time  $t_{i+1}$  (designated  $\omega_1$ ) is computed from the value for  $\omega$  at time  $t_i$

<sup>1</sup> Note that at time  $t_i$  the angular acceleration  $\alpha$  is designated  $\alpha_0$ , the rotational velocity  $\omega$  is designated  $\omega_0$  and the (permanent wall) rotation  $\theta$  is designated  $\theta_0$ .

(designated  $\omega_0$ ) plus the positive area under the linear angular acceleration relationship over the time-step  $DT$ , designated  $Area_a$  in this figure. By the trapezoidal rule,  $\omega_1$  at time  $t_{i+1}$  is

$$\omega_1 = \omega_0 + \frac{DT}{2} \cdot (\alpha_0 + \alpha_1) \quad 3.38$$

with the values for  $\omega_0$  and  $\alpha_0$  now known values that were computed in the previous solution step. Note the wall is in motion at time  $t_i$ , as reflected by a positive value for  $\omega_0$  (designated  $\omega_0$  in Figure 3.11). Similarly, the wall rotation  $\theta$  at time  $t_{i+1}$  (designated  $\theta_1$ ) is computed from the value for  $\theta$  at time  $t_i$  (designated  $\theta_0$ ) plus the positive area under the quadratic rotational velocity relationship over the time-step  $DT$ , designated  $Area_o$  in this figure. For this linear acceleration method,  $\theta_1$  at time  $t_{i+1}$  is

$$\theta_1 = \theta_0 + DT \cdot \omega_0 + \frac{DT^2}{6} \cdot (2 \cdot \alpha_0 + \alpha_1) \quad 3.39$$

with the value for  $\theta_0$  being a known value that was computed in the previous solution step. The value for rotational velocity  $\omega$  and (permanent wall) rotation  $\theta$  at time  $t_{i+1}$  are also described in terms of the area relationships contained in Figure 3.11. In this manner a step-by-step solution scheme is followed throughout the entire time-history of earthquake shaking in order to obtain the wall velocity,  $\omega$ , and rotation,  $\theta$ , at each increment in time in the Figure 3.11 case of positive values for  $\alpha$  at times  $t_i$  and  $t_{i+1}$ .

In summary, Figure 3.11 outlines a numerical procedure to obtain values for  $\omega$  and for  $\theta$  at time  $t_{i+1}$  in situations for which values of  $\alpha$  at times  $t_i$  and  $t_{i+1}$  are both positive. However, there are three other situations that can arise during the step-by-step solution: (a) the case of a negative value for  $\alpha$  at time  $t_i$  and a positive value for  $\alpha$  at time  $t_{i+1}$ ; (b) the case of wall rotation decelerating over the entire time-step  $DT$  for which the values of  $\alpha$  are negative at both times  $t_i$  and  $t_{i+1}$ ; and (c) the case of a positive value for  $\alpha$  at time  $t_i$  and a negative value for  $\alpha$  at time  $t_{i+1}$ . In all four cases, the assumption of **linear angular acceleration** over time-step  $DT$  is made and the basic concept of **integrating** positive areas above and/or negative areas below the time line of angular acceleration  $\alpha$  to obtain the *change* in



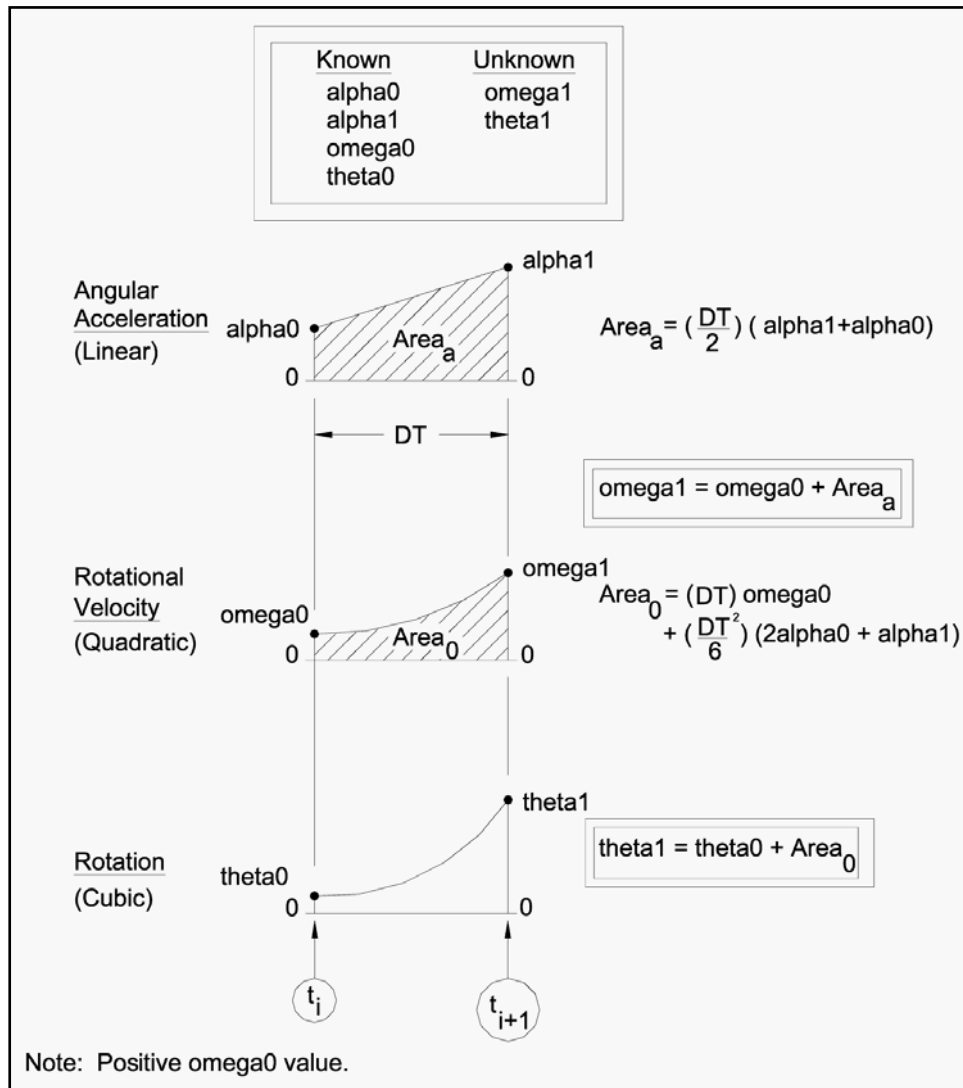


Figure 3.11. Rotational velocity and rotations at the end of time increment DT based on linearly varying angular acceleration.

rotational velocity  $\omega$  and then, in turn, the integration of positive and/or negative areas above and/or below the time line of  $\omega$  to obtain the *change* in rotation  $\theta$  is used to determine the values for  $\omega$  and  $\theta$ , respectively, at time  $t_{i+1}$ . These three additional step-by-step solutions will be discussed next. Note the frequent use of the trapezoidal rule for  $\omega$  and the linear acceleration method for  $\theta$  in the solution processes to be described.

**3.8.3 Positive angular acceleration  $\alpha_0$  at time  $t_i$  and negative angular acceleration  $\alpha_1$  at  $t_{i+1}$**

Next consider a wall in motion (i.e., with a positive value for  $\omega$ ) at time  $t_i$  but with the Figure 3.12 case of a negative value for  $\alpha$  computed using

Equation 3.26 at time-step  $t_i$  and positive value for  $\alpha$  computed using Equation 3.26 at the next time-step of  $t_{i+1}$ .<sup>1</sup> The first step is to determine the time instant [ $t_i$  plus lhsDT] at which the angular acceleration  $\alpha$  is equal to zero, as labeled in the figure. By linear interpolation, this time increment lhsDT is

$$lhsDT = \left| \alpha_0 \cdot \left( \frac{DT}{\alpha_1 - \alpha_0} \right) \right| \quad 3.40$$

The negative area between the negative portion of the linear acceleration line and the time line over the Figure 3.12 time increment lhsDT is

$$NegativeArea_{-\alpha+} = \frac{1}{2} \cdot lhsDT \cdot (\alpha_0 + 0) \quad 3.41$$

Recall that the wall is in motion at time  $t_i$  when  $\omega$  (designated  $\omega_0$  in the figure) is positive. There are two possible outcomes for the Figure 3.12 step-by-step numerical solutions for values of  $\omega$  and of  $\theta$  at time  $t_{i+1}$ , depending upon the magnitude of  $\omega_0$  relative to the magnitude of  $NegativeArea_{-\alpha+}$ . These possible scenarios are depicted by two columns of figures in Figure 3.12, labeled as the Case 1 and Case 2 figure groups.

**Case 1:** This case results when the positive value for  $\omega$  at time  $t_i$  is greater than the magnitude of  $NegativeArea_{-\alpha+}$  (i.e., the negative area between the negative portion of the linear acceleration line and the time line over the portion of the Figure 3.12 time increment labeled lhsDT). The three left-hand side figures in Figure 3.12 are used to describe the Case 1 step-by-step solution scheme: The top figure describes the angular acceleration  $\alpha$ , the middle figure describes the rotational velocity  $\omega$ , and the lower figure describes the permanent wall rotation  $\theta$ .

The top Case 1 figure depicts the case of a (labeled) negative triangular area between the linear angular deceleration  $\alpha$  line and the time line (i.e.,  $NegativeArea_{-\alpha+}$  by Equation 3.41), being of less magnitude than the positive value for  $\omega$  at time  $t_i$  (designated  $\omega_0$ ). Consequently, the wall will remain in rotation during the entire time-step  $DT$ . At the increment in time lhsDT after time  $t_i$ , a portion of the negative deceleration area reduces

---

<sup>1</sup> Note the assumption of a linear variation in angular acceleration  $\alpha$  over the time-step  $DT$  in Figure 3.12.

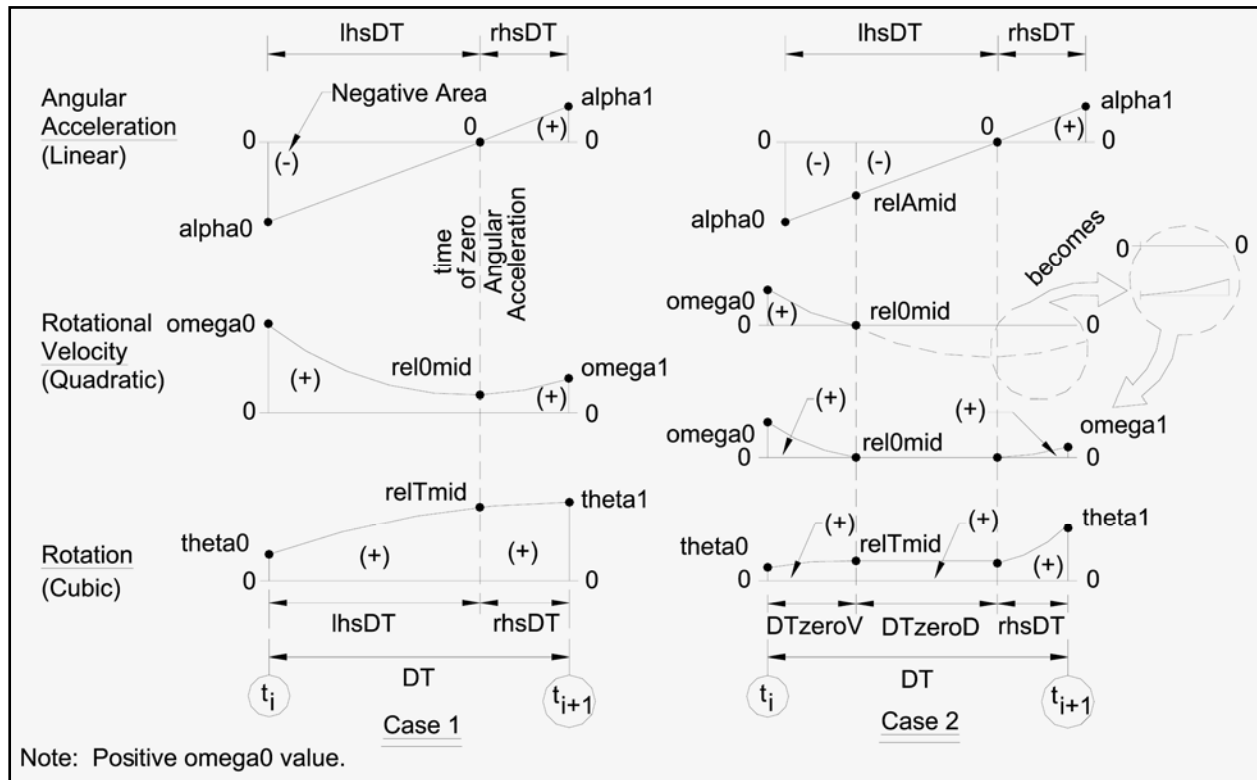


Figure 3.12. Two possible outcomes for the case of a negative angular acceleration at time  $t_i$  and a positive angular acceleration at time  $t_{i+1}$ .

the value of rotational velocity  $\omega$  from the positive value of magnitude  $\omega_{00}$  at time  $t_i$  to a smaller magnitude value at time  $[t_i \text{ plus } lhsDT]$ , as shown in this figure. The rotational velocity  $\omega$  at time  $[t_i \text{ plus } lhsDT]$  is

$$rel\omega_{mid} = \omega_{00} + \frac{1}{2} \cdot lhsDT \cdot (\alpha_{00} + 0) \tag{3.42}$$

The *change* in rotation from time  $t_i$  to time  $[t_i \text{ plus } lhsDT]$  is equal to the labeled positive area between the quadratic  $\omega$  curve and the time line. At time  $[t_i \text{ plus } lhsDT]$  the wall rotation increases in magnitude from  $\theta_{00}$  to  $rel\theta_{mid}$ .

$$rel\theta_{mid} = \theta_{00} + lhsDT \cdot \omega_{00} + \frac{(lhsDT)^2}{6} \cdot (2 \cdot \alpha_{00} + 0) \tag{3.43}$$

The wall continues in motion, with positive angular velocity  $\omega$  and with additional permanent rotation  $\theta$  after time  $[t_i \text{ plus } lhsDT]$  when the angular acceleration of the wall is positive. At time  $[t_i \text{ plus } lhsDT]$  the magnitude of wall rotational velocity  $\omega$  begins to increase in magnitude as

a result of the positive angular reacceleration of the wall. The positive (labeled) triangular area between the time line and the linear angular acceleration  $\alpha$  line, shown in the top Case 1 figure, equals the *change* in  $\omega$  and for the wall, consequently, the value for  $\omega$  at time  $t_{i+1}$  (labeled  $\omega_{i+1}$  in the Case 1 middle figure) is

$$\omega_{i+1} = \omega_{mid} + \frac{1}{2} \cdot \alpha_{DT} \cdot (0 + \alpha_{i+1}) \quad 3.44$$

The *change* in wall rotation from time  $[t_i \text{ plus } \Delta t]$  to time  $t_{i+1}$  is equal to the integral of the positive rotational velocity of the middle  $\omega$ -figure. The permanent wall rotation,  $\theta$ , increases in value from  $\theta_{mid}$  to  $\theta_{i+1}$ , as depicted in the bottom figure.

$$\theta_{i+1} = \theta_{mid} + \Delta t \cdot \omega_{mid} + \frac{(\Delta t)^2}{6} \cdot (2 \cdot 0 + \alpha_{i+1}) \quad 3.45$$

**Case 2:** This case results when the positive value for  $\omega$  at time  $t_i$  is less than the magnitude of  $\text{NegativeArea}_{-\alpha}$  (i.e., the negative area between the negative portion of the linear acceleration line and the time line over the portion of the Figure 3.12 time increment labeled  $\Delta t$ ). The four right-hand side figures in Figure 3.12 are used to describe the Case 2 step-by-step solution scheme. From the top to bottom, one figure describes the angular acceleration,  $\alpha$ , two figures describe the rotational velocity,  $\omega$ , and one figure describes the permanent wall rotation,  $\theta$ .

The top, right-hand side, Case 2 figure depicts the case of a (labeled) negative triangular area between the linear angular deceleration  $\alpha$  line and the time line, being of greater magnitude than the positive value for  $\omega$  at time  $t_i$  (designated  $\omega_0$ ). Consequently, the wall will come to rest before time  $t_{i+1}$  is achieved. At an increment in time  $\Delta t_{zeroV}$  after time  $t_i$ , a portion of the negative deceleration area reduces the value of rotational velocity  $\omega$  from the positive value of magnitude  $\omega_0$  at time  $t_i$  to a value of 0 at time  $[t_i \text{ plus } \Delta t_{zeroV}]$ , as shown in this figure. At time  $[t_i \text{ plus } \Delta t_{zeroV}]$  the angular acceleration is

$$\alpha_{mid} = \Delta t_{zeroV} \cdot \left( \frac{\alpha_0}{\Delta t} \right) \quad 3.46$$

where DTzeroD is the time increment shown in Figure 3.12. The Figure 3.12 negative  $\alpha$  area below time increment DTzeroV is

$$AreaTrapezoid_{-\alpha+} = \frac{1}{2} \bullet DTzeroV \bullet (\alpha0 + relAmid) \quad 3.47$$

The Figure 3.12 negative  $\alpha$  area below time increment DTzeroD is

$$AreaTriangle_{-\alpha+} = \frac{1}{2} \bullet DTzeroD \bullet (relAmid + 0) \quad 3.48$$

Thus, the total Figure 3.12 negative  $\alpha$  area below time increment lhsDT is

$$NegativeArea_{-\alpha+} = AreaTrapezoid_{-\alpha+} + AreaTriangle_{-\alpha+} \quad 3.49$$

The rotational velocity  $\omega$  at time [t<sub>i</sub> plus DTzeroV] is

$$rel0mid = \omega0 + AreaTrapezoid_{-\alpha+} \quad 3.50$$

With a value for relomid equal to zero, Equation 3.50 becomes

$$0 = \omega0 + AreaTrapezoid_{-\alpha+} \quad 3.51$$

Expanding by adding the term AreaTriangle<sub>- $\alpha$ +</sub> to both sides, Equation 3.51 becomes

$$AreaTriangle_{-\alpha+} = \omega0 + AreaTrapezoid_{-\alpha+} + AreaTriangle_{-\alpha+} \quad 3.52$$

Which by introducing Equation 3.49, becomes

$$AreaTriangle_{-\alpha+} = \omega0 + NegativeArea_{-\alpha+} \quad 3.53$$

Introducing Equations 3.48 and 3.46 and solving for DTzeroD, Equation 3.53 becomes

$$DTzeroD = \sqrt{2 \bullet \left( \frac{lhsDT}{\alpha0} \right) \bullet (\omega0 + NegativeArea_{-\alpha+})} \quad 3.54$$

Recognizing the time increment lhsDT is equivalent to

$$lhsDT = DTzeroV + DTzeroD \quad 3.55$$

and by introducing Equation 3.55 and 3.47 into Equation 3.54 and solving for DTzeroV,

$$DTzeroV = lhsDT - \sqrt{2 \cdot \left( \frac{lhsDT}{alpha0} \right) \cdot (\omega_0 + NegativeArea_{-\alpha+})} \quad 3.56$$

The *change* in rotation from time  $t_i$  to time  $[t_i \text{ plus } DTzeroV]$  is equal to the labeled positive area between the quadratic  $\omega$  curve and the time line. At time  $[t_i \text{ plus } DTzeroV]$  the wall rotation increases in magnitude from  $\theta_0$  to  $relTmid$ . The rotational velocity  $\omega$  at time  $[t_i \text{ plus } DTzeroV]$ , expressed in terms of DTzeroV, is

$$relOmid = \omega_0 + \frac{1}{2} \cdot DTzeroV \cdot (\alpha_0 + relAmid) \quad 3.57$$

with the angular acceleration at time  $[t_i \text{ plus } DTzeroV]$  equal to

$$relAmid = \alpha_0 + \left( \frac{\alpha_1 - \alpha_0}{DT} \right) \cdot DTzeroV \quad 3.58$$

The *change* in rotation from time  $t_i$  to time  $[t_i \text{ plus } DTzeroV]$  is equal to the labeled positive area between the quadratic  $\omega$  curve and the time line. At time  $[t_i \text{ plus } DTzeroV]$  the wall rotation increases in magnitude from  $\theta_0$  to  $relTmid$ .

$$relTmid = \theta_0 + DTzeroV \cdot \omega_0 + \frac{(DTzeroV)^2}{6} \cdot (2 \cdot \alpha_0 + relAmid) \quad 3.59$$

The wall remains at rest with zero angular velocity,  $\omega$ , and with no additional permanent rotation,  $\theta$ , from time  $[t_i \text{ plus } DTzeroV]$  until time  $[t_i \text{ plus } lhsDT]$  when the angular acceleration of the wall begins (again). At time  $[t_i \text{ plus } lhsDT]$  the wall begins to develop further permanent rotation about its toe as a result of the positive angular reacceleration of the wall. The positive (labeled) triangular area between the time line and the linear angular deceleration  $\alpha$  line, shown in the right-hand side of the top figure, equals the *change* in  $\omega$  and with the wall at rest, consequently, the value for  $\omega$  at time  $t_{i+1}$  (labeled  $\omega_1$  in the lower  $\omega$  figure) is

$$\omega_1 = \frac{1}{2} \cdot \alpha_{DT} \cdot (0 + \alpha_1) \quad 3.60$$

The *change* in wall rotation from time  $[t_i \text{ plus } \Delta t]$  to time  $t_{i+1}$  is equal to the integral of the positive rotational velocity, as depicted in the middle two, right-hand side  $\omega$ -figures. The top  $\omega$  figure being a computational figure, and the bottom  $\omega$  figure being the  $\omega$  curve-shift figure that properly accounts for zero wall rotational velocity over time increment  $\Delta t_{zero}$ , with an insert detailed, curve-shift figure for  $\omega$  shown of this computational  $\omega$  figure in Figure 3.12. The permanent wall rotation,  $\theta$ , increases in value from  $\theta_{mid}$  to  $\theta_1$ , as depicted in the bottom figure.

$$\theta_1 = \theta_{mid} + \alpha_{DT} \cdot 0 + \frac{(\alpha_{DT})^2}{6} \cdot (2 \cdot 0 + \alpha_1) \quad 3.61$$

### 3.8.4 Negative angular accelerations $\alpha_0$ and $\alpha_1$ at times $t_i$ and $t_{i+1}$

Next consider a wall in motion (i.e., with a positive value for  $\omega$ ) at time  $t_i$  but with the Figure 3.13 case of a negative value for  $\alpha$  computed using Equation 3.26 at time-steps  $t_i$  and  $t_{i+1}$ .<sup>1</sup> The first step is to determine if the wall, which is in motion at time  $t_i$ , comes to rest during the time-step  $\Delta t$ .

The negative area between the negative portion of the linear acceleration line and the time line over the Figure 3.13 time increment  $\Delta t$  is

$$\text{NegativeArea}_{-\alpha} = \frac{1}{2} \cdot \Delta t \cdot (\alpha_0 + \alpha_1) \quad 3.62$$

There are two possible outcomes for the Figure 3.13 step-by-step numerical solution for  $\omega$  and of  $\theta$  at time  $t_{i+1}$ , depending upon the magnitude of  $\omega_0$  relative to the magnitude of Equation 3.62  $\text{NegativeArea}_{-\alpha}$ . These possible scenarios are depicted by two columns of figures in Figure 3.13, labeled as Case 1 and Case 2 figure groups.

<sup>1</sup> Again, note the assumption of a linear variation in angular acceleration  $\alpha$  over the time-step  $\Delta t$  shown in Figure 3.13.

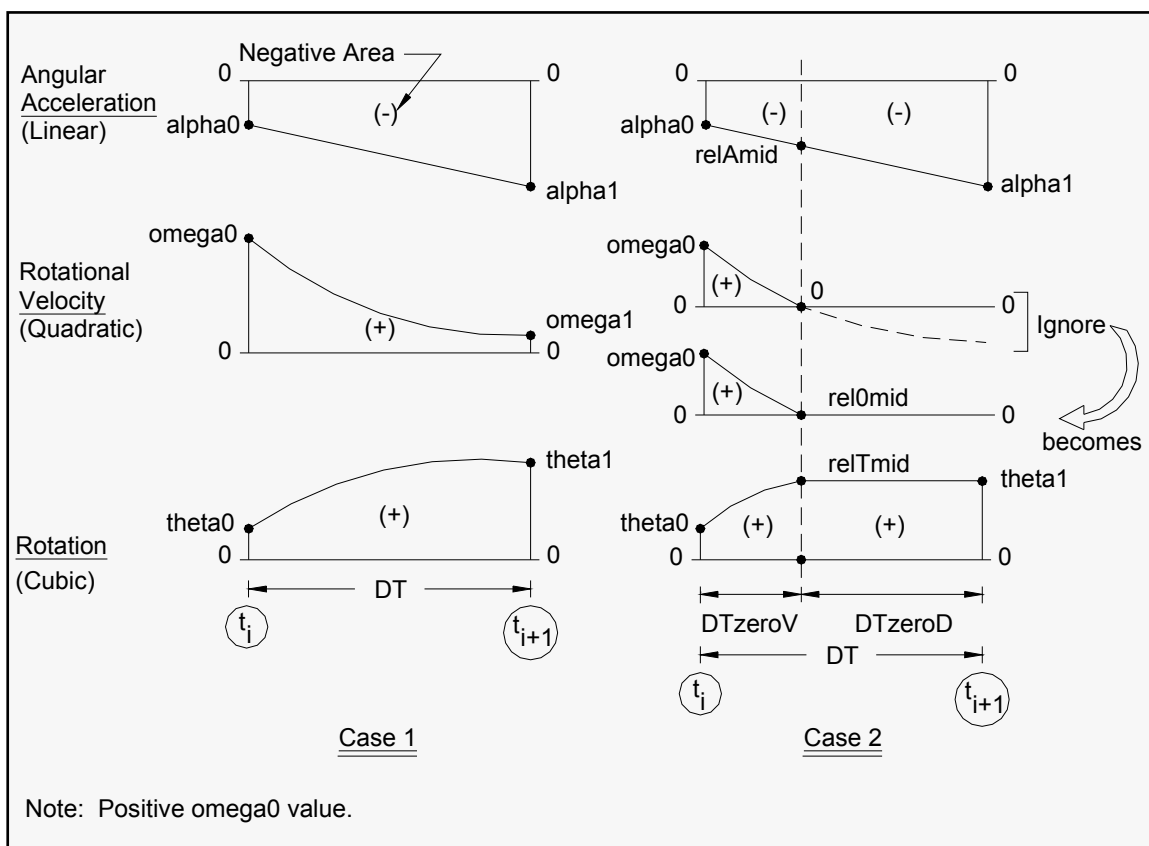


Figure 3.13. Two possible outcomes for the case of negative angular accelerations at times  $t_i$  and  $t_{i+1}$ .

**Case 1:** This case results when the positive value for  $\omega$  at time  $t_i$  is greater than the magnitude of  $NegativeArea_{-\alpha-}$  (i.e., the negative area between the negative portion of the linear acceleration line and the time line over the Figure 3.13 time-step  $DT$ ). The three left-hand side figures in Figure 3.13 are used to describe the Case 1 step-by-step solution scheme: The top figure describes the angular acceleration,  $\alpha$ , the middle figure describes the rotational velocity,  $\omega$ , and the lower figure describes the permanent wall rotation,  $\theta$ .

The top Case 1 figure depicts the case of a (labeled) negative area between the linear angular deceleration,  $\alpha$ , line and the time line (i.e.,  $NegativeArea_{-\alpha-}$  by Equation 3.62), being of less magnitude than the positive value for  $\omega$  at time  $t_i$  (designated  $\omega_{00}$ ). Consequently, the wall will remain in rotation during the entire time-step  $DT$ . At the time-step  $DT$  after time  $t_i$ , the negative deceleration area reduces the value of rotational velocity,  $\omega$ , from the positive value of magnitude  $\omega_{00}$  at time  $t_i$  to a smaller magnitude value at time  $[t_i \text{ plus } DT]$ , as shown in this figure. The rotational velocity,  $\omega$ , at time  $[t_i \text{ plus } DT]$  is



$$\omega_1 = \omega_0 + \frac{1}{2} \cdot DT \cdot (\alpha_0 + \alpha_1) \quad 3.63$$

The *change* in rotation from time  $t_i$  to time  $[t_i \text{ plus } DT]$  is equal to the labeled positive area between the quadratic  $\omega$  curve and the time line. At time  $[t_i \text{ plus } DT]$  the wall rotation increases in magnitude from  $\theta_0$  to  $\theta_1$ .

$$\theta_1 = \theta_0 + DT \cdot \omega_0 + \frac{(DT)^2}{6} \cdot (2 \cdot \alpha_0 + \alpha_1) \quad 3.64$$

**Case 2:** This case results when the positive value for  $\omega$  at time  $t_i$  is less than the magnitude of  $\text{NegativeArea}_{-\alpha-}$  (i.e., the negative area between the negative portion of the linear acceleration line and the time line over the portion of the Figure 3.13 time increment labeled  $\text{lhsDT}$ ). The four right-hand side figures in Figure 3.13 are used to describe the Case 2 step-by-step solution scheme. From the top to bottom, one figure describes the angular acceleration,  $\alpha$ , two figures describe the rotational velocity,  $\omega$ , and one figure describes the permanent wall rotation,  $\theta$ .

The top, right-hand side, Case 2 figure depicts the case of a (labeled) negative area between the linear angular deceleration  $\alpha$  line and the time line (i.e.,  $\text{NegativeArea}_{-\alpha-}$  by Equation 3.62), being of greater magnitude than the positive value for  $\omega$  at time  $t_i$  (designated  $\omega_0$ ). Consequently, the wall will come to rest before time  $t_{i+1}$  is achieved. At an increment in time  $DT_{\text{zeroV}}$  after time  $t_i$ , a portion of the negative deceleration area reduces the value of rotational velocity,  $\omega$ , from the positive value of magnitude  $\omega_0$  at time  $t_i$  to a value of 0 at time  $[t_i \text{ plus } DT_{\text{zeroV}}]$ , as shown in this figure. At time  $[t_i \text{ plus } DT_{\text{zeroV}}]$  the angular acceleration is

$$\text{relAmid} = \alpha_0 + DT_{\text{zeroV}} \cdot \left( \frac{\alpha_1 - \alpha_0}{DT} \right) \quad 3.65$$

where  $DT_{\text{zeroV}}$  is the time increment shown in Figure 3.13. The Figure 3.13 negative  $\alpha$  area below time increment  $DT_{\text{zeroV}}$  is

$$\text{AreaTrapezoid}_{-\alpha-} = \frac{1}{2} \cdot DT_{\text{zeroV}} \cdot (\alpha_0 + \text{relAmid}) \quad 3.66$$

Introducing Equations 3.65, Equation 3.66 becomes

$$AreaTrapezoid_{-\alpha-} = \left\{ \begin{array}{l} \frac{1}{2} \cdot DTzeroV \cdot \alpha0 + \frac{DTzeroV}{2} \\ \bullet \left[ \alpha0 + DTzeroV \cdot \left( \frac{\alpha1 - \alpha0}{DT} \right) \right] \end{array} \right\} \quad 3.67$$

This simplifies to

$$AreaTrapezoid_{-\alpha-} = DTzeroV \cdot \alpha0 + \frac{(DTzeroV)^2}{2} \bullet \left( \frac{\alpha1 - \alpha0}{DT} \right) \quad 3.68$$

The *change* in rotation from time  $t_i$  to time  $[t_i \text{ plus } DTzeroV]$  is equal to the labeled positive area between the quadratic  $\omega$  curve and the time line. At time  $[t_i \text{ plus } DTzeroV]$  the wall rotation increases in magnitude from  $\theta_{\alpha0}$  to  $relTmid$ . The rotational velocity  $\omega$  at time  $[t_i \text{ plus } DTzeroV]$  is

$$relOmid = \omega_{\alpha0} + AreaTrapezoid_{-\alpha-} \quad 3.69$$

With a value for  $relOmid$  equal to zero, Equation 3.69 becomes

$$0 = \left[ \frac{1}{2} \bullet \left( \frac{\alpha1 - \alpha0}{DT} \right) \right] \bullet (DTzeroV)^2 + \alpha0 \bullet DTzeroV + \omega_{\alpha0} \quad 3.70$$

This quadratic equation has a general solution of

$$DTzeroV = \frac{-\alpha0 \pm \sqrt{(\alpha0)^2 - 4 \bullet \left[ \frac{1}{2} \bullet \left( \frac{\alpha1 - \alpha0}{DT} \right) \right] \bullet \omega_{\alpha0}}}{2 \bullet \left[ \frac{1}{2} \bullet \left( \frac{\alpha1 - \alpha0}{DT} \right) \right]} \quad 3.71$$

Even though this solution provides for two possible values for  $DTzeroV$ , only the positive value is assigned to  $DTzeroV$  in  $C_{orps}W_{allRotate}$ .

The *change* in rotation from time  $t_i$  to time  $[t_i \text{ plus } DTzeroV]$  is equal to the labeled positive area between the quadratic  $\omega$  curve and the time line.

At time  $[t_i \text{ plus } DT_{zeroV}]$  the wall rotation increases in magnitude from  $\theta_0$  to  $relT_{mid}$ .

$$relT_{mid} = \theta_0 + DT_{zeroV} \cdot \omega_0 + \frac{(DT_{zeroV})^2}{6} \cdot (2 \cdot \alpha_0 + relA_{mid}) \quad \text{bis 3.59}$$

The wall remains at rest with zero angular velocity  $\omega$  and with no additional permanent rotation  $\theta$  from time  $[t_i \text{ plus } DT_{zeroV}]$  until time  $[t_i \text{ plus } DT]$ . Consequently, at time  $t_{i+1}$  the permanent wall rotation  $\theta$  is constant, as depicted in the bottom figure.

$$\theta_1 = relT_{mid} \quad 3.72$$

with the value for  $relT_{mid}$  given by Equation 3.59.

### 3.8.5 Positive angular acceleration $\alpha_0$ at time $t_i$ and negative angular acceleration $\alpha_1$ at $t_{i+1}$

Next consider a wall in motion (i.e., with a positive value for  $\omega$ ) at time  $t_i$  but with the Figure 3.14 case of a positive value for  $\alpha$  computed using Equation 3.26 at time-step  $t_i$  and negative value for  $\alpha$  computed using Equation 3.26 at the next time-step of  $t_{i+1}$ .<sup>1</sup> The first step is to determine the time instant  $[t_i \text{ plus } lhsDT]$  at which the angular acceleration  $\alpha$  is equal to zero, as labeled in the figure. By linear interpolation, this time increment  $lhsDT$  is

$$lhsDT = \left| \alpha_0 \cdot \left( \frac{DT}{\alpha_1 - \alpha_0} \right) \right| \quad \text{bis 3.40}$$

The positive area between the positive portion of the linear acceleration line and the time line over the Figure 3.14 time increment  $lhsDT$  is

$$PositiveArea_{+\alpha-} = \frac{1}{2} \cdot lhsDT \cdot (\alpha_0 + 0) \quad 3.73$$

The Figure 3.14 time increment  $rhsDT$  is given by

---

<sup>1</sup> Again, observe the assumption of a linear variation in angular acceleration  $\alpha$  over the time-step  $DT$  shown in Figure 3.14.

$$rhsDT = DT - lhsDT \quad 3.74$$

The negative area between the negative portion of the linear acceleration line and the time line over the Figure 3.14 time increment rhsDT is

$$NegativeArea_{+\alpha-} = \frac{1}{2} \bullet rhsDT \bullet (0 + \alpha_1) \quad 3.75$$

There are two possible outcomes for the Figure 3.14 step-by-step numerical solution for  $\omega$  and of  $\theta$  at time  $t_{i+1}$ , depending upon the magnitude of  $\omega_0$  relative to the magnitude of the sum of the  $PositiveArea_{+\alpha-}$  plus the  $NegativeArea_{+\alpha-}$ . These possible scenarios are depicted by two columns of figures in Figure 3.14, labeled as Case 1 and Case 2 figure groups.

**Case 1:** This case results if (a) the  $NegativeArea_{+\alpha-}$  exceeds  $PositiveArea_{+\alpha-}$  but the positive value for  $\omega$  at time  $t_i$  is greater than the magnitude of the negative sum of  $PositiveArea_{+\alpha-}$  plus  $NegativeArea_{+\alpha-}$ , or (b) the  $NegativeArea_{+\alpha-}$  is less than  $PositiveArea_{+\alpha-}$ , consequently the positive value for  $\omega_0$  at time  $t_i$  will increase to a larger value of  $\omega_1$  at time  $t_{i+1}$  (with an increase equal to the positive sum of  $PositiveArea_{+\alpha-}$  plus  $NegativeArea_{+\alpha-}$ ). The three left-hand side figures in Figure 3.14 are used to describe the Case 1 step-by-step solution scheme: The top figure describes the angular acceleration,  $\alpha$ , the middle figure describes the rotational velocity,  $\omega$ , and the lower figure describes the permanent wall rotation,  $\theta$ .

The top Case 1 figure depicts the case of a wall remaining in rotation during the entire time-step DT because either (a) the  $NegativeArea_{+\alpha-}$  exceeds  $PositiveArea_{+\alpha-}$  but the positive value for  $\omega$  at time  $t_i$  is greater than the magnitude of the sum of  $PositiveArea_{+\alpha-}$  plus  $NegativeArea_{+\alpha-}$ , or because (b) the  $NegativeArea_{+\alpha-}$  is less than  $PositiveArea_{+\alpha-}$ . At the increment in time lhsDT after time  $t_i$ , the positive acceleration area increases the value of rotational velocity,  $\omega$ , from the positive value of magnitude  $\omega_0$  at time  $t_i$  to a larger magnitude value at time  $[t_i$  plus

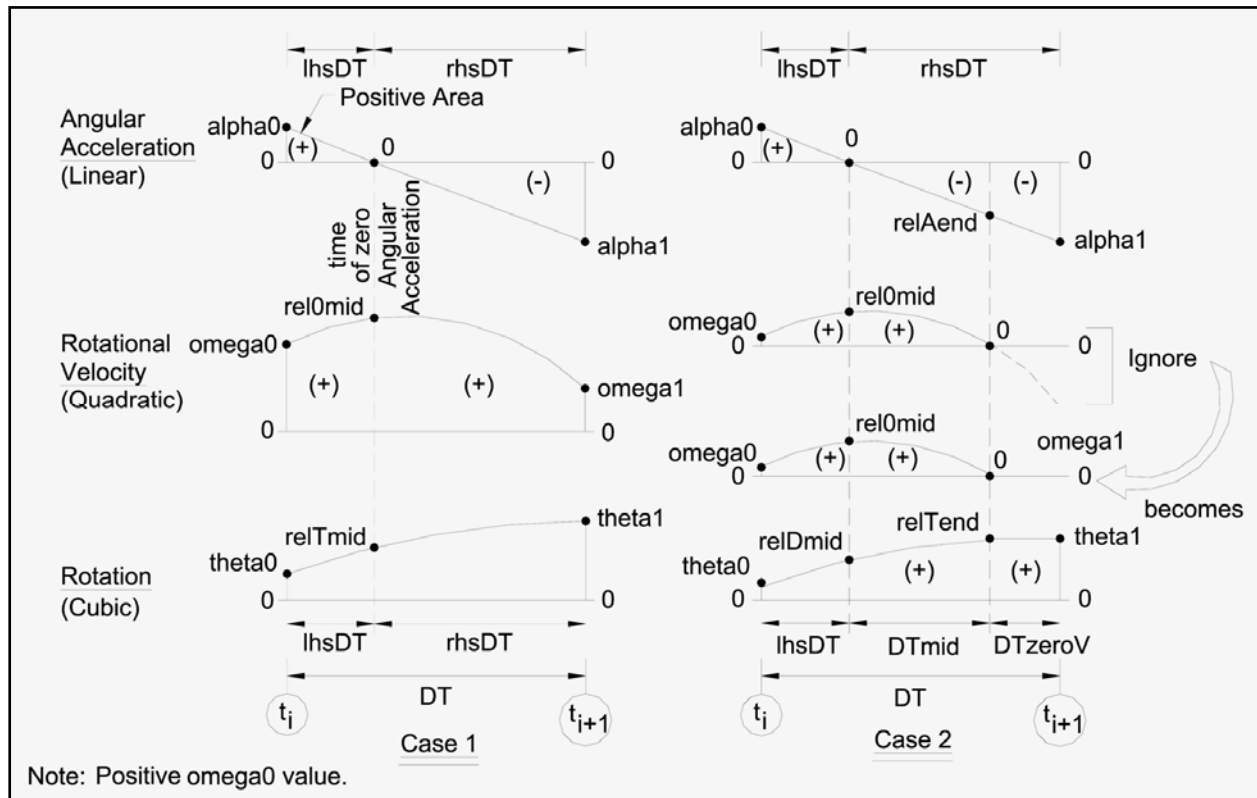


Figure 3.14. Two possible outcomes for the case of a positive angular acceleration at time  $t_i$  and a negative angular acceleration at time  $t_{i+1}$ .

lhsDT], as shown in this figure. The rotational velocity,  $\omega$ , at time  $[t_i$  plus lhsDT] is

$$relOmid = \omega_0 + \frac{1}{2} \cdot lhsDT \cdot (\alpha_0 + 0) \tag{bis 3.42}$$

The *change* in rotation from time  $t_i$  to time  $[t_i$  plus lhsDT] is equal to the labeled positive area between the quadratic  $\omega$  curve and the time line. At time  $[t_i$  plus lhsDT] the wall rotation increases in magnitude from  $\theta_{tao}$  to  $relTmid$ .

$$relTmid = \theta_{tao} + lhsDT \cdot \omega_0 + \frac{(lhsDT)^2}{6} \cdot (2 \cdot \alpha_0 + 0) \tag{bis 3.43}$$

The wall continues in motion, with positive angular velocity,  $\omega$ , and with additional permanent rotation,  $\theta$ , after time  $[t_i$  plus lhsDT] when the angular acceleration of the wall is positive. At time  $[t_i$  plus lhsDT] the

magnitude of wall rotational velocity,  $\omega$ , begins to decrease in magnitude as a result of the angular deceleration of the wall. The negative (labeled) triangular area between the time line and the linear angular deceleration  $\alpha$  line, shown in the top Case 1 figure, equals the *change* in  $\omega$  and for the wall. Consequently, the value for  $\omega$  at time  $t_{i+1}$  (labeled  $\omega_{a1}$  in the Case 1 middle figure) is

$$\omega_{a1} = \omega_{mid} + \frac{1}{2} \cdot \alpha_{DT} \cdot (0 + \alpha_{a1}) \quad \text{bis 3.44}$$

The *change* in wall rotation from time  $[t_i \text{ plus } \Delta t]$  to time  $t_{i+1}$  is equal to the integral of the positive rotational velocity of the middle  $\omega$ -figure. The permanent wall rotation,  $\theta$ , increases in value from  $\theta_{mid}$  to  $\theta_{a1}$ , as depicted in the bottom figure.

$$\theta_{a1} = \theta_{mid} + \Delta t \cdot \omega_{mid} + \frac{(\Delta t)^2}{6} \cdot (2 \cdot \omega_{mid} + \alpha_{a1}) \quad \text{bis 3.45}$$

**Case 2:** This case results when the  $\text{NegativeArea}_{+\alpha-}$  exceeds  $\text{PositiveArea}_{+\alpha-}$  and the positive value for  $\omega$  at time  $t_i$  is less than the magnitude of the sum of  $\text{PositiveArea}_{+\alpha-}$  plus  $\text{NegativeArea}_{+\alpha-}$ . The four right-hand side figures in Figure 3.14 are used to describe the Case 2 step-by-step solution scheme. From the top to bottom, one figure describes the angular acceleration,  $\alpha$ , two figures describe the rotational velocity,  $\omega$ , and one figure describes the permanent wall rotation,  $\theta$ .

The top, right-hand side, Case 2 figure depicts the case of the sum of a (labeled) positive triangular area between the linear angular deceleration  $\alpha$  line and the time line (i.e.,  $\text{PositiveArea}_{+\alpha-}$  by Equation 3.73) plus a (labeled) negative triangular area between the linear angular deceleration  $\alpha$  line and the time line (i.e.,  $\text{NegativeArea}_{+\alpha-}$  by Equation 3.75), being negative and of greater magnitude than the positive value for  $\omega$  at time  $t_i$  (designated  $\omega_{a0}$ ). Consequently, the wall will come to rest before time  $t_{i+1}$  is achieved.

At time  $[t_i \text{ plus } \Delta t]$  the wall's rotational velocity increases in magnitude from  $\omega_{a0}$  to  $\omega_{mid}$ . The rotational velocity  $\omega$  at time  $[t_i \text{ plus } \Delta t]$  is

$$relOmid = \omega_0 + \frac{1}{2} \cdot l_{hsDT} \cdot (\alpha_0 + 0) \quad \text{bis 3.42}$$

with the angular acceleration at time [  $t_i$  plus  $l_{hsDT}$ ] equal to zero.

The *change* in rotation from time  $t_i$  to time [  $t_i$  plus  $l_{hsDT}$ ] is equal to the labeled positive area between the quadratic  $\omega$  curve and the time line. At time [  $t_i$  plus  $l_{hsDT}$ ] the wall rotation increases in magnitude from  $\theta_0$  to  $relDmid$ .

$$relDmid = \theta_0 + l_{hsDT} \cdot \omega_0 + \frac{(l_{hsDT})^2}{6} \cdot (2 \cdot \alpha_0 + 0) \quad 3.76$$

At an increment in time [  $l_{hsDT} + DT_{mid}$ ] after time  $t_i$ , a portion of the negative deceleration area reduces the value of rotational velocity  $\omega$  from the positive value of magnitude  $relOmid$  at time [  $t_i$  plus  $l_{hsDT}$ ] to a value of 0 at time [  $t_i$  plus  $(l_{hsDT} + DT_{mid})$ ], as shown in this figure. At time [  $t_i$  plus  $(l_{hsDT} + DT_{mid})$ ] the angular acceleration is

$$relAend = DT_{mid} \cdot \left( \frac{\alpha_1}{r_{hsDT}} \right) \quad 3.77$$

where  $DT_{mid}$  is the time increment shown in Figure 3.14. The Figure 3.14 negative  $\alpha$  area below time increment  $DT_{mid}$  is

$$AreaTriangle_{+\alpha-} = \frac{1}{2} \cdot DT_{mid} \cdot (0 + relAend) \quad 3.78$$

The Figure 3.14 negative  $\alpha$  area below time increment  $DT_{zeroV}$  is

$$AreaTrapezoid_{+\alpha-} = \frac{1}{2} \cdot DT_{zeroV} \cdot (relAend + \alpha_1) \quad 3.79$$

Thus, the total Figure 3.14 negative  $\alpha$  area below time increment  $r_{hsDT}$  is

$$NegativeArea_{+\alpha-} = AreaTrapezoid_{+\alpha-} + AreaTriangle_{+\alpha-} \quad 3.80$$

With the rotational velocity  $\omega$  at time [  $t_i$  plus  $(l_{hsDT} + DT_{mid})$ ] equal to zero,

$$0 = relOmid + AreaTriangle_{+\alpha-} \quad 3.81$$

By introducing Equations 3.42, 3.73, 3.77, and 3.78, and solving for DTmid, Equation 3.81 becomes

$$DTmid = \sqrt{-2 \cdot \left( \frac{rhsDT}{alpha1} \right) \cdot (\omega_0 + PositiveArea_{+\alpha-})} \quad 3.82$$

At time [t<sub>i</sub> plus (lhsDT+DTmid)] the wall comes to rest with

$$relTend = relDmid + DTmid \cdot relOmid + \frac{(DTmid)^2}{6} \cdot (2 \cdot 0 + relAend) \quad 3.83$$

The wall remains at rest with zero angular velocity,  $\omega$ , and with no additional permanent rotation,  $\theta$ , from time [t<sub>i</sub> plus (lhsDT+DTmid)] until time t<sub>i+1</sub>. The permanent wall rotation,  $\theta$ , at this time t<sub>i+1</sub> is

$$theta1 = relTend \quad 3.84$$

### 3.8.6 Starting the C<sub>orps</sub>W<sub>all</sub>Rotate analysis and the initiation of wall rotation during a DT time-step

*Start of the step-by-step time-history analysis:* The numerical formulation used in the step-by-step time-history analysis by C<sub>orps</sub>W<sub>all</sub>Rotate assumes that the wall is at rest at the start of the analysis (i.e., at time t<sub>i</sub> equal to 0 and with i = 1). Consequently,  $\alpha$ ,  $\omega$ , and  $\theta$  are equal to zero as an initial boundary condition at the first time-step (i.e., with i = 1).

*Initiation of wall rotation during the first DT time-step:* At the end of the first DT time-step, at time increment t<sub>2</sub> (i.e., t<sub>i+1</sub> and with i = 1 so the subscript i + 1 becomes 2), a *trial* angular acceleration value is computed by C<sub>orps</sub>W<sub>all</sub>Rotate using Equation 3.26. If a positive value for  $\alpha$  is computed at time increment t<sub>2</sub>, the system is in motion during this first time-step DT. This means that the correct value for  $\alpha$  was computed using Equation 3.26.

However, if a negative value for  $\alpha$  is computed and the system has been at rest and with zero angular acceleration at time t<sub>1</sub> = 0 (i.e., t<sub>i</sub> and for i = 1), the system is at rest at time t<sub>2</sub>. This means that the correct value for  $\alpha$  is



zero at time  $t_2$  and not the negative value computed using Equation 3.26. Stating this another way and referring to Equation 3.26, a negative value for  $\alpha$  results when negative moments due to the clockwise stabilizing forces acting about the toe of the wall are greater than the moments due to the counterclockwise overturning (i.e., destabilizing) forces acting about the toe. Consequently a fictitious, negative value results from Equation 3.26 and the correct value for  $\alpha$  is zero at time  $t_2$  (or more generally,  $t_{i+1}$ ).

*Initiation of wall rotation during a DT time-step:* A wall is at rest at the beginning of any DT time-step (designated time  $t_i$  in Figures 3.10 through 3.14) when  $\omega$  and  $\theta$  are equal to zero. At all DT time-steps other than the first time-step, the values at time  $t_i$  for  $\alpha$ ,  $\omega$ , and  $\theta$  were computed during the previous time-step and then assigned as known values for this next time-step. The step-by-step numerical procedure implemented in `CorpsWallRotate` allows for wall rotation to initiate during any DT time-step during earthquake shaking. This will occur for a wall at rest at time  $t_i$ , i.e., the start of the time-step, when a positive value is computed for  $\alpha$  using Equation 3.26 at time  $t_{i+1}$ . The numerical procedure outlined in Figure 3.11 allows for the computation of  $\omega$  and  $\theta$  at time  $t_{i+1}$  for this case.

### 3.8.7 Cessation of wall rotation

A wall is in motion at the start of any DT time-step (designated time  $t_i$  in Figures 3.10 through 3.14) when  $\omega$  is nonzero. The step-by-step numerical procedure implemented in `CorpsWallRotate` allows for wall rotation to terminate during any DT time-step during earthquake shaking. This occurs when the deceleration of the wall is sufficiently large during time-step DT. The applicable numerical procedures are labeled as Case 2 in Figures 3.13 and 3.14.

In the case of wall rotation decelerating and with negative values for  $\alpha$  at times  $t_i$  and  $t_{i+1}$  during time-step DT, the rotational velocity,  $\omega$ , at time  $t_{i+1}$  (designated  $\omega_1$ ) and the wall rotation,  $\theta$ , at time  $t_{i+1}$  (designated  $\theta_1$ ) are made using the Case 2 approach outlined in Figure 3.13. The value for  $\alpha$  at time  $t_{i+1}$  (designated  $\alpha_1$ ) is made using Equation 3.26. Note the rotational velocity reduces to zero at a time increment  $DT_{zeroV}$  after time  $t_i$ . The wall remains at rest and with zero rotational velocity over time increment  $DT_{zeroD}$ , as shown in this figure.

In the case of wall rotation decelerating and with a positive value for  $\alpha$  at time  $t_i$  and a negative value for  $\alpha$  at time  $t_{i+1}$  during time-step DT, the

rotational velocity,  $\omega$ , at time  $t_{i+1}$  (designated  $\omega_{i+1}$ ) and the wall rotation,  $\theta$ , at time  $t_{i+1}$  (designated  $\theta_{i+1}$ ) are made using the Case 2 approach outlined in Figure 3.14. The value for  $\alpha$  at time  $t_{i+1}$  (designated  $\alpha_{i+1}$ ) is made using Equation 3.26. Note the rotational velocity reduces to zero at a time increment  $[\text{lhsDT} + \text{DTmid}]$  after time  $t_i$ . The wall remains at rest and with zero rotational velocity over time increment  $\text{DTzeroV}$ , as shown in this figure.

Note that wall rotation can begin again at a later point in time, as described in the subsection 3.8.6 paragraph entitled “initiation of wall rotation during a DT time-step.”

### **3.9 New rotational analysis model of a wall retaining a partially submerged backfill and rotating about its toe and buttressed by a reinforced concrete slab**

The formulation for a rock-founded wall retaining a partially submerged backfill and for the case of a pool in front of the retaining wall is summarized in this subsection. The formulation presented is an extension of the moist backfill formulation discussed in the previous sections of this chapter. Water pressures are assumed to act along three faces of the structural wedge denoted as the toe, base, and the heel regions of Figure 3.15. Forces acting on the toe are due to the presence of a pool of water in front of the wall. A leaking vertical joint is assumed between the base slab and the structural wedge with water pressures above the toe controlled by the presence of the pool. The computation of water pressures acting on this partially submerged structural wedge is discussed in detail in Appendix D.<sup>1</sup> The Figure 3.15 distributions of water pressures are converted into equivalent resultant forces, expressed in global x- and y-coordinates, and their points of application along each of the three regions. These resultant water pressure forces are used in an effective stress based stability analysis of the structural wedge. Dynamic considerations for the pool during earthquake shaking are accounted for in the analysis using hydrodynamic water pressures computed using the Westergaard (1931) procedure of analysis (see Appendix D). The hydrodynamic water pressure resultant force,  $P_{wd}$  (Equation D.5), is shown acting on the structural wedge in this figure (and shown acting in a

---

<sup>1</sup> In the initial  $C_{\text{orpsWallRotate}}$  version, no excess pore water pressures due to earthquake-induced shear strains within the soil regions are included in the current  $C_{\text{orpsWallRotate}}$  formulation (i.e., the excess pore water pressure ratio  $r_u$  is equal to zero). Refer to Ebeling and Morrison (1992) for a complete description and discussion of  $r_u$ .

direction consistent with the direction of positive horizontal acceleration,  $+a_h$ ).

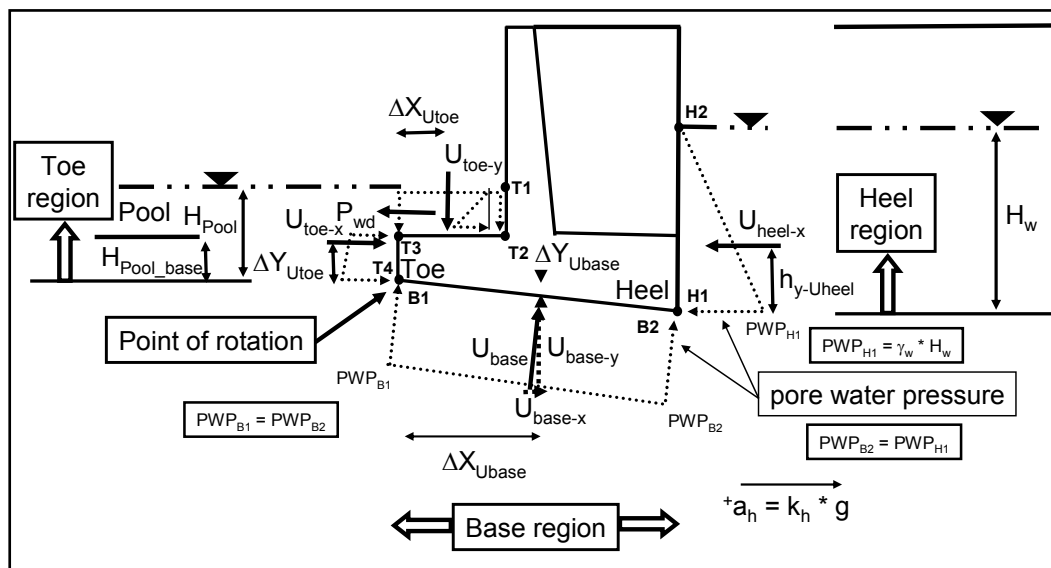


Figure 3.15. Control points, water pressures, and corresponding resultant forces acting normal to faces of the three regions of a structural wedge rotating about its toe—effective stress analysis.

In the case of rotation about the toe, contact between the base of the structural wedge and the foundation is lost sometime during earthquake shaking. Recall that a simplistic rigid base assumption is made in this formulation for rock-founded earth retaining structures. Due to the possible formation of a gap sometime during earthquake shaking, the Figure 3.15 pore water pressure distribution is used along the base. Note that this distribution differs from the steady-state pore water pressures resulting from a structural wedge in full contact with the rock foundation, shown in Figure D.1. The exact pore water distribution within the structure-to-foundation gap is a complex problem and a subject for state-of-the-art research. In *C<sub>orps</sub>W<sub>all</sub>Rotate*, it is recognized that the Figure 3.15 (or, equivalently, Figure D.4) pore water pressure distribution along the base of the structural wedge makes the simplistic assumption of the hydrostatic pore water pressure at the heel of the wall extends along the entire base of the structural wedge. It is based on the assumption that a gap opens early on during earthquake shaking during rotation about the toe of the retaining wall.

The resultant water pressure forces  $U_{toe}$ ,  $U_{base}$ ,  $U_{heel}$ , and  $P_{wd}$  shown in Figure 3.15 are superimposed on the free-body diagram of forces acting on

the Figure 3.5 structural wedge, resulting in the Figure 3.16 free-body diagram. Recall  $P_{resist}$  is the force provided by the reinforced concrete (toe) slab.

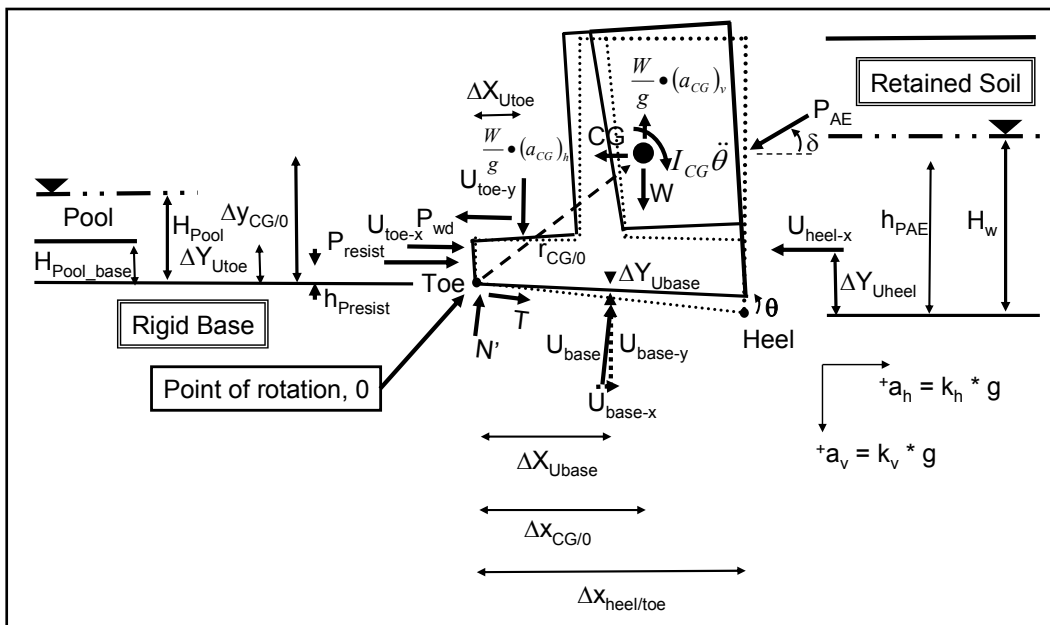


Figure 3.16. Inertia forces and resultant force vectors acting on a rigid block model of a (inclined base) cantilever wall retaining a partially submerged backfill with rotation about the toe of the wall during horizontal and vertical shaking of the inclined rigid base—effective stress analysis.

### 3.9.1 Threshold value of acceleration corresponding to incipient lift-off of the base of the wall in rotation—partially submerged backfill

At the onset of lift-off of the (inclined) base of the Figure 3.16 retaining wall subject to pure rotation about its toe, the rotating (i.e., overturning) moment equals the stabilizing (i.e., restoring) moment. The summation of moments about point o of the Figure 3.16 forces acting on a rigid body with results in the following modified form of Equation 3.8,

$$\begin{aligned}
 & \frac{W}{g} \cdot (a_{CG})_h \cdot \Delta y_{CG/0} + \frac{W}{g} \cdot (a_{CG})_v \cdot \Delta x_{CG/0} + P_{AE} \cdot \cos(\delta) \cdot [(y_{heel} + h_{PAE}) - y_{toe}] \\
 & + U_{heel-x} \cdot [(y_{heel} + \Delta Y_{Uheel}) - y_{toe}] + U_{base-y} \cdot \Delta X_{Ubase} + U_{base-x} \cdot \Delta Y_{Ubase} + \\
 & P_{wd} \cdot [H_{Pool\_base} + 0.4 \cdot (H_{Pool} - H_{Pool\_base})] = \qquad \qquad \qquad 3.85 \\
 & P_{resist} \cdot h_{Presist} + W \cdot \Delta x_{CG/0} + P_{AE} \cdot \sin(\delta) \cdot \Delta x_{heel/toe} \\
 & + U_{toe-x} \cdot \Delta Y_{Utoe} + U_{toe-y} \cdot \Delta X_{Utoe}
 \end{aligned}$$

Note that  $\ddot{\theta}$  is a very small number at the *onset* of lift-off and is set equal to zero as its limiting value when deriving this relationship. The component of the threshold acceleration occurring at lift-off of the base is designated as

$$(a_{CG})_{\text{threshold-rotation-h}} = (k_{CG})_{\text{threshold-rotation-h}} \cdot g \quad \text{bis 3.9}$$

where  $(k_{CG})_{\text{threshold-rotation-h}}$  is a value of horizontal ground acceleration, expressed in decimal fraction. Note that the horizontal acceleration value  $[(k_{CG})_{\text{threshold-rotation-h}} \text{ times } g]$  is not a user-specified constant.

For a user-specified constant<sup>1</sup> for vertical acceleration [i.e.,  $(a_{CG})_v = \text{constant}$ ], CorpsWallRotate solves Equation 3.85 by introducing  $(a_{CG})_{\text{threshold-rotation-h}}$  and  $(k_{CG})_{\text{threshold-rotation-h}}$  for  $(a_{CG})_h$  and  $(k_{CG})_h$ . Because of the inclusion of acceleration in  $P_{AE}$  formulation (refer to Appendix A), CorpsWallRotate solves Equation 3.85 using a trial-and-error numerical approach. The value of horizontal acceleration at incipient lift-off in rotation is reported in the WORKrotate.TMP output file generated in each CorpsWallRotate analysis. This file may be viewed using the visual modeler boxes labeled Show Lift-Off Evaluation on the Analysis tab.

In CorpsWallRotate output data files the Equation 3.85 moments acting about the point of rotation (set equal to toe position of the toe in this initial version of CorpsWallRotate) of the structural wedge are grouped into Overturning Moments and Restoring Moments, which are defined as

$$\begin{aligned} \text{Overturning Moments} = & \\ & \frac{W}{g} \cdot (a_{CG})_h \cdot \Delta y_{CG/O} + \frac{W}{g} \cdot (a_{CG})_v \cdot \Delta x_{CG/O} + P_{AE} \cdot \cos(\delta) \cdot [(y_{heel} + h_{PAE}) - y_{toe}] \\ & + U_{heel-x} \cdot [(y_{heel} + \Delta Y_{Uheel}) - y_{toe}] + U_{base-y} \cdot \Delta X_{Ubase} + U_{base-x} \cdot \Delta Y_{Ubase} + \\ & P_{wd} \cdot [H_{Pool\_base} + 0.4 \cdot (H_{Pool} - H_{Pool\_base})] \end{aligned} \quad 3.86$$

and

<sup>1</sup> A procedure for determining the value for this constant (for vertical acceleration) is discussed in Section 4.10.

$$\begin{aligned}
 &\text{Restoring Moments} = \\
 &P_{resist} \cdot h_{Presist} + W \cdot \Delta X_{CG/0} + P_{AE} \cdot \sin(\delta) \cdot \Delta X_{heel/toe} \\
 &+ U_{toe-x} \cdot \Delta Y_{Utoe} + U_{toe-y} \cdot \Delta X_{Utoe}
 \end{aligned} \tag{3.87}$$

In a total stress analysis the internal pore water pressure force terms  $U_{base}$  and  $U_{heel}$  are excluded from Equations 3.85 through 3.87 and  $c'$  is set equal to  $S_u$  with  $\phi'$  set equal to zero. Additionally,  $N'$  is set equal to  $N$ .

Since the horizontal limiting acceleration is of interest, another option is a simplified form of Equation 3.85 that may be derived by setting the vertical component of acceleration in the incipient lift-off in rotation equal to zero, as done by Nadim and Whitman (1984). By making this assumption and introducing Equation 3.9, Equation 3.85 becomes

$$\begin{aligned}
 &(k_{CG})_{threshold-rotation-h} = \\
 &\frac{
 \begin{aligned}
 &P_{resist} \cdot h_{Presist} + W \cdot \Delta X_{CG/0} + P_{AE} \cdot \sin(\delta) \cdot \Delta X_{heel/toe} + \\
 &U_{toe-x} \cdot \Delta Y_{Utoe} + U_{toe-y} \cdot \Delta X_{Utoe} - P_{AE} \cdot \cos(\delta) \cdot [(y_{heel} + h_{PAE}) - y_{toe}] - \\
 &U_{heel-x} \cdot [(y_{heel} + \Delta Y_{Uheel}) - y_{toe}] - U_{base-y} \cdot \Delta X_{Ubase} - U_{base-x} \cdot \Delta Y_{Ubase} - \\
 &P_{wd} \cdot [H_{Pool\_base} + 0.4 \cdot (H_{Pool} - H_{Pool\_base})]
 \end{aligned}
 }{
 W \cdot \Delta y_{CG/0}
 }
 \end{aligned} \tag{3.88}$$

Because of the inclusion of acceleration in  $P_{AE}$  formulation (refer to Appendix A),  $C_{orps}W_{all}Rotate$  solves Equation 3.88 using a trial-and-error numerical approach.

In a total stress analysis the internal pore water pressure force terms  $U_{base}$  and  $U_{heel}$  are excluded from Equations 3.85 and 3.88.

### 3.9.2 Moments due to external forces acting about the toe of the structural wedge—partially submerged backfill

The Figure 3.16 (inclined base) cantilever wall retaining partially submerged backfill and with pool, is subjected to the nine *external* forces of the weight of the structural wedge,  $W$ , the dynamic active earth pressure force,  $P_{AE}$ , the resisting force,  $P_{resist}$ , provided by the reinforced concrete slab at the toe of the wall, and the horizontal and vertical components of the rigid base-to-wall reaction forces  $T$  and  $N'$ , respectively, acting through the toe of the wall as well as the resultant water pressure forces  $U_{toe}$ ,  $U_{base}$ ,

$U_{heel}$ , and  $P_{wd}$ . For the partially submerged backfill with pool in front of the wall, the moment due to these external forces about the point o at toe of the wall (counterclockwise positive) is

$$\begin{aligned} \sum M_o = & -W \cdot \Delta x_{CG/o} - P_{resist} \cdot h_{Presist} - P_{AE} \cdot \sin(\delta) \cdot \Delta x_{heel/toe} \\ & + P_{AE} \cdot \cos(\delta) \cdot [(y_{heel} + h_{PAE}) - y_{toe}] - U_{toe-y} \cdot \Delta X_{Utoe} - U_{toe-x} \cdot \Delta Y_{Utoe} \\ & + U_{base-y} \cdot \Delta X_{Ubase} + U_{base-x} \cdot \Delta Y_{Ubase} + U_{heel-x} \cdot [(y_{heel} + \Delta Y_{Uheel}) - y_{toe}] \\ & + P_{wd} \cdot [H_{Pool\_base} + 0.4 \cdot (H_{Pool} - H_{Pool\_base})] \end{aligned} \quad 3.89$$

Since the foundation reaction shear force  $T$  and normal force  $N'$  act through point o during rotation, they do not contribute to the moment. At each instant in time during earthquake shaking, the horizontal and vertical accelerations vary in direction. Thus, the magnitudes of  $P_{AE}$  and  $h_{PAE}$  and  $P_{wd}$  vary as well.

In a total stress analysis the internal pore water pressure force terms  $U_{base}$  and  $U_{heel}$  are excluded from Equation 3.89.

### 3.9.3 Angular acceleration of the structural wedge wall retaining a partially submerged backfill—formulation implemented in CorpsWallRotate

The relationship defining the angular acceleration of the retaining wall structural wedge that is implemented in CorpsWallRotate is derived by introducing Equation 3.89 into Equation 3.19. When rotation has initiated, the angular acceleration of the structural wedge is

$$\alpha = \frac{\left\{ \begin{aligned} & -W \cdot \Delta x_{CG/o} - P_{resist} \cdot h_{Presist} - P_{AE} \cdot \sin(\delta) \cdot \Delta x_{heel/toe} \\ & + P_{AE} \cdot \cos(\delta) \cdot [(y_{heel} + h_{PAE}) - y_{toe}] - U_{toe-y} \cdot \Delta X_{Utoe} - U_{toe-x} \cdot \Delta Y_{Utoe} \\ & + U_{base-y} \cdot \Delta X_{Ubase} + U_{base-x} \cdot \Delta Y_{Ubase} + U_{heel-x} \cdot [(y_{heel} + \Delta Y_{Uheel}) - y_{toe}] \\ & + P_{wd} \cdot [H_{Pool\_base} + 0.4 \cdot (H_{Pool} - H_{Pool\_base})] \\ & + \frac{W}{g} \cdot [(k_h \cdot g) \cdot \Delta y_{CG/o} + (k_v \cdot g) \cdot \Delta x_{CG/o}] \end{aligned} \right\}}{I_o} \quad 3.90$$

with the mass moment of inertia about the point o (the of rotation) given by

$$I_o = I_{CG} + \frac{W}{g} \cdot (r_{CG/o})^2 \quad \text{bis 3.16}$$

Recall  $\alpha$  (or, equivalently,  $\ddot{\theta}$ ) is the angular acceleration of the structural wedge of (total) mass  $M$  ( $=W/g$ ) about point of rotation, point  $o$ . The resulting engineering formulation is implemented in the corresponding software  $C_{orps}W_{all}Rotate$  and will perform a rotating analysis of each user-specified retaining wall section. The output files for  $C_{orps}W_{all}Rotate$  report the Overturning Moments (Equation 3.86) and Restoring Moments (Equation 3.87) as well as the angular acceleration  $\alpha$  at each time-step  $t_i$ . Consequently, when viewing computed results using the visual Post-Processor of  $C_{orps}W_{all}Rotate$ , it is more convenient to express Equation 3.90 as

$$\alpha = \frac{\{OverturningMoments - Restoring Moments\}}{I_o} \quad 3.91$$

In a total stress analysis the internal pore water pressure force terms  $U_{base}$  and  $U_{heel}$  are excluded from Equations 3.90 and 3.91.

#### **3.9.4 Numerical method for computing the rotational time-history of a rigid block retaining structure rotating about its toe**

Earthquake acceleration time-histories are used to represent the earthquake demand in a rotational analysis of rigid body structural wedge (permanent) rotation. A step-by-step solution scheme is followed in order to obtain the wall's rotational velocity,  $\omega$ , and rotation,  $\theta$ , in the time domain by  $C_{orps}W_{all}Rotate$ . An overview of the characteristics of this numerical formulation is given in section 3.8. Equation 3.26 for angular acceleration,  $\alpha$ , is replaced by Equation 3.90 in this discussion for the case of a wall retaining a partially submerged backfill with a pool in front.

#### **3.10 Effective vertical acceleration constant value for the incipient lift-off in rotation evaluation process**

In a rotational analysis (i.e., KEYanalysis = 2 of Group 7, Appendix F) the complete, user-specified vertical acceleration (time-history) may be requested for use in the time-history analysis. Alternatively, a constant value for vertical acceleration may be used during the time-history analysis of permanent wall rotation and/or in the analysis of the threshold horizontal acceleration at incipient lift-off in rotation. This section



describes a new procedure for determining an effective, representative constant value for vertical acceleration.

In Section 4.6, a new procedure for determining an approximate, constant, effective value for vertical acceleration in a Newmark (1965) sliding block maximum transmissible acceleration analysis of earth retaining structures is proposed. This same procedure may also be used to determine the effective constant vertical acceleration for the acceleration pulses generating wall rotation for the incipient lift-off evaluation process and computation of the horizontal acceleration value  $[(k_{CG})_{\text{threshold-rotation-h}} \text{ times } g]$ .

In an incipient lift-off in wall rotation evaluation analysis of a retaining structure,  $C_{\text{orps}}W_{\text{allRotate}}$  allows the user to specify a constant value for vertical acceleration to be used in the equilibrium Equation 3.85 when computing (in a trial-and-error numerical procedure) the value for horizontal acceleration  $[(k_{CG})_{\text{threshold-rotation-h}} \text{ times } g]$ . This software implements the following two new methods to help determine a representative value for the constant vertical acceleration:

**Method 1 - average vertical acceleration value:** Using the user-specified horizontal acceleration time-history and the user-provided constant value for vertical (Y) acceleration, the value for horizontal acceleration at incipient lift-off in wall rotation,  $(a_{CG})_{\text{threshold-rotation-h}}$  is computed and a rotating block time-history analysis is performed. The software then identifies at which  $i$  time increments that *incremental* rotation,  $(\theta_r)_i$ , takes place and the total number of incremental time-step increments  $i$  during which rotation occurs, designated  $n_{\text{rotation}}$ . The average vertical acceleration value for the user-specified vertical acceleration time-history is computed for all these  $i$  time increments using the relationship

$$(a_{CG})_{v\text{-ave}} = \frac{\sum_i^{n_{\text{rotation}}} (a_v)_i}{n_{\text{rotation}}} \quad 3.92$$

The sign for the average vertical acceleration,  $(a_v)_i$ , during each select time increment  $i$  for which incremental rotation occurs is maintained in this calculation.

A trial-and-error procedure is used to determine the appropriate value for the constant vertical acceleration value. The primary author of this report usually starts with a constant vertical (Y) acceleration value set equal to zero. An incipient lift-off in wall rotation evaluation analysis is made, including a computation made by  $C_{orps}W_{all}Rotate$  using Equation 3.92 to determine a value for  $(a_{CG})_{v-ave}$ . Then a second incipient lift-off in wall rotation evaluation analysis is made in which the constant vertical acceleration value is set equal to the previously computed value for  $(a_{CG})_{v-ave}$  by the user. This second computation results in an updated value for  $(a_{CG})_{v-ave}$ . The iterative process is repeated until the difference between old and new values is minor; usually within four computations.

**Method 2 - weighted vertical acceleration value:** This approach is a variation of Method 1. Using the user specified horizontal acceleration time-history and the user-provided constant value for vertical (Y) acceleration, the value for horizontal acceleration at incipient lift-off in wall rotation,  $(a_{CG})_{threshold-rotation-h}$ , is computed and a rotational time-history analysis is performed. The software then identifies at which  $i$  time increments during which incremental rotation,  $(\theta_r)_i$ , takes place and the total number of time increments  $i$  during which rotation occurs is designated  $n_{rotation}$ . The total rotation is

$$\theta_r = \sum_i^{n_{rotation}} (\theta_r)_i \quad 3.93$$

A weighted vertical acceleration value is computed for the user-specified vertical acceleration time-history with average vertical acceleration value,  $(a_v)_i$ , computed for each time increment  $i$  of incremental rotations using the following relationship

$$(a_{CG})_{v-weighted} = \sum_i^{n_{rotation}} \left\{ (a_v)_i \cdot \left[ \frac{(\theta_r)_i}{\theta_r} \right] \right\} \quad 3.94$$

Again, the sign for the average vertical acceleration,  $(a_v)_i$ , during each select time increment  $i$  of incremental rotations is maintained in this calculation.

A trial-and-error procedure is used to determine the appropriate value for the constant vertical acceleration value. The primary author of this report usually starts with a constant vertical (Y) acceleration value set equal to

zero. An incipient lift-off in wall rotation and rotational time-history analysis is made, including a computation made by  $C_{\text{orps}}W_{\text{allRotate}}$  using Equations 3.93 and 3.94 to determine a value for  $(a_{\text{CG}})_{\text{v-weighted}}$ . Then a second incipient lift-off in wall rotation analysis is made in which the constant vertical (Y) acceleration value is set equal to the previously computed value for  $(a_{\text{CG}})_{\text{v-weighted}}$  by the user. This second computation results in an updated value for  $(a_{\text{CG}})_{\text{v-weighted}}$ . The process is repeated until the difference between old and new values is minor; usually within four computations.

Method 2 differs from Method 1 in that the weighting factor applied to each of the average vertical acceleration,  $(a_v)_i$ , values at the  $i$  time increments of incremental rotation is assigned according to the relative magnitude of incremental rotations occurring at each time increment. Method 1 applies a uniform weighting factor.

## 4 New Translational Block Analysis Model of a Retaining Structure Buttressed by a Reinforced Concrete Slab

### 4.1 Introduction

This chapter describes a new engineering formulation developed for computing the permanent translational response to earthquake ground motions of *toe-restrained*, rock-founded retaining walls. The resulting engineering formulation is implemented within corresponding PC software  $C_{\text{orps}}W_{\text{all}}\text{Rotate}$  using a GUI for input of geometry, input of material properties, input/verification of earthquake time-history files, and visualization of results. (Key aspects of the visual modeler and visual post-processor  $C_{\text{orps}}W_{\text{all}}\text{Rotate}$  are described in Chapter 5.)

A key result from the translational (i.e., sliding) block method of analysis is the computation of the permanent deformation of a retaining structural system due to a user-specified design earthquake event. This design earthquake event is represented by an acceleration time-history specified within the rock-foundation base. Chapter 1 discussed the numerous variations of rigid sliding block methods of seismic analysis as applied to slopes, earthen dams, retaining wall systems, and foundations. They all have their roots in the methodology outlined in Newmark (1965) and what has come to be known as the Newmark sliding block model (Section 1.1.3). This chapter discusses the formulation of the translational (rigid) block analysis of the Figure 4.1 cantilever retaining structure buttressed by, e.g., a concrete slab at its toe, as implemented in  $C_{\text{orps}}W_{\text{all}}\text{Rotate}$  for Corps retaining walls. The effect of this reinforced concrete slab is represented by the user-specified force  $P_{\text{resist}}$  acting on a vertical section extending upwards from the toe of the wall. Strom and Ebeling (2004) present a simplified engineering procedure to estimate the magnitude of  $P_{\text{resist}}$ .

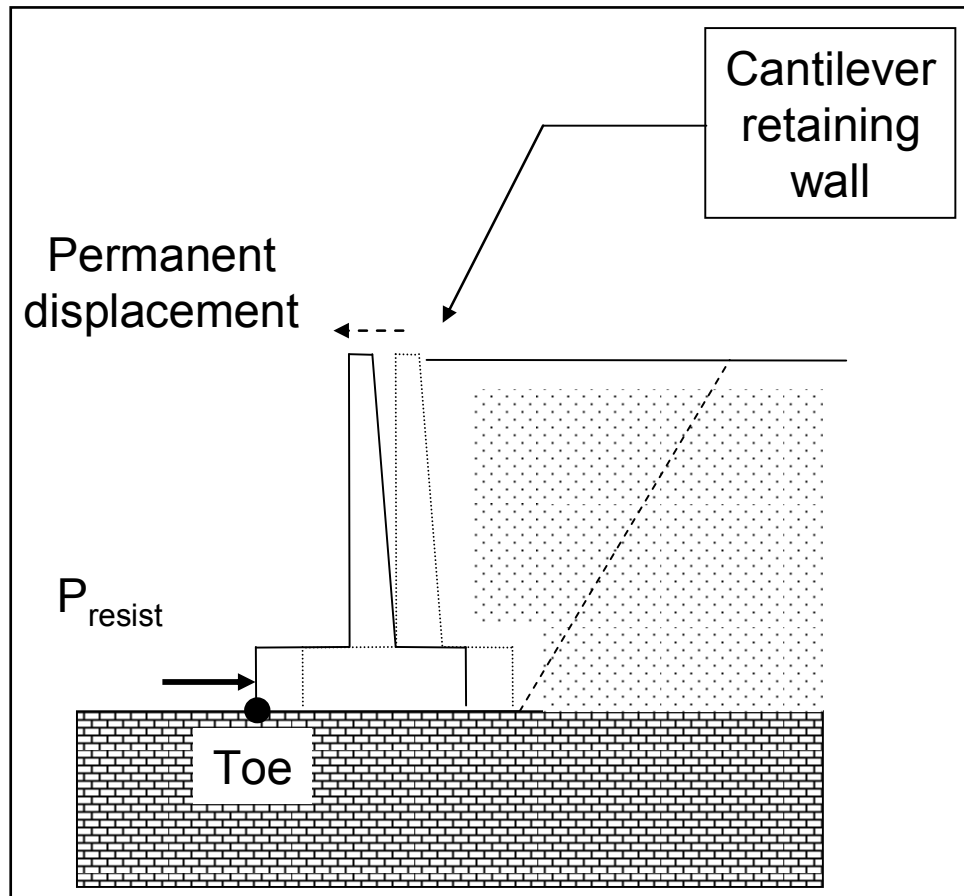


Figure 4.1. Permanent, seismically induced displacement of a rock-founded cantilever wall retaining moist backfill and with toe restraint, computed using CorpsWallRotate.

## 4.2 Contrasting a translational with the rotational analysis of a rigid block

A rotational analysis of permanent deformation of a retaining wall during earthquake shaking was discussed in Chapter 3. An important difference between the translational (i.e., Newmark sliding) block method of analysis for earth retaining structures and the rotational analysis of a retaining structure modeled as a rigid block is *the acceleration imparted to the rigid block*. When a rigid block undergoes permanent *sliding* displacement during earthquake shaking, the largest magnitude horizontal acceleration felt by the rigid block (and the retaining structure contained within the rigid block model) is *less* than the peak value for ground acceleration, as depicted in Figure 1.8. Ebeling and Morrison (1992) designated the value for a retaining wall's maximum transmissible acceleration as  $N^*g$ . The maximum transmissible acceleration,  $N^*g$ , is sometimes referred to as the yield acceleration; it is not the user-defined, horizontal ground (or, equivalently, the rigid base) acceleration. Contrast this to the response of a

rigid block that undergoes *rotation* during earthquake shaking; the accelerations felt by this rigid block during shaking are those of the ground acceleration time-history. This is because continuous contact between the rigid block undergoing rotation and the ground (modeled as a rigid base) is maintained at the point of rotation (e.g., the toe of the Figure 3.1 retaining wall) during the entire earthquake shaking process. The acceleration imparted to the center of mass of a rotating rigid block is discussed in Sections 1.2 and 3.2.

### ***Does a wall slide or does it rotate during earthquake shaking?***

The first step in determining if the retaining wall will rotate prior to sliding during earthquake shaking, or vice versa, is to compute (1) the value of acceleration that is needed for lift-off of the wall from its base in rotation about the toe of the wall using the procedure outlined in Chapter 3; and (2) the limiting acceleration required to reduce the factor of safety against sliding to a limiting value of 1.0 (commonly referred to as the maximum transmissible acceleration using the procedure outlined in this chapter). These two computations are accomplished by the software `CorpsWallRotate`. The second step is to compare these limiting acceleration values. For the simplified decoupled analyses outlined in this report, the mode of deformation is dictated by the smaller of the two acceleration values.

## **4.3 Maximum transmissible acceleration**

In the earthquake-induced translational displacement analysis of a retaining wall, the primary variable is the permanent displacement. A user-defined (ground) acceleration time-history is applied to the Figure 4.2 rigid base on which the retaining wall is founded in the idealized model. The seismic inertia coefficient ( $N^*$  in Ebeling and Morrison (1992) terminology) that reduces the sliding factor of safety for the driving soil wedge and the structural wedge to unity is first determined. The value for the maximum transmissible acceleration (i.e.,  $N^*g$ ; the yield acceleration in Ebeling and Morrison (1992) terminology) is the horizontal acceleration imparted to the retaining wall system, consisting of the driving wedge and structural wedge (see Figure 1.7), that will nominally exceed the shear resistance provided by the foundation along (or immediately below) the interface between the base of the retaining structure and the foundation. The driving soil wedge (Figure A.1) is represented by the dynamic force  $P_{AE}$  in the Figure 4.2 free-body diagram of the structural wedge figure showing the dynamic forces acting on a rigid block model of the structural

wedge with sliding along its base during shaking of the rigid base.<sup>1</sup> This cantilever wall, which retains moist backfill, is subjected to the five external forces of the weight of the structural wedge  $W$ , the dynamic active earth pressure force  $P_{AE}$ , the resisting force  $P_{resist}$  provided by the reinforced concrete slab at the toe of the wall, and the rigid base-to-wall reaction shear and normal forces  $T$  and  $N'$ , respectively. The procedure outlined in Section 3.6 and Appendix A are used to compute the value of  $P_{AE}$  at each acceleration time-history time-step. The structural wedge and driving soil wedges are assumed to act as a single rigid body, as shown in Figure 1.7. Thus, inertial forces due to the acceleration values applied at a given time-step to the structural and driving wedges impact the magnitude of  $P_{AE}$ , as outlined in the sweep-search soil wedge solution procedure summarized in Appendix A. Consequently, when the value for acceleration of the rigid block changes with time-steps, the value of  $P_{AE}$  changes as well.

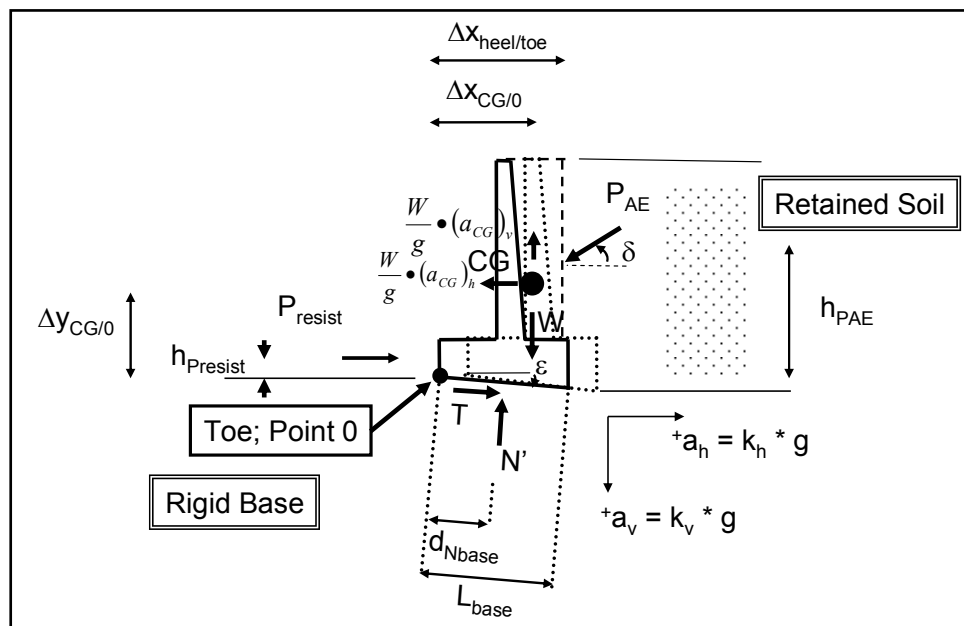


Figure 4.2. Inertia forces and resultant force vectors acting on a rigid block model of a cantilever wall retaining moist backfill with sliding along its base during horizontal and vertical shaking of the inclined rigid base.

At the onset of sliding of the Figure 4.2 retaining wall, the horizontal driving force equals the stabilizing (i.e., restoring) force. The summation of the Figure 4.2 horizontal forces acting on the rigid body results in

<sup>1</sup> The inertial forces are applied according to D'Alembert's principle. The advantage of the inertia-force method based on D'Alembert's principle is that it converts a dynamics problem into an equivalent problem in equilibrium.

$$\frac{W}{g} \cdot (a_{CG})_h + P_{AE} \cdot \cos(\delta) = P_{resist} + T \cdot \cos(\varepsilon) + N' \cdot \sin(\varepsilon) \quad 4.1$$

T is the shear force required for equilibrium of forces acting on the structural wedge. At incipient sliding, the shear strength along the base to foundation interface becomes fully mobilized (i.e.,  $FS_{slide} = 1.0$ ). Assuming a full mobilization of shear resistance along the base (of length  $L_{base}$ ), the shear force may be computed utilizing the Mohr-Coulomb failure criteria, in an effective stress analysis, as

$$T = c'_{base} \cdot L_{base} + N' \cdot \tan(\delta'_{base}) \quad 4.2$$

Introducing Equation 4.2, Equation 4.1 becomes

$$\begin{aligned} \frac{W}{g} \cdot (a_{CG})_h + P_{AE} \cdot \cos(\delta) = \\ P_{resist} + [c' \cdot L_{base} + N' \cdot \tan(\delta'_{base})] \cdot \cos(\varepsilon) + N' \cdot \sin(\varepsilon) \end{aligned} \quad 4.3$$

Simplifying, Equation 4.3 becomes

$$\begin{aligned} \frac{W}{g} \cdot (a_{CG})_h + P_{AE} \cdot \cos(\delta) = \\ P_{resist} + c' \cdot L_{base} \cdot \cos(\varepsilon) + N' \cdot [\tan(\delta'_{base}) \cdot \cos(\varepsilon) + \sin(\varepsilon)] \end{aligned} \quad 4.3$$

The summation of the Figure 4.2 vertical forces acting on the rigid body results in

$$0 = N' \cdot \cos(\varepsilon) - T \cdot \sin(\varepsilon) - W + \frac{W}{g} \cdot (a_{CG})_v - P_{AE} \cdot \sin(\delta) \quad 4.4$$

Introducing Equation 4.2, Equation 4.4 becomes

$$\begin{aligned} 0 = N' \cdot \cos(\varepsilon) - [c' \cdot L_{base} + N' \cdot \tan(\delta'_{base})] \cdot \sin(\varepsilon) \\ - W + \frac{W}{g} \cdot (a_{CG})_v - P_{AE} \cdot \sin(\delta) \end{aligned} \quad 4.5$$

Simplifying, Equation 4.5 becomes



$$N' = \frac{c' \cdot L_{base} \cdot \sin(\varepsilon) + W - \frac{W}{g} \cdot (a_{CG})_v + P_{AE} \cdot \sin(\delta)}{\cos(\varepsilon) - \tan(\delta'_{base}) \cdot \sin(\varepsilon)} \quad 4.6$$

Introducing Equation 4.6, Equation 4.3 becomes

$$\frac{W}{g} \cdot (a_{CG})_h + P_{AE} \cdot \cos(\delta) = P_{resist} + c' \cdot L_{base} \cdot \cos(\varepsilon) + \left\{ \frac{c' \cdot L_{base} \cdot \sin(\varepsilon) + W - \frac{W}{g} \cdot (a_{CG})_v + P_{AE} \cdot \sin(\delta)}{\cos(\varepsilon) - \tan(\delta'_{base}) \cdot \sin(\varepsilon)} \right\} \cdot [\tan(\delta'_{base}) \cdot \cos(\varepsilon) + \sin(\varepsilon)] \quad 4.7$$

Equation 4.7 represents the equilibrium relationship for the (rigid) structural wedge when the earthquake accelerations are such that the factor of safety against sliding along its base is equal to 1.0. For a factor of safety > 1.0 against sliding, the retaining wall does not slide. The rigid body CG accelerations are the same as the rigid base accelerations (i.e., within the rock foundation). However, the accelerations felt by the rigid body (i.e., at its center of gravity, CG) will differ from the rigid base accelerations for user-defined rigid base acceleration (time-history) values that exceed the value for acceleration that results in a factor of safety against sliding equal to 1.0. During sliding, the acceleration felt by the rigid body at its center of gravity, CG, is of constant magnitude.

The component of the threshold acceleration occurring at translation (i.e., sliding) along the base is designated as

$$(a_{CG})_{threshold-sliding-h} = (k_{CG})_{threshold-sliding-h} \cdot g \quad 4.8$$

where  $(k_{CG})_{threshold-sliding-h}$  is a value of horizontal ground acceleration, expressed in decimal fraction. In Ebeling and Morrison (1992), the acceleration  $(a_{CG})_{threshold-sliding-h}$  is referred to as the maximum transmissible acceleration ( $N \cdot g$ ) or as the yield acceleration. Note that the horizontal acceleration value [ $(k_{CG})_{threshold-sliding-h}$  times  $g$ ] is a not a user-specified constant. Since the horizontal limiting acceleration is of interest, one option is to set the vertical component of acceleration occurring at

sliding equal to zero, as done by Richards and Elms (1979) and others.<sup>1</sup> By making this assumption and introducing Equation 4.8, Equation 4.7 becomes

$$(k_{CG})_{\text{threshold-sliding-h}} = \frac{\left\langle \begin{aligned} &P_{\text{resist}} + c' \cdot L_{\text{base}} \cdot \cos(\varepsilon) - P_{\text{AE}} \cdot \cos(\delta) + \\ &\left\{ \frac{c' \cdot L_{\text{base}} \cdot \sin(\varepsilon) + W + P_{\text{AE}} \cdot \sin(\delta)}{\cos(\varepsilon) - \tan(\delta'_{\text{base}}) \cdot \sin(\varepsilon)} \right\} \cdot [\tan(\delta'_{\text{base}}) \cdot \cos(\varepsilon) + \sin(\varepsilon)] \end{aligned} \right\rangle}{W} \quad 4.9$$

Because of the inclusion of acceleration in  $P_{\text{AE}}$  formulation (refer to Appendix A) in this equation,  $\text{CorpsWallRotate}$  solves Equation 4.9 using a trial-and-error numerical approach. Note that no safety factor need be applied to the weight of the wall/structural wedge nor to its shear strength in this calculation.

The summation of overturning and resisting moments about the toe (i.e., point o) of the Figure 4.2 forces acting on the rigid body results in

$$\begin{aligned} &\frac{W}{g} \cdot (a_{CG})_h \cdot \Delta y_{CG/0} + \frac{W}{g} \cdot (a_{CG})_v \cdot \Delta x_{CG/0} \\ &+ P_{\text{AE}} \cdot \cos(\delta) \cdot [(y_{\text{heel}} + h_{\text{PAE}}) - y_{\text{toe}}] + N' \cdot d_{\text{Nbase}} = \\ &P_{\text{resist}} \cdot h_{\text{Presist}} + W \cdot \Delta x_{CG/0} + P_{\text{AE}} \cdot \sin(\delta) \cdot \Delta x_{\text{heel/toe}} \end{aligned} \quad 4.10$$

Recall the computation of  $h_{\text{PAE}}$  as well as the distribution of earth pressure forces corresponding to  $P_{\text{AE}}$  are discussed in Section 3.6 and in Appendix C. Solving for the location of the result effective force normal to the base,  $d_{\text{Nbase}}$ , Equation 4.10 becomes

$$d_{\text{Nbase}} = \frac{\left[ \begin{aligned} &-\frac{W}{g} \cdot (a_{CG})_h \cdot \Delta y_{CG/0} - \frac{W}{g} \cdot (a_{CG})_v \cdot \Delta x_{CG/0} \\ &-P_{\text{AE}} \cdot \cos(\delta) \cdot [(y_{\text{heel}} + h_{\text{PAE}}) - y_{\text{toe}}] \\ &+P_{\text{resist}} \cdot h_{\text{Presist}} + W \cdot \Delta x_{CG/0} + P_{\text{AE}} \cdot \sin(\delta) \cdot \Delta x_{\text{heel/toe}} \end{aligned} \right]}{N'} \quad 4.11$$

<sup>1</sup> Another option, implemented in  $\text{CorpsWallRotate}$ , is to assign a constant value to the vertical acceleration component. A procedure for determining the value for this constant is discussed in Sections 4.5 and 4.6.

Because of the inclusion of acceleration in  $P_{AE}$  formulation (refer to Appendix A) in this equation,  $C_{orps}W_{all}Rotate$  solves Equation 4.11 using a trial-and-error numerical approach. Introducing the horizontal limiting acceleration (i.e., Equation 4.8) in the case of a wall sliding along its base and setting the vertical component of acceleration occurring at sliding equal to zero, Equation 4.11 simplifies to

$$d_{Nbase} = \frac{\begin{bmatrix} -W \cdot (k_{CG})_{threshold-sliding-h} \cdot \Delta y_{CG/0} \\ -P_{AE} \cdot \cos(\delta) \cdot [(y_{heel} + h_{PAE}) - y_{toe}] \\ + P_{resist} \cdot h_{Presist} + W \cdot \Delta x_{CG/0} + P_{AE} \cdot \sin(\delta) \cdot \Delta x_{heel/toe} \end{bmatrix}}{N'} \quad 4.12$$

During sliding, the value of  $P_{AE}$  is computed using the horizontal acceleration value  $[(k_{CG})_{threshold-sliding-h} \text{ times } g]$ , the maximum transmissible acceleration ( $N \cdot g$  in Ebeling and Morrison (1992) notation). Recall that full contact is maintained between the base of the wall and its foundation during sliding in this formulation.

#### 4.4 Time-history of permanent wall displacement

Earthquake shaking of the rock foundation is represented by time-histories of acceleration in the translational block formulation implemented in  $C_{orps}W_{all}Rotate$ .<sup>1</sup> Since the ground acceleration varies with time, let the horizontal ground acceleration be represented by variable fraction  $A$  times the constant acceleration of gravity,  $g$ , in Figure 1.8. Recall that the integral of the acceleration time-history is equal to the velocity time-history and the integral of velocity is displacement (i.e., the permanent wall displacement in this case). For a “rigid block” (i.e., retaining wall structural wedge and driving wedge) subjected to an acceleration of value larger than the Figure 1.8 maximum transmissible acceleration, labeled  $N \cdot g$  in this figure, the rigid block will displace. When this occurs over several time-steps, the total permanent displacement of a sliding structural wedge relative to the base (i.e., the rock foundation) is the sum of the increments of displacement occurring during a number of individual pulses of ground motion as shown in this figure. These incremental relative displacements are determined as follows: For each time the acceleration of the ground, equal to  $A$  times  $g$ , is greater than the

<sup>1</sup> Baseline-corrected, horizontal and vertical acceleration time-histories are to be used to represent the earthquake ground motions in  $C_{orps}W_{all}Rotate$ .

constant  $N^*$  times  $g$  shown in this figure, relative displacements (between the retaining wall mass and the foundation) will *initiate*. The integral of the difference in velocities between the sliding structural wedge and the rock foundation velocity is equal to the incremental, relative displacement of the sliding structural wedge.

This section describes the numerical method implemented within  $C_{\text{CorpsWallRotate}}$  to compute the translational time-history of a rigid block retaining structure during earthquake shaking. It mirrors the numerical procedure used to compute the rotational time-history of a rigid block rotating about its toe, discussed in Section 3.8.

#### 4.4.1 Introduction to a step-by-step solution scheme

Earthquake acceleration time-histories are used to represent the earthquake demand in this formulation. They are specified within the rigid base of Figure 4.2. It is the experience of the primary author of this report that the duration of ground acceleration time-histories used on Corps projects is on the order of tens of seconds, and up to about one minute of earthquake shaking. The number of time increments (i.e., discrete acceleration point values) contained in the acceleration time-history corresponds to the number of solutions made in the translational wall analysis by  $C_{\text{CorpsWallRotate}}$ . The number of time increments is defined by the duration of earthquake shaking and the time increment  $DT$  used in digitization of the acceleration time-history.<sup>1</sup> There is no standard time increment  $DT$  for the digitization and subsequent processing of acceleration time-histories for Corps projects. However, Ebeling, Green, and French (1997) observe that a  $DT$  equal to 0.02, 0.01, or 0.005 sec is the most common. For example, an earthquake acceleration time-history with 40 seconds of shaking and a time-step of 0.02 sec will contain 2,000 discretized acceleration points. If the acceleration time-history was processed with a  $DT$  equal to 0.01 or 0.005 sec, then the discretized acceleration time-histories would contain 4,000 and 8,000 acceleration points, respectively.

A step-by-step solution scheme is followed in order to obtain the wall's permanent translational relative velocity,  $relV$ , and displacement,  $relD$ , in the time domain by  $C_{\text{CorpsWallRotate}}$ . An overview of the characteristics of

---

<sup>1</sup> Note that  $C_{\text{CorpsWallRotate}}$  requires the time-step  $DT$  for the horizontal and vertical acceleration time-histories used in the same analysis be the same value.

this numerical formulation is depicted in Figure 4.3. A key feature of the numerical formulation used is the assumption of a *linear* variation in relative acceleration  $relA$  over time-step  $DT$ , from time  $t_i$  to time  $t_{i+1}$ . Values of the user-provided ground acceleration (specified within the rigid base model) are compared against the maximum transmissible acceleration value  $[(k_{CG})_{\text{threshold-sliding-h}} \text{ times } g]$  at each time-step. (Recall the value for maximum transmissible acceleration value  $[(k_{CG})_{\text{threshold-sliding-h}} \text{ times } g]$  is a constant.) This idealized figure assumes that the wall is undergoing positive relative acceleration (i.e., value for acceleration of the ground is greater than the value of  $[(k_{CG})_{\text{threshold-sliding-h}} \text{ times } g]$ ), positive relative velocity, and positive (permanent) displacement at time  $t_i$ , which continues through time  $t_{i+1}$ . The relative acceleration values  $relA_0$  and  $relA_1$  are equal to the difference between the horizontal ground acceleration value minus the constant value of  $[(k_{CG})_{\text{threshold-sliding-h}} \text{ times } g]$  at times  $t_i$  and  $t_{i+1}$ , respectively, and assumed positive at both time-steps. (Other cases will be considered later.) The idealized figure also assumes that the relative acceleration increases in magnitude over this time-step  $DT$ , as depicted in this figure. The relative velocity is computed by integrating the relative acceleration during each segment of wall translation.

$$relV = \int_0^t relA \, dt \quad \text{when } relV > 0 \quad 4.13$$

or

$$relV = 0 \quad \text{when Equation 4.13 gives } relV < 0 \quad 4.14$$

So for a linear variation in relative acceleration over time-step  $DT$ , the relative velocity,  $relV$ , is a quadratic relationship. Note that  $C_{\text{orps}}W_{\text{all}}\text{Rotate}$  assumes that the wall cannot slide back into the retained soil, which is expressed by Equation 4.14. Similarly, with the permanent relative displacement of the wall being the integration of the relative velocity, the relative displacement of the wall is a cubic relationship listed in Figure 4.3. The permanent relative displacement of the wall is the integration of the relative velocity

$$relD = \int_0^t relV \, dt \quad 4.15$$

This series of computations using relative accelerations and Equations 4.13 through 4.15 are repeated for each sequence of wall translations that occurs for the duration of earthquake shaking. The experience of the primary author of this report is that when the acceleration time-histories used as input to  $C_{\text{orps}}W_{\text{all}}\text{Rotate}$  are based on previously recorded earthquake events (a typical scenario), the permanent displacement occurs during several, separate pulses occurring throughout the duration of shaking.

In Figure 4.3, the value for relative acceleration  $\text{rel}A$ , relative velocity  $\text{rel}V$ , and (permanent wall) relative displacement  $\text{rel}D$  at any point in time  $\Delta t$  after  $t_i$  and before time  $t_{i+1}$  are given by the linear, quadratic, and cubic relationships contained on the right-hand side of these three figures (with  $\Delta t$  less than or equal to  $DT$ ).

Recall that during sliding the acceleration felt by the wall equals the maximum transmissible acceleration. Thus, the sliding (rigid) block model effectively isolates the sliding block from the shaking (rigid) base below.

#### 4.4.2 Positive relative accelerations $\text{rel}A0$ and $\text{rel}A1$ at times $t_i$ and $t_{i+1}$

Expanding on the details of the computations for the numerical formulation depicted in Figure 4.3, the computation of the relative acceleration,  $\text{rel}A$ , relative velocity,  $\text{rel}V$ , and relative displacement,  $\text{rel}D$ , at time  $t_{i+1}$  are made as follows: Values for  $\text{rel}A$ ,  $\text{rel}V$ ,  $\text{rel}D$ , at time  $t_i$  are known from the previous computation step in the step-by-step solution scheme. The value for  $\text{rel}A$  at time  $t_{i+1}$  (designated  $\text{rel}A1$  in the figure) is computed as the difference between horizontal ground acceleration minus the constant value of  $[(k_{CG})_{\text{threshold-sliding-h}} \text{ times } g]$ . Referring to Figure 4.4, the relative velocity at time  $t_{i+1}$  (designated  $\text{rel}V1$ ) is computed from the value for relative velocity at time  $t_i$  (designated  $\text{rel}V0$ ) plus the positive area under the linear relative acceleration relationship over the time-step  $DT$ , designated  $\text{Area}_a$  in this figure. By the trapezoidal rule,  $\text{rel}V1$  at time  $t_{i+1}$  is

$$\text{rel}V1 = \text{rel}V0 + \frac{DT}{2} \cdot (\text{rel}A0 + \text{rel}A1) \quad 4.16$$

with the values for  $\text{rel}V0$  and  $\text{rel}A0$  now known values that were computed in the previous solution step. Note the wall is in motion at time  $t_i$ , as reflected by a positive value for relative velocity (designated  $\text{rel}V0$  in

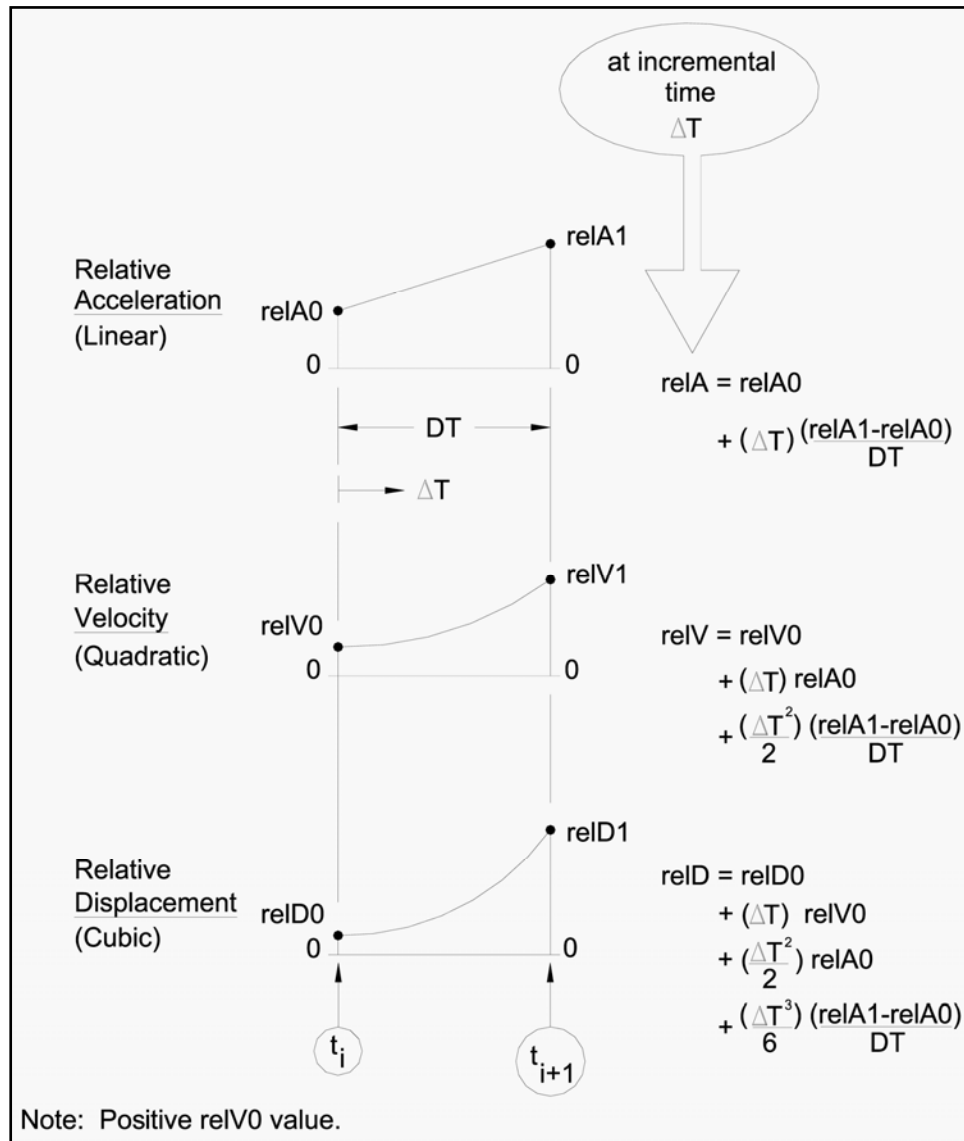


Figure 4.3. Complete equations for relative motions over time increment DT based on linearly varying acceleration.

Figure 4.4). Similarly, the permanent relative wall displacement at time  $t_{i+1}$  (designated relD1) is computed from the value for relative displacement at time  $t_i$  (designated relD0) plus the positive area under the quadratic relative velocity relationship over the time-step DT, designated Area<sub>v</sub> in this figure. For this linear acceleration method, relD1 at time  $t_{i+1}$  is

$$relD1 = relD0 + DT \cdot relV0 + \frac{DT^2}{6} \cdot (2 \cdot relA0 + relA1) \tag{4.17}$$

with the value for relD0 being a known value that was computed in the previous solution step. The value for relative velocity relV and (permanent

wall) displacement  $relD$  at time  $t_{i+1}$  are also described in terms of the area relationships contained in Figure 4.4. In this manner a step-by-step solution scheme is followed throughout the entire time-history of earthquake shaking in order to obtain the wall velocity,  $relV$ , and relative displacement,  $relD$ , at each increment in time in the Figure 4.4 case of positive values for  $relA$  at times  $t_i$  and  $t_{i+1}$ .

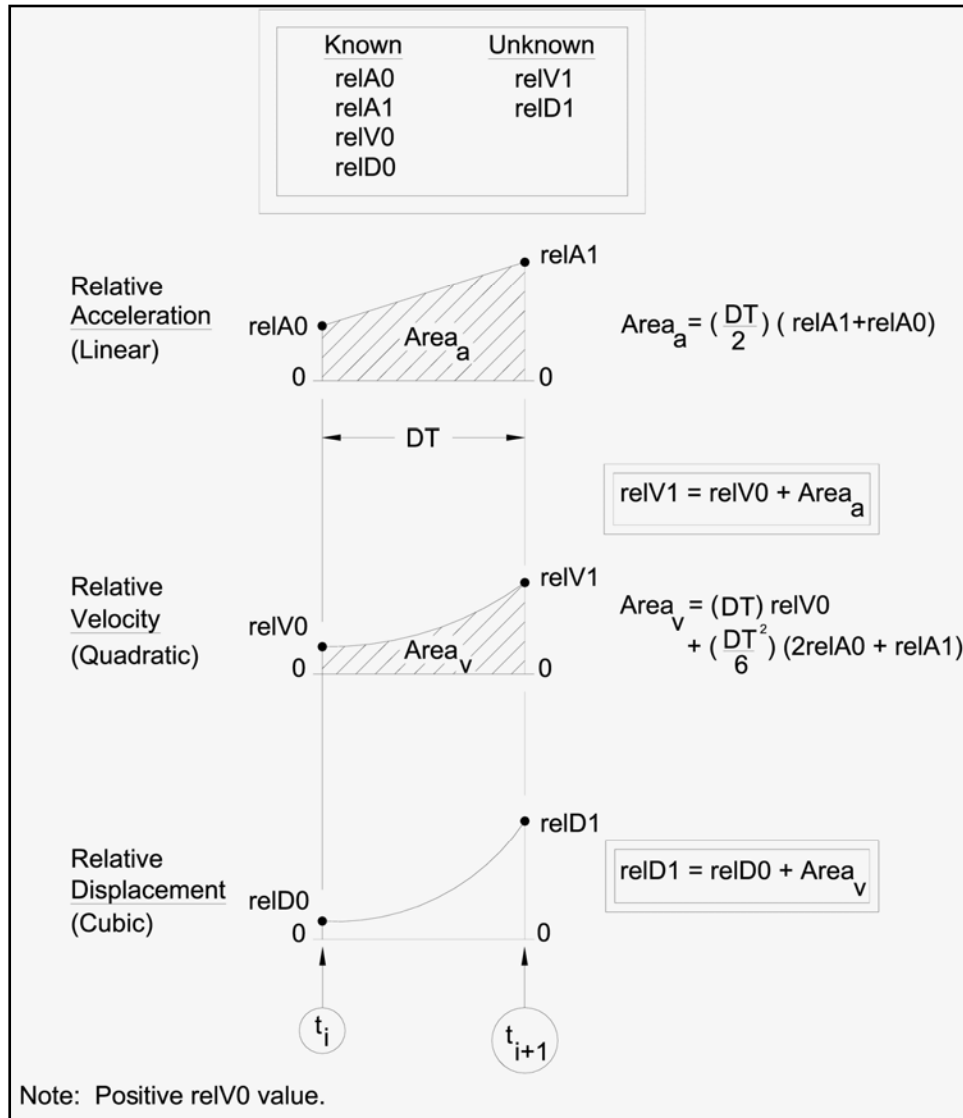


Figure 4.4. Relative velocity and displacements at the end of time increment DT based on linearly varying relative acceleration.

In summary, Figure 4.4 outlines a numerical procedure to obtain values for relative velocity and for relative displacement at time  $t_{i+1}$  in situations for which values of relative acceleration  $relA$  at times  $t_i$  and  $t_{i+1}$  are both positive. However, there are three other situations that can arise during



the step-by-step solution: (a) the case of a negative value for relA at time  $t_i$  and a positive value for relA at time  $t_{i+1}$ ; (b) the case of wall decelerating over the entire time-step DT for which the values of relA are negative at both times  $t_i$  and  $t_{i+1}$ ; and (c) the case of a positive value for relA at time  $t_i$  and a negative value for relA at time  $t_{i+1}$ . In all four cases, the assumption of **linear relative acceleration** over time-step DT is made and the basic concept of **integrating** positive areas above and/or negative areas below the time line of relative acceleration, relA, to obtain the *change* in relative velocity, relV, and then, in turn, the integration of positive and/or negative areas above and/or below the time line of relV to obtain the *change* in relative displacement, relD, is used to determine the values for relV and relD, respectively, at time  $t_{i+1}$ . These three additional step-by-step solutions are discussed next. Note the frequent use of the trapezoidal rule for relV and the linear acceleration method for relD in the solution processes to be described.

#### 4.4.3 Positive relative acceleration relA0 at time $t_i$ and negative relative acceleration relA1 at $t_{i+1}$

Next consider a wall in motion (i.e., with a positive value for relV) at time  $t_i$  but with the Figure 4.5 case of a negative value for relA0 computed at time-step  $t_i$  and positive value for relA1 computed at the next time-step of  $t_{i+1}$ .<sup>1</sup> The first step is to determine the time instant [ $t_i$  plus lhsDT] at which the relative acceleration relA is equal to zero, as labeled in the figure. By linear interpolation, this time increment lhsDT is

$$lhsDT = \left| relA0 \cdot \left( \frac{DT}{relA1 - relA0} \right) \right| \quad 4.18$$

The negative area between the negative portion of the linear acceleration line and the time line over the Figure 4.5 time increment lhsDT is

$$NegativeArea_{-A+} = \frac{1}{2} \cdot lhsDT \cdot (relA0 + 0) \quad 4.19$$

Recall that the wall is in motion at time  $t_i$  when relative velocity (designated relV0 in the figure) is positive. There are two possible outcomes for the Figure 4.5 step-by-step numerical solutions for values of relV and of relD at time  $t_{i+1}$ , depending upon the magnitude of relV0

<sup>1</sup> Note the assumption of a linear variation in relative acceleration over the time-step DT in Figure 4.5.

relative to the magnitude of  $NegativeArea_{-A+}$ . These possible scenarios are depicted by two columns of figures in Figure 4.5, labeled as the Case 1 and Case 2 figure groups.

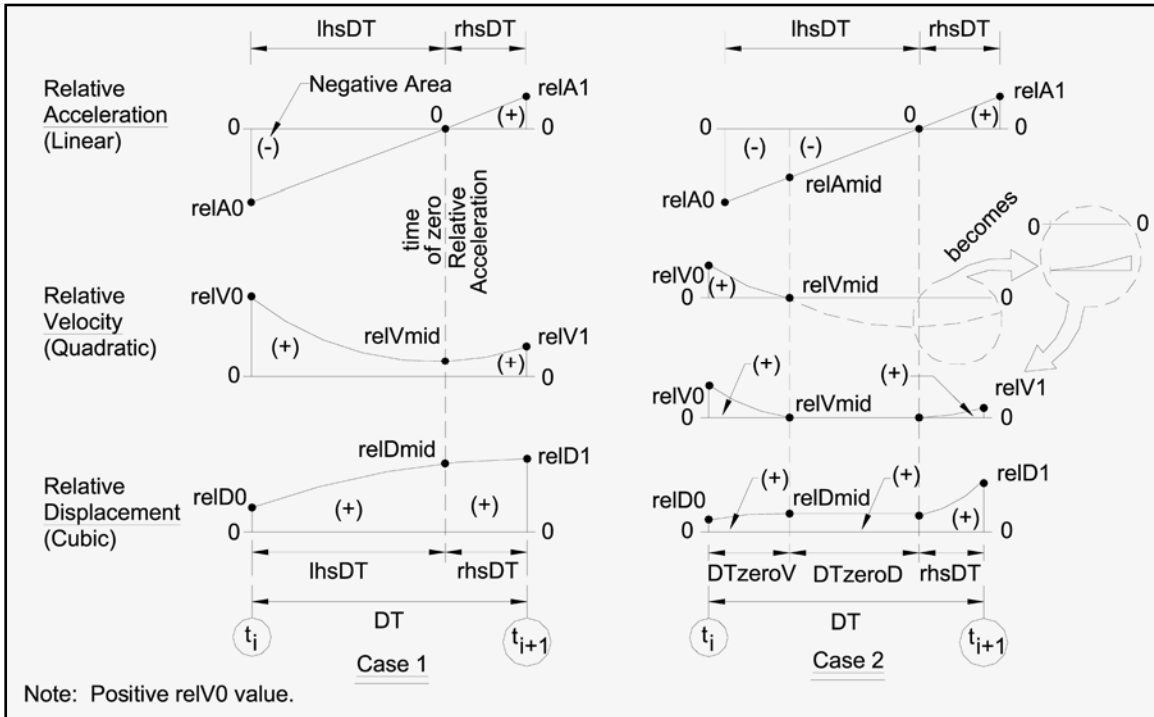


Figure 4.5. Two possible outcomes for the case of a negative relative acceleration at time  $t_i$  and a positive relative acceleration at time  $t_{i+1}$ .

**Case 1:** This case results when the positive value for  $relV$  at time  $t_i$  is greater than the magnitude of  $NegativeArea_{-A+}$  (i.e., the negative area between the negative portion of the linear acceleration line and the time line over the portion of the Figure 4.5 time increment labeled  $lhsDT$ ). The three left-hand side figures in Figure 4.5 are used to describe the Case 1 step-by-step solution scheme: The top figure describes the relative acceleration,  $relA$ , the middle figure describes the relative velocity,  $relV$ , and the lower figure describes the (permanent) relative wall displacement,  $relD$ .

The top Case 1 figure depicts the case of a (labeled) negative triangular area between the linear relative deceleration  $relA$  line and the time line (i.e.,  $NegativeArea_{-A+}$  by Equation 4.19), being of less magnitude than the positive value for relative velocity at time  $t_i$  (designated  $relV_0$ ). Consequently, the wall will remain in displacement (i.e., sliding) during the entire time-step  $DT$ . At the increment in time  $lhsDT$  after time  $t_i$ , a

portion of the negative deceleration area reduces the value of relative velocity from the positive value of magnitude  $relV_0$  at time  $t_i$  to a smaller magnitude value at time  $[t_i \text{ plus } lhsDT]$ , as shown in this figure. The relative velocity at time  $[t_i \text{ plus } lhsDT]$  is

$$relV_{mid} = relV_0 + \frac{1}{2} \cdot lhsDT \cdot (relA_0 + 0) \quad 4.20$$

The *change* in relative displacement from time  $t_i$  to time  $[t_i \text{ plus } lhsDT]$  is equal to the labeled positive area between the quadratic relative velocity curve and the time line. At time  $[t_i \text{ plus } lhsDT]$  the relative wall displacement increases in magnitude from  $relD_0$  to  $relD_{mid}$ .

$$relD_{mid} = relD_0 + lhsDT \cdot relV_0 + \frac{(lhsDT)^2}{6} \cdot (2 \cdot relA_0 + 0) \quad 4.21$$

The wall continues in motion, with positive relative velocity and with additional permanent deformation after time  $[t_i \text{ plus } lhsDT]$  when the relative acceleration of the wall is positive. At time  $[t_i \text{ plus } lhsDT]$  the magnitude of the wall's relative velocity begins to increase as a result of the positive relative acceleration of the wall. The positive (labeled) triangular area between the time line and the linear acceleration line, shown in the top Case 1 figure, equals the *change* in relative velocity and for the wall, consequently, the value for relative velocity at time  $t_{i+1}$  (labeled  $relV_1$  in the Case 1 middle figure) is

$$relV_1 = relV_{mid} + \frac{1}{2} \cdot rhsDT \cdot (0 + relA_1) \quad 4.22$$

The *change* in wall displacement from time  $[t_i \text{ plus } lhsDT]$  to time  $t_{i+1}$  is equal to the integral of the positive relative velocity of the middle  $relV$  figure. The permanent wall displacement increases in value from  $relD_{mid}$  to  $relD_1$ , as depicted in the bottom figure.

$$relD_1 = relD_{mid} + rhsDT \cdot relV_{mid} + \frac{(rhsDT)^2}{6} \cdot (2 \cdot 0 + relA_1) \quad 4.23$$

**Case 2:** This case results when the positive value for relative velocity at time  $t_i$  is less than the magnitude of  $NegativeArea_{-A+}$  (i.e., the negative area between the negative portion of the linear acceleration line and the time

line over the portion of the Figure 4.5 time increment labeled lhsDT). The four right-hand side figures in Figure 4.5 are used to describe the Case 2 step-by-step solution scheme. From the top to bottom, one figure describes the relative acceleration, two figures describe the relative velocity, and one figure describes the permanent relative wall displacement.

The top, right-hand side, Case 2 figure depicts the case of a (labeled) negative triangular area between the linear relative deceleration line and the time line, being of greater magnitude than the positive value for relative velocity at time  $t_i$  (designated relV0). Consequently, the wall will come to rest before time  $t_{i+1}$  is achieved. At an increment in time DTzeroV after time  $t_i$ , a portion of the negative deceleration area reduces the value of relative velocity from the positive value of magnitude relV0 at time  $t_i$  to a value of 0 at time [ $t_i$  plus DTzeroV], as shown in this figure. At time [ $t_i$  plus DTzeroV] the relative acceleration is

$$relAmid = DTzeroD \cdot \left( \frac{relAO}{lhsDT} \right) \quad 4.24$$

where DTzeroD is the time increment shown in Figure 4.5. The Figure 4.5 negative (relative) deceleration area below time increment DTzeroV is

$$AreaTrapezoid_{-A+} = \frac{1}{2} \cdot DTzeroV \cdot (relAO + relAmid) \quad 4.25$$

The Figure 4.5 negative relative deceleration area below time increment DTzeroD is

$$AreaTriangle_{-A+} = \frac{1}{2} \cdot DTzeroD \cdot (relAmid + 0) \quad 4.26$$

Thus, the total Figure 4.5 negative relative deceleration area below time increment lhsDT is

$$NegativeArea_{-A+} = AreaTrapezoid_{-A+} + AreaTriangle_{-A+} \quad 4.27$$

The relative velocity at time [ $t_i$  plus DTzeroV] is

$$relVmid = relV0 + AreaTrapezoid_{-A+} \quad 4.28$$

With a value for  $relV_{mid}$  equal to zero, Equation 4.28 becomes

$$0 = relVO + AreaTrapezoid_{-A+} \quad 4.29$$

Expanding by adding the term  $AreaTriangle_{-A+}$  to both sides, Equation 4.29 becomes

$$AreaTriangle_{-A+} = relVO + AreaTrapezoid_{-A+} + AreaTriangle_{-A+} \quad 4.30$$

Which by introducing Equation 4.27, becomes

$$AreaTriangle_{-A+} = relVO + NegativeArea_{-A+} \quad 4.31$$

Introducing Equations 4.26 and 4.24 and solving for  $DTzeroD$ , Equation 4.31 becomes

$$DTzeroD = \sqrt{2 \cdot \left( \frac{lhsDT}{relAO} \right) \cdot (relVO + NegativeArea_{-A+})} \quad 4.32$$

Recognizing the time increment  $lhsDT$  is equivalent to

$$lhsDT = DTzeroV + DTzeroD \quad 4.33$$

and by introducing Equations 4.33 and 4.25 into Equation 4.32 and solving for  $DTzeroV$ ,

$$DTzeroV = lhsDT - \sqrt{2 \cdot \left( \frac{lhsDT}{relAO} \right) \cdot (relVO + NegativeArea_{-A+})} \quad 4.34$$

The *change* in relative displacement from time  $t_i$  to time [  $t_i$  plus  $DTzeroV$  ] is equal to the labeled positive area between the quadratic relative velocity curve and the time line. At time [  $t_i$  plus  $DTzeroV$  ] the wall displacement increases in magnitude from  $relDO$  to  $relD_{mid}$ . The relative velocity at time [  $t_i$  plus  $DTzeroV$  ], expressed in terms of  $DTzeroV$ , is

$$relV_{mid} = relVO + \frac{1}{2} \cdot DTzeroV \cdot (relAO + relA_{mid}) \quad 4.35$$

with the relative acceleration at time [  $t_i$  plus  $DTzeroV$  ] equal to

$$relA_{mid} = relA_0 + \left( \frac{relA_1 - relA_0}{DT} \right) \bullet DT_{zeroV} \quad 4.36$$

The *change* in relative displacement from time  $t_i$  to time  $[t_i \text{ plus } DT_{zeroV}]$  is equal to the labeled positive area between the quadratic relative velocity curve and the time line. At time  $[t_i \text{ plus } DT_{zeroV}]$  the wall displacement increases in magnitude from  $relD_0$  to  $relD_{mid}$ .

$$relD_{mid} = relD_0 + DT_{zeroV} \bullet relV_0 + \frac{(DT_{zeroV})^2}{6} \bullet (2 \bullet relA_0 + relA_{mid}) \quad 4.37$$

The wall remains at rest with zero relative velocity and with no additional permanent relative displacement from time  $[t_i \text{ plus } DT_{zeroV}]$  until time  $[t_i \text{ plus } lhsDT]$  when the relative acceleration of the wall begins (again). At time  $[t_i \text{ plus } lhsDT]$  the wall begins to develop further permanent displacement as a result of the positive relative reacceleration of the wall. The positive (labeled) triangular area between the time line and the linear relative acceleration line, shown in the right-hand side of the top figure, equals the *change* in relative velocity; and with the wall at rest, consequently, the value for relative velocity at time  $t_{i+1}$  (labeled  $relV_1$  in the lower relative velocity figure) is

$$relV_1 = \frac{1}{2} \bullet rhsDT \bullet (0 + relA_1) \quad 4.38$$

The *change* in wall displacement from time  $[t_i \text{ plus } lhsDT]$  to time  $t_{i+1}$  is equal to the integral of the positive relative velocity, as depicted in the middle two, right-hand side  $relV$  figures. The top  $relV$  figure being a computational figure, and the bottom  $relV$  figure being the  $relV$  curve-shift figure that properly accounts for zero wall relative velocity over time increment  $DT_{zeroD}$ , with an insert detailed, curve-shift figure for  $relV$  shown of this computational  $relV$  figure in Figure 4.5. The permanent relative wall displacement increases in value from  $relD_{mid}$  to  $relD_1$ , as depicted in the bottom figure.

$$relD_1 = relD_{mid} + rhsDT \bullet 0 + \frac{(rhsDT)^2}{6} \bullet (2 \bullet 0 + relA_1) \quad 4.39$$

#### 4.4.4 Negative relative accelerations $relA0$ and $relA1$ at times $t_i$ and $t_{i+1}$

Next consider a wall in motion (i.e., with a positive value for relative velocity) at time  $t_i$  but with the Figure 4.6 case of a negative values for relative acceleration computed at time-steps  $t_i$  and  $t_{i+1}$ .<sup>1</sup> The first step is to determine if the wall, which is in motion at time  $t_i$ , comes to rest during the time-step  $DT$ .

The negative area between the negative portion of the linear acceleration line and the time line over the Figure 4.6 time increment  $DT$  is

$$NegativeArea_{-A-} = \frac{1}{2} \cdot DT \cdot (relA0 + relA1) \quad 4.40$$

There are two possible outcomes for the Figure 4.6 step-by-step numerical solution for relative velocity and relative displacement at time  $t_{i+1}$ , depending upon the magnitude of  $relV0$  relative to the magnitude of Equation 4.40  $NegativeArea_{-A-}$ . These possible scenarios are depicted by two columns of figures in Figure 4.6, labeled as Case 1 and Case 2 figure groups.

**Case 1:** This case results when the positive value for relative velocity at time  $t_i$  is greater than the magnitude of  $NegativeArea_{-A-}$  (i.e., the negative area between the negative portion of the linear acceleration line and the time line over the Figure 4.6 time-step  $DT$ ). The three left-hand side figures in Figure 4.6 are used to describe the Case 1 step-by-step solution scheme: The top figure describes the relative acceleration, the middle figure describes the relative velocity, and the lower figure describes the permanent relative wall displacement.

---

<sup>1</sup> Again, note the assumption of a linear variation in relative acceleration over the time-step  $DT$  shown in Figure 4.6.

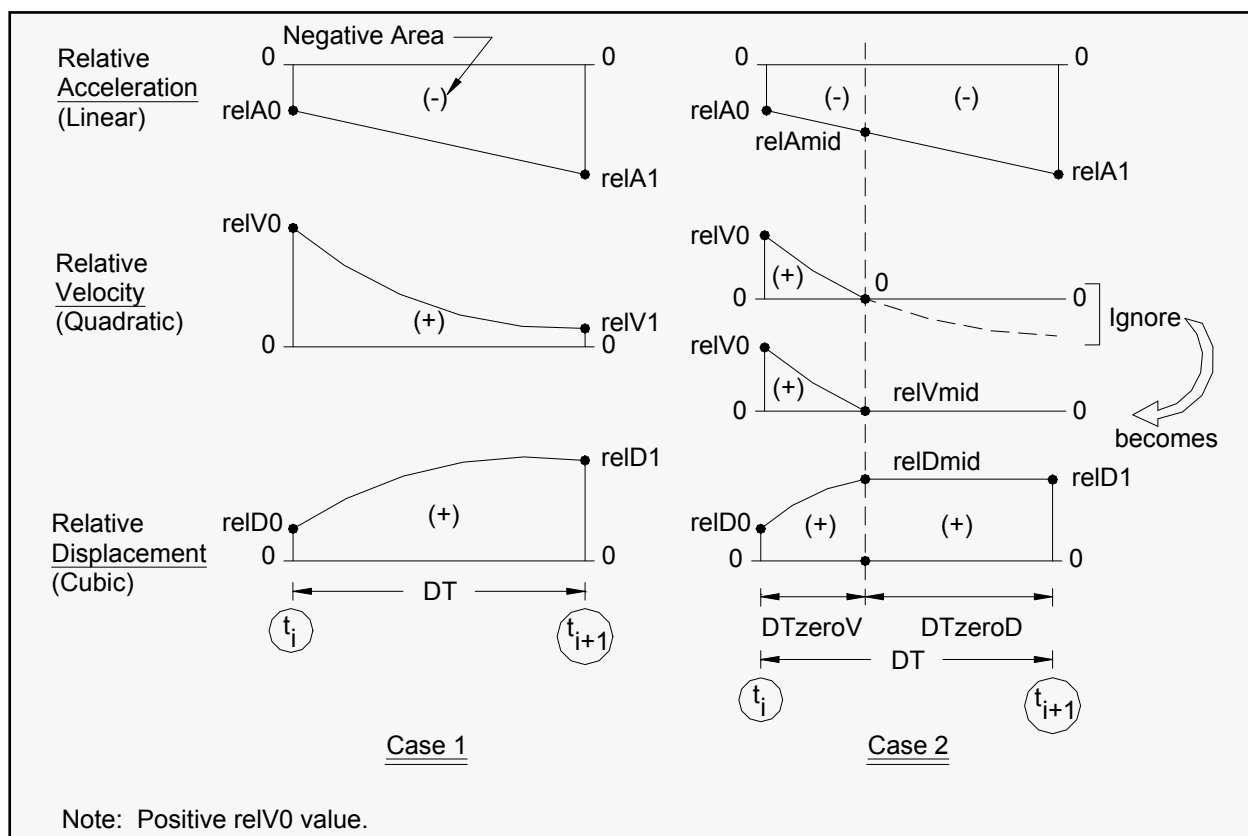


Figure 4.6. Two possible outcomes for the case of negative relative accelerations at times  $t_i$  and  $t_{i+1}$ .

The top Case 1 figure depicts the case of a (labeled) negative area between the linear relative deceleration line and the time line (i.e., NegativeArea<sub>A-</sub> by Equation 4.40), being of less magnitude than the positive value for relative velocity at time  $t_i$  (designated  $relV0$ ). Consequently, the wall will remain in motion during the entire time-step  $DT$ . At the time-step  $DT$  after time  $t_i$ , the negative deceleration area reduces the value of relative velocity from the positive value of magnitude  $relV0$  at time  $t_i$  to a smaller magnitude value at time  $[t_i$  plus  $DT]$ , as shown in this figure. The relative velocity at time  $[t_i$  plus  $DT]$  is

$$relV1 = relV0 + \frac{1}{2} \cdot DT \cdot (relA0 + relV1) \tag{4.41}$$

The *change* in relative displacement from time  $t_i$  to time  $[t_i$  plus  $DT]$  is equal to the labeled positive area between the quadratic relative velocity curve and the time line. At time  $[t_i$  plus  $DT]$  the wall displacement increases in magnitude from  $relD0$  to  $relD1$ .



$$relD1 = relD0 + DT \cdot relV0 + \frac{(DT)^2}{6} \cdot (2 \cdot relA0 + relA1) \quad 4.42$$

**Case 2:** This case results when the positive value for relative velocity at time  $t_i$  is less than the magnitude of NegativeArea<sub>-A-</sub> (i.e., the negative area between the negative portion of the linear acceleration line and the time line over the portion of the Figure 4.6 time increment labeled lhsDT). The four right-hand side figures in Figure 4.6 are used to describe the Case 2 step-by-step solution scheme. From the top to bottom, one figure describes the relative acceleration, two figures describe the relative velocity, and one figure describes the permanent relative wall displacement.

The top, right-hand side, Case 2 figure depicts the case of a (labeled) negative area between the linear relative deceleration line and the time line (i.e., NegativeArea<sub>-A-</sub> by Equation 4.40), being of greater magnitude than the positive value for relative velocity at time  $t_i$  (designated relV0). Consequently, the wall will come to rest before time  $t_{i+1}$  is achieved. At an increment in time DTzeroV after time  $t_i$ , a portion of the negative deceleration area reduces the value of relative velocity from the positive value of magnitude relV0 at time  $t_i$  to a value of 0 at time [ $t_i$  plus DTzeroV], as shown in this figure. At time [ $t_i$  plus DTzeroV] the relative acceleration is

$$relAmid = relA0 + DTzeroV \cdot \left( \frac{relA1 - relA0}{DT} \right) \quad 4.43$$

where DTzeroV is the time increment shown in Figure 4.6. The Figure 4.6 negative relative deceleration area below time increment DTzeroV is

$$AreaTrapezoid_{-A-} = \frac{1}{2} \cdot DTzeroV \cdot (relA0 + relAmid) \quad 4.44$$

Introducing Equations 4.43, Equation 4.44 becomes

$$AreaTrapezoid_{-A-} = \left\{ \begin{array}{l} \frac{1}{2} \cdot DTzeroV \cdot relA0 + \\ \frac{DTzeroV}{2} \cdot \left[ relA0 + DTzeroV \cdot \left( \frac{relA1 - relA0}{DT} \right) \right] \end{array} \right\} \quad 4.45$$

This simplifies to

$$AreaTrapezoid_{-A-} = DTzeroV \cdot relAO + \frac{(DTzeroV)^2}{2} \cdot \left( \frac{relA1 - relAO}{DT} \right) \quad 4.46$$

The *change* in rotation from time  $t_i$  to time  $[t_i \text{ plus } DTzeroV]$  is equal to the labeled positive area between the quadratic relative velocity curve and the time line. At time  $[t_i \text{ plus } DTzeroV]$  the wall displacement increases in magnitude from  $relDO$  to  $relDmid$ . The relative velocity at time  $[t_i \text{ plus } DTzeroV]$  is

$$relVmid = relVO + AreaTrapezoid_{-A-} \quad 4.47$$

With a value for  $relVmid$  equal to zero, Equation 4.47 becomes

$$0 = \left[ \frac{1}{2} \cdot \left( \frac{relA1 - relAO}{DT} \right) \right] \cdot (DTzeroV)^2 + relAO \cdot DTzeroV + relVO \quad 4.48$$

This quadratic equation has a general solution of

$$DTzeroV = \frac{-relAO \pm \sqrt{(relAO)^2 - 4 \cdot \left[ \frac{1}{2} \cdot \left( \frac{relA1 - relAO}{DT} \right) \right] \cdot relVO}}{2 \cdot \left[ \frac{1}{2} \cdot \left( \frac{relA1 - relAO}{DT} \right) \right]} \quad 4.49$$

Even though this solution provides for two possible values for  $DTzeroV$ , only the positive value is assigned to  $DTzeroV$  in  $C_{orps}W_{all}Rotate$ .

The *change* in displacement from time  $t_i$  to time  $[t_i \text{ plus } DTzeroV]$  is equal to the labeled positive area between the quadratic relative velocity curve and the time line. At time  $[t_i \text{ plus } DTzeroV]$  the relative wall displacement increases in magnitude from  $relDO$  to  $relDTmid$ .

$$relDmid = relDO + DTzeroV \cdot relVO + \frac{(DTzeroV)^2}{6} \cdot (2 \cdot relAO + relA_{mid}) \quad \text{bis 4.37}$$

The wall remains at rest with zero relative velocity and with no additional permanent displacement from time  $[t_i \text{ plus } DTzeroV]$  until time  $[t_i \text{ plus } DT]$ . Consequently, at time  $t_{i+1}$  the permanent relative wall displacement is constant, as depicted in the bottom figure.

$$relD1 = relDmid \quad 4.50$$

with the value for relDmid given by Equation 4.37.

#### 4.4.5 Positive relative acceleration relA0 at time $t_i$ and negative relative acceleration relA1 at $t_{i+1}$

Next consider a wall in motion (i.e., with a positive value for relative velocity) at time  $t_i$  but with the Figure 4.7 case of a positive value for relative acceleration at time-step  $t_i$  and negative value for relative acceleration at the next time-step of  $t_{i+1}$ .<sup>1</sup> The first step is to determine the time instant [ $t_i$  plus lhsDT] at which the relative acceleration is equal to zero, as labeled in the figure. By linear interpolation, this time increment lhsDT is

$$lhsDT = \left| relA0 \cdot \left( \frac{DT}{relA1 - relA0} \right) \right| \quad \text{bis 4.18}$$

The positive area between the positive portion of the linear acceleration line and the time line over the Figure 4.7 time increment lhsDT is

$$PositiveArea_{+A-} = \frac{1}{2} \cdot lhsDT \cdot (relA0 + 0) \quad 4.51$$

The Figure 4.7 time increment rhsDT is given by

$$rhsDT = DT - lhsDT \quad 4.52$$

The negative area between the negative portion of the linear acceleration line and the time line over the Figure 4.7 time increment rhsDT is

$$NegativeArea_{+A-} = \frac{1}{2} \cdot rhsDT \cdot (0 + relA1) \quad 4.53$$

There are two possible outcomes for the Figure 4.7 step-by-step numerical solution for relative velocity and relative displacement at time  $t_{i+1}$ , depending upon the magnitude of relVo relative to the magnitude of the sum of the PositiveArea<sub>+A-</sub> plus the NegativeArea<sub>+A-</sub>. These possible

<sup>1</sup> Again, observe the assumption of a linear variation in relative acceleration over the time-step DT shown in Figure 4.7.

scenarios are depicted by two columns of figures in Figure 4.7, labeled as Case 1 and Case 2 figure groups.

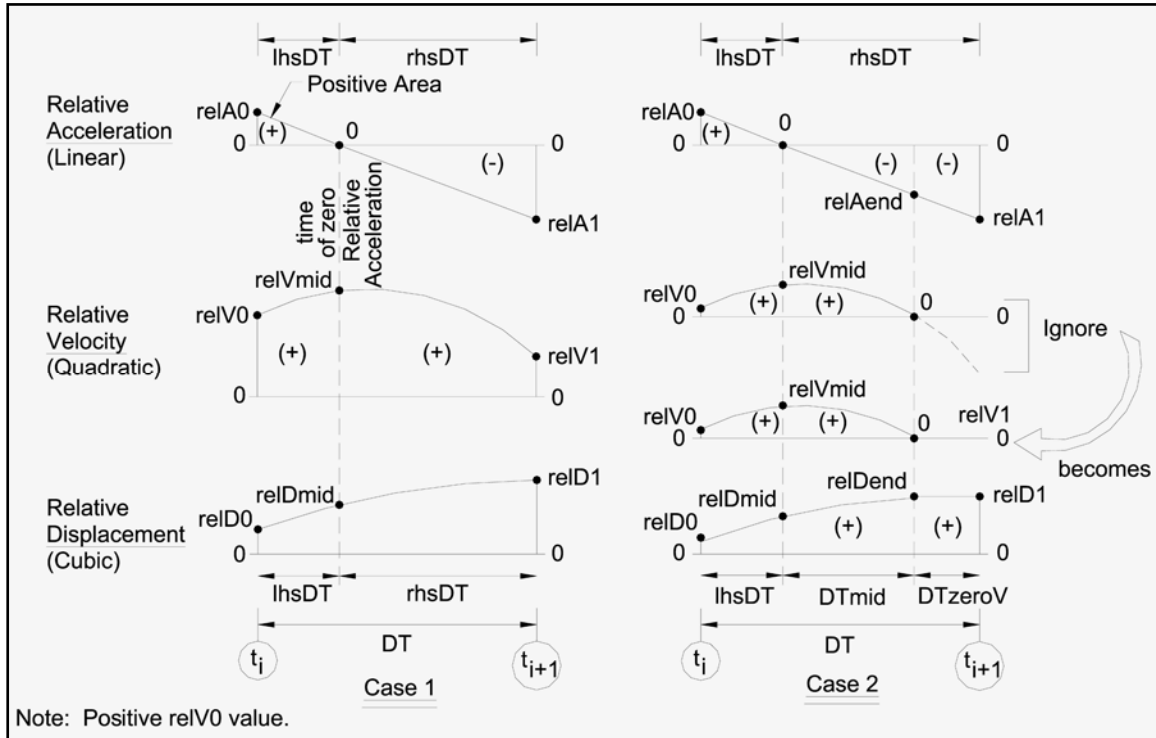


Figure 4.7. Two possible outcomes for the case of a positive relative acceleration at time  $t_i$  and a negative relative acceleration at time  $t_{i+1}$ .

**Case 1:** This case results if (a) the  $NegativeArea_{+A-}$  exceeds  $PositiveArea_{+A-}$  but the positive value for relative velocity at time  $t_i$  is greater than the magnitude of the negative sum of  $PositiveArea_{+A-}$  plus  $NegativeArea_{+A-}$ , or (b) the  $NegativeArea_{+A-}$  is less than  $PositiveArea_{+A-}$ , consequently the positive value for  $relV0$  at time  $t_i$  will increase to a larger value of  $relV1$  at time  $t_{i+1}$  (with an increase equal to the positive sum of  $PositiveArea_{+A-}$  plus  $NegativeArea_{+A-}$ ). The three left-hand side figures in Figure 4.7 are used to describe the Case 1 step-by-step solution scheme: The top figure describes the relative acceleration, the middle figure describes the relative velocity, and the lower figure describes the permanent relative wall displacement.

The top Case 1 figure depicts the case of a wall sliding during the entire time-step  $DT$  because either (a) the  $NegativeArea_{+A-}$  exceeds  $PositiveArea_{+A-}$  but the positive value for relative velocity at time  $t_i$  is greater than the magnitude of the sum of  $PositiveArea_{+A-}$  plus  $NegativeArea_{+A-}$ , or because (b) the  $NegativeArea_{+A-}$  is less than

PositiveArea<sub>+A-</sub>. At the increment in time lhsDT after time t<sub>i</sub>, the positive acceleration area increases the value of relative velocity from the positive value of magnitude relV<sub>0</sub> at time t<sub>i</sub> to a larger magnitude value at time [t<sub>i</sub> plus lhsDT], as shown in this figure. The relative velocity at time [t<sub>i</sub> plus lhsDT] is

$$relV_{mid} = relV_0 + \frac{1}{2} \cdot lhsDT \cdot (relA_0 + 0) \quad \text{bis 4.20}$$

The *change* in displacement from time t<sub>i</sub> to time [t<sub>i</sub> plus lhsDT] is equal to the labeled positive area between the quadratic relative velocity curve and the time line. At time [t<sub>i</sub> plus lhsDT] the wall displacement increases in magnitude from relD<sub>0</sub> to relD<sub>mid</sub>.

$$relD_{mid} = relD_0 + lhsDT \cdot relV_0 + \frac{(lhsDT)^2}{6} \cdot (2 \cdot relA_0 + 0) \quad \text{bis 4.21}$$

The wall continues in motion, with positive relative velocity and with additional permanent relative displacement after time [t<sub>i</sub> plus lhsDT] when the relative acceleration of the wall is positive. At time [t<sub>i</sub> plus lhsDT] the magnitude of wall relative velocity begins to decrease in magnitude as a result of the relative deceleration of the wall. The negative (labeled) triangular area between the time line and the linear relative deceleration line, shown in the top Case 1 figure, equals the *change* in relative velocity for the wall. Consequently, the value for relative velocity at time t<sub>i+1</sub> (labeled relV<sub>1</sub> in the Case 1 middle figure) is

$$relV_1 = relV_{mid} + \frac{1}{2} \cdot rhsDT \cdot (0 + relA_1) \quad \text{bis 4.22}$$

The *change* in wall displacement from time [t<sub>i</sub> plus lhsDT] to time t<sub>i+1</sub> is equal to the integral of the positive relative velocity of the middle relV-figure. The permanent relative wall displacement increases in value from relD<sub>mid</sub> to relD<sub>1</sub>, as depicted in the bottom figure.

$$relD_1 = relD_{mid} + rhsDT \cdot relV_{mid} + \frac{(rhsDT)^2}{6} \cdot (2 \cdot 0 + relA_1) \quad \text{bis 4.23}$$

**Case 2:** This case results when the NegativeArea<sub>+A-</sub> exceeds PositiveArea<sub>+A-</sub> and the positive value for relative velocity at time t<sub>i</sub> is less

than the magnitude of the sum of  $\text{PositiveArea}_{+\Delta-}$  plus  $\text{NegativeArea}_{+\Delta-}$ . The four right-hand side figures in Figure 4.7 are used to describe the Case 2 step-by-step solution scheme. From the top to bottom, one figure describes the relative acceleration, two figures describe the relative velocity, and one figure describes the permanent relative wall displacement.

The top, right-hand side, Case 2 figure depicts the case of the sum of a (labeled) positive triangular area between the linear relative deceleration line and the time line (i.e.,  $\text{PositiveArea}_{+\Delta-}$  by Equation 4.51) plus a (labeled) negative triangular area between the linear relative deceleration line and the time line (i.e.,  $\text{NegativeArea}_{+\Delta-}$  by Equation 4.53), being negative and of greater magnitude than the positive value for relative velocity at time  $t_i$  (designated  $\text{relVO}$ ). Consequently, the wall will come to rest before time  $t_{i+1}$  is achieved.

At time  $[t_i \text{ plus lhsDT}]$  the wall's relative velocity increases in magnitude from  $\text{relVO}$  to  $\text{relVmid}$ . The relative velocity at time  $[t_i \text{ plus lhsDT}]$  is

$$\text{relVmid} = \text{relVO} + \frac{1}{2} \cdot \text{lhsDT} \cdot (\text{relAO} + 0) \quad \text{bis 4.20}$$

with the relative acceleration at time  $[t_i \text{ plus lhsDT}]$  equal to zero.

The *change* in displacement from time  $t_i$  to time  $[t_i \text{ plus lhsDT}]$  is equal to the labeled positive area between the quadratic relative velocity curve and the time line. At time  $[t_i \text{ plus lhsDT}]$  the wall displacement increases in magnitude from  $\text{relDO}$  to  $\text{relDmid}$ .

$$\text{relDmid} = \text{relDO} + \text{lhsDT} \cdot \text{relVO} + \frac{(\text{lhsDT})^2}{6} \cdot (2 \cdot \text{relAO} + 0) \quad 4.54$$

At an increment in time  $[\text{lhsDT} + \text{DTmid}]$  after time  $t_i$ , a portion of the negative deceleration area reduces the value of relative velocity from the positive value of magnitude  $\text{relVmid}$  at time  $[t_i \text{ plus lhsDT}]$  to a value of 0 at time  $[t_i \text{ plus } (\text{lhsDT} + \text{DTmid})]$ , as shown in this figure. At time  $[t_i \text{ plus } (\text{lhsDT} + \text{DTmid})]$  the relative acceleration is

$$\text{relAend} = \text{DTmid} \cdot \left( \frac{\text{relA1}}{\text{rhsDT}} \right) \quad 4.55$$

where  $DT_{mid}$  is the time increment shown in Figure 4.7. The Figure 4.7 negative relative acceleration area below time increment  $DT_{mid}$  is

$$AreaTriangle_{+A-} = \frac{1}{2} \cdot DT_{mid} \cdot (0 + relA_{end}) \quad 4.56$$

The Figure 4.7 negative relative acceleration area below time increment  $DT_{zeroV}$  is

$$AreaTrapezoid_{+A-} = \frac{1}{2} \cdot DT_{zeroV} \cdot (relA_{end} + relA1) \quad 4.57$$

Thus, the total Figure 4.7 negative relative acceleration area below time increment  $rhsDT$  is

$$NegativeArea_{+A-} = AreaTrapezoid_{+A-} + AreaTriangle_{+A-} \quad 4.58$$

With the relative velocity at time  $[t_i \text{ plus } (lhsDT + DT_{mid})]$  equal to zero,

$$0 = relV_{mid} + AreaTriangle_{+A-} \quad 4.59$$

By introducing Equations 4.20, 4.51, 4.55 and 4.56, and solving for  $DT_{mid}$ , Equation 4.59 becomes

$$DT_{mid} = \sqrt{-2 \cdot \left( \frac{rhsDT}{relA1} \right) \cdot (relV0 + PositiveArea_{+A-})} \quad 4.60$$

At time  $[t_i \text{ plus } (lhsDT + DT_{mid})]$  the relative wall displacement comes to rest with

$$relD_{end} = relD_{mid} + DT_{mid} \cdot relV_{mid} + \frac{(DT_{mid})^2}{6} \cdot (2 \cdot 0 + relA_{end}) \quad 4.61$$

The wall remains at rest with zero relative velocity and with no additional permanent relative displacement from time  $[t_i \text{ plus } (lhsDT + DT_{mid})]$  until time  $t_{i+1}$ . The permanent relative wall displacement at this time  $t_{i+1}$  is

$$relD1 = relD_{end} \quad 4.62$$

#### 4.4.6 Starting the $C_{orps}W_{all}Rotate$ analysis and the initiation of wall translation during a DT time-step

*Start of the step-by-step time-history analysis:* The numerical formulation used in the step-by-step time-history analysis by  $C_{orps}W_{all}Rotate$  assumes that the wall is at rest at the start of the analysis (i.e., at time  $t_i$  equal to 0 and with  $i = 1$ ). Consequently, relative acceleration, relative velocity, and relative displacement are equal to zero as an initial boundary condition at the first time-step (i.e., with  $i = 1$ ). Recall the relative acceleration at time  $t_i$  is equal to the difference between the horizontal ground acceleration value at time  $t_i$  minus the constant value of  $[(k_{CG})_{threshold-sliding-h} \text{ times } g]$ .

*Initiation of wall displacement during the first DT time-step:* At the end of the first DT time-step, at time increment  $t_2$  (i.e.,  $t_{i+1}$  and with  $i = 1$  so the subscript  $i + 1$  becomes 2), a relative acceleration value is computed by  $C_{orps}W_{all}Rotate$ . If a positive value for relative acceleration is computed at time increment  $t_2$  then the system is in motion (i.e., sliding) during this first time-step DT.

However, if a negative value for relative acceleration is computed and the system has been at rest and with zero relative acceleration at time  $t_1 = 0$  (i.e.,  $t_i$  and for  $i = 1$ ) then the system is at rest at time  $t_2$ . This means that the correct value for relative acceleration is zero at time  $t_2$ .

*Initiation of wall displacement during a DT time-step:* A wall is at rest at the beginning of any DT time-step (designated time  $t_i$  in Figures 4.3 through 4.7) when relative velocity and relative displacement are equal to zero. At all DT time-steps other than the first time-step, the values at time  $t_i$  for relative acceleration, relative velocity, and relative displacement were computed during the previous time-step and then assigned as known values for this next time-step. The step-by-step numerical procedure implemented in  $C_{orps}W_{all}Rotate$  allows for wall displacement to initiate during any DT time-step during earthquake shaking. This will occur for a wall at rest at time  $t_i$ , i.e., the start of the time-step, when a positive value is computed for relative acceleration at time  $t_{i+1}$ . The numerical procedure outlined in Figure 4.4 allows for the computation of relative velocity and relative displacement at time  $t_{i+1}$  for this case.



#### 4.4.7 Cessation of wall translation

A wall is in motion at the start of any DT time-step (designated time  $t_i$  in Figures 4.3 through 4.7) when relative velocity (i.e.,  $relV$ ) is nonzero. The step-by-step numerical procedure implemented in  $C_{orps}W_{all}Rotate$  allows for wall translation (i.e., sliding) to terminate during any DT time-step during earthquake shaking. This occurs when the deceleration of the wall is sufficiently large during time-step DT. The applicable numerical procedures are labeled as Case 2 in Figures 4.6 and 4.7.

In the case of wall translation decelerating and with negative values for relative acceleration at times  $t_i$  and  $t_{i+1}$  during time-step DT, the relative velocity at time  $t_{i+1}$  (designated  $relV_1$ ) and the relative wall displacement at time  $t_{i+1}$  (designated  $relD_1$ ) are made using the Case 2 approach outlined in Figure 4.6. Note the relative velocity reduces to zero at a time increment  $DT_{zeroV}$  after time  $t_i$ . The wall remains at rest and with zero relative velocity over time increment  $DT_{zeroD}$ , as shown in this figure.

In the case of wall translation decelerating and with a positive value for relative acceleration at time  $t_i$  and a negative value for relative acceleration at time  $t_{i+1}$  during time-step DT, the relative velocity at time  $t_{i+1}$  (designated  $relV_1$ ) and the relative wall displacement at time  $t_{i+1}$  (designated  $relD_1$ ) are made using the Case 2 approach outlined in Figure 4.7. Note the relative velocity reduces to zero at a time increment  $[lhsDT + DT_{mid}]$  after time  $t_i$ . The wall remains at rest and with zero relative velocity over time increment  $DT_{zeroV}$ , as shown in this figure.

Note that wall translation can begin again at a later point in time, as described in the subsection 4.4.6 paragraph entitled “initiation of wall rotation during a DT time-step.”

### 4.5 New translational analysis model of a wall retaining a partially submerged backfill and buttressed by a reinforced concrete slab

#### 4.5.1 Introduction

The formulation for a rock-founded wall retaining a partially submerged backfill and for the case of a pool in front of the retaining wall is summarized in this subsection. The formulation presented is an extension of the moist backfill formulation discussed in the previous sections of this chapter. Water pressures are assumed to act along three faces of the

structural wedge denoted as the toe, base, and the heel regions of Figure 4.8. Forces acting on the toe are due to the presence of a pool of water in front of the wall. A leaking vertical joint is assumed between the base slab and the structural wedge with water pressures above the toe controlled by the presence of the pool. The computation of water pressures acting on this partially submerged structural wedge is discussed in detail in Appendix D.<sup>1</sup> The Figure 4.8 distributions of water pressures are converted into equivalent resultant forces, expressed in global x- and y-coordinates, and their points of application along each of the three regions. These resultant water pressure forces are used in an effective stress-based stability analysis of the structural wedge. Dynamic considerations for the pool during earthquake shaking are accounted for in the analysis using hydrodynamic water pressures computed using the Westergaard (1931) procedure of analysis (see Appendix D). The hydrodynamic water pressure resultant force  $P_{wd}$  (Equation D.5) is shown acting on the structural wedge in this figure (and shown acting in a direction consistent with the direction of positive horizontal acceleration,  $+a_h$ ).

---

<sup>1</sup> In the initial  $C_{orps}W_{all}Rotate$  version, no excess pore water pressures due to earthquake-induced shear strains within the soil regions are included in the current  $C_{orps}W_{all}Rotate$  formulation (i.e., the excess pore water pressure ratio  $r_u$  is equal to zero). Refer to Ebeling and Morrision (1992) for a complete description and discussion of  $r_u$ .

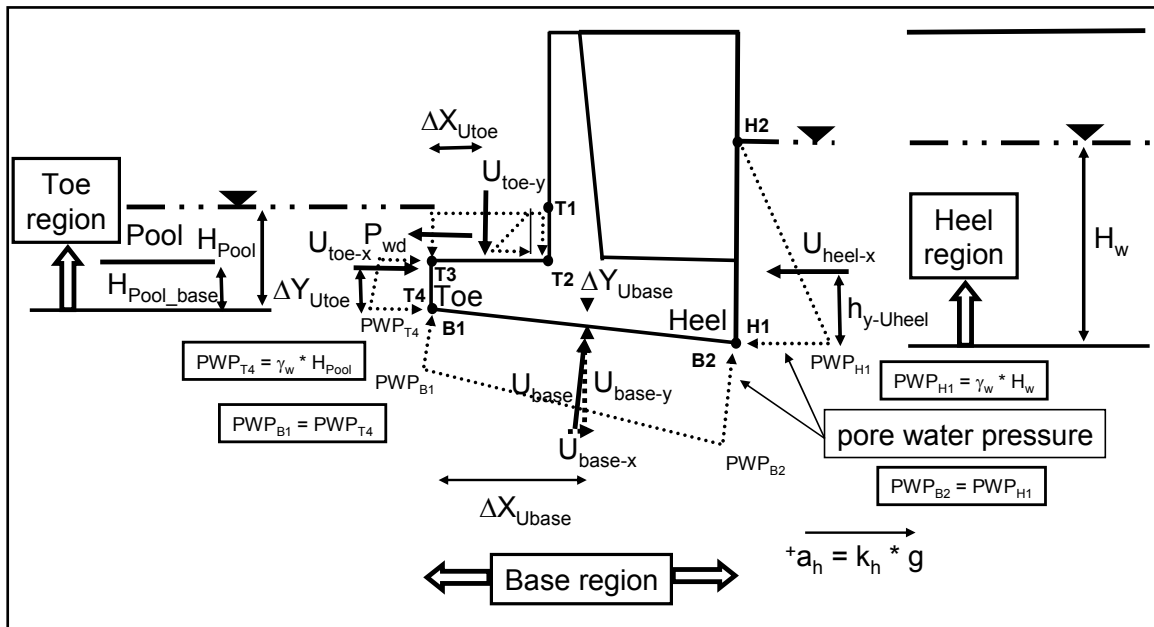


Figure 4.8. Control points, water pressures, and corresponding resultant forces acting normal to faces of the three regions of a structural wedge sliding along its base—effective stress analysis.

In the case of a wall sliding along its base, contact between the base of the structural wedge and the foundation is maintained during earthquake shaking. Recall that a simplistic rigid base assumption is made in this formulation for rock-founded earth retaining structures. There is no formation of a gap sometime during earthquake shaking. Note that the Figure 4.8 water pressure distribution is the steady-state pore water pressures resulting from a structural wedge in full contact with the rock foundation, shown in Figure D.1.

The resultant water pressure forces  $U_{toe}$ ,  $U_{base}$ ,  $U_{heel}$ , and  $P_{wd}$  shown in Figure 4.8 are superimposed on the free-body diagram of forces acting on the Figure 4.2 structural wedge, resulting in the Figure 4.9 free-body diagram. Recall  $P_{resist}$  is the force provided by the reinforced concrete (toe) slab.

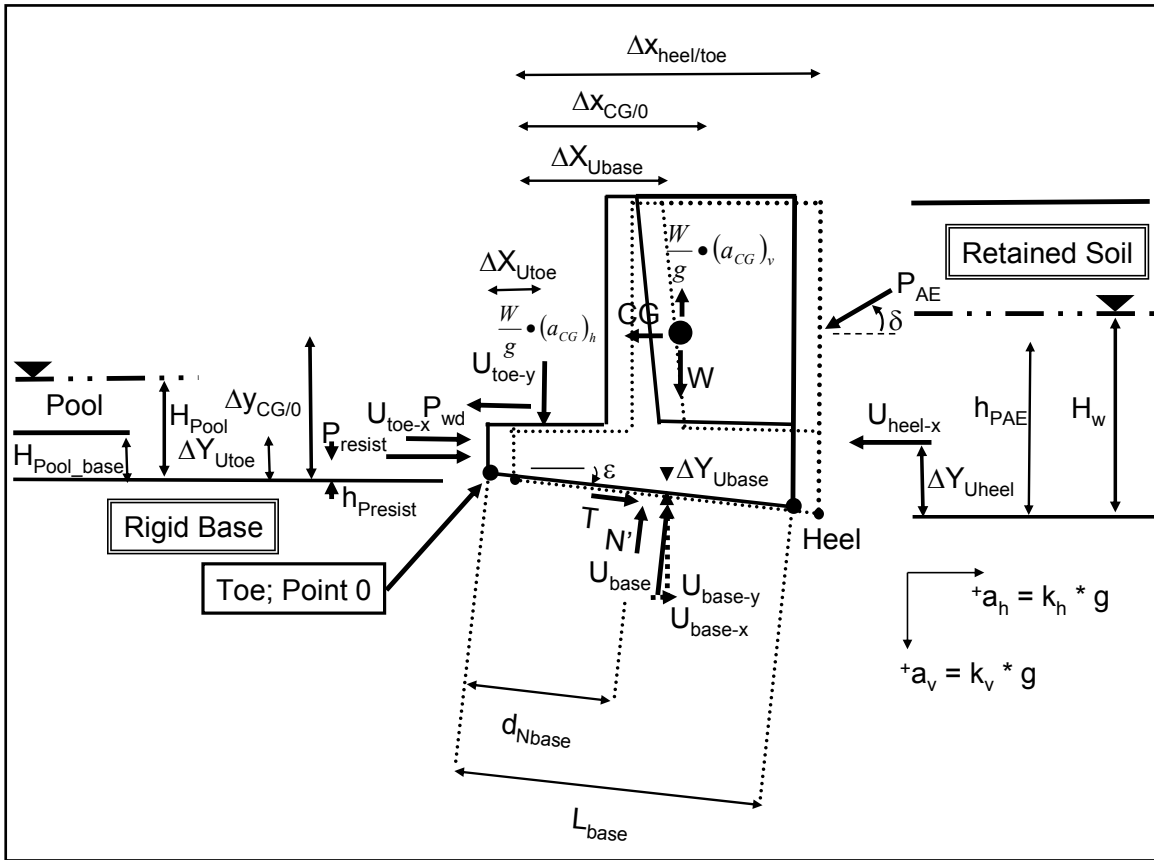


Figure 4.9. Inertia forces and resultant force vectors acting on a rigid block model of a (inclined base) cantilever wall retaining a partially submerged backfill with sliding along the base of the wall during earthquake shaking of the inclined rigid base—effective stress analysis.

#### 4.5.2 Threshold value of acceleration corresponding to incipient lift-off of the base of the wall in rotation—partially submerged backfill

At the onset of sliding of the Figure 4.9 retaining wall, the horizontal driving force equals the stabilizing (i.e., restoring) force. The summation of the Figure 4.9 horizontal forces acting on the rigid body results in

$$\frac{W}{g} \cdot (a_{CG})_h + P_{AE} \cdot \cos(\delta) + U_{heel-x} + P_{wd} = P_{resist} + T \cdot \cos(\varepsilon) + N' \cdot \sin(\varepsilon) + U_{base-x} + U_{toe-x} \tag{4.63}$$

T is the shear force required for equilibrium of forces acting on the structural wedge (i.e.,  $FS_{slide} = 1.0$ ). At incipient sliding, the shear strength along the base to foundation interface becomes fully mobilized. Assuming a full mobilization of shear resistance along the base (of length  $L_{base}$ ), the

shear force may be computed utilizing the Mohr-Coulomb failure criteria, in an effective stress analysis, as

$$T = c'_{base} \bullet L_{base} + N' \bullet \tan(\delta'_{base}) \quad \text{bis 4.2}$$

The summation of the Figure 4.9 vertical forces acting on the rigid body results in

$$0 = N' \bullet \cos(\varepsilon) - T \bullet \sin(\varepsilon) - W + \frac{W}{g} \bullet (a_{CG})_v - P_{AE} \bullet \sin(\delta) + U_{base-y} - U_{toe-y} \quad 4.64$$

Introducing Equation 4.2 for T, Equation 4.64 becomes

$$N' = \frac{c' \bullet L_{base} \bullet \sin(\varepsilon) + W - \frac{W}{g} \bullet (a_{CG})_v + P_{AE} \bullet \sin(\delta) - U_{base-y} + U_{toe-y}}{\cos(\varepsilon) - \tan(\delta'_{base}) \bullet \sin(\varepsilon)} \quad 4.65$$

Introducing Equations 4.2 and 4.65 and collecting variables, Equation 4.63 becomes

$$\begin{aligned} & \frac{W}{g} \bullet (a_{CG})_h + P_{AE} \bullet \cos(\delta) + U_{heel-x} + P_{wd} = \\ & P_{resist} + c' \bullet L_{base} \bullet \cos(\varepsilon) + U_{toe-x} + U_{base-x} + \\ & \left\{ \frac{c' \bullet L_{base} \bullet \sin(\varepsilon) + W - \frac{W}{g} \bullet (a_{CG})_v + P_{AE} \bullet \sin(\delta) - U_{base-y} + U_{toe-y}}{\cos(\varepsilon) - \tan(\delta'_{base}) \bullet \sin(\varepsilon)} \right\} \quad 4.66 \\ & \bullet [\tan(\delta'_{base}) \bullet \cos(\varepsilon) + \sin(\varepsilon)] \end{aligned}$$

Equation 4.66 represents the equilibrium relationship for the (rigid) structural wedge when the earthquake accelerations are such that the factor of safety against sliding along its base is equal to 1.0. For a factor of safety > 1.0 against sliding, the retaining wall does not slide. The rigid body CG accelerations are the same as the rigid base accelerations (i.e., within the rock foundation). However, the accelerations felt by the rigid body (i.e., at its center of gravity, CG) will differ from the rigid base accelerations for user-defined rigid base acceleration (time-history) values that exceed the value for acceleration that results in a factor of safety

against sliding equal to 1.0. During sliding, the acceleration felt by the rigid body at its center of gravity is of constant magnitude.

The component of the threshold acceleration occurring at translation (i.e., sliding) along the base is designated as

$$(a_{CG})_{\text{threshold-sliding-h}} = (k_{CG})_{\text{threshold-sliding-h}} \bullet g \quad \text{bis 4.8}$$

where  $(k_{CG})_{\text{threshold-sliding-h}}$  is a value of horizontal ground acceleration, expressed in decimal fraction. In Ebeling and Morrision (1992), the acceleration  $(a_{CG})_{\text{threshold-sliding-h}}$  is referred to as the maximum transmissible acceleration ( $N \bullet g$ ) or as the yield acceleration. Note that the horizontal acceleration value [ $(k_{CG})_{\text{threshold-sliding-h}}$  times  $g$ ] is a not a user-specified constant.

For a user-specified constant<sup>1</sup> for vertical acceleration [i.e.,  $(a_{CG})_v = \text{constant}$ ],  $C_{\text{orps}}W_{\text{allRotate}}$  solves Equation 4.66 by introducing  $(a_{CG})_{\text{threshold-sliding-h}}$  and  $(k_{CG})_{\text{threshold-sliding-h}}$  for  $(a_{CG})_h$  and  $(k_{CG})_h$ . Because of the inclusion of acceleration in  $P_{AE}$  formulation (refer to Appendix A) in this equation,  $C_{\text{orps}}W_{\text{allRotate}}$  solves Equation 4.66 using a trial-and-error numerical approach. Note that no safety factor need be applied to the weight of the wall/structural wedge nor to its shear strength in this calculation. The value of maximum transmissible (horizontal) acceleration at incipient sliding is reported in the WORKslide.TMP output file generated in each  $C_{\text{orps}}W_{\text{allRotate}}$  analysis. This file may be viewed using the Visual Modeler boxes labeled Show Sliding Evaluation on the Analysis tab.

In  $C_{\text{orps}}W_{\text{allRotate}}$  output data files, the Equation 4.66 horizontal forces acting on the structural wedge are grouped into driving forces and resisting forces, which are defined as

$$\text{Driving Forces} = \frac{W}{g} \bullet (a_{CG})_h + P_{AE} \bullet \cos(\delta) + U_{\text{heel-x}} + P_{wd} \quad 4.67$$

and

---

<sup>1</sup> A procedure for determining the value for this constant (for vertical acceleration) is discussed in Section 4.6.

$$\begin{aligned}
 \text{Resisting Forces} = & P_{\text{resist}} + c' \bullet L_{\text{base}} \bullet \cos(\varepsilon) + U_{\text{toe-x}} + U_{\text{base-x}} + \\
 & \left\{ \frac{c' \bullet L_{\text{base}} \bullet \sin(\varepsilon) + W - \frac{W}{g} \bullet (a_{\text{CG}})_v + P_{\text{AE}} \bullet \sin(\delta) - U_{\text{base-y}} + U_{\text{toe-y}}}{\cos(\varepsilon) - \tan(\delta'_{\text{base}}) \bullet \sin(\varepsilon)} \right\} \\
 & \bullet [\tan(\delta'_{\text{base}}) \bullet \cos(\varepsilon) + \sin(\varepsilon)]
 \end{aligned} \tag{4.68}$$

Introducing Equation 4.65, the resisting forces is also expressed as

$$\begin{aligned}
 \text{Resisting Forces} = & \\
 & P_{\text{resist}} + c' \bullet L_{\text{base}} \bullet \cos(\varepsilon) + U_{\text{toe-x}} + U_{\text{base-x}} + \\
 & \{N'\} \bullet [\tan(\delta'_{\text{base}}) \bullet \cos(\varepsilon) + \sin(\varepsilon)]
 \end{aligned} \tag{4.69}$$

In a total stress analysis, the internal pore water pressure force terms  $U_{\text{base}}$  and  $U_{\text{heel}}$  are excluded from Equations 4.66 through 4.69 and  $c'$  is set equal to  $S_u$  with  $\phi'$  set equal to zero. Additionally,  $N'$  is set equal to  $N$  in Equations 4.63 through 4.69.

Since the horizontal limiting acceleration is of interest, another option is a simplified form of Equation 4.66 that may be derived by setting the vertical component of acceleration occurring at sliding equal to zero, as done by Richards and Elms (1979) and others. By making this assumption and introducing Equation 4.8, Equation 4.66 becomes

$$\begin{aligned}
 (k_{\text{CG}})_{\text{threshold-sliding-h}} = & \\
 & \left\langle \frac{P_{\text{resist}} + c' \bullet L_{\text{base}} \bullet \cos(\varepsilon) + U_{\text{toe-x}} + U_{\text{base-x}} - P_{\text{AE}} \bullet \cos(\delta) - U_{\text{heel-x}} - P_{\text{wd}} + \right. \\
 & \left. \left\{ \frac{c' \bullet L_{\text{base}} \bullet \sin(\varepsilon) + W + P_{\text{AE}} \bullet \sin(\delta) - U_{\text{base-y}} + U_{\text{toe-y}}}{\cos(\varepsilon) - \tan(\delta'_{\text{base}}) \bullet \sin(\varepsilon)} \right\} \right. \\
 & \left. \bullet [\tan(\delta'_{\text{base}}) \bullet \cos(\varepsilon) + \sin(\varepsilon)] \right\rangle \\
 & W
 \end{aligned} \tag{4.70}$$

Because of the inclusion of acceleration in  $P_{\text{AE}}$  formulation (refer to Appendix A) in this equation,  $C_{\text{orps}} W_{\text{allRotate}}$  solves Equation 4.70 using a trial-and-error numerical approach.

In a total stress analysis, the internal pore water pressure force terms  $U_{\text{base}}$  and  $U_{\text{heel}}$  are excluded from Equations 4.63 through 4.70.

The summation of overturning and resisting moments about the toe (i.e., point o) of the Figure 4.9 forces acting on the rigid body results in

$$\begin{aligned}
 & \frac{W}{g} \cdot (a_{CG})_h \cdot \Delta y_{CG/O} + \frac{W}{g} \cdot (a_{CG})_v \cdot \Delta x_{CG/O} + P_{AE} \cdot \cos(\delta) \cdot [(y_{heel} + h_{PAE}) - y_{toe}] \\
 & + N' \cdot d_{Nbase} + U_{heel-x} \cdot [(y_{heel} + \Delta Y_{Uheel}) - y_{toe}] + U_{base-y} \cdot \Delta X_{Ubase} + U_{base-x} \\
 & \cdot \Delta Y_{Ubase} + P_{wd} \cdot [H_{Pool\_base} + 0.4 \cdot (H_{Pool} - H_{Pool\_base})] = \quad \quad \quad 4.71 \\
 & P_{resist} \cdot h_{Presist} + W \cdot \Delta x_{CG/O} + P_{AE} \cdot \sin(\delta) \cdot \Delta x_{heel/toe} \\
 & + U_{toe-x} \cdot \Delta Y_{Utoe} + U_{toe-y} \cdot \Delta X_{Utoe}
 \end{aligned}$$

Solving for the location of the result effective force normal to the base,  $d_{Nbase}$ , Equation 4.10 becomes

$$d_{Nbase} = \frac{\left[ \begin{aligned} & -\frac{W}{g} \cdot (a_{CG})_h \cdot \Delta y_{CG/O} - \frac{W}{g} \cdot (a_{CG})_v \cdot \Delta x_{CG/O} \\ & - P_{AE} \cdot \cos(\delta) \cdot [(y_{heel} + h_{PAE}) - y_{toe}] \\ & - U_{heel-x} \cdot [(y_{heel} + \Delta Y_{Uheel}) - y_{toe}] - U_{base-y} \cdot \Delta X_{Ubase} - U_{base-x} \cdot \Delta Y_{Ubase} \\ & - P_{wd} \cdot [H_{Pool\_base} + 0.4 \cdot (H_{Pool} - H_{Pool\_base})] \\ & + P_{resist} \cdot h_{Presist} + W \cdot \Delta x_{CG/O} + P_{AE} \cdot \sin(\delta) \cdot \Delta x_{heel/toe} \\ & + U_{toe-x} \cdot \Delta Y_{Utoe} + U_{toe-y} \cdot \Delta X_{Utoe} \end{aligned} \right]}{N'} \quad 4.72$$

Because of the inclusion of acceleration in  $P_{AE}$  formulation (refer to Appendix A) in this equation,  $C_{orps}W_{all}Rotate$  solves Equation 4.72 using a trial-and-error numerical approach. Introducing the horizontal limiting acceleration (i.e., Equation 4.8) in the case of a wall sliding along its base and setting the vertical component of acceleration occurring at sliding equal to zero, Equation 4.72 can be simplified to



$$d_{N_{base}} = \frac{\left[ \begin{aligned} & -\frac{W}{g} \cdot (k_{CG})_{\text{threshold-sliding-h}} \cdot \Delta y_{CG/0} \\ & -P_{AE} \cdot \cos(\delta) \cdot [(y_{heel} + h_{PAE}) - y_{toe}] \\ & -U_{heel-x} \cdot [(y_{heel} + \Delta Y_{U_{heel}}) - y_{toe}] - U_{base-y} \cdot \Delta X_{U_{base}} - U_{base-x} \cdot \Delta Y_{U_{base}} \\ & -P_{wd} \cdot [H_{Pool\_base} + 0.4 \cdot (H_{Pool} - H_{Pool\_base})] \\ & + P_{resist} \cdot h_{presist} + W \cdot \Delta x_{CG/0} + P_{AE} \cdot \sin(\delta) \cdot \Delta x_{heel/toe} \\ & + U_{toe-x} \cdot \Delta Y_{U_{toe}} + U_{toe-y} \cdot \Delta X_{U_{toe}} \end{aligned} \right]}{N'} \quad 4.73$$

During sliding, the value of  $P_{AE}$  is computed using the horizontal acceleration value  $[(k_{CG})_{\text{threshold-sliding-h}} \text{ times } g]$ , the maximum transmissible acceleration ( $N \cdot g$  in Ebeling and Morrison (1992) notation). Recall that full contact is maintained between the base of the wall and its foundation during sliding in this formulation.

In a total stress analysis, the internal pore water pressure force terms  $U_{base}$  and  $U_{heel}$  are excluded from Equations 4.71 through 4.73.

#### 4.5.3 Numerical method for computing the translational time-history of a rigid block retaining structure

Earthquake acceleration time-histories are used to represent the earthquake demand in a displacement analysis of rigid body structural wedge (permanent) translation. A step-by-step solution scheme is followed in order to obtain the wall's relative velocity and relative displacement in the time domain by  $C_{orps}W_{all}Rotate$ . An overview of the characteristics of this numerical formulation is given in section 4.4.

#### 4.6 Vertical acceleration in the new translational analysis model of a wall retaining a partially submerged backfill and buttressed by a reinforced concrete slab

Vertical accelerations can be included in the Newmark (1965) sliding block analysis of earth retaining structures. However, several sliding block formulations, e.g., Richards and Elms (1979) and others, set the vertical component of acceleration occurring at sliding equal to zero in their formulations. Whitman and Liao (1985, pages 30 and 74) observe that the vertical earthquake ground motion component is generally not considered to be of as much significance as the horizontal component and has generally been ignored in sliding block analyses. From their study of the

effect of vertical accelerations using 14 earthquake records on wall displacements (summarized in Section 6.5 of their report), they conclude that incorporating vertical ground accelerations causes greater residual displacement.

Current Corps projects often involve the development of horizontal and vertical acceleration time-histories for use in the design of various project features. One of the Corps projects leading to the development of *C<sub>orps</sub>W<sub>all</sub>Rotate* is sited in a high seismic region on the West coast and situated in close proximity to an active fault that dominates the ground motion hazard. Initial assessments of the Maximum Credible Earthquake design events led to the development of horizontal and vertical acceleration time-histories with positive/negative peak values of 1.2g/-1.02g and 0.83g/-1.2g, respectively. Normally the polarity of ground motions is not retained in their development so that in a sliding block analysis four combinations of horizontal and vertical ground motions are investigated, with two due to the reverse in sign for the horizontal and two due to the reverse in sign for the vertical acceleration time-histories. This can easily be accomplished by selecting the option to invert a time-history in the *C<sub>orps</sub>W<sub>all</sub>Rotate* Visual Modeler in the horizontal and/or vertical earthquake time-history tabs. For the case of a “dry” site (i.e., no pool nor water table within the retained soil), with cohesionless soils, interface friction  $\delta$  between the driving and structural wedges equal to zero, the computed value for the effective normal force acting along the base of a structural wedge would be less than or equal to zero according to Equation 4.6 or Equation 4.65. The shear force resistance along the base of the structural wedge would be less than or equal to zero by Equation 4.2, resulting in infinite relative displacements. Consequently, a vertical acceleration time-history with magnitudes (at time-steps) approaching or exceeding 1g cannot be used in the current formulation.

In an attempt to answer questions regarding the impact of a vertical acceleration time-history of significant amplitude on seismic response, as is the case for the Corps project discussed in the previous paragraph, an alternative method to incorporate the effects of vertical accelerations in a Newmark (1965) sliding block analysis is proposed. This new approach is incorporated in *C<sub>orps</sub>W<sub>all</sub>Rotate* program.

In a Newmark sliding block analysis of a retaining structure, *C<sub>orps</sub>W<sub>all</sub>Rotate* allows the user to specify a constant value for vertical

acceleration to be used (a) in the equilibrium Equation 4.7 or 4.66 when computing (in a trial-and-error numerical procedure) the value of maximum horizontal transmissible acceleration,  $(a_{CG})_{\text{threshold-sliding-h}}$ , and (b) during the entire horizontal sliding block time-history analysis. This software implements the following two new methods for determining an approximate, constant, effective value for vertical acceleration:

**Method 1 - average vertical acceleration value:** Using the user-specified horizontal acceleration time-history and the user-provided constant value for vertical acceleration, the value for maximum horizontal transmissible acceleration,  $(a_{CG})_{\text{threshold-sliding-h}}$ , is computed and a sliding block time-history analysis is performed. The software then identifies at which  $i$  time increments that *incremental* sliding  $(d_r)_i$  takes place and the total number of incremental time-step increments  $i$  during which sliding occurs, designated  $n_{\text{slide}}$ . The average vertical acceleration value for the user-specified vertical acceleration time-history is computed for all these  $i$  time increments using the relationship

$$(a_{CG})_{v\text{-ave}} = \frac{\sum_i^{n_{\text{slide}}} (a_v)_i}{n_{\text{slide}}} \quad 4.74$$

The sign for the average vertical acceleration,  $(a_v)_i$ , during each select time increment  $i$  for which incremental sliding occurs is maintained in this calculation.

A trial-and-error procedure is used to determine the appropriate value for the constant vertical acceleration value. The primary author of this report usually starts with a constant vertical (Y) acceleration value set equal to zero. A Newmark sliding block analysis is made, including a computation made by  $C_{\text{orps}} W_{\text{all}} \text{Rotate}$  using Equation 4.74 to determine a value for  $(a_{CG})_{v\text{-ave}}$ . Then a second Newmark sliding block analysis is made in which the constant vertical acceleration value is set equal to the previously computed value for  $(a_{CG})_{v\text{-ave}}$  by the user. This second computation results in an updated value for  $(a_{CG})_{v\text{-ave}}$ . The iterative process is repeated until the difference between old and new values is minor, usually within four computations.

**Method 2 - weighted vertical acceleration value:** This approach is a variation of Method 1. Using the user-specified horizontal acceleration

time-history and the user-provided constant value for vertical (Y) acceleration, the value for maximum horizontal transmissible acceleration,  $(a_{CG})_{\text{threshold-sliding-h}}$ , is computed and a sliding block time-history analysis is performed. The software then identifies at which  $i$  time increments during which incremental sliding  $(d_r)_i$  takes place and the total number of time increments  $i$  during which sliding occurs is designated  $n_{\text{slide}}$ . The total horizontal displacement is

$$d_r = \sum_i^{n_{\text{slide}}} (d_r)_i \quad 4.75$$

A weighted vertical acceleration value is computed for the user-specified vertical acceleration time-history with average vertical acceleration value,  $(a_v)_i$ , computed for each time increment  $i$  of incremental displacements using the following relationship

$$(a_{CG})_{v\text{-weighted}} = \sum_i^{n_{\text{slide}}} \left\{ (a_v)_i \cdot \left[ \frac{(d_r)_i}{d_r} \right] \right\} \quad 4.76$$

Again, the sign for the average vertical acceleration,  $(a_v)_i$ , during each select time increment  $i$  of incremental displacements is maintained in this calculation.

A trial-and-error procedure is used to determine the appropriate value for the constant vertical acceleration value. The primary author of this report usually starts with a constant vertical (Y) acceleration value set equal to zero. A Newmark sliding block analysis is made, including a computation made by  $C_{\text{orps}} W_{\text{all}} \text{Rotate}$  using Equations 4.75 and 4.76 to determine a value for  $(a_{CG})_{v\text{-weighted}}$ . Then a second Newmark sliding block analysis is made in which the constant vertical (Y) acceleration value is set equal to the previously computed value for  $(a_{CG})_{v\text{-weighted}}$  by the user. This second computation results in an updated value for  $(a_{CG})_{v\text{-weighted}}$ . The process is repeated until the difference between old and new values is minor, usually within four computations.

Method 2 differs from Method 1 in that the weighting factor applied to each of the average vertical acceleration,  $(a_v)_i$ , values at the  $i$  time increments of incremental sliding is assigned according to the relative magnitude of incremental displacements occurring at each time increment. Method 1 applies a uniform weighting factor.

## 5 The Visual Modeler and Visual Post-Processor — CorpsWallRotate

### 5.1 Introduction

This chapter discusses the Visual Modeler, how to perform a CorpsWallRotate analysis, and how to interpret the results using the Visual Post-Processor. It also provides guidance for using the CorpsWallRotate software package. The software package is referred to by its abbreviated name, CWRotate, throughout this chapter.

### 5.2 Visual modeler and visual post-processor

#### 5.2.1 Introduction to the visual modeling environment

CWRotate is a program for performing rotational or translational time-history analysis of a variety of wall structures during earthquake loading. This chapter is intended to give the user an understanding of how the CWRotate program is to be used to its greatest potential. To that end it also tries to imbue the user with an understanding of the work-flow in creating and executing a CWRotate analysis.

Input data for the CWRotate program falls into six different groups, and the user-interface reflects those groupings using tabs. The input groupings are:

- **Horizontal earthquake time-history data**
- **Vertical earthquake time-history data**
- **Structural geometry**
- **Structural wedge information**
- **Driving wedge information**
- **Analysis specific data**

There is one other tab, a “splash” tab that shows a typical example of the type of problem handled by the CWRotate program; this is labeled as the Introduction tab. Above the Introduction tab shown in Figure 5.1 is a drop down menu entitled “File.” Activating this menu allows the user to open an existing, user-created, **\*\*\*.CWR** file that replenishes the contents of all

tabs. Also on the Analysis tab are the controls to run an analysis and post-processing options.

**Introduction Tab:** The first tab, labeled **Introduction**, shows the structural wedge, idealized as a rigid body, and the forces acting on it (Figure 5.1). The rock-founded cantilever retaining wall is buttressed at its toe by, e.g., an invert spillway slab (not shown). The rotation of the structural wedge about its toe is assumed to occur during earthquake shaking.

**Forces Shown on the Introduction Tab:**  $P_{AE}$  is the dynamic active earth pressure force due to the driving, moist soil wedge (not shown) or the partially submerged soil wedge (when a water table is present in the retained soil). Inertial effects due to earthquake shaking are incorporated in  $P_{AE}$ .  $W$  is the weight of the structural wedge, including both the weight of the (cantilever) retaining wall as well as the weight of the soil contained within this idealized structural wedge.  $W$  times  $k_h$  and  $W$  times  $k_v$  are the horizontal and vertical inertial forces, respectively, acting on the structural wedge during earthquake shaking. The reactions of the rock foundation on the structural wedge are represented through the horizontal and vertical forces  $T$  and  $N'$ , respectively.  $P_{resist}$  is the force provided to the toe of the (cantilever) retaining wall by the invert spillway slab (not shown) during earthquake shaking.

### 5.2.2 Earthquake time-history input

Both horizontal and vertical time-history input follow the same input pattern. First an appropriate, base-line corrected acceleration time-history data file is selected for the Corps project by the user. Given the non-standardized nature of earthquake time-history data files, certain attributes need to be specified to correctly read the input (ASCII) data file. These attributes are entered in the Format section of the Earthquake Time-history (EQTH) tabs – Horizontal and Vertical. This is an exceptionally powerful tool for handling any format EQTH files. Figure 5.2 shows the **Horizontal Earthquake Time-History** tab.

To read in an appropriate EQTH data file, the user must first specify a file to be read in. The user can type a specific filename or select a file using the **Find** button that exists on the **Earthquake Time-History** tabs.

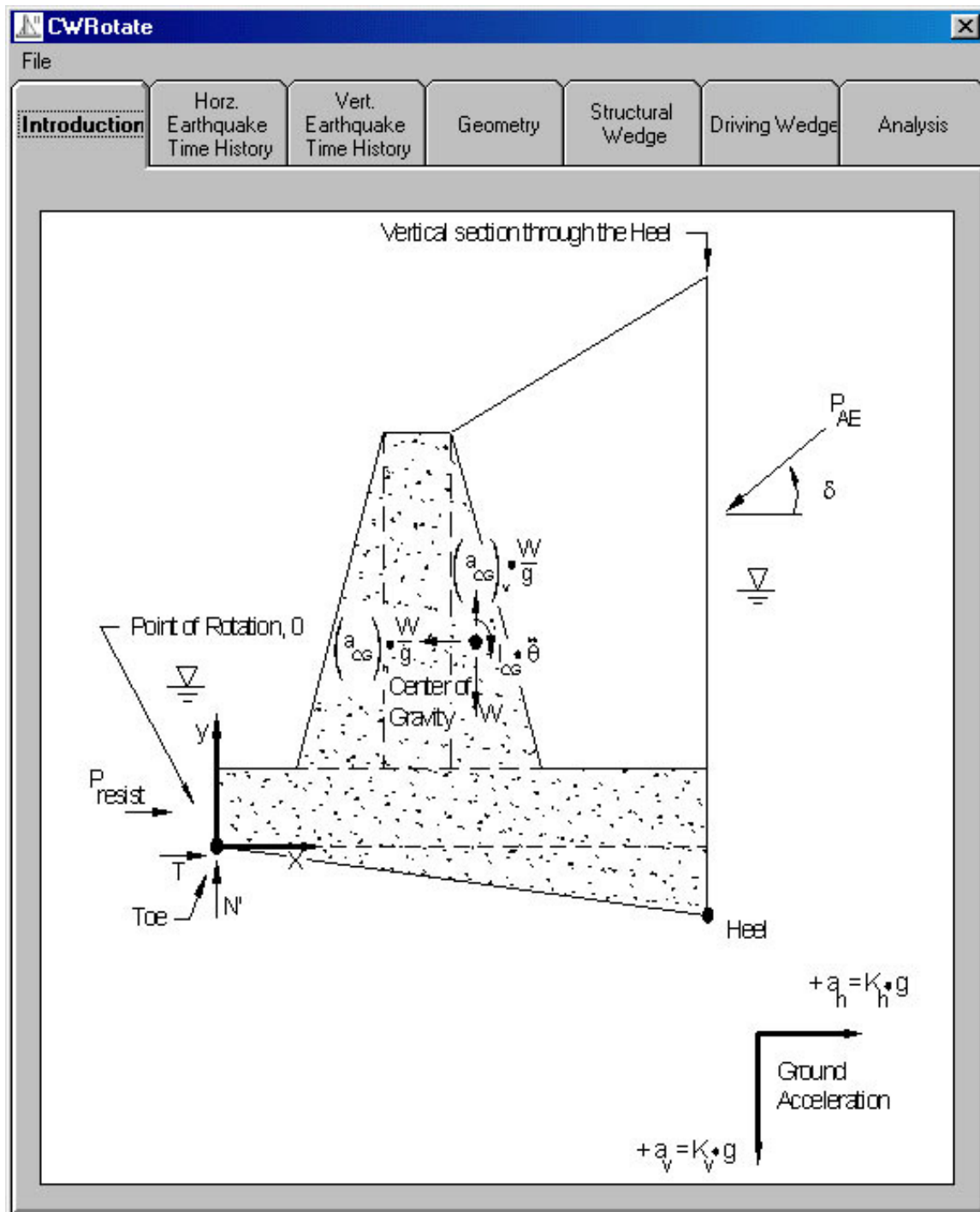


Figure 5.1. The **Introduction** tab features and idealized structural wedge diagram.

When a file has been selected, a format must be built. All specifications for reading a file are grouped in a frame labeled **EQTH Format**. To know what information to enter for reading the file, it will be beneficial to be able to peruse the file to find each section of data.

The first data in each EQTH file are a number of header lines. These are of no concern to the CWRotate program, so entering how many header lines there are allows the program to skip those lines. Also of no concern to the program CWRotate are line numbers in the input. In order to ignore them, the user must specify whether these line numbers exist, and if they do, which side of the data are they on.

It is more important to know how many data samples are on each line. Entering the **Number of Values/Line** keeps the program from entering blank samples or ignoring samples. The value entered for **Time-step** should be the amount of time that occurs between samples, establishing the sampling frequency and the total time for the earthquake data.

Since CWRotate works from the beginning of an earthquake, it is to be assumed that the first sample, time-step 0, will be of value 0.0 in whatever units are to be chosen. If the EQTH file does not have this zero point, it will have to be added. This can be done using the combo box provided.

In the same manner, the units in which the data were recorded can be specified. NOTE: The vertical EQTH file uses the same units as the Horizontal EQTH file. EQTH units must be consistent.

Finally, there is a combo box that shows several options for a data format. These formats are displayed as if they were in a FORTRAN FORMAT statement. These are especially important in areas where data text may run together.

After an EQTH format has been built for a particular file, the user can read in the Earthquake Time-history. When the button has been pressed, the actual values of the maximum and minimum values for that file are displayed in the **Data Limits** sub-frame of the **EQTH Format** frame. A plot of the input data also is displayed at the bottom of the tab. The **Edit EQTH Data** frame is also enabled.

The **Edit EQTH Data** frame is a tool that allows the user to scale the EQTH data to values more appropriate for modeling the problem at hand. There is a combo box that allows the user to invert the user-specified earthquake acceleration time-history values, which is valuable for determining how the direction of peak values influences the computed results.



There are also two possible ways of scaling the input data, either by setting an absolute scale value to multiply the samples by or by setting an absolute maximum value for the positive peak value and scaling the other samples to match. To choose the scale method, click the radio button beside that option. Then type in the value desired.

When this is done the inactive choice will be updated with the related value. Also, the scaled minimum and maximum values will be displayed, and the data plot at the bottom of the form will reflect the changes.

If the user desires a hardcopy of the scaled data in the same format as at the bottom of the tab, there is a button labeled **Print Plot**.

Vertical acceleration time-histories are handled in a similar fashion as the horizontal acceleration time-histories.

### 5.2.3 Structural geometry input

For simplification of the geometric modeling and engineering analysis required to configure the structural wedge for analysis, it is assumed that the structural geometry of any structure designed by this program will be described in axis-aligned right-triangular and rectangular regions. Using this idea, a structural region template was created (see the lower image in Figure 5.3) that allows the user to specify regions as widths and heights for an accurate representation of the wall. There are a total of ten different regions that may be used. Each region is placed in relation to the other regions, and most regions can be represented as zero width and/or height, effectively removing them from the structure. The result of this modeling technique is the possibility to model almost any standard Corps retaining wall cross section.

The diagrams in Figures 5.4 and 5.5 illustrate how the sections can be used to create different wall cross sections. Figure 5.4 displays each of the ten sections as well as their widths and heights. Each section is either rectangular or right triangular, and can therefore be defined by specifying the width and height of each of the sections that, when assembled together, form the structural wedge. Three material regions of concrete, moist soil, and saturated soil are allowed. The concrete material regions are assigned to material region numbers 1, 2, 6, 7, and 10. Moist soil material regions are assigned numbers 4, 5, and 9, while saturated soil

material regions are assigned numbers 3 and 8. Values for the three material unit weights are specified by the user as part of the input data.

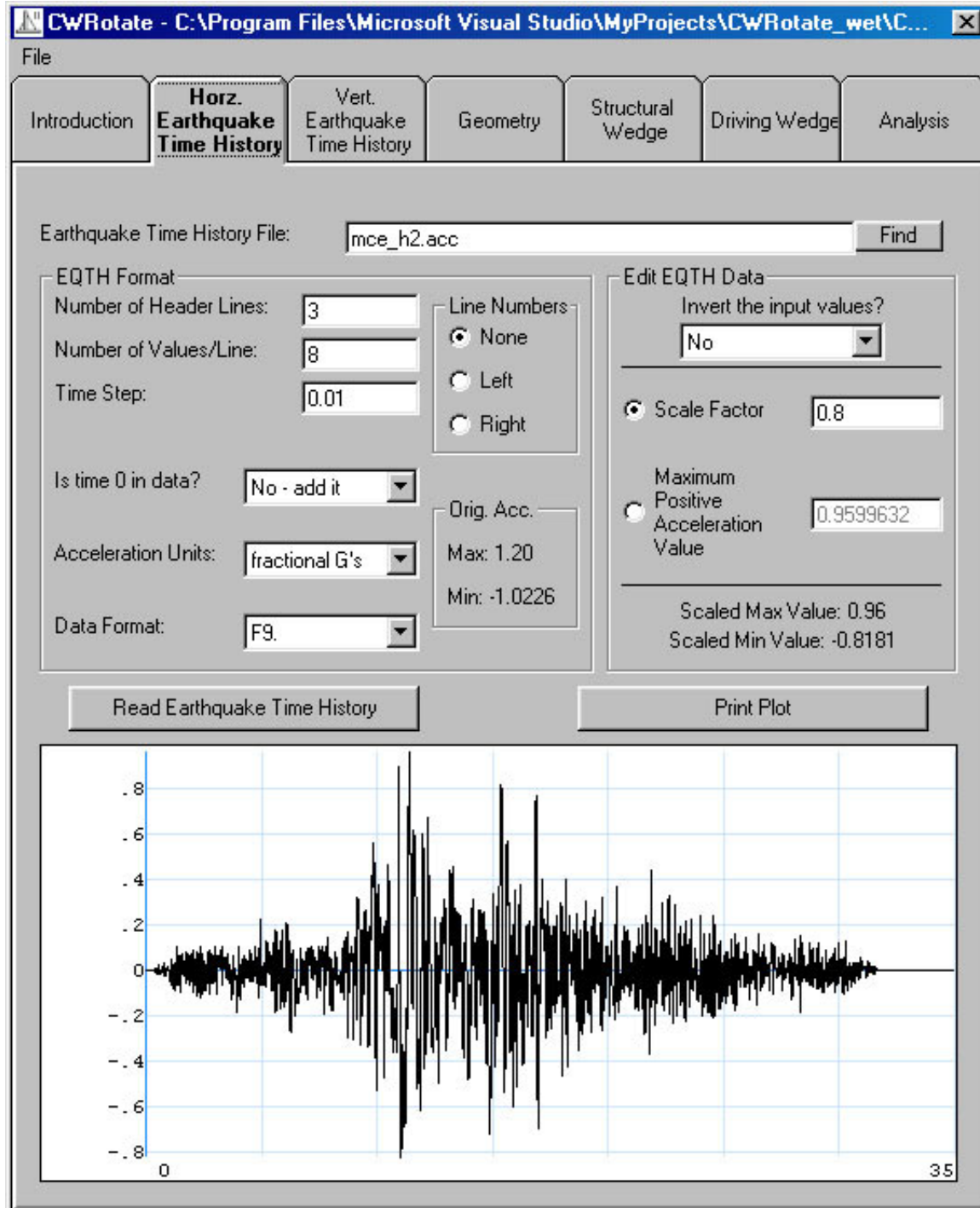


Figure 5.2. A strong earthquake time-history ground motion shown in the **Earthquake** tab.

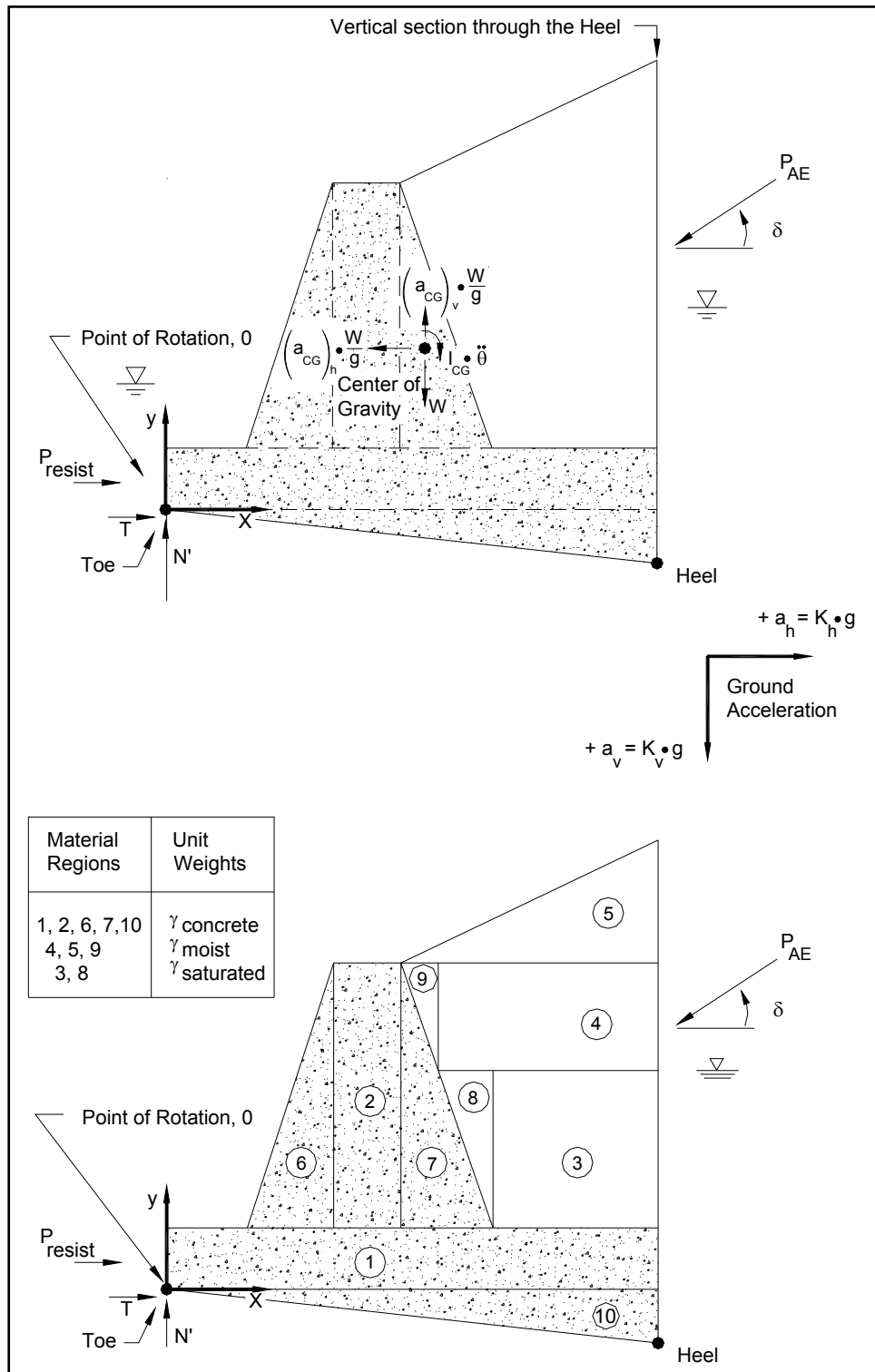


Figure 5.3. Dynamic forces acting on the free-body section of the structural wedge and its material regions.

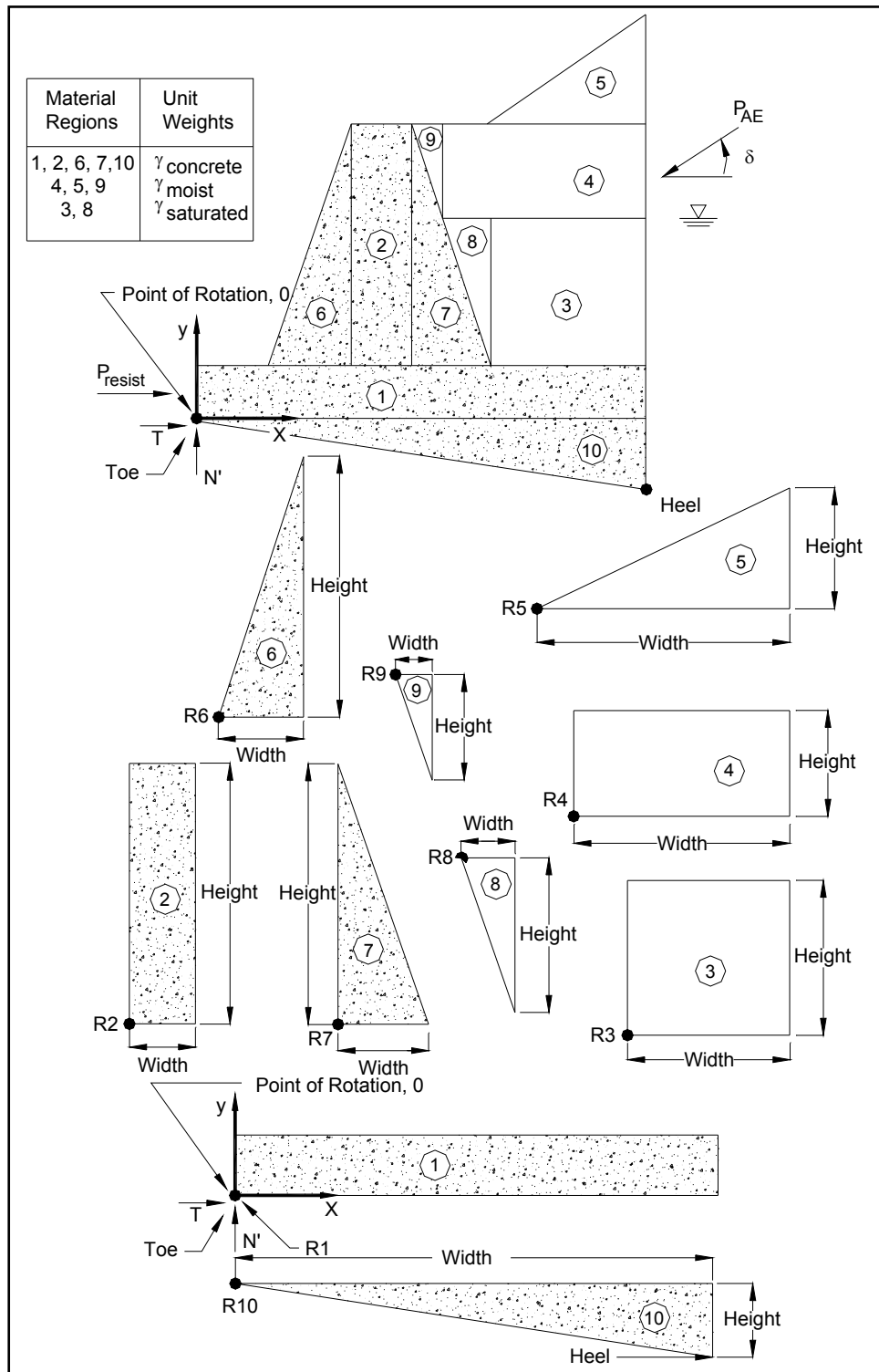
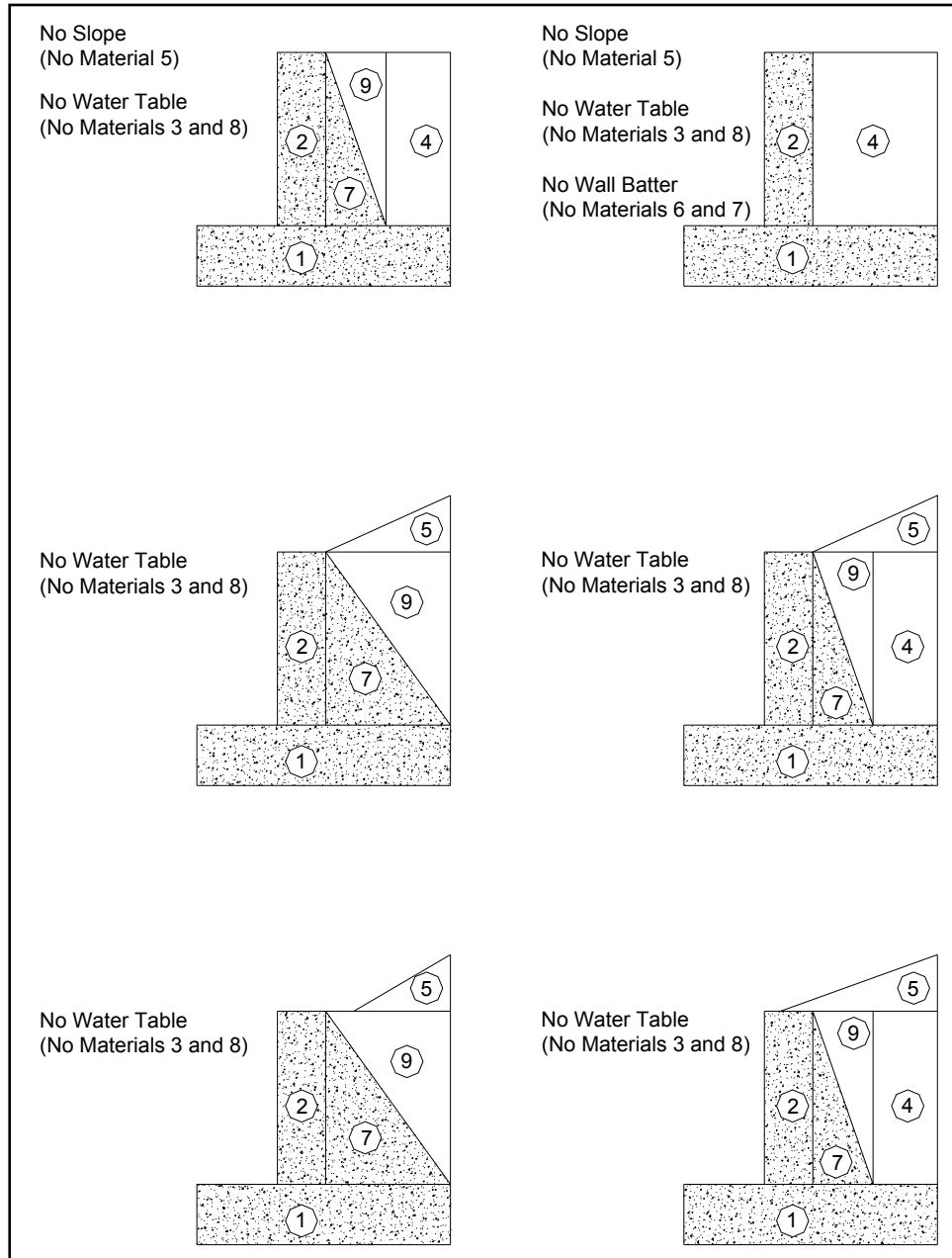


Figure 5.4. Examples of width and height definition for each of the ten structural wedge material regions.

Figure 5.5 shows examples of how different walls may be configured using the ten sections. Entering a width or height of zero enables sections to be

entirely ignored for a structural wedge. For example, in the first diagram, region 6 is not used and therefore its width (or height) is set to zero as user input.

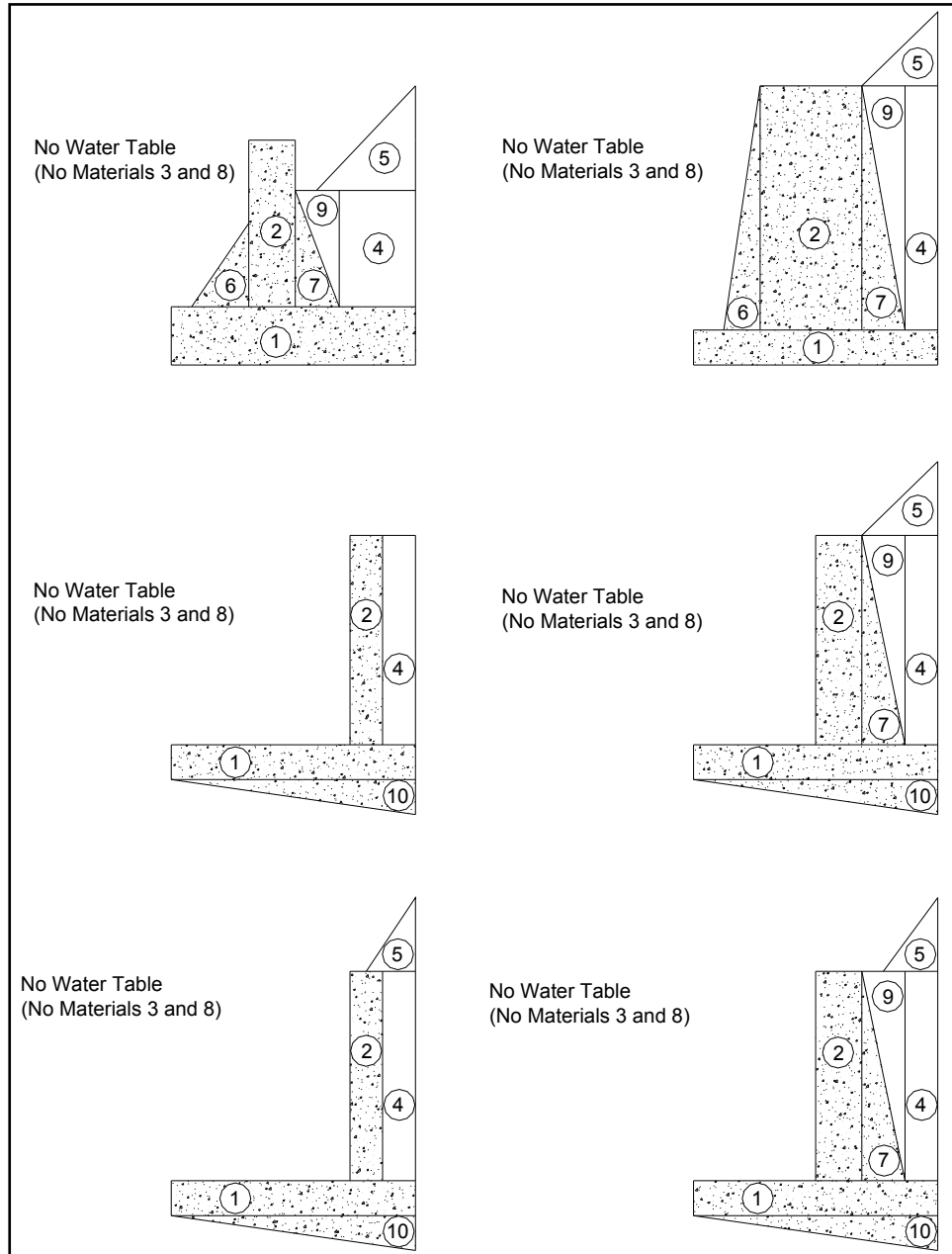


a. Moist backfill (Continued)

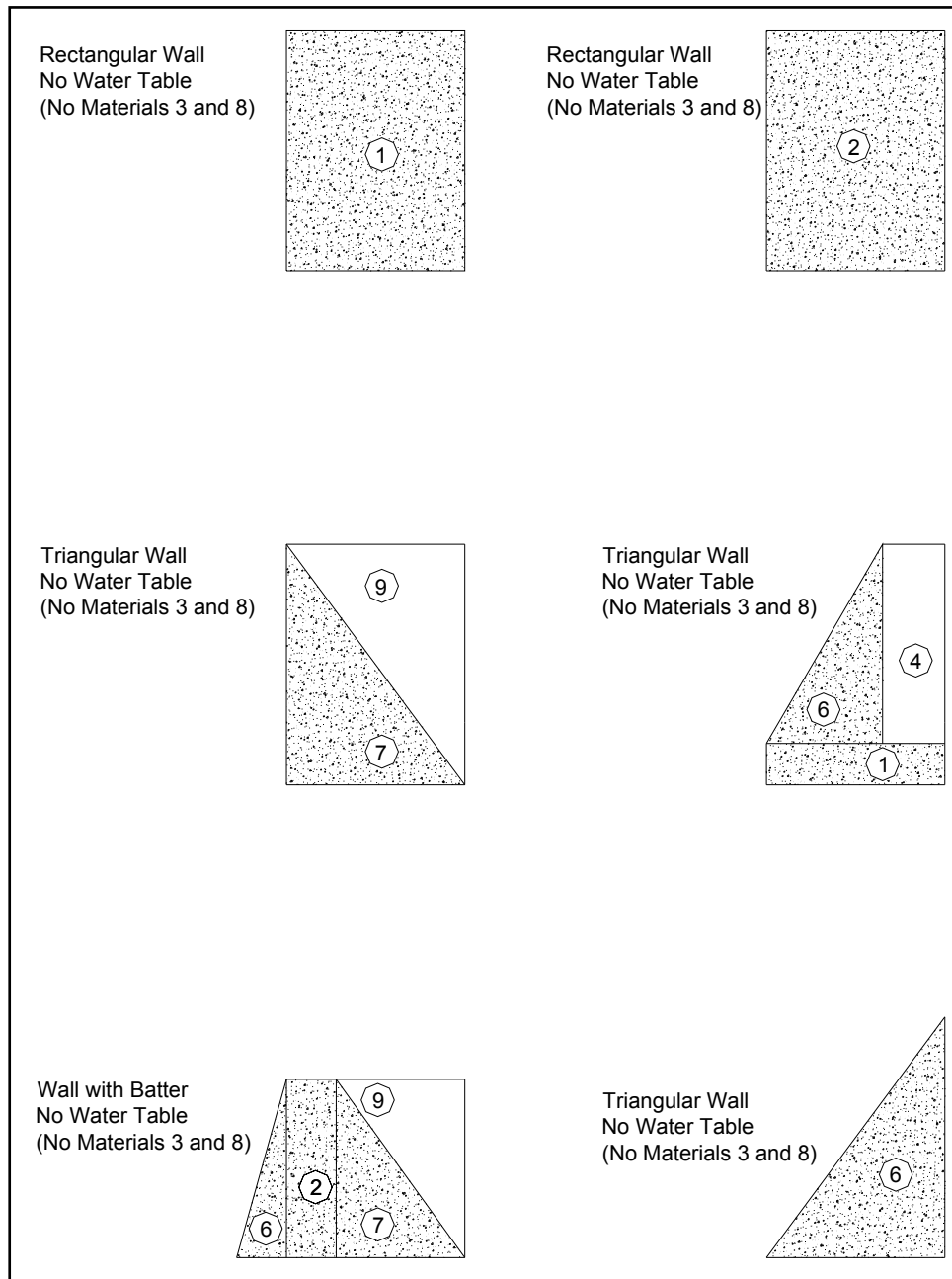
Figure 5.5. Examples of structural wedge material regions (Sheet 1 of 4).

When region 10 is specified, as in the case of some of the hypothetical wall geometries shown in Figure 5.5, the user is allowed to input the height of the region but not its width. The width of region 10 is dictated by the

geometry (specifically, the width) of region 1, as shown in these figures. When this region is present, the user specifies its height.

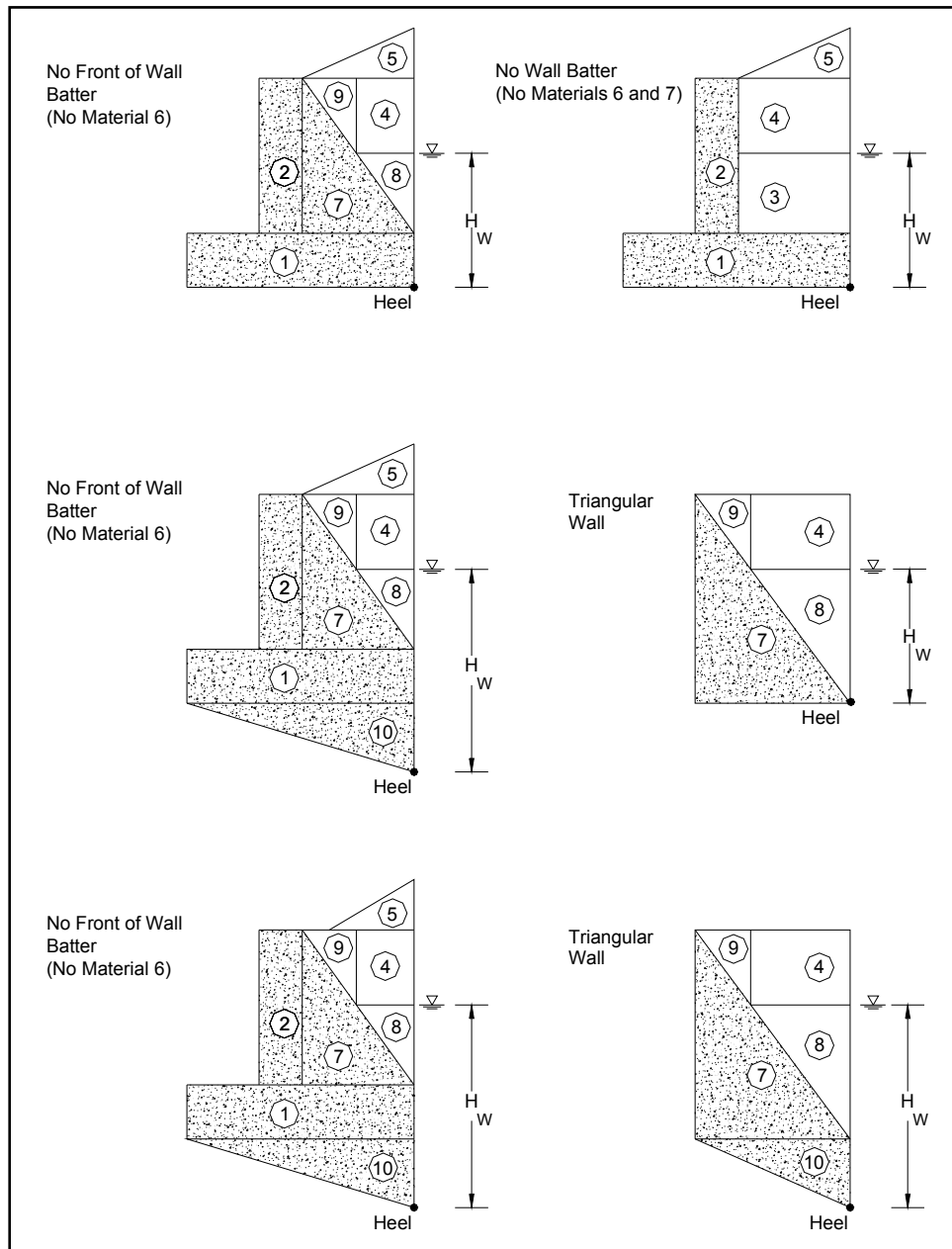


a. Moist backfill (Continued).  
Figure 5.5. (Sheet 2 of 4).



a. Moist backfill (Concluded).  
 Figure 5.5. (Sheet 3 of 4).

Figure 5.5b shows the configurations possible if a water table is specified in the retained soil. Regions 3 and 8 are created when a table within the retained soil is higher than the concrete structure above the heel point.



b. Partially submerged backfill.  
Figure 5.5. (Sheet 4 of 4).

The Figure 5.6 **Geometry** input tab is designed around this template scheme and provides a visual confirmation for the user. At the upper left of the tab, there is a region template that shows all of the regions that can be used in CWRotate. Each region is color-coded to show which of the three materials it belongs to. The currently selected region (chosen in the **Region Information** box) is highlighted to show the user which geometry is being changed.



At the upper right of the tab is a drawing of the geometry as created by the user. Three data points are also displayed for the structure (*although overlapping points may hide others*). The toe point is the lower leftmost point of the wall and it is displayed in purple. All geometry is placed relative to this toe location. Its coordinate is entered in the **Toe Position** box, using the units specified in the **Units of Length** combo box. Since all data are relative to this point, changing the toe position will not change the input geometry plot.

Another point displayed on the input geometry plot is the rotation point. In this initial version of  $C_{\text{orps}}W_{\text{all}}\text{Rotate}$ , the rotation point will be specified by default to be the same as the toe point and will hide the toe point dot in the input geometry plot. The rotation point, displayed in red, is the point at the base, coincident with the toe of the wall. It is the point about which the structural wedge will rotate. Note that the rotation point is restricted to the toe point in the **Rotation Point** data box display. *The boxes for the coordinate entries are gray, signifying a fixed value that the user may not change.*

The last point that is displayed on the input geometry plot is the center of gravity for the structural wedge, displayed in light green. The center of gravity is computed for the user, based on the geometry for the model and the material unit weights for each region of the geometry. The actual absolute coordinates of the center of gravity are displayed in the **Center of Gravity** box. *Because it is a computed value, its (coordinate) entry boxes are gray to designate that the user need not perform this tedious calculation.*

There are four unit weights for the model. These unit weights are for concrete, moist soil, saturated soil, and water. They are user-specified input in the **Unit Weights** data box, using the units displayed in the title for the box.

The input geometry is input using the **Region Information** box. The user can select a region to edit, which will be highlighted in the region template plot, and then specify a width and height for that region. Any other affected regions are adjusted to fit the new region and the results are displayed in the input geometry window.

Another way to change the geometry of the model is to specify the **Backfill Water Table Height**. The water table height specifies the separation point between moist and saturated soil, in the input geometry (and in the driving wedge, discussed later). The water table height is specified relative to the heel of the model, defined as the lower rightmost point, possibly below the toe.

On the pool side, the water must be taken into account for rotation or sliding, too. The **Pool Base** height is set by the top of the buttressing, reinforced concrete toe slab, and is measured (vertically) from the toe. The **Pool Height** is also measured relative to the toe. These two heights define the total height of the pool for hydrodynamic water pressure calculations (see Appendix D).

The last bit of input data to be entered on the input geometry tab is a force representing the buttressing action of the reinforced concrete slab acting on the vertical face extending upwards from the toe of the wall. This is a user-specified force which acts horizontally at a user-specified height above the toe of the retaining wall. (Refer to Strom and Ebeling (2004) for a method to determine the magnitude of this force.) The relative height and magnitude are specified in the **Resisting Force** box, using the units in the title of the box. Its height is measured relative to the toe.

From the **Geometry** tab, a button click can let the user view the water pressures for the structural geometry, relative to the water heights (Figures 5.7 and 5.8). (Refer to Appendix D for a complete description of the assumptions made for water pressures in this initial version.) Another tab shows the computed data for the structural wedge (Figure 5.9). Tables showing the current input and computed values (center of gravity, moment about the rotation point, etc.) can be viewed, saved to a file, or printed. It is also possible to print a plot of the input data from this window.

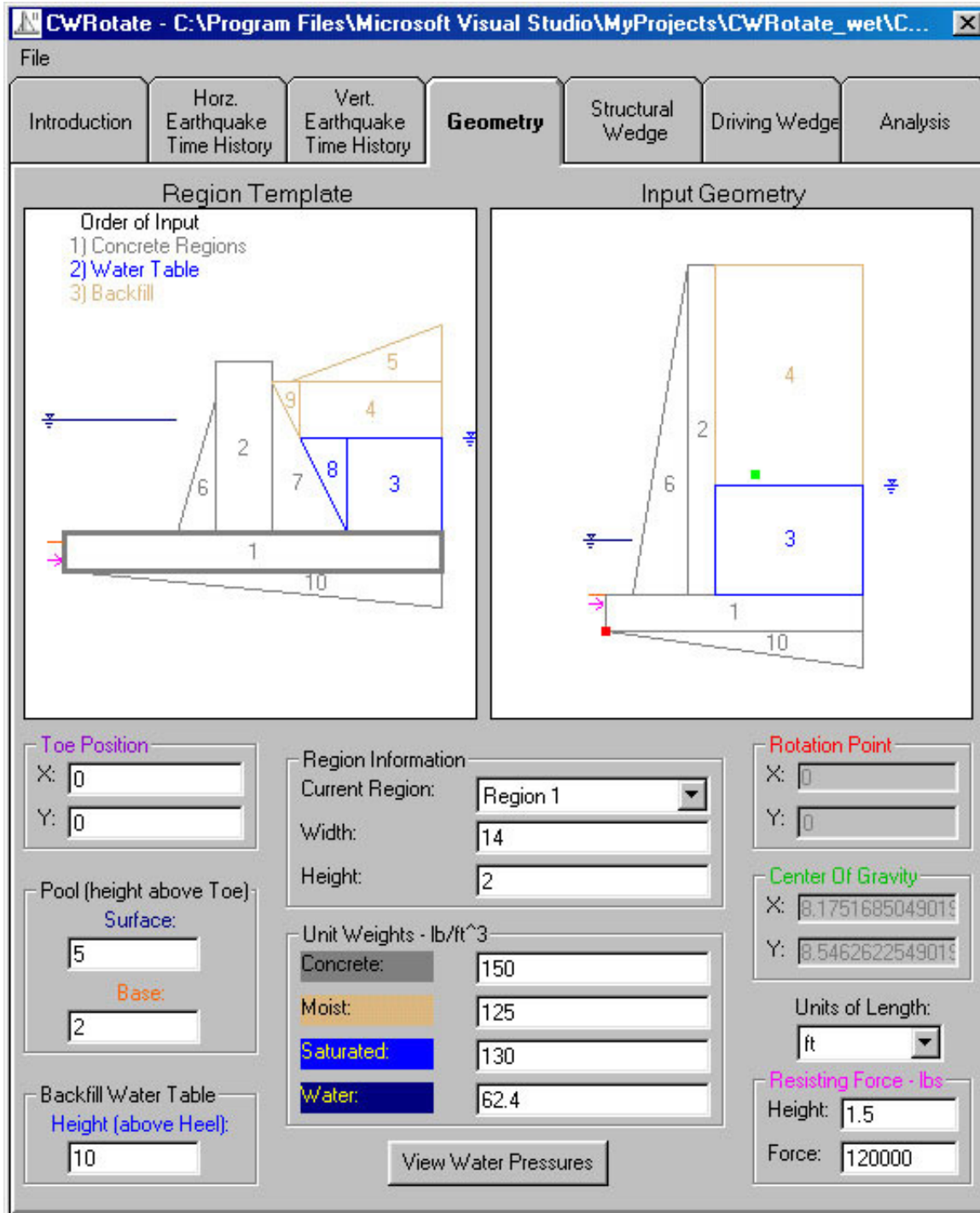


Figure 5.6. The input **Geometry** tab in action.

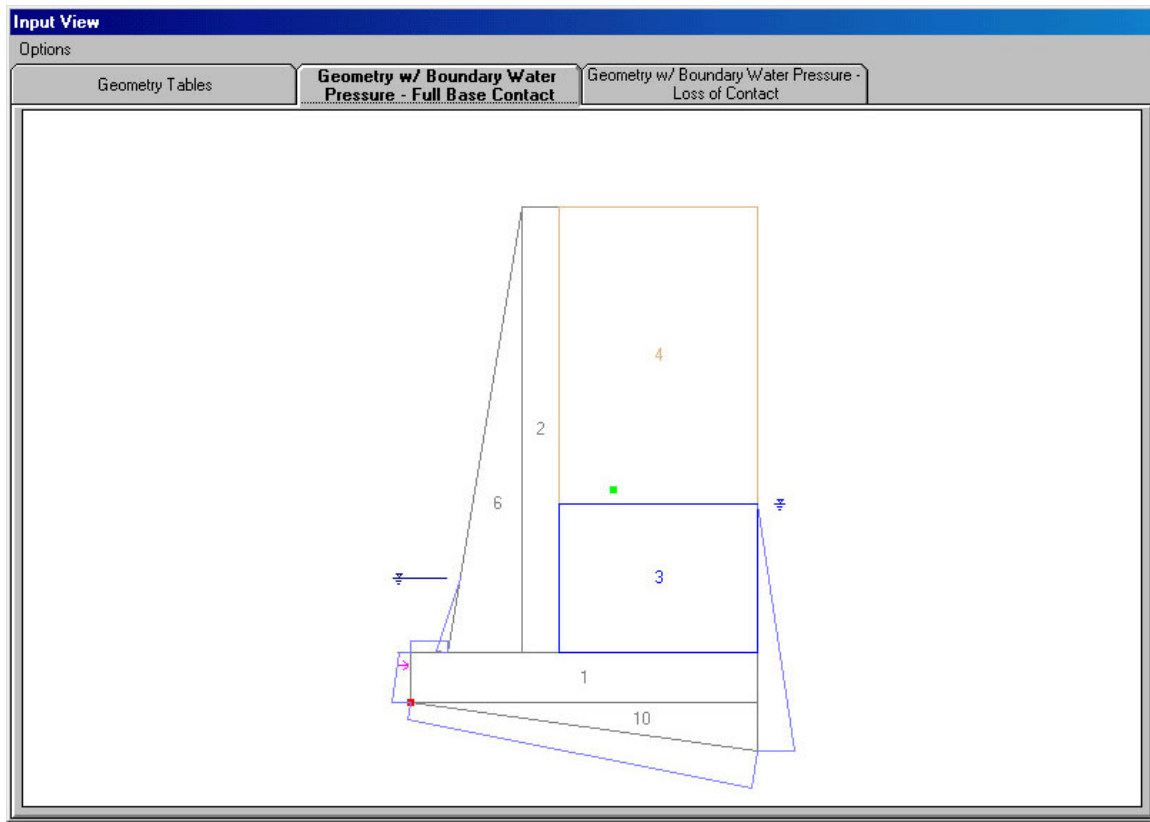


Figure 5.7. Boundary water pressure diagram – full contact along the base of the retaining wall with its foundation in a sliding block analysis.

#### 5.2.4 Structural wedge data

To simplify the computation of forces upon a wall, the model of the retaining system was split into two wedges: The structural wedge contains the retaining wall geometry, and the driving wedge to the right of the structure that “pushes” against the structural wedge.

From the **Structural Wedge** data tab, it is possible to enter the engineering material properties for the structural wedge. Soil strength can be entered using parameters associated with either the **Effective Stress** or **Total Stress** method of analysis, with either choice determining what is input. Consideration of seismically induced permanent deformations is part of the material property specification process. These data input tabs for the structural wedge are shown in Figures 5.10 and 5.11, respectively.

If **Effective Stress** method of analysis is chosen, then the effective angle of internal friction and the effective cohesion need to be entered for both

the foundation soil and the soil-to-concrete interface at the base of the retaining wall.

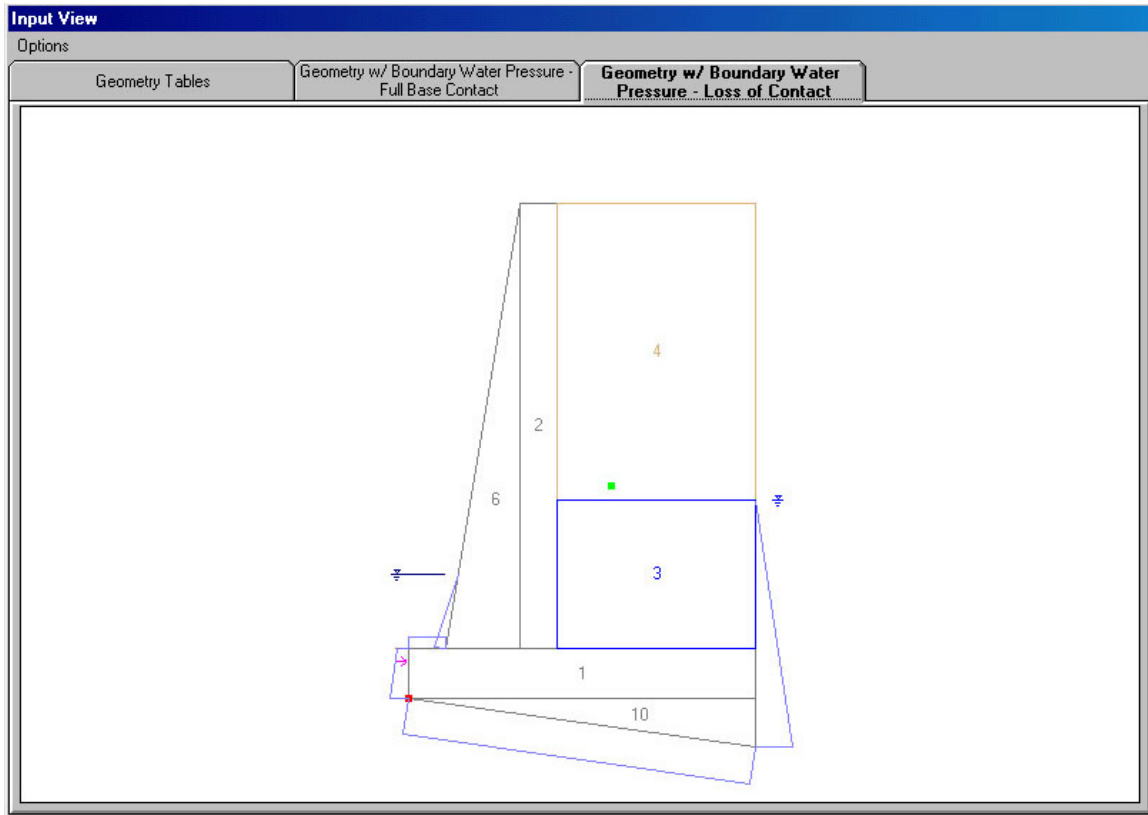


Figure 5.8. Boundary water pressure diagram – loss of contact (i.e., development of a gap) along the base of the retaining wall with its foundation in a rotational analysis.

If **Total Stress** is chosen then the undrained shear strength is required for both foundation soil and the soil-to-concrete interface. The tab changes reflect the different input. Note that in a total stress analysis the friction angle (PHI) box does not accept user input and its value is internally set equal to zero by CWRotate.

**Input View**

Options

**Geometry Tables**      Geometry w/ Boundary Water Pressure - Full Base Contact      Geometry w/ Boundary Water Pressure - Loss of Contact

\*\*\*\*\* Region Information \*\*\*\*\*

#	Width	Height	Unit Weight	Area	Unit Mass	Total Mass
1	14.00	2.00	150.00	28.00	4.662	130.540
2	1.50	18.00	150.00	27.00	4.662	125.878
3	8.00	6.00	130.00	48.00	4.041	193.945
4	8.00	12.00	125.00	96.00	3.885	372.972
5	0.00	0.00	125.00	0.00	3.885	0.000
6	3.00	18.00	150.00	27.00	4.662	125.878
7	0.00	0.00	150.00	0.00	4.662	0.000
8	0.00	0.00	130.00	0.00	4.041	0.000
9	0.00	0.00	125.00	0.00	3.885	0.000
10	14.00	2.00	150.00	14.00	4.662	65.270

#	Center of Gravity X	Center of Gravity Y	Distance from Center of Gravity to Rotation Point	Total Weight	Reference Point X	Reference Point Y
1	7.00	1.00	7.07	4200.00	0.00	0.00
2	5.25	11.00	12.19	4050.00	4.50	2.00
3	10.00	5.00	11.18	6240.00	6.00	2.00
4	10.00	14.00	17.20	12000.00	6.00	8.00
5	14.00	20.00	24.41	0.00	14.00	20.00
6	3.50	8.00	8.73	4050.00	1.50	2.00
7	6.00	2.00	6.32	0.00	6.00	2.00
8	6.00	2.00	6.32	0.00	6.00	2.00
9	6.00	2.00	6.32	0.00	6.00	2.00

Figure 5.9. Summary of the user-defined geometry and computed weight, mass and moments of inertia for the structural wedge as defined in the **Geometry** tab.

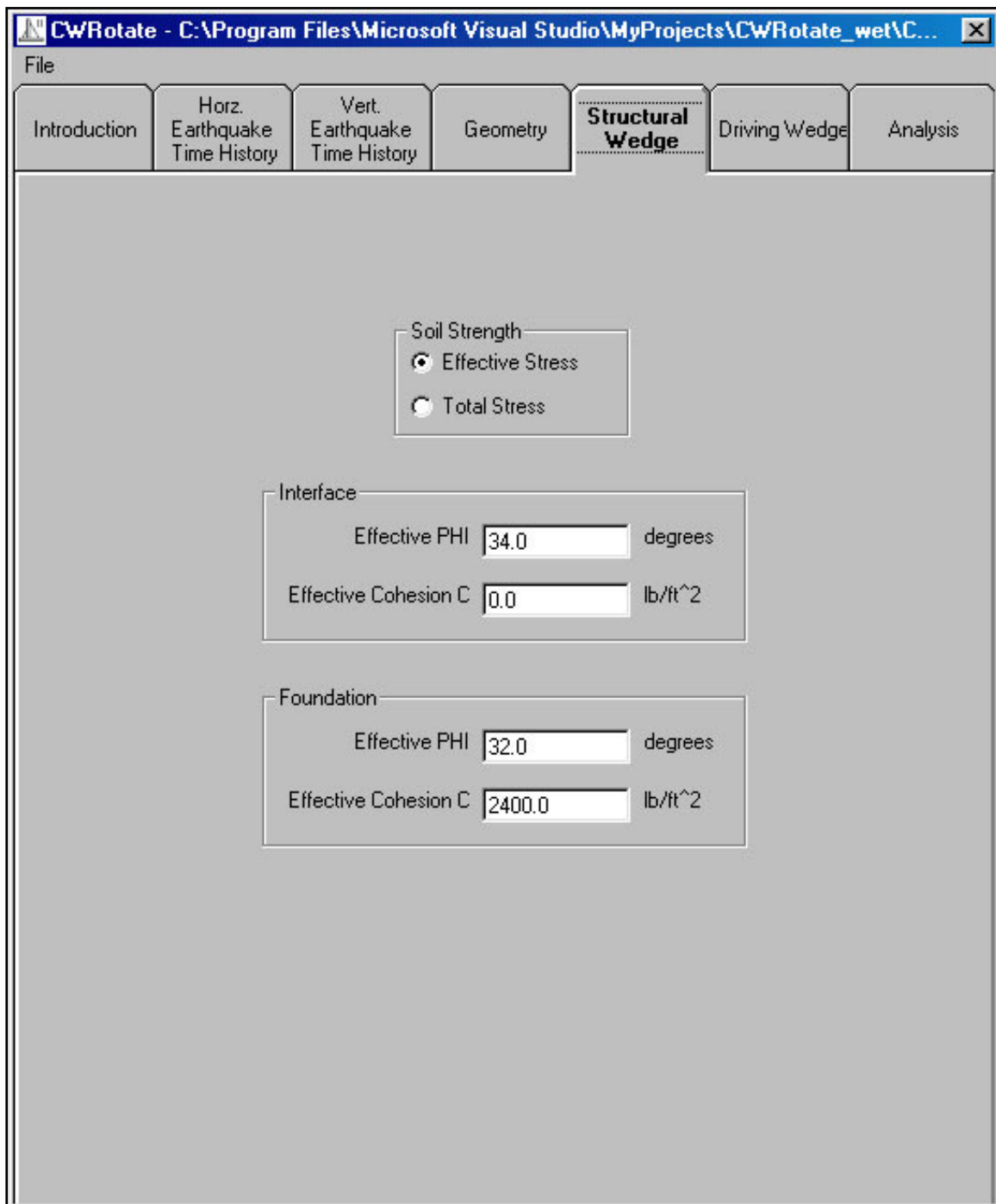


Figure 5.10. Defining the material properties using the **Structural Wedge** tab for an effective stress analysis.

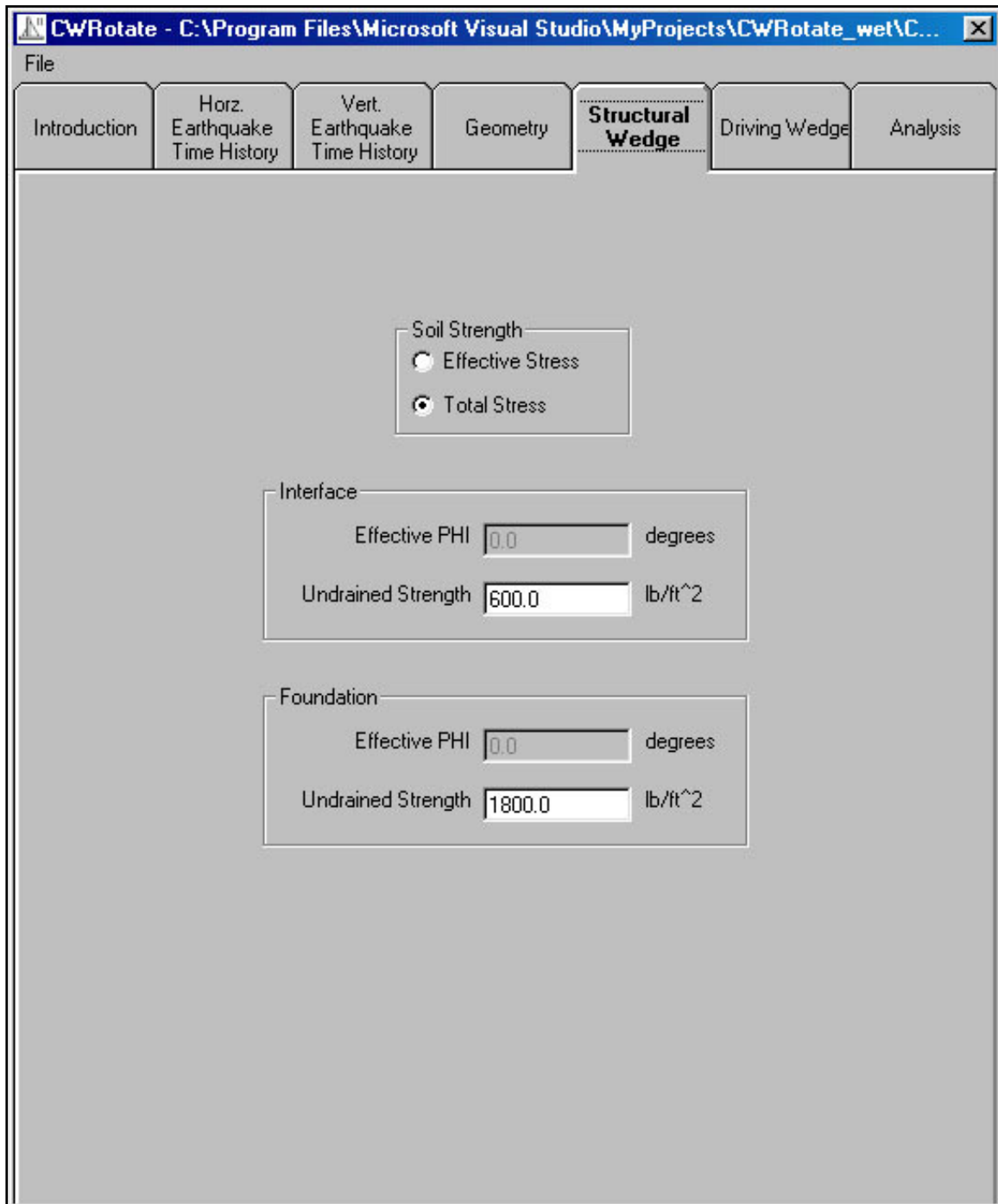


Figure 5.11. Defining the material properties using the **Structural Wedge** tab for a total stress analysis.



### 5.2.5 Driving wedge data

Modeled after the input to the PC-based program EQWedge (developed by the primary author of this report), the driving wedge data allow the input of engineering data for determining the force imposed by the driving wedge on the structural wedge. The sweep-search wedge formulation is used to compute this force, as discussed in Appendix A. Some structural wedge geometry data are also displayed on this tab as a reminder for the user.

Once again, the method for determining the soil strength determines the data that are input for the driving wedge soil properties. If **Effective Stress** is chosen then the effective angle of internal friction and the effective cohesion need to be entered for the retained soil of the driving wedge (Figure 5.12). (The effective angle of interface friction is also specified.) Otherwise, if **Total Stress** is chosen then only the undrained shear strength is required for the retained soil of the driving wedge (Figure 5.13). The tab changes to reflect the different input. All other inputs for this tab stay the same.

The value entered for **Delta** is the effective angle of interface friction between the driving wedge and the structural geometry. This interface is the imaginary vertical section that extends upwards from the heel of the wall and delineates the driving wedge from the structural wedge.

The height of the vertical section is determined from the structural wedge geometry. It is provided to give the user knowledge of the length of the vertical interface between the structural wedge geometry and the driving wedge.

The height to level backfill and backfill slope entries define the shape of the driving wedge. It is assumed that the retained soil geometry is as high as or higher than the structural wedge geometry, as defined by the height to level backfill. If the retained soil is higher than the structural geometry, then a slope must be specified for the backfill, until it reaches the level backfill limit.

The next three values shown are the moist unit weight, the saturated unit weight, and the hydrostatic water table. These values were all entered in the structural wedge **Geometry** tab, and are provided here as a reminder.

The next value,  $r_u$ , is the excess pore water pressure ratio due to earthquake shaking in an effective stress analysis. It is disabled in this program (at this time). However, provisions are made to add this option to CWRotate in the future.

The final value for entry is the minimum angle for the slip plane. Using a sweep-search method of analysis, CWRotate will evaluate all potential slip planes in 1-degree increments, between the user-provided **Min. angle for slip plane** value (in degrees) and 89 degrees, from horizontal. If a maximum thrust force is not found (refer to insert figure to Figure A.1) then the driving wedge defined by the user-provided minimum angle for slip plane is used to compute the thrust force acting on the structural wedge. A low value for this angle is typically specified by the primary author of this report (e.g., on the order of 5 degrees or so) unless there are geometrical constraints.

CWRotate - C:\Program Files\Microsoft Visual Studio\MyProjects\CWRotate\_wet\C...

File

Introduction    Horz. Earthquake Time History    Vert. Earthquake Time History    Geometry    Structural Wedge    **Driving Wedge**    Analysis

Soil Strength

Effective Stress

Total Stress

Input Values

Effective PHI  degrees

Effective Cohesion C  lb/ft<sup>2</sup>

Delta  degrees

Height of Vertical Section  (from Heel)

Height to Level Backfill  (from Heel)

Backfill Slope  degrees

Moist Unit Weight  lb/ft<sup>3</sup>

Saturated Unit Weight  lb/ft<sup>3</sup>

Hydrostatic Water Table  (from Heel)

ru

Min. angle for slip plane  degrees (from horizontal)

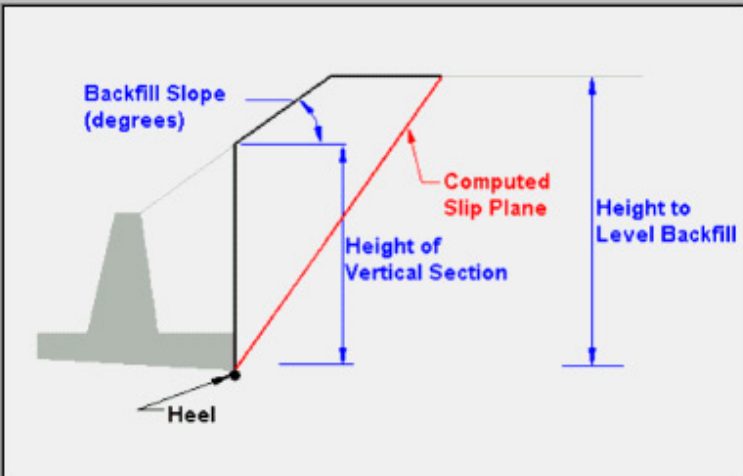


Figure 5.12. Defining the material parameter for the **Driving Wedge** tab – effective stress method of analysis.

CWRotate - C:\Program Files\Microsoft Visual Studio\MyProjects\CWRotate\_wet\C...

File

Introduction    Horz. Earthquake Time History    Vert. Earthquake Time History    Geometry    Structural Wedge    **Driving Wedge**    Analysis

Soil Strength

Effective Stress

Total Stress

Input Values

Effective PHI  degrees

Undrained Strength  lb/ft<sup>2</sup>

Delta  degrees

Height of Vertical Section  (from Heel)

Height to Level Backfill  (from Heel)

Backfill Slope  degrees

Moist Unit Weight  lb/ft<sup>3</sup>

Saturated Unit Weight  lb/ft<sup>3</sup>

Hydrostatic Water Table  (from Heel)

ru

Min. angle for slip plane  degrees (from horizontal)

The diagram illustrates a retaining wall cross-section. A vertical line represents the wall face, with a point at the bottom labeled 'Heel'. To the right of the wall, a red line represents the 'Computed Slip Plane'. The 'Backfill Slope (degrees)' is indicated by a blue arc between the horizontal ground surface and the backfill slope. The 'Height of Vertical Section' is shown as a blue vertical dimension from the heel to the top of the wall. The 'Height to Level Backfill' is shown as a blue vertical dimension from the heel to the top of the backfill. A small green trapezoidal shape is shown to the left of the wall, representing the soil behind the wall.

Figure 5.13. Defining the material properties for the **Driving Wedge** tab – total stress method of analysis.

### 5.2.6 Analysis results and visual post-processor

The Figure 5.14 **Analysis** tab is broken into three sections: **Input Parameters, Run CWRotate Analyzer, View Output**. The Input Parameters section allows the user to enter last-minute analysis options. The Run CWRotate Analyzer section is a button to execute the program. The View Output section contains options for viewing the many outputs of the CWRotate Analysis, including an option to view the total rotation and/or slide of the structure.

Immediately prior to execution of CWRotate it is a good idea to create a restart file containing all the input information. This is accomplished by using the file drop down menu and the save option. The file created has a “CWR” extension. This file may be read in by CWRotate using this same file drop down menu and populate the data contained within all tabs at a later point in time.

After the **Run CWRotate Analyzer** button is activated, a CWRotate.IN ASCII data input file, described in Appendix F, is created by the Visual Modeler and the FORTRAN engineering program is executed. This FORTRAN engineering program creates the output and plot data files that are used in the Figure 5.14 **Visual Output** frame of the **Analysis** tab. Appendix G lists and summarizes the contents of these output and plot data files.

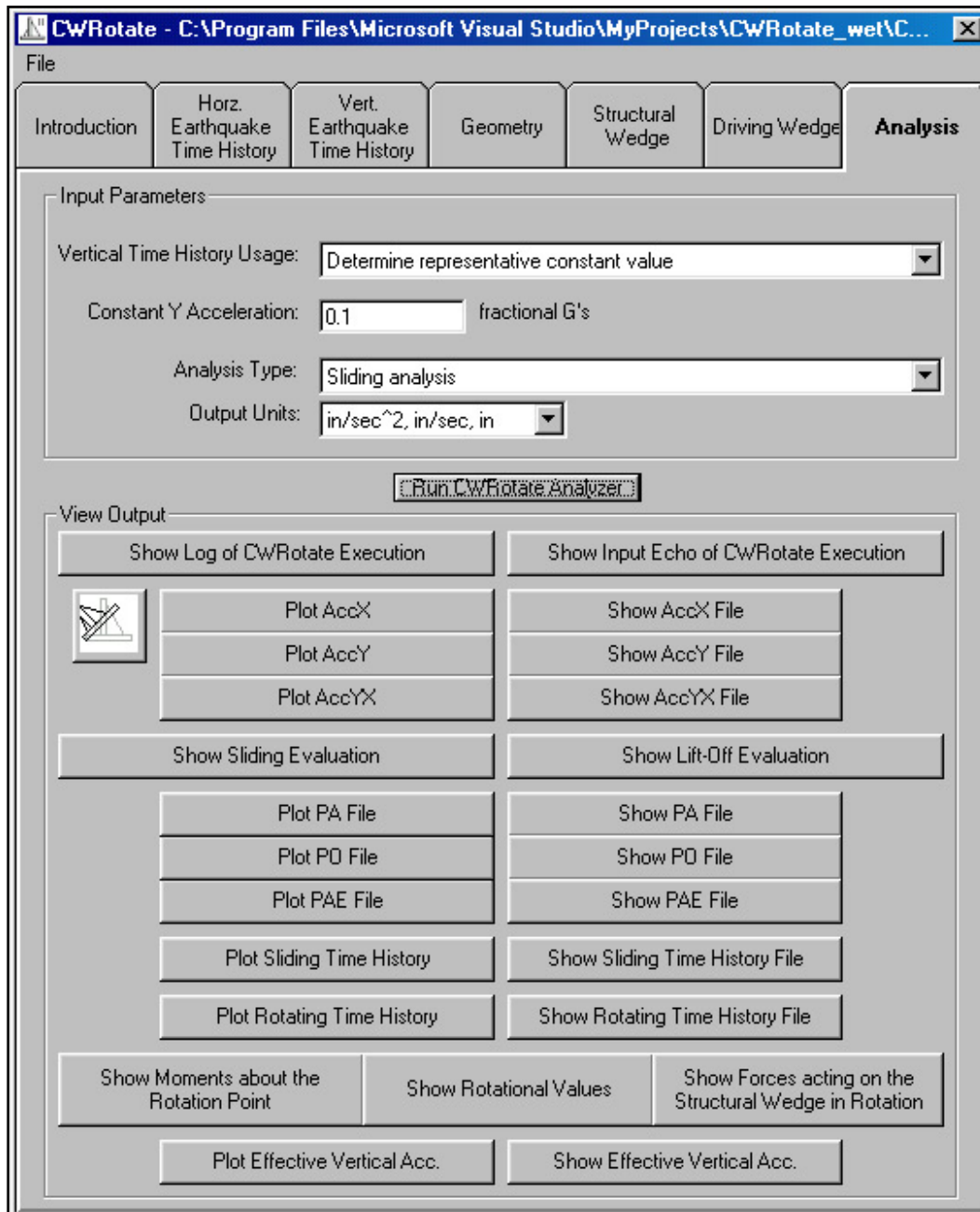


Figure 5.14. The **Analysis** tab.

In the **Input Parameters** frame allows for the user to select/specify the following four pieces of information:

1. **Vertical Time-History Usage** combo box:
  - Determine representative constant value
  - Evaluate with representative constant value
  - Evaluate with current time-history

2. **Constant Y Acceleration** data box.
3. **Analysis Type** combo box:
  - Sliding Analysis
  - Rotating Analysis
  - Sliding and Rotating Analysis
4. **Output Units** combo box.

Input Parameters selection is best described by the following staged seismic evaluation approach: The first step in the process is to determine if the user-specified retaining wall will slide or rotate during shaking when subjected to the Corps Project Design Earthquake:

1. Select a **Sliding Analysis Type** and select **Vertical Time-history Usage: Determine a representative constant value** for the vertical time-history (which will be a trial-and-error, iterative process). In the first iteration specify a **Constant Y Acceleration** set equal to zero. Select **Run CWRotate Analyzer** and view the results to determine the average and the weight vertical acceleration during sliding (definitions given in Section 4.6), as reported by the **Show Sliding Evaluation** button (or, equivalently, in the WORKslide.TMP ACSII output file). Perform a second CWRotate analysis using an updated **Constant Y Acceleration** value based on this vertical acceleration information. Repeat the analysis until conversion is achieved. Read the updated value for the maximum transmissible acceleration and the updated value for the incipient lift-off in rotation acceleration as reported by the **Show Lift-Off Evaluation** button (or, equivalently, in the WORKrotate.TMP ACSII output file). Note that both analyses are using the same **Constant Y Acceleration** values in their respective computations. The smaller of the two horizontal acceleration constants dictates if the wall will slide or rotate for the given wall geometry, soil shear strengths, and ground motions. If the values for the maximum transmissible acceleration and the value for the incipient lift-off in rotation acceleration are close, it may be worthwhile to perform a second series of rotating block analyses to determine a more accurate value for the **Constant Y Acceleration** that is consistent with the acceleration pulses generating wall rotation for the lift-off evaluation process, rather than using the value determined by using the results based on a sliding block evaluation process.
2. In order to determine a value for the **Constant Y Acceleration** that is consistent with the acceleration pulses generating wall rotation for the

lift-off evaluation process, select a **Rotating Analysis Type** and select **Vertical Time-history Usage: Determine a representative constant value** for the vertical time-history (which will be a trial-and-error, iterative process). In the first iteration specify a **Constant Y Acceleration** (set equal to zero or the value determined from the final sliding block analysis discussed in the previous paragraph). Select **Run CWRotate Analyzer** and view the results to determine the average and the weight vertical acceleration during sliding (definitions given in Section 4.6), as reported by the **Show Lift-Off Evaluation** button (or, equivalently, in the WORKrotate.TMP ACSII output file). Perform a second CWRotate analysis using an updated **Constant Y Acceleration** value based on the vertical acceleration information. Repeat the analysis until conversion is achieved. Read the updated value for the incipient lift-off in rotation acceleration as reported by the **Show Lift-Off Evaluation** button (or, equivalently, in the WORKrotate.TMP ACSII output file). The smaller of the two horizontal acceleration constants, the maximum transmissible acceleration value and the value for the incipient lift-off in rotation acceleration, dictates if the wall will slide or rotate for the given wall geometry, soil shear strengths, and ground motions.

If the wall will slide before it will rotate, then for the sliding block analysis using the final **Constant Y Acceleration** value (determined during the sliding pulses<sup>1</sup>), continue viewing the results of the Newmark time-history analysis using the as reported in the figure(s) activated by the **Plot Sliding Time-History** button. **Show Sliding Evaluation** button (or, equivalently, in the WORKslide.TMP ACSII output file) also reports the value for the cumulative (permanent) horizontal relative wall displacement. Forces acting on the structural wedge are reported in this same data output box and file.

If the wall rotates before it slides, then another CWRotate analysis is required. Select a **Rotating Analysis Type** and select **Evaluate with current time-history** for the **Vertical Time-history Usage**. View the results of the rotating structural wedge time-history analysis as reported in the figure, is activated by the **Plot Rotating Time-history** button. **Show Lift-Off Evaluation** button (or, equivalently, in the WORKrotate.TMP ACSII output file) also reports the cumulative

---

<sup>1</sup> Based on Input Parameter selection for the **Analysis** tab of a **Sliding Analysis Type** and **Vertical Time-History Usage: Determine a representative constant value** or with **Evaluate with representative constant value**.



(permanent) wall rotation. Moments and Forces acting on the structural wedge are reported in other output button activated files (refer to Appendix G for a description of output file contents).

If the user were to select a **Sliding and Rotating Analysis Type**, select **Evaluate with a representative constant value** for the **Vertical Time-history Usage** and specify a **Constant Y Acceleration** value, and **Run CWRotate Analyzer**. During the CWRotate analysis, the program would automatically determine if the wall will slide or rotate and perform the appropriate time-history analysis (but not both complete time-history analyses).

The two examples discussed in the following two subsections demonstrate this process.

#### **5.2.7 Example 1 – Earth retaining wall at a dry soil site – No reinforced concrete slab buttress at the wall's toe**

In this first example consider the case of the seismic stability evaluation of the Figure 5.15 reinforced concrete earth retaining structure. No buttressing toe slab exists in this evaluation. This 22-ft high earth retaining structure retains moist cohesionless soil, dense sand, and is founded on rock. During construction, a thin layer of dense sand was used to level the top of rock before pouring the base of the reinforced concrete retaining wall. It is assumed that this Corps project is sited in a high seismic region on the West coast and situated in close proximity to an active fault that dominates the ground motion hazard. The projects horizontal and vertical strong ground motion component time-histories were provided (by the District) and possess scaled horizontal and vertical acceleration time-histories with positive/negative peak values of 0.96g/-0.82g and 0.68g/-0.96g, respectively. Both acceleration time-histories are baseline corrected. The polarity of ground motions was not retained during their development.

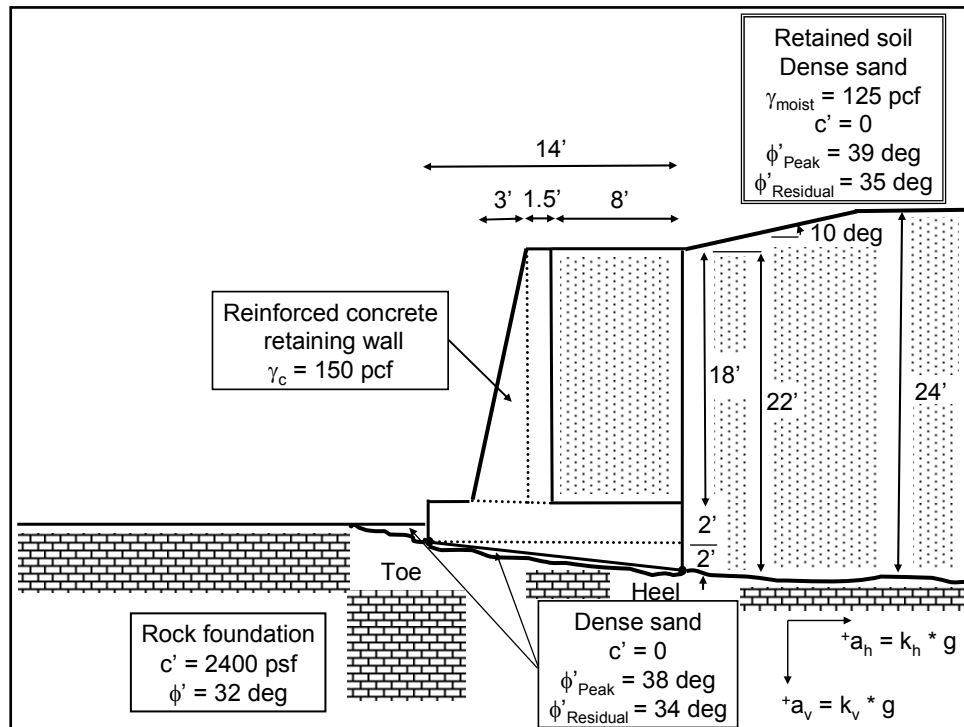


Figure 5.15. Rock-founded earth retaining wall for Example 1.

Figure 5.16 shows the input **Geometry** tab data for this problem. Material region numbers 1, 2, 4, 6, and 10 are used to define the geometry of the structural wedge. Note a resisting force at the toe of the wall is set equal to zero since a reinforced concrete buttress slab is not present.

A minimum angle for slip plane of 3 degrees from horizontal is specified in the **Driving Wedge** tab (not shown). Additionally, residual shear strength parameter values of  $\phi' = 35$  degrees and  $\phi' = 34$  degrees are specified for the retained soil and the cohesionless soil immediately in contact with the base of the structural wedge, respectively.

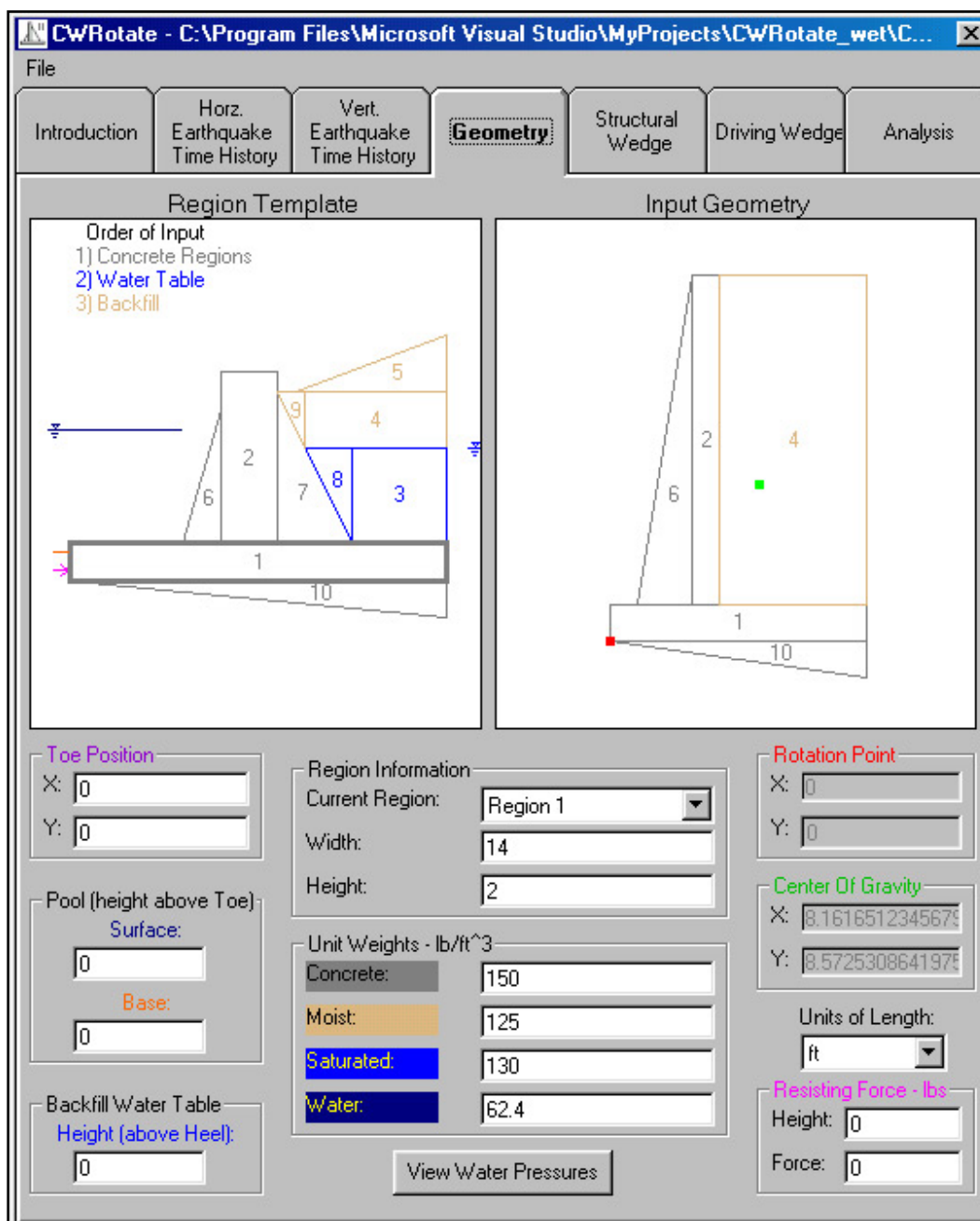


Figure 5.16. Data contained within the input **Geometry** tab for Example 1.

The first step in the CWRotate analysis is to determine if the Figure 5.15 retaining wall will slide or rotate during shaking when subjected to the District's Project Evaluation Earthquake. Select a **Sliding Analysis Type** and select **Determine a representative constant value** for the **Vertical Time-history Usage** (which will be a trial-and-error, iterative process). Table 5.1 summarizes the computed results from this two-iteration process. In the first iteration, a **Constant Y Acceleration** is set equal to

zero. The program is executed via select **Run CWRotate Analyzer** button and the results used to determine the average and the weighted vertical acceleration during sliding (definitions given in Section 4.6), are viewed by the **Show Sliding Evaluation** button (or, equivalently, in the WORKslide.TMP ACSII output file). Based on the computed average and weighted vertical acceleration values, a second CWRotate analysis is conducted using a **Constant Y Acceleration** set equal to 0.01g. Figure 5.17 shows the **Analysis** tab input and settings for this computation. This second iteration/Newmark sliding block computation is made with **Constant Y Acceleration** set equal to a constant 0.01 g. Conversion is achieved in this computation as demonstrated in the tabulated values. The bottom figure in Figure 5.18 shows the magnitude of vertical acceleration for each time-step during which sliding occurs (specifically, the average acceleration during each time increment of sliding) for this second Newmark sliding block analysis (activated by the **Plot Effective Vertical Acc.** button). The Table 5.1 average and weighted vertical acceleration values are computed using the Section 4.6 Equations 4.74 and 4.76, respectively. Note that even though the peak positive/negative vertical accelerations are 0.68g/-0.96g, respectively, for the time-history figure second from the top in Figure 5.18, these peak values are not concurrent with the times of sliding. The vertical accelerations that occur during sliding are far lower in magnitude and are labeled effective vertical accelerations (that occur during sliding) in this bottom figure. In this manner, a vertical acceleration time-history possessing peak positive/negative vertical accelerations of 0.68g/-0.96g, respectively, becomes a constant Y acceleration of (positive) 0.01g for the sliding analysis.

The computed value for the (horizontal) maximum transmissible acceleration is equal to 0.34 g (reported by the **Show Sliding Evaluation** button or, equivalently, in the WORKslide.TMP ASCII output file). For the incipient lift-off in rotation the computed horizontal acceleration is computed to be 0.37g (reported by the **Show Lift-Off Evaluation** button or, equivalently, in the WORKrotate.TMP ASCII output file). These computations are also made with a **Constant Y Acceleration** of 0.01g. (It is reasoned that those horizontal acceleration pulses during which sliding occurs will also dominate the pulses during which rotation will occur.) Since the maximum transmissible acceleration is the smaller of the two horizontal acceleration constants, the wall will slide during earthquake shaking (for the given wall geometry, soil shear strengths, and ground motions used in this particular analysis).

A separate analysis to determine a value for the **Constant Y Acceleration** that is consistent with the acceleration pulses generating wall rotation for the lift-off evaluation process was also conducted.<sup>1</sup> After iteration, the computed results were the same as for the sliding block based analyses; a **Constant Y Acceleration** value of 0.01g with the horizontal acceleration for incipient lift-off in rotation computed to be 0.37g (reported by the **Show Lift-Off Evaluation** button or, equivalently, in the WORKrotate.TMP ASCII output file).

Table 5.1. Assessment of constant Y acceleration, the effective vertical acceleration for Example 1.

Iteration No.	User Specified Acceleration (kCG) <sub>v</sub> *g	Average Vertical Acceleration (kCG) <sub>v-ave</sub> *g	Weighted Vertical Acceleration (kCG) <sub>v-weighted</sub> *g	Maximum Transmissible Acceleration
1	0	0.0124g	0.0121g	0.35g
2	0.01g	0.0128g	0.0136g	0.34g

<sup>1</sup> Based on Input Parameter selection for the **Analysis** tab of a **Rotating Analysis Type** and **Vertical Time-history Usage: Determine a representative constant value**.

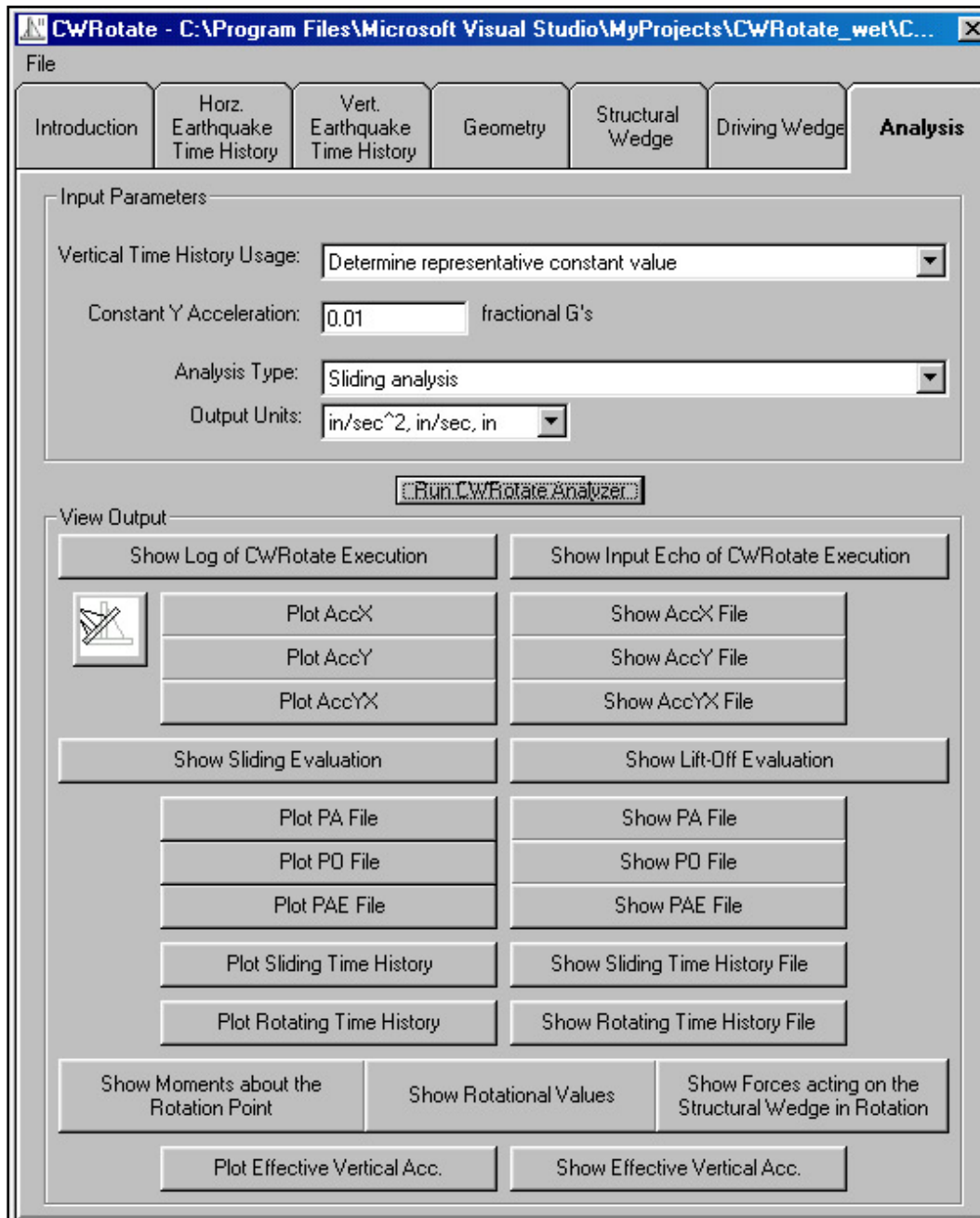


Figure 5.17. The final **Analysis** tab for Example 1.

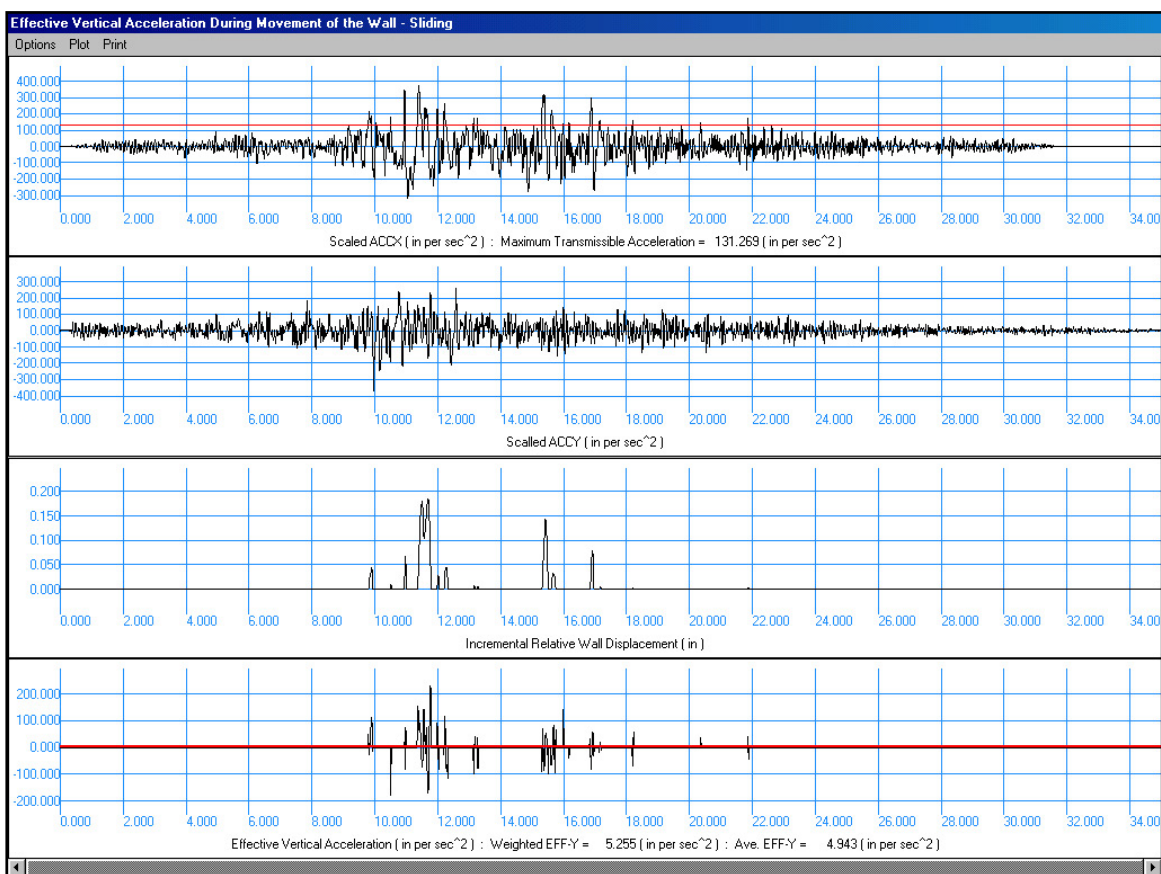


Figure 5.18. Time-history of the evaluation of the effective vertical acceleration.

Since the Figure 5.15 retaining wall will slide before it will rotate, then continue viewing the results for the Newmark time-history permanent deformation analysis results, which for this problem is shown in Figure 5.19. This figure is seen by activating the Plot **Sliding Time-history** button on the **Analysis** tab. (Note that the **Show Sliding Evaluation** button (or, equivalently, in the WORKslide.TMP ASCII output file) also reports the value for the cumulative (permanent) horizontal relative wall displacement.) The upper figure is a plot of the horizontal acceleration time-history and the red line designates the maximum transmissible acceleration value of 0.34g. Wall displacements start to occur the first time the acceleration trace plots above this red line. Observe that permanent wall translation starts at about 10 seconds after initial shaking and concludes by about 17 seconds out of a total of 35 seconds of ground shaking. The cumulative permanent displacement is about 9 inches, which occurs over about six significant relative (wall) velocity and displacement pulses (refer to the second and third figure down from the top, respectively). During sliding the maximum inertial force imparted to the structural wedge and to the driving soil wedge (and

to  $P_{AE}$ ) is due to a horizontal acceleration of  $0.34g$ , the value for the maximum transmissible acceleration (with a constant vertical acceleration of  $0.01g$ ). Forces acting on the structural wedge are reported by the **Show Sliding Evaluation** button (or, equivalently, in the WORKslide.TMP ASCII output file). By allowing the retaining wall structural wedge and soil wedge are not subjected to inertia forces due to the higher accelerations values, i.e., up to  $0.96g$  of horizontal acceleration. Thus, allowing the wall to slide during earthquake shaking provides for lower design forces than would otherwise occur should translational wall movements have been constrained.

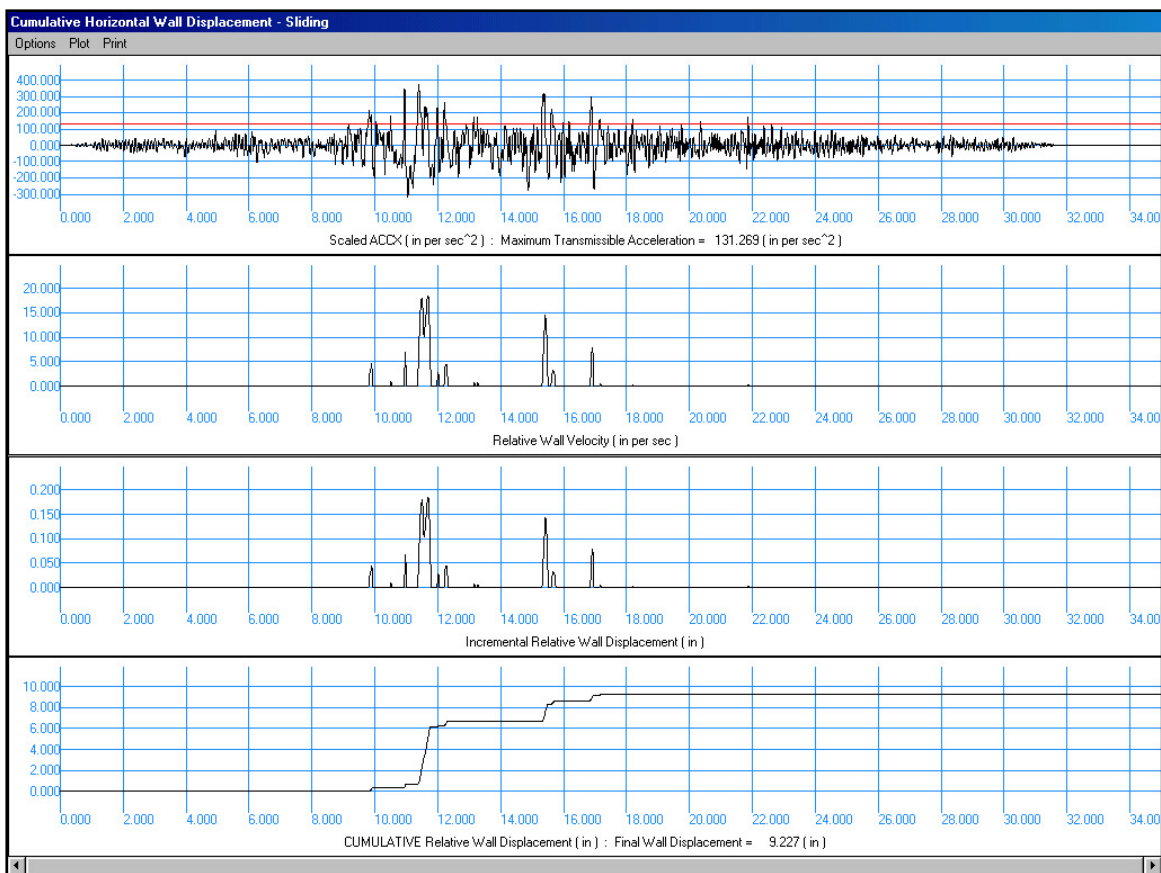


Figure 5.19. Newmark sliding block time-history results for Example 1.

Selected output for the driving soil wedge forces and pressures acting on the structural wedge during sliding are as follows:



```
*****
**** Earth Pressure Forces ****
*****
```

```
PAEqSLIDE =      17817.83 lbs
ALPHAESLIDE = 43.00 degrees
HPAEqSLIDE =   10.23 ft
DCaeSLIDE =    0.00 ft
```

```
=====
Pressure Distributions acting at an angle 0.00 degrees
from normal to the vertical plane through the heel
=====
```

Height above Heel (ft)	Static (lb/ft <sup>2</sup> )	Incremental EQ (lb/ft <sup>2</sup> )	Total EQ (lb/ft <sup>2</sup> )
22.00	0.00	638.30	638.30
3.54	691.52	236.55	928.07
0.00	811.06	159.57	970.64

For a dense sand, the Table 1.1 guidelines indicate that for a 22-ft-high section, active earth pressures may be used in the analysis if wall movements exceed 1/4 in. (=0.001 times 22 ft times 12 in./ft). With predicted wall movements on the order of 9 inches, the use of active earth pressures in the dynamic time-history permanent displacement calculations is deemed appropriate.

Since the polarity of ground motions was not retained in their development, this analysis would be repeated three more times with the user reversing the polarity of the horizontal and vertical input ground motions to determine the most critical results.

Using the forces provided in the output file<sup>1</sup>, the user is advised to determine if the bearing capacity of the foundation is adequate.

**5.2.8 Example 2 – Earth retaining wall at a dry soil site – 1-foot thick reinforced concrete slab buttress at the wall’s toe**

Consider the case of the Figure 5.15 earth retaining structure buttressed by a 1-ft-thick reinforced concrete slab as shown in Figure 5.20. As was the

<sup>1</sup> Appendix G summarizes the contents of the output files.

case in Example 1, the 22-ft-high earth retaining structure retains moist cohesionless soil, a dense sand, and is founded on rock. During construction, a thin layer of dense sand was used to level the top of rock before pouring the base of the reinforced concrete retaining wall. It is assumed that this Corps project is sited in a high seismic region on the West coast and situated in close proximity to an active fault that dominates the ground motion hazard. The same pair of ground motions are used in both examples: The projects horizontal and vertical strong ground motion component time-histories were provided (by the District) and possess scaled horizontal and vertical acceleration time-histories with positive/negative peak values of 0.96g/-0.82g and 0.68g/-0.96g, respectively. Both acceleration time-histories are baseline corrected. The polarity of ground motions was not retained during their development.

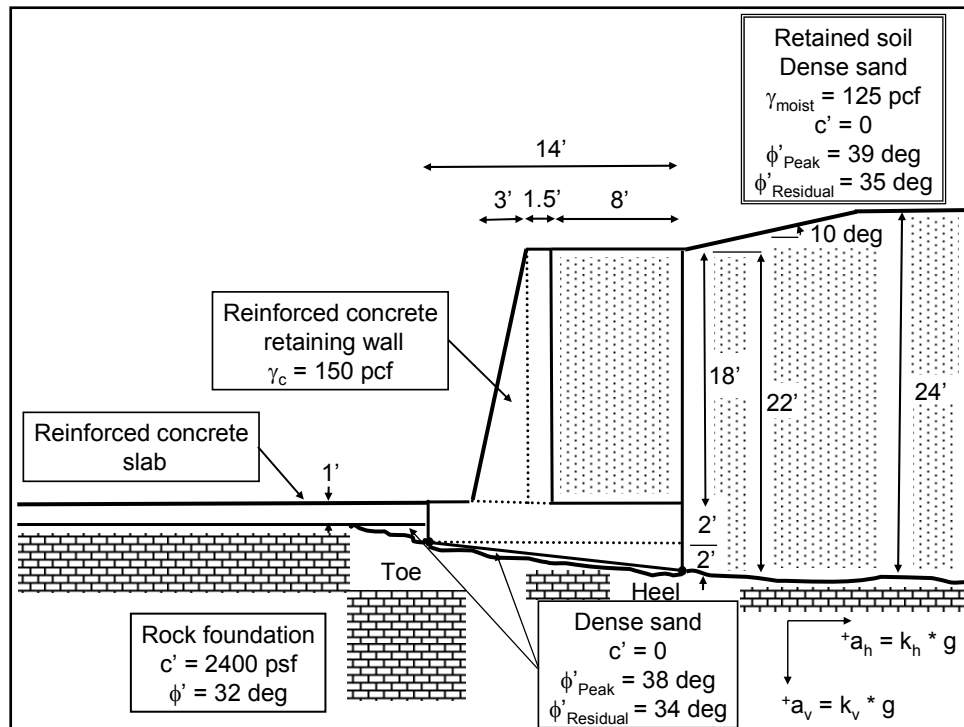


Figure 5.20. Rock-founded earth retaining wall buttressed at the toe of the wall by a 1-ft-thick reinforced concrete slab for Example 2.

Figure 5.21 shows the input **Geometry** tab data for this problem. Material region numbers 1, 2, 4, 6, and 10 are used to define the geometry of the structural wedge. Note that a 120 kip per ft run of wall resisting force is specified at the toe of the wall and acts at height of 1.5 ft above the toe. Its magnitude is determined using the procedure outlined in Strom and Ebeling (2004).

A minimum angle for slip plane of 3 degrees from horizontal is specified in the **Driving Wedge** tab (not shown). Additionally, residual shear strength parameter values of  $\phi' = 35$  degrees and  $\phi' = 34$  degrees are specified for the retained soil and the cohesionless soil immediately in contact with the base of the structural wedge, respectively.

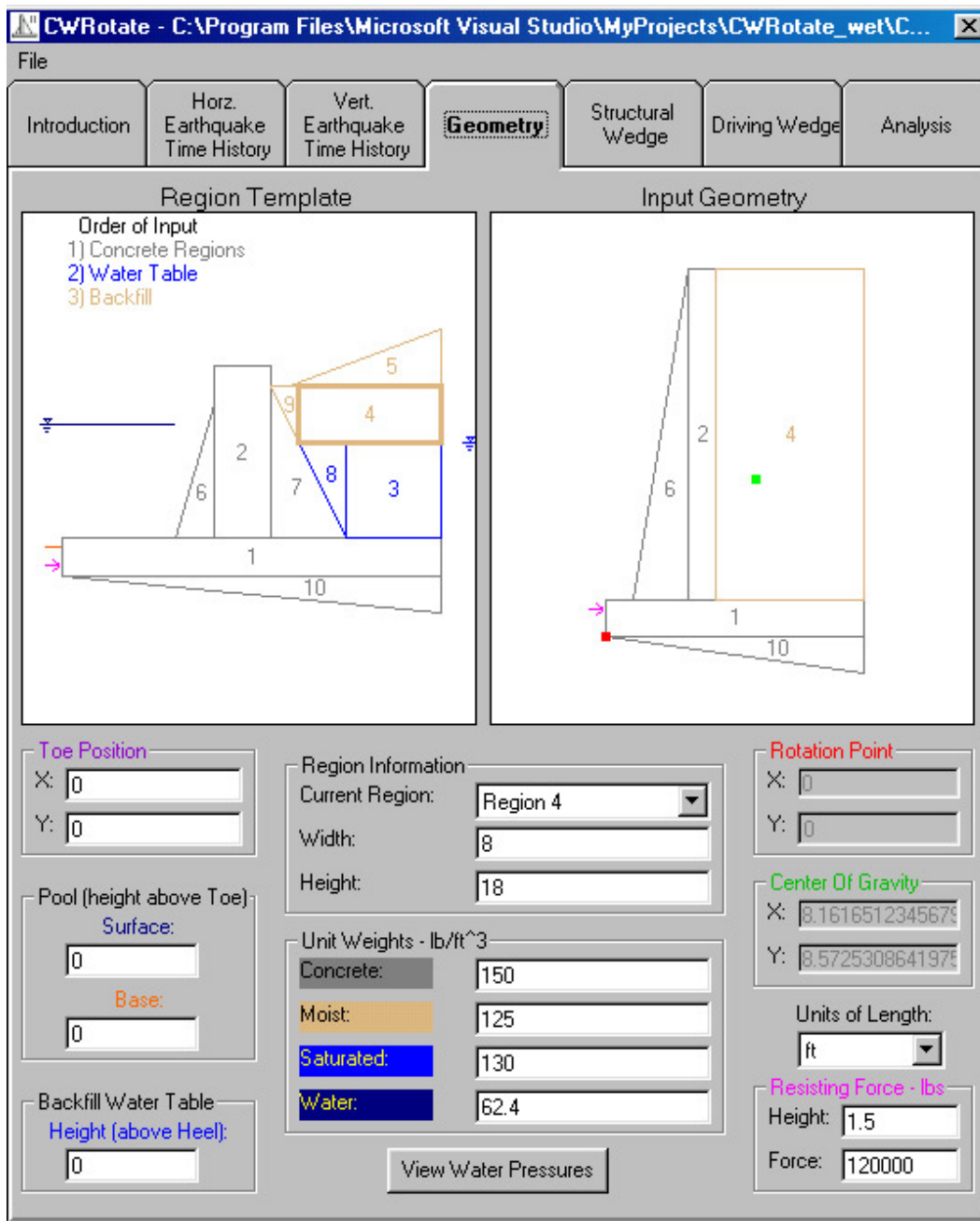


Figure 5.21. The input **Geometry** tab for Example 2.

The first step in the CWRotate analysis is to determine if the Figure 5.20 retaining wall will slide or rotate during shaking when subjected to the District's Project Evaluation Earthquake. Select a **Sliding Analysis Type** and select **Determine a representative constant value** for the **Vertical Time-history Usage** (which will be a trial-and-error, iterative process). Table 5.2 summarizes the computed results from this three-iteration process. In the first iteration, the value for **Constant Y Acceleration** is set equal to zero. The program is executed via the **Run CWRotate Analyzer** button and the results are used to determine the average and the weighted vertical acceleration during sliding (definitions given in Section 4.6). These results are observed by activating the **Show Sliding Evaluation** button (or, equivalently, in the WORKslide.TMP ASCII output file). Based on the computed average and weighted vertical acceleration values, a second CWRotate analysis is conducted. This second computation is made using a **Constant Y acceleration** set equal to 0.15g. The second iteration is followed by a third iteration. Figure 5.22 shows the **Analysis** tab input and settings for this third computation. This third iteration/Newmark sliding block computation with **Constant Y Acceleration** set equal to a constant 0.13 g provides reasonable convergence, as demonstrated in the tabulated values. The Table 5.2 average and weighted vertical acceleration values are computed using the Section 4.6 Equations 4.74 and 4.76, respectively. Recall the peak positive/negative vertical accelerations are 0.68g/-0.96g, respectively, for the vertical acceleration time-history. The vertical accelerations that occur during sliding are far lower in magnitude as reflected by in the plot used to compute the effective vertical acceleration that occurs during sliding (the plot is activating the **Plot Effective Vertical Acc** button). In this manner, a vertical acceleration time-history possessing peak positive/negative vertical accelerations of 0.68g/-0.96g, respectively, becomes a constant Y acceleration of (positive) 0.13g. It is referred to as the effective vertical acceleration during sliding and is a constant.

Table 5.2. Assessment of constant Y acceleration, the effective vertical acceleration for Example 2 – Sliding Evaluation.

Iteration No.	User-Specified Acceleration (kcg) <sub>v</sub> *g	Average Vertical Acceleration (kcg) <sub>v-ave</sub> *g	Weighted Vertical Acceleration (kcg) <sub>v-weighted</sub> *g	Maximum Transmissible Acceleration
1	0	0.0835g	0.187g	0.804g
2	0.15g	0.0361g	0.1097g	0.71g
3	0.13g	0.042g	0.1216g	0.72g

The computed value for the (horizontal) maximum transmissible acceleration is equal to 0.72 g (reported by the **Show Sliding Evaluation** button or, equivalently, in the WORKslide.TMP ASCII output file). For the incipient lift-off in rotation the computed horizontal acceleration is computed to be 0.522g (reported by the **Show Lift-Off Evaluation** button or, equivalently, in the WORKrotate.TMP ASCII output file). These computations are made with a **Constant Y Acceleration** of 0.13g.

A separate analysis to determine a value for the **Constant Y Acceleration** that is consistent with the acceleration pulses generating wall rotation for the lift-off evaluation process was also conducted<sup>1</sup>. Two iterations are required. Figure 5.23 shows the **Analysis** tab input and settings for the second computation. This second iteration of the rotational block computation with **Constant Y Acceleration** set equal to a constant 0.05g provides reasonable convergence, as demonstrated in the tabulated values of Table 5.3, based on the computed average and weighted vertical acceleration values. The horizontal acceleration of incipient lift-off in rotation is computed to be 0.552g (reported by the **Show Lift-Off Evaluation** button or, equivalently, in the WORKrotate.TMP ASCII output file). Figure 5.23 shows the **Analysis** tab settings for the second iteration. Observe that after the second rotational analysis results of 0.552 g, horizontal acceleration of incipient lift-off in rotation with a **Constant Y Acceleration** value of 0.05 g is only slightly different from those lift-off of the base results obtained for the sliding block-based analysis (0.522 g for a Constant Y Acceleration of 0.13 g).

Table 5.3. Assessment of constant Y acceleration, the effective vertical acceleration for Example 2 – Rotational Evaluation.

Iteration No.	User-Specified Acceleration (kcg) <sub>v</sub> *g	Average Vertical Acceleration (kcg) <sub>v-ave</sub> *g	Weighted Vertical Acceleration (kcg) <sub>v-weighted</sub> *g	Maximum Transmissible Acceleration
1	0.13g	0.0412g	0.0515g	0.522g
2	0.05g	0.0412g	0.0515g	0.552g

Since the incipient lift-off in rotation acceleration is the smaller of the two horizontal acceleration constants, the wall will rotate during earthquake

<sup>1</sup> Based on Input Parameter selection for the **Analysis** tab of a **Rotating Analysis Type** and **Vertical Time-history Usage: Determine a representative constant value.**

shaking (for the given wall geometry, soil shear strengths, and ground motions used in this particular analysis).

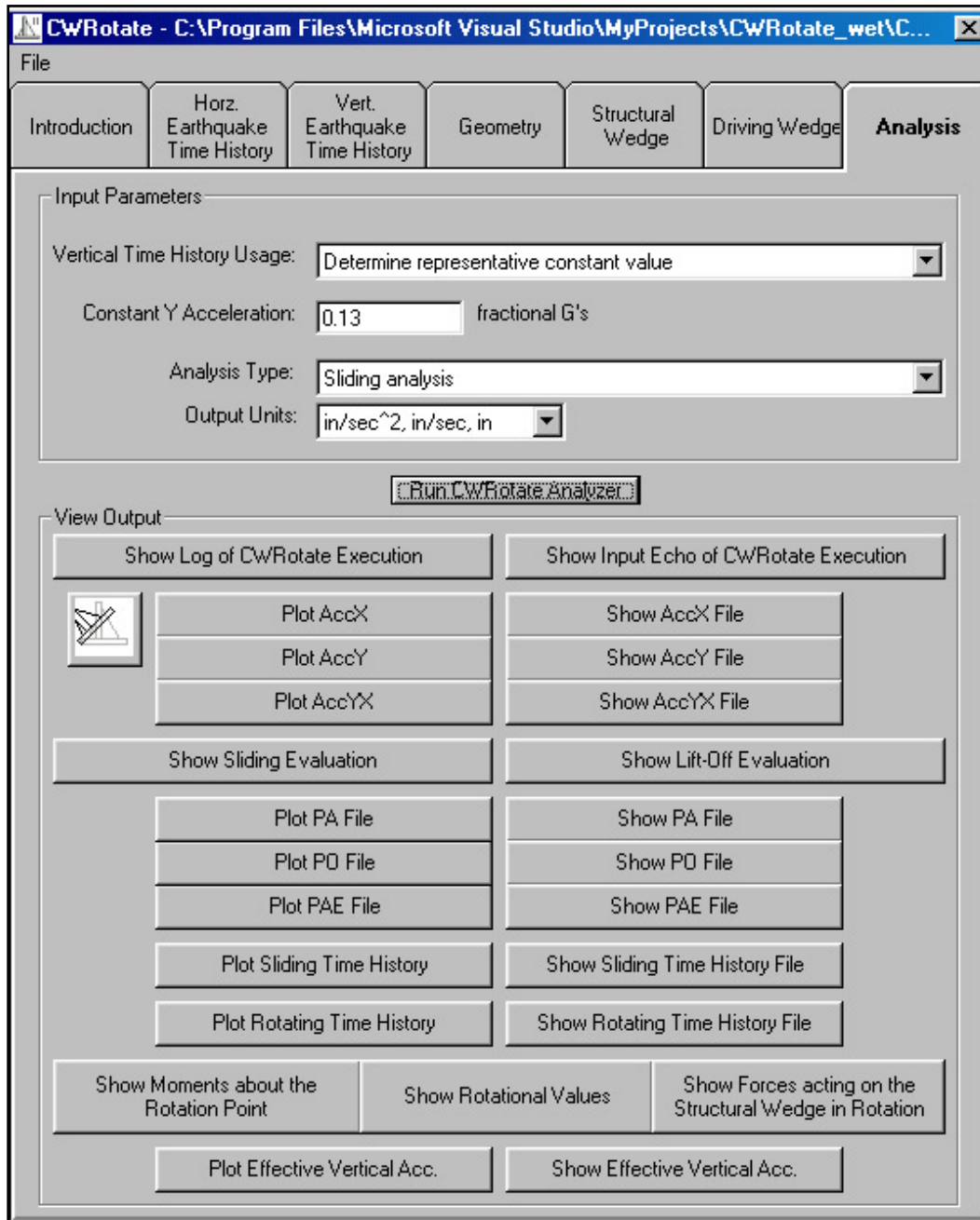


Figure 5.22. The third iteration **Analysis** tab settings for Example 2 – Sliding Evaluation.

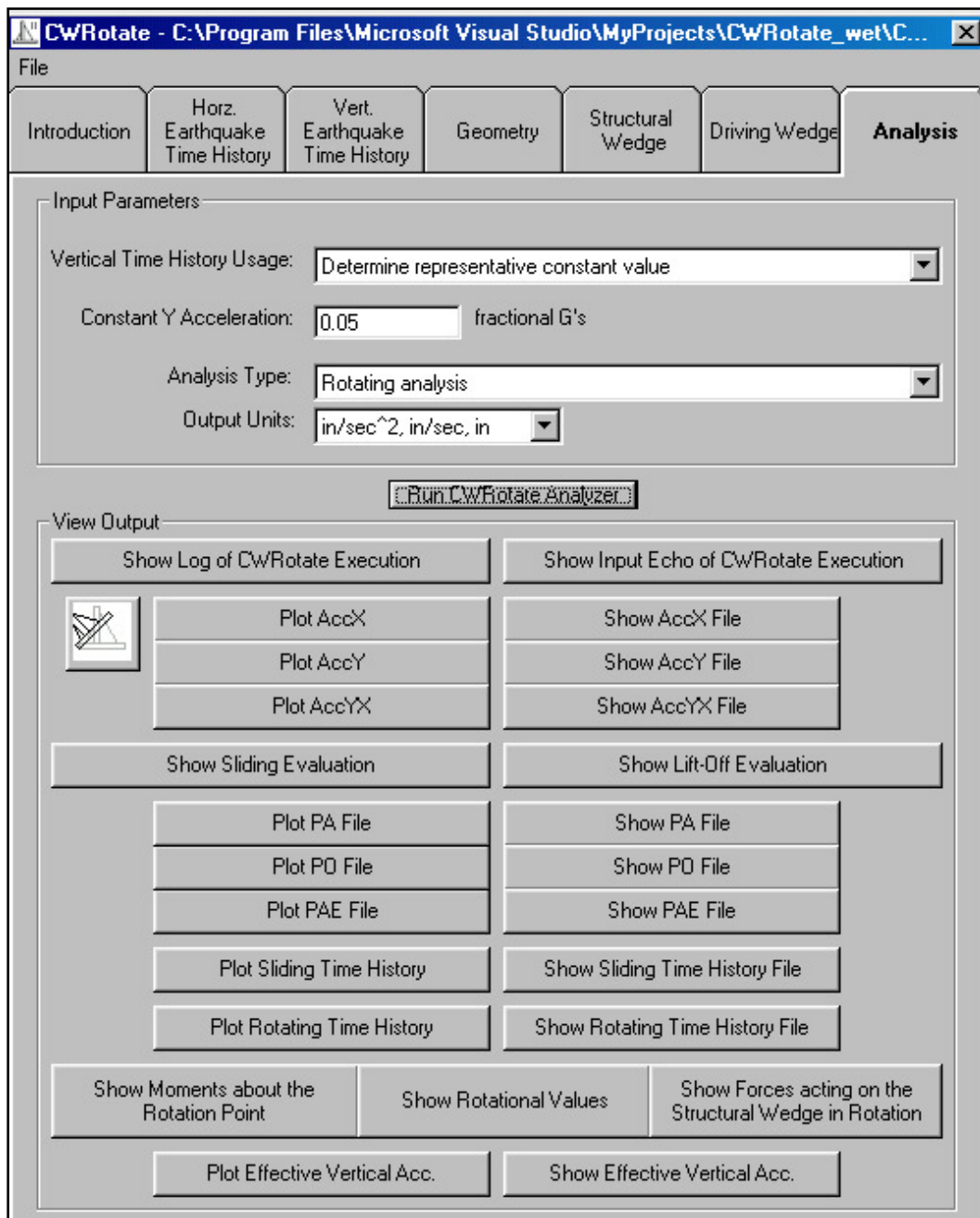


Figure 5.23. The second iteration **Analysis** tab settings for Example 2 – Rotational Evaluation.

Since the wall rotates before it slides, a final CWRotate analysis is conducted. Select a **Rotating Analysis Type** and select **Evaluate with current time-history** for the **Vertical Time-history Usage** as shown in Figure 5.24. Note with the **Vertical Time-history Usage** option of current (vertical) time-history being selected for the analysis, the value contained in the **Constant Y Acceleration** box, displaying a value of

0.05g (displayed as a value entry in gray rather than black), is not used in the permanent wall rotation analysis. View the results of the rotating structural wedge time-history analysis as reported in the figure, is activated by the **Plot Rotating Time-history** button. **Show Lift-Off Evaluation** button (or, equivalently, in the WORKrotate.TMP ASCII output file) also reports the cumulative (permanent) wall rotation. Figure 5.25 shows the results of the rotational time-history analysis. Note that the total permanent rotation of approximately 29 degrees occurs over five rotational pulses. Moments and Forces acting on the structural wedge are reported using other output buttons and files (refer to Appendix G for a description of output file contents). Figure 5.26 shows the resulting position for the rigid block after earthquake shaking ends.



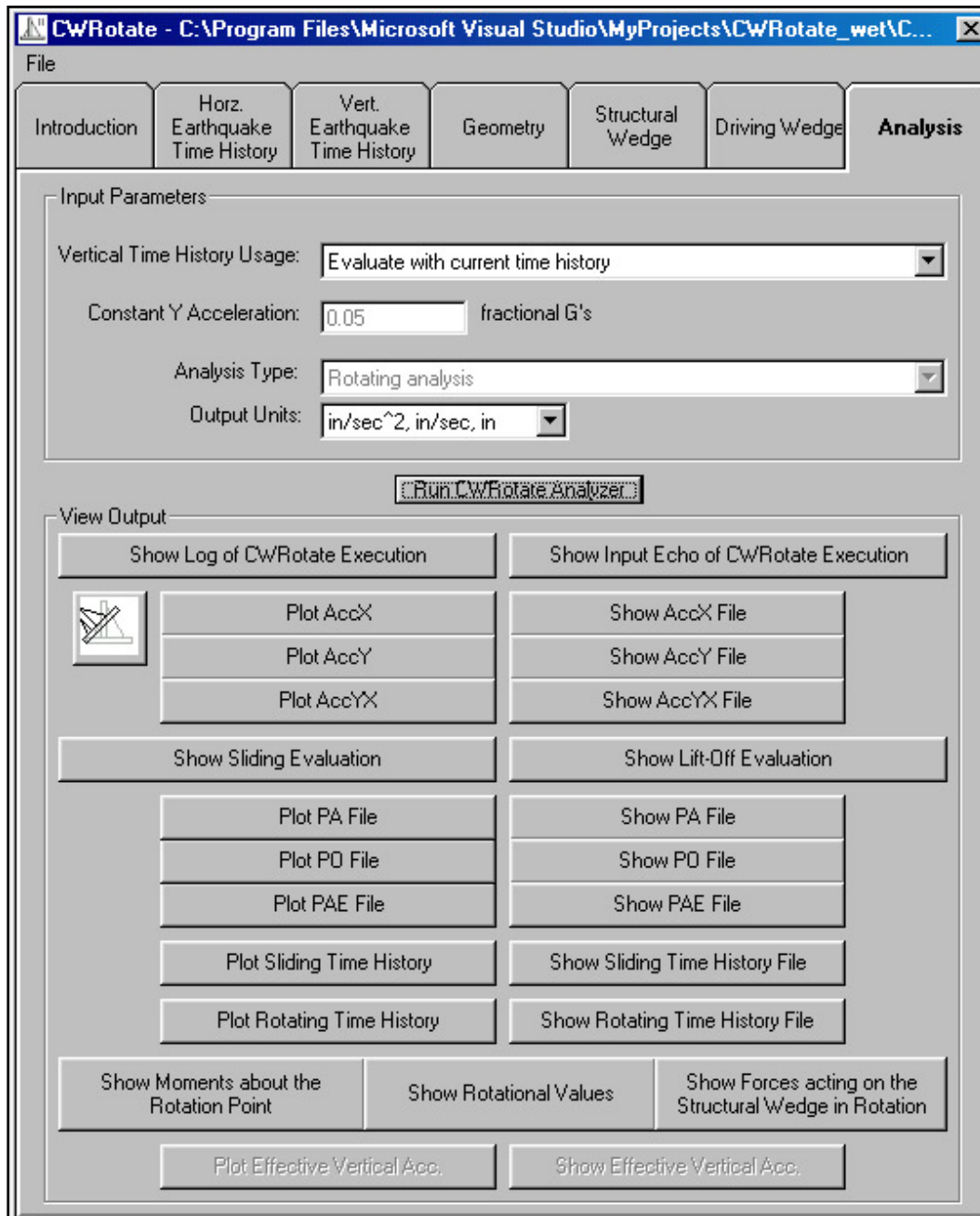


Figure 5.24. The rotational **Analysis** tab settings for final Example 2 – Computation.

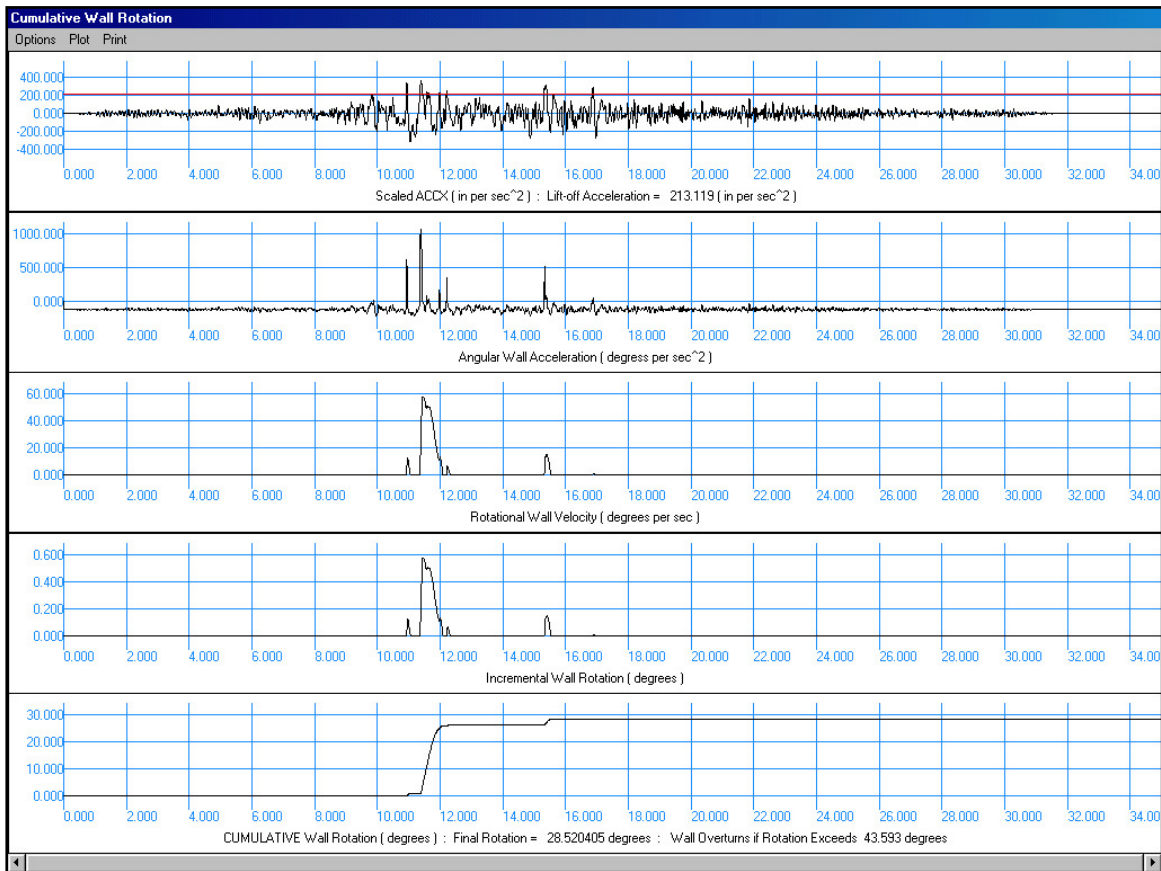


Figure 5.25. Rotational block time-history results for Example 2.

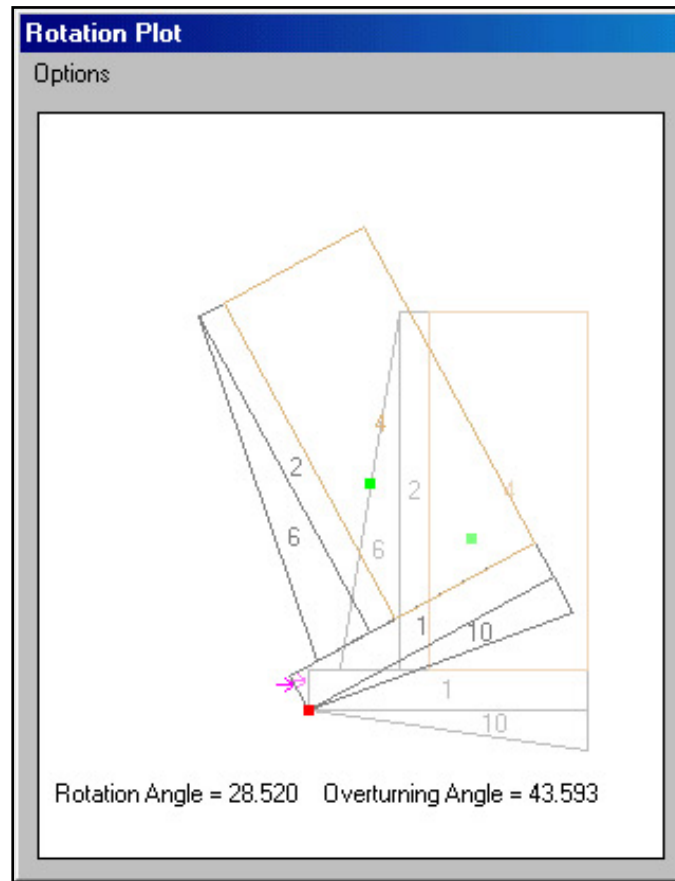


Figure 5.26. Permanent rotation of the rigid block after earthquake shaking ends for Example 2.

Selected output for the driving soil wedge forces and pressures acting on the structural wedge at a time of 11.38 seconds that results in maximum angular acceleration of the wall during rotation are as follows:

MAXIMUM Angular Wall Acceleration = 18.7262131106 (rad per sec<sup>2</sup>)  
at time = 11.3800 (sec) with

Scaled ACCX = 0.9162968000 in g's

Scaled ACCY = 0.3122528000 in g's

Overturning Moment = 3937112.54 ft-lb

Interface Overturning Moment = 3937112.54 ft-lb

Foundation Overturning Moment = 3937112.54 ft-lb

Restoring Moment = 361866.15 ft-lb

PAE = 333527.87 lbs

Slip plane angle from horizontal = 3.00 (deg)

Minimum slip plane angle from horizontal = 3.00 (deg)

Height of PAE above the Heel = 13.04 ft

PAE run number = 1189

Normal force to Base = 24909.47 lbs

Shear force to Base = 16801.65 lbs

For a dense sand, the Table 1.1 guidelines indicate that for a 22-ft-high section, active earth pressures may be used in the analysis if wall movements exceed  $\frac{1}{4}$  in. (=0.001 times 22 ft times 12 in./ft). With predicted wall rotation on the order of 29 degrees, the use of active earth pressures in the dynamic time-history permanent displacement calculations is deemed appropriate (calculations not shown).

Since the polarity of ground motions was not retained in their development, this analysis would be repeated three more times with the user reversing the polarity of the horizontal and vertical input ground motions to determine the most critical results.

Using the forces provided in the output file<sup>1</sup>, the user is advised to determine if the bearing capacity of the foundation is adequate.

The difference between the Figure 5.20 retaining wall of Example 2 and the Figure 5.15 retaining wall system of Example 1 is the addition of a 1-ft thick reinforced concrete slab at the toe of the wall. Due to the buttressing effect of the reinforced concrete slab, the wall will now rotate before it translates during the user-specified seismic event. This results in higher forces acting on the wall. For example, the maximum  $P_{AE}$  dynamic earth loading for Example 2 is 333,528 lb per ft run of wall while for Example 1 it is 17,818 lb per ft run of wall. This is because the accelerations felt by this rigid block during shaking are those of the ground acceleration time-history plus the contribution of angular acceleration and angular velocity during rotation of the rigid body about its point of rotation, a result of the continuous contact between the rigid block and the ground being maintained at the point of rotation (refer to Section 3.2).

---

<sup>1</sup> Appendix G summarizes the contents of the output files.

## 6 Summary, Conclusions, and Recommendations

### 6.1 Summary and conclusions

Engineer Manual 1110-2-2502 Retaining and Flood Walls gives engineering procedures that are currently being used by District Engineers in their *initial* assessment of seismic wall performance of existing earth retaining structures and the preliminary sizing of new retaining structures. The engineering procedures given in EM 1110-2-2502 for retaining walls make extensive use of the simplified pseudo-static procedure of analysis of earth retaining structures and expresses wall performance criteria in terms of computed factors of safety against sliding and bearing failure, and base area in compression. The simplified pseudo-static procedure of analysis makes it difficult to interpret the actual wall performance for Corps projects subjected to “strong” design ground motions because of simplifications made in the procedure of analysis. In a pseudo-static analysis an oversimplification occurs when the engineer is forced to render the complex, horizontal and vertical earthquake acceleration time-history events to constant values of accelerations and assume a constant direction for each. These constant values are denoted as the pseudo-static acceleration coefficients in the horizontal and vertical directions (refer to Section 1.1.1 of this report). The engineer is also required to assume a constant direction for each of these components. An acceleration time-history, in actuality, varies both in magnitude and in direction with time.

The simplified pseudo-static procedure does not allow for interpretation of *actual* wall performance by District Engineers. Intense shaking imparted by the OBE and MCE design events makes the interpretation of the simplified procedure of analysis even more difficult. The more important questions for the wall are whether the wall slides into the spillway basin, or rotates into the spillway basin, or even tips over onto its side during the earthquake event. The simplified pseudo-static procedure of analysis is not capable of answering these questions. The answers depend on the magnitude of the pseudo-static coefficient used in the calculations compared to the magnitude of the peak values for the acceleration pulses as well as the number and duration of these strong shaking acceleration pulses in the design earthquake event time-history. When considering

both horizontal and vertical accelerations, the resulting wall response is further complicated by the time-history of phasing between the pulses of horizontal and vertical accelerations. Only the permanent wall sliding displacement/wall rotation method of time-history analysis can answer these questions. Again, wall displacements will influence the seismic earth pressure forces imparted on the wall by the retained soil.

Formal consideration of the permanent seismic wall displacement in the seismic design process for Corps-type retaining structures is given in Ebeling and Morrison (1992). The key aspect of the engineering approach presented in this Corps document is that simplified procedures for computing the seismically-induced earth loads on retaining structures are also dependent upon the amount of permanent wall displacement that is expected to occur for each specified design earthquake. The Ebeling and Morrison simplified engineering procedures for Corps retaining structures are geared towards hand calculations. The engineering formulation and corresponding user friendly, PC-based software discussed in this report extend these simplified procedures.

This research report describes the engineering formulation developed for the permanent rotational response of rock-founded, toe-restrained retaining walls to earthquake ground motions. The corresponding PC software  $C_{\text{corps}}W_{\text{all}}\text{Rotate}$  developed to perform a rotating or sliding analysis of each user-specified retaining wall section was discussed. Baseline-corrected, horizontal and vertical acceleration time-histories are used to represent the earthquake ground motions in the formulation implemented within  $C_{\text{corps}}W_{\text{all}}\text{Rotate}$ . A particular formulation of the permanent sliding displacement response of Corps retaining walls for a user-specified earthquake acceleration time-history was also described. The engineering methodology and software are particularly applicable to rock-founded L-walls and T-walls (usually referred to as cantilever retaining walls) and semi-gravity walls.  $C_{\text{corps}}W_{\text{all}}\text{Rotate}$  is applicable to a variety of retaining walls buttressed at their toe by a structural feature such as a reinforced concrete slab. The presence of the structural feature at the toe of the retaining wall may result in a tendency for the earth retaining structure to rotate rather than slide during earthquake shaking. Other examples of Corps earth retaining structures having this structural feature include navigation walls, spillway chute walls, spillway discharge channel walls, approach channel walls to outlet works structures, highway and railway relocation retaining walls, and floodwall channels.  $C_{\text{corps}}W_{\text{all}}\text{Rotate}$  may

also be used to predict permanent seismically induced (rotational or translational) displacements of retaining walls without toe restraint.

**The engineering methods contained in this report and implemented within CorpsWallRotate allow the engineer to determine if a given retaining wall has a tendency to rotate or to slide for a specified seismic event. This is a new capability for the seismic design/evaluation process for Corps retaining structures.**

CorpsWallRotate was designed for ease of use in a PC environment and to render the complex problem of seismic evaluation/design of retaining walls that tend to permanently displace during earthquakes to a more straight-forward and rapid engineering process. The computed permanent wall rotation and other pertinent information allow for a rapid investigation of retaining wall configurations by District Engineers.

***Minimum Wall Displacement:*** Recall that CorpsWallRotate applies an active earth pressure force to the structural wedge in the permanent rotation analysis, as is done in most sliding block formulations for retaining walls. Table 1.1 lists the approximate magnitudes of movements required to reach minimum active earth pressure conditions. Although this Clough and Duncan (1969) guidance is for static loading, after careful evaluation Ebeling and Morrison (1992, in Section 2.2.2) concluded that the Table 1.1 values may also be used as rough guidance for minimum retained soil seismic displacement to fully mobilize a soil shear resistance, resulting in dynamic active earth pressures. That is, the permanent displacements resulting from rotations computed using CorpsWallRotate must equal or exceed the Table 1.1 values (given as displacement-normalized wall heights in this table). If not, then the dynamic earth pressures are underestimated in the analysis.

## 6.2 Recommendations for future research

Engineering formulations and software provisions based on sound seismic engineering principles are needed for a wide variety of the Corps retaining walls that (1) rotate or (2) slide during earthquake shaking and (3) for massive concrete retaining walls constrained to rocking. The engineering formulation discussed in this report and implemented within CorpsWallRotate was developed to address the first two of these three modes of retaining wall responses to earthquake shaking.

The formulation of complete engineering procedures and corresponding software are needed to compute the seismic response of Corps-type earth retaining structures that slide or rock in place during earthquake shaking. A particular formulation of the permanent sliding displacement response of retaining walls for a user-specified earthquake acceleration time-history is incorporated in  $C_{\text{Corps}}W_{\text{all}}\text{Rotate}$ . However, a more versatile, simplified sliding block formulation that eliminates the need for an acceleration time-history is in the final stages of development by the primary author of this report (Ebeling et al. 2007),  $C_{\text{Corps}}W_{\text{all}}\text{SLIP}$ . An ERDC research effort is needed to develop simplified engineering formulations and corresponding GUI-based PC software for analyzing Corps retaining walls that rock in place during seismic shaking due to their sizeable mass or due to lower levels of ground shaking. Their seismically induced wall movements will not be sufficient to fully mobilize the shear resistance within the retained soils and the resulting (seismic) earth pressures will be larger than the resultant active earth pressure force  $P_{\text{AE}}$ , whose formulation is given in Appendix A and implemented within  $C_{\text{Corps}}W_{\text{all}}\text{Rotate}$ .

In addition, the engineering methodology and corresponding software  $C_{\text{Corps}}W_{\text{all}}\text{Rotate}$  were formulated for rock-founded retaining structures. Research is needed to extend this formulation to soil-founded Corps retaining structures.

For the initial version of  $C_{\text{Corps}}W_{\text{all}}\text{Rotate}$ , a simplified assumption is made that for steady-state conditions, hydrostatic water pressures exist within the heel region of the backfill. This implies that all head loss occurs due to flow within the foundation below the base of the structural wedge as discussed in Appendix D. Future improvements should include the formulation and inclusion of more refined steady-state seepage analyses implemented within  $C_{\text{Corps}}W_{\text{all}}\text{Rotate}$ .

Most Corps hydraulic structures that act as earth retaining structures possess a vertical face in contact with the pool (when present). Consequently, hydrodynamic water pressures acting on this front “wet” face are approximated in the  $C_{\text{Corps}}W_{\text{all}}\text{Rotate}$  using the Westergaard (1931) procedure (see Appendix D). This procedure needs to be expanded to include consideration of hydrodynamic water pressures acting on inclined “wetted” structural faces during sliding of the structural wedge. In addition, a more rigorous hydrodynamic water pressure formulation that accounts for the variation in horizontal acceleration along the “wetted”



face of rigid block models of walls that rotate about a point of rotation (specified as the toe in this initial  $C_{orps}W_{all}Rotate$  version) during earthquake shaking needs to be developed and implemented within  $C_{orps}W_{all}Rotate$ .

The evaluation of the adequacy of the bearing capacity of the foundation for loadings imposed by walls that rotate needs to be evaluated. This is currently being done using hand computations by engineers using the computed forces provided by  $C_{orps}W_{all}Rotate$ . This evaluation needs to be formulated and then incorporated within  $C_{orps}W_{all}Rotate$ .

Excess pore water pressures may be generated by earthquake shaking of contractive backfill and foundation soils. The procedures outlined in Ebeling and Morrison (1992) to account for  $r_u > 0$  needs to be incorporated within  $C_{orps}W_{all}Rotate$ .

## References

- Ambraseys, N. N., and J. M. Menu. 1988. Earthquake-induced ground displacements. *Earthquake Engineering and Structural Dynamics* 16:985-1006.
- American Society of Civil Engineers (ASCE) Standard. 1986. Seismic analysis of safety-related nuclear structures and commentary on standard for seismic analysis of safety related nuclear structures. ASCE 4-86.
- Bowles, J. N. 1968. *Foundation analysis and design*. New York: McGraw-Hill.
- Chang, C.-J., W. F. Chen, and J.T.P. Yao. 1984. Seismic displacements in slopes by limit analysis. ASCE. *Journal of Geotechnical Engineering* 110(GT7):860-874.
- Chopra, A. K. 1967. Hydrodynamic pressures on dams during earthquakes. ASCE. *Journal of Engineering Mechanics Division* 93(EM6):205-223.
- Clough, G. W., and J. M. Duncan. 1969. *Finite element analyses of Port Allen and Old River Locks*. Contract Report S-69-6. Vicksburg, MS: U.S. Army Engineer Waterways Experiment Station.
- \_\_\_\_\_. 1991. Earth pressures. In *Foundation engineering handbook*, 2nd ed., Chap 6, ed. H. Y. Fang, 223-235. New York: Van Nostrand Reinhold.
- Duncan, J. M., and A. L. Buchignani. 1975. *An engineering manual for slope stability studies*. Berkeley, CA: University of California Department of Civil Engineering, Geotechnical Engineering.
- Ebeling, R. M. 1992. *Introduction to the computation of response spectrum for earthquake engineering*. Technical Report ITL-92-4. Vicksburg, MS: U.S. Army Engineer Waterways Experiment Station.
- Ebeling, R. M., A. Chase, and B. C. White. 2007. *Translational response of toe-restrained retaining walls to earthquake ground motions*. ERDC/ITL TR-07-XX. Vicksburg, MS: U.S. Army Engineer Research and Development Center.
- Ebeling, R. M., R. A. Green, and S. E. French. 1997. *Accuracy of response of single-degree-of-freedom systems to ground motion*. Technical Report ITL-97-7. Vicksburg, MS: U.S. Army Engineer Waterways Experiment Station.
- Ebeling, R. M., and E. E. Morrison. 1992. *The seismic design of waterfront retaining structures*. Technical Report ITL-92-11. Vicksburg, MS: U.S. Army Engineer Waterways Experiment Station.
- Ebeling, R. M., and R. L. Mosher. 1996. Red River U-frame Lock No. 1, Backfill-structure-foundation interaction. ASCE. *Journal of Geotechnical Engineering* 122(3): 216-225.

- Ebeling, R. M., R. L. Mosher, K. Abraham, and J. F. Peters. 1993. *Soil-structure interaction study of Red River Lock and Dam No. 1 subjected to sediment loading*. Technical Report ITL-93-3. Vicksburg, MS: U.S. Army Engineer Waterways Experiment Station.
- Ebeling, R. M., M. E. Pace, and E. E. Morrison. 1997. *Evaluating the stability of existing massive concrete gravity structures founded on rock*. Technical Report REMR-CS-54. Vicksburg, MS: U.S. Army Engineer Waterways Experiment Station.
- Ebeling, R. M., J. F. Peters, and G. W. Clough. 1992. *Users guide for the incremental construction, soil-structure interaction program SOILSTRUCT*. Technical Report ITL-90-6. Vicksburg, MS: U.S. Army Engineer Waterways Experiment Station.
- Ebeling, R. M., J. F. Peters, and R. L. Mosher. 1997. The role of non-linear deformation analyses in the design of a reinforced soil berm at Red River U-frame Lock No. 1. *International Journal for Numerical and Analytical Methods in Geomechanics* 21:753-787.
- Ebeling, R. M., and R. E. Wahl. 1997. *Soil-structure-foundation interaction analysis of new roller-compacted concrete north lock wall at McAlpine Locks*. Technical Report ITL-97-5. Vicksburg, MS: U.S. Army Engineer Waterways Experiment Station.
- Fishman, K. L., and R. Richards, Jr. 1997. *Seismic analysis and design of bridge abutments considering sliding and rotation*. Technical Report NCEER-97-0009. National Center for Earthquake Engineering Research. Buffalo, NY: State University of New York at Buffalo.
- Fishman, K. L., and R. Richards, Jr. 1998. Seismic analysis and model studies of bridge abutments. In *Analysis and Design of Retaining Structures Against Earthquakes*. ASCE Geotechnical Special Publication No. 80, 77-99.
- Franklin, A. G., and F. K. Chang. 1977. *Earthquake resistance of earth and rockfill dams: Report 5: Permanent displacement of earth embankments by Newmark sliding block analysis*. Miscellaneous Paper S-71-17. Vicksburg, MS: U.S. Army Engineer Waterways Experiment Station.
- Green, R. A., and R. M. Ebeling. 2002. *Seismic analysis of cantilever retaining walls, Phase I*. ERDC/ITL TR-02-3. Vicksburg, MS: U.S. Army Engineer Research and Development Center.
- Headquarters, Department of the Army. 1989. *Retaining and flood walls*. Engineer Manual 1110-2-2502. Washington, DC: Headquarters, Department of the Army.
- Headquarters, Department of the Army. 1990. *Retaining and flood walls*. Engineer Technical Letter 1110-2-322. Washington, DC: Headquarters, Department of the Army.
- Headquarters, Department of the Army. 1995. *Earthquake design and evaluation for Civil Works projects*. Engineer Regulation 1110-2-1806. Washington, DC: Headquarters, Department of the Army.

- Headquarters, Department of the Army. 2005. *Stability analysis of concrete structures*. Engineer Manual 1110-2-2100. Washington, DC: Headquarters, Department of the Army.
- Hibbler, R.C. 2001. *Engineering mechanics; Statics & dynamics*. 9th ed. Upper Saddle River, NJ: Prentice-Hall.
- Hynes-Griffin, M. E., and A. G. Franklin. 1984. *Rationalizing the seismic coefficient method*. Miscellaneous Paper GL-84-13. Vicksburg, MS: U.S. Army Engineer Waterways Experiment Station.
- Idriss, I. M. 1985. Evaluating seismic risk in engineering practice. In *Proceeding 11th International Conference on Soil Mechanics and Foundation Engineering* 1:255-320.
- Lysmer, J., T. Udaka, C.-F. Tsai, and H. B. Seed. 1975. FLUSH - A computer program for approximate 3-D analysis of soil-structure interaction problems. Report No. EERC 75-30, Earthquake Engineering Research Center. Berkeley: University of California.
- Makdisi, F. I., and H. B. Seed. 1978. Simplified procedure for estimating dam and embankment earthquake-induced deformations. ASCE. *Journal of the Geotechnical Engineering Division* 104(GT7):849-867.
- Mononobe, N., and H. Matsuo. 1929. On the determination of earth pressures during earthquakes. In *Proceedings, World Engineering Congress* 9:177-185.
- Nadim, F. 1980. Tilting and sliding of gravity retaining walls during earthquakes. MS thesis, Department of Civil Engineering, Massachusetts Institute of Technology.
- Nadim, F., and R. V. Whitman. 1984. Coupled sliding and tilting of gravity retaining walls during earthquakes. In *Proceedings of the Eighth World Conference on Earthquake Engineering, San Francisco III*: 477-484.
- Newmark, N. 1965. Effects of earthquakes on dams and embankments. *Geotechnique* 15(2):139-160.
- Okabe, S. 1924. General theory of earth pressures and seismic stability of retaining walls. *Journal Japan Society of Civil Engineering* 10(6).
- Okabe, S. 1926. General theory of earth pressures. *Journal Japan Society of Civil Engineering* 12(1).
- Richards, R., Jr., and D. Elms. 1979. Seismic behavior of gravity retaining walls. ASCE. *Journal of Geotechnical Engineering Division* 105(GT4):449-464.
- Richards, R., Jr., K. L. Fishman, and R. C. Divito. 1996. Threshold acceleration for rotation and sliding of bridge abutments. ASCE. *Journal of Geotechnical Engineering* 112(9):752-759.
- Schnabel, P. B., J. Lysmer, and H. B. Seed. 1972. SHAKE: A computer program for earthquake response analysis of horizontally layered sites. Report EERC-72-12. Earthquake Engineering Research Center. Berkeley: University of California.

- Seed, H. B., and R. V. Whitman. 1970. *Design of earth retaining structures for dynamic loads*. ASCE Specialty Conference on Lateral Earth Stresses in the Ground and Design of Earth Retaining Structures, 103-147.
- Siddharthan, R., S. Ara, and J. Anderson. 1990. Seismic displacement of rigid retaining walls. In *Proceedings of Fourth U.S. National Conference on Earthquake Engineering*, 673-680.
- Siddharthan, R., S. Ara, and G. M. Norris. 1992. Simple rigid plastic model for seismic tilting of rigid wall. ASCE. *Journal of Structural Engineering* 118(2):469-487.
- Siddharthan, R., P. Gowda, and G. M. Norris. 1991. Displacement based design of retaining walls. In *Proceedings, Second International Conference on Recent Advances in Geotechnical Earthquake Engineering and Soil Dynamics*, 657-661.
- Steedman, R. S., and X. Zeng. 1996. Rotation of large gravity walls on rigid foundations under seismic loading. In *Analysis and design of retaining structures against earthquakes*, Proc. of sessions sponsored by the Soil Dynamics Committee of the Geo-Institute of ASCE, ed. S. Prakash, ASCE Geotechnical Special Publication No. 60, 38-56.
- Strom, R. W., and R. M. Ebeling. 2004. Simplified methods used to estimate the limit-state axial load capacity of spillway invert slabs. ERDC/ITL TR-04-3. Vicksburg, MS: U.S. Army Engineer Research and Development Center.
- Westergaard, H. 1931. Water pressures on dams during earthquakes. *Transactions of ASCE*, Paper No. 1835, 418-433.
- Whitman, R. V. 1990. Seismic design behavior of gravity retaining walls. In *Proceedings of ASCE Specialty Conference on Design and Performance of Earth Retaining Structures*, Geotechnical Special Publication No. 25, 817-842.
- Whitman, R. V. 1992. Predicting earthquake-induced tilt of gravity retaining walls. In *Retaining Structures, Proceedings of a Conference*, Institution of Civil Engineers, pp. 750-758.
- Whitman, R. V. 2000. *Fifty years of soil dynamics*. Fifteenth Nabor Carrillo Lecture. Delivered during the XX National Meeting of Soil Mechanics, Oaxaca, Mexico, November, 88 p.
- Whitman, R. V., and S. Liao. 1985. *Seismic design of retaining walls*. Miscellaneous Paper GL-85-1. Vicksburg, MS: U.S. Army Waterways Experiment Station.
- Wong, C. 1982. *Seismic analysis and improved seismic design procedure for gravity retaining walls*. Research Report 82-32. Cambridge, MA: Department of Civil Engineering, Massachusetts Institute of Technology.
- Wood, J. 1975. Earthquake induced pressures on rigid wall structure. *Bulletin of New Zealand Society for Earthquake Engineering* 8(3): 175-186.
- Zarrabi, K. 1979. Sliding of gravity retaining wall during earthquakes considering vertical acceleration and changing inclination of failure surface. MS thesis, Department of Civil Engineering, Massachusetts Institute of Technology.

---

Zeng, X., and R. S. Steedman. 2000. Rotating block method for seismic displacement of gravity walls. ASCE. *Journal of Geotechnical and Geoenvironmental Engineering* 126(8): 709-717.

# Appendix A: Computation of the Dynamic Active Earth Pressure Forces for a Partially Submerged Retained Soil Using the Sweep-Search Wedge Method

## A.1 Introduction

This appendix describes the derivation of the dynamic active earth pressure force for partially submerged backfills using the sweep-search wedge method. The effect of earthquakes is incorporated through the use of a constant horizontal acceleration,  $a_h = k_h \cdot g$ , and a constant vertical acceleration,  $a_v = k_v \cdot g$ , acting on the soil mass comprising the active wedge within the backfill, as shown in Figure A.1.

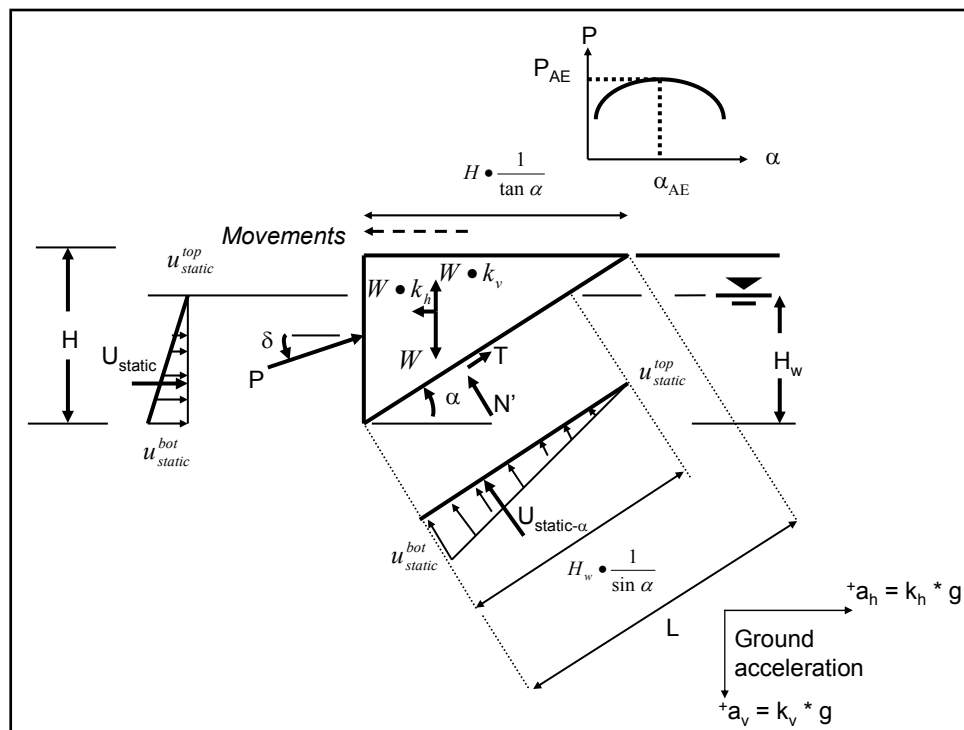


Figure A.1. Dynamic active sweep-search wedge analysis (hydrostatic water table).

The Mohr-Coulomb  $\tau = c + \sigma_n \cdot \tan \phi$  relationship is used to define the shear strength along a potential slip plane in the sweep-search soil wedge formulation derived in this appendix and implemented in  $C_{orps}W_{all}Rotate$ . For granular soils the cohesion intercept  $c$  is usually set equal (with a

non-zero  $\phi$  value) to zero after consideration is given to the anticipated level of permanent deformation associated with anticipated permanent wall movements and the development of the active earth pressure force,  $P_{AE}$ . The purpose for including the cohesion intercept in the shear strength used to define the sliding wedge formulation given in Section A.2 is to derive a set of equations that may be easily adapted to both effective and total stress analyses. In a total stress analysis  $\phi$  is set equal to zero, the cohesion intercept,  $c$ , is set equal to the undrained shear strength,  $S_u$ , and the internal pore water pressures are ignored.

In Section A.2 the relationships used in a sweep-search wedge formulation used to determine the magnitude of the dynamic active earth pressure force,  $P_{AE}$ , is derived for an effective stress analysis using Mohr-Coulomb shear strength parameters  $c'$  and  $\phi'$  for the retained soil.<sup>1,2</sup> The earth and water pressure forces acting on the trial soil wedge are derived for the case of a hydrostatic water table. Any increase in the pore water pressures

---

<sup>1</sup>A key item is the selection of suitable shear strength parameters. In an effective stress analysis, the issue of the suitable friction angle is particularly troublesome when the peak friction angle is significantly greater than the residual friction angle. In the displacement controlled approach examples given in Section 6.2 of Ebeling and Morrison (1992), effective stress-based shear strength parameters (i.e., effective cohesion,  $c'$ , and effective angle of internal friction,  $\phi'$ ) were used to define the shear strength of the dilative granular backfills, with  $c'$  set equal to zero in all cases due to the level of deformations anticipated in a sliding block analysis during seismic shaking. In 1992 Ebeling and Morrison concluded that it is conservative to use the residual friction angle in a sliding block analysis, and this should be the usual practice for displacement-based analysis of granular retained soils. The primary author of this report would broaden the concept to the assignment of effective (or total) shear strength parameters for the retained soil be consistent with the level of shearing-induced deformations encountered for each design earthquake in a rotational analysis and note that active earth pressures are used to define the loading imposed on the structural wedge by the driving soil wedge. (Refer to Table 1.1 for guidance regarding wall movements required to fully mobilize the shear resistance within the retained soil during earthquake shaking.) Therefore, engineers are cautioned to carefully consider the reasonableness of including a nonzero value for effective cohesion,  $c'$ , in their permanent deformation analyses.

<sup>2</sup> CorpsWallRotate performs a permanent displacement analysis of a retaining wall due to earthquake shaking. Reversal in the direction of the horizontal component of the time-history of earthquake ground shaking occurs many times during the typical tens of seconds of ground motion. Consequently, a reversal in direction of the inertial force imparted to the structural wedge and to the soil driving wedge occurs many times during the course of the analysis using CorpsWallRotate. In a traditional soil wedge formulation for static loading, a crack is typically considered to exist within the upper portion of the soil driving wedge for a cohesive soil (with shear strength,  $S_u$ , specified in a total stress analysis or  $c'$  specified in an effective stress analysis) and the planer wedge slip surface is terminated when it intersects the "zone of cracking" at a depth,  $d_{crack}$ , below the ground surface (e.g., see Appendix H in EM 1110-2-2502). This assumption is not made in the CorpsWallRotate formulation for dynamic loading. Instead, it is assumed that in the dynamic wedge formulation, the crack within the "zone of cracking" at the top of the retained cohesive soil of the driving wedge will not remain open during earthquake shaking due to the inertial load direction reversals during this time-history based CorpsWallRotate analysis. So, even for cohesive soils, the Figure A.1 planar slip surface, obtained from the sweep-search method of analysis used by CorpsWallRotate to obtain a value for the earthquake-induced resultant driving force,  $P_{AE}$  (acting on the structural wedge), extends uninterrupted within the driving soil wedge (in the retained soil) to the ground surface and is not terminated by a vertical crack face to the ground surface when it enters the zone of cracking.



above their steady state values in response to the shear stains induced within the saturated portion of the backfill during earthquake shaking is typically reflected in a value of excess pore water pressure ratio,  $r_u > 0$ , as discussed in Ebeling and Morrison (1992). No excess pore water pressures are included in the submerged portion of the backfill in this derivation (i.e.,  $r_u$  is equal to zero) although provisions are made to add this option to *C<sub>orps</sub>W<sub>all</sub>Rotate* in the future. Appendix A in Ebeling and Morrison (1992) provides a complete wedge solution derivation that includes excess pore water pressures (using  $r_u$ ).

Section A.3 briefly discusses the computation made by *C<sub>orps</sub>W<sub>all</sub>Rotate* of the static active earth pressure force,  $P_A$ , for partially submerged backfills using the sweep-search wedge method.

Section A.4 summarizes the computations made by *C<sub>orps</sub>W<sub>all</sub>Rotate* of the dynamic active earth pressure force,  $P_{AE}$ , for a total stress analysis in which a value for the shear strength,  $S_u$ , of the retained soil is specified by the user. The dynamic active earth pressure force,  $P_{AE}$ , is again computed using the sweep-search wedge method.

Section A.5 summarizes the computations made by *C<sub>orps</sub>W<sub>all</sub>Rotate* of the static active earth pressure force,  $P_A$ , for a total stress analysis in which a value for the shear strength,  $S_u$ , of the retained soil is specified by the user. The static active earth pressure force,  $P_A$ , is again computed using the sweep-search wedge method.

Section A.6 discusses the computation of the weight of a soil wedge with a bilinear ground surface.

For cohesive soils, including  $c'-\phi'$  soils, no adhesion force is included along the vertical imaginary section extending upwards through the retained soil from the heel of the wall that delineates the Figure A.1 driving soil wedge from the adjacent structural wedge.

## **A.2 Dynamic Active Earth Pressure Force, $P_{AE}$ — Effective Stress Analysis**

Figure A.1 represents a free body diagram for the derivation, which follows. The base of the wedge is the *trial* planar slip surface representing the active failure plane, which is inclined at angle alpha ( $\alpha$ ) to the horizontal. The top of the Figure A.1 wedge is bounded by a horizontal

ground surface and a vertical face along the interface between the driving soil wedge and the structural wedge.

The weight of the soil wedge acts at the center of mass and is computed as

$$W = \frac{1}{2} \gamma_t \bullet H^2 \bullet \frac{1}{\tan \alpha} \quad \text{A.1}$$

with  $\gamma_t$  being the total unit weight for the soil wedge.<sup>1,2</sup>

The three forces acting along the planar slip surface are represented by an effective normal force,  $N'$ , a shear force,  $T$ , and the pore water pressure force. Assuming a full mobilization of shear resistance along the slip surface, the shear force may be computed utilizing the Mohr-Coulomb failure criteria as

$$T = N' \tan \phi' + c' \bullet L \quad \text{A.3}$$

Note that the length of the potential slip plane,  $L$ , relates to the height of the soil wedge,  $H$ , at an angle  $\alpha$  from horizontal by

$$L = H \bullet \left( \frac{1}{\sin \alpha} \right) \quad \text{A.4}$$

Recall the entire slip plane length,  $L$ , is used in the analysis of the driving soil wedge for cohesive soils to compute  $P_{AE}$  due to the assumption that the “zone of cracking” at the top of the retained cohesive soil of the driving soil wedge will not remain open during earthquake shaking due to load direction reversals during this time-history based  $C_{orps} W_{all} Rotate$  analysis.<sup>2</sup>

The total pore water pressures acting along the submerged faces of the soil wedge are described in terms of the steady state pore water pressure.

---

<sup>1</sup> Using the Figure 4.13 Ebeling and Morrison (1992) relationship,  $\gamma_t$  for the Figure A.1 soil wedge (with a planer slip surface and level backfill) is computed to be

$$\gamma_t = \left( \frac{H_w}{H} \right)^2 \bullet \gamma_{saturated} + \left[ 1 - \left( \frac{H_w}{H} \right)^2 \right] \bullet \gamma_{moist} \quad \text{A.2}$$

with  $\gamma_{moist}$  the moist unit weight of the soil above the water table and  $\gamma_{saturated}$  the saturated unit weight below the water table. An alternative method for determining the value for  $W$  based on the geometry of the trial soil wedge cross sectional area with regions of moist and saturated unit weights is given in Section A.6.

<sup>2</sup> In the case of a soil wedge defined by the Figure 3.7.b bilinear ground surface, the total weight  $W$  is computed using the relationships given in Section A.6.

**A.2.1 Calculation of Water Pressure Forces for a Hydrostatic Water Table**

The pore water pressure at the ground water table (Figure A.2) is

$$u_{static}^{top} = 0 \tag{A.5}$$

For a hydrostatic water table, the pore water pressure distribution is linear with depth, and at the bottom of the wedge is computed as

$$u_{static}^{bot} = \gamma_w \cdot H_w \tag{A.6}$$

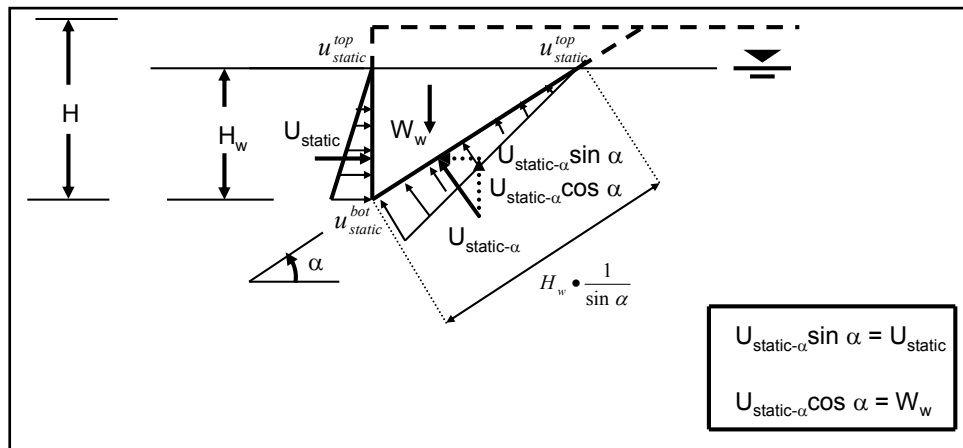


Figure A.2. Equilibrium of horizontal and vertical hydrostatic water pressure forces acting on the retained soil wedge.

**A.2.2 Static Water Pressure Forces Acting on the Wedge**

The static pore pressure distribution immediately behind the structural wedge is triangular and the resultant force may be calculated as

$$U_{static} = \frac{1}{2} \gamma_w \cdot H_w^2 \tag{A.7}$$

The static pore pressure force acting normal to the planar slip surface (of angle  $\alpha$  from horizontal) is also triangular and the resultant force may be computed as

$$U_{static-\alpha} = \frac{1}{2} \gamma_w \cdot H_w^2 \cdot \frac{l}{\sin \alpha} \tag{A.8}$$

### A.2.3 Equilibrium of Vertical Forces

Equilibrium of vertical forces acting on the Figure A.1 soil wedge (with a potential slip plane at an angle  $\alpha$  from horizontal) results in the relationship

$$-P \bullet \sin \delta + W(1 - k_v) - [T] \sin \alpha - N' \bullet \cos \alpha - (U_{static-\alpha} + U_{shear-\alpha}) \cos \alpha = 0 \quad A.9$$

Introducing Equation A.3 into Equation A.9 results in

$$\begin{aligned} -P \bullet \sin \delta + W(1 - k_v) - [c' \bullet L + N' \bullet \tan \phi'] \sin \alpha \\ - N' \bullet \cos \alpha - (U_{static-\alpha} + U_{shear-\alpha}) \cos \alpha = 0 \end{aligned} \quad A.10$$

and solving for the normal effective force,  $N'$ , becomes

$$\begin{aligned} N' = -P \frac{\sin \delta}{\tan \phi' \bullet \sin \alpha + \cos \alpha} + W \frac{(1 - k_v)}{\tan \phi' \bullet \sin \alpha + \cos \alpha} \\ - (U_{static-\alpha}) \frac{\cos \alpha}{\tan \phi' \bullet \sin \alpha + \cos \alpha} - c' \bullet L \frac{\sin \alpha}{\tan \phi' \bullet \sin \alpha + \cos \alpha} \end{aligned} \quad A.11$$

### A.2.4 Equilibrium of Forces in the Horizontal Direction

Equilibrium of horizontal forces acting on the Figure A.1 soil wedge (with a potential slip plane at an angle  $\alpha$  from horizontal) results in the relationship

$$\begin{aligned} P \bullet \cos \delta - N' \bullet \sin \alpha - (U_{static-\alpha}) \sin \alpha \\ + [T] \cos \alpha - W \bullet k_h + (U_{static}) = 0 \end{aligned} \quad A.12$$

Substituting Equation A.3 into Equation A.12, and with the horizontal components of water pressure forces of equal magnitude and opposite direction (refer to Figure A.2), Equation A.12 simplifies to

$$P \bullet \cos \delta - N' \bullet \sin \alpha + [c' \bullet L + N' \tan \phi'] \cos \alpha - W \bullet k_h = 0 \quad A.13$$

Combining the  $N'$  terms results in

$$P \bullet \cos \delta - N' (\sin \alpha - \tan \phi' \bullet \cos \alpha) - W \bullet k_h + c' \bullet L \bullet \cos \alpha = 0 \quad A.14$$

Multiplying Equation A.11 (for  $N'$ ) by  $[-(\sin \alpha - \tan \phi' \cdot \cos \alpha)]$  and simplifying<sup>1</sup> becomes

$$-N'(-\tan \phi' \cdot \cos \alpha + \sin \alpha) = +P \sin \delta \cdot \tan(\alpha - \phi') - W(1 - k_v) \tan(\alpha - \phi') + c' \cdot L \tan(\alpha - \phi') \cdot \sin \alpha + (U_{static-\alpha}) \cos \alpha \cdot \tan(\alpha - \phi') \quad \text{A.16}$$

Substituting Equation A.16 into Equation A.14 gives

$$P \cdot \cos \delta + P \cdot \sin \delta \cdot \tan(\alpha - \phi') - W(1 - k_v) \tan(\alpha - \phi') + c' \cdot L \cdot \tan(\alpha - \phi') \cdot \sin \alpha + c' \cdot L \cdot \cos \alpha + (U_{static-\alpha}) \cos \alpha \cdot \tan(\alpha - \phi') - W \cdot k_h = 0 \quad \text{A.17}$$

Combining terms results in

$$P[\cos \delta + \sin \delta \cdot \tan(\alpha - \phi')] = W[(1 - k_v) \tan(\alpha - \phi') + k_h] - c' \cdot L \cdot \tan(\alpha - \phi') \cdot \sin \alpha - c' \cdot L \cdot \cos \alpha - (U_{static-\alpha}) \cos \alpha \cdot \tan(\alpha - \phi') \quad \text{A.18}$$

Solving for the resultant force,  $P$ , which acts at angle  $\delta$  for the trial soil wedge with a potential slip plane at an angle  $\alpha$  from horizontal,

$$P = \frac{CONSTANT_{A1} - CONSTANT_{A2}}{\cos \delta + \sin \delta \cdot \tan(\alpha - \phi')} \quad \text{A.19}$$

where

$$CONSTANT_{A1} = W[(1 - k_v) \tan(\alpha - \phi') + k_h] \quad \text{A.20}$$

and

$$CONSTANT_{A2} = +c' \cdot L \cdot \tan(\alpha - \phi') \cdot \sin \alpha + c' \cdot L \cdot \cos \alpha + (U_{static-\alpha}) \cos \alpha \cdot \tan(\alpha - \phi') \quad \text{A.21}$$

---

<sup>1</sup> Note:  $\tan(\alpha - \phi) = \frac{\sin \alpha - \tan \phi' \cdot \cos \alpha}{\cos \alpha + \tan \phi' \cdot \sin \alpha} \cdot \frac{1}{\frac{1}{\cos \alpha}} = \frac{\tan \alpha - \tan \phi'}{1 + \tan \phi' \cdot \tan \alpha}$  A.15

The dynamic active earth pressure force,  $P_{AE}$ , is equal to the maximum value of  $P$  for the trial wedges analyzed and  $\alpha_{AE} = \alpha$  for this critical wedge, as shown in Figure A.1.

In order to assign a location to  $P_{AE}$ , the static value for  $P_A$  is needed (refer to Equation 3.24 for the moist backfill, level ground case and to Appendix C for all other cases).  $C_{orps}W_{all}Rotate$  proceeds with the computation of  $h_{PAE}$ , the location of the resultant force,  $P_{AE}$ , using the value for  $P_A$  computed by procedure discussed in this next section. The computation of  $h_{PAE}$  by  $C_{orps}W_{all}Rotate$  in an effective stress analysis is described in Sections C.1 through C.3 of Appendix C.

### A.3 Static Active Earth Pressure Force, $P_A$ – Effective Stress Analysis

The solution for the static active earth pressure force for an effective stress analysis of a partially submerged backfill is calculated by using a variation of the sweep-search wedge method derived in Section A.2. Hydrostatic water pressures are assumed within the submerged portion of the retained soil, including within the zone of cracking. The relationships needed are developed by setting  $P$  equal to  $P_{Static-effective\ stress}$ ,  $k_h$  and  $k_v$  equal to zero, and  $L$  equal to  $L_{net}$  in Equations A.19 through A.21. The portion of the trial wedge planar slip plane that is below the zone of cracking has the length  $L_{net}$  as shown in Figure A.3. Mohr-Coulomb shear strength parameters  $c'$  and  $\phi'$  are used to characterize the shear strength of the retained soil. In a traditional soil wedge formulation for static loading, a crack is typically considered to exist within the upper portion of the soil driving wedge for a cohesive soil (with a cohesive shear strength  $c'$  specified in an effective stress analysis) and the planer wedge slip surface is terminated when it intersects the zone of cracking at a depth  $d_{crack}$  below the ground surface (e.g., see Appendix H in EM 1110-2-2502). This assumption is made in the  $C_{orps}W_{all}Rotate$  formulation for static loading (but not when computing  $P_{AE}$  for dynamic loading as discussed previously). A sweep-search wedge method of analysis as idealized in Figure A.3 is used by the  $C_{orps}W_{all}Rotate$  to determine the value of the active earth pressure force,  $P_A$ .

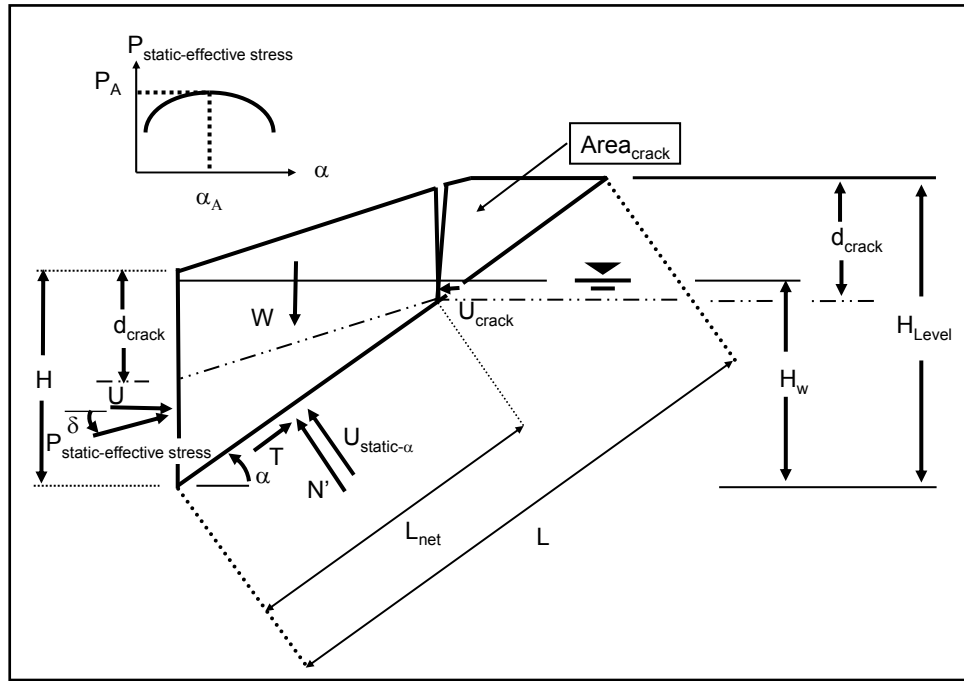


Figure A.3. Static active sweep-search wedge analysis, effective stress analysis with a hydrostatic water table (zone of cracking of depth  $d_{crack}$ ).

For a given trial soil wedge with a potential slip plane at an angle  $\alpha$  from horizontal, the resultant force  $P_{\text{Static-effective stress}}$ , which acts at angle  $\delta$  for the trial soil wedge, is given by

$$P_{\text{Static-effective stress}} = \frac{\text{CONSTANT}_{A1\text{-Static}} - \text{CONSTANT}_{A2\text{-Static}}}{\cos \delta + \sin \delta \cdot \tan(\alpha - \phi')} \tag{A.22}$$

where

$$\text{CONSTANT}_{A1\text{-Static}} = W [\tan(\alpha - \phi')] \tag{A.23}$$

and

$$\text{CONSTANT}_{A2\text{-Static}} = +c' \cdot L_{\text{net}} \cdot \tan(\alpha - \phi') \cdot \sin \alpha + c' \cdot L_{\text{net}} \cdot \cos \alpha + (U_{\text{static-}\alpha}) \cos \alpha \cdot \tan(\alpha - \phi') \tag{A.24}$$

The weight,  $W$ , of the soil wedge for the Figure A.3 bilinear soil surface problem (with cracking) is calculated using one of the procedures described in Section A.6. The static active earth pressure force,  $P_A$ , is equal to the maximum value of  $P_{\text{Static-effective stress}}$  for the trial wedges analyzed and

$\alpha_A = \alpha$  for this critical wedge using the (graphical) procedure depicted in Figure A.3.

In preparation for determining the location of resultant for location for  $P_{AE}$  (to be described in Appendix C) Equation A.22 is recast in the following form to distinguish the contribution of the weight and the frictional component of the soil wedge resultant force,  $P_{\text{Static-effective stress}}$ , from the cohesive component:

$$P_{\text{Static-effective stress}} = P_{\text{Static-}\phi\text{-weight}} - P_{\text{Static-C}} \quad \text{A.25}$$

with

$$P_{\text{Static-}\phi\text{-weight}} = \frac{W[\tan(\alpha - \phi')] - (U_{\text{static-}\alpha}) \cos(\alpha) \cdot \tan(\alpha - \phi')}{\cos \delta + \sin \delta \cdot \tan(\alpha - \phi')} \quad \text{A.26}$$

and

$$P_{\text{Static-C}} = \frac{c' \cdot L_{\text{net}} \cdot [\tan(\alpha - \phi')] \cdot \sin \alpha + c' \cdot L_{\text{net}} \cdot \cos \alpha}{\cos \delta + \sin \delta \cdot \tan(\alpha - \phi')} \quad \text{A.27}$$

Note that the frictional/weight component,  $P_{\text{static-}\phi\text{-weight}}$ , of resultant force  $P_{\text{static-effective stress}}$  (Equation A.25) is reduced by the cohesion force component,  $P_{\text{static-C}}$ . The subtraction the force  $P_{\text{static-C}}$  in Equation A.25 reflects a resultant force component  $P_{\text{static-C}}$  for a *tensile stress* distribution component, to be discussed in Appendix C.

A depth of cracking is considered in an effective stress analysis of  $P_A$  with the assignment of a nonzero value for cohesion ( $c'$ ). CorpsWallRotate uses a trial-and-error procedure to determine the value for  $d_{\text{crack}}$  when computing  $P_A$ . In this iterative procedure, (1) an initial value for  $d_{\text{crack}}$  is assumed (set equal to zero in the first iteration); (2) the trial wedge procedure of analysis discussed in this section is performed and a corresponding trial value for  $P_A$  is computed, along with values for its frictional/weight force component,  $P_{\text{static-}\phi\text{-weight}}$ , and for cohesion force component,  $P_{\text{static-C}}$ ; (3) a new depth of crack is computed based on values for  $P_{\text{static-}\phi\text{-weight}}$  and  $P_{\text{static-C}}$  and their corresponding earth pressure distributions that are determined using the procedure outlined in Section C.3 for  $P_A$ ; (4) repeat these steps (1) through (3) until convergence in the value for  $d_{\text{crack}}$  is achieved.



$C_{orps}W_{all}Rotate$  uses the  $P_A$  value in the computation of  $h_{PAE}$ , the location of the resultant force  $P_{AE}$  as discussed in Appendix C, using the last value for  $P_A$  computed by this trial-and-error procedure.

#### A.4 Dynamic Active Earth Pressure Force, $P_{AE}$ — Total Stress Analysis

In a total stress analysis, the value for the dynamic active earth pressure force,  $P_{AE}$ , is computed based on a user-specified shear strength,  $S_u$ , for the retained soil. The dynamic active earth pressure force is also computed for this situation using the sweep-search wedge method described in Section A.2 but with the following two changes; (1) cohesion term  $c'$  is set equal to  $S_u$ , with  $\phi'$  and the interface friction angle  $\delta$  set to zero, and (2) the pore water pressures internal to the soil wedge are set equal to zero. The relationships needed are developed from Equations A.19 through A.21. For a given trial soil wedge with a potential slip plane at an angle  $\alpha$  from horizontal, the resultant force  $P_{Su}$  is given by

$$P_{Su} = CONSTANT_{A1-Su} - CONSTANT_{A2-Su} \quad A.28$$

where

$$CONSTANT_{A1-Su} = W \left[ (1 - k_v) \tan(\alpha) + k_h \right] \quad A.29$$

and

$$CONSTANT_{A2-Su} = +S_u \cdot L \cdot \tan(\alpha) \cdot \sin \alpha + S_u \cdot L \cdot \cos \alpha \quad A.30$$

The dynamic active earth pressure force,  $P_{AE}$ , is equal to the maximum value of  $P_{Su}$  for the trial wedges analyzed and  $\alpha_{AE} = \alpha$  for this critical wedge, analogous to the (graphical) procedure depicted in Figure A.1 for determining the value of  $P_{AE}$  from all values for  $P$ .

Recall the entire slip plane length,  $L$ , is used in the analysis of the driving soil wedge for cohesive soils to compute  $P_{AE}$  due to the assumption that the zone of cracking at the top of the retained cohesive soil of the driving soil wedge will not remain open during earthquake shaking due to load direction reversals during this time-history based  $C_{orps}W_{all}Rotate$  analysis.

In order to assign a location to  $P_{AE}$  the static value for  $P_A$  is needed.  $C_{orps}W_{all}Rotate$  proceeds with the computation of  $h_{PAE}$ , the location of the

resultant force  $P_{AE}$ , using the value for  $P_A$  computed by procedure discussed in this next section. The computation of  $h_{PAE}$  by  $C_{orps}W_{all}Rotate$  in a total stress analysis is described in Section C.4 of Appendix C.

### **A.5 Static Active Earth Pressure Force, $P_A$ – Total Stress Analysis**

In a traditional soil wedge formulation for static loading, a crack is typically considered to exist within the upper portion of the soil driving wedge for a cohesive soil (with a undrained shear strength,  $S_u$ , specified in an total stress analysis) and the planer wedge slip surface is terminated when it intersects the zone of cracking at a depth,  $d_{crack}$ , below the ground surface (e.g., see Appendix H in EM 1110-2-2502). This assumption is made in the  $C_{orps}W_{all}Rotate$  formulation for static loading (but not when computing  $P_{AE}$  for dynamic loading as discussed previously). A sweep-search wedge method of analysis as idealized in Figure A.4 is used by the  $C_{orps}W_{all}Rotate$  to determine the value of the active earth pressure force  $P_A$ . The solution for the static active earth pressure force for a total stress analysis of a partially submerged backfill is calculated by using a variation of the sweep-search wedge method derived in Section A.3. The static active earth pressure force is computed for this situation using the sweep-search wedge method described in Section A.3 but with the following three changes; (1) the term  $P_{Static-effective\ stress}$  is set equal to  $P_{Static-total\ stress}$ , (2) cohesion term  $c'$  is set equal to  $S_u$ , with  $\phi'$  and the interface friction angle  $\delta$  set to zero, and (3) the pore water pressures internal to the soil wedge are set equal to zero. Hydrostatic water pressures due to the presence of water within the cracks in the zone of cracking are considered.

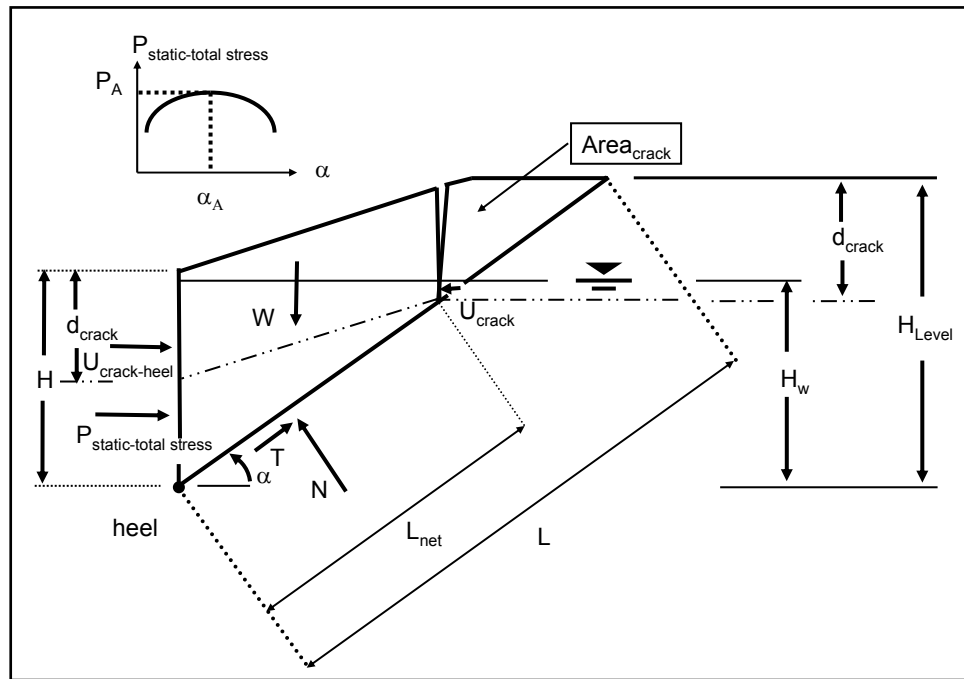


Figure A.4. Static active sweep-search wedge analysis, total stress analysis with a hydrostatic water table (zone of cracking of depth  $d_{\text{crack}}$ ).

The relationships needed are developed from Equations A.22 through A.24. For a given trial soil wedge with a potential slip plane at an angle  $\alpha$  from horizontal, the resultant force  $P_{\text{Static-total stress}}$  is given by

$$P_{\text{static-total stress}} = P_{\text{Static-weight}} - P_{\text{Static-Su}} - \Delta U \quad \text{A.31}$$

$$P_{\text{Static-weight}} = W \cdot \tan(\alpha) \quad \text{A.32}$$

$$P_{\text{Static-Su}} = Su \cdot L_{\text{net}} \cdot \tan(\alpha) \cdot \sin(\alpha) + Su \cdot L_{\text{net}} \cdot \cos(\alpha) \quad \text{A.33}$$

with the difference in water pressure force within the cracks on both sides and acting on soil driving wedge is given by

$$\Delta U = U_{\text{crack-heel}} - U_{\text{crack}} \quad \text{A.34}$$

The weight,  $W$ , of the soil wedge for the Figure A.4 bilinear soil surface problem (with cracking) is calculated using one of the procedures described in Section A.6. The static active earth pressure force,  $P_A$ , is equal to the maximum value of  $P_{\text{static-total stress}}$  for the trial wedges analyzed and  $\alpha_A = \alpha$  for this critical wedge, using the (graphical) procedure depicted in Figure A.4.

Equation A.31 distinguishes the contribution of the weight component of the soil wedge to  $P_{\text{static-total stress}}$  from the cohesive component. Note that the weight component,  $P_{\text{static-weight}}$ , of resultant force  $P_{\text{static-total stress}}$  (Equation A.31) is reduced by the cohesion force component,  $P_{\text{static-Su}}$ . The subtraction the force  $P_{\text{static-Su}}$  in Equation A.31 reflects a resultant force component,  $P_{\text{static-Su}}$ , for a *tensile stress* distribution component, to be discussed in Appendix C.

A depth of cracking is considered in a total stress analysis of  $P_A$  with the assignment of a nonzero value for cohesion ( $S_u$ ).  $C_{\text{orps}}W_{\text{allRotate}}$  uses a trial-and-error procedure to determine the value for  $d_{\text{crack}}$  when computing  $P_A$ . In this iterative procedure, (1) an initial value for  $d_{\text{crack}}$  is assumed (set equal to zero in the first iteration); (2) the trial wedge procedure of analysis discussed in this section is performed and a corresponding trial value for  $P_A$  is computed, along with values for its weight force component,  $P_{\text{static-weight}}$ , and for cohesion force component,  $P_{\text{static-Su}}$ ; (3) a new depth of crack is computed based on values for  $P_{\text{static-weight}}$  and  $P_{\text{static-Su}}$  and their corresponding earth pressure distributions that are determined using the procedure outlined in Section C.4 for  $P_A$ ; (4) repeat these steps (1) through (3) until convergence in the value for  $d_{\text{crack}}$  is achieved.  $C_{\text{orps}}W_{\text{allRotate}}$  proceeds with the computation of  $h_{\text{PAE}}$ , the location of the resultant force  $P_{\text{AE}}$  as discussed in Appendix C, using the last value for  $P_A$  computed by this trial-and-error procedure.

## A.6 Weight Computation of a Soil Wedge with a Bilinear Ground Surface

$C_{\text{orps}}W_{\text{allRotate}}$  computes the value for  $P_{\text{AE}}$  and  $P_A$  via the Figure 3.7 sweep-search method. An advantage of the sweep-search method is that it allows for the analysis of the more practical case of the bilinear ground surface depicted in Figure 3.7.b. The computation of the area of soil wedge above and below the water table and total weight,  $W$ , are made as follows:

### A.6.1 $\alpha$ greater than $\alpha_{\text{corner}}$

For the case of the soil wedge with a potential slip plane at an angle  $\alpha$  from horizontal being greater than the angle designated  $\alpha_{\text{corner}}$ , defining the line between the point corresponding to the heel of the wall and the intersection of the level backfill and the sloping ground surface point 4 in Figure A.5, the total cross-sectional area is

$$Area_{total} = \frac{1}{2} \cdot \{x_1 \cdot [y_2 - y_3] + x_2 \cdot [y_3 - y_1] + x_3 \cdot [y_1 - y_2]\} \quad A.35$$

with  $(x_1, y_1)$ ,  $(x_2, y_2)$ , and  $(x_3, y_3)$  being the vertices of the triangle of the trial soil wedge shown in this figure. Point 5 denotes the intersection of the hydrostatic water table with the planar trial wedge that extends from point 1 to point 2. The area of the trial soil wedge below the water table is designated AreaW in this figure.

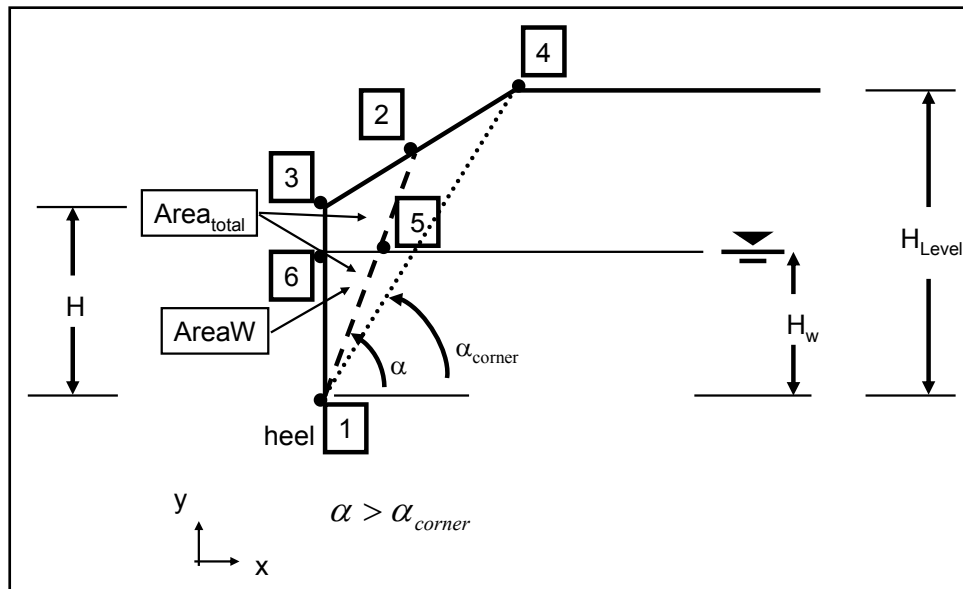


Figure A.5. Soil wedge defined by a bilinear ground surface with  $\alpha$  greater than  $\alpha_{corner}$  and no crack.

Figure A.6 extends the Figure A.5 case to consider a crack within a retained (cohesive) soil. The case shown is for a crack depth that extends to below the hydrostatic water table. Note the depth of cracking extends from the ground surface to a depth,  $d_{crack}$ , below the sloping ground surface as well as below the level portion of the retained soil. Point 7 denotes the intersection of the depth,  $d_{crack}$ , with the planar trial wedge that extends from point 1 to point 2. Points 7, 2, and 8 delineate a triangular region of the trial soil wedge that is fully contained within the depth of cracking.

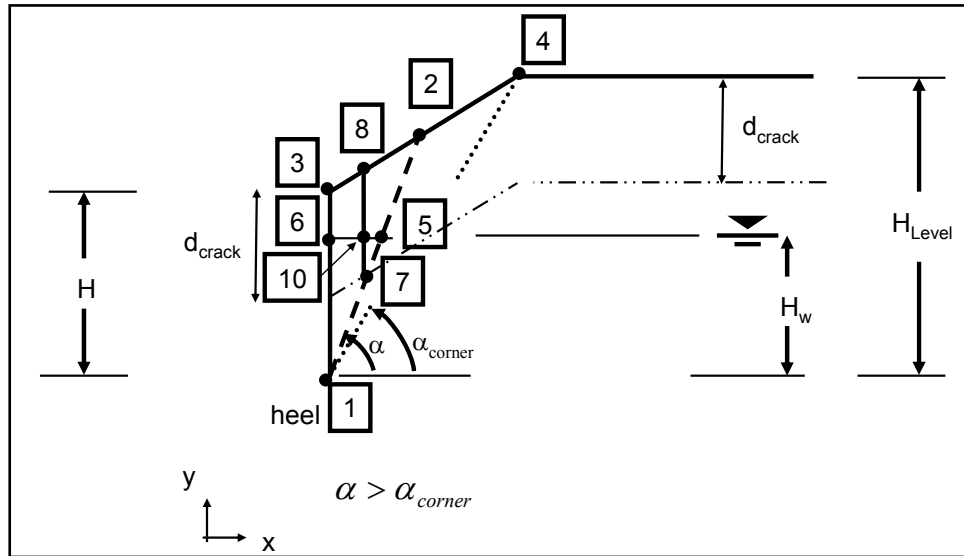


Figure A.6. Soil wedge defined by a bilinear ground surface with  $\alpha$  greater than  $\alpha_{corner}$  and crack depth  $d_{crack}$  that extends below the water table.

The portion of the total cross-sectional area (i.e.,  $Area_{total}$  by Equation A.35) entirely contained within the depth of cracking zone is given by

$$Area_{crack} = \frac{1}{2} \cdot \{x_7 \cdot [y_2 - y_8] + x_2 \cdot [y_8 - y_7] + x_8 \cdot [y_7 - y_2]\} \quad A.36$$

with  $(x_7, y_7)$ ,  $(x_2, y_2)$  and  $(x_8, y_8)$  being the vertices of the triangle of the trial soil wedge identified Figure A.7. Consequently, the total soil wedge area less this triangular zone of cracking ( $Area_{crack}$ ) is designated as the  $Area_{net}$  and is computed to be

$$Area_{net} = Area_{total} - Area_{crack} \quad A.37$$

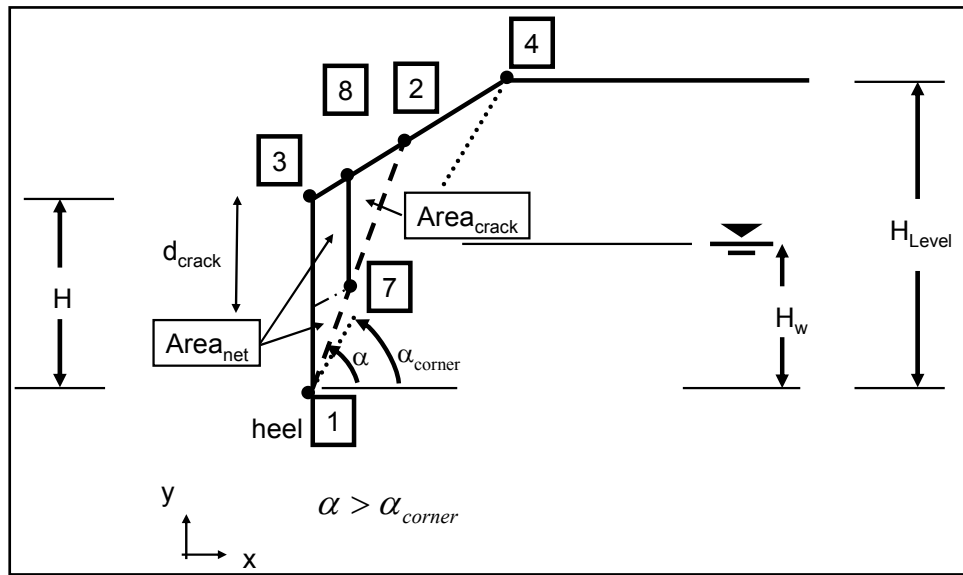


Figure A.7.  $Area_{net}$  and  $Area_{crack}$  within the soil wedge defined by a bilinear ground surface with  $\alpha$  greater than  $\alpha_{corner}$  for a crack depth  $d_{crack}$  that extends below the water table.

The cross-sectional area of the entire submerged portion of the trial soil wedge (with crack) is

$$AreaW = \frac{1}{2} \cdot \{x_1 \cdot [y_5 - y_6] + x_5 \cdot [y_6 - y_1] + x_6 \cdot [y_1 - y_5]\} \tag{A.38}$$

with  $(x_1, y_1)$ ,  $(x_5, y_5)$ , and  $(x_6, y_6)$  being the vertices of the triangle of the submerged portion of the soil wedge, as shown in Figure A.5. The portion of the area given by Equation A.38, i.e., the total submerged cross-sectional area (i.e.,  $AreaW$ ), contained within the depth of cracking is

$$AreaW_{crack} = \frac{1}{2} \cdot \{x_7 \cdot [y_5 - y_{10}] + x_5 \cdot [y_{10} - y_7] + x_{10} \cdot [y_7 - y_5]\} \tag{A.39}$$

with  $(x_7, y_7)$ ,  $(x_5, y_5)$ , and  $(x_{10}, y_{10})$  being the vertices of the triangle of the trial soil wedge identified Figure A.8. The total cross-sectional area of the submerged portion of the trial soil wedge (with crack) less the triangular zone of cracking below the water table, is designated in Figure A.8 as  $AreaW_{net}$  and given by

$$AreaW_{net} = AreaW - AreaW_{crack} \tag{A.40}$$

Consequently, the net moist cross-sectional area of the trial soil wedge above the water table is equal to

$$Area_{moist-net} = Area_{net} - AreaW_{net} \tag{A.41}$$

and identified in Figure A.8.

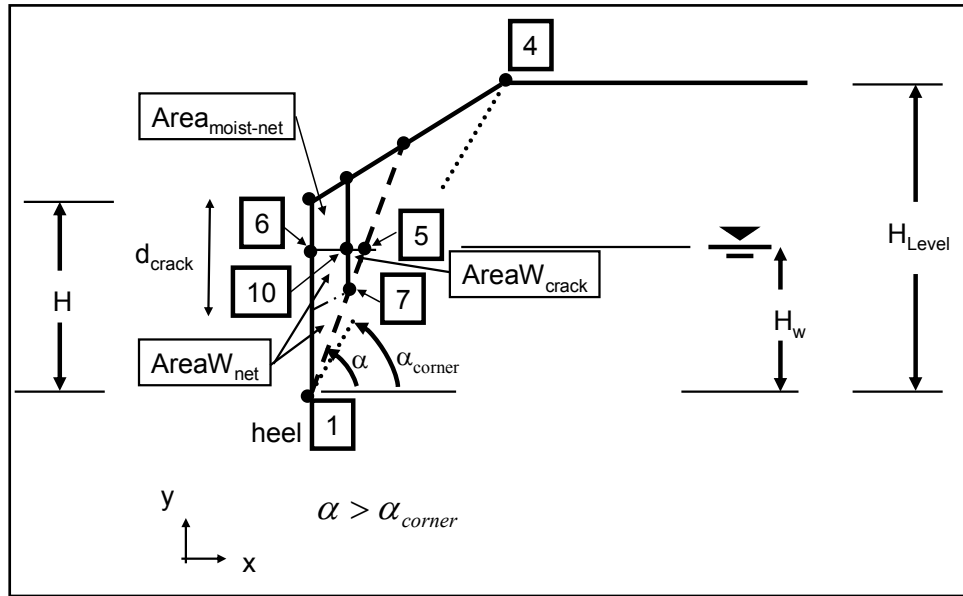


Figure A.8.  $Area_{moist-net}$ ,  $AreaW_{net}$ , and  $AreaW_{crack}$  within the soil wedge defined by a bilinear ground surface with  $\alpha$  greater than  $\alpha_{corner}$  and crack depth  $d_{crack}$  that extends below the water table.

The weight of the net submerged portion of the trial soil wedge,  $W_{saturated}$ , is

$$W_{saturated} = \gamma_{saturated} \bullet AreaW_{net} \tag{A.42}$$

with the weight of the net moist portion of the soil wedge

$$W_{moist} = \gamma_{moist} \bullet Area_{moist-net} \tag{A.43}$$

The total weight for the net trial soil wedge, considering a depth of crack,  $d_{crack}$ , is equal to

$$W = W_{saturated} + W_{moist} \tag{A.44}$$

This and the other relationships given in this subsection are also valid in the case of  $d_{crack}$  equal to zero, i.e., cohesionless soils.



**A.6.2  $\alpha_{corner}$  greater than  $\alpha$**

For the case in which the angle  $\alpha_{corner}$  (from horizontal), defining the line between the point corresponding to the heel of the wall and point 4 in Figure A.9 that designates the intersection of the level backfill and the sloping ground surface, is greater than the angle  $\alpha$  of soil wedge for the potential slip plane, the total cross-sectional area is

$$Area_{total} = \frac{1}{2} \cdot \left\{ \begin{aligned} &x_1 \cdot [y_2 - y_4] + x_2 \cdot [y_4 - y_1] + x_4 \cdot [y_1 - y_2] + \\ &x_1 \cdot [y_4 - y_3] + x_4 \cdot [y_3 - y_1] + x_3 \cdot [y_1 - y_4] \end{aligned} \right\} \quad A.45$$

with  $(x_1, y_1)$ ,  $(x_2, y_2)$ , and  $(x_4, y_4)$ , and with  $(x_1, y_1)$ ,  $(x_4, y_4)$ , and  $(x_3, y_3)$  being the vertices of the two triangles that form the soil wedge shown in this figure. The area of the trial soil wedge below the water table is designated AreaW in this figure and is defined by the vertices  $(x_1, y_1)$ ,  $(x_5, y_5)$ , and  $(x_6, y_6)$ .

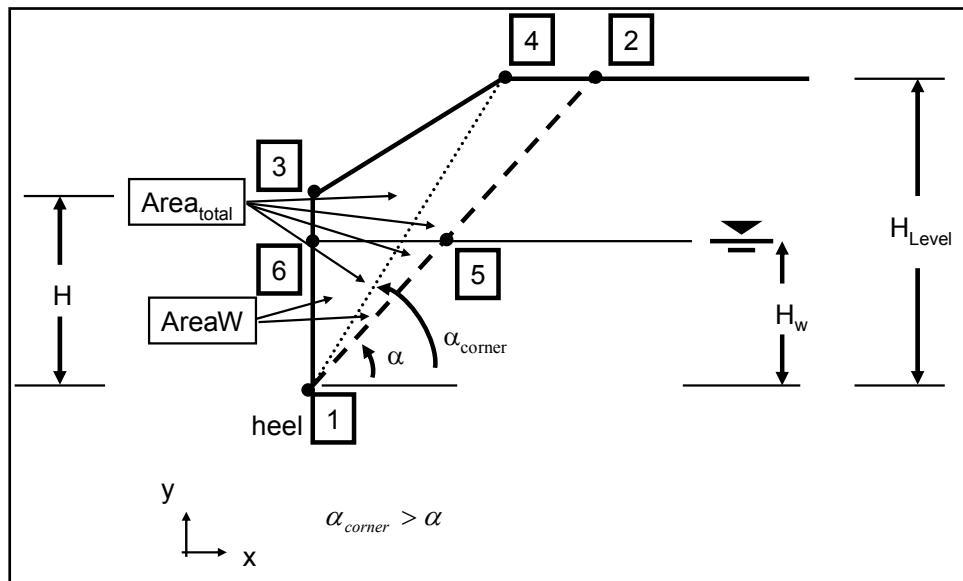


Figure A.9. Soil wedge defined by a bilinear ground surface with  $\alpha_{corner}$  greater than  $\alpha$ .

**A.6.2.1  $d_{crack} > \Delta_{4to9}$**

Figure A.10 extends the Figure A.9 case to consider a crack within a retained (cohesive) soil. Note the depth of cracking extends from the ground surface to a depth,  $d_{crack}$ , below the sloping ground surface as well as below the level portion of the retained soil. The case shown is for a crack depth that intersects the planer trial slip plane (extending from points 1 to 2) below the sloping ground surface of slope  $\beta$  (versus below the level

ground surface region). This intersection point is designated as point 7 in this figure, corresponding to the case of  $d_{crack} > \Delta_{4to9}$ . Point 9 defines the point along the planar trial slip surface (extending from point 1 to point 2) that is below point 4. The case shown in Figure A.10 is for point 7 above the hydrostatic water table. Points 7, 2, 4, and 8 delineate a region of the trial soil wedge that is fully contained within the depth of cracking (i.e.,  $Area_{crack}$ ).

$$Area_{crack} = \left[ \frac{(x_4 - x_8) + (x_9 - x_7)}{2} \right] \cdot \left[ \frac{(y_4 - y_9) + (y_8 - y_7)}{2} \right] + \frac{1}{2} \cdot \{ x_9 \cdot (y_2 - y_4) + x_2 \cdot (y_4 - y_9) + x_4 \cdot (y_9 - y_2) \} \tag{A.46}$$

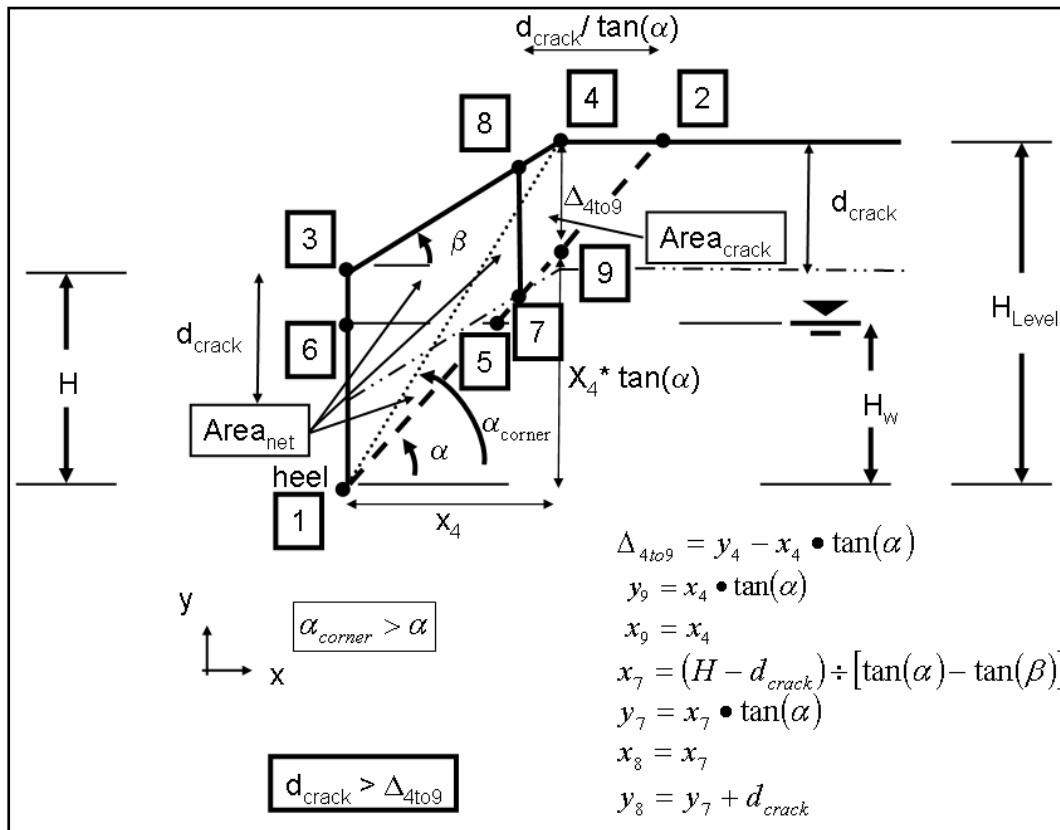


Figure A.10. Soil wedge defined by a bilinear ground surface with  $\alpha_{corner}$  greater than  $\alpha$  and crack depth,  $d_{crack}$ , that extends below the water table ( $d_{crack} > \Delta_{4to9}$ ).

The total soil wedge area less this triangular zone of cracking ( $Area_{crack}$ ) is designated as the  $Area_{net}$  in Figure A.10 and is computed to be

$$Area_{net} = Area_{total} - Area_{crack} \tag{bis A.37}$$

The cross-sectional area of the entire submerged portion of the trial soil wedge, designated AreaW, is given by Equation A.38. Figure A.11 extends Figure A.10 so as to distinguish the moist net area, designated Area<sub>moist-net</sub>, from the submerged net area, designated AreaW<sub>net</sub>.

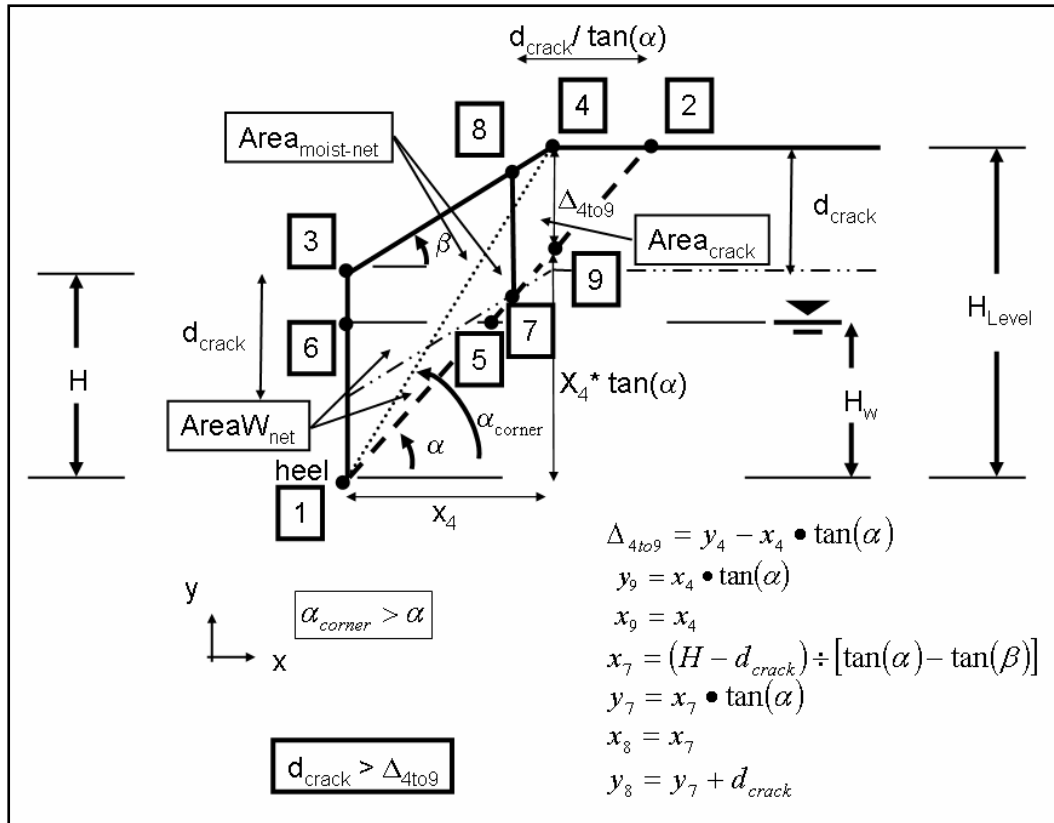


Figure A.11. Area<sub>moist-net</sub>, AreaW<sub>net</sub>, and AreaW<sub>crack</sub> within the soil wedge defined by a bilinear ground surface with  $\alpha_{corner}$  greater than  $\alpha$  and crack depth,  $d_{crack}$  ( $d_{crack} > \Delta_{4to9}$ ).

In the Figures A.9 through A.10 case, the zone of cracking is above the hydrostatic water table. Should the crack zone include a region of cracking below the water table as is the case for Figure A.8 when  $y_7$  is less than  $H_w$ , the total cross-sectional area of the submerged portion of the trial soil wedge (with crack) less the triangular zone of cracking below the water table is equal to AreaW<sub>net</sub> and is given by

$$AreaW_{net} = AreaW - AreaW_{crack} \tag{bis A.40}$$

AreaW<sub>crack</sub> is given by Equation A.39. Consequently, the net moist cross-sectional area of the trial soil wedge above the water table is equal to

$$Area_{moist-net} = Area_{net} - AreaW_{net} \tag{bis A.41}$$

and identified in Figure A.11.

The weight of the net submerged portion of the trial soil wedge,  $W_{\text{saturated}}$ , is

$$W_{\text{saturated}} = \gamma_{\text{saturated}} \bullet \text{Area}W_{\text{net}} \quad \text{bis A.42}$$

with the weight of the net moist portion of the soil wedge

$$W_{\text{moist}} = \gamma_{\text{moist}} \bullet \text{Area}_{\text{moist-net}} \quad \text{bis A.43}$$

The total weight for the net trial soil wedge, considering a depth of crack,  $d_{\text{crack}}$ , is equal to

$$W = W_{\text{saturated}} + W_{\text{moist}} \quad \text{bis A.44}$$

This and the other relationships given in this subsection are also valid in the case of  $d_{\text{crack}}$  equal to zero, i.e., cohesionless soils.

#### A.6.2.2 $d_{\text{crack}} < \Delta_{4\text{to}9}$

Figure A.12 extends the Figure A.9 case to consider a crack within a retained (cohesive) soil and for a crack depth that intersects the planer trial slip plane (extending from points 1 to 2) below the level ground surface region of retained soil (versus below the sloping ground surface retained soil region). This intersection point is designated as point 7 in this figure, corresponding to the case of  $d_{\text{crack}} < \Delta_{4\text{to}9}$ . Point 9 defines the point along the planar trial slip surface (extending from point 1 to point 2) that is below point 4. The case shown in Figure A.10 is for point 7 above the hydrostatic water table. Points 7, 2, and 8 delineate a triangular region of the trial soil wedge that is fully contained within the depth of cracking (i.e.,  $\text{Area}_{\text{crack}}$ ). The portion of the total cross-sectional area (i.e.,  $\text{Area}_{\text{total}}$  by Equation A.45) entirely contained within the depth of cracking zone is given by

$$\text{Area}_{\text{crack}} = \frac{1}{2} \bullet \{x_7 \bullet [y_2 - y_8] + x_2 \bullet [y_8 - y_7] + x_8 \bullet [y_7 - y_2]\} \quad \text{bis A.36}$$

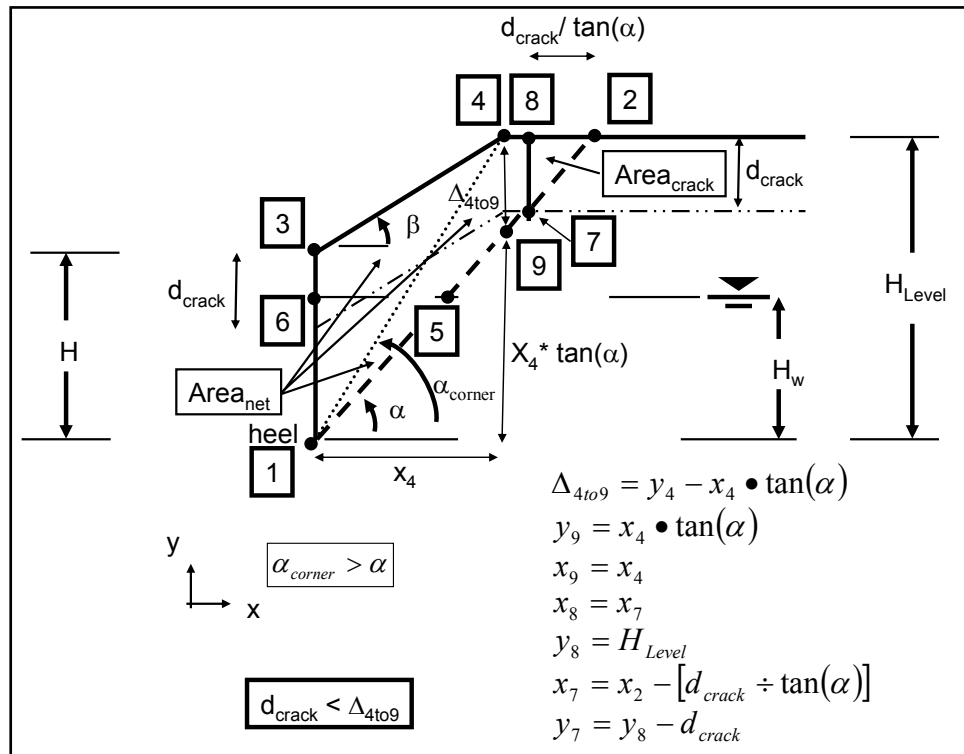


Figure A.12. Soil wedge defined by a bilinear ground surface with  $\alpha_{corner}$  greater than  $\alpha$  and crack depth  $d_{crack}$  that extends below the water table ( $d_{crack} < \Delta_{4to9}$ ).

The total soil wedge area less this triangular zone of cracking ( $Area_{crack}$ ) is designated as the  $Area_{net}$  in Figure A.12 and is computed to be

$$Area_{net} = Area_{total} - Area_{crack} \quad \text{bis A.37}$$

The cross-sectional area of the entire submerged portion of the trial soil wedge, designated  $Area_w$ , is given by Equation A.38. Figure A.13 extends Figure A.12 so as to distinguish the moist net area, designated  $Area_{moist-net}$ , from the submerged net area, designated  $Area_{w-net}$ .

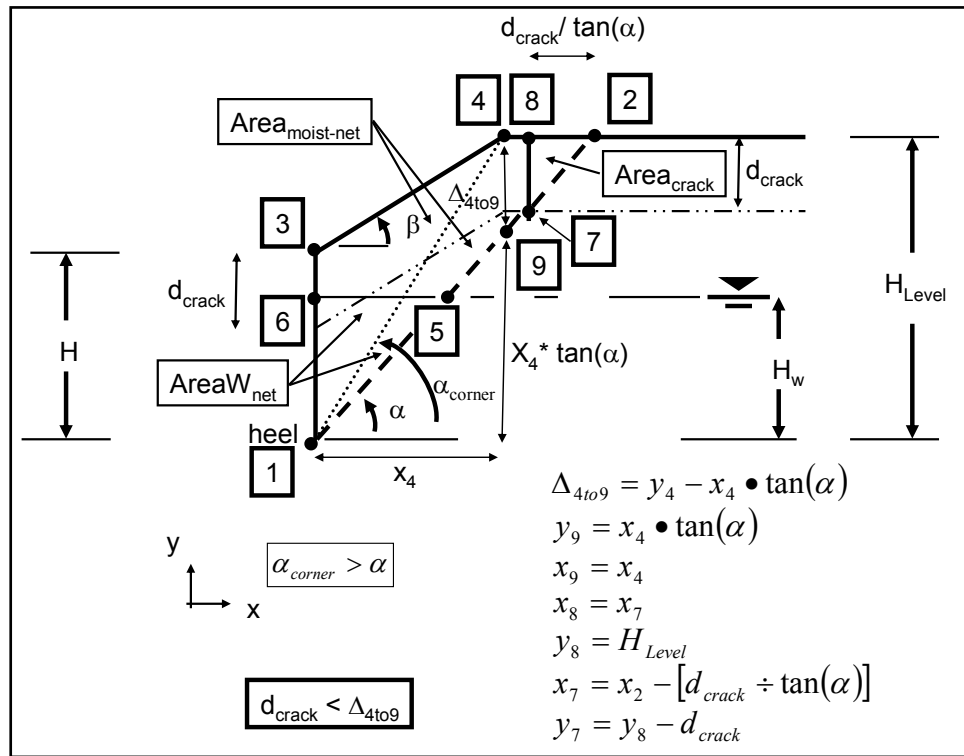


Figure A.13.  $Area_{moist-net}$ ,  $AreaW_{net}$ , and  $AreaW_{crack}$  within the soil wedge defined by a bilinear ground surface with  $\alpha_{corner}$  greater than  $\alpha$  and crack depth,  $d_{crack}$  ( $d_{crack} < \Delta_{4to9}$ ).

In the Figures A.12 and A.13 case, the portion of the soil wedge contained within the zone of cracking (designated  $Area_{crack}$ ) is above the hydrostatic water table. Should this crack zone include a region of cracking below the water table as is the case for Figure A.8 when  $y_7$  is less than  $H_w$ , the total cross-sectional area of the submerged portion of the trial soil wedge (with crack) less the triangular zone of cracking below the water table is equal to  $AreaW_{net}$  and is given by

$$AreaW_{net} = AreaW - AreaW_{crack} \tag{bis A.40}$$

$AreaW_{crack}$  is given by Equation A.39. Consequently, the net moist cross-sectional area of the trial soil wedge above the water table is equal to

$$Area_{moist-net} = Area_{net} - AreaW_{net} \tag{bis A.41}$$

and identified in Figure A.11.

The weight of the net submerged portion of the trial soil wedge,  $W_{\text{saturated}}$ , is

$$W_{\text{saturated}} = \gamma_{\text{saturated}} \bullet \text{Area}W_{\text{net}} \quad \text{bis A.42}$$

with the weight of the net moist portion of the soil wedge

$$W_{\text{moist}} = \gamma_{\text{moist}} \bullet \text{Area}_{\text{moist-net}} \quad \text{bis A.43}$$

The total weight for the net trial soil wedge, considering a depth of crack,  $d_{\text{crack}}$ , is equal to

$$W = W_{\text{saturated}} + W_{\text{moist}} \quad \text{bis A.44}$$

This and the other relationships given in this subsection are also valid in the case of  $d_{\text{crack}}$  equal to zero, i.e., cohesionless soils.

## Appendix B: An Abbreviated Review of Dynamics of a Rigid Body

This appendix provides an abbreviated review of dynamics of a rigid body. The reader is cautioned that the notation used herein is not universally consistent with the notation used in the main body of this report.

### B.1 Dynamic Equilibrium of a Particle under Planar Motion

Newton's second law of motion relates the accelerated motion of a particle to the forces acting on it. It expresses in mathematical form, for a particle of mass  $m$ , the relationship between the displacement of the particle and time,

$$\mathbf{f}_r = m \cdot \mathbf{a} \quad \text{B.1}$$

where  $\mathbf{f}_r$  is the *resultant force* acting on the particle that experiences an acceleration  $\mathbf{a}$  that *has the same direction* as the resultant force  $\mathbf{f}_r$  shown in the Figure B.1 free-body diagram. A free-body diagram of the particle considers it to be free of its surroundings and shows all forces acting on it<sup>1</sup>. The kinetic diagram is also shown in this figure. Kinetics is the analysis of forces which cause the motion of the particle depicted in this figure. Note that the measurements of motion are made from an inertial coordinate system. That is, one that does not rotate and is either fixed or translates with constant velocity. According to rectilinear kinematics (i.e., the study of the geometry of motion without consideration of the forces causing the motion) for a particle, its acceleration,  $\mathbf{a}$ , is equal to its change in velocity with time,  $d\mathbf{v}/dt$ , and its velocity,  $\mathbf{v}$ , is equal to its change in position with time,  $d\mathbf{s}/dt$ , with  $d\mathbf{s}$  the change in a particle's position with time. It is easily shown mathematically that acceleration,  $\mathbf{a}$ , is the second derivative of the position vector with time,  $d^2\mathbf{s}/dt^2$ . Consequently, the equation of motion is a differential equation of second order.

*Interpretation of the equation of motion:* The equation of motion states that the unbalanced force on a rigid body causes it to accelerate.

---

<sup>1</sup> Bold text symbolizes a vector in this appendix.



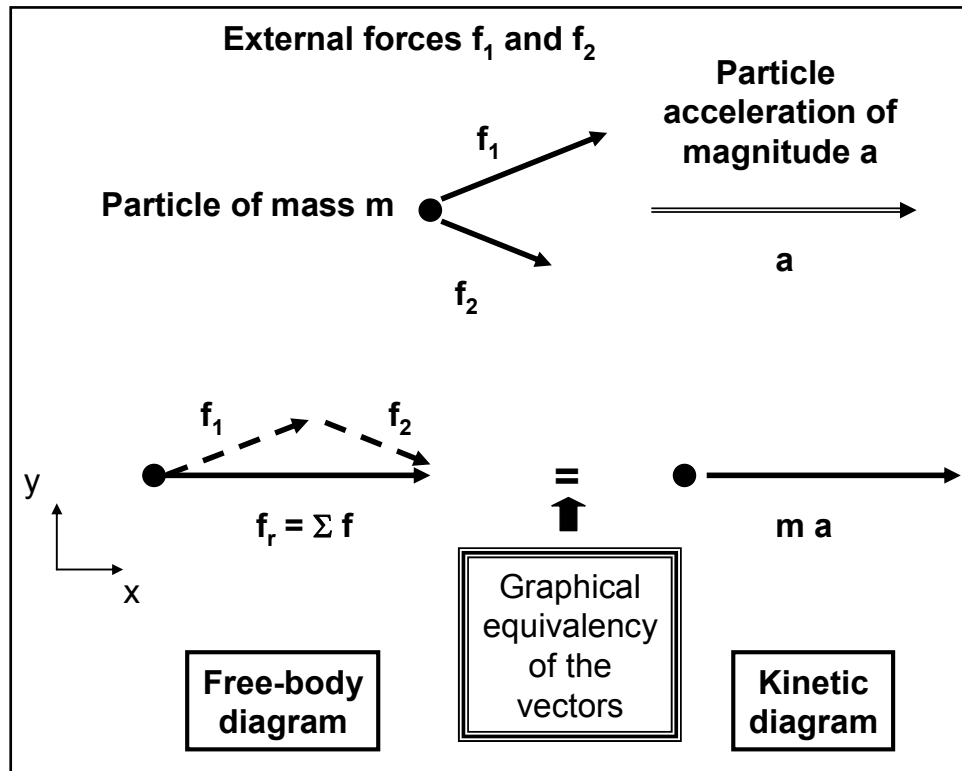


Figure B.1. Free-body and kinetic diagrams of a particle subjected to external forces  $f_1$  and  $f_2$ .

The resultant of the externally applied forces  $f_1$  and  $f_2$ , i.e.,  $f_r (= \Sigma f)$  vectorial sum of all external forces, produces the vector  **$m$  times  $a$**  whose magnitude and direction is represented by the kinetic diagram in Figure B.1. A key concept depicted in this figure is the *graphical equivalency* (in both magnitude and direction) of the resultant force  $f_r$  of the free-body diagram and the vector  **$m a$**  of the kinetic diagram.

***Inertial force vector:*** By rewriting the resultant force vector  $f_r$  as  $\Sigma f$ , and transferring the term  **$m$  times  $a$**  to the left-hand side, the equation of motion of particle mass  $m$  is expressed as

$$\Sigma f - m \bullet a = 0 \quad \text{B.2}$$

where the vector  **$m$  times  $a$**  is referred to as *inertia force vector*. The concept of the inertia force vector acting on the particle is best understood by referring to Figure B.2. If this vector is treated in the same way as the “force vector”  $\Sigma f$  then the state of “equilibrium” created is referred to as dynamic equilibrium. This method for application of the equation of motion is referred to as D’Alembert’s principle. The key concept is that acceleration component *produces an inertia force (i.e., the second term in*

Equation B.2) in the direction opposite to the acceleration component and acts at the center of mass of the particle.

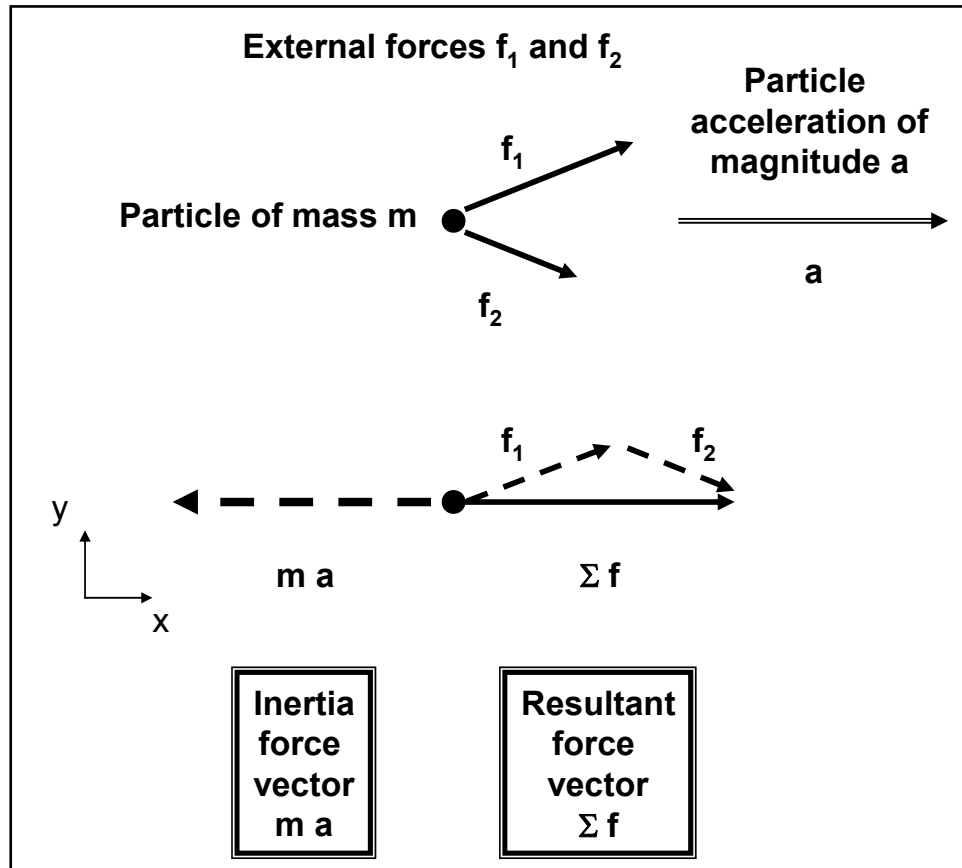


Figure B.2. Inertia force and resultant force vectors for an accelerating particle.

*Interpretation of the inertial force vector:* Recall from elementary mechanics that the inertia of the particle mass is the resistance of the mass to a change in velocity. The change in velocity with respect to time is acceleration. Thus, the inertial mass is considered to be a measure of the particle's resistance to acceleration. By D'Alembert's principle the laws of static equilibrium apply to a dynamic system if the inertia forces, as well as the actual external forces, are considered as forces acting on the system and *the vector sum is zero*. In a sense, the dynamics problem has been reduced to a statics problem at every time  $t$  during the particles motion. The inertial force is sometimes described as a *fictitious force* or as an *imaginary force* in this zero vector sum application of D'Alembert's principle to establishing dynamic equilibrium.

Lastly, the equation of motion of a particle of mass,  $m$ , can also be rewritten in vector form in terms of its components along coordinate axes  $x$  and  $y$ ,

$$\sum f_x - m \cdot a_x = 0 \quad \text{B.3}$$

$$\sum f_y - m \cdot a_y = 0 \quad \text{B.4}$$

where  $\Sigma \mathbf{f}_x$  and  $\Sigma \mathbf{f}_y$  are the resultant force vectors (algebraic sums of the components of all external forces along the respective  $x$ - and  $y$ -axis; positive sense for these forces along the respective positive  $x$ - and  $y$ -axis), and the vectors  $m$  times  $\mathbf{a}_x$  and  $m$  times  $\mathbf{a}_y$  are *inertia force vectors* acting at the center of mass of the particle and in the direction of the respective orthogonal axes. (Note that the resultant force vector  $\mathbf{f}$  is equivalent to the vector sum of  $\Sigma \mathbf{f}_x$  and  $\Sigma \mathbf{f}_y$ .) Each of the acceleration components in the  $x$ - and  $y$ -coordinates *produces an inertia force in the direction opposite to each acceleration component.*

## B.2 Dynamic Equilibrium of a Rigid Mass under Planar Motion

Although Newton's law of motion is directly applicable only to the motion of a single particle of finite mass (but no volume), it is easily extended using elementary mechanics to cover the *translational motion* of rigid bodies that are idealized as a collection of particles that remain at fixed distances with respect to each other. The planar motion of the mass center,  $G$ , of the rigid body is expressed as

$$\mathbf{F}_r = M \cdot \mathbf{a}_G \quad \text{B.5}$$

where  $\mathbf{F}_r$  is the resultant of all external forces acting on the rigid body of mass,  $M$ , and  $\mathbf{a}_G$  is the instantaneous linear acceleration of the mass center of the rigid body relative to an inertial reference frame and in the direction of result force  $\mathbf{F}_r$ . The result force  $\mathbf{F}_r$  is equal to the vector sum of all external forces,  $\Sigma \mathbf{F}$ . The mass center,  $G$ , of the rigid body moves (i.e., translates) as though the rigid body were a single particle subjected to the resultant force  $\mathbf{F}_r$  as exemplified in the Figure B.3 rigid body subjected to the coplanar force vectors  $\mathbf{F}_1$ ,  $\mathbf{F}_2$ , and  $\mathbf{W}$ . The weight of the body,  $W = M \cdot g$ , is included on the free body diagram since it represents an external force acting on the body. Note that all three force vectors are concurrent at mass center point,  $G$ . This equation is satisfied at every time

t during transient (i.e., time-varying) loading of a rigid body. Note that for a rigid body in translation and without rotation, the line of action of the resultant force vector  $\mathbf{F}_r$  passes through the mass center,  $G$ .

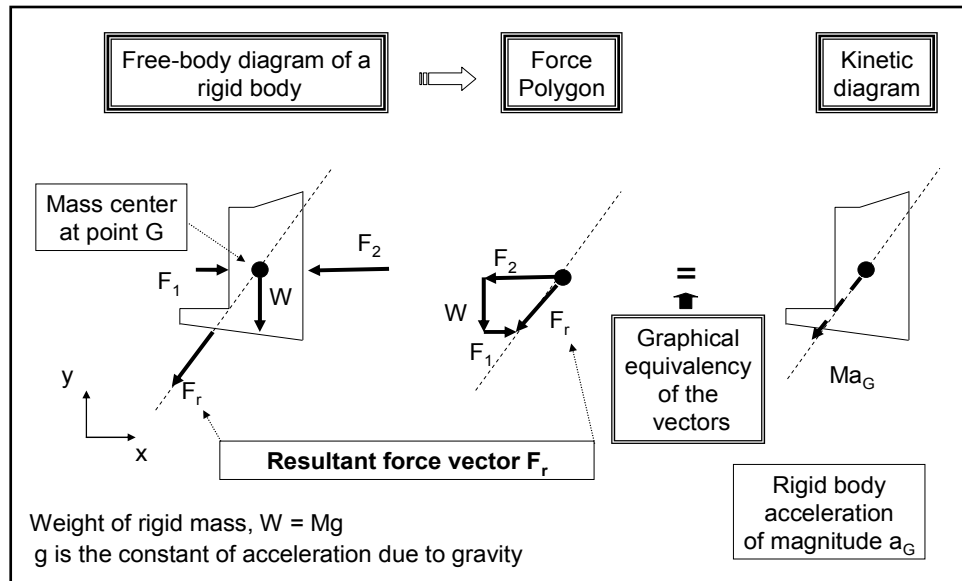


Figure B.3. Free-body and kinetic diagrams of a rigid body subjected to forces  $F_1$ ,  $F_2$ , and  $W$ .

Figure B.3 shows a rigid body with an acceleration of magnitude  $\mathbf{a}_G$ . Assuming that the (Figure B.3) planar rigid body cross section is an idealization of a cross section of a retaining structure, the reaction force vector of the foundation acting on the retaining structure is not included. The exclusion of this force results in a nonzero resultant force vector  $\mathbf{F}_r$  acting on the rigid body, thus the rigid body is in motion by Equation B.5. Inclusion of a foundation-to-retaining structure reaction force  $\mathbf{R}$  (external to the rigid body) as depicted in Figure B.4 results in a rigid body in static equilibrium (i.e. a body at rest with a zero resultant force vector  $\mathbf{F}_r$  acting on the rigid body and a zero  $\mathbf{M}$  times  $\mathbf{a}_G$  vector). Note that the Figure B.4 rigid body is subjected to the coplanar force vectors  $\mathbf{F}_1$ ,  $\mathbf{F}_2$ ,  $\mathbf{W}$ , and  $\mathbf{R}$ , with all four force vectors concurrent at mass center point,  $G$ .

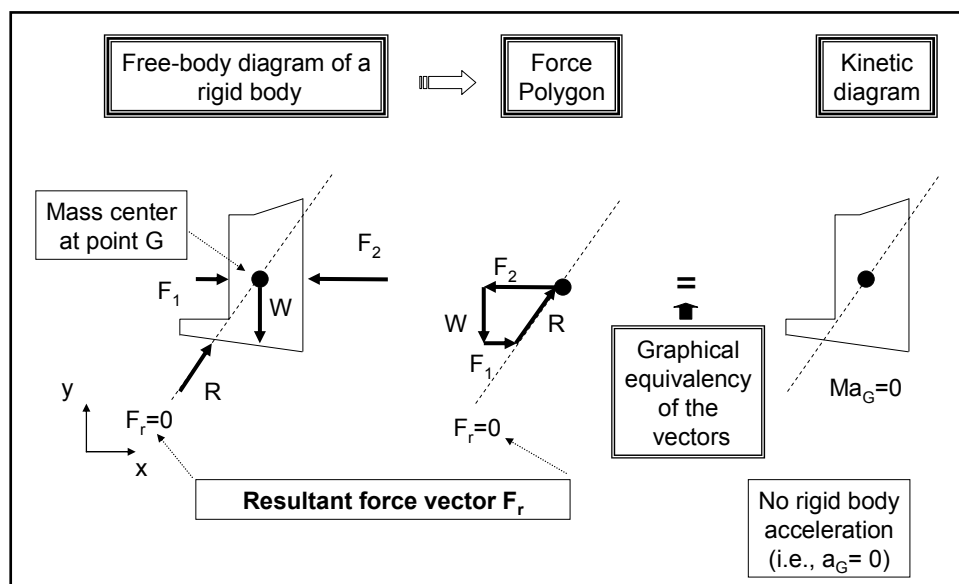


Figure B.4. Free-body and kinetic diagram of a retaining structure subjected to forces  $F_1$ ,  $F_2$ ,  $W$ , and  $R$  that is in static equilibrium.

The equation of motion (Equation B.5) of mass center,  $G$  (e.g., refer to Figure B.3), can also be rewritten in vector form in terms of its components along coordinate axes  $x$  and  $y$ ,

$$\sum F_x - M \cdot (a_G)_x = 0 \quad \text{B.6}$$

$$\sum F_y - M \cdot (a_G)_y = 0 \quad \text{B.7}$$

where the vectors  $M \text{ times } (a_G)_x$  and  $M \text{ times } (a_G)_y$  are referred to as inertia force vectors. If each of these vectors is treated in the same way as the “resultant force vectors,”  $\Sigma F_x$  and  $\Sigma F_y$ , then the state of “equilibrium” created is referred to as dynamic equilibrium. Note that the resultant force vector  $\mathbf{F}_r$  is equivalent to the vector sum of  $\Sigma F_x$  and  $\Sigma F_y$ , the algebraic sums of the components of all external forces along the respective  $x$ - and  $y$ -axis; positive sense for these forces are in the direction along the respective positive  $x$ - and  $y$ -axis shown in this figure. This method for application of the equation of motion is often referred to as D’Alembert’s principle. Each of the acceleration components  $(a_G)_x$  and  $(a_G)_y$  (which are not shown in Figure B.3 but are the components of vector  $\mathbf{a}_G$  along the  $x$ - and  $y$ -axes) produces inertia forces (i.e., the second term in Equations B.3 and B.4) in the direction opposite to these acceleration components that act at the center of gravity of the rigid mass. The inertia force vector  $M \text{ times } \mathbf{a}_G$  for the Figure B.3 rigid body subjected to external force

vectors  $F_1$ ,  $F_2$ , and  $W$  is depicted in Figure B.5. Note this vector acts in the direction opposite to the resultant force vector  $F_r$  (and opposite to acceleration vector  $a_G$ ).

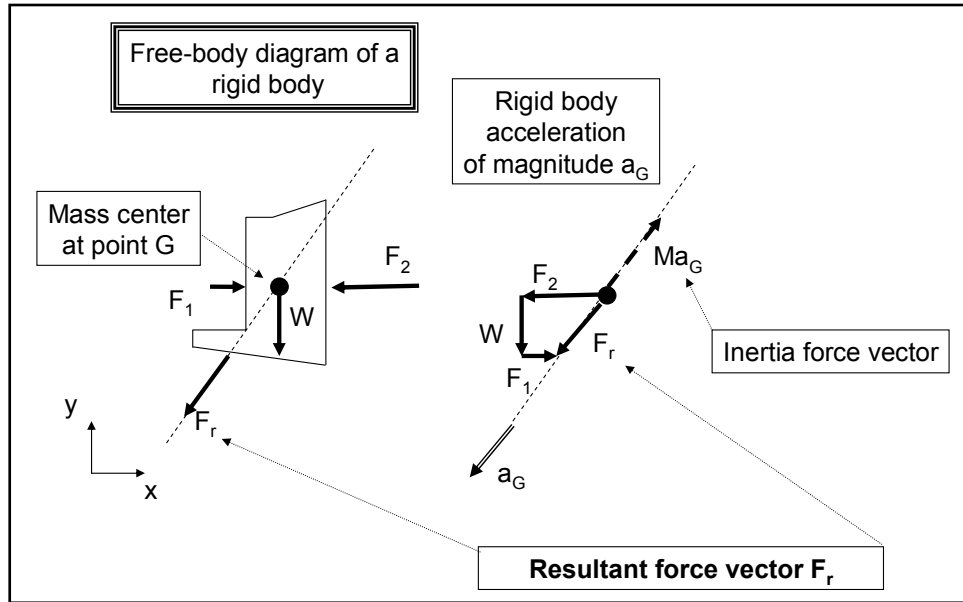


Figure B.5. Inertia force and resultant force vectors for an accelerating rigid body subjected to forces  $F_1$ ,  $F_2$ , and  $W$ .

### B.3 Mass of a Rigid Body

The mass,  $m$ , per unit volume at any point within a body is given by

$$m = \frac{\gamma}{g} \tag{B.8}$$

where at any point within the body  $\gamma$  is the total unit weight per unit volume, and  $g$  is the constant of acceleration due to gravity (equal to 32.174 ft/sec<sup>2</sup>, 386.086 in./sec<sup>2</sup>, 980.665 m/sec<sup>2</sup>, or 980.665 gal).

The total mass,  $M$ , of the planar rigid body is defined as

$$M = \iint_{Area} m \, dx \, dy \tag{B.9}$$

Equivalently, this total mass,  $M$ , is

$$M = \frac{W}{g} \tag{B.10}$$

where  $W$  is the total weight of the entire rigid body.

In order to compute the center of mass of a rigid body, it is often convenient to discretize the rigid body into regular geometrical and/or material regions (e.g., see Figure B.6), each with a constant material unit weight and thus a constant mass per unit volume. The mass for each region  $i$ ,  $\bar{m}_i$ , is

$$\bar{m}_i = \iint_{\text{Area } i} m \, dx \, dy \quad \text{B.11}$$

and for regular geometry, its region mass center (denoted as  $x_i$  and  $y_i$ ) is easily computed.

For a rigid body comprised of regions of different masses, the center of mass (point  $G$ ) of the rigid body is computed by

$$\bar{x} = \frac{\sum \bar{m}_i \cdot x_i}{\sum \bar{m}_i} \quad \text{B.12}$$

and

$$\bar{y} = \frac{\sum \bar{m}_i \cdot y_i}{\sum \bar{m}_i} \quad \text{B.13}$$

where  $\sum \bar{m}_i$  is equal to the sum of masses of each of the discretized regions, which is also the total rigid body mass  $M$ , and  $x_i$  and  $y_i$  are the individual coordinate centers of each mass region  $i$ .

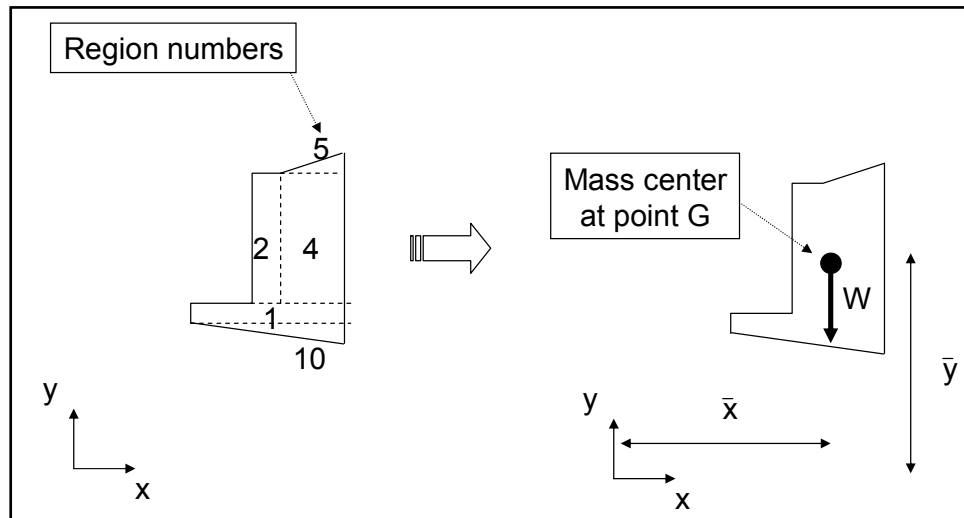


Figure B.6. Example discretization of a rigid body into regular geometrical and material regions.

#### B.4 Equation of Rotational Motion of a Rigid Mass

If a rigid body is acted on by external forces and the resultant force vector does not pass through the mass center of the rigid body, the body may rotate as well as translate. A body subjected to general plane motion undergoes a combination of translation and rotation. In the special case of the translational component of motion along a straight path, then the body travels along a cycloidal path under the combined translational and rotational motions. Considering the rotational component separately, rotation is produced by a moment equal to the resultant force  $\mathbf{F}_r$  about the body's mass center, G, or, equivalently, the sum of moments of each external force about mass center, G. When the rigid body rotates about an axis through mass center, G, perpendicular to the x-y plane (and denoted as the z-axis), any point in the body travels along a circular path. The equation of motion governs the translational aspect of the kinetic problem. The rotational aspects of the kinetic problem are governed by the equation

$$\sum M_G = I_G \cdot \alpha \quad \text{B.14}$$

where  $\sum M_G$  is the sum of moments of all external forces acting on the rigid body with respect to the an axis through mass center, G, perpendicular to the x-y plane (and denoted as the z-axis),  $I_G$  is the mass moment of inertia of the body with respect to an axis through G, and  $\alpha$  is the angular



acceleration.<sup>1</sup> Note that positive sense for moment(s) agrees with the assumed sense of the angular acceleration  $\alpha$ .

The angular acceleration vector  $\alpha$  is positive for counter-clockwise angular acceleration about the z-axis. Similarly, the vector  $\Sigma \mathbf{M}_G$  is defined as being positive for counter-clockwise moments of external forces about the z-axis according to the right-hand rule. Recall that the x, y, and z axes are orthogonal. The vector for a positive resultant moment  $\Sigma \mathbf{M}_G$  points out of the drawing, along the positive z-axis.

Consider the Figure B.7 rigid body subjected to force vectors  $\mathbf{F}_1$ ,  $\mathbf{F}_2$ , and  $\mathbf{W}$ . Note that two of the three coplanar force vectors are not concurrent at mass center point, G, as they were in Figure B.3. The resultant force vector  $\mathbf{F}_R$  is shown in Figure B.7; recall that the resultant force vector  $\mathbf{F}_R$  is the vector sum of the all external forces as shown in the force polygon. Because the resultant force vector is nonzero, the body of mass, M, translates at an acceleration,  $\mathbf{a}_G$ , according to Equation B.5 (or, equivalently, Equations B.6 and B.7). Additionally, because force vectors  $\mathbf{F}_1$  and  $\mathbf{F}_2$  do not act along a line that projects through the center of mass, the rigid body is also subject to a resultant moment vector  $\Sigma \mathbf{M}_G$  (the sum of moments of all forces about mass center point, G), of magnitude

$$\sum M_G = F_1 \cdot h_1 + F_2 \cdot h_2 \quad \text{B.17}$$

where  $h_1$  and  $h_2$  are the perpendicular distances between the lines of action of vectors  $\mathbf{F}_1$  and  $\mathbf{F}_2$ , respectively, and parallel lines that pass through mass center, G, as shown in Figure B.7. The action of the vector  $\Sigma \mathbf{M}_G$  on the rigid body results in the angular rotation of the body. An alternate,

---

<sup>1</sup> For a body undergoing planar motion, the mass moment of inertia  $I_G$  is the integral of the “second moment” about the z-axis and passing through point G of all the elements of mass  $dm$  which compose the body.

$$I_G = \int_m r^2 dm \quad \text{B.15}$$

The “moment arm”  $r$  is the perpendicular distance from the z-axis to the arbitrary element  $dm$ . In planar kinetics, the axis chosen for analysis passes through the body’s mass center, G, and is always perpendicular to the plane of motion. With  $x$  and  $y$  being the distance from  $dm$  to mass center, G, (as measured along the x- and y-axes, respectively) and substituting  $r^2 = (x^2 + y^2)$ , Equation B.15

becomes

$$I_G = \int_m (x^2 + y^2) dm \quad \text{B.16}$$

The mass moment of inertia,  $I_G$ , is a measure of the resistance of a rigid body to the angular acceleration  $\alpha$  in the same manner as mass is a measure of the rigid body’s resistance to the acceleration,  $\mathbf{a}_G$ .

equivalent expression for the resultant moment vector  $\Sigma \mathbf{M}_G$  is given in terms of the resultant force vector  $\mathbf{F}_r$  as

$$\Sigma M_G = F_r \cdot d \quad \text{B.18}$$

where  $d$  is the perpendicular distance between the line of action of vector  $\mathbf{F}_r$  and a parallel line passing through mass center,  $G$ , as shown in Figure B.7. The angular acceleration of the Figure B.7 rigid body about mass center point,  $G$ , is given by Equation B.14. This equation is satisfied at every time  $t$  during transient (i.e., time-varying) loading of a rigid body. The mass center,  $G$ , of the rigid body moves (i.e., translates and rotates) as though the rigid body were a single particle subjected to the resultant force  $\mathbf{F}_r$  acting at lever arm  $d$  from mass center.

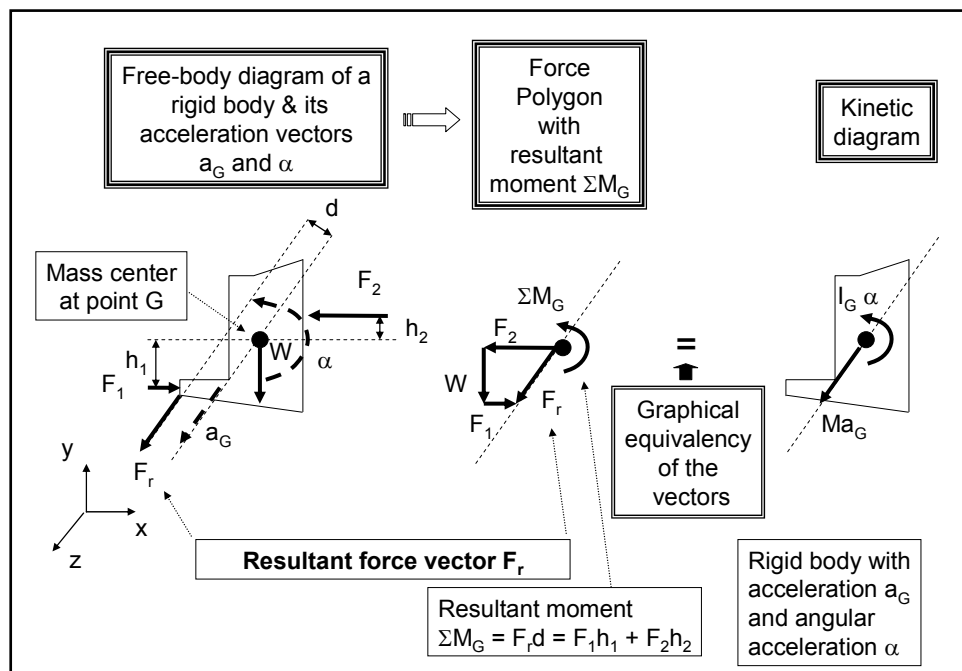


Figure B.7. Free-body and kinetic diagrams of a rigid body subjected to the forces  $F_1$ ,  $F_2$ , and  $W$ .  $F_1$  and  $F_2$  are eccentric to mass center,  $G$ .

According to planar kinematics of a rigid body, its angular acceleration  $\alpha$  is equal to its change in angular velocity with time,  $d\omega/dt$ , and its angular velocity,  $\omega$ , is equal to its change in angular displacement with time,  $d\theta/dt$ , with  $d\theta$  representing the change in angular position with time.<sup>1</sup>

<sup>1</sup> Planar kinematics of a rigid body is the study of the geometry of motion without consideration of the forces causing the motion.

It is easily shown mathematically that angular acceleration,  $\alpha$ , is the second derivative of the angular position with time,  $d^2\theta/dt^2$ .

It is useful to keep in mind that the two vectors  $\mathbf{M}$  times  $\mathbf{a}_G$  and  $\mathbf{I}_G$  times  $\alpha$  are not the same as a force and a moment of a force, respectively. Rather, they are the *result* of external forces acting on the rigid body.

Equation B.14 can also be rewritten in vector form as

$$\sum \mathbf{M}_G - \mathbf{I}_G \cdot \alpha = 0 \quad \text{B.19}$$

where the vector  $\mathbf{I}_G$  times  $\alpha$  is considered as the moment that acts counter to sum of moments of all external forces acting on the rigid body  $\sum \mathbf{M}_G$  about the center of mass,  $G$ , resulting in a vector sum of zero (D'Alembert's principle). The inertia force vector  $\mathbf{M}$  times  $\mathbf{a}_G$  and the inertia vector  $\mathbf{I}_G$  times  $\alpha$  for the Figure B.7 rigid body subjected to external force vectors  $\mathbf{F}_1$ ,  $\mathbf{F}_2$ , and  $\mathbf{W}$  are depicted in Figure B.8. Observe in this figure that these two inertial vectors act in the direction opposite to the resultant force vector,  $\mathbf{F}_r$ , (and opposite to acceleration vector,  $\mathbf{a}_G$ ) and opposite to sum of moments of all external forces about the center of mass,  $G$ ,  $\sum \mathbf{M}_G$ , (and opposite to the angular acceleration vector  $\alpha$ ), respectively.

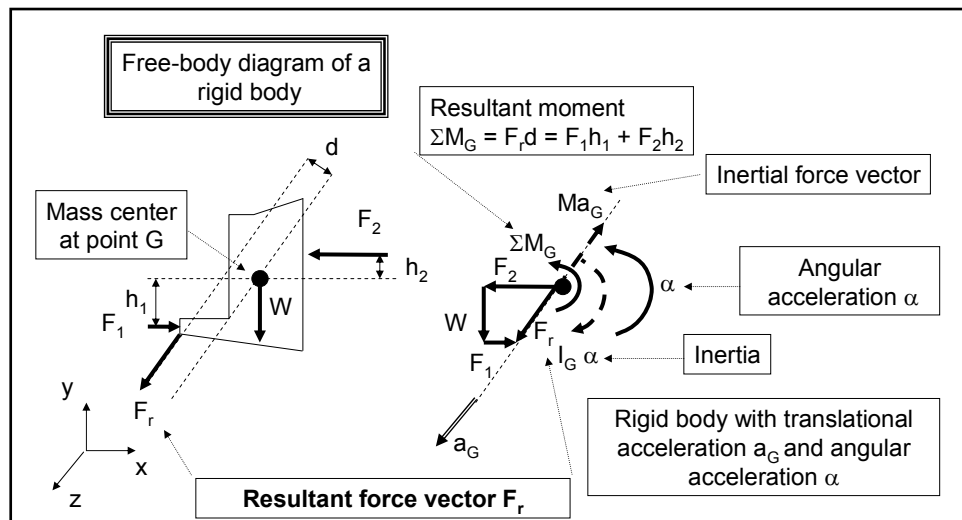


Figure B.8. Inertia force and resultant force vectors for a rigid body subjected to the forces  $F_1$  and  $F_2$ , eccentric to mass center,  $G$ , and subjected to force  $W$ .

## B.5 Equations of Motion: Rotation about a Fixed Axis

Consider the Figure B.7 (or B.8) rigid body of mass center, G, shown in Figure B.9, which is now constrained to rotate in the x-y plane about a fixed axis perpendicular to the page and passing through a pin at point O. The angular velocity,  $\omega$ , and angular acceleration,  $\alpha$ , are caused by the external force and couple moment system acting on the body. Because the body's center of mass, G, moves in a circular path about point O, the acceleration of this point is represented by its tangential and normal components.<sup>1</sup> The tangential component of acceleration has a magnitude

$$a_t = \alpha \bullet r_{G/O} \quad \text{B.26}$$

and must act in a direction which is consistent with the body's angular acceleration,  $\alpha$ . The magnitude of the normal component of acceleration is

$$a_n = \omega^2 \bullet r_{G/O} \quad \text{B.27}$$

This component is always directed from the center of mass point, G, to point O, regardless of the direction of  $\omega$ , as shown in Figure B.10.

---

<sup>1</sup> The tangential velocity  $\mathbf{v}$  vector of mass center, G, along its Figure B.9 circular path about point O is the cross product of  $\omega$  and  $\mathbf{r}_{G/O}$

$$\mathbf{v} = \omega \times \mathbf{r}_{G/O} \quad \text{B.20}$$

Recall that the angular velocity,  $\omega$ , is the time rate of change in angular position and equals  $d\theta/dt$ .

Given that  $a_t = dv/dt$  and  $a_n = v^2/r_{G/O}$ , and with  $v = \omega \bullet r_{G/O}$  and  $\alpha = d\omega/dt$ , the magnitude of tangential acceleration becomes

$$a_t = \alpha \bullet r_{G/O} \quad \text{B.21}$$

and the magnitude of normal acceleration becomes

$$a_n = \omega^2 \bullet r_{G/O} \quad \text{B.22}$$

Like velocity, the acceleration of mass center point, G, may be expressed in terms of vector cross product. Taking the time derivatives of the vector Equation B.20 results in

$$\mathbf{a} = \alpha \times \mathbf{r}_{G/O} + \omega \times (\omega \times \mathbf{r}_{G/O}) \quad \text{B.23}$$

Which is equivalent to

$$\mathbf{a} = \mathbf{a}_t + \mathbf{a}_n \quad \text{B.24}$$

Performing the vector cross products results in the following two acceleration vector components

$$\mathbf{a} = \alpha \times \mathbf{r}_{G/O} - \omega^2 \bullet \mathbf{r} \quad \text{B.25}$$

Note  $\mathbf{a}_n$  is directed from point G towards point O, hence the negative sign. Additionally,  $\mathbf{a}_t$  and  $\mathbf{a}_n$  are perpendicular to one another. Refer to pages 294-295 in Hibbler (2001) for additional details regarding the cross products of the vectors discussed in this footnote and the direction of the resulting vector by the right-hand rule.

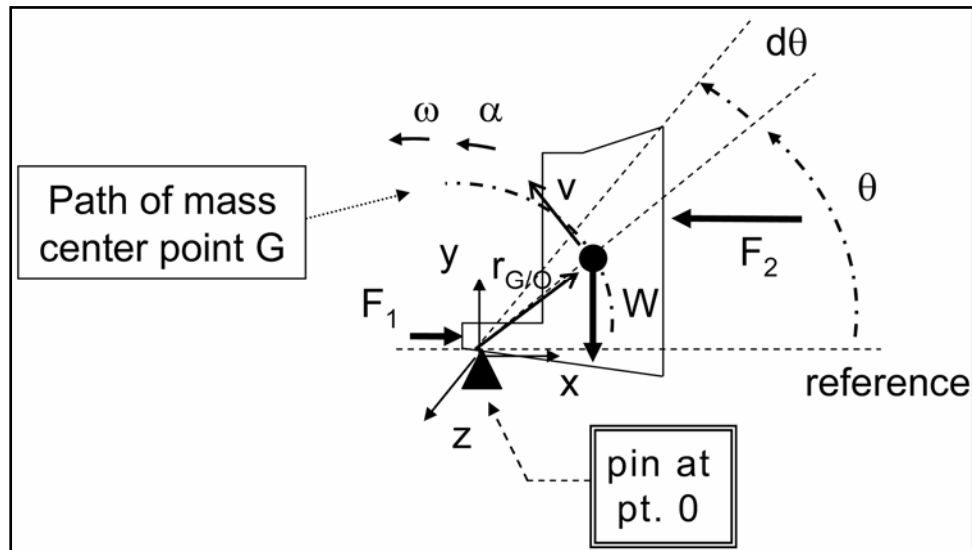


Figure B.9. Free-body diagram of a rigid body subjected to the forces  $F_1$ ,  $F_2$ , and  $W$  which is attached to a pin at point  $O$ . (Pin reaction force at point  $O$  not shown.)

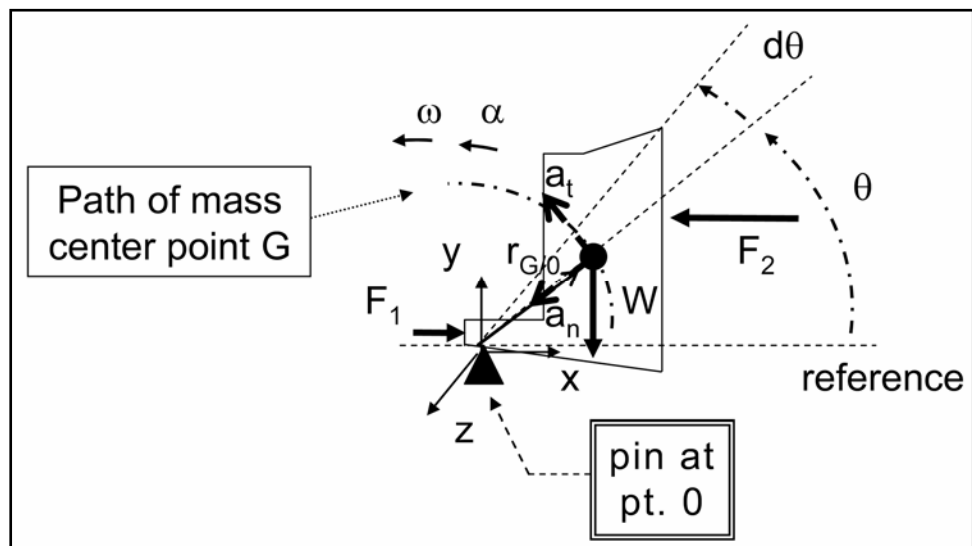


Figure B.10. Tangential and normal acceleration vectors of mass center point,  $G$ , for the free-body diagram of a rigid body subjected to the forces  $F_1$ ,  $F_2$ , and  $W$  which is attached to a pin at point  $O$ . (Pin reaction force at point  $O$  not shown.)

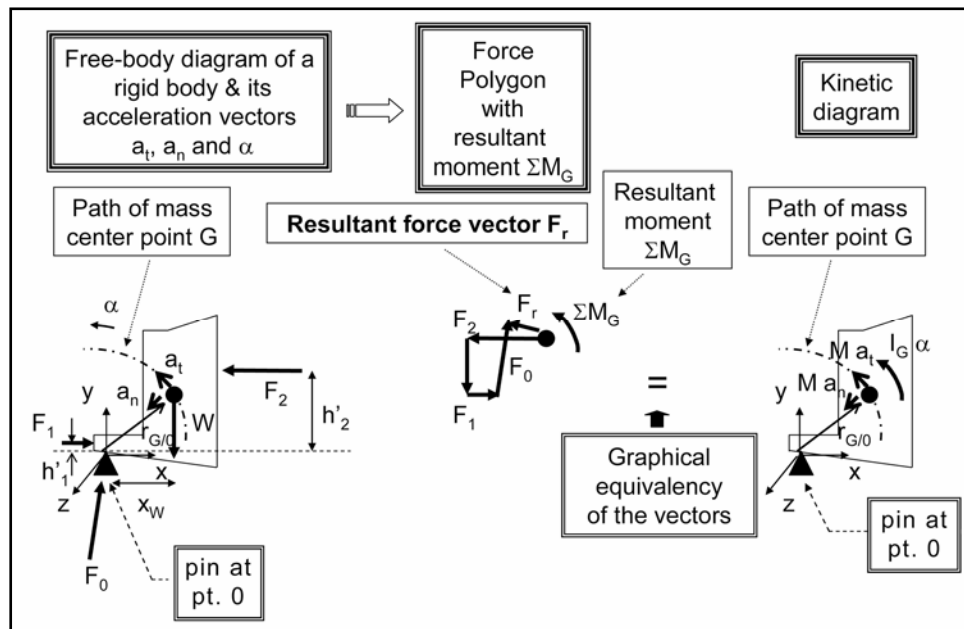
The free-body and kinetic diagrams for the body are shown in Figure B.11. The two components,  $\mathbf{m}$  times  $\mathbf{a}_t$  and  $\mathbf{m}$  times  $\mathbf{a}_n$ , shown on the kinetic diagram, are associated with the tangential and normal acceleration components of the body's mass center,  $G$ . These vectors act in the same direction as the acceleration components of the body's mass center. The  $\mathbf{I}_G$  times  $\boldsymbol{\alpha}$  vector in the kinetic diagram acts in the same direction as  $\boldsymbol{\alpha}$ . The equations of motion which apply to the rigid body are

$$\sum F_n = M \cdot a_n = M \cdot \omega^2 \cdot r_{G/O} \tag{B.28}$$

$$\sum F_t = M \cdot a_t = M \cdot \alpha \cdot r_{G/O} \tag{B.29}$$

$$\sum M_G = I_G \cdot \alpha \tag{B.14 bis}$$

The resultant force vector  $F_r$ , shown in the Figure B.11 force polygon (middle diagram), is the vector resultant of the forces  $F_1$ ,  $F_2$ ,  $W$ , and reaction force  $F_0$  (acting at pin o). The left-hand sides of Equations B.28 and B.29 define the magnitude of the resultant force vector  $F_r$  with its vector components oriented along the normal and tangential axes defined



by the Figure B.11 vectors  $a_n$  and  $r_{G/O}$ , respectively.<sup>1</sup>

Figure B.11. Free-body and kinetic diagrams of a rigid body subjected to the forces  $F_1$ ,  $F_2$ ,  $W$ , and reaction force  $F_0$  acting at pin O. (Resultant vector  $F_r$  not shown in the free-body diagram, the left-hand side diagram.)

In the case of Figure B.11 planar motion about a fixed axis of rotation (i.e., axis z, perpendicular to the x-y plane) that does not pass through mass point, G, Equation B.14 is replaced by

<sup>1</sup> The magnitude of vector  $F_r$  is given by

$$F_r = \sqrt{(\sum F_n)^2 + (\sum F_t)^2}$$

$$\sum M_o = I_o \cdot \alpha \quad \text{B.31}$$

where  $\Sigma \mathbf{M}_O$  (not shown in Figure B.11) is now the sum of moments of all external forces (four forces in the case of Figure B.11;  $\mathbf{F}_1$ ,  $\mathbf{F}_2$ ,  $\mathbf{W}$ , and reaction force  $\mathbf{F}_O$ ) acting on the rigid body with respect to this fixed axis of rotation through point O and  $I_o$  is the mass moment of inertia of the body with respect to point O. The resulting moment  $\Sigma \mathbf{M}_O$  is equal to the moments of forces  $\mathbf{F}_1$ ,  $\mathbf{F}_2$ , and  $\mathbf{W}$  about point O, which are eccentric to the pin. Since reaction force  $\mathbf{F}_O$  acts at pin o, it does not contribute to this resultant moment. Summing moments due to these three forces about pin O, with counterclockwise moments positive, the magnitude of the resultant moment vector  $\Sigma \mathbf{M}_O$  (the sum of moments of all forces about point O) is

$$\sum M_o = -F_1 \cdot h'_1 + F_2 \cdot h'_2 - W \cdot x_w \quad \text{B.32}$$

where  $h'_1$ ,  $h'_2$ , and  $x_w$  are the perpendicular distances between the lines of action of vectors  $\mathbf{F}_1$ ,  $\mathbf{F}_2$ , and  $\mathbf{W}$ , respectively, and parallel lines that pass through pin O, as shown in Figure B.11. The action of the vector  $\Sigma \mathbf{M}_O$  (not shown) acting about pin O on the rigid body results in the angular rotation of the body and is graphically equivalent to the Figure B.11 vector  $\mathbf{I}_G$  **times**  $\alpha$  shown in the kinetic diagram (the right-hand side diagram).

The two mass moments of inertia  $I_G$  and  $I_o$  are related by the parallel axis theorem,

$$I_o = I_G + M \cdot r_{G/O}^2 \quad \text{B.33}$$

where  $M$  is the mass of the rigid body and  $r_{G/O}$  is the perpendicular distance between the parallel z-axes (perpendicular to the x-y plane) passing through points G and O. It is used to transfer the mass moment of inertia,  $I_G$ , from a set of three orthogonal planes passing through the body's mass center, G, to a corresponding set of orthogonal planes passing

through some other point O.<sup>1</sup> For applications, one should remember that “ $I_O\alpha$ ” accounts for the “moment” of both  $M$  times  $a_t$  and  $I_G$  times  $\alpha$  about point O. An alternate, equivalent expression for  $I_O$  is

$$I_O = I_G + M \cdot (x_{O \text{ to } G}^2 + y_{O \text{ to } G}^2) \quad \text{B.37}$$

## B.6 Planar Kinematics of a Rigid Body: Noncentroidal Rotation about a Fixed Axis

Planar kinematics of a rigid body is the study of the geometry of motion without consideration of the forces causing the motion. The rigid body shown in Figure B.9 is an example of a body undergoing noncentroidal rotation. The rigid body’s mass center, G, travels along a circular path of radius  $r_{G/O}$  centered at the point O in this figure, where the axis of rotation intersects the plane of reference.

*Angular displacement:* The change in the angular position of the of the Figure B.9 radius vector from point O to G, which can be measured as a differential  $d\theta$  and is a vector quantity, is called the angular displacement. Since motion is always about a fixed axis (whose origin is point O) the direction of vector  $d\theta$  is always along the axis. Specifically, the direction is determined by the right-hand rule. In Figure B.9 both  $\theta$  and  $d\theta$  are directed counterclockwise. Thus the directional sense of  $\omega$  is outward from the Figure B.9 drawing.

*Angular Velocity:* The angular velocity vector,  $\omega$ , is the time rate of change in angular position

$$\omega = \frac{d\theta}{dt} \quad \text{B.38}$$

<sup>1</sup> Introducing Equation B.33 into the relationship

$$\sum M_o = I_o \cdot \alpha \quad \text{bis B.31}$$

results in

$$\sum M_o = (I_G + M \cdot r_{G/O}^2) \cdot \alpha \quad \text{B.34}$$

Expanding terms, Equation B.32 becomes

$$\sum M_o = I_G \cdot \alpha + M \cdot r_{G/O} \cdot (r_{G/O} \cdot \alpha) \quad \text{B.35}$$

and by introducing Equation B.26, simplifies to

$$\sum M_o = I_G \cdot \alpha + M \cdot r_{G/O} \cdot a_t \quad \text{B.36}$$



and is often measured in radians/sec. Its direction is always along the axis of rotation, i.e., in the same direction as  $d\theta$ . When indicating the angular motion of the Figure B.9 rigid body we *arbitrarily* chose counterclockwise rotations as positive; the directional sense of  $\omega$  is outward from the Figure B.9 drawing.

**Angular Acceleration:** The angular acceleration,  $\alpha$ , measures the time rate of change of the angular velocity

$$\alpha = \frac{d\omega}{dt} \quad \text{B.39}$$

or, equivalently,

$$\alpha = \frac{d^2\theta}{dt^2} \quad \text{B.40}$$

The line of action of  $\alpha$  is the same as that for  $\omega$ . However, its sense of direction depends on whether  $\omega$  is decreasing or increasing. Note that if  $\omega$  is decreasing, then  $\alpha$  is the angular *deceleration* and it has a sense of direction *opposite* to  $\omega$ .

The similarity between the differential relations for angular motion and for rectilinear motion of a particle (i.e.,  $v = ds/dt$ ;  $a = dv/dt$ ) should be apparent.

## B.7 Planar Kinetics of a Rigid Body

A rigid body undergoing general plane motion undergoes a combination of translation and rotation. Returning to the Figure B.7 (discussed in Section B.5), this rigid body of mass  $M$  is subjected to the external forces  $\mathbf{F}_1$ ,  $\mathbf{F}_2$ , and  $\mathbf{W}$  contained in the plane of the rigid body. (Note that no displacement and/or rotational constraints are placed on this body.) The motion of the rigid body is completely defined by the resultant of the external forces and moment of these forces about its mass center,

$$\sum F_x = M \cdot (a_G)_x \quad \text{B.41}$$

$$\sum F_y = M \cdot (a_G)_y \quad \text{B.42}$$

$$\sum M_G = I_G \cdot \alpha \quad \text{bis B.14}$$

Equations B.41 and B.42 describe the magnitude of the x- and y-components of the resultant force  $\mathbf{F}_r$  (refer to Equation B.30) which may also be expressed as

$$F_r = M \cdot a_G \quad \text{bis B.5}$$

where the vectors  $\mathbf{F}_r$  and  $\mathbf{a}_G$  are shown in Figure B.7.

Considering the rotational component separately, rotation is produced by a moment equal to the Figure B.7 resultant force vector  $\mathbf{F}_r$  about the body's mass center, G, or equivalently, the sum of moments of each external force about mass center, G (as discussed in the Section B.4). Note that if the resultant of external forces acting on the Figure B.7 rigid body had passed through the mass center, G, it would be constrained to move in translation with zero angular acceleration. In this case the resultant force  $\mathbf{F}_r$  acting on the Figure B.7 rigid body does not pass through the mass center, resulting in an angular rotation about point G.

Considering the rotational component separately for the Figure B.7 rigid body, rotation is produced by the sum of moments of each external force about the body's mass center, G, resulting in this case with centroidal rotation. However, if the motion of the body is constrained to rotate about a fixed axis which does not pass through its mass center, noncentroidal rotation results. A rigid body subjected to this constraint was discussed in Sections B.5 and B.6 and shown in Figures B.9, B.10, and B.11.

## Appendix C: An Approach for Computing the Dynamic Active Earth Pressure Distribution for a Partially Submerged Retained Soil

This appendix provides an approach for computing the dynamic active earth pressure distribution equivalent to the pseudo-static force  $P_{AE}$  and its corresponding point of application. The computation of the resultant location of  $P_{AE}$  and a corresponding pressure distribution for a granular backfill is discussed in Section C.1 in which Mohr-Coulomb effective stress shear strength parameter  $\phi'$  (with  $c'$  set equal to zero) is used to characterize the shear strength of the retained soil. Wall movements sufficient to fully mobilize the shear strength of the backfill are assumed in the formulation, thus allowing for the use of active earth pressures. A hydrostatic water table is assumed in this formulation. Section C.2 discusses the computation of the resultant location of the static  $P_A$  force component of  $P_{AE}$  and a corresponding pressure distribution for a granular backfill with a non-level backfill surface.

Section C.3 discusses the computation of the resultant location of  $P_{AE}$  and a corresponding pressure distribution for a backfill in which Mohr-Coulomb effective stress shear strength parameter  $\phi'$  and  $c'$  are nonzero. Section C.4 discusses the computation of the resultant location of  $P_{AE}$  and a corresponding pressure distribution for a backfill in which Mohr-Coulomb total stress shear strength parameter  $c$  is set equal to the undrained shear strength,  $S_u$ , and  $\phi$  is set equal to zero.

### C.1 Earth Pressure Distribution for the Dynamic Active Earth Pressure Force, $P_{AE}$ , of a Partially Submerged, Cohesionless, Level Backfill – Effective Stress Analysis with $c'$ Equal to Zero

In Section 3.5 of Chapter 3, an approach to convert the resultant active earth pressure force,  $P_{AE}$  (calculated using the approach outlined in Appendix A), into an equivalent pressure diagram for a wall retaining moist granular backfill was outlined. Key to this approach is the construction and use of *pressure distributions* for each of the two force components of  $P_{AE}$ ,

$$P_{AE} = P_A + \Delta P_{AE}$$

bis 3.23

The procedure was outlined in Figure 3.9 for a *granular, moist backfill with a level ground surface*. This figure demonstrates that the resulting total pressure distribution acting on the structural wedge is the sum of the triangular distribution of static active earth pressures plus the trapezoidal stress distribution consistent with  $\Delta P_{AE}$ . For this moist backfill condition, the static pressures are consistent with  $P_A$  for the  $c'=0$ , moist granular backfill (with no water table), the equivalent resultant force for the static active earth pressure distribution acts at a height of  $H/3$  and the equivalent resultant force for the incremental dynamic earth pressure distribution acts at a height equal to 0.6 times  $H$ . For partially submerged backfills, Equation 3.24 and Ebeling and Morrison (1992) describe an extension of this procedure to the case of a *level, granular backfill with a partially submerged backfill containing a hydrostatic water table*. This procedure is outlined below using a four-step computational process:

**Step 1: Convert the static active earth pressure force,  $P_A$ , into an equivalent active earth pressure diagram**

The active earth pressure coefficient,  $K_A$ , is first computed using the relationship

$$K_A = \frac{P_A}{\int_0^H \sigma'_{vertical} dh} \quad C.1$$

with  $P_A$  computed by the sweep-search method in  $C_{orps}W_{all}Rotate$  (refer to Section A.3) and the denominator equal to the integral of the vertical effective stress (i.e., the effective overburden pressure distribution). For level backfill with a hydrostatic water table of height  $H_w$  above the heel of the wall (and no surcharge), the denominator of Equation C.1 is computed using the simplified relationship

$$\int_0^H \sigma'_{vertical} dh = \left\{ \begin{array}{l} \frac{1}{2} \cdot \gamma_{moist} \cdot (H - H_w)^2 + \gamma_{moist} \cdot [(H - H_w) \cdot H_w] \\ + \frac{1}{2} \cdot (\gamma_{saturated} - \gamma_w) \cdot (H_w)^2 \end{array} \right\} \quad C.2$$

with

- $\gamma_{\text{moist}}$  = moist unit weight of the retained soil (above the water table)  
 $\gamma_{\text{saturated}}$  = saturated unit weight of the retained soil (below the water table)  
 $H$  = height of the imaginary section as measured vertically from the heel of the wall to the horizontal ground surface (and equal to the height of the imaginary section taken at the interface of the driving soil wedge with the structural wedge)  
 $(H-H_w)$  = thickness of the backfill above the hydrostatic water table

Note that the height term  $H_w$  in Equation C.2 is used to denote the thickness of the submerged backfill above the heel of the wall.

The static active earth pressure  $\sigma_A$ , acting at an effective interface friction angle of  $\delta$  to the normal of the vertical imaginary section, is computed at any depth,  $d$ , below the ground surface as

$$\sigma_A = K_A \bullet (\gamma_{\text{moist}} \bullet d) \quad \text{with } d \leq (H - H_w) \quad \text{C.3.a}$$

above the water table, and

$$\sigma_A = K_A \bullet \left\{ \gamma_{\text{moist}} \bullet (H - H_w) + (\gamma_{\text{saturated}} - \gamma_w) \bullet [d - (H - H_w)] \right\} \quad \text{C.3.b}$$

*with*  $d > (H - H_w)$

below the hydrostatic water table, as shown in Figure C.1.

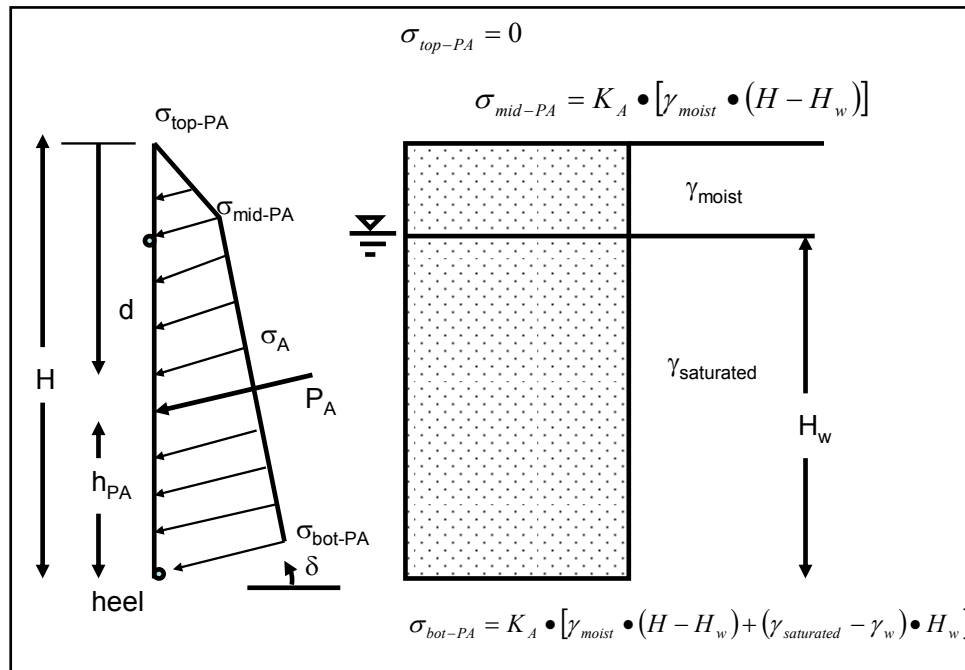


Figure C.1. Static active earth pressure  $\sigma_A$  distribution acting at an effective interface friction angle of  $\delta$  to the normal of the vertical imaginary section through the heel of the wall – effective stress analysis.

The area under the Figure C.1 active earth pressure diagram is equal to  $P_A$ .

The  $h_{PA}$  location of the equivalent resultant force ( $P_A$ ) for the Figure C.1 earth pressure distribution is computed in a two-step process: First, the active earth pressure distribution is converted into an equivalent set of Figure C.2 forces  $F_1$ ,  $F_2$ ,  $F_3$ , and  $F_4$

$$F_1 = \frac{1}{(H - H_w)} \cdot \left[ \frac{\sigma_{top-PA}}{3} + \frac{\sigma_{mid-PA}}{6} \right] \tag{C.4}$$

$$F_2 = \frac{1}{(H - H_w)} \cdot \left[ \frac{\sigma_{top-PA}}{6} + \frac{\sigma_{mid-PA}}{3} \right] \tag{C.5}$$

$$F_3 = \frac{1}{H_w} \cdot \left[ \frac{\sigma_{mid-PA}}{3} + \frac{\sigma_{bot-PA}}{6} \right] \tag{C.6}$$

$$F_4 = \frac{1}{H_w} \cdot \left[ \frac{\sigma_{mid-PA}}{6} + \frac{\sigma_{bot-PA}}{3} \right] \tag{C.7}$$

Secondly, from the moment equilibrium relationship for the horizontal components of the four forces about the heel,

$$\left\{ \sum_{i=1}^4 F_i \right\} \bullet \cos(\delta) \bullet h_{PA} = \{ F_1 \bullet H + (F_2 + F_3) \bullet H_w + F_4 \bullet 0 \} \bullet \cos(\delta) \quad \text{C.8}$$

the  $h_{PA}$  location of the equivalent resultant active earth pressure force  $P_A$  is computed using

$$h_{PA} = \frac{F_1 \bullet H + (F_2 + F_3) \bullet (H - H_w) + F_4 \bullet 0}{\sum_{i=1}^4 F_i} \quad \text{C.9}$$

Note that

$$\sum_{i=1}^4 F_i = P_A \quad \text{C.10}$$

with  $P_A$  being the value computed by the sweep-search trial wedge solution discussed in Section A.3.

Observe in Figure C.2 that the location of the resultant force  $P_A$  for a level, granular ( $c'=0$ ) backfill with a partially submerged backfill containing a hydrostatic water table is above the  $H/3$  height for a moist backfill (with no water table).

### **Step 2: Create an incremental dynamic force component pressure diagram**

The incremental dynamic force component  $\Delta P_{AE}$  is next converted into an equivalent earth pressure diagram. Using the relationship

$$\Delta P_{AE} = P_{AE} - P_A \quad \text{C.11}$$

and with values for  $P_{AE}$  and  $P_A$  provided by the dynamic and static sweep-search solutions made by  $C_{ORPS}W_{all}Rotate$  using the procedures outlined in Appendix A. The Ebeling and Morrison (1992) simplified procedure assumes a trapezoidal distribution for the corresponding incremental stress distribution, acting at an effective interface friction angle of  $\delta$  to the normal of the vertical imaginary section, as shown in Figure C.3. The

resulting force corresponding to the area under the pressure distribution is equal to  $\Delta P_{AE}$  and acts at a height to 0.6 times H.

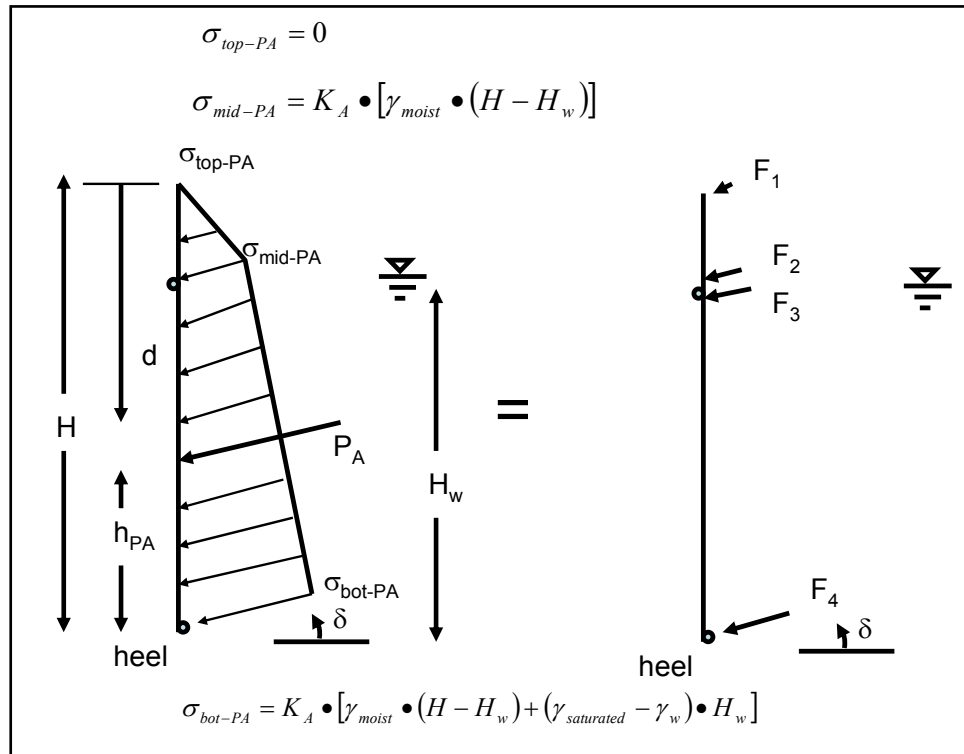


Figure C.2. The static active earth pressure distribution and its equivalent set of forces – effective stress analysis.

**Step 3: Create the dynamic active earth pressure diagram**

The dynamic active earth pressure diagram is created by adding the earth pressure diagrams created in steps 1 and 2. The resulting force corresponds to the area under the combined pressure distribution and is equal to  $P_{AE}$  (recall  $P_{AE} = P_A + \Delta P_{AE}$ ). Its point of application above the heel of the wall is given by

$$h_{PAE} = \frac{P_A \cdot (h_{PA}) + \Delta P_{AE} \cdot (0.6 \cdot H)}{P_{AE}} \tag{C.12}$$

**Step 4: Complete the pressure diagram by adding in the pore water pressure distribution.**

In this effective stress analysis, pore water pressures will be added to the Figure C1  $P_A$  and Figure C3  $\Delta P_{AE}$  component earth pressure distributions in order to obtain a total diagram of pressures acting on the structural



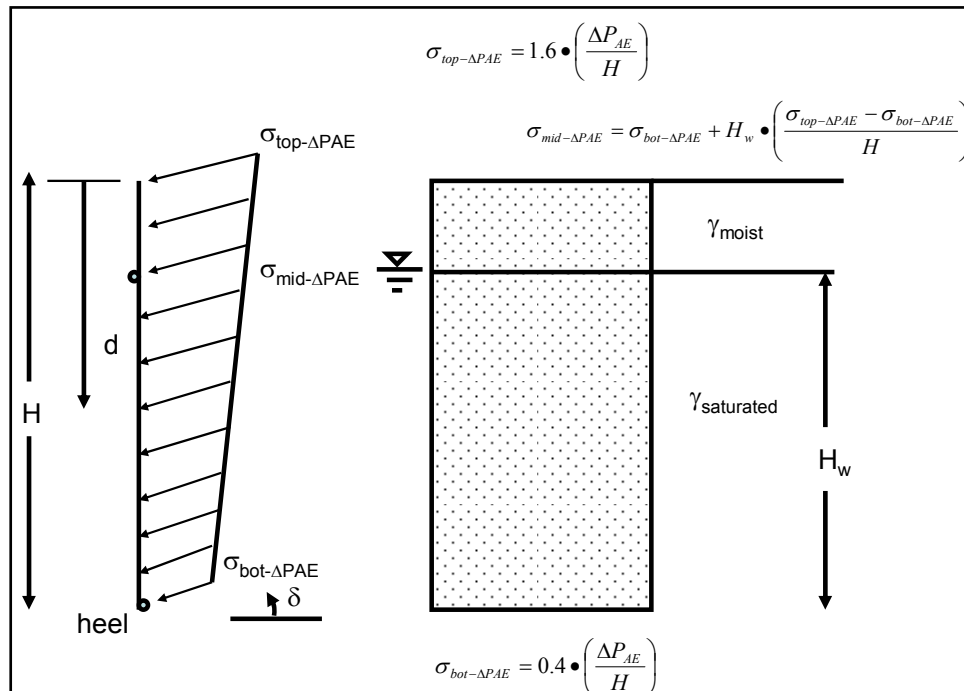


Figure C.3. The dynamic earth pressure distribution corresponding to the incremental dynamic force component  $\Delta P_{AE}$ , acting at an effective interface friction angle of  $\delta$  to the normal of the vertical imaginary section through the heel of the wall (after Ebeling and Morrison (1992)).

wedge (and not to be confused with a total stress analysis). Pore water pressures act normal to the imaginary vertical section through the heel of the wall in this effective stress characterization of earth pressures acting on the structural wedge. For a hydrostatic water table, the pore water pressure at depth,  $d$ , below the ground surface is given by

$$u = 0 \quad \text{with} \quad d \leq (H - H_w) \tag{C.13.a}$$

above the water table, and

$$u = \gamma_w \cdot [d - (H - H_w)] \quad \text{with} \quad d > (H - H_w) \tag{C.13.b}$$

below the hydrostatic water table, as shown in Figure C.5.

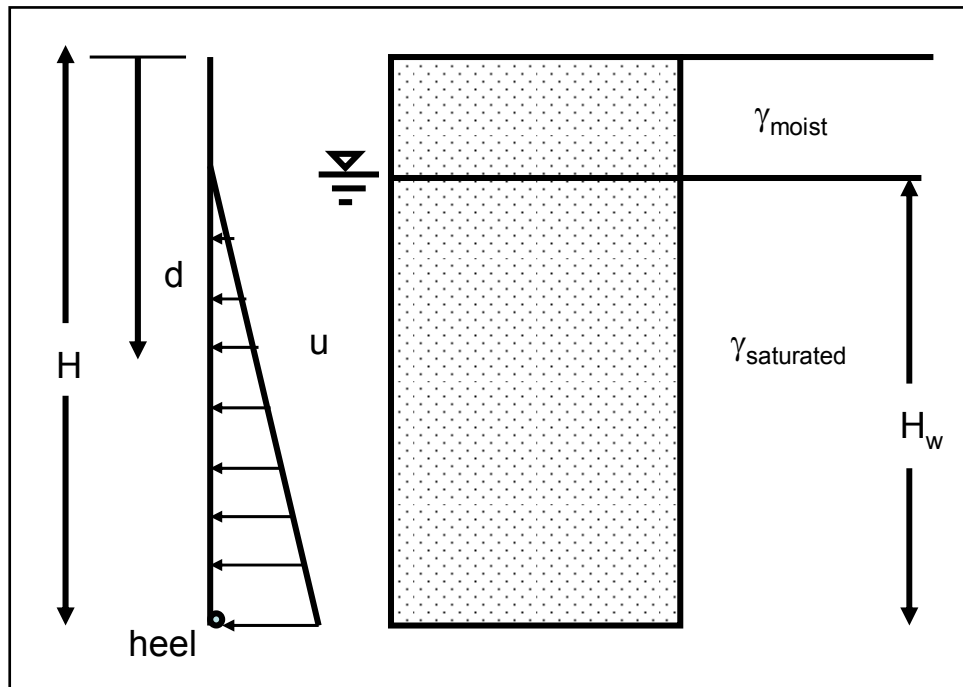


Figure C.5. Hydrostatic pore water pressure distribution acting normal of the vertical imaginary section through the heel of the wall.

Thus, a total diagram of pressures acting on the structural wedge consists of the Figure C1  $P_A$  distribution, plus the Figure C3  $\Delta P_{AE}$  distribution, plus the Figure C.5 pore water pressure distribution.

## C.2 Earth Pressure Distribution for the Static Active Earth Pressure Force, $P_A$ , component of $P_{AE}$ of a Cohesionless, Backfill with a Sloping or a Bilinear Ground Surface – Effective Stress Analysis with $c'$ Equal to Zero

The previous section describes an approach to convert the resultant active earth pressure force,  $P_{AE}$ , (calculated using the approach outlined in Appendix A) into an equivalent pressure diagram for a wall retaining moist granular backfill with  $c'$  equal to zero. This procedure starts with the computation of an equivalent static active earth pressure force  $P_A$  and an equivalent active earth pressure diagram for a *level* backfill ground surface. This section expands on the Section C.1 procedure for determining the distribution and resultant location of  $P_A$  for a sloping and a bilinear ground surface backfill following a procedure outlined in ETL 1110-2-322.

### **C.2.1 The Basic Procedure to Compute the Active Effective Stress Distribution Corresponding to $P_A$ for a Moist Retained Soil with a Sloping Ground Surface**

The procedure to calculate the active earth pressure distribution for resultant static force  $P_A$  due to the geometry of the backfill is outlined using the information contained within Figure C.6 for a moist, granular frictional ( $\phi' > 0$  and  $c' = 0$ ) retained soil with a constant slope for the ground surface. The sweep-search wedge procedure described in Section A.3 is used to first compute the value for  $P_A$  as well as the orientation of the planar slip surface,  $\alpha_A$ , for the critical soil wedge that originates at point 1. The equation to compute the active earth pressure (designated as  $\sigma_A$ ) at key points is given in this figure and is equal to the active earth pressure coefficient,  $K_A$ , times the vertical effective stress at depth  $z$  in the moist retained soil. The key feature for this formulation is that at a given point along the vertical imaginary section through the heel of the structural wedge (and labeled in this figure), the effective vertical stress (designated as  $\sigma_{v-z}$  in the brackets) is computed *using a depth*  $z$ , the depth below the ground surface as shown in this figure. A computation of  $\sigma_{v-z}$  and, subsequently,  $\sigma_A$  are made in this figure for point 1 (at the heel). Note that depth  $z$ , designated as  $z_1$  for point 1, is determined by extending the critical, planar slip plane from point 1 until it intersects the ground surface. This same procedure is followed to compute a different value for  $z$ ,  $\sigma_{v-z}$  and for  $\sigma_A$  at any other point of interest along the imaginary vertical section of height  $H$ . To determine the value for the active earth pressure coefficient,  $K_A$ , the value for the force  $P_A$  from the sweep-search method of analysis is divided by the integral of the  $\sigma_{v-z}$  distribution along the imaginary vertical section of height  $H$  (refer to the  $K_A$  equation given in this figure). For the case of a moist granular retained soil with a constant surface slope, the equation for  $\sigma_{v-z}$  and  $\sigma_A$  at key points and for  $K_A$  are straight-forward and given in this figure.

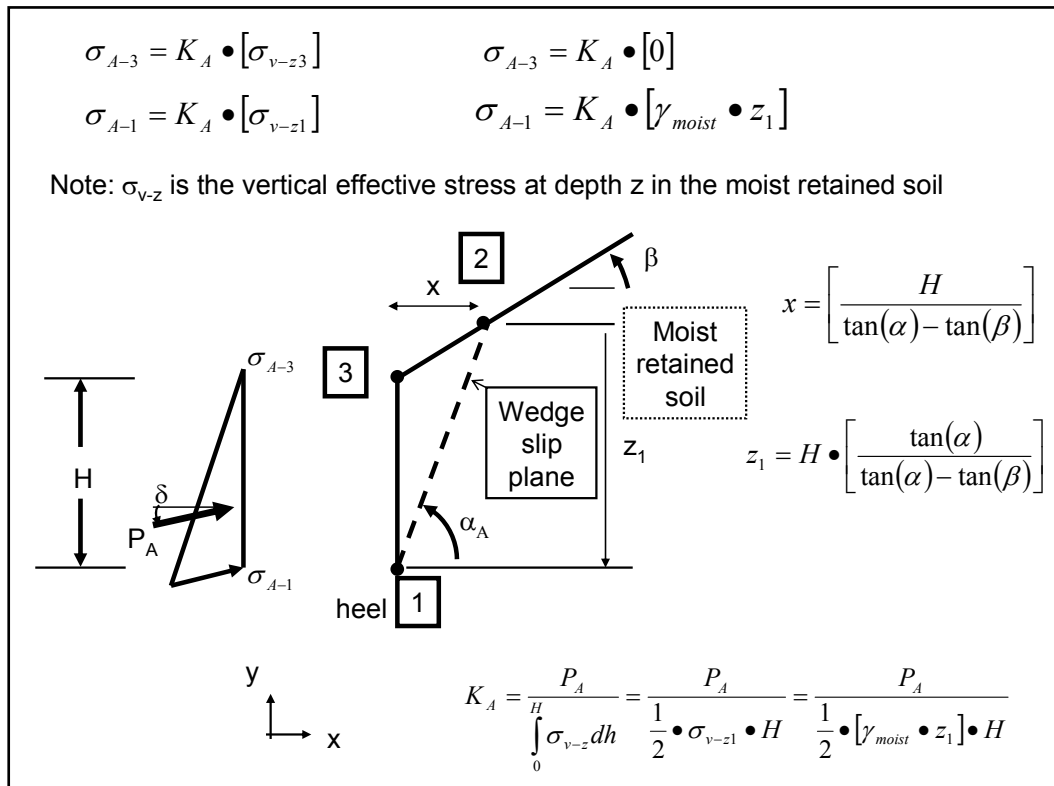


Figure C.6. The active earth pressure distribution corresponding to the incremental static force component  $P_A$ , acting at an effective interface friction angle of  $\delta$  to the normal of the vertical imaginary section through the heel of the wall – moist retained soil with  $\phi' > 0$  and  $c' = 0$ .

The procedure outlined in Step 1 in Section C.1 that converts the  $\sigma_A$  distribution into equivalent forces (see Figure C.2) is used to compute the resultant location  $h_{PA}$  of  $P_A$  for use in Equation C.12 for the resultant location  $h_{PAE}$  of  $P_{AE}$ . The procedure outlined in Step 2 and Step 3 in Section C.1 are used to compute the incremental dynamic force component  $\Delta P_{AE}$  and its corresponding equivalent earth pressure diagram.

**C.2.2 The Basic Procedure to Compute the Active Effective Stress Distribution Corresponding to  $P_A$  for a Partially Submerged Retained Soil with a Sloping Ground Surface**

This section expands upon the procedure outlined in Section C.2.1 by including the case of a partially submerged granular backfill (with a hydrostatic water table). The procedure to calculate the active earth pressure distribution for resultant static force  $P_A$  due to the geometry of the backfill is outlined using the information contained within Figure C.7 for a granular frictional ( $\phi' > 0$  and  $c' = 0$ ) retained soil with the critical planar wedge slip plane that passes through point 1 (with  $\alpha_A > \alpha_{corner}$ ) and

*intersects the sloping portion of the ground surface.* The sweep-search wedge procedure described in Section A.3 is used to first compute the value for  $P_A$  as well as the orientation of the planar slip surface,  $\alpha_A$ , for the critical soil wedge that originates at point 1. The equation to compute the active earth pressure (designated as  $\sigma_A$ ) at the key points identified in this figure as 1, 6, and 3, is equal to the active earth pressure coefficient,  $K_A$ , times the vertical effective stress at depth  $z$  in the retained soil. The key feature for this formulation is that at a given point along the vertical imaginary section through the heel of the structural wedge (identified in this figure as points 1, 6, and 3), the effective vertical stress (designated as  $\sigma'_{v-z}$  in the brackets) is computed using a depth  $z$ , the depth below the ground surface as shown in this figure. A computation of  $\sigma'_{v-z}$  and, subsequently,  $\sigma_A$  are made in this figure for point 1 (at the heel). Note that depth  $z$ , designated as  $z_1$  for point 1, is determined by extending the critical, planar slip plane from point 1 until it intersects the ground surface (at point 2). This same procedure is followed to compute the value for  $z$ ,  $\sigma'_{v-z}$ , and  $\sigma_A$  at the other key point 6 (and point 3) along the imaginary vertical section of height  $H$ . A plane oriented at  $\alpha_A$  from horizontal is projected from the point of interest, e.g., point 6, up through the retained soil until it intersects the sloping ground surface.  $\sigma'_{v-z6}$  is computed using the resulting vertical height  $z_6$  of this planar surface, as shown in this figure. Moist unit weights above the water table and buoyant unit weights below the water table (assuming a hydrostatic water table in the retained soil) are used to compute the vertical effective stress  $\sigma'_{v-z}$ . To determine the value for the active earth pressure coefficient,  $K_A$ , the value for the force  $P_A$  from the sweep-search method of analysis is divided by the integral of the  $\sigma'_{v-z}$  distribution along the imaginary vertical section of height  $H$  (refer to the equation given in this figure). [ $\sigma'_{v-z}$  is contained within the brackets of the  $\sigma_A$  relationships in this figure.] For the case of a granular retained soil with a constant surface slope, the equation for  $\sigma'_{v-z}$  and  $\sigma_A$  at key points and for  $K_A$  are straight-forward and given in this figure.

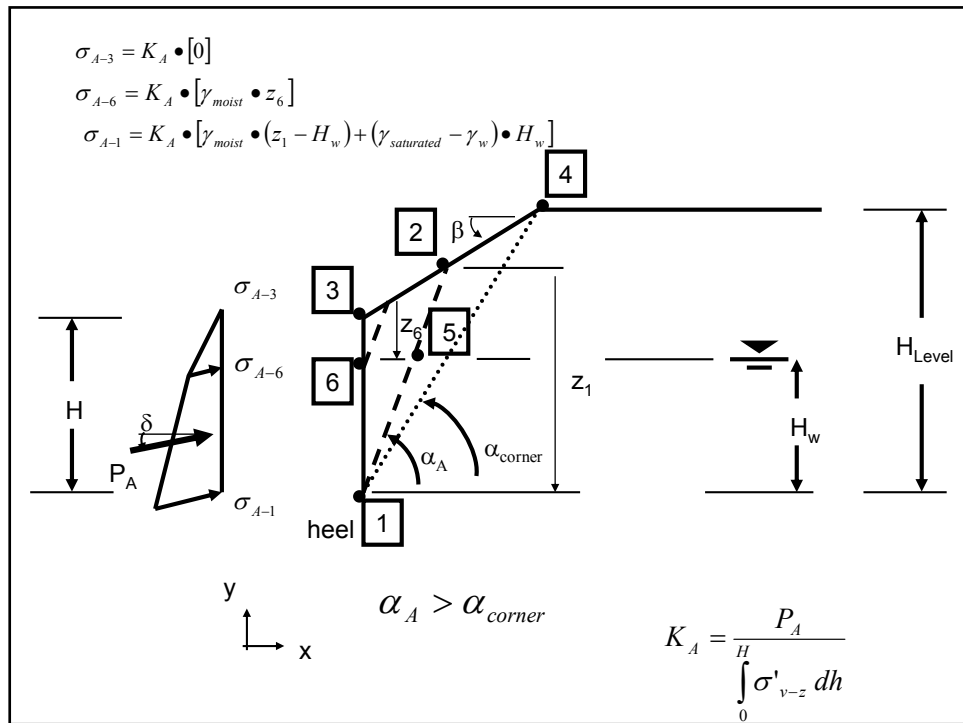


Figure C.7. The active earth pressure distribution corresponding to the incremental static force component  $P_A$ , acting at an effective interface friction angle of  $\delta$  to the normal of the vertical imaginary section through the heel of the wall – partially submerged backfill with  $\phi' > 0$  and  $c' = 0$ .

The procedure outlined in Step 1 in Section C.1 that converts the  $\sigma_A$  distribution into equivalent forces (as generalized in Figure C.8) is used to compute the resultant location  $h_{PA}$  of  $P_A$  for use in Equation C.12 for the resultant location  $h_{PAE}$  of  $P_{AE}$ . The procedures outlined in Step 2 and Step 3 in Section C.1 are used to compute the incremental dynamic force component,  $\Delta P_{AE}$ , and its corresponding equivalent earth pressure diagram.

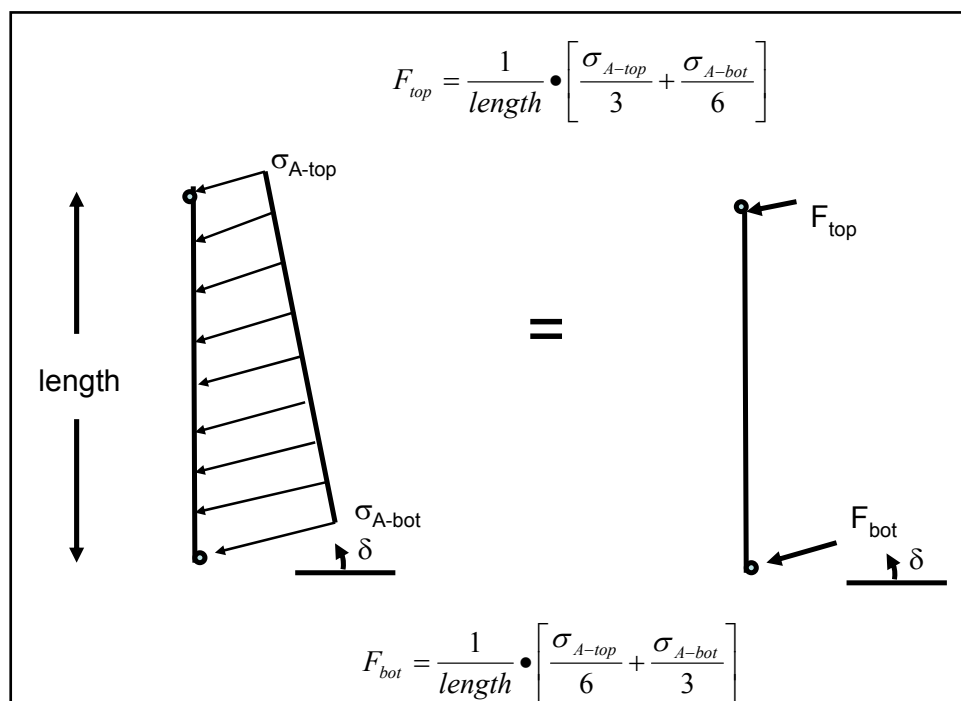


Figure C.8. Conversion of a linear stress distribution into an equivalent set of forces.

### C.2.3 The Basic Procedure to Compute the Active Effective Stress Distribution Corresponding to $P_A$ for a Partially Submerged Retained Soil with a Bilinear Ground Surface

This section expands upon the procedure outlined in Section C.2.2 in the case of a partially submerged granular backfill. The procedure to calculate the active earth pressure distribution for resultant static force  $P_A$  due to the geometry of the backfill is outlined using the information contained within Figure C.9 for a granular, frictional ( $\phi' > 0$  and  $c' = 0$ ) retained soil for which the critical planar wedge slip plane that passes through point 1 (with  $\alpha_{corner} > \alpha_A$ ) and *intersects the horizontal portion of the bilinear ground surface*. The sweep-search wedge procedure described in Section A.3 is used to first compute the value for  $P_A$  as well as the orientation of the planar slip surface,  $\alpha_A$ , for the critical soil wedge that originates at point 1. The equation to compute the active earth pressures (designated as  $\sigma_A$ ) at the Figure C.9 key points 1, 12, 6, and 3 is equal to the active earth pressure coefficient,  $K_A$ , times the vertical effective stress at depth  $z$  in the moist retained soil. The key feature for this formulation is that at a given point along the vertical imaginary section through the heel of the structural wedge (identified in this figure as points 1, 12, 6, and 3), the effective vertical stress (designated as  $\sigma'_{v-z}$  in the brackets) is computed using a depth  $z$ , the depth below the ground surface as shown in this

figure. A computation of  $\sigma'_{v-z}$  and, subsequently,  $\sigma_A$  are made in this figure for point 1 (at the heel). Note that depth  $z$ , designated as  $z_1$  for point 1, is determined by extending the critical, planar slip plane from point 1 until it intersects the *horizontal* ground surface. This same procedure is followed to compute the value for  $z$ ,  $\sigma'_{v-z}$ , and  $\sigma_A$  at the other key points 12, 6, and 3 along the imaginary vertical section of height  $H$ . A plane oriented at  $\alpha_A$  from horizontal is projected from the point of interest (e.g., point 6) up through the retained soil until it intersects the *sloping* ground surface.  $\sigma'_{v-z_6}$  is computed using the resulting vertical height  $z_6$  of this planar surface, as shown in this figure. The computations outlined in Figure C.9 differ from the Figure C.7 computations because the deepest soil wedge slip plane (originating at point 1) intersects the horizontal rather than the sloping portion of the ground surface. Thus an additional key point 12 is needed to define the  $\sigma_A$  distribution. Moist unit weights above the water table and buoyant unit weights below the water table (assuming a hydrostatic water table in the retained soil) are used to compute the vertical effective stress  $\sigma'_{v-z}$ . To determine the value for the active earth pressure coefficient,  $K_A$ , the value for the force  $P_A$  from the sweep-search method of analysis is divided by the integral of the  $\sigma'_{v-z}$  distribution along the imaginary vertical section of height  $H$  (refer to the equation given in this figure). [ $\sigma'_{v-z}$  is contained within the brackets of the  $\sigma_A$  relationships given in this figure.] For the case of a granular retained soil with a bilinear ground surface, the equation for  $\sigma'_{v-z}$  and  $\sigma_A$  at key points and for  $K_A$  are straight-forward and given in this figure.



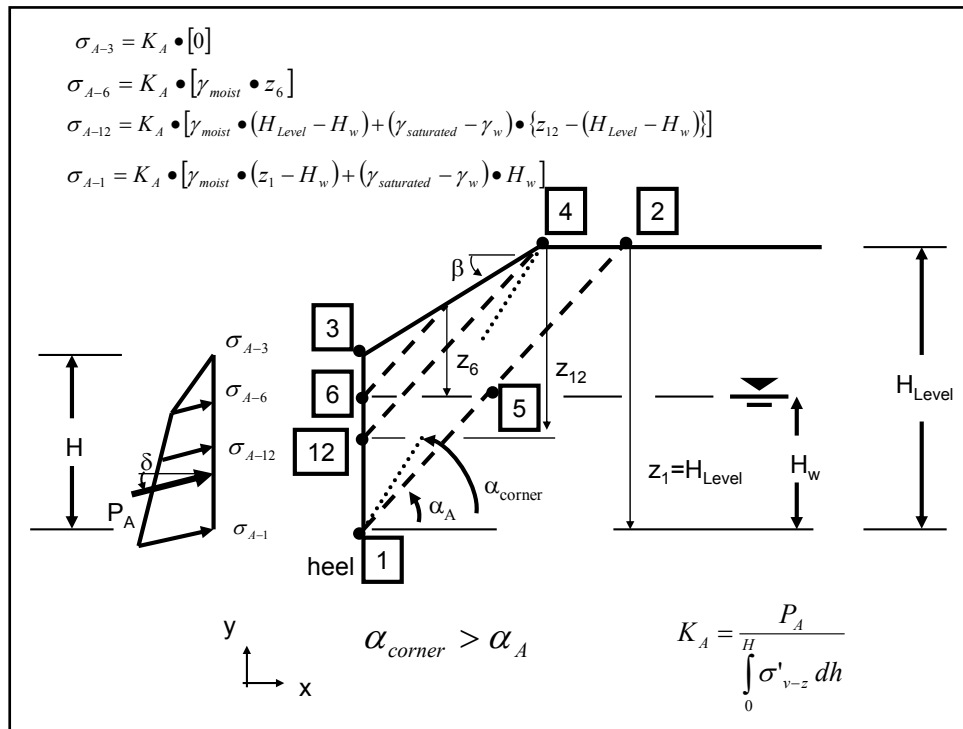


Figure C.9. The active earth pressure distribution corresponding to the incremental static force component  $P_A$ , acting at an effective interface friction angle of  $\delta$  to the normal of the vertical imaginary section through the heel of the wall for a bilinear ground surface – partially submerged backfill with  $\phi' > 0$  and  $c' = 0$ .

The procedure outlined in Step 1 in Section C.1 that converts the  $\sigma_A$  distribution into equivalent forces (see Figure C.8) is used to compute the resultant location  $h_{PA}$  of  $P_A$  for use in Equation C.12 for the resultant location  $h_{PAE}$  of  $P_{AE}$ . The procedures outlined in Step 2 and Step 3 in Section C.1 are used to compute the incremental dynamic force component  $\Delta P_{AE}$  and its corresponding equivalent earth pressure diagram.

### C.3 Earth Pressure Distribution for the Dynamic Active Earth Pressure Force, $P_{AE}$ , for a Backfill with Mohr-Coulomb Shear Strength Parameters $c'$ and $\phi'$ – Effective Stress Analysis

This section discusses the computation of the resultant location of  $P_{AE}$  and a corresponding pressure distribution for a backfill in which Mohr-Coulomb effective stress shear strength parameter  $\phi'$  and  $c'$  are both

nonzero.<sup>1</sup>  $P_{AE}$  is equal to the sum of  $P_A$  plus  $\Delta P_{AE}$  by Equation 3.23. The same four-step computational process outlined in Section C.1 is used to determine the earth pressure distribution and resultant location for  $P_{AE}$  for a backfill with nonzero  $c'$  and  $\phi'$  effective stress based Mohr-Coulomb shear strength parameters assigned to the backfill:

*Step 1: Convert the static active earth pressure force,  $P_A$ , into an equivalent active earth pressure diagram.*

Equation A.25 of the sweep-search wedge solution method described in Section A.3 demonstrates that  $P_A$  is made up of two forces, (1) a frictional and weight force component and (2) a cohesive force component. The frictional/weight resultant force component is reduced by the cohesion force component. The subtraction of the cohesion force component in Equation A.25 reflects a cohesion force component for a *tensile stress* distribution component of the resulting (effective) active earth pressure  $\sigma_A$  distribution of stresses with depth,

$$\sigma_A = K_{A-\phi\text{-weight}} \bullet \sigma'_{v-z} - SIGc \quad \text{C.14}$$

The component of (effective) active earth pressure distribution due to cohesion is designated as  $SIGc$  in this report and is of constant magnitude with depth.  $SIGc$  is computed by

$$SIGc = \frac{P_{A-C}}{H} \quad \text{C.15}$$

---

<sup>1</sup> A key item is the selection of suitable shear strength parameters. In an effective stress analysis, the issue of the suitable friction angle is particularly troublesome when the peak friction angle is significantly greater than the residual friction angle. In the displacement controlled approach examples given in Section 6.2 of Ebeling and Morrison (1992), effective stress based shear strength parameters (i.e., effective cohesion  $c'$  and effective angle of internal friction  $\phi'$ ) were used to define the shear strength of the dilative granular backfills, *with  $c'$  set equal to zero in all cases due to the level of deformations anticipated in a sliding block analysis during seismic shaking*. In 1992 Ebeling and Morrison concluded that it is conservative to use the residual friction angle in a sliding block analysis, and this should be the usual practice for displacement based analysis of granular retained soils. The primary author of this report would broaden the concept to the assignment of effective (or total) shear strength parameters for the retained soil be consistent with the level of shearing-induced deformations encountered for each design earthquake in a rotational analysis and note that active earth pressures are used to define the loading imposed on the structural wedge by the driving soil wedge. (Refer to Table 1.1 for guidance regarding wall movements required to fully mobilize the shear resistance within the retained soil during earthquake shaking.) Therefore, engineers are cautioned to carefully consider the reasonableness of including a nonzero value for effective cohesion  $c'$  in their permanent deformation and permanent rotation analyses.

with  $P_{A-C}$  corresponding to the cohesion component of  $P_A$  computed using Equation A.25 in the sweep-search wedge method of analysis with a critical wedge oriented at angle  $\alpha_A$ . The active earth pressure coefficient,  $K_{A-\phi\text{-weight}}$ , is computed using

$$K_{A-\phi\text{-weight}} = \frac{P_{A-\phi\text{-weight}}}{H} \int_0^H \sigma'_{v-z} dh \quad \text{C.16}$$

with  $P_{A-\phi\text{-weight}}$  corresponding to the frictional/weight component of  $P_A$  computed using Equation A.25 in the sweep-search wedge method of analysis. The effective vertical stress  $\sigma'_{v-z}$  is computed using a depth  $z$ , the depth below the ground surface using the procedure outlined in the Section C.2. In a moist backfill (i.e., with no water table) the depth to zero stress (i.e., depth of cracking) is computed as

$$d_{crack} = \frac{SIGc}{\gamma_{moist} \cdot K_{A-\phi\text{-weight}} \cdot \left[ \frac{\tan(\alpha_A)}{\tan(\alpha_A) - \tan(\beta)} \right]} \quad \text{C.17}$$

The effective vertical stress at the deepest point in the crack in moist soil (and above a water table) is computed equal to

$$\sigma'_{v-z-dcrack} = \gamma_{moist} \cdot z_{dcrack} \quad \text{C.18}$$

which, for a plane at angle  $\alpha_A$  (from horizontal) intersecting the sloping ground becomes

$$z_{dcrack} = d_{crack} \cdot \left[ \frac{\tan(\alpha)}{\tan(\alpha) - \tan(\beta)} \right] \quad \text{C.19}$$

and  $\sigma_{A-dcrack}$  is equal to zero at the crack tip

$$\sigma_{A-dcrack} = 0 = K_{A-\phi\text{-weight}} \cdot \sigma'_{v-z-dcrack} - SIGc \quad \text{C.20}$$

In the case of a crack extending below a hydrostatic water table within a retained soil, the effective vertical stress at the deepest point in the crack in Equation C.20 is computed using

$$\sigma'_{v-z-dcrack} = \gamma_{moist} \bullet z_{11toWT} + (\gamma_{saturated} - \gamma_w) \bullet z_{WTtoCrack} \tag{C.21}$$

with  $z_{11toWT}$  and  $z_{WTtoCrack}$  dimensions as shown in Figures C.10.a and C.10.b. In retained soils with a hydrostatic water table an iterative approach, using Equations C.20 and C.21, is used by CorpsWallRotate to determine the value of  $d_{crack}$ .

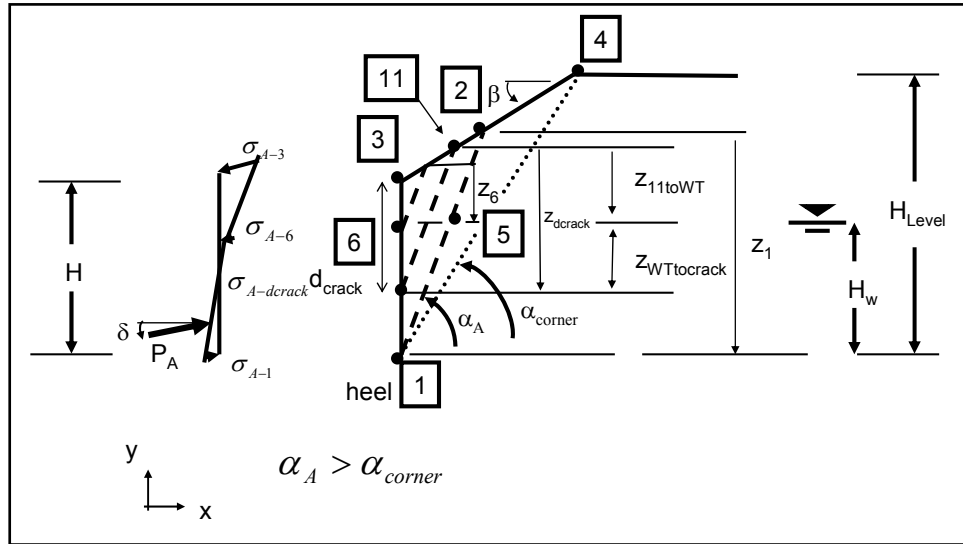


Figure C.10.a Graphical definition of  $z_{11toWT}$  and  $z_{WTtoCrack}$  in the effective vertical stress  $\sigma'_{v-z-dcrack}$  computation with  $x_{11} < x_4$ .

For the partially submerged retained soil case of Figure C.10.a, the depth to crack,  $d_{crack}$ , extends below the hydrostatic water table, and point 11 is located on the slope of the retained soil's ground surface (as indicated by  $x_{11} < x_4$ ). Equations C.19 through C.21 are used in a trial-and-error procedure to compute the value of  $d_{crack}$  (and  $y_{dcrack}$ ). The following relationships, based on the Figure C.10.a geometry, are also used in the solution process,

$$x_{11} = z_{dcrack} / \tan(\alpha) \tag{C.22}$$

$$z_{11toWT} = z_{dcrack} - z_{WTtoCrack} \tag{C.23}$$

with

$$z_{WTtoCrack} = y_6 - y_{dcrack} \tag{C.24}$$

For

$$y_6 = H_w \tag{C.25}$$

the variable  $z_{WTto\text{crack}}$  is also expressed as

$$z_{WTto\text{crack}} = d_{\text{crack}} - (H - H_w) \tag{C.26}$$

Note that for  $y_3$  equal to  $H$ ,

$$y_{\text{crack}} = H - d_{\text{crack}} \tag{C.27}$$

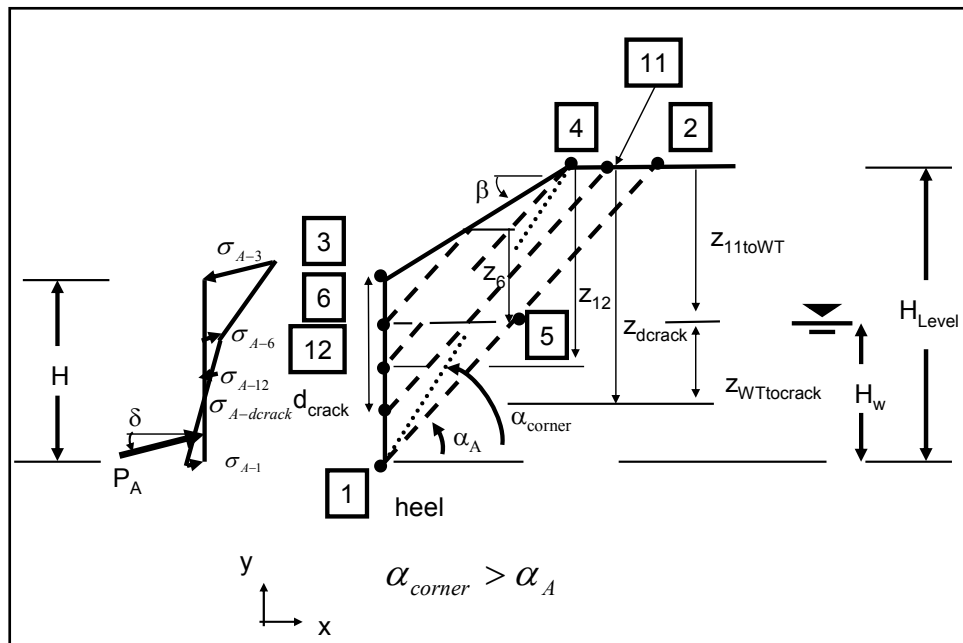


Figure C.10.b Graphical definition of  $z_{11toWT}$  and  $z_{WTto\text{crack}}$  in the effective vertical stress  $\sigma'_v\text{-}z\text{-}d_{\text{crack}}$  computation with  $x_{11} > x_4$ .

For the partially submerged retained soil case of Figure C.10.b, the depth to crack,  $d_{\text{crack}}$ , also extends below the hydrostatic water table but with point 11 located on the level ground surface of the retained soil (as indicated by  $x_{11} > x_4$ ). The Equation C.19 relationship between  $z_{d\text{crack}}$  and  $d_{\text{crack}}$  is not applicable. The following equation is substituted,

$$z_{d\text{crack}} = (H_{\text{Level}} - H) + d_{\text{crack}} \quad \text{with } x_{11} > x_4 \tag{C.28}$$

or, equivalently,

$$z_{d\text{crack}} = z_{12} + (x_{11} - x_4) \cdot \tan(\alpha) \quad \text{with } x_{11} > x_4 \tag{C.29}$$

Equations C.20 and C.21 are used in a trial-and-error procedure to compute the value of  $d_{crack}$  (and  $y_{dcrack}$ ). The following relationships, based on the Figure C.10.b geometry, are also used in the solution process,

$$x_{11} = z_{dcrack} / \tan(\alpha) \quad \text{bis C.22}$$

$$z_{12} = x_4 \bullet \tan(\alpha) \quad \text{C.30}$$

$$z_{11toWT} = z_{dcrack} - z_{WTto crack} \quad \text{bis C.23}$$

with

$$z_{WTto crack} = y_6 - y_{dcrack} \quad \text{bis C.24}$$

substituting

$$y_6 = H_w \quad \text{bis C.25}$$

and for  $y_3$  equal to H,

$$y_{dcrack} = H - d_{crack} \quad \text{bis C.27}$$

Recognizing that  $z_{11toWT}$  is a constant, equal to the difference between  $H_{Level}$  and  $H_w$  (in the case of  $x_{11} > x_4$ ), the variable  $z_{WTto crack}$  is also expressed as

$$z_{WTto crack} = z_{dcrack} - (H_{Level} - H_w) \quad \text{bis C.26}$$

Another useful geometrical Figure C.10.b relationships is

$$y_{12} = y_3 - \left\{ \frac{z_{12}}{\left[ \frac{\tan(\alpha)}{\tan(\alpha) - \tan(\beta)} \right]} \right\} \quad \text{C.31}$$

$C_{orps}W_{all}R_{otate}$  performs a permanent displacement analysis of a retaining wall due to earthquake shaking. Reversal in the direction of the horizontal component of the time-history of earthquake ground shaking occurs many times during the typical tens of seconds of ground motion. Consequently, a reversal in direction of the inertial force imparted to the structural wedge

and to the soil driving wedge occurs many times during the course of the analysis using  $C_{orps}W_{all}Rotate$ . In a traditional soil wedge formulation for static loading, a crack is typically considered to exist within the upper regime of the soil driving wedge for a cohesive soil and the planer wedge slip surface is terminated when it intersects the zone of cracking at a depth  $d_{crack}$  below the ground surface (e.g., see Appendix H in EM 1110-2-2502). This assumption is not made the  $C_{orps}W_{all}Rotate$  formulation for dynamic loading. Instead, it is assumed that in the dynamic wedge formulation, the crack within the zone of cracking at the top of the retained cohesive soil of the driving wedge will not remain open during earthquake shaking *due to the inertial load direction reversals*. So even for cohesive soils, the Figure A.1 planar slip surface obtained from the sweep-search method of analysis used by  $C_{orps}W_{all}Rotate$  to obtain a value for the earthquake-induced resultant driving force  $P_{AE}$  (acting on the structural wedge), extends uninterrupted within the driving soil wedge (in the retained soil) to the ground surface and is not terminated by a vertical crack face to the ground surface when it enters the zone of cracking. Since  $P_A$  is used solely to determine the value for  $h_{PAE}$ , the resultant location for  $P_{AE}$  with the procedure outlined in this appendix, a continuous planar slip surface is also assumed in  $P_A$  computations. A sweep-search wedge formulation is used to compute  $P_A$ . Equation C.17 for crack depth,  $d_{crack}$ , in moist backfill and Equation C.20 in partially submerged backfill are used solely to establish the static earth pressure diagram component of  $P_{AE}$  pressures along the imaginary vertical section passing through the heel of the wall, consistent with the Equation 3.23 formulation. This assumption is made for the earth pressure distribution corresponding to  $P_A$  with consideration of  $d_{crack}$  because the permanent displacement of the structural wedge is away from the backfill, and it is likely that at this vertical section a vertical crack may occur. Thus,  $d_{crack}$  is accounted for in the  $h_{PAE}$  computation using Equation C.12. The static tensile  $\sigma_A$  stresses along the driving soil wedge-to-structural wedge interface (i.e., located along the vertical imaginary section extending through the heel) are neglected over the depth of cracking due to the presence of the crack by  $C_{orps}W_{all}Rotate$ .

*Step 2: Create an incremental dynamic force component pressure diagram.*

The incremental dynamic force component,  $\Delta P_{AE}$ , is next converted into an equivalent earth pressure diagram using the relationship

$$\Delta P_{AE} = P_{AE} - P_A$$

bis C.11

and with values for  $P_{AE}$  and  $P_A$  provided by the dynamic and static sweep-search solutions made by CorpsWallRotate using the procedures outlined in Appendix A (Sections A.4 and A.5). The Ebeling and Morrison (1992) simplified procedure assumes a trapezoidal distribution for the corresponding incremental stress distribution with an interface friction angle of  $\delta = 0$  to the normal of the vertical imaginary section in a total stress analysis (refer to Figure C.3). The resulting force corresponding to the area under the pressure distribution is equal to  $\Delta P_{AE}$  and acts at a height to 0.6 times  $H$ .

*Step 3: Create the dynamic active earth pressure diagram.*

The dynamic active earth pressure diagram is created by adding the earth pressure diagrams created in Steps 1 and 2. The resulting force corresponds to the area under the combined pressure distribution and is equal to  $P_{AE}$  (recall  $P_{AE} = P_A + \Delta P_{AE}$ ). Its point of application above the heel of the wall is given by

$$h_{PAE} = \frac{P_A \cdot (h_{PA}) + \Delta P_{AE} \cdot (0.6 \cdot H)}{P_{AE}} \quad \text{bis C.12}$$

In the special case of cohesive soils, the CorpsWallRotate analysis disregards the tensile stresses when defining the static active earth pressures and the corresponding resulting static active earth pressure force to be applied to the structural wedge, as well as when computing  $h_{PA}$  for this modified stress distribution. A trapezoidal earth pressure distribution is still used to define  $\Delta P_{AE}$ .

*Step 4: Complete the pressure diagram by adding in the pore water pressure distribution.*

Refer to discussion in Step 4 of Section C.1.

### **C.3.1 The Basic Procedure to Compute the Active Effective Stress Distribution Corresponding to $P_A$ for a Partially Submerged Retained Soil with a Sloping Ground Surface**

The procedure outlined in Section C.2.2 is expanded to consider the case of a partially submerged backfill with nonzero effective cohesion and friction shear strength parameters (i.e.,  $c' > 0$  and  $\phi' > 0$ ). The procedure to calculate the active earth pressure distribution for resultant static force



$P_A$  due to the geometry of the backfill is outlined using the information contained within Figure C.11 for which the critical planar wedge slip plane that passes through point 1 (with  $\alpha_A > \alpha_{\text{corner}}$ ) intersects the sloping portion of the bilinear ground surface. The sweep-search wedge procedure described in Section A.3 is used to first compute the value for  $P_A$  as well as the orientation of the planar slip surface,  $\alpha_A$ , for the critical soil wedge that originates at point 1. The equation to compute the active earth pressures (designated as  $\sigma_A$ ) at the Figure C.11 key points designated as 1, 6,  $d_{\text{crack}}$ , and 3 is, by Equation C.14, equal to the active earth pressure coefficient,  $K_{A-\phi\text{-weight}}$ , times the vertical effective stress at depth  $z$  in the retained soil minus  $\text{SIGc}$ . The key feature for this formulation is that at a given point along the vertical imaginary section through the heel of the structural wedge (identified in this figure as points 1, 6,  $d_{\text{crack}}$ , and 3), the effective vertical stress (designated as  $\sigma'_{v-z}$  in the brackets and for a hydrostatic water table) is computed using a depth  $z$ , the depth below the ground surface as shown in this figure. A computation of  $\sigma'_{v-z}$  and, subsequently,  $\sigma_A$  are made in this figure for point 1 (at the heel). Note that depth  $z$ , designated as  $z_1$  for point 1, is determined by extending the critical, planar slip plane from point 1 until it intersects the *sloping* ground surface. This same procedure is followed to compute the value for  $z$ ,  $\sigma'_{v-z}$ , and  $\sigma_A$  at the other key points 6,  $d_{\text{crack}}$ , and 3 along the imaginary vertical section of height  $H$ . A plane oriented at  $\alpha_A$  from horizontal is projected from the point of interest (e.g., point  $d_{\text{crack}}$ ) up through the retained soil until it intersects the sloping ground surface.  $\sigma'_{v-z-d_{\text{crack}}}$  is computed using the resulting vertical height,  $z_{d_{\text{crack}}}$ , of this planar surface, as shown in this figure. The computations outlined in Figure C.11 differ from the Figure C.7 computations because of the depth of cracking. Thus an additional key point,  $d_{\text{crack}}$ , is needed to define the  $\sigma_A$  distribution. Moist unit weights above the water table and buoyant unit weights below the water table (assuming a hydrostatic water table in the retained soil) are used to compute the vertical effective stress  $\sigma'_{v-z}$ . To determine the value for the active earth pressure coefficient,  $K_{A-\phi\text{-weight}}$ , the value for the force component  $P_{A-\phi\text{-weight}}$  from the sweep-search method of analysis is divided by the integral of the  $\sigma'_{v-z}$  distribution along the imaginary vertical section of height  $H$  (refer to the equation given in this figure). [ $\sigma'_{v-z}$  is contained within the brackets of the  $\sigma_A$  relationships given in this figure.] For the Figure C.11 case of a granular retained soil with a constant surface slope (as far as this effective vertical stress computational procedure is concerned), the equation for  $\sigma'_{v-z}$  and  $\sigma_A$  at key points and for  $K_{A-\phi\text{-weight}}$  are straight-forward and given in this figure.

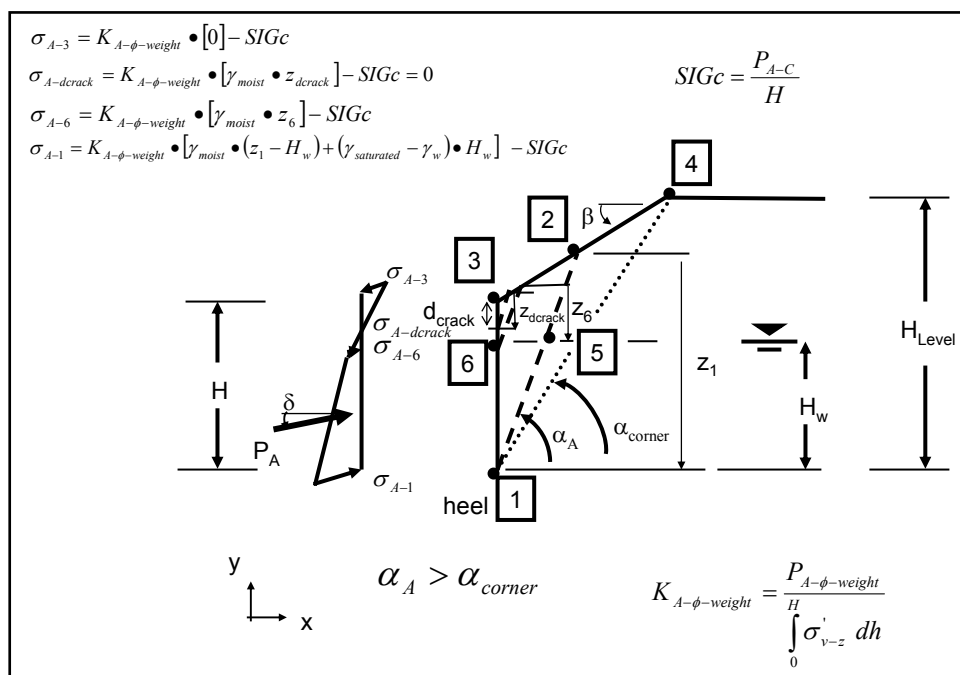


Figure C.11. The active earth pressure distribution corresponding to the incremental static force component,  $P_A$ , acting at an effective interface friction angle of  $\delta$  to the normal of the vertical imaginary section through the heel of the wall for a bilinear ground surface – partially submerged backfill with  $\phi' > 0$  and  $c' > 0$ .

The procedure outlined in Step 1 in Section C.1 that converts the  $\sigma_A$  distribution into equivalent forces (see Figure C.8) is used to compute the resultant location  $h_{PA}$  of  $P_A$  for use in Equation C.12 for the resultant location  $h_{PAE}$  of  $P_{AE}$ . The procedures outlined in Step 2 and Step 3 in Section C.1 are used to compute the incremental dynamic force component,  $\Delta P_{AE}$ , and its corresponding equivalent earth pressure diagram.

### C.3.2 The Basic Procedure to Compute the Active Effective Stress Distribution Corresponding to $P_A$ for a Partially Submerged Retained Soil with a Bilinear Ground Surface

The procedure outlined in Section C.2.3 is expanded to consider the Figure C.12 geometry of a partially submerged backfill with nonzero effective cohesion and friction shear strength parameters (i.e.,  $c' > 0$  and  $\phi' > 0$ ). The procedure to calculate the active earth pressure distribution for resultant static force  $P_A$  due to the geometry of the backfill is outlined using the information contained within Figure C.12 for which the critical planar wedge slip plane that passes through point 1 (with  $\alpha_A > \alpha_{corner}$ ), intersecting the level portion of the bilinear ground surface. The sweep-

search wedge procedure described in Section A.3 is used to first compute the value for  $P_A$  as well as the orientation of the planar slip surface,  $\alpha_A$ , for the critical soil wedge that originates at point 1. The equation to compute the active earth pressures (designated as  $\sigma_A$ ) at the Figure C.12 key points designated as 1, 12, 6,  $d_{\text{crack}}$ , and 3 is, by Equation C.14, equal to the active earth pressure coefficient,  $K_{A-\phi\text{-weight}}$ , times the vertical effective stress at depth  $z$  in the retained soil minus  $\text{SIGc}$ . The key feature for this formulation is that at a given point along the vertical imaginary section through the heel of the structural wedge (identified in this figure as points 1, 12, 6,  $d_{\text{crack}}$ , and 3), the effective vertical stress (designated as  $\sigma'_{v-z}$  in the brackets and for a hydrostatic water table) is computed using a depth  $z$ , the depth below the ground surface as shown in this figure. A computation of  $\sigma'_{v-z}$  and, subsequently,  $\sigma_A$  are made in this figure for point 1 (at the heel). Note that depth  $z$ , designated as  $z_1$  for point 1, is determined by extending the critical, planar slip plane from point 1 until it intersects the horizontal ground surface. This same procedure is followed to compute the value for  $z$ ,  $\sigma'_{v-z}$ , and  $\sigma_A$  at the other key points 12, 6,  $d_{\text{crack}}$ , and 3 along the imaginary vertical section of height  $H$ . A plane oriented at  $\alpha_A$  from horizontal is projected from the point of interest (e.g., point  $d_{\text{crack}}$ ) up through the retained soil until it intersects the sloping ground surface.  $\sigma'_{v-z-d_{\text{crack}}}$  is computed using the resulting vertical height  $z_{d_{\text{crack}}}$  of this planar surface, as shown in this figure. The computations outlined in Figure C.12 differ from the Figure C.9 computations because of the depth of cracking. Thus an additional key point,  $d_{\text{crack}}$ , is needed to define the  $\sigma_A$  distribution. Moist unit weights above the water table and buoyant unit weights below the water table (assuming a hydrostatic water table in the retained soil) are used to compute the vertical effective stress  $\sigma'_{v-z}$ . To determine the value for the active earth pressure coefficient,  $K_{A-\phi\text{-weight}}$ , the value for the force component  $P_{A-\phi\text{-weight}}$  from the sweep-search method of analysis is divided by the integral of the  $\sigma'_{v-z}$  distribution along the imaginary vertical section of height  $H$  (refer to the equation given in this figure). [ $\sigma'_{v-z}$  is contained within the brackets of the  $\sigma_A$  relationships given in this figure.] For the case of the Figure C.12 retained soil with a constant surface slope (as far as this effective vertical stress computational procedure is concerned), the equation for  $\sigma'_{v-z}$  and  $\sigma_A$  at key points and for  $K_{A-\phi\text{-weight}}$  are straight-forward and given in this figure.

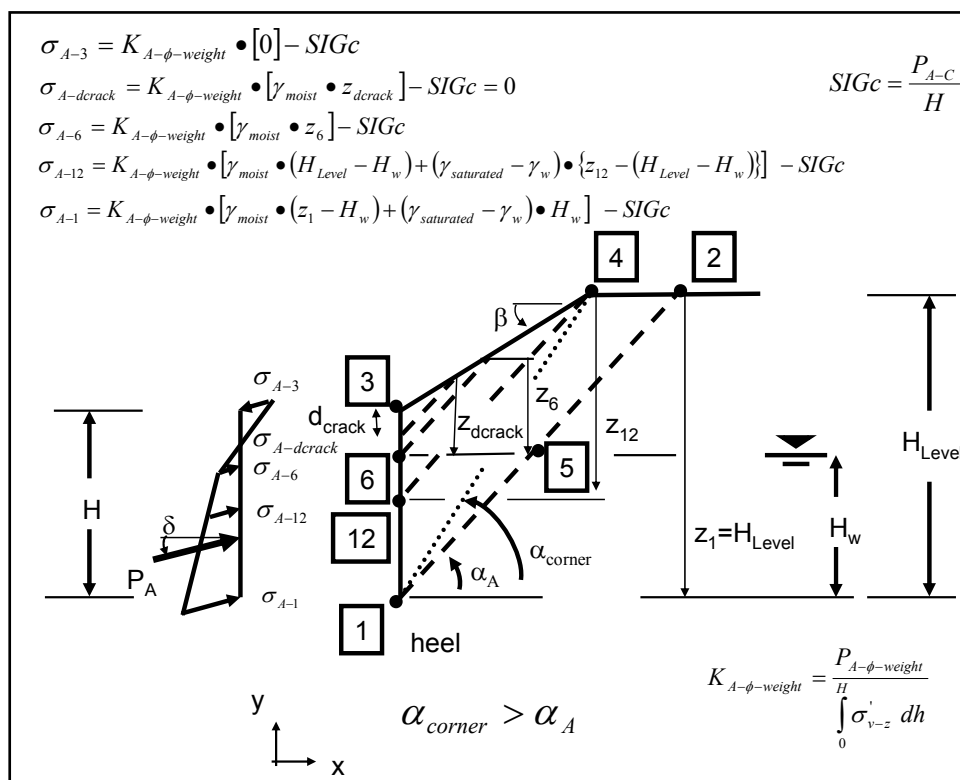


Figure C.12 The active earth pressure distribution corresponding to the incremental static force component,  $P_A$ , acting at an effective interface friction angle of  $\delta$  to the normal of the vertical imaginary section through the heel of the wall for a bilinear ground surface – partially submerged backfill with  $\phi' > 0$  and  $c' > 0$ .

The procedure outlined in Step 1 in Section C.1 that converts the  $\sigma_A$  distribution into equivalent forces (see Figure C.8) is used to compute the resultant location  $h_{PA}$  of  $P_A$  for use in Equation C.12 for the resultant location  $h_{PAE}$  of  $P_{AE}$ . The procedures outlined in Step 2 and Step 3 in Section C.1 are used to compute the incremental dynamic force component  $\Delta P_{AE}$  and its corresponding equivalent earth pressure diagram.

#### C.4 Earth Pressure Distribution for the Dynamic Active Earth Pressure Force, $P_{AE}$ , for a Backfill with Mohr-Coulomb Shear Strength Parameters, $S_u$ – Total Stress Analysis

This section discusses the computation of the resultant location of  $P_{AE}$  and a corresponding pressure distribution for a backfill in which Mohr-Coulomb total stress (undrained) shear strength parameter,  $S_u$ , is

nonzero.<sup>1</sup>  $P_{AE}$  is equal to the sum of  $P_A$  plus  $\Delta P_{AE}$  by Equation 3.23. The first three steps of the computational process outlined in Section C.1 are used to determine the earth pressure distribution and resultant location for  $P_{AE}$  for a backfill with nonzero  $S_u$  total stress shear strength parameter assigned to the backfill:

*Step 1: Convert the static active earth pressure force,  $P_A$ , into an equivalent active earth pressure diagram.*

Equation A.31 of the (total stress) sweep-search wedge solution method described in Section A.5 demonstrates that  $P_A$  is made up of two forces, (1) a force component due to the weight of the soil (driving) wedge and (2) a cohesive force component. The resultant force component due to the weight of the soil wedge is reduced by the cohesion force component. The subtraction of the cohesion force component in Equation A.31 reflects a cohesion force component for a *tensile stress* distribution component of the resulting (effective) active earth pressure  $\sigma_A$  distribution of stresses with depth,

$$\sigma_A = K_{A\text{-weight}} \bullet \sigma_{v-z} - SIG_{Su} \quad \text{C.32}$$

The component of (total) active earth pressure distribution due to cohesion is designated as  $SIG_{Su}$  in this report and is of constant magnitude with depth.  $SIG_{Su}$  is computed by

$$SIG_{Su} = \frac{P_{A-Su}}{H} \quad \text{C.33}$$

with  $P_{A-Su}$  corresponding to the cohesion component of  $P_A$  computed using Equation A.31 in the sweep-search wedge method of analysis with a critical wedge oriented at angle  $\alpha_A$ . The active earth pressure coefficient,  $K_{A\text{-weight}}$ , is computed using

---

<sup>1</sup> A key item is the selection of suitable shear strength parameters. The assignment of total (or effective) shear strength parameter(s) for the retained soil to be consistent with the level of shearing-induced deformations encountered for each design earthquake in a rotational analysis and note that active earth pressures are used to define the loading imposed on the structural wedge by the driving soil wedge. (Refer to Table 1.1 for guidance regarding wall movements required to fully mobilize the shear resistance within the retained soil during earthquake shaking.)

$$K_{A\text{-weight}} = \frac{P_{A\text{-weight}}}{H \int_0^H \sigma_{v-z} dh} \quad \text{C.34}$$

with  $P_{A\text{-weight}}$  corresponding to the weight component of  $P_A$  computed using Equation A.31 in the sweep-search wedge method of analysis. The total vertical stress  $\sigma_{v-z}$  is computed using a depth  $z$ , the depth below the ground surface using the procedure similar to that outlined in the Section C.2. In a moist backfill (i.e., with no water table) the depth to zero stress (i.e., depth of cracking) is computed as

$$d_{\text{crack}} = \frac{SIG_{Su}}{\gamma_{\text{moist}} \bullet K_{A\text{-weight}} \bullet \left[ \frac{\tan(\alpha_A)}{\tan(\alpha_A) - \tan(\beta)} \right]} \quad \text{C.35}$$

The total vertical stress at the deepest point in the crack in moist soil (and above a water table) is computed equal to

$$\sigma_{v-z\text{-dcrack}} = \gamma_{\text{moist}} \bullet Z_{\text{dcrack}} \quad \text{C.36}$$

which, for a slip plane intersecting the sloping ground is

$$Z_{\text{dcrack}} = d_{\text{crack}} \bullet \left[ \frac{\tan(\alpha)}{\tan(\alpha) - \tan(\beta)} \right] \quad \text{bis C.19}$$

and  $\sigma_{A\text{-dcrack}}$  is equal to zero at the crack tip

$$\sigma_{A\text{-dcrack}} = 0 = K_{A\text{-weight}} \bullet \sigma_{v-z\text{-dcrack}} - SIG_{Su} \quad \text{C.37}$$

In the case of a crack extending below a hydrostatic water table within a retained soil, the total vertical stress at the deepest point in the crack in Equation C.37, is computed using

$$\sigma_{v-z\text{-dcrack}} = \gamma_{\text{moist}} \bullet Z_{11\text{toWT}} + \gamma_{\text{saturated}} \bullet Z_{\text{WTtoCrack}} \quad \text{C.38}$$

with  $Z_{11\text{toWT}}$  and  $Z_{\text{WTtoCrack}}$  dimensions are the same as were shown in Figures C.10.a and C.10.b for the effective stress based analysis. In retained soils with a hydrostatic water table an iterative approach, using Equations C.37 and C.38, is used by  $C_{\text{orps}}W_{\text{allRotate}}$  to determine the value

of  $d_{\text{crack}}$ . Note that pore water pressure internal to the soil wedge is not included in the Equation C.38 total vertical stress computation.

$C_{\text{orps}}W_{\text{all}}\text{Rotate}$  performs a permanent displacement analysis of a retaining wall due to earthquake shaking. Reversal in the direction of the horizontal component of the time-history of earthquake ground shaking occurs many times during the typical tens of seconds of ground motion. Consequently, a reversal in direction of the inertial force imparted to the structural wedge and to the soil driving wedge occurs many times during the course of the analysis using  $C_{\text{orps}}W_{\text{all}}\text{Rotate}$ . In a traditional soil wedge formulation for static loading, a crack is typically considered to exist within the upper regime of the soil driving wedge for a cohesive soil and the planar wedge slip surface is terminated when it intersects the zone of cracking at a depth,  $d_{\text{crack}}$ , below the ground surface (e.g., see Appendix H in EM 1110-2-2502). This assumption is not made the  $C_{\text{orps}}W_{\text{all}}\text{Rotate}$  formulation for dynamic loading. Instead, it is assumed that in the dynamic wedge formulation, the crack within the zone of cracking at the top of the retained cohesive soil of the driving wedge will not remain open during earthquake shaking *due to the inertial load direction reversals*. So even for cohesive soils, the Figure A.1 planar slip surface obtained from the sweep-search method of analysis used by  $C_{\text{orps}}W_{\text{all}}\text{Rotate}$  to obtain a value for the earthquake induced resultant driving force  $P_{\text{AE}}$  (acting on the structural wedge) extends uninterrupted within the driving soil wedge (in the retained soil) to the ground surface and is not terminated by a vertical crack face to the ground surface when it enters the zone of cracking. Since  $P_{\text{A}}$  is used solely to determine the value for  $h_{\text{PAE}}$ , the resultant location for  $P_{\text{AE}}$  with the procedure outlined in this appendix, a continuous planar slip surface is also assumed in  $P_{\text{A}}$  computations. A sweep-search wedge formulation is used to compute  $P_{\text{A}}$ . Equation C.35 for crack depth  $d_{\text{crack}}$  in moist backfill and Equation C.37 in partially submerged backfill are used solely to establish the static earth pressure diagram component of  $P_{\text{AE}}$  pressures along the imaginary vertical section passing through the heel of the wall, consistent with the Equation 3.23 formulation. This assumption is made for the earth pressure distribution corresponding to  $P_{\text{A}}$  with consideration of  $d_{\text{crack}}$  because the permanent displacement of the structural wedge is away from the backfill, and it is likely that at this vertical section a vertical crack may occur. Thus,  $d_{\text{crack}}$  is accounted for in the  $h_{\text{PAE}}$  computation using Equation C.12. The static tensile  $\sigma_{\text{A}}$  stresses along the driving soil wedge-to-structural wedge interface (i.e., located along the vertical imaginary section extending through the heel) are

neglected over the depth of cracking due to the presence of the crack by  $C_{\text{orps}}W_{\text{allRotate}}$ .

*Step 2: Create an incremental dynamic force component pressure diagram.*

The incremental dynamic force component,  $\Delta P_{\text{AE}}$ , is next converted into an equivalent earth pressure diagram using the relationship

$$\Delta P_{\text{AE}} = P_{\text{AE}} - P_{\text{A}} \quad \text{bis C.11}$$

and with values for  $P_{\text{AE}}$  and  $P_{\text{A}}$  provided by the dynamic and static sweep-search solutions made by  $C_{\text{orps}}W_{\text{allRotate}}$  using the procedures outlined in Appendix A (Sections A.4 and A.5). The Ebeling and Morrison (1992) simplified procedure assumes a trapezoidal distribution for the corresponding incremental stress distribution with an interface friction angle of  $\delta = 0$  to the normal of the vertical imaginary section in a total stress analysis (refer to Figure C.3). The resulting force corresponding to the area under the pressure distribution is equal to  $\Delta P_{\text{AE}}$  and acts at a height to 0.6 times  $H$ .

In the case of a Figure A.4 water filled crack,  $\Delta P_{\text{AE}}$  is given by

$$\Delta P_{\text{AE}} = P_{\text{AE}} - P_{\text{A}} - \Delta U \quad \text{C.39}$$

with values for  $P_{\text{AE}}$  and  $P_{\text{A}}$  provided by the dynamic and static sweep-search solutions made by  $C_{\text{orps}}W_{\text{allRotate}}$  using the procedures outlined in Appendix A (Sections A.4 and A.5).  $P_{\text{A}}$  is set equal to  $P_{\text{static-total stress}}$  (Equation A.31) for the critical slip plane (i.e., at angle  $\alpha = \alpha_{\text{A}}$ )  $\Delta U$  (Equation A.34) is the difference in water pressure force within the cracks on both sides of the Figure A.4 driving soil wedge. Recall that in a total stress analysis, internal pore water pressures are not applied along the imaginary vertical sections and slip plane defining the driving soil wedge. However, should a crack extend to below the water table, the boundary water pressures and their resultant forces are included along the imaginary vertical sections in the free-body diagram for the static soil wedge, as depicted in Figure A.4, and in the computation of  $P_{\text{A}}$ . Further, it is assumed that in the dynamic wedge formulation used to compute  $P_{\text{AE}}$ , the crack within the zone of cracking at the top of the retained cohesive soil of the driving wedge will not remain open during earthquake shaking *due to the inertial load direction reversals* during this time-history based



analysis. So, no crack depth is included in the  $C_{orps}W_{all}Rotate$  analysis of the dynamic resultant force,  $P_{AE}$ , for cohesive soils.

*Step 3: Create the dynamic active earth pressure diagram.*

The dynamic active earth pressure diagram is created by adding the earth pressure diagrams created in Steps 1 and 2. The resulting force corresponds to the area under the combined pressure distribution and is equal to  $P_{AE}$  (recall  $P_{AE} = P_A + \Delta P_{AE}$ ). Its point of application above the heel of the wall is given by

$$h_{PAE} = \frac{P_A \cdot (h_{PA}) + \Delta P_{AE} \cdot (0.6 \cdot H)}{P_{AE}} \quad \text{bis C.12}$$

In the case of a Figure A.4 water filled crack, the point of application of  $P_{AE}$  is

$$h_{PAE} = \frac{P_A \cdot (h_{PA}) + \Delta U \cdot h_{\Delta U} + \Delta P_{AE} \cdot (0.6 \cdot H)}{P_{AE}} \quad \text{C.40}$$

with  $P_A$  set equal to  $P_{static-total\ stress}$  (Equation A.31) for the critical slip plane (i.e., at angle  $\alpha = \alpha_A$ );  $\Delta U$  is (Equation A.34) the difference in water pressure force within the cracks on both sides of the Figure A.4 driving soil wedge, and  $h_{PA}$  and  $h_{\Delta U}$  are the resultant locations of these respective forces.

In the special case of cohesive soils, the  $C_{orps}W_{all}Rotate$  analysis disregards the tensile stresses when defining the static active earth pressures and the corresponding resulting static active earth pressure force to be applied to the structural wedge, as well as when computing  $h_{PA}$  for this modified stress distribution. A trapezoidal earth pressure distribution is still used to define  $\Delta P_{AE}$ .

#### **C.4.1 The Basic Procedure to Compute the Active Total Stress Distribution Corresponding to $P_A$ for a Partially Submerged Retained Soil with a Sloping Ground Surface**

The procedure outlined in this subsection considers the case of a partially submerged backfill in which Mohr-Coulomb total stress (undrained) shear strength parameter,  $S_u$ , is nonzero (i.e., a nonzero cohesion). The

procedure to calculate the active earth pressure distribution for resultant static force,  $P_A$ , due to the geometry of the backfill is outlined using the information contained within Figure C.13 for which the critical planar wedge slip plane that passes through point 1 (with  $\alpha_A > \alpha_{\text{corner}}$ ) intersects the sloping portion of the bilinear ground surface. The sweep-search wedge procedure described in Section A.5 is used to first compute the value for  $P_A$  as well as the orientation of the planar slip surface,  $\alpha_A$ , for the critical soil wedge that originates at point 1. The equation to compute the active earth pressures (designated as  $\sigma_A$ ) at the Figure C.13 key points designated as 1, 6,  $d_{\text{crack}}$ , and 3 is, by Equation C.32, equal to the active earth pressure coefficient,  $K_{A\text{-weight}}$ , times the vertical total stress at depth  $z$  in the retained soil minus  $\text{SIG}_{\text{Su}}$ . The key feature for this formulation is that at a given point along the vertical imaginary section through the heel of the structural wedge (identified in this figure as points 1, 6,  $d_{\text{crack}}$ , and 3), the total vertical stress (designated as  $\sigma_{v-z}$  in the brackets) is computed using a depth  $z$ , the depth below the ground surface as shown in this figure. A computation of  $\sigma_{v-z}$  and, subsequently,  $\sigma_A$  are made in this figure for point 1 (at the heel). Note that depth  $z$ , designated as  $z_1$  for point 1, is determined by extending the critical, planar slip plane from point 1 until it intersects the *sloping* ground surface. This same procedure is followed to compute the value for  $z$ ,  $\sigma_{v-z}$ , and  $\sigma_A$  at the other key points 6,  $d_{\text{crack}}$ , and 3 along the imaginary vertical section of height  $H$ . A plane oriented at  $\alpha_A$  from horizontal is projected from the point of interest (e.g., point  $d_{\text{crack}}$ ) up through the retained soil until it intersects the sloping ground surface.  $\sigma_{v-z-d_{\text{crack}}}$  is computed using the resulting vertical height  $Z_{d_{\text{crack}}}$  of this planar surface, as shown in this figure. Moist unit weights above the water table and submerged unit weights below the water table are used to compute the vertical total stress  $\sigma_{v-z}$ . To determine the value for the active earth pressure coefficient,  $K_{A\text{-weight}}$ , the value for the force component  $P_{A\text{-weight}}$  from the sweep-search method of analysis is divided by the integral of the  $\sigma_{v-z}$  distribution along the imaginary vertical section of height  $H$  (refer to the equation given in this figure). [ $\sigma_{v-z}$  is contained within the brackets of the  $\sigma_A$  relationships given in this figure.] For the Figure C.13 case of a retained soil with a constant surface slope (as far as this total vertical stress computational procedure is concerned), the equation for  $\sigma_{v-z}$  and  $\sigma_A$  at key points and for  $K_{A\text{-weight}}$  are straight-forward and given in this figure.

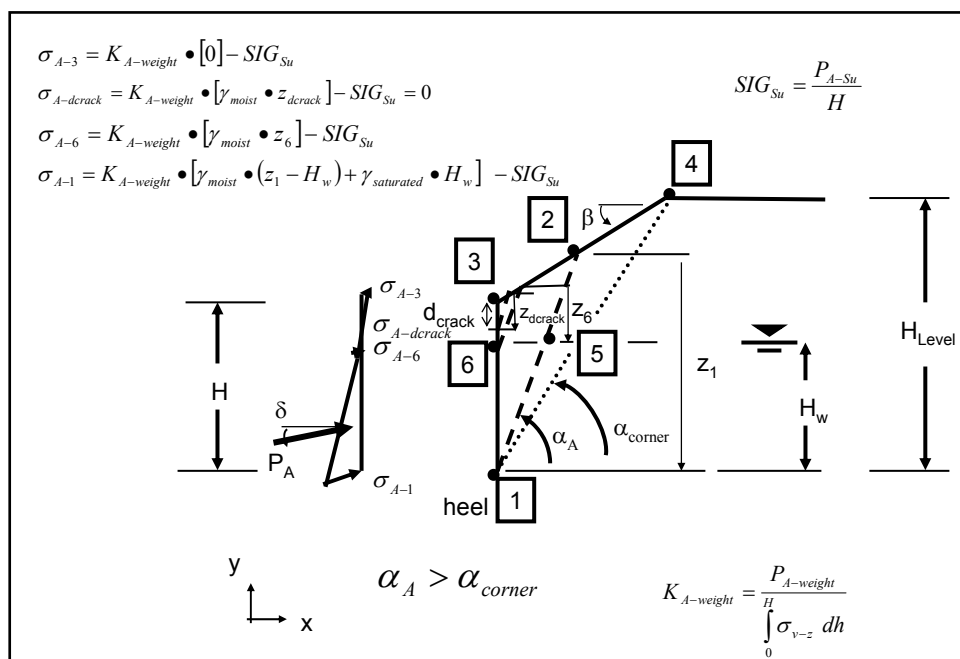


Figure C.13. The active earth pressure distribution corresponding to the incremental static force component,  $P_A$ , acting at an interface friction angle of  $\delta = 0$  to the normal of the vertical imaginary section through the heel of the wall for a bilinear ground surface – partially submerged backfill with  $S_u > 0$ .

The same procedure outlined in Step 1 in Section C.1 that converts the  $\sigma_A$  distribution into equivalent forces (see Figure C.8) is used to compute the resultant location  $h_{PA}$  of  $P_A$  for use in Equation C.12 for the resultant location  $h_{PAE}$  of  $P_{AE}$ . The procedures outlined in Step 2 and Step 3 in Section C.4 are used to compute the incremental dynamic force component,  $\Delta P_{AE}$ , and its corresponding equivalent earth pressure diagram.

#### C.4.2 The Basic Procedure to Compute the Active Total Stress Distribution Corresponding to $P_A$ for a Partially Submerged Retained Soil with a Bilinear Ground Surface

The procedure used to calculate the active earth pressure distribution for resultant static force  $P_A$  due to the geometry of the backfill is outlined using the information contained within Figure C.14 for which the critical planar wedge slip plane that passes through point 1 (with  $\alpha_A > \alpha_{corner}$ ), *intersecting the level portion* of the bilinear ground surface. It considers the case of a partially submerged backfill in which Mohr-Coulomb total stress (undrained) shear strength parameter,  $S_u$ , is nonzero (i.e., a nonzero cohesion). The sweep-search wedge procedure described in Section A.5 is used to first compute the value for  $P_A$  as well as the orientation of the

planar slip surface,  $\alpha_A$ , for the critical soil wedge that originates at point 1. The equation to compute the active earth pressures (designated as  $\sigma_A$ ) at the Figure C.14 key points designated as 1, 12, 6,  $d_{\text{crack}}$ , and 3 is, by Equation C.32, equal to the active earth pressure coefficient,  $K_{A\text{-weight}}$ , times the vertical total stress at depth  $z$  in the retained soil minus  $\text{SIG}_{\text{Su}}$ . The key feature for this formulation is that at a given point along the vertical imaginary section through the heel of the structural wedge (identified in this figure as points 1, 12, 6,  $d_{\text{crack}}$ , and 3), the total vertical stress (designated as  $\sigma_{v-z}$  in the brackets) is computed using a depth  $z$ , the depth below the ground surface as shown in this figure. A computation of  $\sigma_{v-z}$  and, subsequently,  $\sigma_A$  are made in this figure for point 1 (at the heel). Note that depth  $z$ , designated as  $z_1$  for point 1, is determined by extending the critical, planar slip plane from point 1 until it intersects the horizontal ground surface. This same procedure is followed to compute the value for  $z$ ,  $\sigma_{v-z}$ , and  $\sigma_A$  at the other key points 12, 6,  $d_{\text{crack}}$ , and 3 along the imaginary vertical section of height  $H$ . A plane oriented at  $\alpha_A$  from horizontal is projected from the point of interest (e.g., point  $d_{\text{crack}}$ ) up through the retained soil until it intersects the sloping ground surface.  $\sigma_{v-z-d_{\text{crack}}}$  is computed using the resulting vertical height,  $Z_{d_{\text{crack}}}$ , of this planar surface, as shown in this figure. Moist unit weights above the water table and submerged unit weights below the water table are used to compute the vertical total stress  $\sigma_{v-z}$ . To determine the value for the active earth pressure coefficient,  $K_{A\text{-weight}}$ , the value for the force component,  $P_{A\text{-weight}}$ , from the sweep-search method of analysis is divided by the integral of the  $\sigma_{v-z}$  distribution along the imaginary vertical section of height  $H$  (refer to the equation given in this figure). [ $\sigma_{v-z}$  is contained within the brackets of the  $\sigma_A$  relationships given in this figure.] For the case of the Figure C.14 retained soil with a constant surface slope (as far as this total vertical stress computational procedure is concerned), the equation for  $\sigma_{v-z}$  and  $\sigma_A$  at key points and for  $K_{A\text{-weight}}$  are straight-forward and given in this figure.

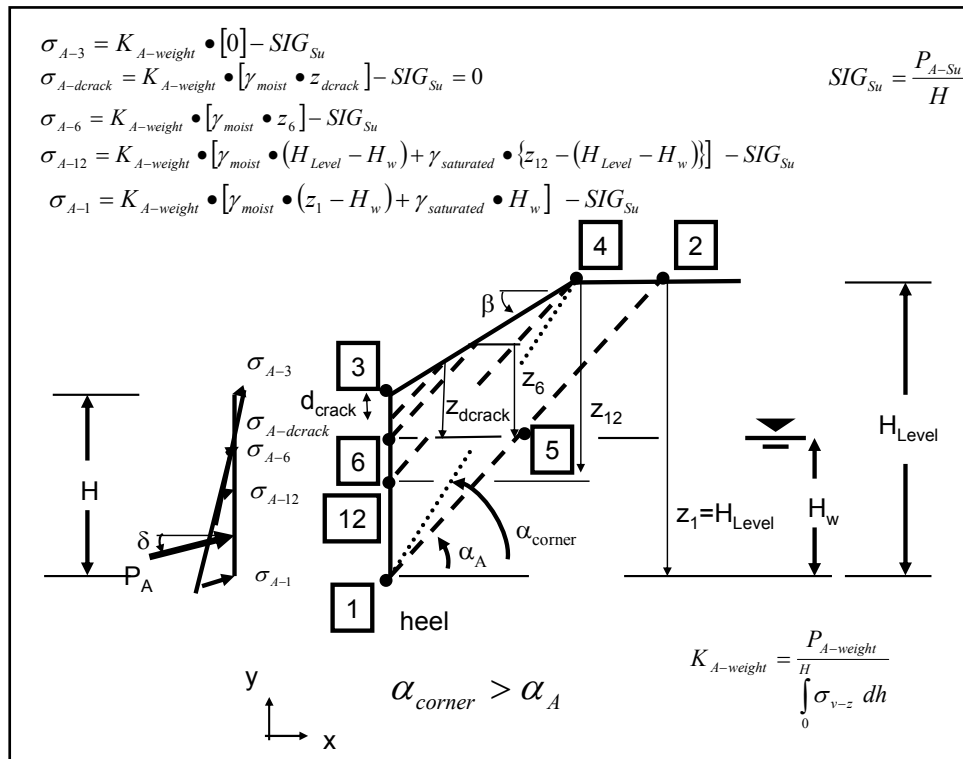


Figure C.14. The active earth pressure distribution corresponding to the incremental static force component,  $P_A$ , acting at an effective interface friction angle of  $\delta = 0$  to the normal of the vertical imaginary section through the heel of the wall for a bilinear ground surface – partially submerged backfill with  $S_u > 0$ .

The same procedure outlined in Step 1 in Section C.1 that converts the  $\sigma_A$  distribution into equivalent forces (see Figure C.8) is used to compute the resultant location  $h_{PA}$  of  $P_A$  for use in Equation C.12 for the resultant location  $h_{PAE}$  of  $P_{AE}$ . The procedures outlined in Step 2 and Step 3 in Section C.4 are used to compute the incremental dynamic force component,  $\Delta P_{AE}$ , and its corresponding equivalent earth pressure diagram.

## Appendix D: Water Pressures Acting on a Partially Submerged Structural Wedge

An earth retaining structure under investigation using CorpsWallRotate may retain a partially submerged backfill and may have a pool of water present in front of the structure. This appendix summarizes the computation of water pressures acting on a partially submerged structural wedge. Dynamic considerations for the pool during earthquake shaking are accounted for in the analysis using hydrodynamic water pressures computed using the Westergaard (1931) procedure of analysis.

### D.1 Steady-State Water Pressures Acting on the Structural Wedge

**Effective Stress Analysis:** In an effective stress based stability analysis, knowledge of the water pressures acting on the structural wedge is required. Figure D.1 shows key points and water pressures acting normal to the faces of the structural wedge that retains a partially submerged backfill and has a pool of water in front of the structure. Accounting for water pressures is an essential feature of an effective stress-based stability analysis.

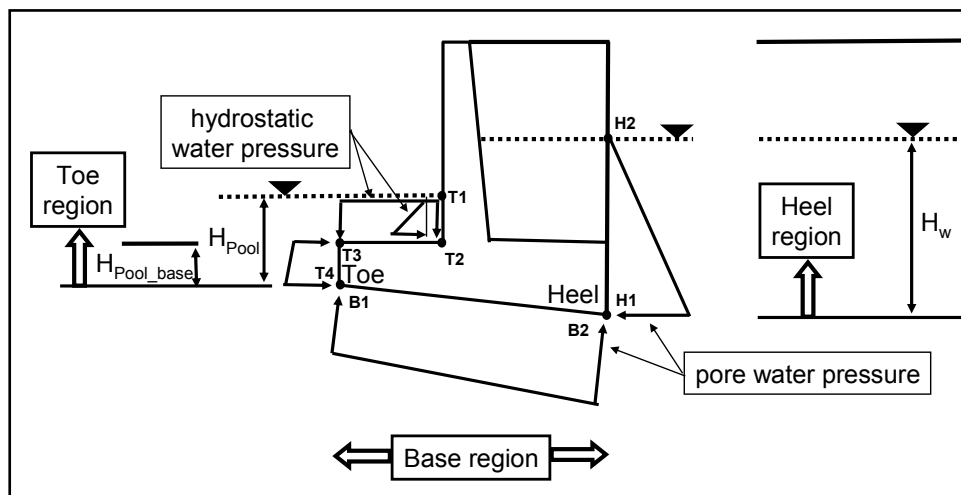


Figure D.1. Control points and steady-state water pressures acting normal to faces within the three regions of a structural wedge in full contact with the foundation – effective stress analysis.

Full contact between the base of the structural wedge and the foundation is assumed in Figure D.1. This is the situation for the sliding block method of analysis.

In  $C_{\text{orps}}W_{\text{all}}\text{Rotate}$  the faces of the structural wedge are divided into three regions: the toe region, the base region, and the heel region. Coordinates of key points defining these three regions are provided as input. These points are specified in a counterclockwise fashion progressing around the wetted perimeter of the structural wedge, as discussed in data input group 5 of Appendix F. For the structural wedge shown in Figure D.1, four points (designated points T1, T2, T3, and T4) define the wetted toe face, two points define the wetted base face (designated points B1 and B2), and two points define the wetted heel face (designated points T1 and T2). For the initial version of  $C_{\text{orps}}W_{\text{all}}\text{Rotate}$ , a simplified assumption is made that for steady-state conditions, hydrostatic water pressures exist within the heel region of the backfill. This implies that all head loss occurs due to flow within the foundation below the base of the structural wedge.<sup>1</sup> Thus, the pore water pressure at point H1 (also labeled as point B2) is equal to  $\gamma_w$  times  $H_w$ . Hydrostatic water pressures are also assumed within the pool at the toe region of the structural wedge. Consequently, the pore water pressure at point T4 (also labeled as point B1) is equal to  $\gamma_w$  times  $H_{\text{Pool}}$ . At points T2 and T3, the boundary water pressure is equal to  $\gamma_w$  times the depth to the point as measured from pool elevation. A linear variation in boundary water pressures is assumed along the base region, from point B1 to point B2. In this fashion, the steady-state boundary water pressures are assigned to the Figure D.1 idealized structural wedge.

$C_{\text{orps}}W_{\text{all}}\text{Rotate}$  converts the Figure D.1 boundary water pressures into equivalent forces and points of application using the procedure outlined in Figure D.2 for the base region. The base region is defined by the two points B1 and B2. The pore water pressure at point B1 is designated  $u_{B1}$ , and the pore water pressure at point B2 is designated  $u_{B2}$ . A linear variation in pore water pressure exists between these two points and acts normal to this linear face. The pressure distribution acting normal to this linear face is then converted to equivalent forces (e.g., forces  $F_{B1}$  and  $F_{B2}$  at points B1 and B2, respectively) using the equations given in this figure. This same approach is used to compute equivalent point forces along each linear segment used to define all faces within the other two regions. Each region

---

<sup>1</sup> Future improvements to  $C_{\text{orps}}W_{\text{all}}\text{Rotate}$  will include other steady-state seepage conditions.

is reduced to linear segments of face geometry of constant or linear variation in pore water pressure with distance (e.g., three line segments are used to define the toe region while one line segment is used to define the heel region).

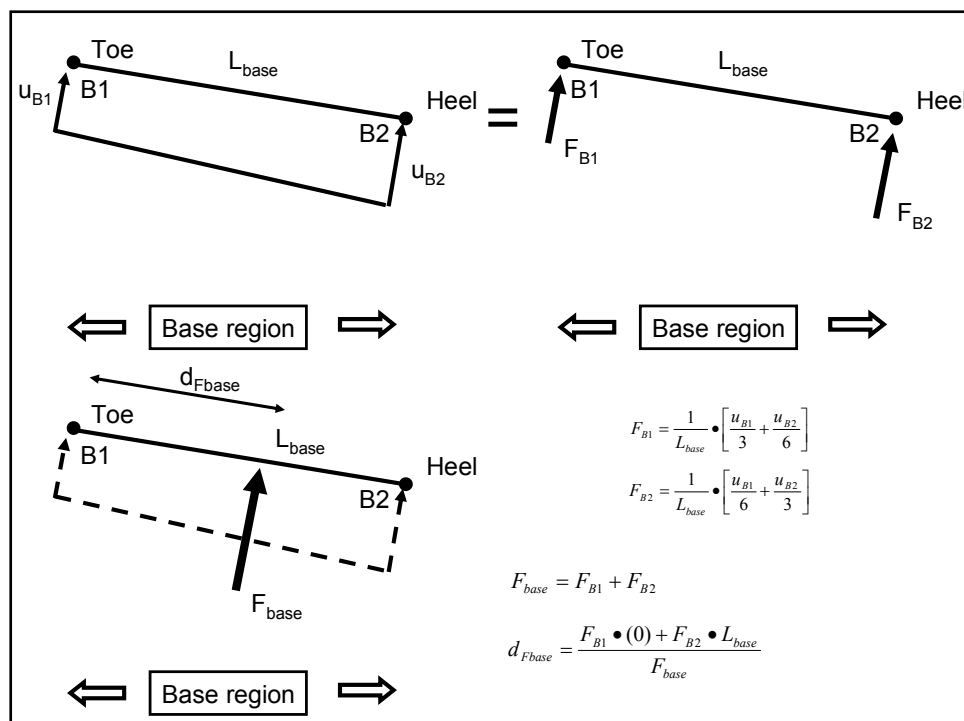


Figure D.2. Distribution of pore water pressures and its equivalent set of forces.

Also shown in Figure D.2 is a method for determining an equivalent resultant force, designated  $F_{base}$ , and its point of application  $d_{Fbase}$  (as measured from the toe) and its point of application. An expanded variation on this procedure is used by CorpsW<sub>all</sub>Rotate to compute the point of application of resultant force acting on each of the three regions identified in Figure D.1.

Global x- and y-coordinate forces are needed for the stability analysis of the structural wedge. They are computed for the equivalent point forces for each linear segment (defined by each adjacent pair of points) within each of the three regions. By specifying the Figure D.1 points in a counterclockwise fashion around the wetted perimeter of the structural wedge, the equivalent point forces acting normal to the wetted perimeter face (refer to Figure D.2) may be converted into x- and y- global coordinates using the procedure shown in Figure D.3. In this generalization, four hypothetical loaded faces, with each face defined by



extending point I to point J, are shown. The face loaded by water pressure for each hypothetical line segment is identified in this figure. The procedure to convert a normal force, for example, at each point J into its x- and y- global force components is outlined using the equations given in this figure. Key to using the equations given in this figure is to determine for a given I-to-J line segment which quadrant this line segment falls into. For the toe region, the three line segments shown in Figure D.1 fall within quadrants IV and II. The single line segment defining the base region falls within quadrant IV and the line segment defining the heel region falls within quadrant I, along the positive Y axis.

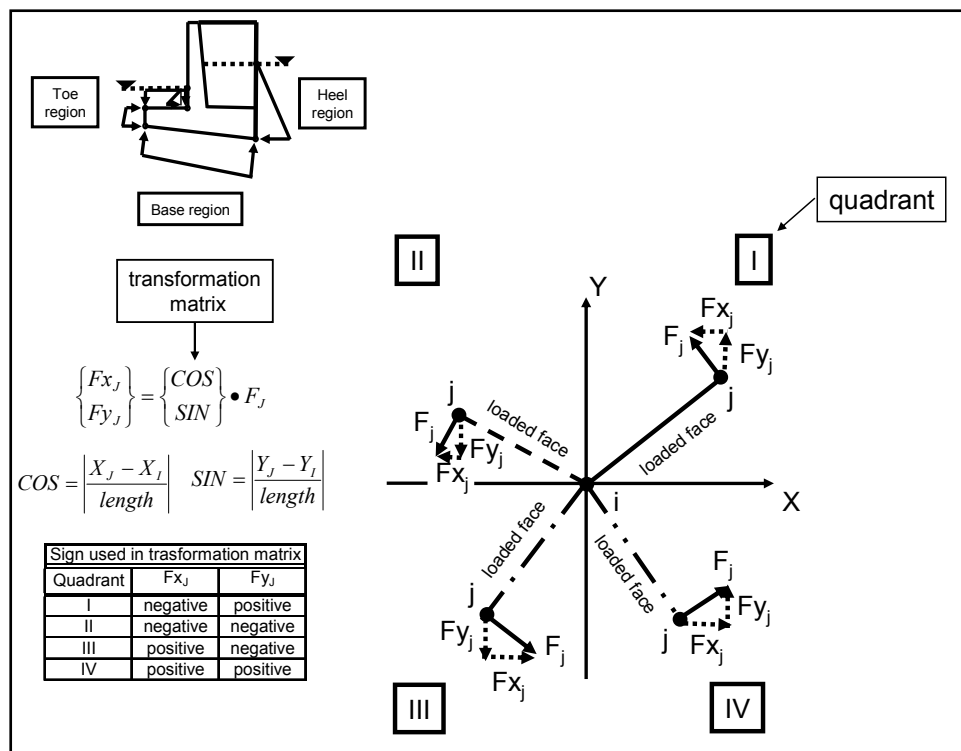


Figure D.3. Conversion of equivalent point forces at point J into global x- and y- coordinate forces.

In the case of rotation about the toe, contact between the base of the structural wedge and the foundation is lost sometime during earthquake shaking. Recall that a simplistic rigid base assumption is made in this formulation for rock-founded retaining structures. Due to the possible formation of a gap sometime during earthquake shaking, pore water pressures along the base may differ from those shown in Figure D.1. (No excess pore water pressures due to earthquake-induced shear strains within the soils are included in the current  $C_{orps}W_{all}Rotate$  formulation.) The exact pore water distribution within the structure-to-foundation gap is

a complex problem and a subject for state-of-the-art research. In  $C_{\text{Corps}}W_{\text{all}}\text{Rotate}$ , a simplistic assumption of the hydrostatic pore water pressure at the heel of the wall is extended to along the entire base of the structure, as shown in Figure D.4. This assumes that a gap opens early on during earthquake shaking during rotation about the toe of the retaining wall.

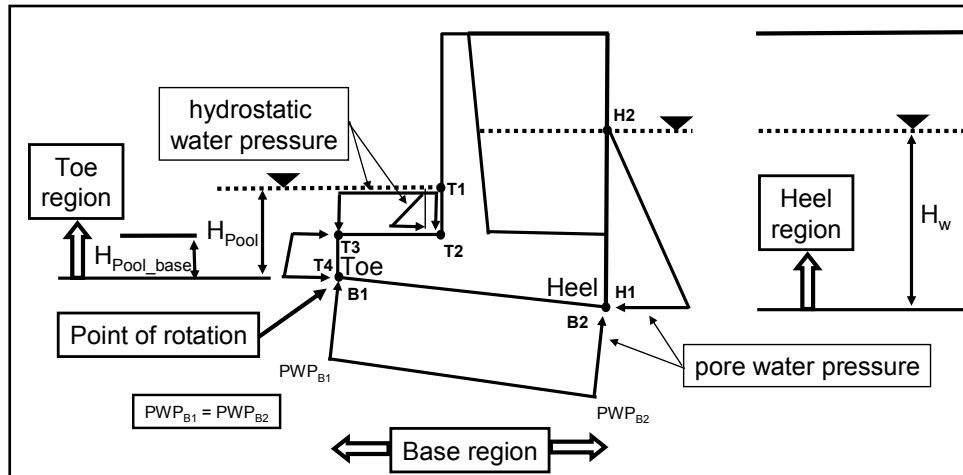


Figure D.4. Control points and water pressures acting normal to faces within the three regions of a structural wedge rotating about its toe – effective stress analysis.

**Total Stress Analysis:** In a total stress-based stability analysis, boundary water pressures are specified along the toe region only of the structural wedge. Knowledge of the internal (with respect to the soil and rock foundation) pore water pressures acting along/within the base region and the heel region of the structural wedge is not required in a total stress analysis.

Water pressure forces acting on the structural wedge are reported in the Workslide.TMP output file and the WORKrotate.TMP output file generated in each  $C_{\text{Corps}}W_{\text{all}}\text{Rotate}$  analysis. These files may be viewed using the visual modeler boxes labeled **Show Sliding Evaluation** and **Show Lift-Off Evaluation** on the **Analysis** tab, respectively.

## D.2 The Westergaard Procedure for Computing Hydrodynamic Water Pressures

Most Corps hydraulic structures that act as earth retaining structures possess a vertical face in contact with the pool (when present). The Westergaard procedure is used by  $C_{\text{Corps}}W_{\text{all}}\text{Rotate}$  for computing the magnitude of the hydrodynamic water pressures along the idealized rigid

walls during earthquake shaking. The solution developed by Westergaard (1931) is for the case of a semi-infinite long water reservoir retained by a concrete dam with a vertical face and subjected to a horizontal earthquake motion. The fundamental period of the concrete dam is assumed to be much smaller than the fundamental period of the earthquake so that the acceleration for the massive structure is approximated as the acceleration of the earthquake motion along the rigid base. This allows the problem of a very stiff concrete dam to be simplified to the case of a rigid vertical face moving at the same horizontal acceleration as the base horizontal acceleration. Using the equations of elasticity of a solid to describe the propagation of sounds in liquids (waves propagate without shear distortions) and with the water considered to be compressible, a solution to the equation of motion of the water was developed for a harmonic motion applied along the base of the reservoir. This solution ignores the effects of surface waves and is valid only when the period of the harmonic excitation is greater than the fundamental natural period of the reservoir (Chopra 1967). The fundamental period for the reservoir,  $T_w$ , is equal to

$$T_w = \frac{4 \cdot H_p}{C} \quad \text{D.1}$$

Where the velocity of sound in water,  $C$ , is given by

$$C = \sqrt{\frac{K}{\rho}} \quad \text{D.2}$$

And the mass density of water,  $\rho$ , is given by

$$\rho = \frac{\gamma_w}{g} \quad \text{D.3}$$

With the bulk modulus of elasticity of water,  $K$ , equal to  $4.32 \times 10^7$  lb/ft<sup>2</sup>, the unit weight for water,  $\gamma_w$ , equal to 62.4 lb/ft<sup>3</sup> and the acceleration due to gravity,  $g$ , equal to 32.17 ft/sec<sup>2</sup>,  $C$  is equal to 4,720 ft/sec. For example, with a depth of pool of water,  $H_p$ , equal to 25 ft,  $T_w$  is equal to 0.02 second (47 Hz) by Equation D.1.

The resulting relationship for hydrodynamic pressure on the face of the dam is a function of the horizontal seismic coefficient,  $k_h$  (expressed as a decimal fraction of acceleration of gravity,  $g$ ), the depth of water,  $Y_w$ , the

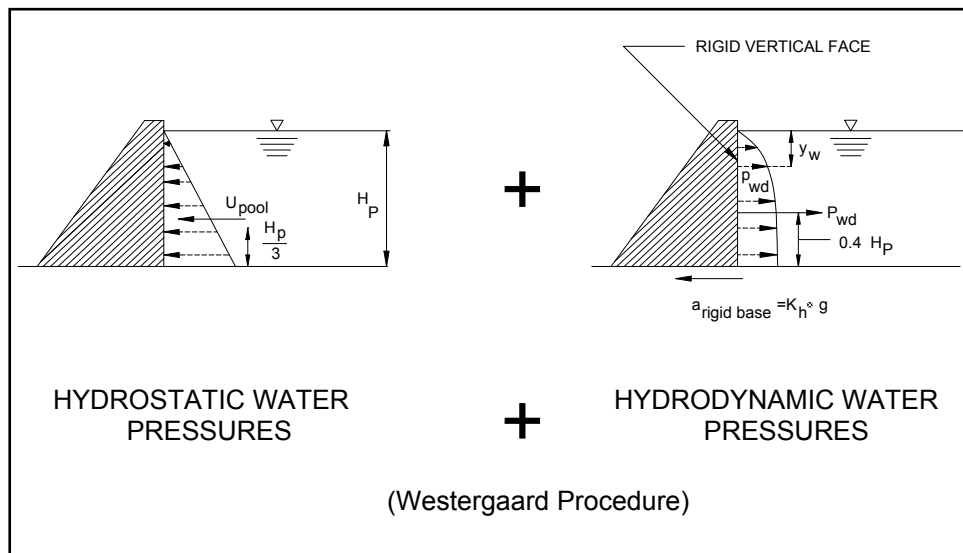
total depth of the pool of water,  $H_p$ , the fundamental period of the earthquake, and the compressibility of the water,  $K$ . The hydrodynamic pressure is opposite in phase to the base application and for positive base accelerations the hydrodynamic pressure is a tensile. Westergaard (1931) proposed the following approximate solution for the hydrodynamic water pressure distribution: a parabolic dynamic pressure distribution,  $p_{wd}$ , described by the relationship

$$p_{wd} = \frac{7}{8} \cdot k_h \cdot \gamma_w \cdot \sqrt{y_w \cdot H_p} \tag{D.4}$$

The resultant dynamic water pressure force,  $P_{wd}$ , is equal to

$$P_{wd} = \frac{7}{12} \cdot k_h \cdot \gamma_w \cdot (H_p)^2 \tag{D.5}$$

acting at an elevation equal to  $0.4 H_p$  above the base of the pool as shown in Figure D.5. This dynamic force does not include the hydrostatic water



pressure force acting along the face of the dam (refer to Figure D.5).

Figure D.5. Hydrostatic and Westergaard hydrodynamic water pressures acting along vertical wall during earthquakes.

Note that the value for  $P_{wd}$  is restricted to  $|P_{wd}| \leq U_{pool}$  in Corps Wall Rotate when acceleration(s) induce a hydrodynamic water pressure  $P_{wd}$  force

acting counter to the direction of the hydrostatic water pressure force,  $U_{\text{pool}}$ . This occurs in the case of the vector configuration for base acceleration(s) as shown in Figure D.5 (i.e., base acceleration(s) directed away from the body of the pool and towards the body of the dam).

In a maximum transmissible acceleration evaluation and during sliding in a Newmark sliding block time-history analysis of permanent displacement, the horizontal acceleration used to compute  $P_{\text{wd}}$  is a constant and equal to the value computed by Equation D.5 with  $k_h$  in this equation set equal to the maximum transmissible acceleration coefficient.  $H_p$  in Equation D.5 is set equal to the difference between the surface and the base height of the pool (i.e.,  $H_{\text{Pool}} - H_{\text{Pool\_base}}$ ) in  $C_{\text{orps}}W_{\text{allRotate}}$ . The initial version of  $C_{\text{orps}}W_{\text{allRotate}}$  implements the Westergaard hydrodynamic water pressure force Equation D.5 approximation in both the sliding and rotating block analysis. For a rigid block approximation and for the Corps hydraulic retaining structures with a vertical “wet” face (pool-side), the Westergaard procedure is considered a reasonable assumption by the primary author of this report. However, it is recognized that this assumption and approach is less accurate for the rotating block analysis than for the sliding block analysis because of the variation in horizontal accelerations along the wetted face of the structural wedge, as may be inferred by reference to the dependence of the horizontal acceleration on not only the ground acceleration as well as the angular acceleration, rotational velocity and *position of the point of interest* as noted in Equation 3.6 for Figure 3.3. In this initial version of  $C_{\text{orps}}W_{\text{allRotate}}$ , only the ground acceleration is used to compute  $P_{\text{wd}}$  using Equation D.5.<sup>1</sup> In a structural wedge analysis of incipient lift-off in rotation, the horizontal acceleration used to compute  $P_{\text{wd}}$  at incipient lift-off is another constant (of different value from the maximum transmissible acceleration value). Consequently, the value for  $P_{\text{wd}}$  is also a constant for the lift-off calculation. During a rotational time-history analysis, the magnitude of horizontal acceleration used to compute  $P_{\text{wd}}$  varies with time during rotation. So  $P_{\text{wd}}$  also varies in magnitude and direction with time in a rotational analysis in  $C_{\text{orps}}W_{\text{allRotate}}$ .

---

<sup>1</sup> Future improvements in  $C_{\text{orps}}W_{\text{allRotate}}$  will include the development of a more complete hydrodynamic water pressure force formulation that accounts for the variation in acceleration along the “wetted” face of the Corps hydraulic earth retaining structure during rotation by considering angular acceleration, rotational velocity, and *position of all points along the wetted face*.

## Appendix E: Mass Moment of Inertia Computation

This appendix outlines the mass moment of inertia computation for the structural wedge. Figure E.1 depicts the dynamic forces acting on the structural wedge as well as the ten material regions used to define this structural wedge that contains the retaining wall.

Each of the ten Figure E.2 material regions are labeled by a material region number and are either rectangular or triangular in shape. The user specifies the width and height of each of the ten material regions to define the geometry of the structural wedge. In the following two sections, the mass moments of inertia of a rectangle and a triangle are first derived. The mass moment of inertia of the entire structural wedge is then assembled from each of the ten material regions using one of these basic formulations.

Figure E.2 defines the reference points on each of the ten material regions. This point defines the left-most point on each material region. For rectangles and triangles with vertical left-hand sides, it is always the lower-most, left point. It is used to determine the position of each material region within  $C_{\text{orps}}W_{\text{all}}\text{Rotate}$ .

### E.1 Mass Moment of Inertia of a Rectangle

For a Figure E.3 rectangle of width  $b$  and height  $h$ , the cross-sectional area is

$$Area_{\text{rectangle}} = b \cdot h \quad \text{E.1}$$

and with a mass of rectangle of

$$M_{\text{rectangle}} = \frac{\gamma \cdot Area_{\text{rectangle}}}{g} \quad \text{E.2}$$

Note that the mass per unit volume is given by

$$m = \frac{\gamma}{g} \quad \text{bis. B.8}$$

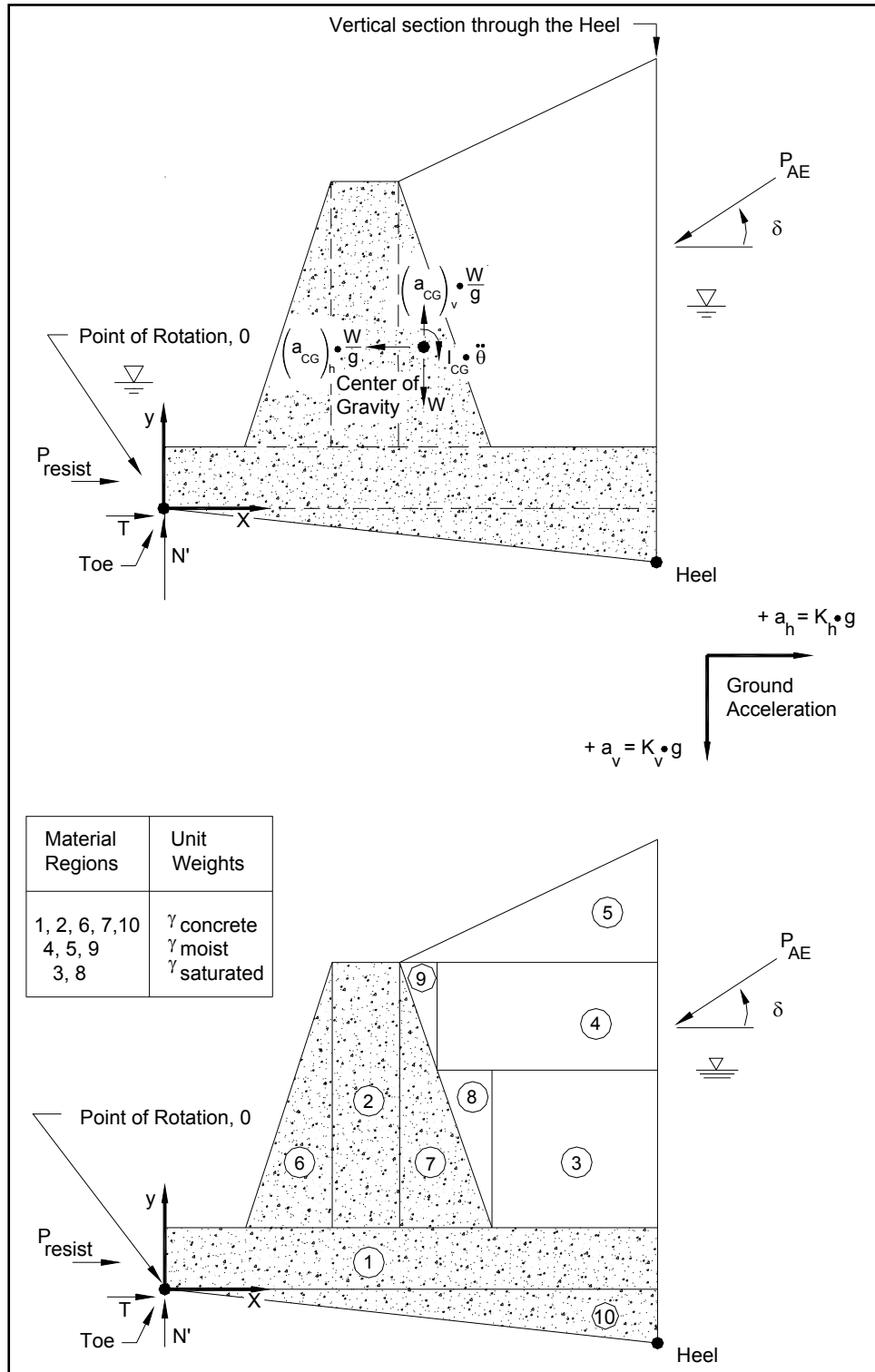


Figure E.1. Dynamic forces acting on the structural wedge and its material regions.

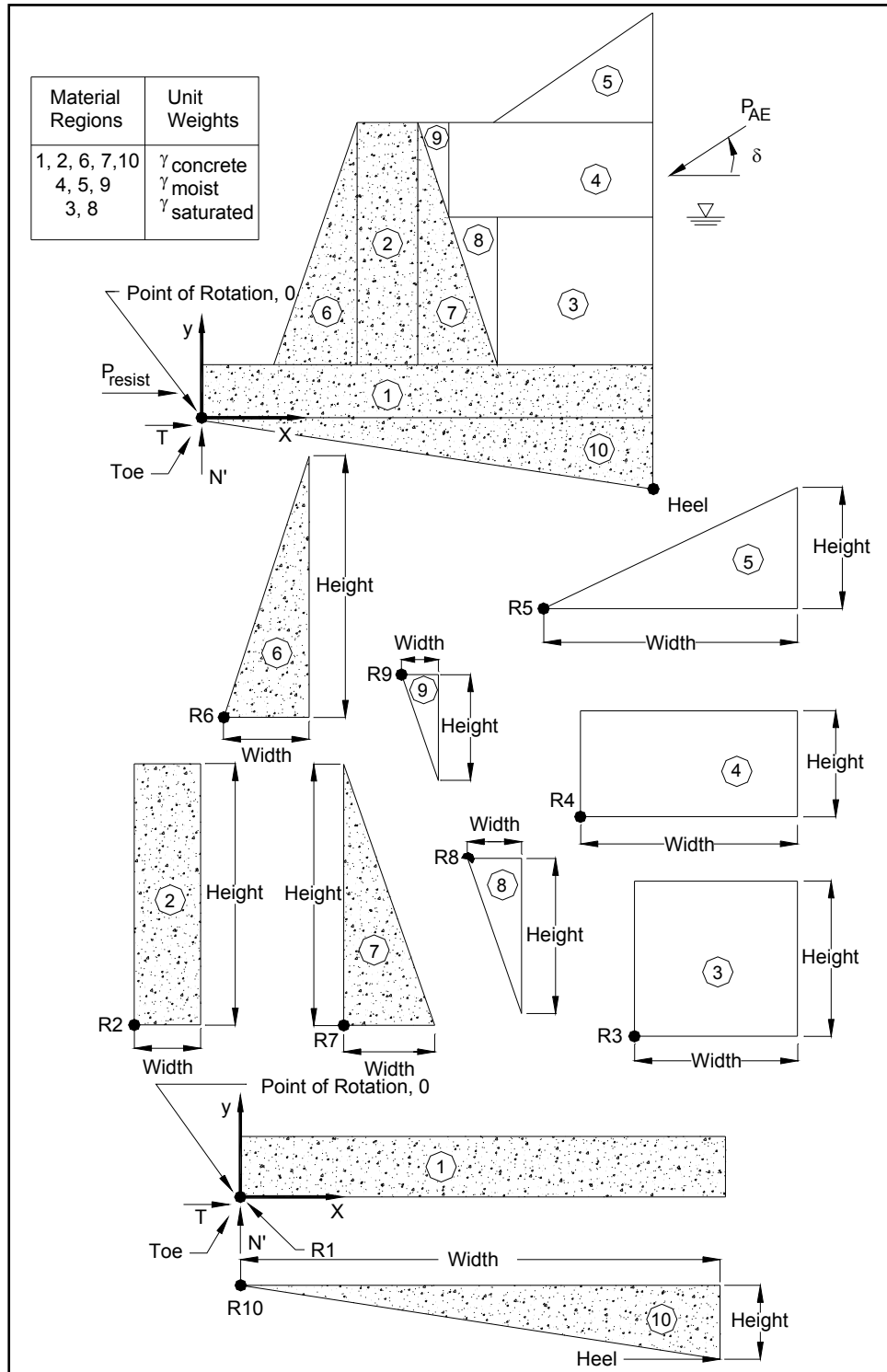


Figure E.2. The structural wedge comprises ten material regions.



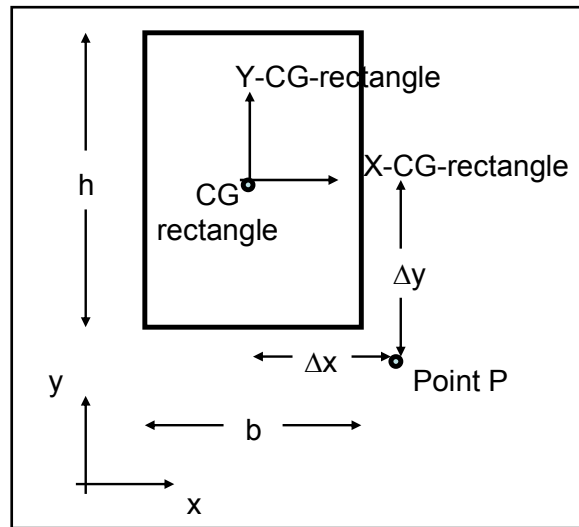


Figure E.3. Rectangle of width  $b$  and height  $h$ .

The x- and y- axes mass moments of inertia of the rectangle about the rectangle's center of gravity, CG, are

$$I_{x\text{-CG-rectangle}} = \left(\frac{\gamma}{g}\right) \cdot \frac{1}{12} \cdot b \cdot (h)^3 \quad \text{E.3}$$

and

$$I_{y\text{-CG-rectangle}} = \left(\frac{\gamma}{g}\right) \cdot \frac{1}{12} \cdot h \cdot (b)^3 \quad \text{E.4}$$

Let the distance between the center of gravity of the rectangle to an arbitrary point P be equal to  $\Delta x$  and  $\Delta y$ .

The x- and y- axes mass moments of inertia of the rectangle about point o are

$$I_{x-P} = I_{x\text{-CG-rectangle}} + \left(\frac{\gamma \cdot \text{Area}_{\text{rectangle}}}{g}\right) \cdot (\Delta y)^2 \quad \text{E.5}$$

and

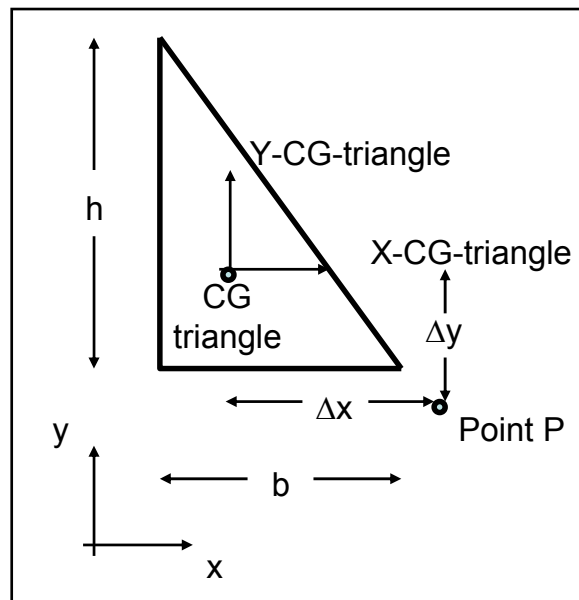
$$I_{y-P} = I_{y\text{-CG-rectangle}} + \left(\frac{\gamma \cdot \text{Area}_{\text{rectangle}}}{g}\right) \cdot (\Delta x)^2 \quad \text{E.6}$$

## E.2 Mass Moment of Inertia of a Triangle

For a Figure E.4 triangle of base width  $b$  and height  $h$ , the cross-sectional area is

$$Area_{triangle} = \frac{1}{2} \cdot b \cdot h \quad E.7$$

and with a mass of triangle of



$$M_{triangle} = \frac{\gamma \cdot Area_{triangle}}{g} \quad E.8$$

Figure E.4. Triangle of base width  $b$  and height  $h$ .

The  $x$ - and  $y$ - axes mass moments of inertia of the triangle about its center of gravity, CG, are

$$I_{x-CG-triangle} = \left( \frac{\gamma}{g} \right) \cdot \frac{1}{36} \cdot b \cdot (h)^3 \quad E.9$$

and

$$I_{y-CG-triangle} = \left( \frac{\gamma}{g} \right) \cdot \frac{1}{36} \cdot h \cdot (b)^3 \quad \text{E.10}$$

Let the distance between the center of gravity of the triangle to an arbitrary point P be equal to  $\Delta x$  and  $\Delta y$ .

The x- and y- axes mass moments of inertia of the triangle about point o are

$$I_{x-P} = I_{x-CG-triangle} + \left( \frac{\gamma \cdot \text{Area}_{triangle}}{g} \right) \cdot (\Delta y)^2 \quad \text{E.11}$$

and

$$I_{y-P} = I_{y-CG-triangle} + \left( \frac{\gamma \cdot \text{Area}_{triangle}}{g} \right) \cdot (\Delta x)^2 \quad \text{E.12}$$

### E.3 Mass Moment of Inertia of the Structural Wedge

The center of gravity of the structural wedge is computed in  $C_{orps}W_{all}Rotate$  following the procedure described in Section B.3. The mass moment of inertia about this center of gravity is computed using either Equations E.5 and E.6 for a rectangle or Equations E.11 and E.12 for a triangle, for each of the ten material regions and with point P assigned to the coordinate of the center of gravity of the structural wedge. The mass moment of inertia about the center of rotation of the structural wedge, point o in Figure E.1, is computed using Equation 3.16.

## Appendix F: Listing and Description of CorpsWallRotate ASCII Input Data File (file name: CWROTATE.IN)

This appendix lists and describes the contents of the ASCII input data file to the FORTRAN engineering computer program portion of CorpsWallRotate. This data file, always designated as CWROTATE.IN, is created by the graphical user interface (GUI), the visual modeler portion of CorpsWallRotate.

### First line/First column – Designate this data input is for a CorpsWallRotate analysis

Type a capital **R** in the first column of the first line.

The ASCII input data to CorpsWallRotate are provided in eight groups of data. They are as follows:

#### Group 1 – Global Geometry of the Structural Wedge that Contains the Retaining Wall

<b>XTOE, YTOE</b>	X and Y coordinates of the toe of the wall.
<b>XROTATE, YROTATE</b>	X and Y coordinates of the point of rotation.
<b>XHEEL, YHEEL</b>	X and Y coordinates of the heel of the wall.
<b>Gweight, Gmass, Gconstant</b>	Weight and mass of the structural wedge. The value for Gconstant identifies the units of length, density, force, and pressure being used according to the table below.
<b>GXCG, GYCG</b>	X and Y coordinates of the center of gravity.
<b>GIXmassptO, GIYmassptO, GjmassptO</b>	X-mass moment of inertia about the point of rotation, Y-mass moment of inertia about the point of rotation, and the mass moment of inertia about the point of rotation.

Value for Gconstant	Units of Length	Units of Soil and Concrete Densities	Units of Force	Units of Pressure
32.174	feet	lb/ft <sup>3</sup>	lb	lb/ft <sup>2</sup>
386.086	inches	lb/in <sup>3</sup>	lb	lb/in <sup>2</sup>
9.80665	meters	kN/m <sup>3</sup>	kN	kN/m <sup>2</sup> (=kPa)
980.665	centimeters	kN/cm <sup>3</sup>	kN	kN/cm <sup>2</sup>
9806.65	millimeters	kN/mm <sup>3</sup>	kN	kN/mm <sup>2</sup>

### Group 2 – Base of Structural Wedge

#### PHI<sub>i</sub>, C<sub>i</sub>, PHI<sub>f</sub>, C<sub>f</sub>, ISTRENGTH<sub>sw</sub>

C<sub>i</sub> and PHI<sub>i</sub> are the Mohr-Coulomb shear strength parameters for the base of wall-to-foundation interface.

C<sub>f</sub> and PHI<sub>f</sub> are the Mohr-Coulomb shear strength parameters for the foundation.

and

ISTRENGTH<sub>sw</sub> = 1 Strength definition below the structural wedge – Effective Stress

ISTRENGTH<sub>sw</sub> = 2 Strength definition below the structural wedge – Total Stress

Note:

In a Total Stress Analysis PHI is set equal to zero, and C is set equal to the value for the undrained shear strength, S<sub>u</sub>, for the base of wall-to-foundation interface and the foundation, respectively. Internal pore water pressures are not considered explicitly in total stress analyses, but the effects of the pore pressures in the undrained tests are reflected in the undrained shear strength value, as discussed in Duncan and Buchignani (1975). Consequently, uplift pressures acting normal to the foundation interface are not included in the free-body force diagram of the structural wedge in a total stress analysis by C<sub>orps</sub>W<sub>all</sub>Rotate.

### Group 3 – Resisting Force Normal to a Vertical Plane Extending up Through the Toe of the Structural Wedge

**XRESIST, YRESIST, FXRESIST** X and Y coordinates of the resisting horizontal force, and the value of the horizontal force in consistent units.

#### **Group 4 – Driving Wedge in the Retained Soil**

**PHI, C, DELTA**

**H, HLEVEL, BETA**

**GAMAMOIST, GAMASAT**

**SLIPMIN**

**ISTRENGTHdw**

C and PHI are the Mohr-Coulomb shear strength parameters for the retained soil (i.e., the backfill), and DELTA is the interface friction along the vertical plane extending up through the heel of the structural wedge.

GAMAMOIST is the moist unit weight of the retained soil and GAMASAT is the saturated unit weight in consistent units (force/length<sup>3</sup>).

H is the height of the vertical plane extending up from the heel of the structural wedge to the ground surface ( $H \leq HLEVEL$ ).

BETA is the slope of the ground surface of the retained soil in degrees (BETA = 0 if HLEVEL = H).

HLEVEL is the height to level retained soil as measured from the heel of the wall/structural wedge ( $HLEVEL \geq H$ ).

Note: For the infinite slope problem, input a large value for HLEVEL such that the critical, planer slip surface computed within the retained soil does not intersect the fictitious (imaginary) level retained soil ground surface.

SLIPMIN is the shallowest planar slip surface that a potential slip surface can achieve in the retained soil. SLIPMIN is measured from horizontal and specified in degrees (a value between 1 and 89 degrees).

with

ISTRENGTHdw = 1 Soil Strength definition within retained soil – Effective Stress

ISTRENGTHdw = 2 Soil Strength definition within retained soil – Total Stress

Note:

In a Total Stress Analysis PHI is set equal to zero and C is set equal to the value for the undrained shear strength,  $S_u$ , of the retained soil (i.e., the backfill). Internal pore water pressures are not considered explicitly in total stress analyses, but the effects of the pore pressures in the undrained tests are reflected in the undrained shear strength value, as discussed in Duncan and Buchignani (1975). Consequently, pore water pressures acting

normal to the potential slip plane within the retained soil are not included in the free-body force diagram of the soil wedge in a total stress analysis by  $C_{\text{ Corps Wall Rotate}}$ .

### **Group 5 – Water Table Height in the Retained Soil and Pool Height, with Input in Four Parts**

#### **Part 1: GAMAW**

#### **HW, HPool, HPool\_base**

with

GAMAW is the unit weight of water in consistent units (units of force/length<sup>3</sup>).

HW is the height of water table in the retained soil (i.e., the backfill) as measured from the heel of the wall of the structural wedge.

HPool is the height of pool in front of the wall as measured from the toe of the wall of the structural wedge.

and

HPool\_base is the height to the base of the pool as measured from the toe of the wall of the structural wedge ( $\text{HPool\_base} \leq \text{HPool}$ ).

Note:

For no water table in the retained soil (i.e., a “dry” backfill), HW is set equal to zero.

For no pool in front of the wall, HPool and HPool\_base are equivalent and set equal to zero.

Data provided in subsequent three parts define points along each of the three wetted perimeter regions of the structural wedge. The first point specified is at the intersection of the pool with the exposed face of the wall. All subsequent points are specified in a counterclockwise fashion progressing around the wetted perimeter of the structural wedge (of toe region to base region to heel region).

*Special case; “dry” site: In the case of a “dry” site, HW, HPool, and HPool\_base are all set to zero. Skip Parts 2, 3 and 4 input.*

**Skip Part 2 input if HPool = 0.**

**Part 2: nWetToePTS****X\_Wet\_Toe<sub>i</sub>, Y\_Wet\_Toe<sub>i</sub> (i=1 to nWetToePTS)**

with

nWetToePTS is the total number of points defining the exposed wetted perimeter face of the wall and progressing from the pool of water to the toe of the wall, including the point defining the intersection of the base of the pool and the wetted wall face.

X\_Wet\_Toe<sub>i</sub>, Y\_Wet\_Toe<sub>i</sub> are the coordinates of the exposed wetted perimeter face of the wall and progressing from the pool of water to the toe of the wall.

Note: The coordinates of the point defined by the intersection of the exposed wetted perimeter and the base of the pool are to be included in the nWetToePTS points.

**Part 3: nWetBasePTS****X\_Wet\_Base<sub>i</sub>, Y\_Wet\_Base<sub>i</sub> (i=1 to nWetBasePTS)**

with

nWetBasePTS is the total number of points defining the wetted perimeter face of the base of structure-to-foundation interface and progressing from the toe to the heel of the wall.

X\_Wet\_Base<sub>i</sub>, Y\_Wet\_Base<sub>i</sub> are the coordinates of the exposed wetted perimeter face of the base of structure-to-foundation interface and progressing from the toe to the heel of the wall of the structural wedge.

Note: nWetBasePTS is set equal to 2 and the coordinates of the toe and the heel of the wall are provided as input.

**Skip Part 4 input if HW = 0.**

**Part 4: nWetHeelPTS****X\_Wet\_Heel<sub>i</sub>, Y\_Wet\_Heel<sub>i</sub> (i=1 to nWetHeelPTS)**

with

nWetHeelPTS is the total number of points defining the wetted perimeter face of the structural wedge to soil driving wedge interface, progressing along a vertical imaginary section extending upwards from the Heel of the wall to the surface of the water table in the retained soil.

X\_Wet\_Heel<sub>i</sub>, Y\_Wet\_Heel<sub>i</sub> are the coordinates of the wetted perimeter face of the structural wedge to soil driving wedge interface, progressing



along a vertical imaginary section extending upwards from the heel of the wall to the surface of the water table in the retained soil.

Note: nWetHeelPTS is set equal to 2 and the coordinates of a line defined by two points, (1) the heel of the wall and (2) the point defined by the intersection of a vertical line extending from the heel to the surface of the water table.

### **Group 6 – Acceleration Time-Histories with Input in Two Parts**

#### **Part 1: NOACC, DT, GACC, XSCALE, YSCALE, KEYACCY**

with

NOACC is the total number of acceleration time-history values.

DT is the time-step in seconds.

GACC is the constant of acceleration due to gravity as given in the table below.

XSCALE is the scale factor applied to the horizontal acceleration time-history (negative value to invert time-history).

YSCALE is the scale factor applied to the vertical acceleration time-history (negative value to invert time-history).

and

KEYACCY is set to 0 in the case of horizontal and vertical acceleration time-histories.

or

KEYACCY is set to 1 in the case of a horizontal acceleration time history and a constant vertical acceleration value. (When KEYACCY = 1, KEYkv must be set equal to 3 in Group 6 Analysis control data.)

Value for GACC	Units
32.174	ft/sec <sup>2</sup>
386.086	in/sec <sup>2</sup>
9.80665	m/sec <sup>2</sup>
980.665	cm/sec <sup>2</sup>
9806.65	mm/sec <sup>2</sup>
1.0	G
980.665	gal

**Part 2:** In the case of KEYACCY = 0, input  
**T(i=1 to NOACC), ACCX(I=1 to NOACC), ACCY(I=1 to NOACC)**

or

In the case of KEYACCY = 1, input  
**T(i=1 to NOACC), ACCX(I=1 to NOACC)**

Note:

1. Horizontal and vertical inertial forces act in the direction opposite to the direction of the horizontal and vertical accelerations.
2. All time-histories are required to have zero acceleration value(s) for T(1) = 0.0 in the data input file.
3. Values for the horizontal accelerations used in C<sub>orps</sub>W<sub>all</sub>Rotate are equal to ACCX(I) times XSCALE times GACC.
4. Values for the vertical accelerations used in C<sub>orps</sub>W<sub>all</sub>Rotate are equal to ACCY(I) times YSCALE times GACC.

### **Group 7 – Analysis Controls**

#### **KEYkv, constACCY, KEYanalysis**

with

KEYkv = 1 Use the vertical acceleration time-history ACCY(I=1 to NOACC) to determine a representative constant value for the vertical acceleration during those time-steps when the structural wedge slides. This requires an iterative process involving sequential executions of C<sub>orps</sub>W<sub>all</sub>Rotate, during which an updated value for the constant constACCY is specified.

Note:

1. KEYanalysis (see input below) must be set equal to 1 in this case and value for constACCY (see input below) is required.
2. Recommendation: For the first evaluation, the value for constACCY is usually set equal to zero.
3. Recommendation: For the second evaluation, the value for constACCY may be set to the average value for the vertical acceleration computed during those time-steps when the structural wedge slides (reported in the C<sub>orps</sub>W<sub>all</sub>Rotate output), determined from the output from the first KEYkv = 1 analysis.
4. The KEYanalysis =1 analysis is repeated using updated constACCY values until the change in constACCY value and the vertical acceleration computed during those time-steps when the structural wedge slides is sufficiently small.

KEYkv = 2 Evaluation using the current vertical acceleration time-history ACCY(I=1 to NOACC).

Note: KEYanalysis (see input below) must be set equal to 2 in this case.

KEYkv = 3 Evaluation using a constant value for the vertical acceleration constACCY (see below).

Note:

1. KEYkv must be set equal to 3 when KEYACCY = 1 (in Group 6 data).
2. KEYanalysis (see below) can be set equal to 1, 2, or 3 in this case.

with

constACCY = Constant value for the vertical acceleration. This can be an average vertical acceleration during sliding or during rotation. Specified in the same units as the acceleration time-histories of Group 6 (Units consistent with the value of GACC).

Note: Value for constACCY is used to compute the value for the horizontal yield acceleration in a sliding analysis (designated as cofkhslide in the output file WORKslide.TMP) or to compute the value for the horizontal acceleration for which there is incipient lift-off of the structural wedge from its foundation in rotation (designated as cofkhrotate in the output file WORKrotate.TMP).

and

KEYanalysis = 1 Sliding analysis of the structural wedge.

KEYanalysis = 2 Rotating analysis of the structural wedge.

KEYanalysis = 3 Conduct either a sliding or rotating rigid block analysis of the Structural Wedge using a constant value for the vertical acceleration (KEYkv must be set equal to 3). A sliding analysis is conducted when the value of the horizontal maximum transmissible acceleration, cofkhslide, is less than the value of the horizontal acceleration for which there is incipient lift-off of the structural wedge from its foundation in rotation, cofkhrotate; otherwise a rotating block analysis is conducted.

### **Group 8 – Units for Output of Acceleration, Velocity, and Displacement Time-Histories**

**DISPACC** The value for DISPACC identifies the units of the scaled acceleration, computed velocity, and computed displacements according to the table below.

Value for DISPACC	Units of Acceleration	Units of Velocity	Units of Displacement
32.174	ft/sec <sup>2</sup>	ft/sec	ft
386.086	in/sec <sup>2</sup>	in/sec	in.
9.80665	m/sec <sup>2</sup>	m/sec	m
980.665	cm/sec <sup>2</sup>	cm/sec	cm
9806.65	mm/sec <sup>2</sup>	mm/sec	mm

## Appendix G: Listing of CorpsW<sub>all</sub>Rotate ASCII Output Files

This appendix lists the CorpsW<sub>all</sub>Rotate ASCII Output Files. Table G.1 lists the output box labels and corresponding (tape) files for the visual modeler **Analysis** tab and briefly describes the contents.

Table G.1. Output data files used by output boxes in the visual modeler Analysis tab.

Visual Modeler Output Box Label	Name of Tape	Description
Show Log of CWRotate Execution	CWROTATE.RUN	Summary of execution steps and limited results.
Show Input Echo of CWRotate Execution	CWROTATE.OUT	Echo of key input variables assigned by the visual modeler.
Plot AccX	PLOTaccX.TMP	Scaled horizontal acceleration time-history.
Show AccX	WORKaccX.TMP	Show data file of scaled horizontal acceleration time-history.
Plot AccY	PLOTaccY.TMP	Scaled vertical acceleration time-history.
Show AccY	WORKaccY.TMP	Show data file of scaled vertical acceleration time-history.
Plot AccYX	PLOTaccYX.TMP	Scaled X- and Y- time-histories and ratio of a scaled-ACCY divided by scaled-ACCX.
Show AccYX	WORKaccYX.TMP	Show data file of scaled X- and Y- time-histories and ratio of a scaled-ACCY divided by scaled-ACCX.
Show Sliding Evaluation	WORKslide.TMP	Iteration results for Maximum Transmissible Acceleration; yield acceleration (horizontal) for structural wedge slide limit state. Boundary water pressures to the structural wedge, when present, are listed in this file. When water is present, the resultant water pressure forces acting on the structural wedge are reported in this file.
Show Lift-Off Acceleration	WORKrotate.TMP	Iteration results for Maximum Acceleration resulting in lift-off of the structural wedge from its foundation with rotation about its toe. Boundary water pressures to the structural wedge, when present, are listed in this file. When water is present, the resultant water pressure forces acting on the structural wedge are reported in this file.
Plot PA File	PLOTpa.TMP	Sweep-search wedge results of $\alpha$ versus P and the resulting static active earth pressure force $P_A$ . A single sweep-search wedge solution is contained in this file using SMF = 1.0.

Visual Modeler Output Box Label	Name of Tape	Description
Show PA File	WORKpa.TMP	Sweep-search wedge results of $\alpha$ versus P and the resulting static active earth pressure force, $P_A$ . A single sweep-search wedge solution is contained in this file, calculated using SMF = 1.0.
Plot PO File	PLOTpo.TMP	Sweep-search wedge results of $\alpha$ versus P and the resulting approximation for the static at-rest earth pressure force $P_o$ . A single sweep-search wedge solution is contained in this file, calculated using SMF = $1/1.5=0.67$ . The value for $P_o$ is not used in the sliding nor rotational rigid block calculations of the initial version of CWRotate.
Show PO File	WORKpo.TMP	Sweep-search wedge results of $\alpha$ versus P and the resulting approximation for the static at-rest earth pressure force $P_o$ . A single sweep-search wedge solution is contained in this file, calculated using SMF = $1/1.5=0.67$ . The value for $P_o$ is not used in the sliding nor rotational rigid block calculations of the initial version of CWRotate.
Plot PAE File	PLOTpae.TMP	Sweep-search wedge results of $\alpha$ versus P and the resulting dynamic active earth pressure force, $P_{AE}$ . This file contains results from multiple analyses. When a rotational rigid block time-history analysis is conducted, this file can become quite large. Drop down menu options can be used to plot user selected $P_{AE}$ plot numbers. $P_{AE}$ run numbers are identified in various output files.
Show PAE File	WORKpae.TMP	Sweep-search wedge results of $\alpha$ versus P and the resulting dynamic active earth pressure force, $P_{AE}$ . This file contains results from multiple analyses. When a rotational rigid block time-history analysis is conducted this file can become quite large. Drop down menu options can be used to view user selected $P_{AE}$ analyses. $P_{AE}$ run numbers are identified in other output files.
Plot Sliding Time-history	PLOTslideTH.TMP	Time-history of sliding block analysis.
Show Sliding Time-history	PLOTslideTH.TMP	Show data file of time-history of sliding block analysis.
Plot Rotating Time-history	PLOTrotatTH.TMP	Time-history of rotating block analysis.
Show Rotating Time-history	PLOTrotatTH.TMP	Show data file of time-history of rotating block analysis.
Show Moments about the Rotation Point	WORKrotatTH1.TMP	Time-histories of overM, restoreM, $P_{AE}$ , ALPHAr1
Show Rotational Values	WORKrotatTH2.TMP	Time-histories of ALPHAr1, OMEGAR1, THETAr1, totTHETAr1

Visual Modeler Output Box Label	Name of Tape	Description
Show Forces acting on the Structural Wedge in Rotation	WORKrotatTH3.TMP	Time-histories of overM, restoreM, Pae, Hpaе, Nbase, Tultbase
Plot Effective Vertical Acc.	PLOTKEYkv1TH.TMP	Time-history of effective vertical acceleration during sliding or rotation analysis with KEYkv = 1
Show Effective Vertical Acc.	PLOTKEYkv1TH.TMP	Show data file of time-history of effective vertical acceleration during sliding or rotation analysis with KEYkv = 1

A second table, Table G.2 lists other tape files generated in each Corps Wall Rotate analysis and briefly describes the contents.

**Table G.2. Output data files used by output boxes in the visual modeler Analysis tab.**

Name of Tape	Description
–	Print to screen a summary of execution steps and limited results. Same information as is contained in CWROTATE.RUN.
OUTPUTpa.TMP	Summary of forces acting on each wedge in a sweep search wedge analysis of $\alpha$ versus $P_A$ (static active earth pressure force). A single sweep-search wedge solution is contained in this file.
OUTPUTpo.TMP	Summary of forces acting on each wedge in a sweep search wedge analysis of $\alpha$ versus $P_o$ (static at-rest earth pressure force). A single sweep-search wedge solution is contained in this file.
OUTPUTpae.TMP	Summary of forces acting on each wedge in a sweep-search wedge analysis of $\alpha$ versus $P_{AE}$ (pseudo-static active earth pressure force). This file contains results from multiple analyses. When a rotational rigid block time-history analysis is conducted, this file can become quite large.

## Appendix H: Earth Pressure Distribution and Depth of Cracking in a Cohesive Retained Soil – Static Active Earth Pressures

This appendix summarizes for static loading the results of sweep-search analyses of two types of cohesive soils, the first being an effective stress analysis with Mohr-Coulomb effective stress shear strength parameters  $c'$  and  $\phi'$  used to characterize the shear strength of the retained soil and the second case for a backfill in which Mohr-Coulomb total stress shear strength parameter  $c$  is set equal to the undrained shear strength,  $S_u$ , and with  $\phi$  set equal to zero. The objective of this appendix is to demonstrate the trial-and-error procedure used to determine the depth of cracking in a cohesive soil as well as the resulting static active earth pressure distribution that is applied to the structural wedge in a  $C_{orps}W_{all}Rotate$  analysis.

Background: The sole purpose of a  $P_A$  computation in a  $C_{orps}W_{all}Rotate$  analysis is to determine the value for  $h_{PAE}$ , the resultant location for  $P_{AE}$ . The procedure used is outlined in Appendix C. The approach used can also be interpreted in terms of an equivalent earth pressure distribution applied to the structural wedge by the driving soil wedge in a  $C_{orps}W_{all}Rotate$  analysis that is made up of two components, the earth pressure distribution due to the static active earth pressures and a trapezoidal earth pressure distribution due to the incremental dynamic force component  $\Delta P_{AE}$  (with  $\Delta P_{AE} = P_{AE} - P_A$ ). The methodologies discussed in Appendix A are used by  $C_{orps}W_{all}Rotate$  to first determine the resultant earth pressure forces,  $P_A$  and  $P_{AE}$ , and then the methodologies discussed in Appendix C are used to compute the resulting earth pressure distributions for  $P_A$  and  $\Delta P_{AE}$ , respectively. In order to compute values of  $P_{AE}$  and  $P_A$  by the dynamic and static sweep-search solutions of trial soil wedges, a depth of cracking needs to be specified in each sweep-search analysis made by  $C_{orps}W_{all}Rotate$  of a cohesive soil. Initial sweep-search soil wedge solutions are always made assuming a zero depth of crack. This is sufficient for the  $P_{AE}$  computation, as discussed previously. However, an iterative procedure is used to determine the value for the depth of cracking in the analysis of  $P_A$  in cohesive soils and the corresponding earth pressure distribution (which includes both compression as well as tensile stresses).



After the resulting static earth pressure force,  $P_A$ , computation is completed, a resulting earth pressure distribution is constructed and new depth of cracking for static loading is determined.  $C_{orps}W_{all}Rotate$  then proceeds with second sweep-search trial wedge analysis of the retained soil for a new value for  $P_A$  corresponding to this new, nonzero crack depth value. A new static earth pressure distribution and new crack depth are determined. The process is repeated until the depth of cracking used in the sweep-search trial wedge analysis and the depth of cracking determined from the static active earth pressure distribution are nearly the same value. This iterative procedure is demonstrated for two examples in this appendix.

In the special case of cohesive soils, the  $C_{orps}W_{all}Rotate$  analysis disregards the tensile stresses when defining the static active earth pressures and the corresponding resulting static active earth pressure force to be applied to the structural wedge, as well as when computing the resulting force location,  $h_{PA}$ , of this modified stress distribution. A trapezoidal earth pressure distribution is used to define  $\Delta P_{AE}$  for cohesive as well as cohesionless soils.

### **H.1 Example No. 1: Effective Stress Analysis of a Cohesive Soil**

Consider the case of the Figure H.1 20-ft high, moist, cohesive, retained soil with  $c' = 200$  psf,  $\phi' = 10$  degrees,  $\delta = 0$  degrees, and  $\gamma_{moist} = 110$  psf. The first step in the  $C_{orps}W_{all}Rotate$  analysis of this static earth pressure problem is a sweep search trial wedge analysis starting with assumption that the depth of cracking is equal to zero. This results in a computed  $P_A$  value equal to 8,105.9 per ft run of wall using the method outlined in Section A.3 of Appendix A for a planar slip surface with  $\alpha_A$  computed to be 50 degrees from horizontal. The second step is to compute the corresponding earth pressure distribution and depth of cracking using the procedure outlined in Section C.3 of Appendix C. This active earth pressure distribution resulted in a depth of cracking equal to 4.767 ft. Ignoring the tensile stresses within the depth of cracking, as is done by  $C_{orps}W_{all}Rotate$ , the resultant net force,  $P_{AstaticPOSa}$ , corresponding to the computed triangular compressive earth pressure stress distribution, is equal to 8,985.9 lb per ft run of wall with a point of application at 5.078 ft at the end of this first iteration. These results are consistent with the results given in Example 6-4 of Bowles (1968). Since the depth of cracking from the active earth pressure distribution (i.e., 4.767 ft) is so different

from the value assumed in the sweep search trial wedge solution for  $P_A$  (i.e., 0 ft), additional analyses are required.

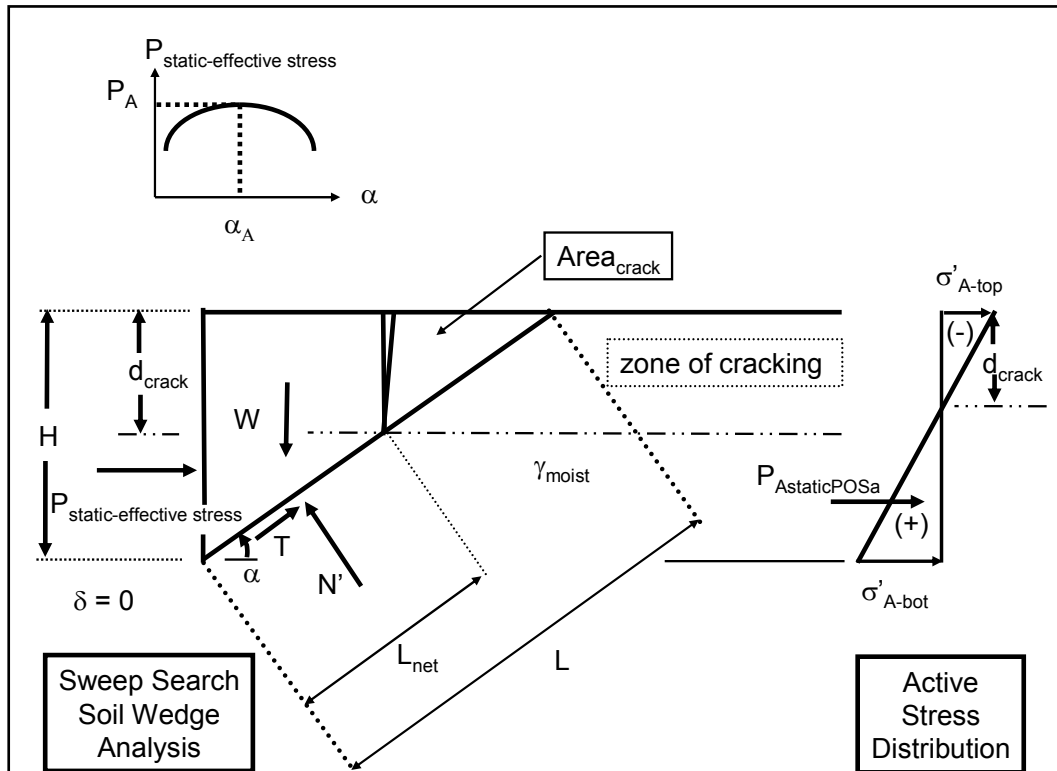


Figure H.1. Sweep-search trial wedge analysis of a cohesive retained soil and the corresponding active earth pressure distribution — effective stress analysis.

The second sweep-search trial wedge analysis starts with an assumption of 4.767 ft for the depth of cracking, as indicated in Table H.1. A total of four iterations are required to converge on a depth of cracking in which the depth of crack used in the sweep-search soil wedge analysis results is consistent with the depth of cracking resulting from the active stress distribution. In the final iteration (i.e., number 4), the net active force corresponding to the compressive stress distribution starting 3.973 ft below top of wall is equal to 9,549.7 lb per ft run of wall. Note that the sweep-search active soil wedge solution for  $\alpha_A$  equal to 50 degrees is computed to be equal to 8,962.9 lb per ft run of wall. These two values differ because  $P_A$  is computed by the sweep-search (active) wedge solution and includes the contribution of tensile stresses due to cohesion in the retained soil (e.g., refer to Equation A.27).

Table H.1. Iterative results from the static sweep-search wedge analysis of a cohesive soil – effective stress.

Iteration No.	Depth of Crack Used in Sweep-Search Soil Wedge Analysis (ft)	$\alpha_A$ (deg)	$P_{AstaticMAXa}$ (lb per ft of run wall)	$\sigma'_{A-top}$ (psf)	$\sigma'_{A-bot}$ (psf)	$P_{AstaticPOSa}$ (lb per ft of run wall)	$H_{PAstatica}$ (ft)	Depth of Crack Resulting from Active Stress Distribution (ft)
1	0	50	8105.9	-369.2	1,179.80	8,985.9	5.078	4.767
2	4.767	50	8985.9	-281.2	1,179.80	9,527.1	5.384	3.849
3	3.849	50	8953.3	-298.1	1,193.40	9,549.2	5.334	3.998
4	3.998	50	8962.9	-295.4	1,191.70	9,549.7	5.342	3.973

## H.2 Example No. 2: Total Stress Analysis of a Cohesive Soil

Consider the case of the Figure H.2 20-ft high, moist, cohesive, retained soil with  $S_u = 600$  psf (with  $\phi = 0$  degrees),  $\delta = 0$  degrees, and  $\gamma_{moist} = 130$  psf. The first step in the  $C_{orps}W_{all}Rotate$  analysis of this static earth pressure problem is a sweep-search trial wedge analysis starting with assumption that the depth of cracking is equal to zero. This results in a computed  $P_A$  value equal to 2,000 per ft run of wall using the method outlined in Section A.5 of Appendix A for a planar slip surface with  $\alpha_A$  computed to be 45 degrees from horizontal. The second step is to compute the corresponding earth pressure distribution and depth of cracking using the procedure outlined in Section C.4 of Appendix C. This active earth pressure distribution resulted in a depth of cracking equal to 9.231 ft. Ignoring the tensile stresses within the depth of cracking, as is done by  $C_{orps}W_{all}Rotate$ , the resultant net force,  $P_{AstaticPOSa}$ , corresponding to the computed triangular compressive earth pressure stress distribution, is equal to 7,538.5 lb per ft run of wall with a point of application at 3.59 ft at the end of this first iteration.

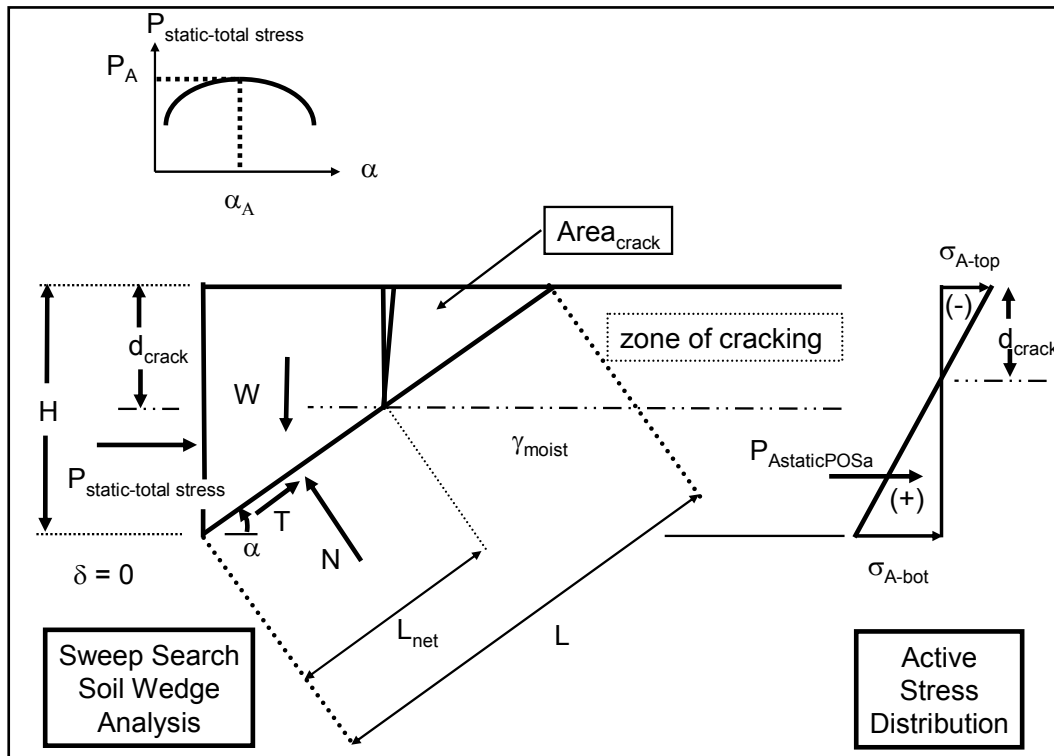


Figure H.2. Sweep-search trial wedge analysis of a cohesive retained soil and the corresponding active earth pressure distribution – total stress analysis.

These Corps Wall Rotate analysis results are consistent with the results for a Rankine active earth pressure distribution, for which the horizontal stress at any depth is given by

$$\sigma_a = K_A \cdot \gamma_{moist} \cdot depth - 2 \cdot c \cdot \sqrt{K_A} \tag{H.1}$$

with

$$K_A = \tan^2 \left( 45 - \frac{\phi}{2} \right) \tag{H.2}$$

Solving Equation H.1 for the depth of zero active horizontal earth pressure, results in a depth of cracking of

$$d_{crack} = \frac{2 \cdot c \cdot \sqrt{K_A}}{K_A \cdot \gamma_{moist}} \tag{H.3}$$

With  $\phi$  equal to zero and  $c$  set equal to  $S_u$  in this problem, Equations H.1 and H.3 simplify to

$$\sigma_a = \gamma_{moist} \cdot depth - 2 \cdot S_u \tag{H.4}$$

and

$$d_{crack} = \frac{2 \cdot S_u}{\gamma_{moist}} \quad \text{H.5}$$

With  $S_u$  equal to 600 psf and  $\gamma_{moist} = 130$  psf, the horizontal active earth pressure at the ground surface and at a 20-ft depth are computed to be -1,200 psf and 1,400 psf, respectively, by Equation H.4. Additionally, the depth of cracking is computed to be 9.231ft below the ground surface. These results are consistent with those from the first iteration of the CorpsWallRotate analysis, summarized in Table H.2. Since the depth of cracking from the active earth pressure distribution (i.e., 9.231 ft) is so much greater than the value assumed in the sweep-search trial wedge solution for  $P_A$  (i.e., 0 ft), additional analyses are required.

Table H.2. Iterative results from the static sweep-search wedge analysis of a cohesive soil – total stress.

Iteration No.	Depth of Crack Used in Sweep Search Soil Wedge Analysis (ft)	$\alpha_A$ (deg)	$P_{AstaticMAXa}$ (lb per ft of run wall)	$\sigma_{A-top}$ (psf)	$\sigma_{A-bot}$ (psf)	$P_{AstaticPOSa}$ (lb per ft of run wall)	$H_{PAstatica}$ (ft)	Depth of Crack Resulting from Active Stress Distribution (ft)
1	0	45	2000.0	-1200.0	1,400.0	7,538.5	3.590	9.231
2	9.231	45	7538.5	-646.2	1,400.0	9,578.9	4.561	6.316
3	6.316	45	6986.1	-821.1	1,519.7	9,866.1	4.328	7.015
4	7.015	45	7219.4	-779.1	1,501.0	9,881.4	4.389	6.834
5	6.834	45	7165.0	-790.0	1,506.5	9,882.5	4.373	6.880

The second sweep-search trial wedge analysis starts with an assumption of 9.231 ft for the depth of cracking, as indicated in Table H.2. A total of five iterations are required to converge on a depth of cracking in which the depth of crack used in the sweep search soil wedge analysis results is consistent with the depth of cracking resulting from the active stress distribution. In the final iteration (i.e., number 5), the net active force corresponding to the compressive stress distribution starting 4.373 ft below top of wall is equal to 9,882.5 lb per ft run of wall. Note that the sweep search active soil wedge solution for  $\alpha_A$  equal to 45 degrees is computed to be equal to 7,165 lb per ft run of wall. These two values differ because  $P_A$  is computed by the sweep search (active) wedge solution and includes the contribution of tensile stresses due to cohesion in the retained soil (e.g., refer to Equation A.31).

# REPORT DOCUMENTATION PAGE

*Form Approved*  
*OMB No. 0704-0188*

Public reporting burden for this collection of information is estimated to average 1 hour per response, including the time for reviewing instructions, searching existing data sources, gathering and maintaining the data needed, and completing and reviewing this collection of information. Send comments regarding this burden estimate or any other aspect of this collection of information, including suggestions for reducing this burden to Department of Defense, Washington Headquarters Services, Directorate for Information Operations and Reports (0704-0188), 1215 Jefferson Davis Highway, Suite 1204, Arlington, VA 22202-4302. Respondents should be aware that notwithstanding any other provision of law, no person shall be subject to any penalty for failing to comply with a collection of information if it does not display a currently valid OMB control number. **PLEASE DO NOT RETURN YOUR FORM TO THE ABOVE ADDRESS.**

<b>1. REPORT DATE (DD-MM-YYYY)</b> December 2006		<b>2. REPORT TYPE</b> Final report		<b>3. DATES COVERED (From - To)</b>	
<b>4. TITLE AND SUBTITLE</b>  Rotational Response of Toe-Restrained Retaining Walls to Earthquake Ground Motions				<b>5a. CONTRACT NUMBER</b>	
				<b>5b. GRANT NUMBER</b>	
				<b>5c. PROGRAM ELEMENT NUMBER</b>	
<b>6. AUTHOR(S)</b>  Robert M. Ebeling and Barry C. White				<b>5d. PROJECT NUMBER</b>	
				<b>5e. TASK NUMBER</b>	
				<b>5f. WORK UNIT NUMBER</b>	
<b>7. PERFORMING ORGANIZATION NAME(S) AND ADDRESS(ES)</b>  Information Technology Laboratory U.S. Army Engineer Research and Development Center 3909 Halls Ferry Road Vicksburg, MS 39180-6199				<b>8. PERFORMING ORGANIZATION REPORT NUMBER</b>  ERDC/ITL TR-06-2	
<b>9. SPONSORING / MONITORING AGENCY NAME(S) AND ADDRESS(ES)</b>  U.S. Army Corps of Engineers Washington, DC 20314-1000				<b>10. SPONSOR/MONITOR'S ACRONYM(S)</b>	
				<b>11. SPONSOR/MONITOR'S REPORT NUMBER(S)</b>	
<b>12. DISTRIBUTION / AVAILABILITY STATEMENT</b> Approved for public release; distribution is unlimited.					
<b>13. SUPPLEMENTARY NOTES</b>					
<b>14. ABSTRACT</b>  This research report describes the engineering formulation and corresponding software developed for the rotational response of rock-founded, toe-restrained Corps retaining walls to earthquake ground motions. The PC software $C_{orps}W_{all}Rotate$ (sometimes referred to as $CWRotate$ ) was developed to perform an analysis of permanent wall rotation for each proposed retaining wall section to a user-specified earthquake acceleration time-history. A particular formulation of the permanent sliding (i.e., translational) displacement response of retaining walls is also described. The resulting engineering methodology and corresponding software are applicable to a variety of retaining walls that are buttressed at their toes by a structural feature (e.g., navigation walls retaining earth, spillway chute walls, spillway discharge channel walls, approach channel walls to outlet works structures, highway and railway relocation retaining walls, and floodwall channels). $C_{orps}W_{all}Rotate$ is particularly applicable to L-walls and T-walls (cantilever retaining walls) and may also be used to predict permanent, seismically induced displacements on retaining walls with or without a toe restraint.  <div style="text-align: right;">(Continued)</div>					
<b>15. SUBJECT TERMS</b>		Earthquake ground motions	Rotation	Translation	
Displacement		Earth retaining structures	Seismic		
Dynamic earth pressures		$C_{orps}W_{all}Rotate$	Soil dynamics		
<b>16. SECURITY CLASSIFICATION OF:</b>			<b>17. LIMITATION OF ABSTRACT</b>	<b>18. NUMBER OF PAGES</b>	<b>19a. NAME OF RESPONSIBLE PERSON</b>
<b>a. REPORT</b>	<b>b. ABSTRACT</b>	<b>c. THIS PAGE</b>			<b>19b. TELEPHONE NUMBER (include area code)</b>
UNCLASSIFIED	UNCLASSIFIED	UNCLASSIFIED		342	

#### 14. ABSTRACT (concluded)

Formal consideration of the permanent seismic wall displacement in the seismic design process for Corps-type retaining structures is given in Ebeling and Morrison (1992). The key aspect of the engineering approach presented in this 1992 document is that simplified procedures for computing the seismically induced earth loads on Corps retaining structures are also dependent upon the amount of permanent wall displacement expected to occur for each specified design earthquake. The Ebeling and Morrison simplified engineering procedures for Corps retaining structures, including waterfront retaining structures, are geared towards hand calculations. The engineering formulation and corresponding PC software *C<sub>orps</sub>W<sub>all</sub>Rotate* discussed in this report extend simplified procedures to walls that rotate or slide during earthquake shaking and make possible the use of acceleration time-histories in the Corps' design/analysis process when time-histories are made available on Corps projects. The engineering methods contained in this report and implemented within *C<sub>orps</sub>W<sub>all</sub>Rotate* allow the engineer to rapidly determine if a given retaining wall system has a tendency to rotate or to slide for a specified seismic event.